AMAM 2000

Proceedings of the International Symposium
on Adaptive Motion of Animals and Machines

August 8-12, 2000

McGill University, Montreal, Canada

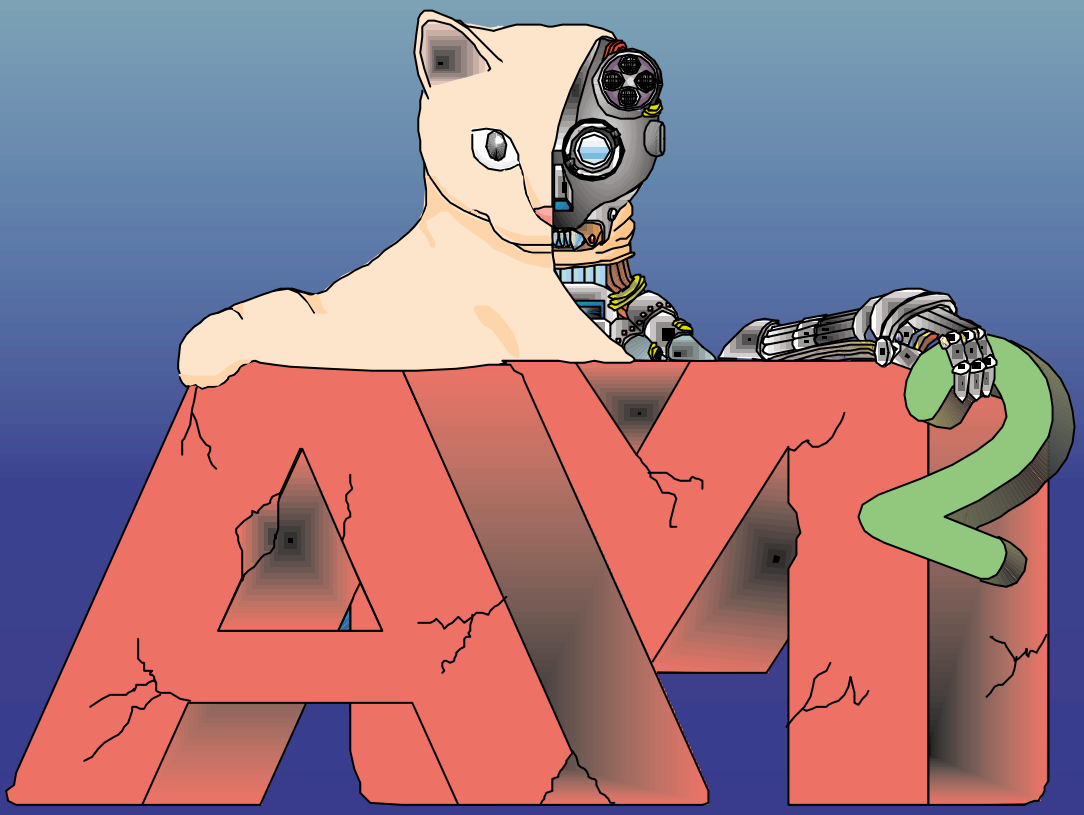

International Symposium on Adaptive Motion of Animals and Machines (AMAM)
Montreal, Canada, August 8-12, 2000

Tuesday August 8, 2000

Wednesday August 9, 2000

Keynote Speech IV

Thursday August 10, 2000

Friday August 11, 2000

Keynote Speech VIII

Session FrA-I: Technical Development of Mechanism and Control
Chairs: *M. Buehler[1] and K. Yoneda[2]*
[1]McGill University
[2]Tokyo Institute of Technology

Session FrP-II: Super Mechano-Systems
Chairs: *F. Matsuno[1] and R. M. Voyles[2]*
[1]Tokyo Institute of Technology
[2]University of Minnesota

Proceedings of the International Symposium on
Adaptive Motion of Animals and Machines,
Montreal, Aug.8-12, 2000

Briefing of AMAM

H.Kimura[1], H.Witte[2] and G.Taga[3]

[1]Univ. of Electro-Comm., Tokyo, hiroshi@kimura.is.uec.ac.jp

[2]Friedrich-Schiller-Universitat Jena, witte@pan.zoo.uni-jena.de

[3]Univ. of Tokyo & PRESTO, JST, Tokyo, taga@complex.c.u-tokyo.ac.jp

Abstract

In this symposium, several functions of skeletal systems (mechanisms), muscles (actuators) and nervous systems (control) in adaptive motion will be discussed. In addition, relations and coupling between them should become important issues for discussion. In vertebrates, the nervous system as the control instance allows to separate into low level (generation and control at spinal cord), medium level (adaptation at cerebellum), and high level (adaptation at cerebrum) control. In invertebrates, on a first glance the underlying morphology is more integrated, making it difficult to identify functional sub-units of control. Musculoskeletal systems more than ever have to be analyzed in view of dynamic properties of mechanisms. The transfer of those molecular physiological and biomechanical concepts into applications on machine design will be an important topic of the conference.

1 Motivation

It is our dream to understand principles of animals' surprising abilities in adaptive motion and to transfer such abilities on a robot. Up to now, mechanisms for generation and control of stereotyped motions and adaptive motions in well-known simple environment were formulated to some extent and successfully applied to robots. However, principles of adaptation to various environments have not yet been clarified, and autonomous adaptation is left unsolved as seriously difficult problem in robotics.

Apparently, the adaptation ability shown by animals and needed by robots in a real world can not be explained or realized by one single function in control system and mechanism. That is, adaptation in motion is induced at every level in a wide spectrum from central neural system to musculoskeletal system. Thus, we organized this symposium for scientists and engineers concerned with adaptation on various levels to be brought in contact, to discuss on principles on each level and to investigate principles governing total systems. We believe that this symposium will stimulate interests of both scientists and engineers.

2 Outlines

Starting with "high level sensory adaptation" (vision), we arranged the following sessions in an order "decreasing level of neural control, increasing intelligence of construction/morphology/mechanisms".

- Visual Adaptation Mechanisms of Systems in Locomotion
- Neuro-Mechanics
- Design of Neural Controller
- Adaptive Locomotion
- Modeling and Analysis of Motion
- Adaptive Mechanics
- Behavior and Motion of Humans & Humanoids
- Technical Development of Mechanism and Control
- Super-Mechano Systems

The backgroud of papers in those sessions widely broaden on biology, physiology, biomechanics, nonlinear system dynamics and robotics. It is usually difficult for people from different disciplines to discuss on particular issues. In order to ease this problem, we invited five keynote speakers impressively studying on each field. We expect from each keynote speaker to give a comprehensive knowledge found in his field to the audience before the start of the more specialized technical sessions. We also asked the first speaker of each session to explain current states of related research field with additional 10 minutes of talk.

Although all presented studies are referring to principles of animals' motion in some sense, each study differs from others in the actual extent of reference. Roughly speaking, two thirds of all contributions are

deeply inspired by principles discovered in animals' motion. In the remaining studies, new ideas are engineeringly proposed and not always constrained by principles of animals' motion. The comparison and competition between biologically inspired methods and engineeringly derived methods in view of ability and complexity in adaptation is important for the future development of novel machines.

3 Key Issues in AMAM

In this section, several key issues in AMAM clarified through discussion between IPC members are enumerated. Terms contrasted in each subsection are not always contrary to each other. But it is very interesting that there are different standing positions in considering generation and adaptation of motion.

3.1 Animals vs. Machines

Animals and machines are quite different in their sensors, actuators, and controlling devices. We would like to know what kind of principles in adaptive motion can be the same, similar or should be different in animals and machines.

3.2 Behavior vs. Motion

There were several interdisciplinary conferences concerned with "Adaptive Behavior": SAB2000[1], for example. In SAB and behavior based robotics, importance of "embodiness" and "dynamics" were emphasized. But these terms usually are used in the sense that a system has sensors and actuators, or that a time factor is considered, since they were proposed in artificial intelligence. The control system in most cases is represented by a diagram consisting of boxes and arrows or a state transition graph.

On the other hand, most of studies presented in AMAM are concerned with "natural dynamics" expressed by dynamic equations. The control system or mechanism for "Adaptive Motion" is described by using differential equations or transfer functions. Therefore, dynamic properties of both control system and musculoskeletal system are important, and adaptation at all levels is required.

Of course, differences between behavior and motion described above are not induced by their linguistic definition, but just the temporary status at this moment.

3.3 Model Based vs. Biologically Inspired

In conventional robotics, since exact models of a robot and environment are necessary and the whole motion of a robot in environment is described as an algorithm based on models, autonomous adaptation requires complicated programs.

On the other hand, such biologically inspired methods like connectionism or behavior based robotics employ a quite different approach. In those methods, motion is not described by using algorithms governing the whole system but by using relations between elements, and adaptive motion is generated through emergent interaction with the environment. Since relations between elements in response to sensor input are sufficient as a description, autonomous adaptation can be derived by simple programs and complicated dynamics of systems in biologically inspired methods. But we have some difficulties in predicting what kind of motion is generated in particular environment.

The comparison between the methods is illustrated in Table 1.

	Model Based	Biologically Inspired
model	robot and environment	not necessary explicitly
description for motion	algorithm governing whole system	relation between elements
prediction/ reappearance	easy	difficult
adaptation	complicated program	emergence in dynamics

Table 1 Comparison between a model based method and a biologically inspired method for adaptive motion

3.4 Control vs. Mechanics

In high speed motion like running, it is difficult to realize effective control in very short stance phase. Therefore, the importance of the passive dynamic properties of the musculo-skeleton is pointed out in biology, and machine design in such view point is emphasized in robotics in these days. The passive dynamic properties yet identified to be relevant in this context are the configuration of joints and links (geometry, morphology, topology) and spring and damping factors in muscles, tendons, soft tissues, joints or exoskeletons (structural or material properties).

On the other hand, one of the reasons why motion generation and adaptation can be derived by using relatively simple neural systems is that part of the dynamics of the musculoskeleton is encoded in neural systems as parameters of CPG(Central Pattern Generator) and reflexes. Therefore, the coupling between the dynamics of neural system and the passive dynamic properties of the musculoskeleton will become increasingly important in biologically inspired robotics.

Studies of "Super-Mechano Systems" also are aiming at the new machine design method by combining control theory and mechanical design.

3.5 Locomotion vs. Manipulation

Are locomotion and manipulation based on the same principles, as far as mechanisms of motion generation and adaptation are concerned? IPC members have no consensus about how to answer this question. At least in robotics, locomotion and manipulation have been developed independently to some extent. For example, fine motion in assembly tasks, and motion planning and control in vision coordination are typical sensor based adaptations in manipulation. Manipulation theories for such motion types are established completely independently of locomotion. But we have established sufficient locomotion theories in neither sensor based nor sensorless dynamic adaptation yet. It seems that this is the reason why a lot of people are interested in biologically inspired locomotion control.

We even would like to provoke any comments from participants from different fields to this topics.

3.6 Visuomotor Adaptation in Locomotion

Even if we accept that basic walking patterns to some extent are generated by CPGs, it is not clear enough how vision based adaptation is related to CPGs. There are several hypotheses:

(1) directive signals based on vision are sent to CPG and CPG itself adjusts motion of a leg,

(2) reflexes based on vision adjust motions of a leg independently of CPGs generating basic walking patterns,

(3) only reflexes generate walking patterns and adjust motion of a leg without CPGs.

We are expecting active discussion in related sessions.

In addition, it is also very important to make it clear how adaptation based on vision is acquired through learning.

3.7 Being Genetically Programmed vs. Learning vs. Development

It is well known that a horse can start walking several hours after its birth perhaps mostly by a genetically programmed mechanism with slight tuning mechanism at spinal cord. However, as sensor informations for adaptation become sophisticated, learning at the cerebellum for adaptation and learning at the basal ganglia for adjustment based on vision becomes more important. When we design control systems for a robot, it will become important to make it clear what kind of combinations of these mechanisms are totally effective in view of costs of programming, experiments and computation. In addition, during ontogenetic development not only parameter tuning but also drastic changes of structure are a very important matter of adaptation.

4 Future

It is important how to combine contrasted issues in Section.**3** according to task level.

No matter what we discuss on, "Science vs. Engineering" or "Biology vs. Robotics" is not one of the key issues in AMAM. When we solve unknown complicated problems, it is desirable to proceed analysis and synthesis concurrently. It is well-known that analysis by synthesis is a really good and important methodology to understand principles. That means the beginning of a new interdisciplinary research field where science and engineering are merged.

References

[1] SAB2000, Int. Conf. on Simulation of Adaptive Behavior, http://www-poleia.lip6.fr/ sab2000/

Keynote Speech I

Proceedings of the International Symposium on
Adaptive Motion of Animals and Machines,
Montreal, Aug.8-12, 2000

Neuronal mechanisms for the adaptive control of locomotion in the cat.

Trevor DREW
Department of Physiology, University of Montréal
P.O. Box 6128, Station "centre-ville", Montréal, Québec, H3C 3J7, Canada
Email: drewt@ere.umontreal.ca

1. Introduction

Locomotion is a highly complex activity whose control is ensured by the coordinated action of a number of diverse structures and nuclei at different levels of the central nervous system. Indeed, an animal in full flight, moving over a surface that is irregular and full of obstacles, needs to call on the full capacity of its nervous system in order to adjust its movements to the terrain. In such a circumstance, locomotion is much more than a simple rhythmical activity that requires alternating activity in flexor and extensor muscles of the limbs. Locomotion become a challenge in which posture and equilibrium must be maintained in the face of self-imposed perturbations as the feet exert forces at angles anything but perpendicular to the ground and limb trajectories must be continually altered to assure that the limbs clear obstacles and are placed appropriately on the support surface. The aim of this brief chapter is to give the reader an overview of some of the neural structures that are involved in such behaviours and of the manner in which they may exert their control. Because of space limitations, the focus in this chapter will be on the role of the motor cortex in the adaptations required during voluntary modifications of gait. However, for those who have little background in the neuronal mechanisms used to control animal locomotion, the chapter will also provide some general information on the role of both spinal and supraspinal structures in the control of locomotion.

2. The basic locomotor rhythm

It is quite clear from the experimental evidence that most mammals(reviewed in: Armstrong 1986; Grillner and Wallen 1985; Rossignol 1996), including non-human primates (Fedirchuk et al. 1998), and probably humans themselves (Calancie et al. 1994; Dietz et al. 1995; Harkema et al. 1997), possess neuronal circuits within the spinal cord that are capable of generating the basic alternating rhythm of locomotion. Evidence for this statement comes from several sources but is best illustrated by the remarkable capacity of adult cats with complete transections of the thoracic spinal cord to execute well coordinated locomotor movements with the hindlimbs when placed on a treadmill (Barbeau and Rossignol 1987; Bélanger et al. 1996; Eidelberg et al. 1980; Giuliani and Smith 1987; Lovely et al. 1990). Such cats are not only capable of generating a locomotor rhythm but also of adapting that rhythm to changes in treadmill speed and, to a small extent, to changes in the orientation of the treadmill either in the pitch tilt (nose up and nose down) or the roll tilt (ear down) conditions. In addition, if the hindlimb of such spinal cats hits an obstruction the spinal cord contains the requisite circuitry to ensure that the leg is appropriately brought away from and then over the obstruction in a manner very similar to that observed in the intact cat.

While experiments in spinal cats show the capacity of the lumbo-sacral cord to generate and, within limits, to adapt locomotion, it must be realised that in these animals there is abundant rhythmical peripheral afferent feedback from the moving limbs that can both entrain and modify the locomotor rhythm (Rossignol 1996). The existence of a locomotor rhythm in such animals, therefore, does not of itself prove that the spinal cord contains the intrinsic circuitry that is necessary for locomotion. However, other experiments have shown unequivocally that the spinal cord is, indeed, capable of generating a pattern of rhythmical activity that closely resembles that observed during locomotion in the intact animal. This has been demonstrated very clearly by recording locomotor activity in animals in which the spinal cord is completely transected and rhythmical movement of the limbs is prevented by applying a paralysing agent, such as curare, that blocks the neuromuscular junction. In such animals, it is possible to record the central locomotor command signals from motor nerves, an electroneurographic recording, instead of by recording electromyographic (EMG) activity from the muscles as one normally does in the intact animal. Such locomotion, in an animal which is paralysed and, therefore, can not walk, is normally referred to as fictive locomotion. In such a preparation, after application of various pharmacological agents, or non-specific electrical stimulation, it is possible to record from the motor nerves a rhythm that shows some of the complexity of the normal locomotor pattern, thus demonstrating the intrinsic capacity of the spinal cord to generate the basic locomotor rhythm (Grillner and Zangger 1975, 1979; Pearson and Rossignol 1991). Details

concerning the organisation of this intrinsic spinal central pattern generator, or CPG, can be found in the chapter by Cohen.

The existence of such a CPG implies that neither peripheral afferents nor supraspinal structures are necessary for the generation of the basic locomotor rhythm. However, both are essential for the adaptation of that rhythm to the take into account the vagaries of the terrain over which it walks. Indeed, one should normally assume that, in the normal, intact, animal, even the most basic locomotion over a flat, even, surface is the result of the integrative action of the spinal rhythm generating circuits and the rhythmical inputs from peripheral afferents and supraspinal structures.

3. Descending control of Locomotion

Descending regulatory signals from supraspinal structures are essential for the full expression of locomotion as has been shown by a wide array of experiments carried out in a large number of different laboratories (for general reviews, see: Armstrong 1986, Rossignol, 1996, Orlovsky et al. 1999). This fact is best appreciated by a consideration of the deficits that are seen following complete transection of the spinal cord at the lower thoracic level. As documented above, adult cats with such complete transections have the remarkable ability to recuperate locomotor activity of the hindlimbs, which are capable of walking on a moving treadmill belt and of adapting their movements to changes in speed and, to a lesser extent, to changes in slope. However, these cats, even after several months of training, show a number of serious deficits that highlight the normal contribution of input from supraspinal structures in the control of locomotion. Among these deficits, the most evident are: i) a loss of adequate weight support and of lateral stability; ii) an inability to voluntarily initiate locomotion; iii) a loss of interlimb coordination between the fore- and hindlimbs; and iv) an inability to make any anticipatory modifications of the locomotor pattern. Separate experimental evidence is available in each case to show that descending signals from the brain are essential for (i, ii, and iv) or contribute to (iii) these functions. In addition, it is probable that loss of descending information also contributes to some of the more subtle deficits seen in these animals; for example, the loss of intralimb coordination evident in cats with both complete and incomplete transections of the spinal cord. In sum then, while the spinal cord produces a basic locomotor rhythm, supraspinal (and peripheral) signals are essential to produce what has been referred to as behaviourally relevant locomotion (Grillner and Wallen 1985).

While a general review of the interactions between the different supraspinal pathways and the basic locomotor rhythm is beyond the scope of this chapter, it is important to emphasize that, in most cases, descending systems probably exert their effect either via the CPG, or through interneuronal pathways that are modulated by the output of the CPG, rather than by a direct action on the motoneurones controlling the muscles themselves. Such a mode of action ensures that the descending signals from the supraspinal structures are appropriately integrated into the base rhythm (McCrea 1996). Evidence for this assertion comes primarily from experiments in which the effects of stimulating different structures during locomotion have been studied. In virtually every case that has been examined, it has been found that the effects of such stimuli are phase-dependent. That is, stimulation in certain phases of the locomotor cycle is effective in eliciting modifications of EMG activity, while stimulation in other phases is ineffective. For example, weak stimulation of the lateral vestibular nucleus (LVN) during stance elicits brief responses in extensor muscles and has no effects on flexor muscles (Orlovsky 1972). The same stimulation applied to the LVN during the swing phase is without effect. Conversely, stimulation of the red nucleus is most effective when applied during the swing phase when it evokes facilitatory responses in most flexor muscles (Orlovsky 1972; Rho et al. 1999); during stance it is either without effect (Orlovsky 1972) or produces a mixture of facilitatory and inhibitory responses in extensor muscles (Rho et al. 1999). Stimulation of the pontomedullary reticular formation (PMRF) always produces complex effects, with stimulation during stance producing a mixture of facilitatory and inhibitory responses in extensor muscles and stimulation during swing generally producing facilitatory responses in flexor muscles (Degtyarenko 1993; Drew and Rossignol 1984; Drew 1991; Orlovsky 1972).

While these effects might be explained simply on the basis of the level of depolarization of motoneurones, examination of the phase at which the maximal response is obtained frequently shows it to be different from the period of peak EMG amplitude, suggesting mediation via phasically active interneuronal pathways. Other experiments, in which the intensity and the duration of the stimulus train has been increased show that many supraspinal structures are also capable of resetting the locomotor rhythm, generally by prolonging either the swing or stance phases of the locomotor cycle (Armstrong and Drew, 1985; Degtyarenko 1993; Drew and Rossignol 1984; Leblond and Gossard 1997; Perreault et al. 1994; Rho et al. 1999; Russell and Zajac 1979). Such a capacity

suggests that these supraspinal structures may act through interneurones that form part of the CPG. Resetting of the rhythm has been observed for all structures in the fictively locomoting cat but is less frequently observed, and less strong, in the intact cat. This suggests that all descending pathways have access to the CPG but that, in the intact cat, the peripheral and cortical pathways have a stabilizing influence that makes it difficult for signals from any one pathway to disrupt the ongoing locomotor rhythm. The exception is the corticospinal pathway which seems to have privileged access to these pathways allowing descending cortical commands to modify the locomotor rhythm (Orlovsky 1972; Rho et al. 1999).

The sum result of this type of organisation is that descending commands will normally produce modifications of locomotor activity that are superimposed onto the locomotor rhythm without undue interruption of that rhythm. Only if the strength of the descending signal is increased is it possible to modify that rhythm, and only in response to signals from the motor cortex does it seem possible, in the intact animal, to produce a change in the overall locomotor cycle.

4. Anticipatory control of locomotion

4.1 An Overview

Efficient locomotion over irregular terrain is impossible without visual information. Experiments have shown that under relatively undemanding circumstances, human subjects do not need to fixate objects or to continuously scan their immediate environment but will rather normally make intermittent visual samples of their environment (Assaiante et al. 1989; Laurent 1991; Laurent and Thomson1988; Patla 1989; Patla and Vickers 1997). However, as the difficulty of the locomotor task increases, so does the frequency of the samples that are made so that under circumstances in which subjects must accurately place their feet in each step, visual information of the environment is, likewise, made in each step (Hollands et al. 1995; Hollands and Marple-Horvat 1996; Patla et al. 1996). These data are reviewed in the chapter by Patla and will not be discussed further here.

Once visual information about the environment has been sampled, it must be transformed into a pattern of muscular activity that is appropriately scaled to produce the gait modification required to avoid or to step around an obstacle, or to place the foot accurately in a given location.

This is a highly complex process of visuomotor transformation that undoubtedly involves parallel processing in several different areas of the brain, including different areas of the cerebral cortex, the cerebellum and the basal ganglia. However, the exact mechanisms by which the various stages of this transformation occur are poorly understood and have been studied in any detail only in primates trained to make reaching movements to a target. The growing consensus from such work is that a major part of this transformation occurs within the parietal cortex where the signal is progressively transformed from one in which the target is represented in spatial coordinates to one in which it is expressed as an internal representation of the kinematics and kinetics of the movement that are needed to attain the target (see, Caminiti et al. 1996; Johnson et al. 1996; Kalaska 1996; Kalsaka and Crammond 1992; Kalaska and Drew, 1993). Although there is presently no direct evidence on the subject, one may assume that similar processes of visuomotor transformation occur during visually guided locomotion and that similar cortical areas participate in this task. However, during locomotion, there is the added complication that the body is in motion and that the modifications of body orientation and limb trajectory required to step around or over an object have also to be planned on the basis of the speed of progression. In such circumstances the animal must also judge the distance to the target, perhaps by using optic flow signals providing information about the time to contact (Gibson, 1968; Goodale et al. 1990; Lee 1976, 1980; Patla and Vickers 1997) and incorporate them into the locomotor pattern. Such a process may use a forward model (Jordan and Rumelhart 1992; Wolpert et al. 1995) to incorporate this visual information into the basic walking rhythm (McFadyen et al. 1994).

Regardless of the exact neuronal mechanisms that are used to plan the gait modification that is to be made, the final step in this process is a signal that encodes the movement that has to be made. There is general agreement that for both reaching movements and for anticipatory, or visually-triggered, gait modifications the final signal used to control the movement is to be found, in part, in the neuronal discharge of neurones within the motor cortex. The remainder of this section will discuss the signal that is contained within these cortical neurones and the manner by which it may produce the changes in limb trajectory required to step over an obstacle.

4.2 Role of the Motor Cortex

The importance of the motor cortex for the adaptation of locomotion to the nature of the surface on which one walks can be simply demonstrated by surgically excising the motor cortex, by pharmacologically inactivating it or by transecting the major descending pathway from the motor cortex,

either in the pyramidal tract or within the spinal cord (reviewed in Drew et al. 1996). In all cases, interruption of this pathway results in only transient deficits in locomotion on a flat surface, but long-lasting, and probably permanent, deficits in the ability of cats to safely negotiate obstacles in their course and to accurately place their paws in the required location. Thus, one may assume that the signal transmitted within the corticospinal tract is necessary for the appropriate adjustments of the locomotor gait required in such circumstances.

The nature of this signal has been studied by recording the activity of individual neurones within the motor cortex during locomotor tasks that require anticipatory modifications of gait. Such studies, in tasks requiring cats to either accurately place their paws on the rungs of a horizontal ladder (Amos et al. 1990; Armstrong and Marple-Horvat 1996), to step over barriers in their path (Beloozerova and Sirota 1993), or to step over obstacles attached to a moving treadmill belt (Drew 1998; Drew 1993; Drew et al. 1996; Widajewicz et al. 1984) have all shown that neurones in the motor cortex exhibit significant modifications of their discharge activity that are tightly linked to the movement that is to be made.

An example of such a modification is illustrated in Fig.1 which shows the change in limb trajectory (Fig. 1B) and the associated change in EMG activity and neuronal activity when a cat steps over an obstacle with a round cross-section that is attached to a moving treadmill belt. The neurone illustrated in this example was recorded from the motor cortex, in the posterior bank of the cruciate sulcus. It was identified as a neurone whose axon (conduction velocity of 44m.s^{-1}) descended at least as far as the pyramidal tract; the neurone could, therefore, be classified as a pyramidal tract neurone (PTN). During the step over the obstacle, there was a modification in the duration, amplitude and, in some cases (e.g. EDC) of the temporal relationships of the muscles that can be seen both in the single step illustrated in Fig. 1C and in the average illustrated in Fig 1D. Associated with the gait modification, there was a large increase in both the duration and, more particularly, the frequency of the discharge in the recorded PTN (Unit). It is to be noted that there was no change in the frequency of cell discharge in the step preceding that over the obstacle, supporting the general view that the motor cortex is involved in the execution of the task and not in its planning (see Kalaska and Drew 1993).

What is the descending signal from the motor cortex controlling? Is the motor cortex producing a signal that is defining the path of the paw over the obstacle, one that defines the changes in angle of the different limb segments, or one that provides more specific information concerning the detailed modifications in muscle activity that are required to produce this modification? The data obtained in my own experiments lead me to suggest that the motor cortex provides a detailed signal that specifies the changes in muscle activation that are required to produce the change in limb trajectory. Details concerning the reasons for this suggestion can be found within the original papers and review article (references above) but can be summarized briefly in the following manner.

Examination of the changes in EMG activity of muscles acting around different joints during voluntary gait modifications shows that the smooth change in limb trajectory that is observed during a gait modification (Fig 1B) is, in fact, produced by a complicated modification of the pattern of activity in most muscles acting around the different joints of the cat forelimb. Modifications range from simple changes in the level or duration of the period of activity through to more complicated changes in the temporal relationships between muscles; in some muscles there are changes in all three parameters. The changes in muscle activation patterns are, as would be expected, sequential so that changes in different muscle groups occur at different times during the modified swing phase of the gait modification. This can be appreciated from inspection of Figs 1 C and D. For example, the ClB shows a large increase in both its amplitude and duration which occupies the entire swing period while the Br shows primarily an increase in its amplitude during the initial period of flexion that would serve to lift the limb above the obstacle. The TrM also shows a relatively brief period of increased activity and this precedes the modification of activity in Br as the shoulder must be retracted to lift the paw from the support surface before the limb is flexed. The EDC shows a more complicated pattern of activity as, during control locomotion, it has a single period of activity in each step cycle and during the gait modification it is active twice.

Examination of the modification of unit activity that is seen during these gait modifications showed a similar pattern. That is, different PTNs also exhibited their major changes in activity at different times during the swing phase of the modified gait cycle. This is illustrated in Fig. 2 for two neurones that increased their discharge activity at different times during the gait cycle. Unit A showed an increase early in the gait modification, coinciding approximately, with the period of increased activity in the TrM, needed to retract the shoulder. In contrast, Unit B discharged realtively later in the gait cycle, approximately in phase with the second period of

increased activity in the EDC which serves to prepare the limb for landing after the obstacle has been cleared. It is also interesting to note that in the Trail condition, in which the limb contralateral to the recording site is the second to pass over the obstacle, both neurones changed their relative phase of activity with respect to the onset of the ClB, but maintained their relationship to the periods of modified activity in the TrM and the EDC, respectively. This suggests that different PTNs are involved in regulating the activity of a select group of muscles and that the relationship between cell and muscle is maintained even if the overall pattern of activity changes.

Overall, the data from the entire population of neurones indicated that different PTNs are active at different times during the gait modification, with some discharging early in the swing phase, as in the example in Fig 2A and others discharging slightly later (not illustrated), as the limb is being lifted above the obstacle. Still others, such as that illustrated in Fig. 2B, discharge at the end of the swing phase, as the limb is being prepared for contact with the support surface, while yet others, similar to the example illustrated in Fig. 1, are active throughout the swing phase. This suggests that the overall change in limb trajectory is produced by the sequential activation of populations of PTNS, with each population involved in specifying the modulation of activity required in small groups of muscles at different times during the gait modification.

4.3 Interaction with the locomotor rhythm

How is the gait modification superimposed upon the basic locomotor cycle? Fig 3. illustrates a conceptual model that we have used previously to discuss this issue. In brief, we follow Grillner (1982) in suggesting that the CPG may be usefully thought of a series of unit CPGs in which separate modules are used to regulate the rhythmical activity around different articulations. Although the basis for this idea of unit pattern generators is based primarily on theoretical considerations of the flexibilty required to produce different movements, some experimental evidence for the idea of modules comes from the work of Stein in the turtle (reviewed in Stein and Smith 1997).

The advantage of a modular organisation for the control of voluntary gait modifications is that descending systems may bias the activity in one or more modules without, necessarily, changing the activity in other modules. Such an ability is essential when one considers the variety of limb trajectories that are required to step over obstacles of different shapes and sizes. For example, stepping over a very wide obstacles requires a large protraction of the limb and consequently a large increase in the duration of the shoulder flexors. However, stepping over a very narrow but high obstacle requires primarily a large flexion of the elbow. Stepping over a cylindrical obstacle (see Fig. 1) requires the coordinated action of both the shoulder and the elbow muscles. The modular organisation illustrated in Fig. 3 allows a descending signal to differentially modulate the activity of one of the modules by itself, or in combination with any other, thus providing the required flexibility. We suggest that the different patterns of discharge in motor cortical neurones provides the neuronal substrate by which the different modules are modified.

The suggestion that the gait modifications act through a modular CPG, although conceptual in nature, is based upon experimental data. First, it must be realized that all corticospinal projections in the cat are directed at interneurones, i.e there are no monosynaptic connections with motoneurones (Illert et al. 1976). Second, the results from experiments in which brief trains of stimuli have been applied to the motor cortex show that the responses are organized in a phase-dependent manner (see above), suggesting that the effects are mediated through interneurones that are either part of, or influenced by the CPG. Third, as described above, longer trains of stimuli are capable of resetting the locomotor rhythm, suggesting that the corticospinal system has access to the CPG. In addition, by acting through the interneuronal networks involved in controlling cycle timing and structure, the nervous system can take advantage of the intrinsic spinal cord circuits to ensure that changes in any one module are fully integrated into changes in the other modules. The interconnections between spinal modules and those between different cortical neurones, together, would ensure that all movements are smoothly integrated into the locomotor pattern.

However, if such mechanisms might act to ensure integration and coordination, what mechanisms ensure specificity? It is well known, for example, that individual corticospinal neurones do not activate interneurones that will affect only one or two muscles but, rather, are more likely to influence the activity of a substantial number of synergists (Fetz et al. 1976; Shinoda et al 1981). Probably, part of the explanation comes from the relative synaptic weight on different muscles. At least for the direct, corticomotoneuronal, projections in primates, it is known that the connections that a motor cortical neurone makes with some motoneurones are stronger than those with others (Fetz et al. 1976; Bennett et al 1996). Similar considerations probably hold for the connections made through interneurones, i.e connections thorough interneuronal pathways to some muscle groups are likely to be stronger than those

through others. In the example illustrated in Fig. 3 we suggest that different populations of neurones active when the limb is lifted above and over the obstacle (referred to in our previous publications as Phase I) would project to different modules of the CPG allowing the differential modification of shoulder, elbow and wrist muscles. Although neurones in each population would project to several modules, each of these populations would have stronger projections to one module than to the others. Neurones active in Phase II, during the time that the limb is prepared for contact with the support surface, are suggested to preferentially activate modules regulating the activity of the distal muscles that are necessary to stabilize the paw at this time. Interestingly, a neural network model (Prentice and Drew 1997), based on the motor cortical data that was obtained in the experiments in cats, has shown that specificity of action on different muscle groups can indeed be maintained by the spatio-temporal organization of the "corticospinal connections", even though the axons of individual populations of neurones branch widely onto "spinal neurones".

5. Coordination of Posture and Movement

In addition to controlling the trajectory of the limb as an animal steps over an obstacle, there is also a requirement to ensure postural stability. As the cat lifts it legs over the obstacle, it needs to modify its posture to ensure stability and equilibrium as the centre of gravity is shifted. Recordings of ground reaction forces (GRFs) and of EMG activity from extensor muscles in each of the four limbs of the cat suggests that these postural responses consist of a coordinated modification of activity in each of the supporting limbs (Lavoie et al. 1995; McFadyen et al. 1999). Moreover, these modifications of postural activity are dynamic and have to be incorporated into the locomotor cycle.

Our recent experiments suggest that the descending signal from the motor cortex that specifies the voluntary gait modification that is to be made also specifies the magnitude and timing of the postural responses that accompany it (Kably and Drew 1998). We base this suggestion both on a consideration of anatomical connections between the cortex and the brainstem and of the physiological properties of certain classes of corticofugal neurones in the motor cortex and in the pontomedullary reticular formation during voluntary gait modifications. The former structure, as we have detailed in the preceding sections, is strongly implicated in the control of voluntary movements. The latter, is a brainstem structure that is implicated in the regulation of flexor and extensor muscle activity during locomotion and which is suggested to be involved in the control of posture (see Mori 1987, 1989; Mori et al. 1992).

It is known that there is a strong projection from the motor cortex to the PMRF, the corticoreticular pathway (Canedo 1997; Canedo and Lamas 1993; Jinnai 1984; Keizer and Kuypers 1984; Matsuyama and Drew 1997; Newman et al. 1989; Rho et al. 1997), that could be used to adjust the motor output of the latter. Experiments in which the terminal projections of motor cortical neurones have been recorded show that many phasically active motor cortical neurones project both to the spinal cord and to the PMRF. As such the signal transmitted to the spinal cord is also transmitted to the PMRF, where many corticoreticular neurones synapse onto reticulospinal neurones. This collateral signal would provide a copy of the descending signal that would provide information concerning the scale and the magnitude of the voluntary movement and which could be used to modify the output of the reticulospinal neurones (RSNs) to produce the requisite changes in postural activity. That RSNs could provide the neural bases of the complex changes in posture that are observed in the supporting limbs during a gait modification (Lavoie et al. 1995) has received some support from our recent studies showing that individual RSNs, including those receiving input from the motor cortex, may show multiple increases in discharge activity, with each burst corresponding to the passage of a single limb over the obstacle (Prentice and Drew 1995). We suggest that this descending signal would provide general information concerning the magnitude and the timing of the required gait modification while the specific nature of the postural changes would be determined by the state of the excitability of the central pattern generating circuits within the spinal cord.

6. Conclusions

Although this review has been restricted to several narrowly defined aspects of locomotor adaptation, the major principals and concepts that can be drawn from the experiments that I have described hold for a much more diverse group of behaviours than those treated here. Certainly, the existence of an intrinsic CPG within the spinal cord simplifies the control issue by removing the need for supraspinal structures to generate locomotion and instead leaving them free to regulate and modify a well defined spinally generated pattern. In addition, the properties of the CPG, at least as far as we understand them, also simplify, to a great extent, the nature of the descending signals that are required for that

modulation. In circumstances that require only relatively simple changes in the level of EMG activity, without changes in the rhythm or the pattern, simple changes in the intensity of the descending commands will lead to modifications of EMG amplitude that are integrated into the locomotor cycle in a phase-dependent manner. Only if the intensity of the descending signal is increased will there be a modification of cycle duration and the possibility of a reset of the cycle. In other words, unless the descending signal specifically specifies that a change in pattern is required, the intrinsic stability of the system (intrinsic rhythm generator, together with the rhythmical peripheral and supraspinal afferent signals) ensures that changes in signal are incorporated into the step cycle and do not result in instability.

On the other hand, the suggested modular organisation of the spinal circuits provides for sufficient flexibility that when there is a need to modify limb trajectory, this can also be accomplished by modifying the activity of the same interneuronal groups implicated in determining the locomotor rhythm and structure, rather than acting outside the generator. In other words, I suggest that voluntary modifications of gait are superimposed upon the basic locomotor pattern rather than replacing it. In this case, the signals from the motor cortex, and probably from the red nucleus, specify the modifications in activity that are required in different modules. The interconnections between modules, necessary to ensure the coordination of activity between different joints, helps ensure that these changes are integrated into the underlying rhythm so that the change in limb trajectory is smoothly superimposed onto the normal locomotor rhythm.

Taken overall, while the existence of a CPG does not remove the necessity for specificity in the descending signals that are used to control locomotion, it does obviate the need for these signals to specify all the details of the changes that have to be made. If such principals have evolved in animals which have had millions of years to determine the best system to control locomotion, one may ask whether similar principals might prove equally fruitful in the control of machines!

References

Amos, A., Armstrong, D.M., and Marple-Horvat, D.E. Changes in the discharge patterns of motor cortical neurones associated with volitional changes in stepping in the cat. Neurosci.Lett. 109:107-112, 1990.

Armstrong, D.M. and Drew, T. Forelimb electromyographic responses to motor cortex stimulation during locomotion in the cat. J.Physiol. 367:327-351, 1985.

Armstrong, D.M. Supraspinal contributions to the initiation and control of locomotion in the cat. Prog.Neurobiol. 26:273-361, 1986.

Armstrong, D.M. and Marple-Horvat, D.E. Role of the cerebellum and motor cortex in the regulation of visually controlled locomotion. Can.J.Physiol.Pharmacol. 74:443-455, 1996.

Assaiante, C., Marchand, A.R., and Amblard, B. Discrete visual samples may control locomotor equilibrium and foot positionning in man. J.Motor.Behav. 21:72-91, 1989.

Barbeau, H. and Rossignol, S. Recovery of locomotion after chronic spinalization in the adult cat. Brain.Res. 412:84-95, 1987.

Beloozerova, I.N. and Sirota, M.G. The role of the motor cortex in the control of accuracy of locomotor movements in the cat. J.Physiol. 461:1-25, 1993.

Bennett, K.M.B. and Lemon, R.N. Corticomotoneuronal contribution to the fractionation of muscle activity during precision grip in the monkey. J.Neurophysiol. 75:1826-1842, 1996.

Bélanger, M., Drew, T., Provencher, J., and Rossignol, S. A comparison of treadmill locomotion in adult cats before and after spinal transection. J.Neurophysiol. 76:471-491, 1996.

Calancie, B., Needham-Shropshire, B., Jacobs, P., Willer, K., Zych, G., and Green, B.A. Involuntary stepping after chronic spinal cord injury. Evidence for a central rhythm generator for locomotion in man. Brain 117:1143-1159, 1994.

Caminiti, R., Ferraina, S., and Johnson, P.B. The sources of visual information to the primate frontal lobe: A novel role for the superior parietal lobule. Cereb.Cortex 6:319-328, 1996.

Canedo, A. and Lamas, J.A. Pyramidal and corticospinal synaptic effects over reticulospinal neurones in the cat. J.Physiol.(Lond.) 463:475-489, 1993.

Canedo, A. Primary motor cortex influences on the descending and ascending systems. Prog.Neurobiol. 51:287-335, 1997.

Degtyarenko, A.M., Zavadskaya, T.V., and Baev, K.V. Mechanisms of supraspinal correction of locomotor activity generator. Neuroscience 52:323-332, 1993.

Dietz, V., Colombo, G., Jensen, L., and Baumgartner, L. Locomotor capacity of spinal cord in paraplegic patients. Ann.Neurol. 37:574-582, 1995.

Drew, T. and Rossignol, S. Phase dependent responses evoked in limb muscles by stimulation of the medullary reticular formation during locomotion in thalamic cats. J.Neurophysiol. 52:653-675, 1984.

Drew, T. and Rossignol, S. A kinematic and electromyographic study of cutaneous reflexes evoked from the forelimb of unrestrained walking cats. J.Neurophysiol. 57:1160-1184, 1987.

Drew, T. Motor cortical cell discharge during voluntary gait modification. Brain Res. 457:181-187, 1988.

Drew, T. Functional organization within the medullary reticular formation of the intact unanaesthetized cat. III. Microstimulation during locomotion. J.Neurophysiol. 66:919-938, 1991.

Drew, T. Motor cortical activity during voluntary gait modifications in the cat. I. Cells related to the forelimbs. J.Neurophysiol. 70:179-199, 1993.

Drew, T., Jiang, W., Kably, B., and Lavoie, S. Role of the motor cortex in the control of visually triggered gait modifications. Can.J.Physiol.Pharmacol. 74:426-442, 1996.

Eidelberg, E., Story, J.L., and Nystel, J. Stepping by chronic spinal cats. Exp.Brain.Res. 40:241-246, 1980.

Fedirchuk, B., Nielsen, J., Petersen, N., and Hultborn, H. Pharmacologically evoked fictive motor patterns in the acutely spinalized marmoset monkey (Callithrix jacchus). Exp.Brain Res. 122:351-361, 1998.

Fetz, E.E., Cheney, P.D., and German, D.C. Corticomotoneuronal connections of precentral cells detected by post-spike averages of EMG activity in behaving monkeys. Brain.Res. 114:505-510, 1976.

Gibson, J.J. What give rise to the perception of motion? Psychol.Rev. 75:335-346, 1968.

Giuliani, C.A. and Smith, J.L. Stepping behaviors in chronic spinal cats with one hindlimb deafferented. J.Neurosci. 7:2537-2546, 1987.

Goodale, M.A., Ellard, C.G., and Booth, L. The role of image size and retinal motion in the computation of absolute distance by the mongolian gerbil(meriones unguilatus). Vision Res. 30:399-413, 1990.

Grillner, S. and Zangger, P. How detailed is the central pattern generation for locomotion. Brain.Res. 88:367-371, 1975.

Grillner, S. and Zangger, P. On the central generation of locomotion in the low spinal cat. Exp.Brain.Res. 34:241-261, 1979.

Grillner, S. Possible analogies in the control of innate motor acts and the production of sound in speech. In: Speech motor control, edited by S. Grillner. Oxford: Pergamon Press, 1982, p. 217-229.

Grillner, S. and Wallen, P. Central pattern generators for locomotion,with special reference to vertebrates. Ann.Rev.Neurosci. 8:233-261, 1985.

Harkema, S.J., Hurley, S.L., Patel, U.K., Requejo, P.S., Dobkin, B.H., and Edgerton, V.R. Human lumbosacral spinal cord interprets loading during stepping. J.Neurophysiol. 77:797-811, 1997.

Hollands, M.A., Marple-Horvat, D.E., Henkes, S., and Rowan, A.K. Human eye movements during visually guided stepping. J.Motor.Behav. 27(2):155-163, 1995.

Hollands, M.A. and Marple-Horvat, D.E. Visually guided stepping under conditions of step cycle- related denial of visual information. Exp.Brain Res. 109:343-356, 1996.

Illert, M., Lundberg, A., and Tanaka, R. Integration in descending motor pathways controlling the forelimb in the cat. 1. Pyramidal effects on motoneurons. Exp.Brain.Res. 26:509-519, 1976.

Jinnai, K. Electrophysiological study on the corticoreticular projection neurons of the cat. Brain.Res. 291:145-149, 1984.

Johnson, P.B., Ferraina, S., Bianchi, L., and Caminiti, R. Cortical networks for visual reaching: Physiological and anatomical organization of frontal and parietal lobe arm regions. Cereb.Cortex 6:102-119, 1996.

Jordan, M.I. and Rumelhart, D.E. Forward models:supervised learning with a distal teacher. Cognit.Scien. 16:307-354, 1992.

Kably, B. and Drew, T. The corticoreticular pathway in the cat: II. discharge characteristics of neurones in area 4 during voluntary gait modifications. J.Neurophysiol 80:406-424, 1998.

Kalaska, J.F. and Crammond, D.J. Cerebral cortical mechanisms of reaching movements. Science 255:1517-1523, 1992.

Kalaska, J.F. and Drew, T. Motor cortex and visuomotor behavior. Exercise Sport Sci.Rev. 21:397-436, 1993.

Kalaska, J.F. Parietal cortex area 5 and visuomotor behavior. Can.J.Physiol.Pharmacol. 74:483-498, 1996.

Keizer, K. and Kuypers, H.G.J.M. Distribution of corticospinal neurons with collaterals to lower brain stem reticular formation in cat. Exp.Brain.Res. 54:107-120, 1984.

Laurent, M. and Thomson, J.A. The role of visual information in control of a constrained locomotion task. J.Motor.Behav. 20:17-37, 1988.

Laurent, M. Visual cues and processes involved in goal-directed locomotion. In: Adaptability of human gait. Implications for the control of locomotion, edited by A.E. Patla. New York: North-Holland, 1991, p. 99-123.

Lavoie, S., McFadyen, B., and Drew, T. A kinematic and kinetic analysis of locomotion during voluntary gait modification in the cat. Exp.Brain Res. 106:39-56, 1995.

Leblond, H. and Gossard, J.P. Supraspinal and segmental signals can be transmitted through separate spinal cord pathways to enhance locomotor activity in extensor muscles in the cat. Exp.Brain Res. 114:188-192, 1997.

Lee, D.N. A theory of visual control of braking based on information about time-to-collision. Perception 5:437-459, 1976.

Lee, D.N. The optic flow field:the foundation of vision. Philos.Trans.R.Soc.Lond.[Biol.] 290:169-179, 1980.

Lovely, R.G., Gregor, R.J., Roy, R.R., and Edgerton, V.R. Weight-bearing hindlimb stepping in treadmill-exercised adult spinal cats. Brain Res. 514:206-218, 1990.

Matsuyama, K. and Drew, T. The organization of the projections from the pericruciate cortex to the pontomedullary brainstem of the cat: a study using the anterograde tracer, Phaseolus vulgaris leucoagglutinin. J.Comp.Neurol. 1997.

McCrea, D.A. Supraspinal and segmental interactions. Can.J.Physiol.Pharmacol. 74:513-517, 1996.

McFadyen, B.J., Winter, D.A., and Allard, F. Simulated control of unilateral, anticipatory locomotor adjustments during obstructed gait. Biol.Cybern. 72:151-160, 1994.

McFadyen, B.J., Lavoie, S., and Drew, T. Kinetic and energetic patterns for hindlimb obstacle avoidance during cat locomotion. Exp.Brain Res 125:502-510, 1999.

Mori, S. Integration of posture and locomotion in acute decerebrate cats and in awake,freely moving cats. Prog.Neurobiol. 28:161-195, 1987.

Mori, S. Contribution of postural muscle tone to full expression of posture and locomotor movements: Multi-faceted analyses of its setting brainstem-spinal cord mechanisms in the cat. Jpn.J.Physiol. 39:785-809, 1989.

Mori, S., Matsuyama, K., Kohyama, J., Kobayashi, Y., and Takakusaki, K. Neuronal constituents of postural and locomotor control systems and their interactions in cats. Brain Dev. 14 Suppl.:S109-S120, 1992.

Newman, D.B., Hilleary, S.K., and Ginsberg, C.Y. Nuclear terminations of corticoreticular fiber systems in rats. Brain Behav.Evol. 34:223-264, 1989.

Orlovsky, G.N. The effect of different descending systems on flexor and extensor activity during locomotion. Brain Res. 40:359-371, 1972.

Orlovsky, G.N., Deliagina, T., and Grillner, S. Neuronal control of locomotion: from mollusc to man. Oxford University Press, 1999.

Patla, A.E. In search of laws for the visual control of locomotion: Some observations. J.Exp.Psychol. 15:624-628, 1989.

Patla, A.E., Adkin, A., Martin, C., Holden, R., and Prentice, S. Characteristics of voluntary visual sampling of the environment for safe locomotion over different terrains. Exp.Brain Res. 112:513-522, 1996.

Patla, A.E. and Vickers, J.N. Where and when do we look as we approach and step over an obstacle in the travel path? Neuroreport 8:3661-3665, 1997.

Pearson, K.G. and Rossignol, S. Fictive motor patterns in chronic spinal cats. J.Neurophysiol. 66:1874-1887, 1991.

Perreault, M.-C., Rossignol, S., and Drew, T. Microstimulation of the medullary reticular formation during fictive locomotion. J.Neurophysiol. 71:229-245, 1994.

Prentice, S.D. and Drew, T. Characteristics of reticulospinal neurons during voluntary gait modifications in the cat. Soc.Neurosci.Abstr. 21:419-419, 1995.

Prentice, S.D. and Drew, T. A neural network model for studying voluntary gait modifications in the cat. Soc.Neurosci.Abstr. 23:1140, 1997

Rho, M.-J., Cabana, T., and Drew, T. The organization of the projections from the pericruciate cortex to the pontomedullary reticular formation of the cat: a quantitative retrograde tracing study. J.Comp.Neurol. 388:228-249, 1997.

Rho, M.-J., Lavoie, S., and Drew, T. Effects of red nucleus microstimulation on the locomotor pattern and timing in the intact cat: a comparison with the motor cortex. J.Neurophysiol 81:2297-2315, 1999.

Rossignol, S. Neural control of stereotypic limb movements. In: Handbook of physiology. Section 12. Regulation and integration of multiple systems, edited by L.B. Rowell and J.T. Sheperd. American Physiological society, 1996, p. 173-216.

Russel, D.F. and Zajac, F.E. Effects of stimulating Deiter's nucleus and medial longitudinal fasciculus on the timing of the fictive locomotor rythm induced in cats by DOPA. Brain.Res. 177:588-592, 1979.

Shinoda, Y., Yokota, J.I., and Fatami, T. Divergent projection of individual corticospinal axons to motoneurons of multiple muscles in the monkey. Neurosci.Lett. 23:7-12, 1981.

Stein, P.S.G. and Smith, J.L. Neural and biomechanical control strategies for different forms of vertebrate hindlimb locomotor tasks. In: Neurons, networks and motor behavior, edited by P.S.G. Stein, S. Grillner, A.I. Selverston and D.G. Stuart. Cambridge, Ma: Bradford, 1997, p. 61-73.

Widajewicz, W., Kably, B., and Drew, T. Motor cortical activity during voluntary gait modifications in the cat. II. Cells related to the hindlimbs. J.Neurophysiol. 72:2070-2089, 1994.

Wolpert, D.M., Ghahramani, Z., and Jordan, M.I. Are arm trajectories planned in kinematic or dynamic coordinates? An adaptation study

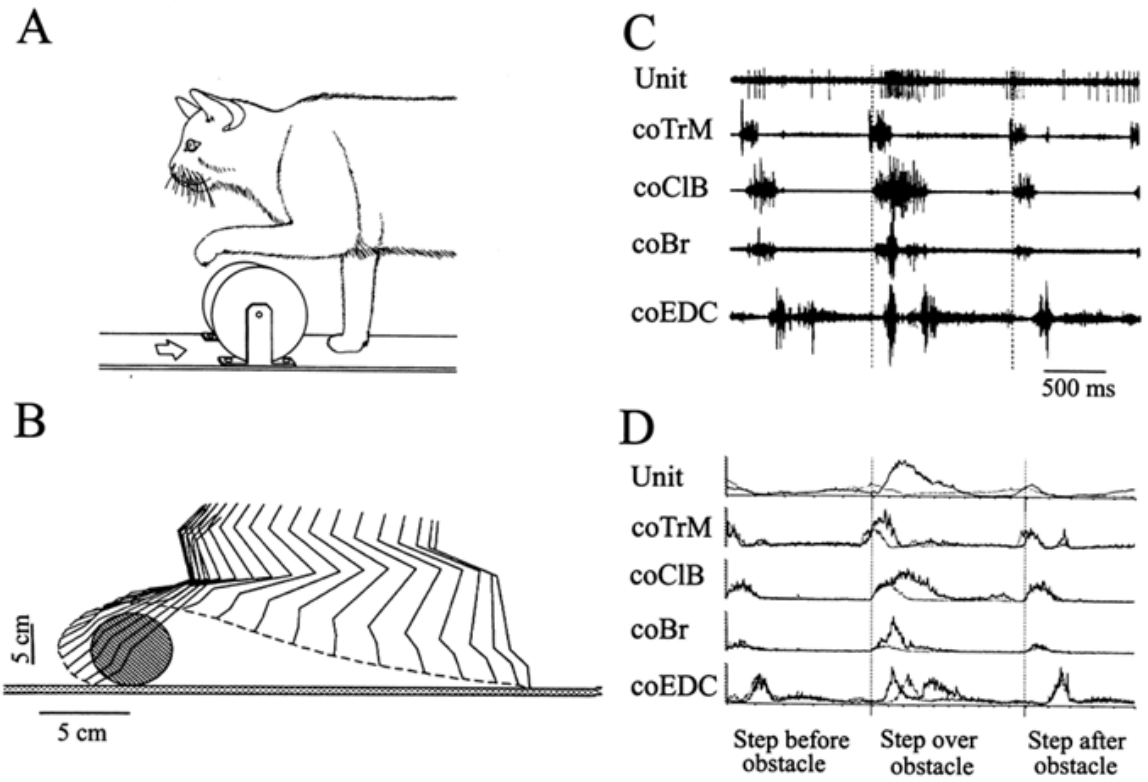

Figure 1: Example of the modification of discharge activity in a PTN during a voluntary gait modification. A: tracing from a video image illustrating the orientation of the forelimb during a step over a cylindrical obstacle attached to the treadmill belt. B: stick figure illustrating the change in trajectory during the swing phase of this step: The leg has been reconstructed from the X and Y coordinates of light reflecting points attached to the skin over identified bony landmarks (see Drew and Rossignol 1987 for details). C: raw data showing activity of four selected flexor muscles (all contralateral to the recording site) acting around the forelimb, together with the activity of a PTN (Unit). The figure shows 3 consecutive cycles with the step over the obstacle being represented by the middle cycle. The vertical dotted lines indicate the time of onset of activity in the ClB. The data is illustrated for the Lead condition, when the forelimb contralateral (co) to the recording site is the first to pass over the obstacle. D: averaged activity of the same cell and muscles, including the cycle illustrated in C:- again each cycle is synchronized on the activity of the ClB. The thinner line indicates the activity of the muscles and cells when no obstacle was attached to the treadmill belt, the thicker line indicates the activity when the cat steps over the obstacle. Abbreviations: Br, brachialis (flexor of the elbow); ClB, cleidobrachialis (protractor of the shoulder and flexor of the elbow); EDC, extensor digitorum communis (dorsiflexor of the wrist and digits); TrM, teres major (retractor of the shoulder).

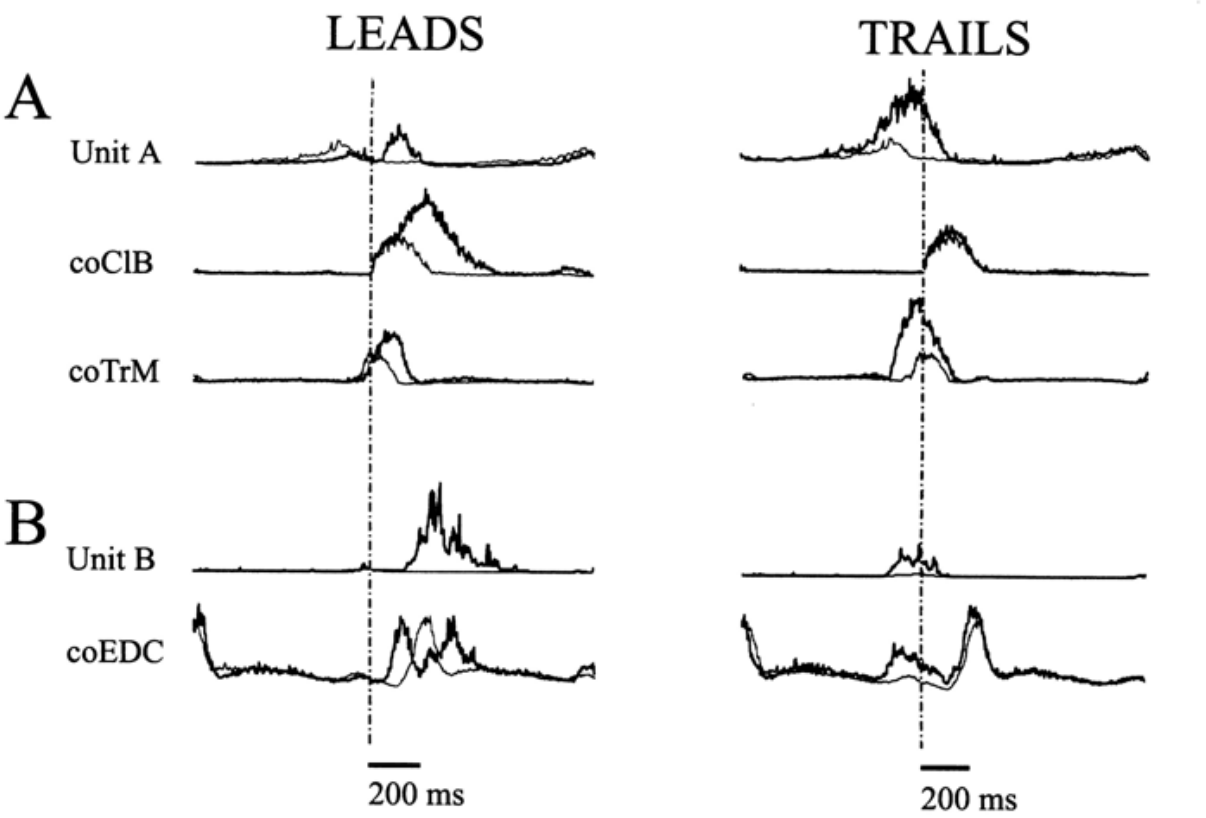

Figure 2: Two examples of PTNs (A and B) that discharged at different times during the gait cycle. As in Fig. 1, the thinner line indicates averaged neuronal and EMG activity during control locomotion and the thicker line the averaged activity during the gait modification. The vertical dotted line indicates the moment of onset of the ClB. Data are shown only for the period just preceding and during the modified step. Data are shown for both the Lead and the Trail condition.

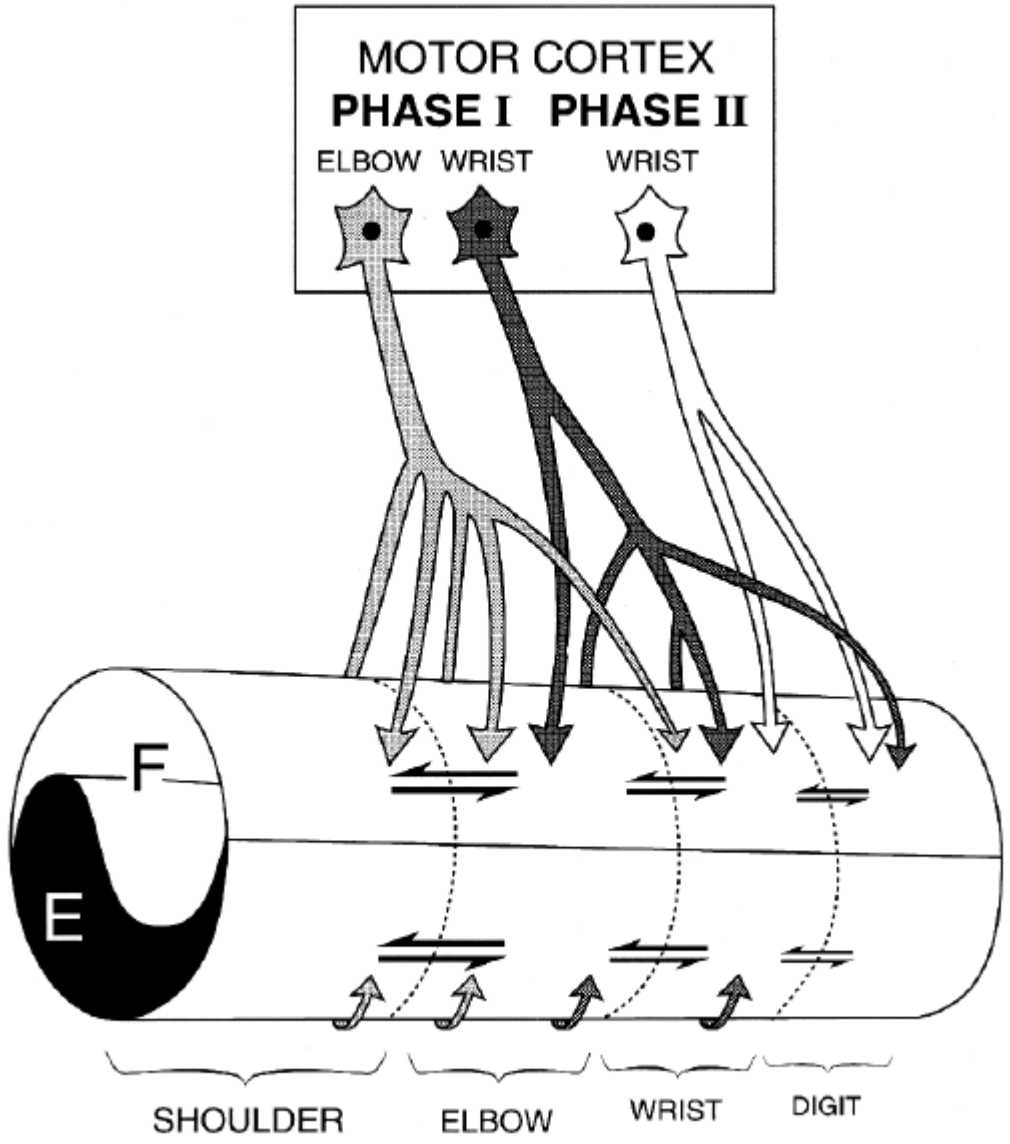

Figure 3: Conceptual model illustrating how the descending command for movement from the motor cortex might act to modify gait by acting through the spinal CPG for locomotion. The spinal CPG is represented as a series of modules, each of which would serve to specify the pattern of activity around a single joint. Each of these modules is coupled, as indicated by the two-way horizontal arrows, and each recieves input from a timing circuit (oscillator) which sets the locomotor rhythm. During the gait modification, a descending signal from the motor cortex differentially modifies the activity of these modules. It is suggested that each population of PTNs, active at different times in the swing phase of the modulated cycle, would influence the activity in a different series of modules. Some would preferentially activate more proximal modules, others those more distally located.

Keynote Speech II

Proceedings of the International Symposium on
Adaptive Motion of Animals and Machines,
Montreal, Aug.8-12, 2000

Nonlinear Dynamics of the Human Motor Control
-Real-Time and Anticipatory Adaptation of Locomotion and Development of Movements-

Gentaro Taga

Department of Pure and Applied Sciences, University of Tokyo & PRESTO, Japan Science and Technology Corporation,
3-8-1 Komaba, Meguro, Tokyo 153-8902, Japan,
taga@complex.c.u-tokyo.ac.jp

Abstract

Nonlinear dynamics of the neuro-musculo-skeletal system and the environment play central roles for the generation and the development of human bipedal locomotion and other movements. This paper highlights a global entrainment that produces adaptive walking, freezing and freeing degrees of freedom during motor development, and chaotic dynamics of spontaneous movements in early infancy.

1. Introduction

The theory of nonlinear dynamics, which claims that spatio-temporal patterns arise spontaneously from the dynamic interaction between the components with many degrees of freedom [1,2], is progressively attracting more attention in the field of motor control. The concept of self-organization in movement was initially applied to describe motor actions such as rhythmic arm movements [3]. On the other hand, neurophysiological studies of animals have revealed that the neural system contains the central pattern generator (CPG), which generates spatio-temporal patterns of activity for the control of rhythmic movements through the interaction of coupled neural oscillators [4]. Moreover, it has been reported that the centrally generated rhythm in the CPG is entrained by the rhythm of sensory signals at rates above and below the intrinsic frequency of the rhythmic activity [4]. This phenomenon is typical for a nonlinear oscillator that is externally driven by a sinusoidal signal.

Inspired by the theoretical and experimental approaches to the motor control in terms of the self-organization, we proposed that the human bipedal locomotion emerges from a global entrainment between the neural system that contains the CPG and the musculo-skeletal system that interacts with a changing environment [5]. A growing number of simulation studies have focused on the dynamic interaction of neural oscillators with mechanical systems to understand the mechanisms of generation of adaptive movements in insects [6], fish [7] and quadruped animals [8]. In the field of robotics, an increasing number of studies have implemented neural oscillators to control movements of real robots [9-11].

The concept of the self-organization argues that movements are generated as a result of dynamic interaction between the neural system, the musculo-skeletal system and the environment. If this is the case, the implicit assumption that the neural system is a controller and that the body is a controlled system is required to be changed. This paper reviews a series of our models of the human bipedal locomotion which show nonlinear properties of the neuro-musculo-skeletal system. The aim of this paper is to provide a framework for understanding the generation of the bipedal locomotion [5, 12], the real-time flexibility in an unpredictable environment [13], the anticipatory adaptation of locomotion when confronted with a visible object [14] and the acquisition of locomotion during development [15]. Our recent study on the analysis of spontaneous movements of young infants also provides evidence that chaotic dynamics may play an important role for the development of varieties of movements [16].

2. Real-Time Adaptation of Locomotion through Global Entrainment

2.1 A model of the neuro-musculo-skeletal system for human locomotion

In principle, bipedal walking of humanoid robots can be controlled if the specific trajectory of all of the joints and of the zero moment point (ZMP) are planned in advance and the feedback mechanisms are incorporated [17]. However, it is obvious that this method of control is not robust against unpredictable changes in the environment.

Is it possible to generate bipedal locomotion by using a neural model of the CPG in a self-organized manner? Let us assume that an entire system is composed of two dynamical systems; a neural system that is responsible for generating locomotion and a musculo-skeletal system that generates forces and moves in an environment. The

neural system is described by differential equations for coupled neural oscillators, which produce motor signals to induce muscle torques and which receive sensory signals indicating the current state of the musculo-skeletal system and the environment. The musculo-skeletal system is described by Newtonian equations for multiple segments of the body and input torque which is generated by the output of the neural system. We proved that a global entrainment between the neural system and the musculo-skeletal system is responsible for generating a stable walking movement by using computer simulation [5].

Here I will present a model of [12]. As shown in Fig.1, the musculo-skeletal system consists of eight segments in the saggital plane. The triangular foot interacts with the ground at its heel and/or toe. According to the output of the neural system, each of twenty "muscles" generates torque at specific joints. It is important to note that a number of studies have demonstrated examples of walking robots which exploit the natural dynamics of the body such as the passive dynamic walkers [18] and the dynamic running machines [19]. The oscillatory property of the musculo-skeletal system is an important determinant to establish the walking pattern.

The neural system was designed based on the following assumptions:

(1) The neural rhythm generator (RG) is composed of neural oscillators, each of which controls the movement of a corresponding joint. As a model neural oscillator, we adopt the half center model, which is composed of two reciprocally inhibiting neurons and which generates alternative activities between the two neurons [20].

(2) All of the relevant information about the body and the environment is taken into account. The angles of the body segments in an earth-fixed frame of reference and ground reaction forces are available to the sensory system. Global information on the position of the center of gravity (COG) with respect to the position of the center of pressure (COP) is also available. We assume that a gait is represented as a cyclic sequence of what we call global states; the double support phase, the first half of the single support phase and the second half of the single support phase. The global states are defined by the sensory information on the alternation of the foot contacting the ground and the orientation of the vector from the COP to the COG.

(3) Reciprocal inhibitions are incorporated between the neural oscillators on the contralateral side, which generates the anti-phase rhythm of muscles between the two limbs. Connections between the neural oscillators on the ipsilateral side change in a phase-dependent manner by using the global state to generate the complex phase relationships of activity among the muscles within a limb.

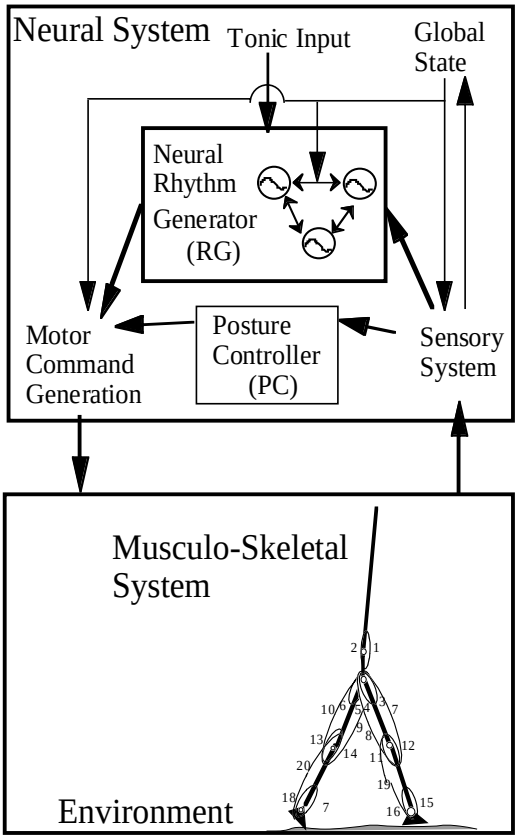

Fig. 1 A model of the neuro-musculo-skeletal system for human locomotion [12].

(4) Both the local information on the angles of the body segments and the global information on the entire body are sent to the neural oscillators in a manner similar to the functional stretch reflex, so that neural oscillation and body movement are synchronized. Sensory information is sent only during the relevant phase of the gait cycle by modulating the gains of the sensory pathways in a phase-dependent manner, which is determined by the global state.

(5) All of the neural oscillators share tonic input from the higher center, which is represented by a single parameter. By changing the value of this parameter, the excitability of each oscillator can be controlled so that different speeds of locomotion are generated.

(6) While the neural rhythm generator induces the rhythmic movement of a limb, a posture controller (PC) is responsible for maintaining the

static posture of the stance limb by producing phase-dependent changes in the impedance of specific joints. The final motor command is a summation of the signals from the neural rhythm generator and the posture controller.

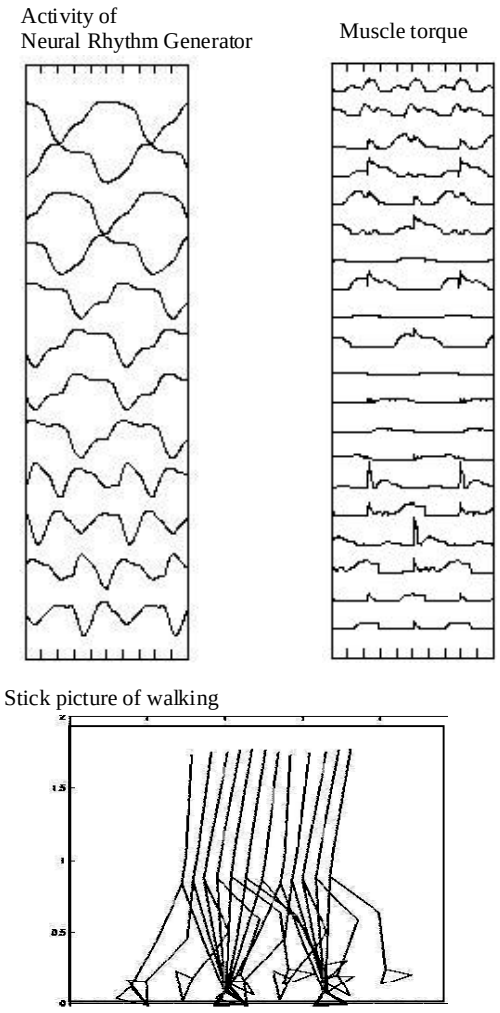

Fig.2 The results of computer simulation of emergence of neural activity, muscle torque and walking movements which are generated in a self-organized manner.

The computer simulation demonstrated that, given a set of initial conditions and values of various parameters, a stable pattern of walking emerged as an attractor which was formed in the state space of both the neural and musculo-skeletal system. Figure 2 shows neural activities, muscle torques and a stick picture of walking within one gait cycle. The attractor was generated by the global entrainment between the oscillatory activity of the neural system and rhythmic movements of the musculo-skeletal system.

When we first proposed the model of bipedal locomotion [5], there was few study to suggest the existence of spinal CPG in humans. Recently, several studies have shown evidence for a spinal CPG in human subjects with spinal cord injury [21,22]. Our model is likely to capture the essential mechanism for the generation of human bipedal locomotion.

2.2 Real-time flexibility of bipedal locomotion in an unpredictable environment

When the solution of the differential equations which were composed of the neural and musculo-skeletal systems converged to a limit cycle that was structurally stable, walking movement was maintained even with small changes in the initial conditions and parameter values [13]. For example, when part of the body was disturbed by a mechanical force, walking was maintained and the steady state was recovered due to the orbital stability of the limit cycle attractor. When part of the body was loaded by a mass, which can be applied by changing the inertial parameters of the musculo-skeletal system, the gait pattern did not change qualitatively but converged to a new steady state, where the speed of walking clearly decreased. When the walking path suddenly changed from level to uneven terrain, stability of walking was maintained but the speed and the step length spontaneously changed as shown in Fig. 3. Naturally, the stability of walking was broken for a heavy load and over a steep and irregular terrain.

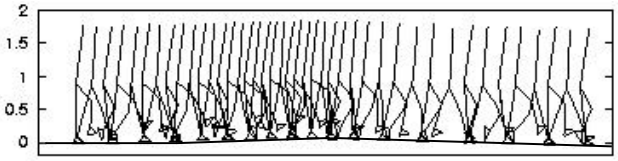

Fig. 3 Walking over uneven terrain.

The real-time adaptability is attributed not only to the afferent control based on the proprioceptive information that is generated by the interaction between the body and the mechanical environment, but also to the efferent control of movements based on intention and planning. In this model, a wide range of walking speeds were available by using the nonspecific input from the higher center to the neural oscillators, which was represented by a single parameter. Changes in the parameter can produce bifurcations of attractors, which correspond to different motor patterns [5,13].

It is open whether a 3D model of the body with a similar model of the neural system will perform dynamic walking with stability and

flexibility. Designing such a model is a crucial step toward constructing a humanoid robot that walks in a real environment [23].

3. Anticipatory Adaptation of Locomotion through Visuo-Motor Coordination

As long as the stability of the attractor is maintained, the locomotor system can produce adaptive movements even in an unpredictable environment. However, this way of generation of motor patterns is not sufficient when the attractor looses stability by drastic changes in the environment. For example, when we step over an obstacle during walking, the path of limb motion must be quickly and precisely controlled using visual information that is available in advance. Given the emergent properties of the neuro-musculo-skeletal system for producing the basic pattern of walking, how the anticipatory adaptation to the environment was realised? Neurophysiological studies in cats have shown that the motor cortex is involved in visuo-motor coordination during anticipatory modification of the gait pattern [24].

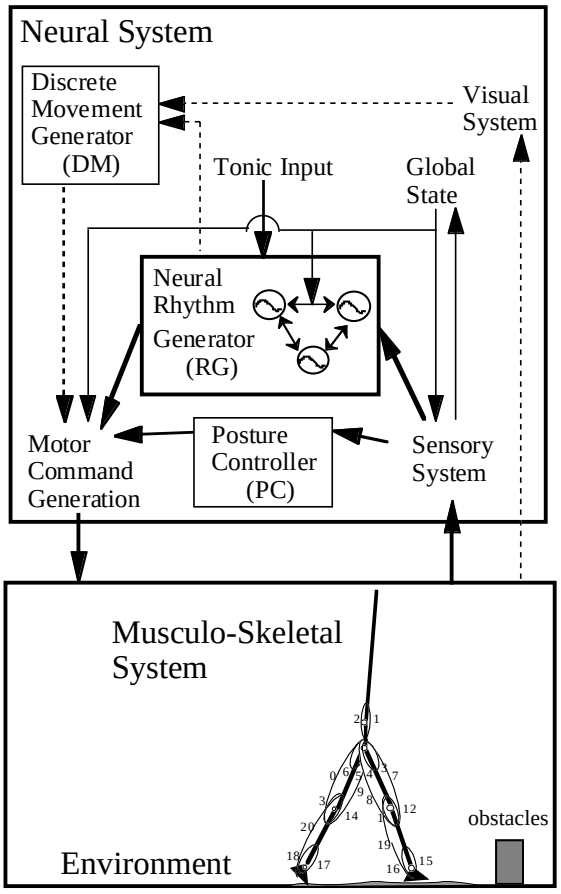

Fig.4 A model of the anticipatory adaptation of locomotion when an obstacle can be seen [15].

It was examined whether modifications of the basic gait pattern could produce rapid changes in the pattern so as to clear an obstacle placed in its path. As shown in Fig. 4, the neural rhythm generator was combined with a system referred to as a discrete movement generator, which receives both the output of the neural oscillators and visual information regarding the obstacle and generates discrete signals for modification of the basic gait pattern [14].

By computer simulation, avoidance of obstacle of varying heights and proximity was demonstrated as shown in Fig. 5. An obstacle placed at an arbitrary position can be cleared by sequential modifications of gait; modulating the step length when approaching the obstacle and modifying the trajectory of the swing limbs while stepping over it. An essential point is that a dynamic interplay between advance information about the obstacle and the on-going dynamics of the neural system produces anticipatory movements. This implies that a planning of limb trajectory is not free from the on-going dynamics of the lower levels of the neural system, the body dynamics and the environmental dynamics.

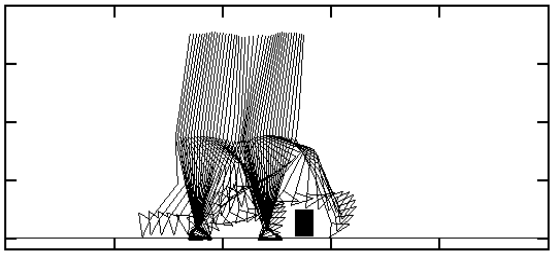

Fig. 5 Result of computer simulation of obstacle avoidance during walking [15].

4. Freezing and Freeing Degrees of Freedom in the Development of Locomotion

Once we had chosen a structure of the neural system and a set of parameter values that produced a walking movement as a stable attractor, the model exhibited the flexibility against various changes in the environmental conditions. However, it was difficult to determine the structure of the model and to tune the parameters, since the entire system was highly nonlinear. A number of studies have used a genetic algorithm to obtain a good performance of locomotion in animals [25] and in humans [26]. Another approach to overcoming the difficulty of

parameter tuning of locomotor systems is to explore the motor development of infants and to unravel a developmental principle of the neuro-musculo-skeletal system. Here I show that a freezing and freeing degrees of freedom is one of the key mechanisms for the acquisition of bipedal locomotion during development.

A prominent feature of locomotor development is that newborn infants who were held erect under their arms perform locomotor-like activity [27]. The existence of the newborn stepping implies that the neural system already contains a CPG for rhythmic movements of the lower limbs. Interestingly, this behavior disappears after the first few months. At around one year of age, infants start walking independently. Why the successive appearance, disappearance and reappearance of stepping were observed in the development of locomotion? According to the traditional neurology, the disappearance of motor patterns is due to the maturation of the cerebral cortex which inhibits the generation of movements on the spinal level. However, it was reported that the stepping of infants of a few months of age can be easily induced on a treadmill [27]. It is likely that the spinal CPG is used for the generation of independent walking.

I hypothesized that this change reflects the freezing and freeing degrees of freedom of the neuro-musculo-skeletal system, which may be produced by the interaction between a neural rhythm generator (RG) with neural oscillators and a posture controller (PC). A computational model was constructed to reproduce qualitative changes in motor patterns during development of locomotion by the following sequence of changes in the structure and parameters of the model as shown in Fig.6 [14].

(1) It was assumed that the RG of newborn infants consists of six neural oscillators which interact through simple excitatory connections and that the PC is not yet functioning. When the body was mechanically supported and the RG was activated, the model produced a stepping movement, which was similar to the newborn stepping. Tightly synchronized movements of the joints were generated by highly synchronized activities of the neural oscillators on the ipsilateral side of the RG, which we called "dynamic freezing" of the neuro-muscular degrees of freedom.

(2) When the PC was recruited and its parameters were adjusted, the model became able to maintain static posture by "static freezing" of degrees of freedom of joints. The disappearance of the stepping was caused by interference between the RG and the PC.

(3) When inhibitory interaction between the RG and the PC was decreased, independent stepping appeared. This movement was lacking in the ability to progress forward. We called this mechanism as "static freeing," since the frozen degrees of freedom of the musculo-skeletal system by the PC were freed.

(4) By decreasing the output of the PC and increasing the input of the sensory information on the segment displacements to the RG, a forward walking was gradually stabilized. The simply synchronized pattern of neural activity in the RG changed into a complex pattern with each neural oscillator generating rhythmic activity asynchronously with respect to one another. By this mechanism, which we called "dynamic freeing," gait patterns became more similar to those of adults.

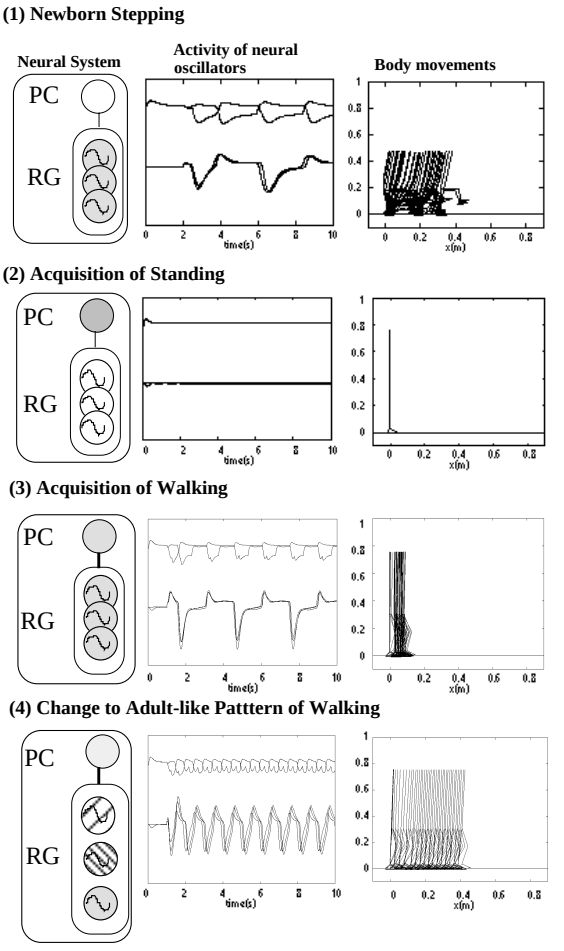

Fig. 6 A model of the development of bipedal locomotion of infants and results of computer simulation.

This model suggests that the u-shaped changes in performance of the stepping movement can be understood as the sequence of dynamic freezing, the static freezing, the static freeing and the dynamic freeing of degrees of freedom of the neuro-musculo-skeletal system. This mechanism is considered to be important to acquire both stability and complexity of movements during development. Parameter tuning for dynamic walking becomes easier after the control of the static posture is established.

5. Chaotic Dynamics of Spontaneous Movements of Young Infants

It remains to be open whether the concept of self-organization in nonlinear dynamical systems can be generalized to unravel the principle of development of complex behaviors including not only rhythmic movements such as walking but also varieties of discrete movements such as reaching arms and touching objects. We focused on what is called general movement (GM) of young infants who have not yet acquired voluntary movements [28]. The GM is a spontaneous movement, which is not just a random movement but a complex one involving head, trunk, arms and legs. The GM emerges during early fetal life and disappears around the age of 4 months post-term when voluntary motor activity gradually appears. Although the GM has attracted attention from a clinical point of view, dynamic properties of the GM have not yet been determined.

We conducted longitudinal observation of the GMs of infants at 4 weeks intervals from 1 to 4 months post-term age [16]. Subjects were 10 infants; 7 normal full-term infants, twin infants born pre-term, one of who was normal but the other was diagnosed as cerebral palsy, and one infant who had midcerebral artery thrombosis. Two-dimensional positions of four reflective markers, which were taped on each of wrists and ankles, were measured using a video camera and a computer with software for digitizing and processing of video images. We finally obtained epochs of spontaneous movements for 150 sec for each observation. Figure 7 shows examples of longitudinal changes in patterns of GMs for two normal infants.

In order to characterize the complexity and variability of GMs, we assumed that time series of GMs were generated by a dynamical system. Dynamic properties of GMs were assessed by the method of nonlinear prediction [29], in which we estimated predictability of trajectories in a phase space that was constructed by embedding of the original time series of x-y coordinate of four limbs. It should be noted that not position but velocity data were used to remove linear trends and to give greater density in phase space. Chaotic dynamics would be revealed by a decrease in the predictability with increasing prediction time steps, whereas linear process with uncorrelated noise would show a non-decreasing predictability. Statistical significance of nonlinearity was also examined using the method of surrogate data processing to exclude a possibility that high predictability can be obtained by random noises with linear auto-correlations [30].

We found evidence that the spontaneous movements of normal subjects were generated by nonlinear dynamics, which can be distinguished from linear processes and correlated noises. We also analyzed developmental trends in the motor pattern changes and detected U-shape changes in the complexity around 2 months of age for 5 infants out of 8 normal infants. Furthermore, movements of the 2 abnormal infants were characterized by loss of complexity; one showed too rhythmic pattern and the other showed a random one.

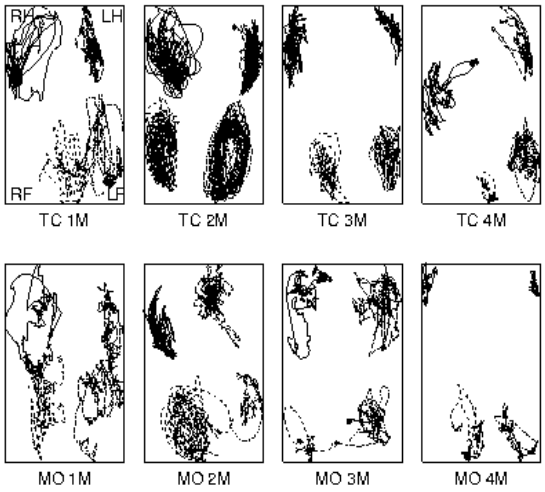

Fig. 7. Longitudinal changes in trajectories of four limbs during general movements of two normal infants for the first 4 months of age [16].

Our findings showed that the development of motor patterns is not a progressive process from a simple to a complex state nor a converging process from a random to an organized state. The developmental changes of the GM around the age of 2 months can be accounted by dynamic freezing and freeing degrees of freedom as shown in the model of development of locomotion. However, the entire processes of developmental changes in the GM are not so simple as the story of the development of locomotion, since the GM includes wide range of motor repertoire such as kicking, reaching arms,

touching one's own body etc. From a point of neural mechanism, the loss of complexity in the patterns of the GM suggests that the cortex is involved in both the generation of complex motor patterns and the transformation of the GM patterns during development. This infers that the chaotic dynamics of the neuro-musuclo-skeletal system may play an important role for acquisition of movements during development. To confirm these findings, three-dimensional measurement of motion of entire body is in progress.

References

[1] Nicolis, G., Prigogine, I., 1977, *Self-organization in Nonequilibrium Systems*, John Wiley and Son..

[2] Haken, H., 1976, *Synergetics - An Introduction*, Springer-Verlag.

[3] Schöner, G., Kelso, J.A.S., 1988, Dynamic pattern generation in behavioral and neural systems, Science, 239, 1513-1520.

[4] Grillner, S., 1985, Neurobiological bases of rhythmic motor acts in vertebrates, *Science*, 228, 143-149.

[5] Taga, G., Yamaguchi, Y., and Shimizu, H., 1991, Self-organized control of bipedal locomotion by neural oscillators in unpredictable environment, *Biol. Cybern.*, 65, 147-159.

[6] Kimura, S., Yano, M., Shimizu, H., 1993, A self-organizing model of walking patterns of insects, *Biol. Cybern.*, 69, 183-193.

[7] Ekeberg, O., 1993, A combined neuronal and mechanical model of fish swimming, *Biol. Cybern.*, 69, 363-374.

[8] Wadden, T., Ekeberg, O., 1998, A neuro-mechanical model of legged locomotion: single leg control. *Biol. Cybern.*, 79, 161-173.

[9] Miyakoshi, S., Yamakita, M., Furata, K., 1994, Juggling control using neural oscillators, *Proc. IEEE/RSJ IROS*, 2, 1186-1193.

[10] Kimura, H., Sakurama, K., Akiyama, S., 1998, Dynamic walking and running of the quadraped using neural oscillators, *Proc. IEEE/RSJ, IROS*, 1, 50-57.

[11] Williamson, M., M., 1998, Neural control of rhythmic arm movements, *Neural Networks*, 11, 1379-1394.

[12] Taga, G., 1995, A model of the neuro-musculo-skeletal system for human locomotion. I. Emergence of basic gait, *Biol. Cybern.*, 73, 97-111.

[13] Taga, G., 1995, A model of the neuro-musculo-skeletal system for human locomotion. II. Real-time adaptibility under various constraints, *Biol. Cybern.*, 73, 113-121.

[14] G.Taga, 1997, Freezing and freeing degrees of freedom in a model neuro-musculo-skeletal system for development of locomotion, *Proc. XVIth Int. Soc. Biomech. Cong.*, 47.

[15] Taga, G., 1998, A model of the neuro-musculo-skeletal system for anticipatory adjustment of human locomotion during obstacle avoidance. *Biol. Cybern.*, 78, 9-17.

[16] Taga, G., Takaya, R., Konishi, Y., 1999, Analysis of general movements of infants towards understanding of developmental principle for motor control, *Proc. IEEE SMC*, V678-683.

[17] Vukobratovic, M., Stokic, D., 1975, Dynamic control of unstable locomotion robots, *Math. Biosci.* 24, 129-157.

[18] McGeer, T., 1993, Dynamics and control of bipedal locomotion, *J. Theor. Biol.* 163, 277-314.

[19] Raibert, M., H., 1984, Hopping in legged systems - modeling and simulation for the two-dimensional one-legged case, *IEEE Trans. SMC*, 14, 451-463.

[20] Matsuoka, K., 1985, Sustained oscillations generated by mutually inhibiting neurons with adaptation, *Biol. Cybern.* 52, 367-376.

[21] Calancie, B., Needham-Shropshire, B., Jacobs, et al., 1994, Involuntary stepping after chronic spinal cord injury, Evidence for a central rhythm generator for locomotion in man, *Brain*, 117, 1143-1159.

[22] Dimitrijevic, M., R., Gerasimenko, Y., Pinter, M., M., 1998, Evidence for a spinal central pattern generator in humans, *Ann NY Acad Sci*, 860, 360-376.

[23] Miyakoshi, S., Taga, G., Kuniyoshi, Y. et al., 1998, Three dimensional bipedal stepping motion using neural oscillators - towards humanoid motion in the real world. *Proc. IEEE/RSJ*, 1, 84-89.

[24] Drew, T., 1988, Motor cortical cell discharge during voluntary gait modification, *Brain Res.*, 457, 181-187.

[25] Lewis, M., A., Fagg, A., H., Bekey, G. A., 1994, Genetic Algorithms for Gait Synthesis in a Hexapod Robot, In Zheng, Y., F., ed. *Recent Trends in Mobile Robots*, World Scientific, New Jersey, 317-331.

[26] Yamazaki, N., Hase, K., Ogihara, N., et al. 1996, Biomechanical analysis of the development of human bopedal walking by a neuro-musculo-skeletal model, *Folia Primatologica*, 66, 253-271.

[27] Thelen, E., Smith, L., B., 1994, *A Dynamic Systems Approaches to the Development of Cognition and Action*, MIT Press.

[28] Prechtl, H., F., R., Hopkins, B., 1986, Developmental transformations of spontaneous movements in early infancy, *Early Hum. Dev.*, 14, 233-238.

[29] Sugihara, G., May, R., M., 1990, Nonlinear forecasting as a way of distinguishing chaos from measurement error in time series, *Nature*, 344, 734-741.

[30] Prichard, D., Theiler, J., 1994, Generating surrogate data for time series with several simultaneously measered variables, *Phys. Rev. Let*. 73, 951-954.

Session

Visual Adaptation Mechanisms of System in Locomotion

Proceedings of the International Symposium on
Adaptive Motion of Animals and Machines,
Montreal, Aug.8-12, 2000

Local path planning during locomotion over irregular terrain

Aftab E. Patla, Ewa Niechwiej, Luiz Santos
Gait and Posture Lab, Department of Kinesiology, University of Waterloo,
Waterloo, Ontario N2L3G1

Abstract

We have been exploring the factors that guide the selection of alternate foot placement during locomotion in a cluttered environment. The results show that when normal landing area is unavailable or undesirable, individuals select an alternate foot placement that minimizes changes to the normal gait trajectory and ensures dynamic stability. These experiments shed light on fundamental issue of local path planning and are relevant to the design of legged robots designed to function in an unstructured environment.

1. Introduction

Path planning is an integral component of locomotion, and most often refers to route plans to goals that are not visible from the start. The choice of a particular travel path is dependent on a number of factors such as energy cost (choosing the shorter of possible paths) and traversability (choosing a path that has been selected and traversed by others) [1]. We consider this global path planning. The focus of this paper is on adjustments to gait that one routinely makes to avoid stepping on or hitting undesirable surfaces, compromising dynamic stability, possibly incurring injuries. These on-line adaptations to gait termed local path planning, include selection of alternate foot placement, control of limb elevation, maintaining adequate head clearance and steering control [2], [3]. This is a hallmark of legged locomotion making it possible to use isolated foot holds for travel [4]. We have been exploring the factors that influence local path planning in several experiments and show that visual input alone does not specify a unique action: other factors play a role in decision making. The focus of the experiments was determining what guides the selection of alternate foot placement during locomotion in a cluttered environment.

In the first series of experiments, individuals were instructed to walk and avoid stepping on a light spot should one appear in the travel path [5]. The position and shape of the light spot was varied such that if an alternate foot placement is not chosen, the normal foot landing would cover different portions of the light spot. The available response time was varied and alternate foot placement chosen were categorized into one of eight choices. The results showed that selection of alternate foot placement was systematic; there is a single dominant choice for each combination of light spot and normal landing spot. A hierarchy of rules was derived from the choices made by the individuals (see Figure 1). First, the selection minimized the displacement of the foot from its normal landing spot. Second, if more than one choice met this criterion, alternate foot placement in the plane of progression was preferred. When there was a choice between stepping long versus short, stepping long was preferred; when there was a choice between stepping inside versus outside, stepping inside was preferred. Analyses of the choices made revealed that the dominant choice requires minimal threat to dynamic stability, allows for a quick initiation of change in ongoing movement and ensures that the locomotor task runs without interruption. These apriori criterion and constraints on the decision making clearly suggests that perception-action coupling mediating foot positioning is dependent not only on visual input acquired by the moving body [6], [7], but also on the prediction of future foot placement from kinesthetic input and constraints posed by dynamic stability requirements.

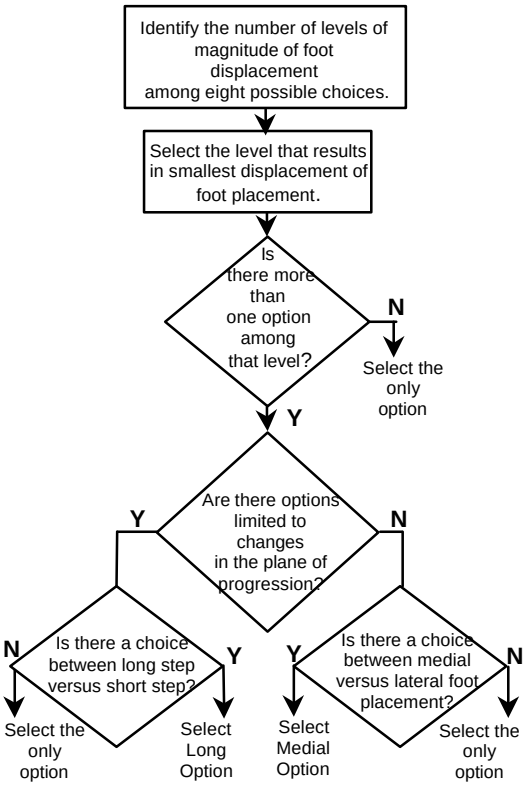

Figure 1: Decision tree that guides foot placement choice developed from experimental data from Patla et al. [5].

2. Computer Simulation of the Adaptive Locomotor Task: Experiment 1

Dynamic stability and ongoing locomotor demands are, we argue, the primary reasons why the control system satisfies the objective and constraints in its selection of alternate foot placement. To indirectly test this reasoning, we decided to keep the perceptual part of the task similar, while changing the action part. Action required in this case involved the use of upper limbs to generate the response, significantly altering the postural/balance requirements. Basically we used the famous yellow pages directory dictum to "let the fingers do the walking".

2.1 Participants

Ten healthy participants with no known neuromuscular pathologies volunteered for the study. Age - mean - 20.1 yrs; range - 18-25 yrs; Gender 5M, 5F; 9 right handed and 1 left handed evaluated using a questionnaire by Bryden [8].

2.2 Computer Simulation of Locomotor Task

A customized program was written to show top view of a travel path on the computer screen. Footprints were shown to travel from the bottom of the screen to the top. In 50% of the trials a light spot was projected where the 4th step would normally land. The trigger for the light spot was the previous foot contact thus giving subjects one step duration to plan and manually move the next foot placement to an alternate location. The light spots were similar in shape and size (with respect to the footprint on the screen) to those used in the previous two locomotor experiments.

2.3 Protocol

Participants were comfortably seated in front of the computer screen and shown sample computer walking trials. They could control the foot placement by a mouse. The mouse was positioned at a comfortable distance and location aligned to the midline of the body. They completed a set of trials with right and left hands. The sequence of right and left hand were randomly assigned.

2.4 Data Analyses

The analysis was identical to the one carried out for the previous experiment by Patla et al. [5].

2.5 Results

There were some small differences in the responses between left and right hand, but in both instances the response choices did not match with those observed in previous experiments. We focus on the responses for the right hand since in the locomotor experiment subjects altered the right foot placement. Chi-square analyses revealed no significant differences in the dominant foot placement for the six experimental conditions (see Figure 2). It is clear from Figure 2 that the dominant response is medial displacement of the footprint, by moving the mouse towards the midline of the body. Success rates for avoiding the light spot were high (98% or greater).

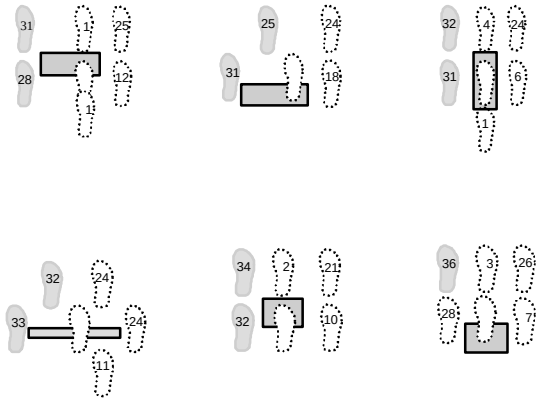

Figure 2: Results of foot placement choices from Experiment 1. Shaded rectangle area represents landing area to be avoided. Foot print location show the landing area chosen by the individual; the shaded footprint represent the dominant choices made by the participants.

2.6 Discussion

It is clear that the dominant responses observed in the computer simulation of the adaptive locomotor task are not the same as those seen in previous experiments. The mouse movement required to avoid the light spot are similar to the operations performed in a graphical computer environment such as dragging a file into the trash can. This file dragging operation has been found to be faster than other ways to perform the same task [9].

What is intriguing is that the dominant response among all the conditions involves movement of the mouse leftward or upward and leftward. Elliott et al [10] have shown that movement adjustments required to point to a target that is perturbed to the left are faster than when the target is perturbed to the right. They have attributed this to different roles of the two cerebral hemispheres. It should be noted that both dominant responses in this study (movement of the mouse to the left or left and upward) involve simple control at a single joint (shoulder rotation for movement to the left which could also be initiated with the wrist and shoulder flexion for movement to the left and upward).

The lack of differential dominant responses for the six experimental conditions clearly suggests that postural/balance constraints, the effector system (upper limb versus whole body) and the ongoing movement/posture used have a tremendous influence on the outcome.

3. Selection of Foot Placement under no time or spatial constraints: Experiment 2

The previous studies where individuals were constrained to modify their steps following a visual cue were useful in elucidating the criteria people use in selecting an alternate foot placement under time and spatial constraints. In other studies of adaptive locomotion, individuals are given the choice to modify their approach phase to step on a target. [11]; [12]); only the goal was specified, not how it was achieved. The changes required in the stepping patterns in these studies were restricted to the plane of progression and the results show that individuals modulate their step length in the last three steps to ensure stepping on the take-off line for a long jump [11]. What would happen to the foot placement selection to avoid landing on a target, if individuals had the freedom to modify their approach phase. An experiment to answer this question was developed and is described next.

3.1 Participants

Twelve healthy participants (6 males and 6 females) with no known neuromuscular pathologies volunteered for the study. (Age - mean - 24 yrs; range – 21-33 yrs). The average step length was 70.8 cm (range 59-78.9 cm), and the average step width was 23.2 cm (range 16-30 cm).

3.2 Schematic of the experimental setup

The top view of the travel path is shown in Figure 3. The rectangles represented possible landing targets and were adjusted to each individuals normal step length. A possible landing target was white in color, whereas a red rectangle represented a landing target to be avoided. A red rectangle was placed at the location indicated by the darkly shaded rectangle, and another one was randomly placed in one of the lightly shaded rectangle.

3.3 Protocol

First, to determine step length and step width, all the participants were asked to walk across a black rubber mat with chalk on the soles of their shoes. Average step length and step width were calculated from four consecutive steps on the mat. Based on the individual measures, a 9.0m pathway of white targets (dimensions 28cm x 14cm) was set up. The white targets were placed medially, laterally, anteriorly, and posteriorly to the participants' expected foot placement. Participants were instructed to walk across the

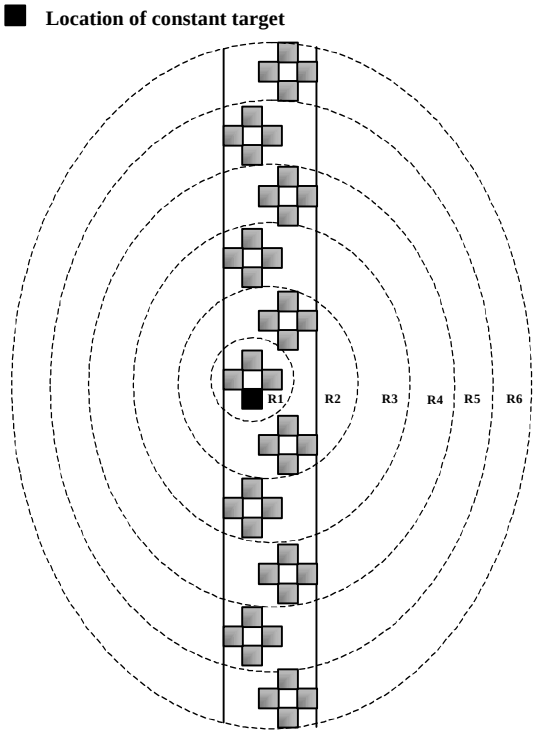

Figure 3: Schematic diagram of the travel path for Experiment 2. Each of the shaded rectangle area represents a possible landing target. A white rectangle in the shaded area represents a target area that can be stepped on, while a red rectangle represents a landing area that has to be avoided. One red rectangle was located in the area shown by the darkly shaded rectangle. The other red rectangle was located randomly in one of the other shaded rectangles

pathway, starting with the right leg and stepping on the white targets only, avoiding the red ones. No other specific instructions regarding where to step were given. There were a total of 55 trials for each participant, 10 of which were control (no red targets in the pathway). A video record of each walking trial was obtained.

3.4 Data Analyses

From the video records, the following measures were determined. Each step was coded with respect to the other foot placement as normal, long, short, medial, lateral or any combination of those. Next, the data was transcribed into x-z co-ordinates system and graphed according to the following convention: in the x-direction, short step was –1, long step was +1; in the z-direction: medial step was –1, lateral step was +1. Figure 4 shows an example of the

changes in step length and width in a given trial for three different participants.

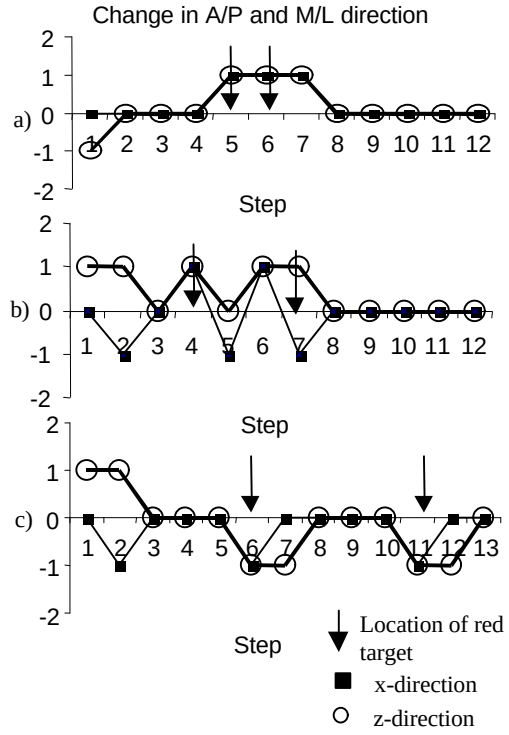

Figure 4 a, b, & c: Stepping pattern of three participants for selected trials.

3.5 Results

The following key results were obtained. Maximum number of consecutive steps modified during a given trial were either 1 (22.9 %) or 2 (68.3 %). The relative location of the two targets that were to be avoided had no effect on whether or not one or two consecutive steps were being modified as shown in figure 5. Greater than 80% of the steps in all the trials across all participants were of normal step length and width. Majority of the adjustments in step length (99 % of the total number) was equal to about an average foot length (28 cm); while majority of step width adjustments (93 % of the total number) was restricted to about an average foot width (14 cm).

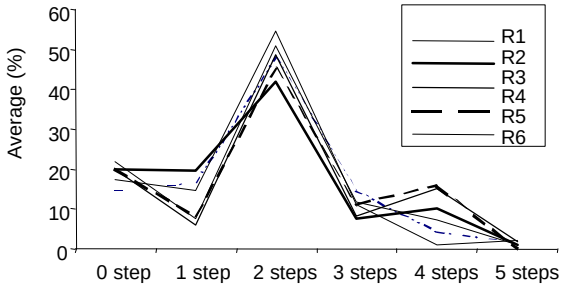

Figure 5: Average % of step modifications if the random target was located within a given radius of the constant target.

3.6 Discussion

These results confirm the findings of previous studies. Individuals do minimize the displacement of the foot from its normal landing spot (selection of stepping wide or narrow). Minimizing the changes to the normal walking patterns ensures that the energy cost for travel is minimized [13], and also reduces the demand on the postural/balance control system [5]. Adjustments to gait patterns are predominately in the plane of progression (almost equal number of step length changes compared to step width changes even though the step length changes are two times the step width changes). Changes in the step metrics in the plane of progression involve modulation of active muscles that are normally very active [14]. In contrast, changes in the step metrics in the frontal plane (step width modulation) require activation of muscles that are not as active [14]. In addition these results do show that adjustments to the stepping patterns are localized to one or two steps, and individuals do return to their normal gait patterns during subsequent steps. These findings are also similar to the observations by Lee et al. [11] that individuals limit the changes to a few steps to ensure that the goal of avoiding or accommodating a landing target for foot placement in the travel path.

4. Conclusions

We have been able to identify the objective and constraints that guide the selection of alternate foot placement during locomotion. Selection of alternate foot placement is not random; there is a single dominant choice for each situation which offers several advantages. The dominant choice requires minimal changes to the ongoing locomotor muscle activity, poses minimal threat to dynamic stability, allows for quick initiation of change in ongoing movement and ensures that the locomotor task runs without interruption. Perception-action coupling mediating this task is dependent not only on visual input but also on prediction of future foot placement and on constraints posed by dynamic stability requirement. Since they are subject to the same perceptual

locomotor constraints, the results from these studies would be useful in the design of bipedal robots.

References

[1] Patla, A.E., Sparrow, W.A., 2000. Factors that have shaped human locomotor structure and bahavior: The "Joules " in the crown. In Metabolic energy Expediture and the Learning and Control of Movement. Edited by: W.A. Sparrow, Human Kinetics, USA (in press)

[2] Patla, A.E. et al. 1989. Visual control of step length during overground locomotion: Task-specific modulation of the locomotion synergy. Journal of Experimental Psychology: Human Perception and Performance, 15(3): 603-617.

[3] Patla, A.E. et al . 1991. Visual control of locomotion: Strategies for changing direction and for going over obstacles. Journal of Experimental Psychology: Human Perception and Performance, 17(3): 603-634.

[4] Raibert, M.H. (1986). Legged Robots That Balance. Cambridge, MA: MIT Press.

[5] Patla, A.E. et al. 1999. What guides the selection of foot placement during locomotion in humans.. Experimental Brain Research, 128:44-450.

[6] Gibson,J.J. (1958) Visually controlled locomotion and visual orientation in animals. British Journal of Psychology, 49:182-189.

[7] Warren, W.H. Jr. (1988). Action modes and laws of control for the visual guidance of action. In: O. Meijer & K. Roth (eds), Movement Behaviour: The Motor-Action Controversy, Amsterdam: North Holland, 339-379.

[8] Bryden, M.P. 1977. Measuring handedness with questionnaires. Neuropsychologia, 15: 617-624.

[9] MacKenzie, I.S. 1992. Movement time prediction in human-computer interfaces. In Human-Computer Interaction: Towards the Year 2000, edited by R.M. Baecker, J. Grudin, W.A.S. Buxton and S. Greenberg. pp 483-493.

[10] Elliott, D. et al. 1995. The influence of target perturbation on manual aiming asymmetries in right handers. Cortex, 31: 685-697.

[11] Lee, D.N., Lishman, J.R., & Thomson, J.A. 1982. Regulation of gait in long jumping. Journal of Experimental Psychology: Human Perception & Performance, 8: 448-459.

[12] Warren, W.H., Jr., Young, D.S. & Lee, D.N. 1986. Visual control of step length during running over irregular terrain. Journal of Experimental Psychology: Human Perception and Performance, 12, 259-266.

[13] Alexander, R. McN (1989). Optimization and gait in the locomotion of vertebrates. Physiological Reviews, 69: 1199-1227.

[14] Winter, D.A. (1991). The Biomechanics and Motor Control of Human Gait: Normal and Pathological. University of Waterloo Press.

6. Acknowledgements

This work was supported by a grant from NSERC Canada.

Proceedings of the International Symposium on
Adaptive Motion of Animals and Machines,
Montreal, Aug.8-12, 2000

Emergence of Quadruped Walk by a Combination of Reflexes

Koh Hosoda, Takahiro Miyashita, and Minoru Asada

Adaptive Machine Systems, Osaka Univ., Suita, Osaka 565-0871, {hosoda,asada}@ams.eng.osaka-u.ac.jp

Abstract

Several behaviors of living things seem to be consequences of combinations of simple reflexes. By this hypothesis, emergence of walk of a quadruped robot is demonstrated by a combination of two reflexes in this paper. One reflex is to move its body according to movement of a target object which the robot gaze at, a vision-cued swaying reflex. The other is a gait reflex, a gait of a free leg so as not to make the robot fall down. As a consequence of these reflexes, the quadruped robot can walk according to the movement of the target object.

1. Introduction

Among mobile abilities of robots, legged locomotion has an advantage to the others owing to its adaptivity/robustness against changes of terrain. There have been numerous studies on legged locomotion in robotics [1] to utilize this advantage. Another reason why legged locomotion receives the attention is that most of natural living things such as human, animals, and insects utilize the ability.

Most common way to realize walking of a legged robot is (1) designing a trajectory of each leg considering kinematics and dynamics of the robot in assumed/estimated terrain, and (2) applying a control scheme to make each leg track the trajectory. Since it is necessary to know the shape of the ground and kinematic/dynamic parameters of the robot beforehand, the resultant robot system cannot be adaptive against changes of environment. There are several attempts (for example [2]) to make the robot adaptive by using external sensors such as cameras, which still lack for a quick response since they need to reconstruct the shape of the ground by the external sensor signal.

Let us consider walking of an infant leaded by his/her mother. The mother may show her hand to the infant, and the infant tries to chase the hand. It does not seem to be true that the infant reconstructs geometry of the ground, calculates desired trajectories, and moves legs. He/she may have primal reflexes such as not to lose balance, to keep the image of the hand constant, and so forth. Following this consideration, we come to the idea that the robot can also be controlled by several reflexes.

In the field of biology and physiology, they assume that several purposive behaviors emerge by combinations of elemental reflexes. Although the reflex of natural creatures should be different from that of artifacts, we can still learn how to construct a behavior of a robot. It may be designed by a combination of elements each of which does not exactly correspond to a behavior. If the element acts in a reactive manner without considering heavy reconstruction, we can call it a reflex of a robot.

The aim of this paper is emergence of walking by a combination of such artificial reflexes. We introduce two relfexes, a vision-cued swaying reflex and a gait reflex. The vision-cued reflex is realized by an adaptive visual servoing controller [3]. The gait reflex is realized by a lifted leg controller that generates a reflective gait which consists of three steps: (1) selecting a leg to be lifted so as to increase the body stability, (2) shifting (lift up, move, and down) one of other legs to enable the selected leg lifted, and (3) shifting the selected leg.

In the rest of this article, we first discuss on emergence of walking by the vision-cued reflex and the gait reflex. Then, an adaptive visual servoing controller and a lifted leg controller are proposed to realize the vision-cued reflex and the gait reflex, respectively. To realize these reflexes simultaneously, a hybrid controller is derived consisting of these controllers. Finally, we show experimental results in a real environment to demonstrate that the proposed combination of reflexes can emgerge quadruped walking.

2. Emergence of Walking

In this paper, we are going to deal with a quadruped robot that has camera(s) on it (Figure 1). The robot is gazing at a visual target and trying to

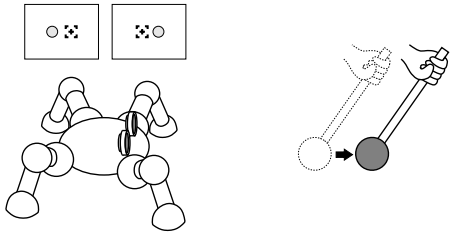

(a) When the visual taget moves,

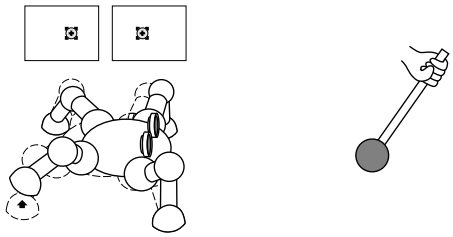

(b) the vision-cued reflex makes the robot sway, and

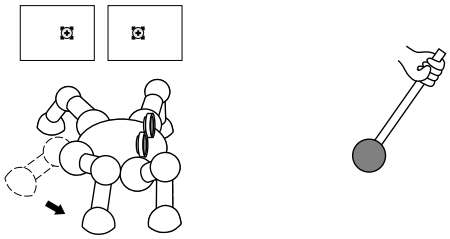

(c) finally, the gait reflex makes another step.

Figure 1: Legged robot walking emerges by tracking a visual target.

keep observed target images constant. Therefore, the robot will sway according to the movement of the target (Figure 1(a)). This is a vision-cued reflex built in the robot.

The robot also has force sensors at its feet. By these force sensors, the robot can observe the ZMP (zero moment point) which is used to calculate a stability measure. Yet another reflex of the robot is a gait reflex by utilizing this stability measure. When the stability is small (Figure 1(b)), the robot will make steps to enlarge it (Figure 1(c)).

Because of a combination of these two reflexes, the robot will sway when the movement of the target is small, and it will walk when the movement is large. Note that these reflexes do not necessarily corresponds to a behavior. We do not explicitly program walking of a quadruped, but it emgerges as a consequence of two reflexes.

3. Vision-cued Swaying Reflex

To realize vision-cued swaying according to the movement of the target, we apply visual servoing [4, 5]. The visual servoing controller feeds the visual information back to control inputs directly, which makes the robot response quick and robust. There have been many studies on visual servoing applied to manipulators, but only one for legged robots [6] to the best of our knowledge. In the paper, to apply visual servoing to a legged robot, stance servoing control is introduced.

Another difficulty to apply visual servoing to the legged robot is that the relation between change of features in the image plane and joint displacement is unknown when the geometry of the terrain is unknown. To estimate the relation, we have to use an on-line estimator [3, 7].

In this section, we quickly introduce adaptive visual servoing control for legged robots to realize a vision-cued swaying reflex, consisting of a stance servoing controller, an on-line estimator, and a visual servoing controller.

3.1. Stance servoing control

First, we introduce the stance servoing controller to keep distances between feet constant. Let ${}^R\boldsymbol{r}_i$ be a position vector of the foot i with respect to the robot coordinate frame Σ_R fixed to the robot body. Since a stance vector $\boldsymbol{l}$, a correction vector of distance between feet, is a function of ${}^R\boldsymbol{r}_i$, we can derive a velocity relation:

$$\dot{\boldsymbol{l}} = \boldsymbol{J}_{lr}\, {}^R\dot{\boldsymbol{r}}, \tag{1}$$

where ${}^R\boldsymbol{r} = [{}^R\boldsymbol{r}_1{}^T\ {}^R\boldsymbol{r}_2{}^T\ \cdots\ {}^R\boldsymbol{r}_2{}^T]^T$, and $\boldsymbol{J}_{lr} = \partial\boldsymbol{l}/\partial\ {}^R\boldsymbol{r}^T$. From eq.(1), we can obtain a stance servoing controller:

$$\boldsymbol{u} = \boldsymbol{J}_{lr}{}^+\boldsymbol{K}_l(\boldsymbol{l}_d - \boldsymbol{l}) + (\boldsymbol{I} - \boldsymbol{J}_{lr}{}^+\boldsymbol{J}_{lr})\boldsymbol{k}_l, \tag{2}$$

where $\boldsymbol{J}_{lr}{}^+$, $\boldsymbol{l}_d$, $\boldsymbol{K}_l$, and $\boldsymbol{k}_l$ denote the pseudo-inverse matrix of $\boldsymbol{J}_{lr}$, the desired stance vector, a gain matrix, and an arbitrary vector that describes redundancy, respectively. Utilizing the second term on the right hand side, we can apply servoing control.

3.2. Visual servoing control

From the camera(s) attached to the robot body, one can get some image features such as position, line length, contour length, and/or area of certain

image patterns. Let a vector of the image features be $\boldsymbol{x}$. Assume that the target is moving so slowly that one can neglect the velocity of the target comparing to the velocity of the robot. If the stance servoing controller (2) keeps the feet distances constant, the image feature vector $\boldsymbol{x}$ is a function of ${}^R\boldsymbol{r}$,

$$\dot{\boldsymbol{x}} = \boldsymbol{J}_{xr}\,{}^R\dot{\boldsymbol{r}}, \tag{3}$$

where $\boldsymbol{J}_{xr} = \partial \boldsymbol{x}/\partial {}^R\boldsymbol{r}^T$.

By utilizing null space of eq.(2), we can derive an adaptive visual servoing controller for a legged robot,

$$\begin{aligned}\boldsymbol{u} &= \boldsymbol{J}_{lr}{}^{+}\boldsymbol{K}_l(\boldsymbol{l}_d - \boldsymbol{l}) \\ &\quad +(\boldsymbol{I} - \boldsymbol{J}_{lr}{}^{+}\boldsymbol{J}_{lr})\left\{\boldsymbol{J}_{xr}(\boldsymbol{I} - \boldsymbol{J}_{lr}{}^{+}\boldsymbol{J}_{lr})\right\}^{+} \\ &\quad \left\{\boldsymbol{K}_x(\boldsymbol{x}_d - \boldsymbol{x}) - \boldsymbol{J}_{xr}\boldsymbol{J}_{lr}{}^{+}\boldsymbol{K}_l(\boldsymbol{l}_d - \boldsymbol{l})\right\}, \end{aligned} \tag{4}$$

where $\boldsymbol{K}_x$ denote a gain matrix for visual servoing.

3.3. On-line estimator

The Jacobian matrix $\boldsymbol{J}_{xr}$ is a function not only of intrinsic camera parameters but also of position/orientation of the visual target w. r. t. Σ_R, and of geometry of the terrain. Since the legged robot is moving in unknown terrain and the position of target is also unknown, the robot must estimate $\boldsymbol{J}_{xr}$ on-line.

We can derive an on-line estimator to identify a non-linear system in the discrete time domain [3],

$$\begin{aligned}\widehat{\boldsymbol{J}}_{xr}(k) &= \widehat{\boldsymbol{J}}_{xr}(k-1) \\ &\quad +\{\Delta\boldsymbol{x}(k) - \widehat{\boldsymbol{J}}_{xr}(k-1)\Delta\boldsymbol{u}(k)\} \\ &\quad \frac{\Delta\boldsymbol{u}(k)^T\boldsymbol{W}(k-1)}{\rho + \Delta\boldsymbol{u}(k)^T\boldsymbol{W}(k-1)\Delta\boldsymbol{u}(k)}, \end{aligned} \tag{5}$$

where $\widehat{\boldsymbol{J}}_{xr}(k)$, $\boldsymbol{u}(k)(= T\dot{\boldsymbol{\theta}})$, ρ, and $\boldsymbol{W}(k)$ denote a constant Jacobian matrix, a control input vector in the k-th step during sampling rate T, an appropriate positive constant and a weighting matrix, respectively. In a case that $\boldsymbol{W}$ is a covariance matrix and that ρ_i is in the range $0 < \rho \leq 1$, the proposed estimator is a well-known weighted recursive least squares estimator [8].

By using estimated $\widehat{\boldsymbol{J}}_{xr}$ instead of $\boldsymbol{J}_{xr}$ in the visual servoing controller (4), we can realize a vision-cued reflex of the legged robot.

4. Gait Reflex to Increase Body Stability

To realize a gait reflex, we proposed a gait stategy based on a body stability measure calculated from the ZMP.

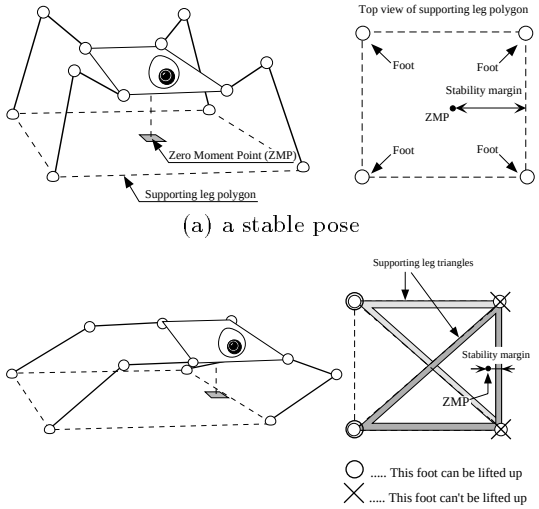

Figure 2: The stability margin is the shortest distance between the ZMP and a side of the supporting leg polygon. If the margin is large, the robot is stable, otherwise it is unstable.

4.1. The reflective gait procedure

We adopt a stability margin [9], the shortest distance between the ZMP and a side of the supporting leg polygon (the boudaries of the support pattern), as a stability measure of the legged robot (see Figure 2). As the robot sways the body, the margin becomes small as shown in Figure 2(b). To recover the stability, the robot has to move one of legs indicated as "$\times$" in the figure so as to increase the margin. However, both legs can not be lifted up immediately because they are included in two supporing triangles where the ZMP is inside. To lift up one of the legs (which we call target leg in the following), therefore, one of the others indicated as "$\circ$" has to be moved as shown in Figure 3. This is a reactive gait procedure since it is reactive to the movement of the ZMP.

4.2. Lifted leg control algorithm

We can realize the reflective gait by a simple algorithm as follows. The positions of the lifted legs fall into two cases with respect to the relationship between the supporting legs and v_{zmp}, the velocity of ZMP (see Figure 4): a hind leg case and a fore leg one.

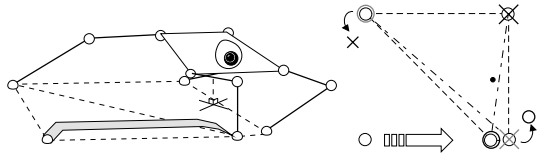

(a) To lift the target leg (right below "×"), the robot have to move one of the others to make the target leg out of one of supporting triangles.

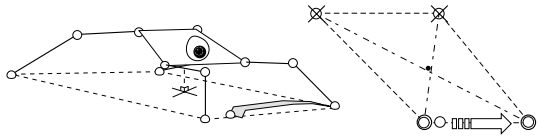

(b) After moving the leg, the target leg can be lifted up since it is no more inside the supporting triangle.

Figure 3: The procedure of the reflective gait

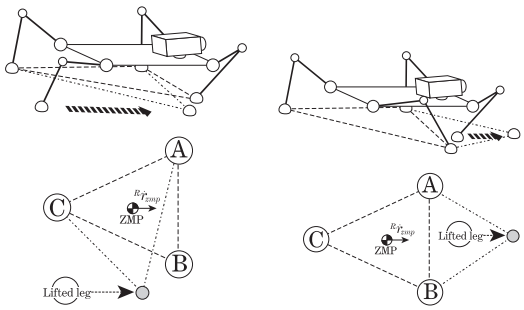

(a) a hind leg case (a) a fore leg case

Figure 4: Supporting leg triangles and a lifted leg

The hind leg case (Figure 4(a): The lifted leg is the diagonal leg of leg(A) or leg(B).) The robot moves the lifted leg to keep ZMP inside the next supporting leg triangle which consists of leg(A) (or leg(B)), leg(C), and the lifted leg. Subsequently, leg(B) (or leg(A)) becomes the lifted leg.

The fore leg case (Figure 4(b): The lifted leg is the diagonal leg of leg (C).) The robot moves the lifted leg to appropriate position in front of it, but does not touch down yet. If the ZMP moves into the next supporting leg triangle which consists of leg(A), leg(B), and the lifted leg, then it is naturally touched down, and subsequently leg(C) becomes the lifted leg.

5. Experiments

We apply the proposed two controllers to a real quadruped robot to realize two reflexes. Emergence of walking is demonstrated in this section.

5.1. A quadruped for experiements

In Figure 5, a legged robot TITAN-VIII [10] and its controller used for the experiment are shown. The legged robot is equipped with one CCD camera (EVI-310, SONY). The image from the camera is sent to a tracking unit (TRV-CPD6, Fujitsu) equipped with a high-speed correlation processor [11]. Before starting an experiment, we give three 16[pixel] × 16[pixel] patterns (called reference patterns) to be tracked. During the experiment the unit feeds coordinates where the correlation coefficient is the highest with respect to the reference patterns to the host computer G6-200 (Gateway2000, CPU:Intel Pentium Pro 200MHz) through a PCI-bus link in real-time (33[ms]).

Each joint of the legged robot is equipped with a potentiometer to observe its angle. Each foot is also equipped with a force sensor to observe its foot force and to estimate the ZMP. The observed joint angles and the foot forces are sent to the computer through an A/D converter board (RIF-01, Fujitsu). The computer calculates the desired joint velocities and sends the commands to the velocity controllers of joints through a D/A converter board (RIF-01, Fujitsu). A hand cart is used as a visual target on which 3 target marks are drawn.

5.2. Experimental results

An example of emerged walking is shown in Figure 6. At t=2.0[s], the cart began to move rightward. The robot was initially supported by right-fore-leg (RF), left-fore-leg (LF), and left-hind-leg (LH). The initial lifted leg was right-hind-leg (RH). The robot was swinging its body as the target motion and switched the lifted leg from RH to LF at t=14.0[s], which was the fore leg case. Subsequently, it switched the lifted leg from LF to RF (the hind leg case) at t=23.0[s], from RF to LH (the fore leg case) at t=32.0[s], from LH to LF (the hind leg case) at t=39.0[s]. In Figure 6, we can see how the legged robot behaved reflectively to track the visual target.

6. Conclusion and Disscussions

Emergence of walk of a quadruped has been demonstrated by a combination of two reflexes in this paper. As a consequence of these reflexes, the real

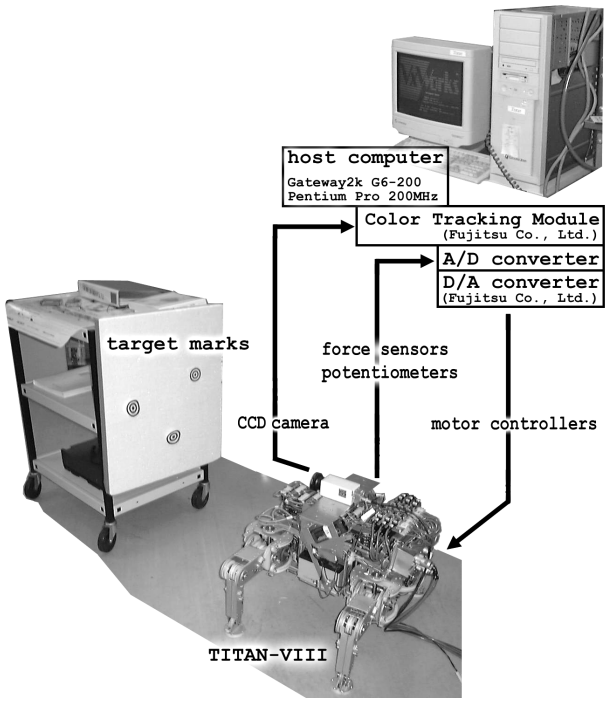

Figure 5: An experimental system: A quadruped "TITAN-VIII" and its controller used for the experiments.

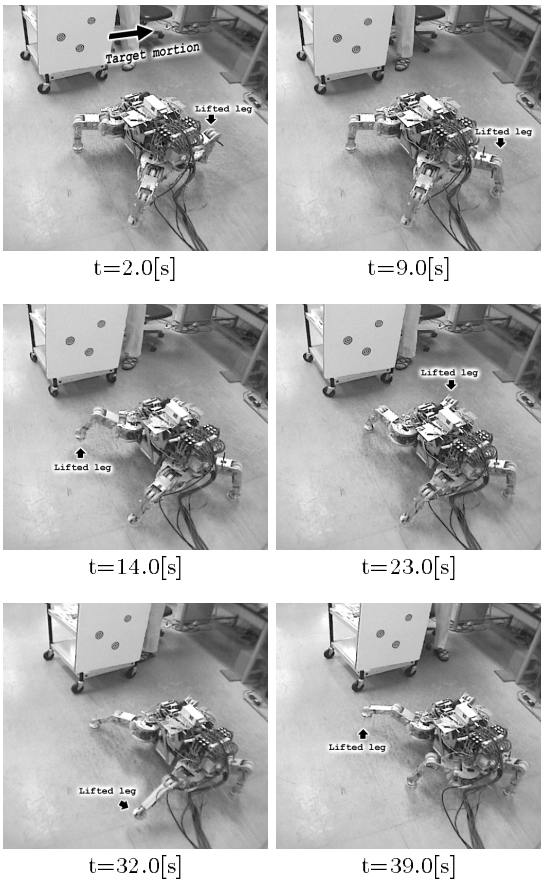

Figure 6: An experimental result: The legged robot walks reflectively to follow the movement of the target.

quadruped walked to track the moving target. We expect that this way of building a robot may be adaptive to changes of the environment, and that an unexpected behavior emerges as a consequence of a combination of reflexes, the robot body, and the environment.

The hypothesis, several purposive behaviors emerge by combinations of elemental reflexes, must be demonstrated by more variety of tasks and robots. We have demonstrated a case of an arm and a case of a hand with several reflexes in other papers[12, 13]. However, still more examples are needed.

A robot, as a universal machine, ought to have adaptivity, ability to estimate appropriate control parameters and/or structure to achieve a given task in an environment. So as to have such adaptivity against changes of task and environment, a robot needs to have larger number of actuators and more variety of sensors. Such many degrees of freedom are expected to be controlled easily by the proposed method.

References

[1] M. H. Raibert et al. Special issue on legged locomotion. Int. J. of Robotics Research, 3(2), 1984.

[2] D. J. Pack. Perception-based control for a quadruped walking robot. In Proc. of IEEE Int. Conf. on Robotics and Automation, pages 2994–3001, 1996.

[3] K. Hosoda and M. Asada. Adaptive visual servoing for various kinds fo robot systems. In A. Casals and A. T. de Almeida, editors, Experimental Robotics V, pages 547–558. Springer, 1998.

[4] L. E. Weiss, A. C. Sanderson, and C. P. Neuman. Dynamic sensor-based control of robots with visual feedback. IEEE J. of Robotics and Automation, RA-3(5):404–417, 1987.

[5] P. I. Corke. Visual control of robot manipulators – a review. In Visual Servoing, pages 1–31. World Scientific, 1993.

[6] K. Hosoda, M. Kamado, and M. Asada. Vision-based servoing control for legged robots. In Proc. of IEEE Int. Conf. on Robotics and Automation, pages 3154–3159, 1997.

[7] K. Hosoda, M. Kamado, and M. Asada. Vision-based servoing control for legged robots. In Proc. of IEEE Int. Conf. on Robotics and Automation, pages 3154–3159, 1997.

[8] P. Eykhoff. System Identification, chapter 7. John Wiley & Sons Ltd., 1974.

[9] S.-M. Song and K. J. Waldron. Machines That Walk: The Adaptive Suspension Vehicle, chapter 3: Level Walking Gaits, page 28. The MIT Press, 1989.

[10] K. Arikawa and S. Hirose. Development of quadruped walking robot TITAN–VIII. In Proc. of the 1996 IEEE/RSJ Int. Conf. on Intelligent Robots and Systems, pages 208–214, 1996.

[11] M. Inaba, T. Kamata, and H. Inoue. Rope handling by mobile hand-eye robots. In Proc. of Int. Conf. on Advanced Robotics, pages 121–126, 1993.

[12] Koh Hosoda and Minoru Asada. How does a robot find redundancy by itself – a control architecture for adaptive multi-dof robots. In Proc. of 8th European Workshop on Learning Robots (EWLR–8), 1999.

[13] Koh Hosoda, Takuya Hisano, and Minoru Asada. Sensor dependent task definition: Object manipulation by fingers with uncalibrated vision. In Proc. of The 6th International Conference on Intelligent Autonomous Systems (IAS–6), 2000(to appear).

Proceedings of the International Symposium on
Adaptive Motion of Animals and Machines,
Montreal, Aug.8-12, 2000

A Model of Visually Triggered Gait Adaptation

M. Anthony Lewis and Lucia S. Simo

Iguana Robotics, Inc.
Mahomet, IL 61853

tlewis@iguana-robotics.com
http://www.iguana-robotics.com/

Abstract-*Walking machines can walk over obstacles without touching them only if they can anticipate contact and make suitable gait modifications. Existing visually guided machines use computationally intense approaches that require construction of a geometrically correct model of both the environment and the robot. We present a model, inspired by research in vertebrates, in which the stride length modification that takes place before stepping over the obstacle is learned based on experience. The key hypothesis introduced here is the use of temporal gating of the visual signal encoding the distance to an obstacle. This hypothesis enables the formulation of the problem as a direct mapping of perception to action. In addition, the use of temporal gating also facilitates learning by simplifying the credit assignment problem. Our approach does not require that a geometric representation of the environment be created and updated based on new observations. Our simulation results indicate that the desired mapping can be learned quickly. The resulting gait modulation is smooth and coordinated with the phase of the central pattern generator controlling the robot. Our model qualitatively reproduces human data where the uncertainty in footsteps decreases with approach to an object.*

1 Introduction

Locomotion and perception have been treated as separate problems in the field of robotics. Under this paradigm, one first solves the 'vision problem' of recovering the three-dimensional geometry of the scene. This information is then passed to a planning system that has access to an explicit model of the robot. A good trajectory is found for each individual leg to move over the obstacle. This solution is computationally intense and, as demonstrated for the Ambler walking machine (Krotkov and Hoffman, 1994; Krotkov and Simmons, 1996), too slow for real-time control using moderate power CPUs. Furthermore, this approach does not exploit the fact that the walking machine will be presented with a similar situation again and again.

The approach considered here is to eliminate the intermediate explicit model and consider creating a direct coupling of perception to action, with the mapping being adaptive and based on experience. For this approach we use a temporal gating hypothesis by which sensory data (distance to the object) is temporally gated to modify the output of the locomotor controller.

Recently, a number of studies have pointed out the necessity of gating mechanisms to control the flow of sensory signals in the brain of vertebrates (Prochazka, 1989; Chapman, 1994; Apps, 1999). In particular, temporal gating during a visual discrimination task prevents extraneous signals occurring around the time of the critical visual event to affect performance (Seidemann et al., 1998).

Continuous visual input is not necessary for accurate stepping. Not all visual samples have the same potential for control limb movements. Samples taken when the foot to be controlled is in stance are by far more effective in modulating gait. It has been suggested that during stepping visual information is used during the stance phase in a feedforward manner to plan and initiate changes in the swing limb trajectory (Holland and Marple-Horvat, 1996; Patla et al., 1996).

Finally, behavioral studies in humans have shown that the regulation of the step depends on the distance to the obstacle. Data from athletes in the long jump have demonstrated that just prior to lift-off the athlete modulates his/her stride length over the last three steps (Lee et al., 1982). Also, the standard deviation of the footsteps decreases over the last three steps.

Taken together, this may indicate that gait is modulated at discrete intervals. This modulation may be a highly stereotyped program that depends on a brief sampling of the visual environment to instantiate it (c.f. Patla et al., 1991). This hypothesis is intriguing because it implies that after a brief sample it is not necessary to store an internal representation of the

world that needs to be shifted and updated during movement.

This shifting and updating is problematic for both neural and traditional robotics models.

2 Elegant Stepping Model

The adaptation problem that we will address can be described abstractly as follows. We wish to make associations between a distance to the obstacle and a change in stride length. We wish to adjust this mapping adaptively and based on experience.

We choose the occurrence of a paw extension and paw placement reflex as training signals. If a reflex is triggered while the leg is extending, then the paw had almost cleared the obstacle. In this case we adjust previous associations between distance and stride length to make longer strides in the future. If a paw placement reflex is triggered when the leg is flexing, we adjust the previous associations between distance and stride length to make shorter strides in the future.

One key difficulty in learning is how to propagate the error back in time in a biologically plausible way. Note that visual information flows into the animal's eyes continuously. However, we note that changes in the step cycle are most effective during narrow time windows. Therefore, we hypothesize that sensory information from visual areas (e.g. distance) is gated periodically and in synchrony with the step cycle. This is our temporal gating hypothesis. This information is then held, decaying exponentially, and is used to modulate the gait over the following step cycle. Thus, as the robot approaches an obstacle, it makes at most three discrete decisions prior to going over the obstacle. These decisions occur at the three footsteps prior to going over the obstacle. This discretization simplifies the credit assignment problem.

The model has four main parts, referring to Fig. 1:

(1) *Range Encoder*— encodes distance to the obstacle using nonoverlapping cells. No spatial ordering of units is assumed. These elements are gating into short-term memory.

(2) *Locomotory Generator*— the central pattern generator (CPG) is modeled as a ring oscillator (Lewis, 1996) that drives two output functions. One drives the muscle of the leg and the other indicates the beginning of each step cycle and is used for the sensory gating. In addition, a "lift reflex" increases the amplitude of the CPG output and is hardwired.

(3) *Mechanical System*— this is the model of environment/leg interaction. We simulate the muscle as a low-pass filter. This muscle drives the flexion of one degree of freedom leg. Each obstacle is simulated as being a rectangle.

(4) *Learning System*— the activity of the units in the range encoder are one-to-one gated into short-term memory cells (STM) in synchrony with the step cycle. The gate used to accomplish this is a shunting inhibition signal originating in the CPG. An adaptive premotor module receives a weighted signal from the STM, and controls the stride length by modulating the burst length (parameter of the CPG controlling the flexion of the leg). The STM activates synapses in the adaptive module. Traces in these synapses maintain a brief memory of having being activated. If a reflex is triggered, then a heuristic is used to modify the weights of the adaptive module. If a paw placement reflex has occurred, then all synapses contributing to this decision should be incrementally decreased. If a paw extension reflex occurs, they should be increased.

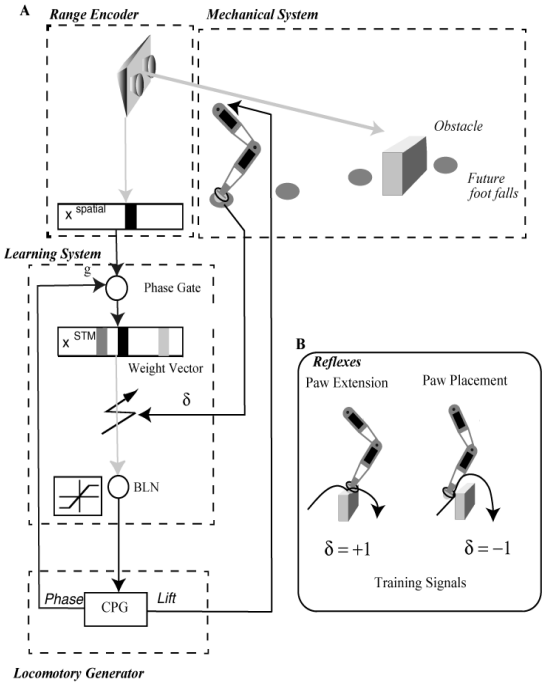

Figure 1. Model of Elegant stepping. (A)Visual input is periodically gated into short term memory by a phase signal ascending from the CPG. Short term memory elements are weighted and the resulting output is used to shorten or lengthen the stride length. (B) Certain reflexes signal error conditions. This supervisory signal is propogated back through time, in a biologically plausible way, and adjusts the short term memory weights.

3 Simulation Experiments

Figure 2 shows a typical foot trajectories before and after learning. As can be seen, the adaptive gait allows the foot to be in a position to clear the obstacle. If stride length adjustments are not made, it may be nearly impossible for the leg to clear the obstacle.

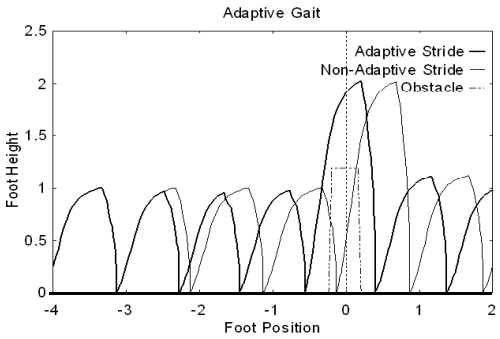

Figure 2. Typical gait trajectories. Example of gait trajectory before and after learning.

Notice that the stride length is adjusted three times before the animal reaches the obstacle.

The learning takes place quickly. The algorithm performs well after about 20 training cycles. After about 100 trials, no more mistakes are made in the gait. Learning is smooth. As the robotic leg moves toward the obstacle, the burst length (parameter of the CPG controlling the flexion of the leg) is gradually altered. After passing the obstacle, the burst length gradually relaxes to its former value. Thus, the gait is altered smoothly.

Interestingly, the variance in footsteps decreases as the robotic leg approaches the obstacle (Fig 3). Just as in long jump athletes the standard deviation of the footsteps decreases just before the final footstep. Thus, the robot found a 'sweet' spot to land on just before going over the obstacle. Furthermore, the variance in footsteps also decreases with increasing object size. The 'sweet' spot is small if the object is large.

The weight distribution after learning is periodic (Fig. 4). The perceptual space is divided into periodic regions.

4 Discussion

In our model perception and action are tightly coupled. The mapping is adaptive and based on experience. The goal of the adaptation is to use distance measurements to smoothly modulate a CPG controlling gait. A key element in our model is the use of a temporal gating hypothesis which simplifies the learning problem.

Our approach does not require that a geometric representation of the environment be created and updated. This is in strong contrast to current practice in machine vision and robotics of surface reconstruction as a prerequisite to planning.

4.1 Separation of Obstacle Clearance and Stride Length adaptation.

The model presented here separates the task of stepping over the obstacle into two components: stride

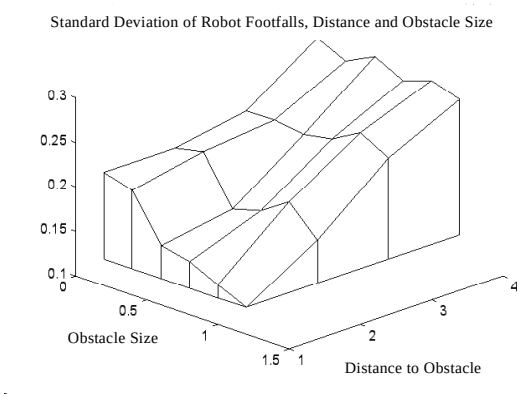

Figure 3. Standard deviation for varying object sizes and distances to object. As the robot approaches the obstacle, its foot fall variance decreases. Variance also decreases with increasing object size.

length adjustment and foot elevation going over the obstacle. The focus of the adaptation in the model is the stride length adjustment. It can be argued that if the stride length is adjusted in anticipation of the obstacle, the task of stepping over the obstacle will be easier. Thus, there is some interaction between the two components. If stride length is poor, then the final step may fail.

Future work should entail strategies for learning the sensory motor transformation for the last step. That is, how does the animal step over the obstacle, while, presumably, optimizing other criteria such as stability, comfort and perhaps energy usage.

Currently, information about the height of the object only impacts stride length. Training occurs for a given set of weights for a single object height only. In the future, object size should be used to give the weights a certain context.

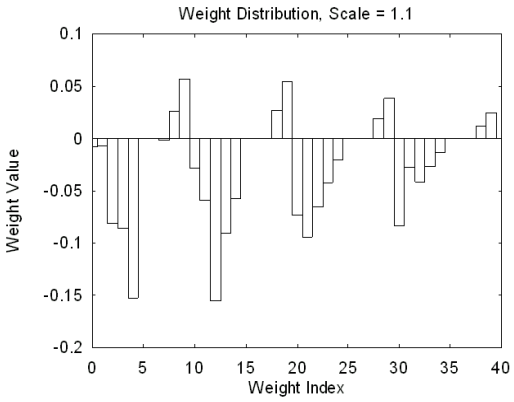

Figure 4. Typical weight distribution after learning. Notice that the weights, or adjustment commands are periodic. Here the weights are ordered according to their correspondence to distances from the obstacle. This ordering is done for the sake of presentation. The algorithm does not assume any particular structure of the sensory space.

4.2 Temporal Gating

Recent studies in cats suggest that during stepping over obstacles premotor signals from the motor cortex may be gated onto the spinal CPG network in synchrony with the step cycle (Drew et al., 1996).

In our model sensory signals (distance) are gated in synchrony with the step cycle. This is our temporal gating hypothesis. Sensory gating has been shown for signals exiting the middle temporal visual area during a visual discrimination task (Seidemann et al., 1998). In addition, movement-related gating of sensory input to the cerebellum via climbing fibers has also been suggested (Apps, 1999).

A recent article by Taga (1996) addresses the problem of adjusting the parameters of a CPG so that a biped figure is able to walk over an object. In that paper Taga proposes a method for synchronizing corrective input to muscles in synchrony with the step cycle. He was inspired by work of Drew and others (see Drew et al., 1996 for a review).

The Taga work is a complement to the work presented here. While our model address the acquisition of a visuomotor mapping, and proposes *sensory gating*. The Taga work supposes that there is a kind of *motor gating of* commands to the muscles. These are compatible interpretations. In practice our adjustment signal might need to be broken up into discrete time intervals to control individual muscles. While our CPG system is rudimentary, Taga's CPG is more complex. It is likely that Taga's biomechanical model could be substituted for the rudimentary biomechanical model presented here. The results should be similar even with a more complex model.

Secondly, the Taga model is concerned with the details of stepping over the object, the system described here considers changes in stride length before the animal or robot reaches the obstacle. We design a system that assumes such programs exists. We are concerned with providing input parameters to such a motor program.

Finally, the model presented by Taga is not concerned with learning.

4.3 Learning Visuomotor Behavior

Asada et al. (1996) describe a system that uses reinforcement learning to automatically generate associations between perceptual stimuli and action. In general the reinforcement learning problem is more difficult than the problem examined here. Using some knowledge of the problem, we were able to deduce that a reflex signal would be an ideal training input. This signal gives the algorithm feedback as to *what* it should do when an error occurs. Thus the learning algorithm used here is a supervised learning problem. The formulation of the this problem as a supervised learning problem undoubtedly accounts for the quick learning observed.

Acknowledgements

The authors acknowledge support of Grant No. N00014-99-0984 from the Office of Naval Research.

5 REFERENCES

Apps, R. (1999) Movement-related gating of climbing fibre input to cerebellar cortical zones. *Progress in Neurobiology*, **57**, 537-562.

Asada, M., Noda, S., Tawaratsumida, S. and Hosada K. (1996) Purposive Behavior Acquisition for a Real Robot by Vision-Based Reinforcement Learning, *Machine Learning*, **23**, 279-303.

Chapman C.E. (1994) Active versus passive touch: factors influencing the transmission of somatosensory signals to primary somatosensory cortex. *Canadian Journal of Physiology and Pharmacology*, **72**, 558-570.

Drew T., Jian W., Kably B., and Lavoie S. (1996) Role of the motor cortex in the control of visually triggered gait modifications. *Canadian Journal of Physiology and Pharmacology*, **74**, 426-442.

Grillner S. and Wallén P. (1985) Central pattern generators for locomotion, with special reference to vertebrates. *Annual Review of Neuroscience*, **8**, 233-61.

Hollands, M.A. and Marple-Horvat, D.E. (1996) Visually guided stepping under conditions of step cycle related denial of visual information. *Experimental Brain Research*, **109**, 343-356.

Krotkov, E. and Simmons, R. (1996) Perception, planning and control for autonomous walking with the ambler planetary rover. *IEEE Transactions on Robotics and Automation*, **15**, 155-180.

Krotkov, E. and Hoffman, R. (1994) Terrain Mapping for a walking planetary rover. *IEEE Transactions on Robotics and Automation*, **10**, 728-736.

Lee, D.N., Lishman, J.R. and Thomson, J.A. (1982) Regulation of gait in long jumping. *Journal of Experimental Psychology: Human Perception and Performance*, **8**, 448-459.

Lewis, M. A. Self Organization of Locomotory Controllers in Animals and Robots, Ph.D. Dissertation, Electrical Engineering Department, University of Southern California, Los Angeles, 1996.

Patla, A.E., Prentice, S.D., Robinson, C. and Neufeld, J. (1991) Visual control of locomotion: strategies for changing direction and for going over obstacles. *Journal of Experimental Psychology: Human Perception and Performance*, **17**, 603-634.

Patla, A.E., Adkin, A., Martin, C., Holden, R. and Prentice, S.D. (1996) Characteristics of voluntary visual sampling of the environment for safe locomotion over different terrains. *Experimental Brain Research*, **112**, 513-522.

Prochazka A. (1989) Sensorimotor gain control: a basic strategy of motor systems? *Progress in Neurobiology*, **33**, 281-307.

Seidemann E, Zohary E, and Newsome WT (1998) Temporal gating of neural signals during performance of a visual discrimination task. *Nature*, **394**, 72-75.

Session

Neuro-Mechanics

Proceedings of the International Symposium on
Adaptive Motion of Animals and Machines,
Montreal, Aug.8-12, 2000

Biologically Inspired Dynamic Walking of a Quadruped Robot on Irregular Terrain - Adaptation at Spinal Cord and Brain Stem -

Hiroshi Kimura and Yasuhiro Fukuoka

Grad. School of Information Systems, Univ. of Electro-Communications, Chofu, Tokyo 182-8585, JAPAN
{hiroshi, fukuoka}@kimura.is.uec.ac.jp

Abstract

We are trying to induce a quadruped robot to walk dynamically on irregular terrain by using a neural system model. In this paper, we integrate several reflexes such as stretch reflex, vestibulospinal reflex, and extensor and flexor reflex into CPG (Central Pattern Generator). The success in walking on terrain of medium degree of irregularity with fixed parameters of CPG and reflexes shows that the biologically inspired control proposed in this study has an ability for autonomous adaptation to unknown irregular terrain. MPEG footage of these experiments can be seen at: http://www.kimura.is.uec.ac.jp.

1. Introduction

Many previous studies of legged robots have been performed. However, autonomous dynamic adaptation in order to cope with an infinite variety of terrain irregularity still remains unsolved.

On the other hand, animals show marvelous abilities in autonomous adaptation. It is well known that the motions of animals are controlled by internal neural systems. Much previous research attempted to generate autonomously adaptable dynamic walking using a neural system model in simulation[1, 2, 3, 4] and real robots[5, 6, 7]. In our previous studies[7], we realized dynamic walking up and down a slope, and over an obstacle by using a CPG (Central Pattern Generator) and reflexes independent of a CPG. However, the irregularity of terrain in that study was low and walking was not smooth.

In this study we propose a new method for combining CPGs and reflexes based on biological knowledge, and show that reflexes via a CPG is much effective in adaptive dynamic walking on terrain of medium degree of irregularity through experiments. In the proposed method, there does not exist adaptation based on trajectory planning commonly used in the conventional robotics and adaptation to irregular terrain is autonomously generated as a result of interaction of the torque-based system consisting of a rhythm pattern generator and reflexes with environment.

2. Dynamic Walking Using CPGs

2.1. Quadruped robot

In order to apply the control using neural system model, we made a quadruped robot, Patrush. Each leg of the robot has three joints, namely the hip, knee, and ankle joint, that rotate around the pitch axis. An ankle joint is passive. The robot is 36 cm in length, 24 cm in width, 33 cm in height and 5.2 kg in weight. The body motion of the robot is constrained on the pitch plane by two poles since the robot has no joint around the roll axis. For a reflex mechanism, 6 axes force/torque sensor is attached on a lower link beneath the knee joint. A rate-gyro as an angular velocity sensor is mounted on a body as vestibule. All control programs below are written in C language and executed on RT-Linux.

In this study, we define the virtual extensor and flexor muscles on a quadruped robot, and origin and direction of joint angle and torque as shown in Fig.1. In addition, we use such notation as L(left), R(right), F(fore), H(hind), S(hip), x(joint angle), f_x and f_z(force sensor value in x and z direction). For example, LFS means the hip joint of the left foreleg, and LFS.x and LF.fx mean the angle at this joint and force sensor value at this leg.

2.2. Walking on flat terrain using CPGs

By investigation of the motion generation mechanism of a spinal cat, it was found that CPGs are located in the spinal cord, and that walking mo-

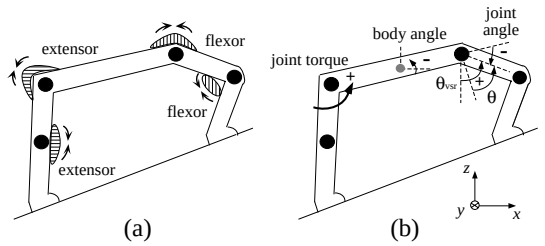

Figure 1: (a) Virtual extensor and flexor muscle on a quadruped robot. (b) Origin and direction of angles and direction of torque.

tions are autonomously generated by the neural systems below the brain stem[8, 9]. Several mathematical models of a CPG were also proposed, and it was pointed out that a CPG has the capability to generate and modulate walking patterns[10], to be mutually entrained with rhythmic joint motion, and to adapt walking motion to the terrain[1, 2].

As a model of a CPG, we used a neural oscillator (NO) proposed by Matsuoka[11] and applied to the biped by Taga[1, 2]. The stability and parameters tuning of a NO was analyzed using describing function method[12]. Single NO consists of two mutually inhibiting neurons (Fig.2-(a)). Each neuron in this model is represented by the nonlinear differential equations:

$$\begin{aligned} \tau \dot{u}_{\{e,f\}i} &= -u_{\{e,f\}i} + w_{fe} y_{\{f,e\}i} - \beta v_{\{e,f\}i} + u_{0i} \\ &\quad + Feed_{\{e,f\}i} + \sum_{j=1}^{n} w_{ij} y_j \qquad (1) \\ y_{\{e,f\}i} &= \max(0, u_{\{e,f\}i}) \\ \tau' \dot{v}_{\{e,f\}i} &= -v_{\{e,f\}i} + y_{\{e,f\}i} \end{aligned}$$

where suffix e, f, and i mean extensor muscle, flexor muscle, and the ith neuron, respectively. u_i is the inner state of neuron; v_i is a variable representing the degree of the self-inhibition effect of the ith neuron; y_i is the output of the ith neuron; u_0 is an external input with a constant rate; $Feed_i$ is a feedback signal from the robot, that is, a joint angle, angular velocity and so on. u_{0i} is constant except for experiments of vision based adaptation described in Section 4.. As a result, a CPG outputs torque proportional to the inner state u_e, u_f to a DC motor of a joint:

$$N\_Tr = -p_e u_e + p_f u_f \qquad (2)$$

The positive or negative value of N_Tr corresponds to activity of flexor or extensor muscle, respectively.

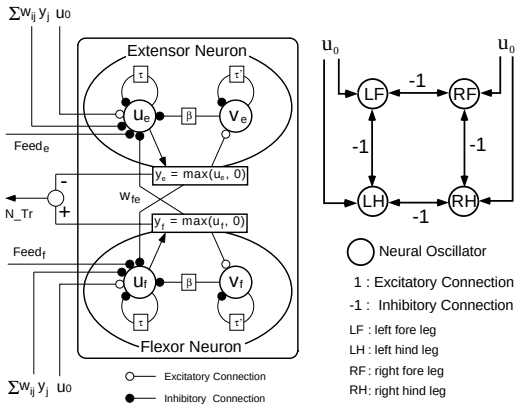

(a) Neural Oscillator (b) Neural Oscillator Network for Trot

Figure 2: Neural oscillator as a model of a CPG.

A stretch reflex in animals acts as feedback loop[13]. The neutral point of this feedback in upright position of a robot is $\theta = 0$, where $\theta =$ (joint angle) $+ \pi/2$ in Fig.1-(b). It is known in biology that there are two different types of stretch reflexes. One is a short term reflex called a "phasic stretch reflex" and another is a long term reflex called a "tonic stretch reflex." When we assume that a tonic stretch reflex occurs on the loop between CPG and muscles, the joint angle feedback to CPG used in Taga's simulation[1, 2] based on biological knowledge[14] corresponds to a tonic stretch reflex. We use such joint angle feedback to a CPG:Eq.(3) in all experiments of this study.

$$Feed_{e \cdot tsr} = k_{tsr}\theta, \quad Feed_{f \cdot tsr} = -k_{tsr}\theta \qquad (3)$$

We also assume that a phasic stretch reflex occurs on the loop between α motor neurons and muscles locally, and use this reflex in Section 2.3..

By connecting NO of a hip joint of each leg, the NOs are mutually entrained and oscillate in the same period and with a fixed phase difference. This mutual entrainment between the NOs of legs results in a gait. We used a trot gait, where the diagonal legs are paired and move together, and two legs supporting phase are repeated.

In all experiments of this study, only hip joints are controlled by a CPG and knee joints are PD-feedback controlled for simplicity. The desired angle of a knee joint in a supporting phase is 4 degrees and that in a swinging phase is calculated based on Eq.(4) by using output torque of a CPG:N_Tr at a hip joint of the same leg.

$$\text{desired angle} = 1.7 N\_Tr + 0.26 \qquad (4)$$

By the experiment using only CPGs and tonic stretch reflexes, where $Feed_e$=$Feed_{e\cdot tsr}$, $Feed_f$=$Feed_{f\cdot tsr}$, we confirmed that Patrush can walk stably on flat terrain. This control was almost same as the one proposed and used in simulation of biped walking by Taga[1, 2]. Patrush walked dynamically with approximately 25 cm stride, 0.8 sec. period and 0.6 m/sec. speed in this experiment.

2.3. Walking on irregular terrain using CPGs and Reflexes

It is well known in biology that adjustment of CPG and reflexes based on somatic sensation such as contact with floor and tension of muscle of supporting legs, and vestibular sensation are very important in adaptive walking[9, 13, 15]. Although it is also well known that activity of CPG is modified by sensory feedback[15], the exact mechanism of such modification in animals is not clear since the neural system of animals is too complicated. Therefore, we consider the following three types of models for adaptation based on sensory information, discuss about which model is better through results of experiments, and propose physical mechanism of relation between CPG and reflexes in view of robotics.

(a) a CPG only involving a tonic stretch reflex

(b) a CPG and reflexes independent of a CPG

(c) a CPG and reflexes via a CPG

By using model (a) (Fig.3-(a)), we realized dynamic walking on flat terrain as described in Section 2.2.. But Patrush failed in walking over an obstacle 3 cm in height and walking up a slope of more than 7 degrees by using this control model[5, 7].

In model (b), we consider reflexes independent of a CPG, and sum of CPG torque and reflexes torque is output to a motor (Fig.3-(b)). By using a phasic stretch reflex, a vestibulospinal reflex and a flexor reflex independent of a CPG, we realized walking up and down a slope of 12 degrees, and walking over an obstacle of 3 cm in height[5, 7]. But following problems were pointed out:

(1) The delay of joint motion from the phase of a CPG in walking up a slope resulted in slipping and stamping with no progress[7].

(2) Since CPGs could not extend the supporting phase corresponding to the extended swinging phase caused by a flexor reflex, it happened for both legs to be in the swinging phase at the same time and Patrush often fell down forward.

(3) Sensor based adjustments to solve such problems increased number of parameters and made control system complicated[7].

In model (c), reflexes torque is output as part of CPG torque by feedback of all sensory information to a CPG (Fig.3-(c)).

3. Reflexes via a CPG

In this section, we consider reflexes via a CPG in response to vestibular sensation, tendon force and contact with floor. Since these reflexes may be confused with such usual reflexes as a vestibulospinal reflex and so on, we call reflexes via a CPG as a vestibulospinal "response" and so on.

3.1. Vestibulospinal response

Since a tonic stretch reflex continues while a muscle is extended, it is appropriate to adjust activity of antigravity muscles for posture control by a tonic stretch reflex utilizing the body angle detected by vestibule. Therefore, the vestibulospinal response for posture control based on vestibular sensation is via a CPG and expressed by:

$$\begin{aligned} \theta_{vsr} &= (\text{joint angle}) + \pi/2 - (\text{body angle}) \\ Feed_{\{e,f\}\cdot tsr\cdot vsr} &= \pm k_{tsr}\theta_{vsr}. \end{aligned} \tag{5}$$

Since excitatory feedback signal to the extensor neuron of a CPG in walking up a slope makes the active period of the extensor neuron of a CPG become longer, difference between phases of a CPG and joint motion becomes small. In Fig.4, we can see that the vestibulospinal response via a CPG in walking up a slope made the active period of the extensor neuron of a CPG and the supporting phase of a leg be longer in comparison with those in walking on flat terrain. This means that autonomous adaptability of a CPG solved the problem (1) mentioned in Section 2.3..

As a result, Patrush succeeded in walking up and down a slope of 12 degrees by using a vestibulospinal response much more stably and smoothly without increasing number of parameters.

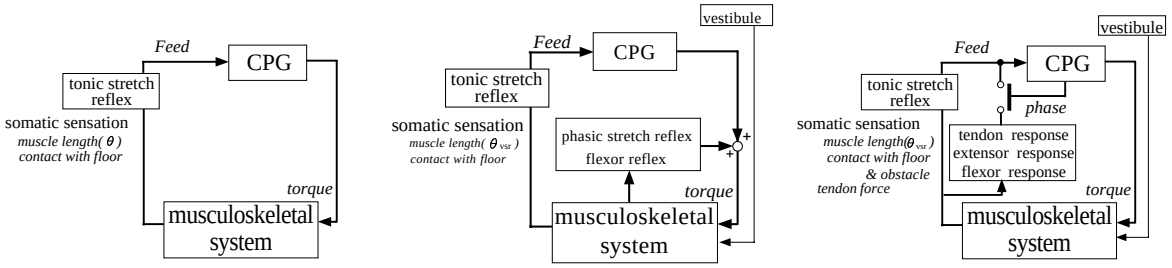

(a) involving tonic stretch reflex (b) reflexes independent of CPG (c) reflexes via CPG

Figure 3: Relation between CPG and reflexes in Taga's model:(a) and models proposed in this study:(b),(c)

3.2. Tendon response

Pearson[16] pointed out that extensor neuron of a CPG gets excitatory signal when the tendon organ detects the load to the ankle joint muscle in a supporting phase. We call this as a tendon response, which acts to complement thrusting force against reaction force from floor in a supporting phase.

We use amount of decrease of $\dot{\theta}$ of a hip joint of a supporting leg for the tendon response instead of the load to the ankle joint muscle. The tendon response via a CPG on a supporting leg is generated by the excitatory feedback signal:$Feed_{e\cdot tr}$ to the extensor neuron of a CPG.

$$Feed_{e\cdot tr} = \begin{cases} k_{tr}(\dot{\theta}+1) & (\dot{\theta} \geq -1) \\ 0 & (\dot{\theta} < -1) \end{cases} \quad (6)$$

$$\begin{aligned} Feed_e &= Feed_{e\cdot tsr\cdot vsr} + Feed_{e\cdot tr} \\ Feed_f &= Feed_{f\cdot tsr\cdot vsr} \end{aligned} \quad (7)$$

By using sensory feedback to a CPG expressed by Eq.(7), Patrush succeeded in walking up and down a slope of 12 degrees (Fig.4). In Fig.4, output torque of the tendon response via a CPG appears as bumps on N_Tr while the extensor neuron of a CPG is active ($N\_Tr < 0$) at 1.9 and 2.3 sec., for example. Although Patrush took 4 sec. to walk up a slope in the experiment without the tendon response in Section 3.1., it took only 2.2 sec. in Fig.4. This means that faster walking up a slope was realized by using the tendon response.

3.3. Extensor and Flexor responses

It is known in biology that the response to stimulus on the paw dorsum in walking of a cat depends on which of extensor or flexor muscles are active:

[a] When extensor muscles are active, a leg is strongly extended in order to avoid falling down.

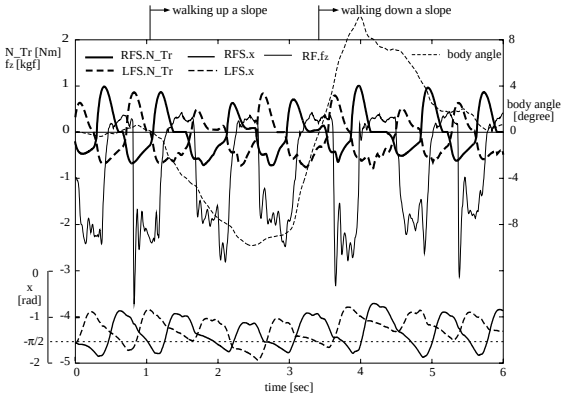

Figure 4: Walking up and down a slope of 12 degrees using feedback:Eq.(7). $N\_Tr < 0$ means the active period of the extensor neuron of a CPG. $f_z < 0$ means the supporting phase of a leg.

[b] When flexor muscles are active, a leg is flexed in order to escape from the stimulus.

We call [a] and [b] as an extensor response and a flexor response respectively, and assume that phase signal from a CPG switches such responses[15].

For the extensor response, we employ the following excitatory feedback signal:$Feed_{e\cdot er}$ to the extensor neuron of a CPG, when reaction force larger than threshold ($f_x > 1.5$[Kgf]) is detected by force sensor while the extensor neuron is active ($N\_Tr < 0$).

$$Feed_{e\cdot er} = \begin{cases} k_{er}\theta_{vsr} & (\theta_{vsr} \geq 0) \\ 0 & (\theta_{vsr} < 0) \end{cases} \quad (8)$$

For the flexor response, we employ the following instant excitatory feedback signal:$Feed_{f\cdot fr}$ to the flexor neuron of a CPG, when reaction force larger than threshold ($f_x > 1.5$[Kgf]) is detected by force sensor while the flexor neuron is active ($N\_Tr > 0$).

$$Feed_{f\cdot fr} = (k_{fr}/0.12)(0.12 - t) \quad (9)$$

where $t = 0$ sec. means the instance when a leg stumbles, and $Feed_{f \cdot fr}$ is active for t=0∼0.2 sec.

Finally, feedback signal to a CPG to avoid falling down after stumbling is expressed by:

$$\begin{aligned} Feed_e &= Feed_{e \cdot tsr \cdot vsr} + Feed_{e \cdot tr} + Feed_{e \cdot er} \\ Feed_f &= Feed_{f \cdot tsr \cdot vsr} + Feed_{f \cdot fr} \end{aligned} \tag{10}$$

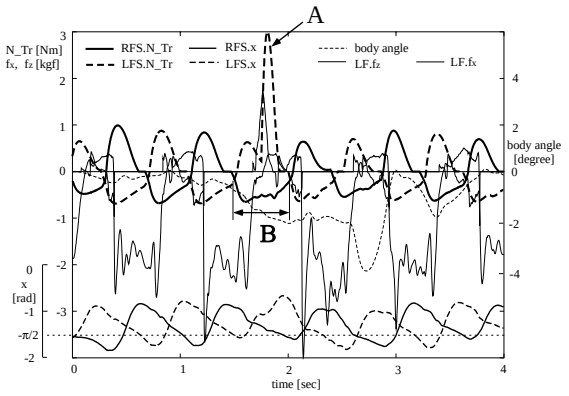

Figure 5: Avoidance of falling down after stumble on an obstacle by using a flexor response.

In Fig.5, the left foreleg stumbled on an obstacle at 1.7 sec., and neuron torque of the left foreleg (LFS.N_Tr) was instantly increased by the flexor response (Fig.5-A). This flexor response made the period of the swinging phase of the left foreleg much longer (1.4∼2.0 sec.). Autonomous adaptability of a CPG made the period of the supporting phase of the right foreleg be longer correspondingly (Fig.5-B) in order to prevent Patrush from falling down by solving the problem (2) mentioned in Section 2.3..

3.4. Adaptation to terrain of medium degree of irregularity

We tried to realize dynamic walking on terrain of medium degree of irregularity, where a slope, an obstacle and undulations continue in series (Fig.6). By realization of such adaptive walking using control method expressed by Eq.(1) and (10) (Fig.7) with fixed values of all parameters, we was able to show that the control method proposed in this section (Fig.7) has ability for adaptation to unknown irregular terrain. The photos of walking on such irregular terrain are shown in Fig.8 and Fig.9.

The experimental results of walking on irregular terrain (Fig.6-(a)) is shown in Fig.10. In Fig.10,

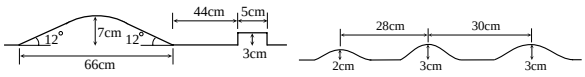

Figure 6: Terrain of medium degree of irregularity

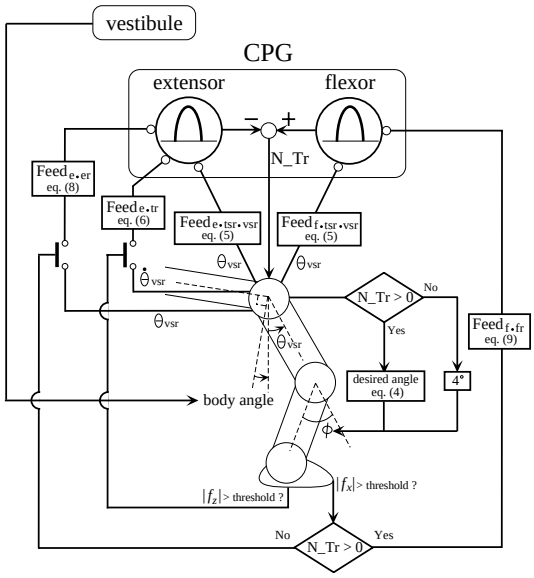

Figure 7: Diagram of actual control of a leg consisting of a CPG and reflexes via a CPG.

Patrush walked up a slope for 1∼3.7[sec] with the tendon response. For 2.8∼3.2[sec], the right hindleg had stumbled on the slope 3 times in a swinghing phase, and CPGs much extended their swinging or supporting phases autonomously influenced by a flexor response. In addition, Patrush walked down a slope (3.7∼4.9) and walked over an obstacle by another flexor response at 5.5[sec]. We can see that RHS.N_Tr in the next supporting phase after those flexor responses was also increased autonomously by CPG and reflexes in order to complement necessary torque after the flexor response.

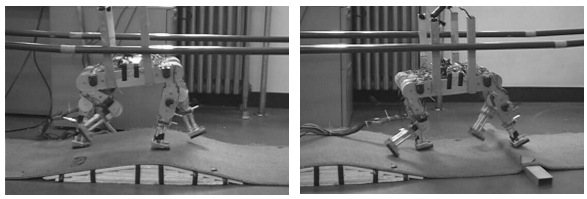

Figure 8: Photos of walking up and down a slope:(a) and walking over an obstacle:(b).

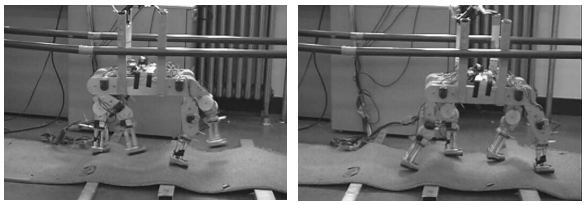

(a) (b)

Figure 9: Photos of walking on terrain undulations.

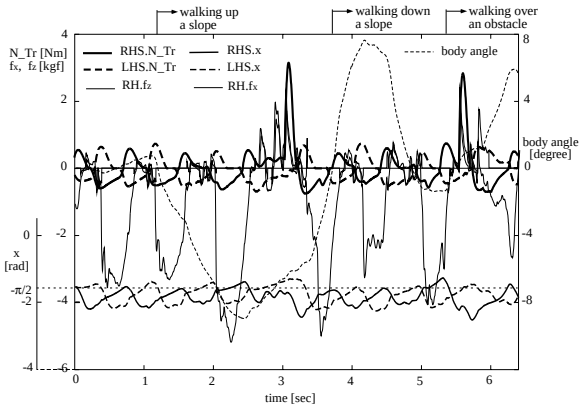

Figure 10: Walking up and down a slope of 12 degrees and over an obstacle 3 cm in height using feedback:Eq.(10).

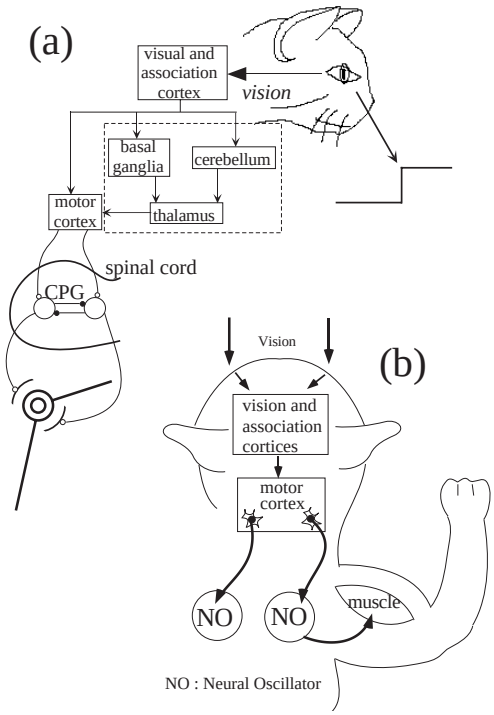

Figure 11: The leg control mechanism of an animal for adaptive walking. (a):a model proposed by Drew[17] and (b):a simplified model used in experiments.

4. Adaptive control based on vision

Drew[17] proposed a model about the adjustment of the directive signal to a CPG based on vision(Fig.11-(a)). When we use neural oscillators as a model of a CPG, the directive signal to a CPG corresponds with external input to neural oscillators: u_0 (Fig.2-(a),(b)). We use a simplified model (Fig.11-(b)) where u_0 for each neural oscillator is determined based on vision and there is neither automatic learning nor adaptation about motion generation at the basal ganglia and cerebellum level. In experiments in this section, we don't use other reflex mechanisms described in Section 3. in order to examine the ability of CPG alone.

The robot succeeded in walking up a step 3 cm in height (Fig.12-(a)) by increasing u_0 based on the height of and distance to the step measured by using stereo vision before start walking.

When a robot had found a marked obstacle on the way, a robot tracked the obstacle while walking forward and succeeded in walking over the obstacle without collision by increasing u_0 of each neural oscillator of a hip joint one by one ((Fig.12-(b)), Fig.13). In Fig.13, we can see that u_0 of each CPG was 5 times increased in swinging phase and 2 times increased in supporting phase in the order of LF, RF, RH and LH, and that CPG torque of a hip joint of each leg became large in the same order.

About adjustment based on vision in walking generated by CPG, Taga[18] and Lewis[19] employed reflex independent of CPG. Since we confirmed that adjustment via CPG is much better than adjustment independent of CPG in Section 3., we employed modification of the directive signal to a CPG referring to Drew's model. But it is still open question that which adjustment is better in visual adaptation of a walking robot. In addition, learning[19] is a key issue in visuomotor adaptation. But we have not yet employed it.

5. Discussion

5.1. What is walking using a CPG?

In order to make the role of CPG be clear, let us consider passive dynamic walking: PDW where a walking machine with no actuator can walk down

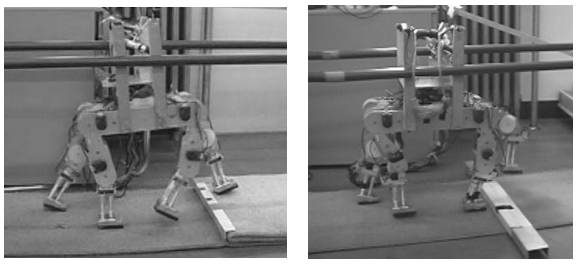

(a) (b)

Figure 12: Photos of the quadruped robot walking up a step:(a) and over an obstacle:(b) by using vision.

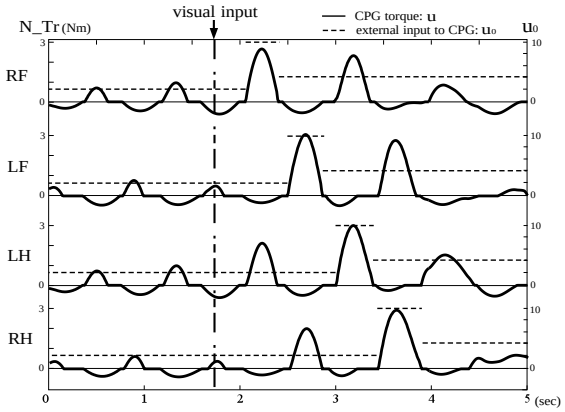

Figure 13: Result of the experiment involving walking over an obstacle 3 cm in height by using adjustment of external input to CPG based on vision.

a slope dynamically[20]. There is similarity between PDW and walking using a CPG in the sense that dynamic walking is autonomously generated on a link mechanism by external force (gravity) or internal torque (CPG torque) as a result of interaction with environment. The result of comparison of additional gravity torque in calculation of PDW with output torque of a CPG in experiment of walking on flat terrain is shown in Fig.14.

In Fig.14, gravity torque on a leg in PDW is reversed at switching of supporting/swinging phases. This shows that walking is exactly passive. On the other hand, switching of torque of extensor/flexor muscles occurs approx. 60 degrees in phase before switching of supporting/swinging phases in walking using a CPG. This switching of torque of extensor/flexor muscles in the latter period of supporting/swinging phases is actually observed in animals' walking[21]. Through this comparison, we can say that active walking using internal torque is nothing but to switch supporting/swinging phases actively by switching of extensor/flexor torque.

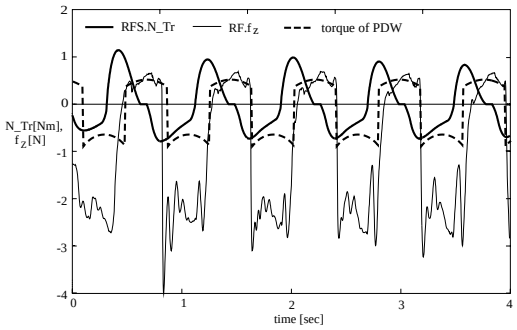

Figure 14: Comparison of CPG torque and additional gravity torque in passive dynamic walking.

This is the reason why active walking using a CPG is much more stable than PDW under errors of initial conditions and disturbances.

Moreover, in dynamic walking on irregular terrain, we can say that the adjustment of phases of CPGs and active switching of supporting/swinging phases of legs are important corresponding to delay of motion caused on a slope and bumps, and extension of phases caused by reflexes CPGs are surely superior in this function because of abilities of mutual entrainment and autonomous adaptation. This is the reason why autonomous adaptive dynamic walking on irregular terrain was realized so simply in this study. As a result, CPGs are much more useful as a lower controller than combination of feedforward torque calculation and feedback control in the conventional robotics method[22].

5.2. CPG and Reflexes

Reflexes independent of CPG had several problems as described in Section 2.3. In the case of reflexes via CPG, it was shown by experiments in Section 3. that the period of phases of CPGs can be appropriately adjusted autonomously by ability of CPG for entrainment while reflexes via CPG output necessary torque for instant adaptation based on sensory information. In addition, the following results obtained in experiments using control system expressed by Eq.(1), (10):

- several reflexes via CPG coincide with each other without improper conflicts,
- adaptive walking on terrain of medium degree of irregularity was realized with fixed value of all parameters,

- strengthening sensory feedback to CPG promotes the autonomous adaptability of walking,

showed that the simple control method using neural system model (Fig.3-(c), Fig.7) has ability for adaptation to unknown irregular terrain.

6. Conclusion

By referring to the neural system of animals, we integrated several reflexes, such as a stretch reflex, a vestibulospinal reflex, and extensor/flexor reflexes, into a CPG. In the case of reflexes via a CPG, it was shown by experiments that the active periods of flexor and extensor neurons of CPGs could be appropriately adjusted autonomously by ability of CPGs for entrainment, while reflexes via a CPG output necessary torque for instant adaptation based on sensory information. The success in walking on terrain of medium degree of irregularity with fixed parameters of CPG and reflexes showed that the biologically inspired control method proposed in this study has an ability for autonomous adaptation to unknown irregular terrain. It was also shown that principles of dynamic walking as a physical phenomenon are identical in animals and robots in spite of difference of actuators and sensors. 3D dynamic walking on 3D irregular terrain is one of the next challenges this study aims for.

Acknowledgments

This study has been supported by a grant from the TEPCO Research Foundation.

References

[1] Taga,G., et al., 1991, "Self-organized control of bipedal locomotion by neural oscillators," Biological Cybernetics, 65, pp.147-159.

[2] Taga,G., 1995, "A model of the neuro-musculoskeletal system for human locomotion II. - Realtime adaptability under various constraints," Biological Cybernetics, 73, pp.113-121.

[3] Ijspeert,A.J., et al., 1998, "From lampreys to salamanders:evolving neural controllers for swimming and walking," Proc. of SAB98, pp.390-399.

[4] Miyakoshi,S., et al., 1998, "Three Dimensional Bipedal Stepping Motion using Neural Oscillators - Towards Humanoid Motion in the Real World," Proc. of IROS98, pp.84-89.

[5] Kimura,H., et al., 1999, "Realization of Dynamic Walking and Running of the Quadruped Using Neural Oscillator," Autonomous Robots, 7-3, pp. 247-258.

[6] Ilg,W., et al., 1999, "Adaptive periodic movement control for the four legged walking machine BISAM," Proc. of ICRA99, pp.2354-2359.

[7] Kimura,H., et al., 2000, "Biologically Inspired Adaptive Dynamic Walking of the Quadruped on Irregular Terrain," Robotics Research 9, J.M.Hollerbach and D.E.Koditschek (Eds), Springer London, pp.329-336.

[8] Shik,M.L. and Orlovsky,G.N., 1976, "Neurophysiology of Locomotor Automatism," Physiol. Review, 56, pp.465-501.

[9] Grillner,S., 1981, " Control of locomotion in bipeds, tetrapods and fish," In Handbook of Physiology II, American Physiol. Society, pp.1179-1236.

[10] Collins,J.J. and Stewart,I.N., 1993, "Coupled nonlinear oscillators and the symmetries of animal gaits," J. of Nonlinear Science, 3, pp.349-392.

[11] Matsuoka,K., 1987, "Mechanisms of frequency and pattern control in the neural rhythm generators," Biological Cybernetics, 56, pp.345-353.

[12] Williamson,M.M., 1999, "Designing rhythmic motions using neural oscillators," Proc. of IROS99, pp.494-500.

[13] Kandel,E.R., et al. (eds.), 1991, Principles of Neural Science, Appleton & Lange, Norwalk, CT..

[14] Andersson,O. and Grillner,S., 1983, "Peripheral control of the cat's step cycle. II Entrainment of the central pattern generators for locomotion by sinusoidal hip movements during fictive locomotion," Acta. Physiol. Scand, 118, pp.229-239.

[15] Cohen,A.H. and Boothe,D.L., 1999, "Sensorimotor interactions during locomotion: principles derived from biological systems," Autonomous Robots, 7-3, pp.239-245.

[16] Pearson,K., et al., 1994, "Corrective responses to loss of ground support during walking II, comparison of intact and chronic spinal cats," J. of Neurophys., 71, pp.611-622.

[17] Drew,T., et al., Role of the motor cortex in the control of visually triggered gait modifications, Can. J. Physiol. Pharmacol., 74, pp.426-442.

[18] Taga,G., 1998, A model of the neuro-musculoskeletal system for anticipatory adjustment of human locomotion during obstacle avoidance, Biological Cybernetics, 78, pp.9-17.

[19] Lewis,M.A. and Simo,L.S., 2000, A Model of Visually Triggered Gait Adaptation, Proc. of AMAM.

[20] McGeer,T., 1990, "Passive Dynamic Walking," Int. J. of Robotics Research, 9-2, pp.62-82.

[21] Pearson,K., 1976, "The Control of Walking," Scientific American, 234-6, pp.72-87.

[22] Kimura,H., et al., 1990, "Dynamics in the dynamic walk of a quadruped robot," Advanced Robotics, 4-3, pp.283-301.

Proceedings of the International Symposium on
Adaptive Motion of Animals and Machines,
Montreal, Aug.8-12, 2000

Adaptive posture control of a four-legged walking machine using some principles of mammalian locomotion

W.Ilg[1], **J. Albiez**[1], **H. Witte**[2], **R. Dillmann**[1]

[1] Forschungszentrum Informatik Karlsruhe,Interactive Diagnosis- and Servicesystems,
Haid–und–Neu–Str. 10–14,76131 Karlsruhe, Germany, ilg@fzi.de

[2] Friedrich Schiller University Jena, Institut für Spezielle Zoologie und Evolutionsbiologie, Erbertstr. 1, D-07743 Jena, Germany

Abstract

This paper presents an adaptive control scheme for the four legged walking machine BISAM. The task of the adaptive control is to learn sensor based reflexes for posture control. For this purpose, an incremental learning scheme is developed based on reinforcement learning. For the planned trajectory of the CoM the data taken from a goat are chosen as a basis, to investigate the transfer potential of biological locomotion to machine motion at this control level.

1. Introduction

Online learning methods for legged robots are investigated to enlarge the flexibility and the adaptivity to different environments, but their use on real walking machines is very complicated due to the high complexity of such robots and only in a few approaches realized. In [8] the leg coordination of a simple six legged walking machine is learned, in [5] the coordination of different behavior controllers for a four legged walking machine is learned. [1] and [7] show two approaches for online learning of biped robots are presented in which the control architecture consists of periodic central pattern generators and peripheral controllers for behaviors like posture control. All these approaches show that an appropriate representation of the control problem is crucial for an efficient and succesful learning process a point that also account the security requirements of real robots.

2. The Walking Machine BISAM

BISAM (Biologically InSpired wAlking Machine) consists of one main body, four equal legs and a head (figure 1). The main body consists of four segments, which are connected by five rotary joints. With the five active degrees of freedom of the body, namely rotation of shoulder and hip, the body supports the stability and higher flexibility in uneven terrain. Each leg consists of four segments, that are connected by three parallel rotary joints and attached to the body by a fourth. The joints are all driven by DC motors and ball-screw gears. The height of the robot is 70 cm, its weight is about 23 kg. A more detailed description of the mechanical construction and the hardware architecture can be found in [2].

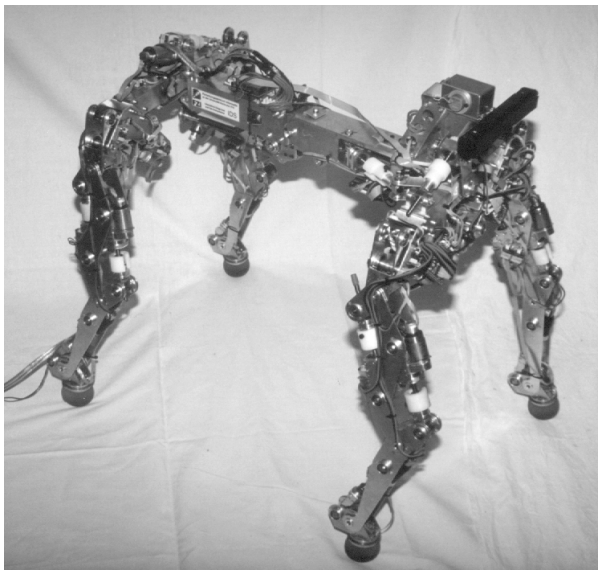

Figure 1: Photograph of the quadrupedal walking machine BISAM in mammal-like position. Due to the five active degrees of freedom in the trunk and the ability to rotate the shoulder and pelvis, the machine realizes key elements of mammal-like locomotion.

3. Control Approach

Based on a classical robotic approach, to determine the joint trajectories by inverse kinematics and pregiven body motion and foot trajectories a statically stable walk ($\beta = 0.8$) and a dynamically stable trot ($\beta = 0.6$) is realized. Special charateristic of the motion is the

hip and shoulder movement, which realize an increasement of the step length.

By analysing this movements following problems have been identified:

- Because of the small feet of BISAM the ZMP-Criterion [9] is not fully adequate for the optimization of movements.
- The movements of BISAM are highly dependent of the load on the machine (camera head, internal PC) and the initial position of CoM.
- In dependency of the machine configuration all working points have to be tuned manually

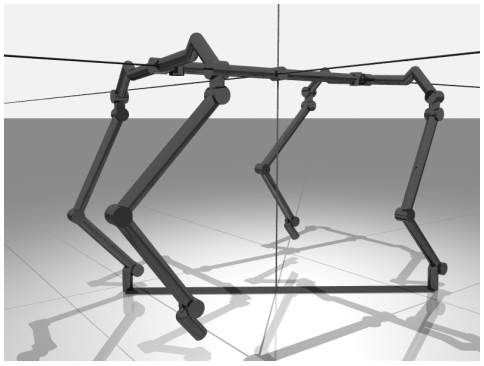

Figure 2: Small Support Area for dynamically stable movements of BISAM.

During animal-like motions with extended excursions not only of the limbs, but with also intense movements of the spine, no simple stability-criterion is definable taking into account the influences of load distribution and initial posture effects. The virtual-leg-mode does not yield closed solutions. A dynamic forward model of the machine at present lacks sufficient informations on the non linear-effects describing the behavior of drive and sensors.

Caused by the described problems we choose the strategy to determine a planned trajectory for the CoM and to learn adaptive reflexes which realize the corrections of the guidance of CoM based on the signals of the foot sensors.

For the modelling of the planned body trajectory, we do not use an analytical optimization criterion but we investigate the use of pregiven CoM-trajectories, which are observed from mammals.

4. Analysis of CoG Trajectory

The CoG Trajectory is analysed in to components on the base of the foot sensors according equations 1, 2 and figure 3.

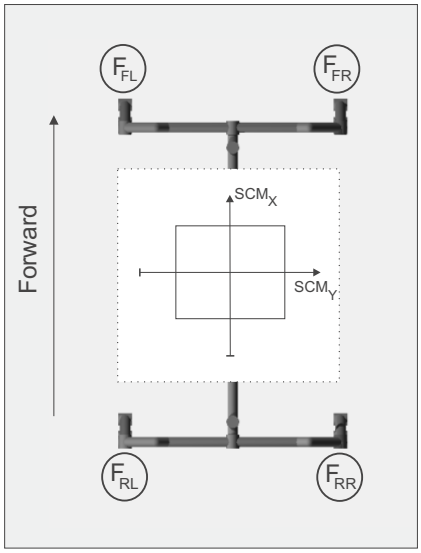

Figure 3: Illustration of the parameters SCM_X and SCM_Y for the sensor based measurement of the COG based on the foot sensors.

$$SCM_X = \frac{F_{FL} + F_{FR} - (F_{RL} + F_{RR})}{\sum_{F_{xy} \in \mathcal{F}} F_{xy}} \quad (1)$$

$$SCM_Y = \frac{F_{FR} + F_{RR} - (F_{FL} + F_{RL})}{\sum_{F_{xy} \in \mathcal{F}} F_{xy}} \quad (2)$$

A typical CoG-Trajectory for a trot with β=0.6 is shown in figure 4.

The description and adaption of the gait on the hand of the CoG-Trajectory have two main advantages:

- The description and of the gait on the hand of the CoG-Trajectory is apprpiate, because the movement experiments show that a right position of the CoG is an fundamental requirement for executing accurate movements
- This representation allows small input and output dimension for the neural networks presented in the next section

5. Learning of reflexes for posture control

For the online learning of the sensor based reflexes for posture control a reinforcement learning method [6] based on an actor/critic approach similar to the SRV-Algorithm [4] is used. This algorithm consists of a critic element which renders an internal evaluation of

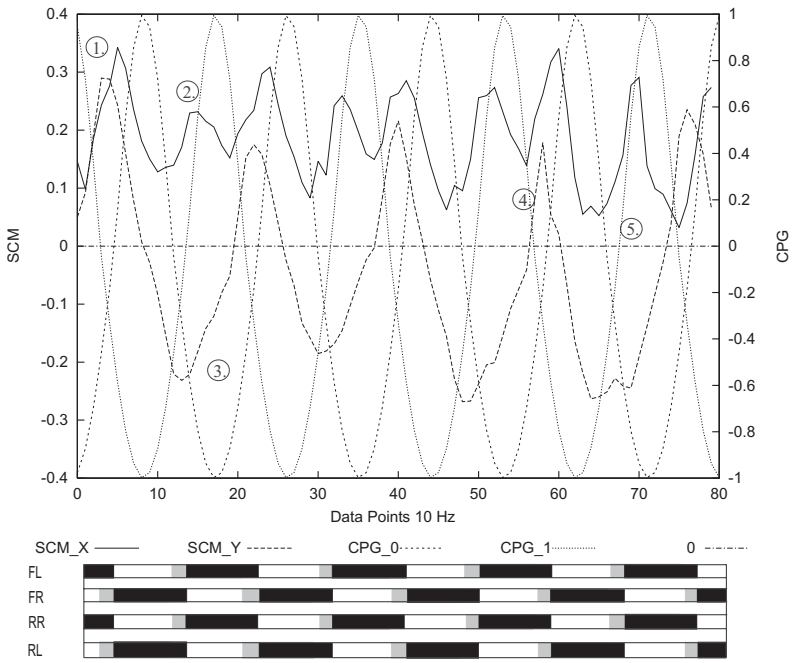

Figure 4: Illustration of a CoG-Trajectory gained by executing a trot with β=0.6. The CoG-Trajectory with the components SCM_X and SCM_Y in dependence of the gait phases can be seen.

the actual state and action elements which determines the next control values. In each control step an adaptation of both components by the TD(λ)-algorithm takes place.

The state space representation used by the learning method is incrementally constructed with self-organizing RBF-networks. The RBF-net builds localized receptive fields which divide the input space into regions of limited size thus allowing localized learning of a function within the boundaries of such a region. This property makes RBFs a suitable tool for online function approximation. In [6] a method is described by which the topology of the RBF network can be constructed according to the learning task.

A critical aspect for online learning processes is the problem modelling with the state and action space. We choose the the level of posture control to realize an adaptive component,

Based on this learning method a learning architecture for incremental learning of the following posture control aspects is developed (Figure 5).

- search for appropriate initial positions
- defined translations of CoM
- adaptive posture reflexes

6. Outlook

Our future work is analyse, in which way the CoG-Trajectories of BISAM can be compared with trajectories of small and medium-sized mammals. Another interesting question is, to which extend rules can derived from the analyses of the mammals for the locomotion of BISAM.

The biological paragon is derived from a huge kinematical and dynamic data base taken on 14 species of small and medium-sized mammals [3]. Techniques applied to determine kinematics were cineradiography (150 frames/sec), high-speed-video (up to 1.000 frames/sec) and marker-based motion analysis (up to 1.000 frames/sec). Ground-reaction forces GRF were taken using Kistler force-plates. The trajectory of CoM in several gaits was derived by two methods:

- "'balancing"' of a multi-segmental model fitted into the outlines of the animal. The triangular finite elements were weighted by mass data taken from dissected cadavers or CT-, MRI- or surface-light laser scans.
- Integration of GRF.

After matching of these data representative points for CoM could be derived. Since the deformations of the body stem are the less the larger the animal is, as a paragon for the control of BISAM the trajectories of

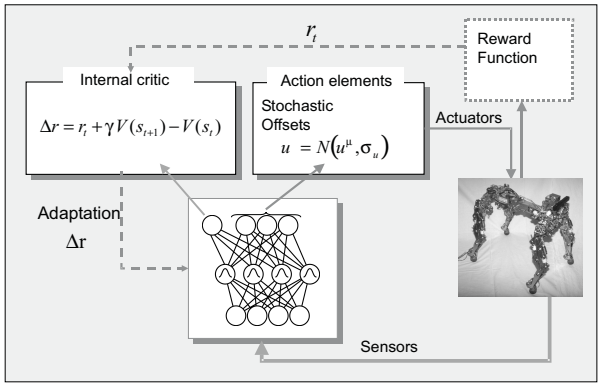

Figure 5: The concept of the adaptive component. The network generates the internal evaluation and prototypical actions. For exploration purposes, stochastic offsets are added to these actions. The stochastic offsets are generated using a normal distribution. The variance of this distribution is determined by the current performance of the net. The executed action sequence caused an external reward. The adaption of the internal evaluation and the action units are based on the successive external and internal evaluations.

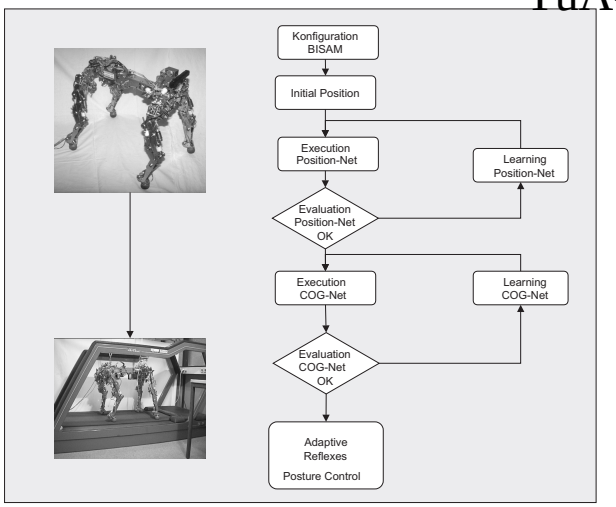

Figure 6: Concept of the incremental learning process for the posture control of BISAM. Based on networks which learn to optimize the initial position and the displacement of the CoM, adaptive reflexes are learned, which do sensor based corrections of the CoM.

CoM of two sub-species of goats were chosen. The kinematical data provided contained informations on the motions of the CoM and the hoofs in walk, trot and bound.

7. Conclusion

The aim of this work is to investigate, to which extend biological data on trajectories of the CoM from mammals can be used as basis for a four-legged walking machine. To adapt this planned motion to different circumstances, posture control reflexes are learned with an online learning method based on reinforcement learning.

Acknowledgments

This research is funded by the Deutsche Forschungsgemeinschaft (DFG), grants DI-10-1 and FI-410-4-1.

References

[1] H. Benbrahim and J. A. Franklin. Biped dynamic walking using reinforcement learning. *Robotics and Autonomous Systems*, 22(3):283–302, december 1997. Special Issue: Robot Learning - The New Wave.

[2] K. Berns, W. Ilg, M. Deck, J. Albiez, and R. Dillmann. Mechanical construction and computer architecture of the four-legged walking machine BISAM. *IEEE Transactions on Mechatronics*, 4(1):1–7, march 1999.

[3] M. S. Fischer and H. Witte. The Functional Morphology of the Three-Segmented Limb of Mammals and its Specialities in Small and Medium-Sized Mammals. In *Proccedings of the European Mechanics Colloquium : Biology and Technology of Walking . Euromech 375*, pages 10–17, 1998.

[4] V. Gullapalli. Learning control under extreme uncertainty. In *Advances in Neural Information Processing Systems 5*, pages 327–343. Morgan Kaufmann Publishers, San Mateo, California, 1992.

[5] M. Huber and R. A. Grupen. Learning to coordinate controllers. In *Proceedings of the 15th International Joint Conference on Artificial Intelligence*, 1997.

[6] W. Ilg, Th. Muehlfriedel, and K.Berns. A Hybrid Learning Architecture based on Neural Networks for Adaptive Control of a Walking Machine. In *IEEE International Conference on Robotics and Automation (ICRA'97)*, Albuquerque, 1997.

[7] A. Kun and W. T. Miller. Adaptive dynamic balance of a biped robot using neural networks. In *Proceedings of the IEEE International Conference on Robotics and Automation*, 1996.

[8] P. Maes and R. Brooks. Learning to coordinate behaviours. In *Proceedings of the 8th AAAI Conference*, pages 796–802. Morgan Kaufmann Publishers, San Mateo, California, 1990.

[9] M. Vukobratovic, B. Borovac, D. Surla, and D. Stokic. *Biped Locomotion*. Springer–Verlag, Heidelberg, Berlin, New York, 1990.

Proceedings of the International Symposium on
Adaptive Motion of Animals and Machines,
Montreal, Aug.8-12, 2000

Stabilization of Periodic Motions
– from Juggling to Bipedal Walking–

Seiichi MIYAKOSHI[1], **Gentaro TAGA**[2] **and Yasuo KUNIYOSHI**[3]

[1]Electrotechnical Laboratory, Tsukuba, Ibaraki 305-8568, smiyakos@etl.go.jp

[2]University of Tokyo and PRESTO JST, Komaba, Tokyo 153-8902, taga@complex.c.u-tokyo.ac.jp

[3]Electrotechnical Laboratory, Tsukuba, Ibaraki 305-8568, kuniyosh@etl.go.jp

Abstract

This paper presents some examples of stabilization of periodic motions. First, the juggling motion controlled by a duplicated simple controller and neural oscillators is discussed. Next, the bipedal stepping motion of the human like lower body and trunk model is discussed. In this model, the stepping motion was accomplished with neural oscillator and simple posture controllers. At the last part, biped walking of a simple compass like model is mentioned with relation to juggling.

1. Introduction

Many researches have been conducted on the Stabilization of periodic motions.

The most typical of such motion is of Walking. Dynamic periodic stepping motion of stilts type biped model mainly controlled in the frontal plane was taken up and experienced[1]. Stabilizing biped system using limit cycle stability of non-linear van der Pol's equation appeared almost same time[2]. On the other hand, passive(neither actuated nor controlled) walker machine was demonstrated and it accomplished bipedal walking only by using human body physical dynamics [3]. Hopping type walking(running?) machine from mono-pod to quardruped are produced and demonstrated with high gymnastic potentiality[4]. Biologically inspired neural oscillator control is proposed and human like biped walking simulation was shown [5].

The other typical example of dynamic(can't stop) periodic motion is Juggling. There has been precedent research(ping-pong robot) which was not classified strictly as periodic control but as rapid motion control[6]. For juggling, 'mirror algorithm' was proposed and spatial two balls by one hand juggling was accomplished[7]. On the contrary, open loop stable juggling strategies were proposed and demonstrated[8].

The characteristics of these systems can be described as follows:

- The transition of the states is mainly Ballistic.
- The structure of the system is time-varying.
- The control input can only affect the states transition of the system for a restricted duration.

Conventional control methods are in many cases neither effective nor natural for these type of systems, but sometimes the characteristics of these systems (from conventional point of view) can be fitted with some special heuristic control law and can accomplish tasks. However, heuristic control laws for such systems are difficult to derive.

2. Juggling

We constructed a robot juggling(padding) system for the research of dynamical periodic stability [9]. That was mostly inspired by Schaal's open loop juggling machine[8] and the Taga's biped walker[5]. The control of motion was purely performed by neural oscillators.

A brief description of the neural oscillator is given in Section 2.1. The design method for our controller is presented in Section 2.2. An example using this method is presented in Section 2.3. The result of this system is presented in Section 2.4.

2.1. Neural oscillator

One neural oscillator is represented two sets of mutual inhibited adaptive(fatigue) neural elements.

$$\begin{aligned}
\tau_1 \dot{x_1} &= -x_1 - \beta f(v_1) - \gamma f(x_2) + u_0 + u_{f1} \\
\tau_2 \dot{v_1} &= -v_1 + f(x_1) \\
\tau_1 \dot{x_2} &= -x_2 - \beta f(v_2) - \gamma f(x_1) + u_0 + u_{f2} \\
\tau_2 \dot{v_2} &= -v_2 + f(x_2) \\
f(x) &= \max(x, \theta)
\end{aligned}$$

where x_i are the state values, τ_i are the time constants, u_0 represents constant input, and u_{fi} are feedback inputs, γ is connection weight and β represents the adaptive strength. $f(x)$ is the threshold function.

The important characteristics of neural oscillators is their ability to entrain to an incoming frequency. The self-excited oscillation of the neural oscillator is synchronized to certain frequency range of oscillation input u_{fi}[5].

2.2. Designing of the controller

The derivation of the juggling controller can be divided into three basic steps:

1. Measuring the restitution coefficient of the paddle and calculating the stable nominal frequency and amplitude of the paddle.
2. Providing a simple feedback input (for the latter neural oscillator), that works only at the hitting instance.
3. Tuning neural oscillator to generate the nominal frequency and amplitude oscillation pattern.

Each step has the role as follows:

1. Finding the suitable trajectory of the state transition that will allow a stabilize the system by itself.
2. Keeping the states of the system to the neighbor of the stable trajectory, while the states can be controlled. Therefor, it works as a local (short term) controller.
3. Preserving the phase difference structure of the states of the system. It works as a global (long term) controller.

2.3. Example of the controller

The following is an example of neural controller system in one ball and one paddle padding case:

1. decide the object ball height and the hitting phase adequately(about $\pi/4$[rad] phase before the paddle top position) and derive the nominal sinusoidal wave trajectory of the paddle.
2. add local feedback for regulate the hitting speed and adjust the parameters of it adequately.
3. tune neural oscillator parameters to fit the nominal sinusoidal wave.

The equations of the local controller is as follows:

$$
\begin{aligned}
v_{bd} &= -\sqrt{2gh_d} \\
v_{ad} &= (1-e)/(1+e)\cdot|v_{bd}| \\
k_s &= k\cdot d/(d^4+\epsilon) \\
u_{f1} &= k_s(k_{ah}(v_{ad}-v_a)+k_{bh}(v_b-v_{bd})) \\
u_{f2} &= -u_{f1}
\end{aligned}
$$

where v_b,v_a,v_{bd} and v_{ad} represent the velocity and desired velocity of the ball and the arm, respectively. h_d is the desired top height of hit ball. e is the restitution coefficient of the arm paddle. d represents the distance between the ball and arm. k and ϵ are constants. k_s means feedback intention scaling coefficient. k_{ah} and k_{bh} are the feedback gain constants. g is the gravitational acceleration. u_{fi} is the feedback input to the neural oscillator.

2.4. Result

We show the one of the results.

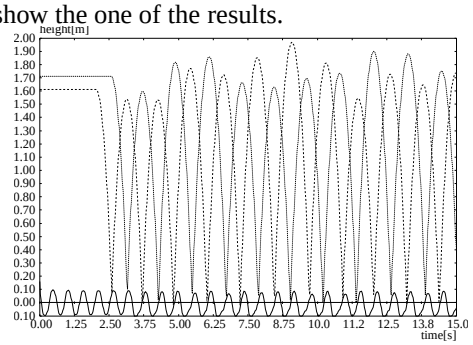

Figure 1: Juggling(padding) with perturbation

On this simulation, we gave perturbations as the fluctuation of the restitution coefficient of the paddle. The open loop wave generator cope with up to $\pm 0.18\%$ range uniform random perturbation. On the contrary, the combination of local and global controller could stabilize up to $\pm 6.15\%$ range. That means the controller expanded the stable basin about 34 times. This result does not mean to impair the value of open loop control method. It prepared the seed to growth. This result is an evidence that the combination of the open loop controller and the neural oscillator has good power.

M. Williamson also analyzed neural oscillator for juggling using the describing function method[10].

3. Stepping

We constructed three dimensional bipedal stepping simulation to prove that adequate interaction and coupling of physical system with neural dynamics produces various behaviors and yield robustness of motions[11].

The three dimensional simulation was an extension of the sagittal two dimensional biped simulation [12].

3.1. Model and controller

The robot model for the simulation is showed in Figure 2. It has a human like biped lower body, but the upper body is simplified to one link. The length and mass of each link correspond to that of humans[13]. The sole

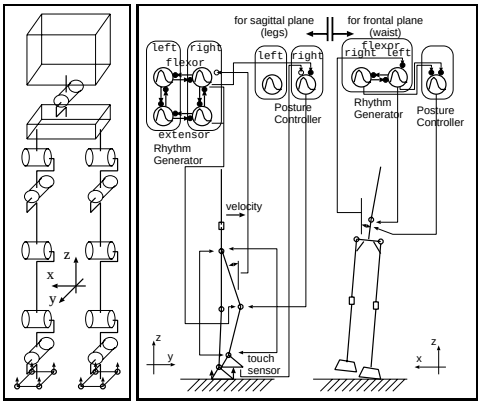

Figure 2: Distribution of degrees of freedom and structure of the system

is a set of 4 contact points.

The neural controller is mainly divided into two parts. One is the stand posture controller and the other is rhythmic motion generator and controller that is constructed by the neural oscillators. These two controllers work in parallel.

The posture controller is a simple PD(Proportional and Derivative) type regulator, and it works on the immediate upper link of each joint standing straight. The posture controller has some inhibit connection from the neural oscillators, that is to ease the fixation of the posture controller for leg bending, allowing rhythmic stepping motion controlled by the neural oscillator.

The rhythmic motion generator and controller is structured by three neural oscillators as shown in Figure 3 [11]. One oscillator corresponds to the waist swing in the frontal plane, and the other two are assigned to each leg for reciprocal bending. These neural oscillators are connected together to keep adequate phase differences of the stepping motion.

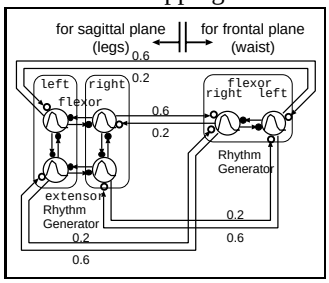

Figure 3: Connection between the leg and the waist oscillators

3.2. Result

The system states move on a stable periodic trajectory. For investigating the stable basin, we added various magnitudes of impact, like perturbation force at various times. Figure 4 shows the stable basin of the trunk in the frontal plane. For comparison, we also show the open loop unstable case for the same perturbations.

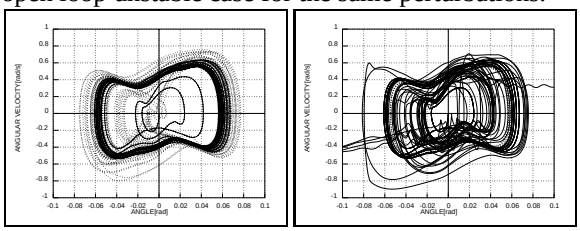

Figure 4: Phase plot of the stability domain(left) and without control(right).

Figure 5 (two rows of left to right sequence in a series)shows the stick figures of the biped facing in the right direction in the view point of the right front upper position. We added perturbation force on the trunk to the forward direction on the upper row third and fourth pictures. That perturbation caused consequent stronger stamp of the left foot and one step forward motion of right foot which was not programmed to do so. This shows the inherent physical stabilization dynamics of the human body.

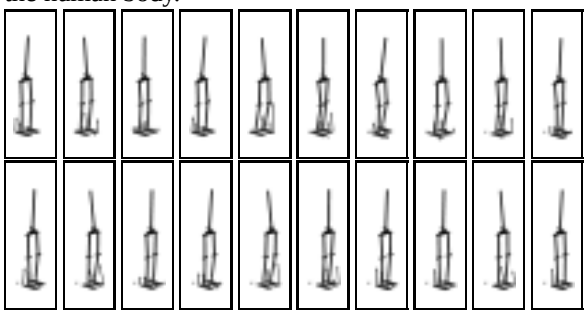

Figure 5: Snapshots of perturbed step motion.

The robot continued the stepping motion with slight motion pattern change, in another perturbation cases(on a slope, waving board and rough terrain).

Neural oscillator base locomotion control is also done by Hase[14] and Kimura[15]. Hase constructed a human whole body model including upper limb and muscle actuators and used genetic algorithms for parameter tuning. Kimura research is based on neural oscillator control of a real physical quadruped robot.

4. Walking

In our current work, we have based our research on the work of passive bipedal walking of [16].

The characteristics of walking and juggling have something in common as mentioned above. Those points pose the question: could open loop control like Schaal's juggler[8] be possible on the bipedal locomotion?

Our biped model is almost the same as the compass-

like point foot biped robot[17] except leg length change.

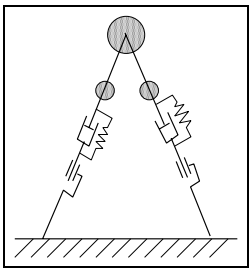

Figure 6: Model of a Compass-like Biped Robot

By setting the leg expansion and contraction sinusoidal frequency 3 times higher than the free motion frequency of the leg swing, this model can walk on a level plane, but the trajectory which we now have is unstable. To get the adequate parameter set and the motion pattern for stable walking is our future work.

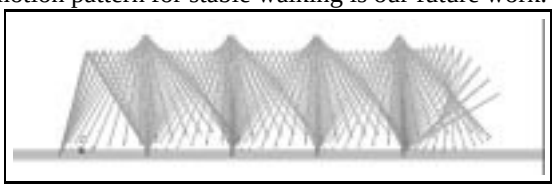

Figure 7: Stick Picture of Open-Loop Walking to the Right

5. Summary

We summarize the results of these case studies as follows.

- It is efficient to use self stabilize mechanism (if it was)of the system as a base.
- The entrainment characteristics of the neural oscillator expands the provided stable basin.
- Interaction between physical and neural system through entrainment generates various motions.

Acknowledgments

This research is financially supported by COE.

We are grateful to Gordon Cheng for helpful suggestions and observations and a critical reading of the manuscript.

References

[1] H. Miura and I. Shimoyama, 1983, "Control System of Stilts Type Biped Locomotion (in Japanese)," *Journal of Robotics Society of Japan*, Vol. 1, No. 3, pp. 16-21.

[2] R. Katoh and M. Mori, 1984, "Control Method of Biped Locomotion Giving Asymptotic Stability of Trajectory," *Automatica*, Vol. 20, No. 4, pp. 405-414.

[3] T. McGeer, 1990, "Passive Walking with Knees," *Proc. of International Conference on R.&A.*, Vol. 3, pp. 1640-1645.

[4] M. H. Raibert, 1986, "Legged Robots That Balance," MIT Press.

[5] G. Taga, Y. Yamaguchi, H. Shimizu, 1991, "Self-Organized Control of Bipedal Locomotion by Neural Oscillators in Unpredictable Environment," *Biological Cybernetics*, Vol. 65, pp. 147-159.

[6] R. L. Andersson, 1989, "Understanding and Applying a Robot Ping-pong Player's Expert Controller," *Proc. of International Conference on R.&A.*, pp. 1284-1289.

[7] A. A. Rizzi and D. E. Koditschek, 1993, "Further Progress in Robot Juggling: The Spatial Two-Juggle," *Proceedings of International Conference on R.&A.*, Vol. 3, pp. 919-937.

[8] S. Schaal et. al., 1993, "Open Loop Stable Control Strategies for Robot Juggling," *Proceedings of International Conference on R.&A.*, Vol. 3, pp. 913-918.

[9] S. Miyakoshi, M. Yamakita and K. Furuta, 1994, "Juggling Control Using Neural Oscillators," *International Conference on Intelligent Robot and Systems*, Vol. 2, pp. 1186-1193.

[10] M. M. Williamson, 1999, "Designing Rhythmic Motions using Neural Oscillators," *International Conference on Intelligent Robot and Systems*, Vol. 1, pp. 494-500.

[11] S. Miyakoshi, G. Taga and Y. Kuniyoshi et. al., 1998, "Three Dimensional Bipedal Stepping Motion using Neural Oscillators –Towards Humanoid Motion in the Real World–," *International Conference on Intelligent Robot and Systems*, Vol. 1, pp. 84-89.

[12] G. Taga, 1997, "A Model of Integration of Posture and Locomotion," *Proceedings of International Symposium on Computer Simulation in Biomechanics*.

[13] G. T. Yamaguchi and F. E. Zajac, 1990, "Restoring Unassisted Natural Gait to Paraplegics Via Functional Neuromuscular Stimulation," *IEEE Transactions on B. M. E.*, Vol. 37, No. 9, pp. 886-902.

[14] N. Yamazaki, K. Hase, N. Ogihara, et. al., 1996, "Biomechanical Analysis of the Development of Human Bipedal Walking by a Neuro-Musculo-Skeletal Model, *Folia Primatol*, Vol. 66, pp. 253-271.

[15] H. Kimura, S. Akiyama and K. Sakurama, 1999, "Realization of Dynamic Walking and Running of the Quardruped Using Neural Oscillator," *Autonomous Robots*, Vol. 7, No. 3, pp. 247-258.

[16] R. Q. van der Linde, 1999, "Passive Bipedal Walking with Phasic Muscle Contraction," *Biological cybernetics*, Vol. 81, pp. 227-237.

[17] B. Thuilot, A. Goswami and B. Espiau, 1997, "Bifurcation and Chaos in a Simple Passive Bipedal Gait," *International Conference on R.& A.*, pp. 792-798.

Proceedings of the International Symposium on
Adaptive Motion of Animals and Machines,
Montreal, Aug.8-12, 2000

Synchronized Robot Drumming with Neural Oscillators

Shin'ya Kotosaka[1] **Stefan Schaal**[1,2]
kotosaka@erato.atr.co.jp sschaal@usc.edu
[1] Kawato Dynamic Brain Project (ERATO/JST), 2-2 Hikari-dai, Seika-cho, Soraku-gun, Kyoto 619-02, Japan
[2]Computer Science and Neuroscience, University of Southern California, Los Angeles, CA 90089-2520

Abstract

Sensorimotor integration and coordination is an important issue in both biological and biomimetic robotic systems. In this paper, we investigate a ubiquitous case of sensorimotor coordination, the synchronization of rhythmic movement with an external rhythmic sound signal, a signal that, however, can change in frequency. The core of our techniques is a network of nonlinear oscillators that can rapidly synchronize with the external sound, and that can generate smooth movement plans for our robot system, a full-body humanoid robot. In order to allow for both frequency synchronisation and phase control for a large range of external frequencies, we develop an automated method of adapting the parameters of the oscillators. The applicability of our methods is exemplified in a drumming task. We demonstrate that our robot can achieve synchronization with an external drummer for a wide range of frequencies with minimal time delays when frequency shifts occur.

1. Introduction

The coordination of movement with external sensory signals is a mode of motor control found commonly in the daily behaviors of humans, e.g., as in dancing, synchronization of locomotion with other humans, playing music, marching in a parade, playing with balls, etc. In our work on humanoid robots, we are interested in equipping autonomous robots with similar sensorimotor skills. Traditional methods of trajectory planning and execution, however, are not always well suited for such sensorimotor coordination. Movement planning in robotics is mostly performed offline by using optimization approaches or other complex planning techniques. In a stochastic environment with quick dynamic changes, such planning approaches cannot adapt fast enough to changes in the environment, and often it would also be unclear what planning criteria to use for complex movement skills as described above ([1]).

In contrast, a framework for movement planning that facilitates sensorimotor coupling can be adopted from work on biological pattern generators ([2]). From a formal point of view, pattern generators are nonlinear dynamical system with attractor dynamics that encodes a robust accomplishing of a task goal. For limb control, pattern generators have been suggested as a method for movement planning: the pattern generator, a set of nonlinear differential equations, creates a desired trajectory that is subsequently converted into motor commands ([3-5]). Sensory information is directly coupled into the pattern generator and can modify the desired movement plan online.

So far, pattern generators for movement planning have just started be used in robotic motor control, mostly hampered by the complexity entailed in manipulating nonlinear dynamical systems. In this paper, we will explore pattern generators for synchronization with an external stimulus. We propose an approach to rhythmic arm movement control based on exploiting the attractor dynamics of nonlinear oscillators (Figure 1). In the next section, we will first introduce the idea of neural oscillators for synchronized drumming and, subsequently, develop our oscillator network for this task. We illustrate the feasibility of our methods with a humanoid robot at the end of the paper and compare its performance to data collected from human subjects.

2. Synchronized Drumming

A sketch of the drumming task that we will investigate is shown in Figure 1: a human drummer provides a rhythmic input pattern, and the robot is to follow this pattern as closely as possible, i.e., as synchronized as possible and without phase lag. In general, neural oscillators have excellent capabilities of synchronizing with external input signals (e.g., [6-8]), and depending on the choice of the oscillator equations, robust synchronization can be accomplished over a large range of frequencies ([9, 10]). However, synchronization breaks down when the input signal deviates too much from the oscillator's natural frequency. Additionally, the phase lag between the oscillator and the input increase the more the input deviates from the natural frequency. For synchronized drumming, such phase lag results in an inappropriate "echo-like" performance. As a last point, synchronization between the input and the oscillator needs to happen rather fast, i.e., long transients as observed in some studies (e.g., [7]) can not be tolerated in drumming. From these viewpoints, entrainment dynamics between the oscillator and the input are a core ingredient for robust performance, but additional tech-

niques will be required to ensure zero phase lag, minimal transients, and wide frequency range applicability. In this paper, we adopted a simple parameter tuning method in an oscillator model to achieve these goals.

Matsuoka ([9, 10]) proposed a mathematical model for mutual inhabitation networks that can generate oscillatory output, and whose parameterization is well suited for automatic parameter adaptation. Equations 1 and 2 provide the core equations of Matsuoka: ***x*** is the membrane potential of a neuron, ***s*** is a tonic input, ***Tr*** and ***Ta*** are the time constants, ***Wij*** is the connecting weight from the ***j***th neuron to the ***i***th neuron, ***b*** is a coefficient of an adaptation effect, and ***f*** is the inner state of the neuron. We add the term ***pulse*** to Equation 1 as a sensory input and define the output of the oscillator described by Equations 1 and 2 as Equation 3 note that only two neurons are need to generate oscillations.

$$T_r \frac{dx_i}{dt} + x_i = -\sum_{j=0, j\neq i}^{n-1} w_{ij} y_j - b_i f_i + s_i + pulse \qquad (1)$$

$$T_a \frac{df_i}{dt} + f_i = y_i, \; y_i = \begin{cases} x_i & (x_i \geq 0) \\ 0 & (x_i < 0) \end{cases} \qquad (2)$$

$$g = (Max(0, x_0) - Max(0, x_1)) \qquad (3)$$

The natural frequency of Matsuoka's oscillator is determined by the two time constants ***Tr*** and ***Ta***. According to Williamson ([8]), if these time constants are changed with a constant ratio, the oscillator produces a signal with a similar waveform, with almost the same amplitude, but different frequency. Thus we define ***Ta*** as ***Tr*** multiplied by a constant coefficient. In our method, the time constants ***Tr*** and ***Ta*** will be modified according to the period of the input signal to produce an output with minimal phase lag. We additionally adopt a technique to control not only the frequency but also the phase of the oscillator to cancel phase lags due to signal processing delays, as explained in the next section.

3. Oscillator Drumming

3.1 System configuration

Figure 2 shows the configuration of the proposed system for robot drumming using neural oscillators. There are multiple oscillators, and we divide the function of the oscillators into two roles, i.e., the production of a synchronized signal and the generation of a stable smooth desired trajectory. The complete system is composed of four parts. The first one is the

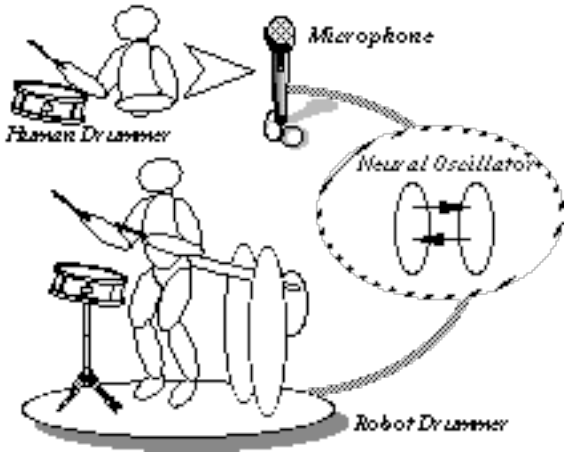

Figure 1: Robot drumming by neural oscillators

sound preprocessing system. The second is the wave generator for producing a wave that is synchronized with an external input signal. The third system is the phase shifter to compensate for delays from the sensor preprocessing and response times of the robot actuator. Together, the latter two systems produce a zero-phase-synchronized signal. The last part of the control system is the oscillator-based trajectory generator where each joint is equipped with a neural oscillator for generating desired trajectory plans.

3.2 Sound preprocessing system

In the sound preprocessing system, a sound signal, as a sensory input from the outside, is acquired by an electronic condenser microphone, and the envelope of the input signal is extracted by a simple integration circuit. Then, the sound signal is converted to digital by an A/D converter with 12 [bit] resolution and 480 [Hz] sampling. Butterworth filtering with a cut off frequency of 40 [Hz] applied to the input signal eliminates high-frequency noise.

3.3 Sync. signal generator

The main role of the sync. signal generator is to create a smooth oscillation that is synchronized with the sound signal and has zero-phase lag. The system is composed of three parts and the functions of these parts are: i) generation of a synchronized signal with a neural oscillator, ii) extraction of the sound period, and iii) calculation of the phase difference between the oscillators wave and the sound signal.

The period of the sound signal is calculated by measuring the peak-to-peak interval of the sound. Peak detection is obtained from a 5 point-moving average method for smoothing the signal and then looking for a peak within the last three sampling points. The extracted sound period, ***tp***, is subsequently

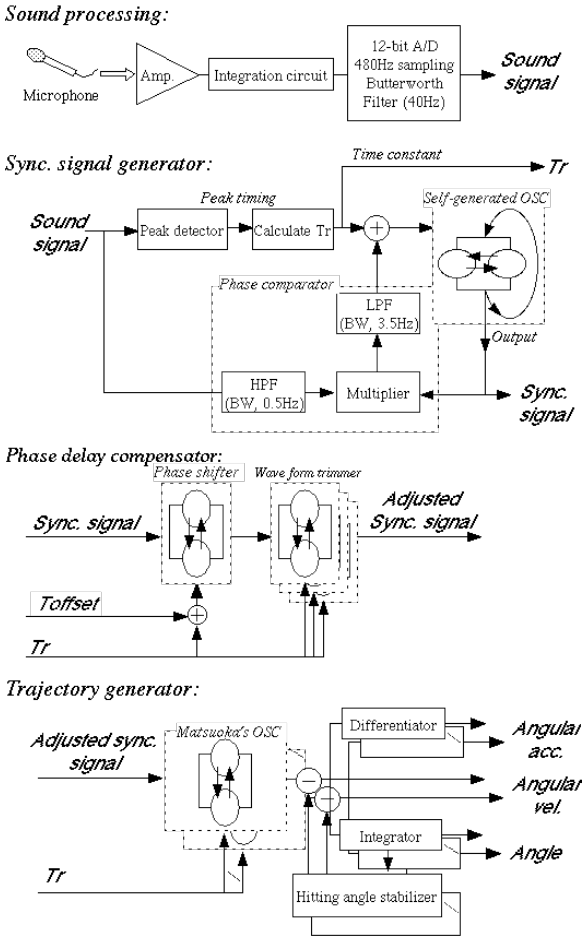

Figure 2: Configuration of a robot synchronized drumming system

converted into appropriate time constants ***Ta*** and ***Tr*** using the following equations.

$$T_r = tp * 0.1309 + 0.0007819 + fdiff * 0.002 \quad (3)$$

$$T_a = T_r * 2.0 \quad (4)$$

The first two terms of equation (3) are a simple linear calibration line that maps ***tp*** into a corresponding ***Tr***. The slope and intercept were determined empirically from Matsuoka's oscillator equations (1-3). Equation (4) just reflects that ***Ta*** is in constant ratio to ***Tr***, as mentioned above. The term ***fdiff*** in (3) is needed for the phase adjustment and explained next.

Using the time constants ***Ta*** and ***Tr,*** the Matsuoka oscillator in the Sync. Signal Generator creates a synchronized oscillation with the sound, but there may be a phase offset. This phase difference can be calculated from the sound signal and the generated pulse. First, a Butterworth high-pass filter with a cut-off frequency of 0.5 [Hz] is applied to the sound signal to remove the DC component. Afterwards, the filtered signal is multiplied with the signal of the oscillator. Then, a Butterworth low-pass filter is applied to the resultant product. The cut-off frequency of this low-pass filter is defined manually to achieve smooth and fast synchronization. This filtered signal is the phase difference, ***fdiff*** used in Equation (3). The method of extracting the phase in the given way corresponds to the Phase-Locked Loop method of electrical engineering.

It should be noted that the Matsuoka oscillator in the Sync. Loop also uses recurrent feedback onto itself. Empirically, this recurrent feedback helped to improve the performance of the Sync. Loop. However, this feedback loop can be avoided by re-parameterizing the Matsuoko oscillator, which we will do in future work.

3.4 Phase delay compensator

To compensate for delays from the information processing of the sensory input and the response time of the actuators, we apply a phase delay compensator to the output pulse from the Sync. Signal Generator. This compensator is a serially connected Matsuoka oscillator. The time constants for this oscillator are set similarly as in Equation (3), however with a small offset ***Toffset*** as shown in Equation 5. ***Toffset***, is tuned to eliminate information processing delays and needs to be determined experimentally. Then, the adjusted pulse is led to other serially connected Matsuoka's oscillators to trim the waveform. This step is needed in order to filter out undesired distortions in the waveform of the adjusted pulse. We basically exploit the ability of Matsuoka oscillator to achieve zero-lag phase coupling with each other, and use them a special kind of low-pass filter. Thus, a distorted wave, run through several synchronization steps with additional oscillators, uncovers the original waveform of the Matusoka oscillator, but retains the phase of the distorted wave. The time constants of the oscillator for the trimming are set to their corresponding values in the frequency of the input sound signal

$$T_r' = tp * 0.1309 + 0.0007819 + T_{offset} \quad (5)$$

3.5 Trajectory generator

Every joint angle is represented by one Matsuoka oscillator ([5]), synchronized by wave coming out of the Phase Delay Compensator. In order to generate a smooth trajectory for each joint, we regard the output signal of each oscillator as a desired angular velocity command. The desired angular acceleration and position are calculated from the angular velocity by using numerical differentiation and integration, respectively. Integration of the velocity signal requires a feedback

term to obtain stability of the angular position. Equations (6-9) demonstrate how this stability can be achieved. We add a feedback term, ***d***, to the oscillator's output in (6). The term ***d*** is calculated by Equation 8 at every moment of impact between drumstick and drum. ***Pbottom*** is the deviation between the desired joint angle at impact (i.e., at the maximal position of the oscillatory wave) and the angle achieved at each impact time ***Pgain*** and ***Igain*** are constants to adjust the feedback effect.

The output of the trajectory generator is finally transformed into a motor command that actuates the robot's joints. Since the magnitude of the output signal of the trajectory generator is not related to any physical quantity, it needs to be multiplied by a coefficient ***Amp*** to be scaled to an appropriate desired angular velocity as shown in Equation (6). The joint angle is calculated by numerical integration and then added a constant value, ***pose,*** as Equation (7) shows to maintain a suitable drumming posture.

$$V = Amp*(Max(0,x_0) - Max(0,x_1)) - d \quad (6)$$

$$P = \int V dt + pose \quad (7)$$

$$d = P_{gain}*P_{bottom} + I_{gain}*c \quad (8)$$

$$c = c + P_{bottom} \quad (9)$$

4. Experiments

4.1 Human drumming experiment

4.1.1 Human drumming

In order to obtain data to compare robot and human drumming, we have examined the drumming movements of a human drummer with a special motion capture device, a Sarcos Sensuit [SARCOS Research Corp.]. The Sensuit measures the whole body movements of human subjects in joint angular coordinates. In our experiment, the human subject grasped a drumstick equipped with an acceleration sensor at the tip of the stick, and hit a snea drum placed directly in front of the body. A computer generated a periodic beep signal for the subject to synchronize. The subject was asked to keep the drumming frequency the same as indicated by the beeps. The sampling frequency of Sensuit was 100 [Hz]. The period of the subject's drumming was computed from the acceleration sensor on the drumstick.

The results of this experiment demonstrated that subjects mainly used the elbow joint to generate drumming movements. Figure 3 shows an observed drumming trajectory of the subject's elbow where the beep frequency changed at 17.25 [sec.]. The upper graph of Figure 4 shows the corresponding drumming period. The small circles on the graph indicate the timing of beeps, while the vertical lines indicate the time of impact of the human subject. The solid line displays the period of drumming of the human subject. The bottom graph of Figure 4 shows the time difference between the time of beep and the corresponding time of impact of the human subject.

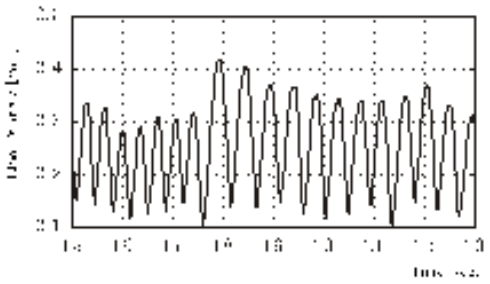

Figure 3: Elbow's trajectory of human subject

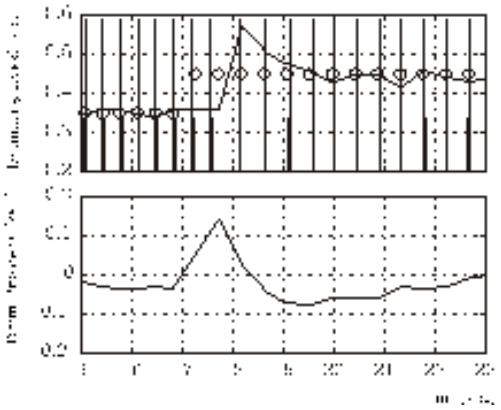

Figure 4: Drumming period and ability to synchronize with the a changing beep frequency

As can be seen in these figures, humans are generally perfectly synchronized with roughly zero phase-lag when the external beep has constant frequency the average phase offset of drumming was less than 20 [msec.]. At an unexpected change of frequency, as shown at 17.25 [sec.] in the graphs, the subject's drumming period undergoes a transient and stabilizes after about 2 seconds at the new drumming frequency. Subjects generally preferred drumming periods between 0.2 [sec.] or 0.5 [sec.]. Larger periods are possible but showed significantly more variance in the phase fluctuations

4.2 Robot Drumming

4.2.1 Robot Setup

The robot used in the following experiments is a full body humanoid robot developed by SARCOS Research Corp., USA (Figure 6). The robot has two arms, two legs, a torso, and a head with a binocular vision system, resulting in a total of 30 hydraulically activated degrees of freedom (DOFs). The height of the robot is approximately 1.85 [m] and its weight is 80 [kg]. The robot's neck has three DOFs and the binocular vision system mounted on the head is equipped with four cameras, one wide angle and one focus camera for each eye, to mimic the foveal vision of human eyes. Each eye has a pan and tilt DOF. The arms have seven DOF like human arms. Legs can only perform planar movements with three DOFS per leg. The robot's trunk has also three DOFs. Every DOF is equipped with a position sensor and a load sensor except for the DOFs of the camera systems, which have only position sensors. Linear and rotary hydraulic actuators control the joints. Due to the control out of a torque loop based on the load cells in each joint, all DOFs of the robot are very compliant (except for the eyes). The robot runs out of a hydraulic pressure of approximately 0.45 [MPa]. A four-bar linkage pivot stand it attached to the robot's pelvis and prevents the robot from falling over laterally. A counter weight is equipped at the opposite side of the four bar linkage to cancel some of the weight of the robot.

The robot's control system is composed of four CPUs in a VME bus (PowerPC 233MHz, 64MB RAM), and D/A, A/D, and AJC (Advanced Joint Controller) cards. AJC cards are special purpose analog signal conditioning cards that drive the hydraulic valves, collect sensory information, and communicate with the VME bus. A color vision system, QuickMag (OKK Inc.), provides information about 3D color-coded objects to the robot from a static stereo camera system attached to the ceiling of the laboratory. Another image processing system is connected to the binocular vision system of the robot. All CPU cards of the robot manage different tasks, e.g., feedback control, signal I/O, feedforward control, movement planning, etc. For the following experiments, the robot was run out of a compute-torque controller. The CPU cards run the real-time operating system VxWork (WindRiver Corp.).

4.2.2 Synchronized Robot Drumming

Figure 5 illustrates the configuration of the humanoid robot system for the drumming task. A snea drum was placed in front of the robot, and, similar as in the human experiments, the drumming timing of the robot was measured from a shock sensor mounted on

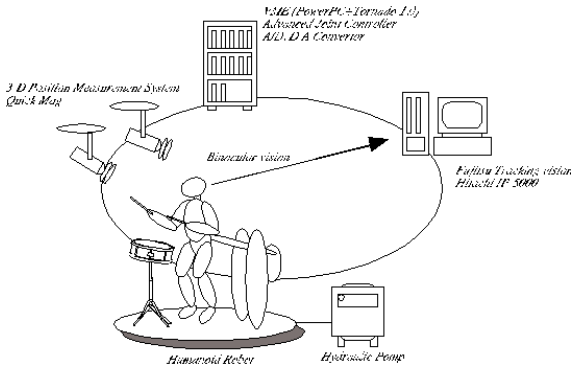

Figure 5 Humanoid robot system

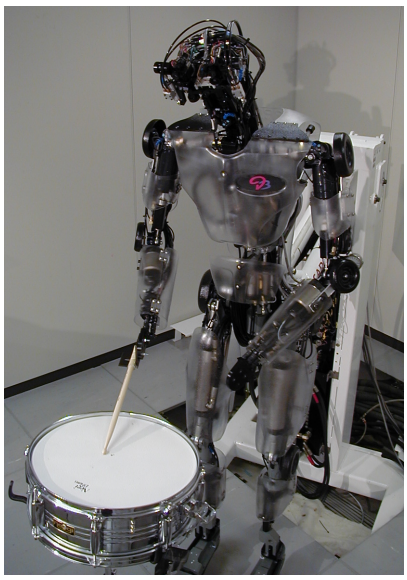

Figure 6 Photograph of our humanoid robot

the drum's surface. A drumstick was attached to the robot's right hand. The trajectory generator produced desired trajectories for the right elbow and wrist abduction/adduction joint to achieve human-like drumming motion.

Figure 7 shows a sound input signal captured by the microphone, the output of the shock sensor, and position and velocity trajectories for the elbow during a typical run of the system. An electric metronome was used to create an accurate rhythmic sound signal. The rising edge of the sound signal coincided well with the rising edge of the shock sensor's output, demonstrating that the proposed system can generate a stable drumming trajectory that is synchronized with the sound. We also confirmed that the system can generate drumming trajectories in a wide period range from 0.2 [sec.] to 0.5 [sec.].

Figure 8 illustrates the accuracy and stability of the drumming period by the proposed system. The upper graph is a sound signal captured by the electric

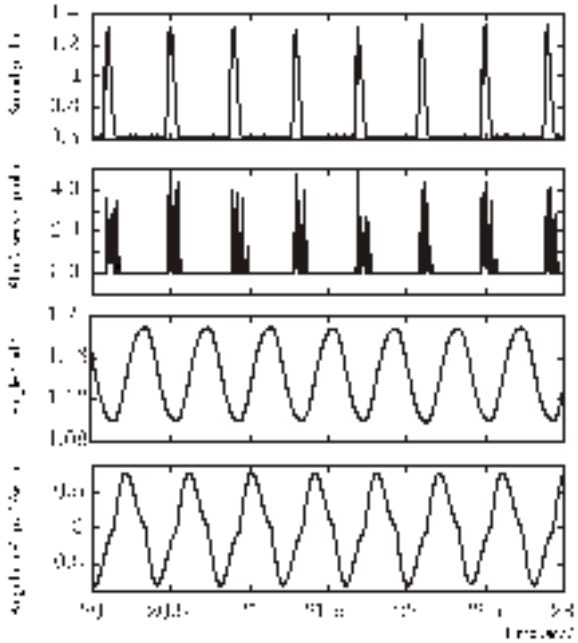

Figure 7 Example trajectory generated by our robot drumming system

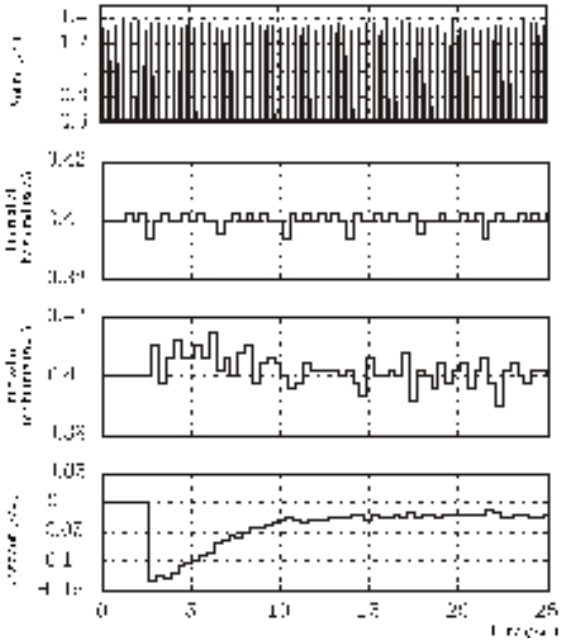

Figure 8 Accuracy and stability of drumming intervals

metronome. The next graph shows the extracted period of the sound signal. The third graph shows the period of drumming generated by the robot. The bottom graph shows the time difference between the rising edge of the sound signal and the rising edge of the shock sensor's output. The interval of the electric metronome was 0.4 [sec.] in this experiment. In this experiment, the motor command was suppressed during the first 10 seconds due to transient behavior of the oscillator startup. After 10 [sec.], the system could follow the sound input very well and had only about 22 [msec.] average phase delay.

Figure 9 shows the following capability of the system if the period of the sound input changed. The upper graph shows a sound signal from the electric metronome. The next graph indicates the robot's drumming period. The third graph shows the time difference between the impact time and the rising time of the sound input. The bottom graph shows the elbow's joint trajectory. The metronome created a sound signal with a period of 0.4 [sec] in the first phase. At some point, the metronome was stopped and then restarted with a shorter period. The robot followed this change in drumming frequency immediately and adjusted the phase of drumming within about 3 [sec.].

Figure 10 shows the following capability of the system for drumming sounds generated by a human drummer. The upper graph indicates a sound signal of the human. The second graph shows the

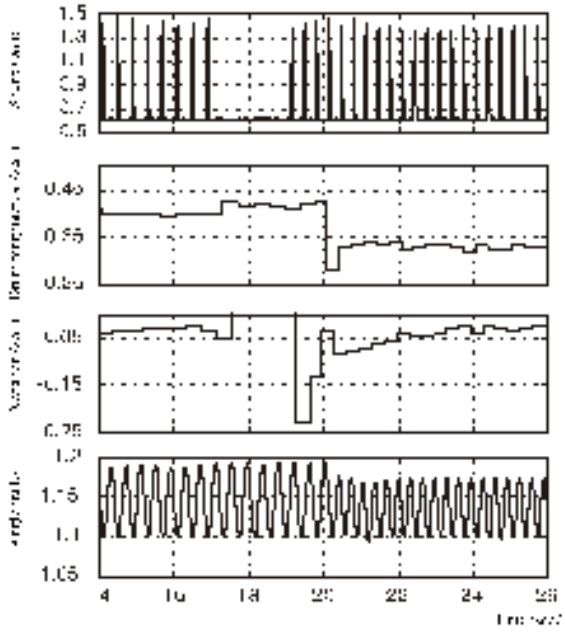

Figure 9 Following capability of our drumming system

elbow joint's trajectory of the robot. The third graph shows the period of the sound signal. The bottom graph shows the time difference between the impact time and the rising time of the sound input, identical to the case above. Although the human drummer changed the drumming period from about 0.2 [sec.] to 0.5 [sec.], the robot was able to follow the drumming sounds without any problems.

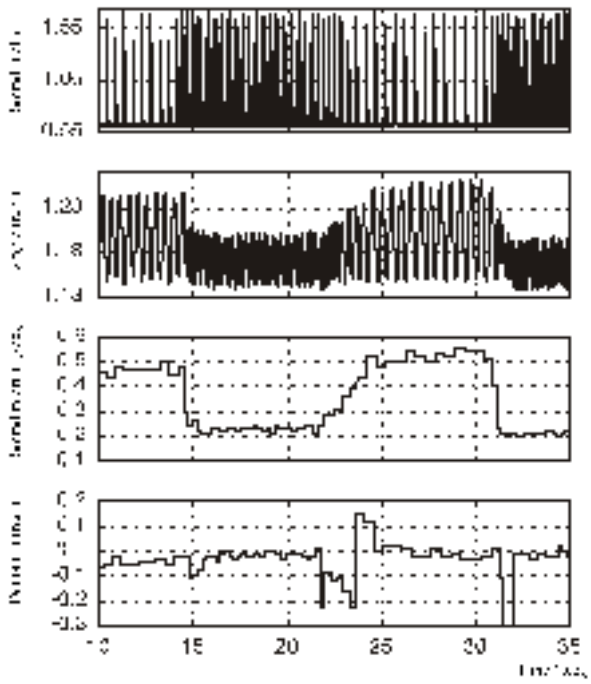

Figure 10 Following capability for drumming sounds generated by a human drummer

5. Conclusion

This paper presented a way of achieving rhythmic movements that are synchronized with an external sensory signal. At the core of our system, neural oscillators produced a synchronized signal with zero phase-lag and generated the desired drumming trajectories for a humanoid robot. Our system was able to synchronize with an external drummer in real-time and showed similar performance as measured from human drumming. Our method can handle several kinds of periodic input signals, like sound, force, and visual stimuli. In the future, we will extend our method to handle the coordination of multiple joints, multiple limbs, and even wider range of input signals.

6. Acknowledgements

We would like to thank Mr. Yoshinori Sasabe for his help in the robot experiments. This work was made possible by Award #9710312 of the National Science Foundation, the ERATO Kawato Dynamic Brain Project funded by the Japanese Science and Technology Cooperation, and the ATR Human Information Processing Research Laboratories.

References

[1] S. Schaal, C. G. Atkeson, and S. Botros, "What should be learned?," presented at Proceedings of Seventh Yale Workshop on Adaptive and Learning Systems, New Haven, CT, 1992.

[2] P. A. Getting, "Understanding central pattern generators: Insights gained from the study of invertebrate systems," presented at Neurobiology of Vertebrate Locomotion, Stockholm, 1985.

[3] A. A. Rizzi and D. E. Koditschek, "Further progress in robot juggling: Solvable mirror laws," presented at IEEE International Conference on Robotics and Automation, San Diego, CA, 1994.

[4] D. Bullock and S. Grossberg, "Neural dynamics of planned arm movements: Emergent invariants and speed-accuracy properties during trajectory formation," *Psychological Review*, vol. 95, pp. 49-90, 1988.

[5] S. Schaal and D. Sternad, "Programmable pattern generators," presented at 3rd International Conference on Computational Intelligence in Neuroscience, Research Triangle Park, NC, 1998.

[6] N. G. Hatsopoulos, "A neural pattern generator that tunes into the physical dynamics of the limb system," presented at Proceedings of the International Joint Conference on Neural Networks, Baltimore, 1992.

[7] N. G. Hatsopoulos and W. H. Warren, Jr., "Resonance tuning in rhythmic arm movements," *Journal of Motor Behavior*, vol. 28, pp. 3-14, 1996.

[8] M. Williamson, "Neural control of rhythmic arm movements," *Neural Networks*, vol. 11, pp. 1379-1394, 1998.

[9] K. Matsuoka, "Sustained oscillations generated by mutually inhibiting neurons with adaptation," *Biological Cybernetics*, vol. 52, pp. 73-83, 1985.

[10] K. Matsuoka, "Mechanisms of frequency and pattern control in the neural rhythm generators," *Biological Cybernetics*, vol. 56, pp. 345-353, 1987.

Session

Design of Neural Controller

Proceedings of the International Symposium on
Adaptive Motion of Animals and Machines,
Montreal, Aug.8-12, 2000

A neuromechanical investigation of salamander locomotion

Auke Jan Ijspeert
Brain Simulation Laboratory, Hedco Neuroscience Building,
University of Southern California, Los Angeles 90089, U.S.A,
ijspeert@rana.usc.edu

Abstract

Understanding biological control of locomotion requires not only good models of the neural mechanisms of pattern generation, but also of the interaction of these neural circuits with the body. In this article, we investigate the neural mechanisms underlying the locomotion of the salamander, an animal capable of both aquatic and terrestrial locomotion. A 3D biomechanical simulation of the salamander's body is developed whose muscle contraction is determined by a locomotion controller simulated as a leaky-integrator neural network. While the connectivity of the neural circuitry underlying locomotion in the salamander has not been decoded for the moment, the neural circuit designed in this article has a a general organization which corresponds to that hypothesized by neurobiologists for the real animal. In particular, the locomotion controller is based on a body *central pattern generator* (CPG) corresponding to a lamprey-like swimming controller, and is extended with a limb CPG for controlling the salamander's limbs. A genetic algorithm is used to instantiate parameters of the neural circuit (e.g. synaptic weights and time parameters) in three stages, with first the evolution of segmental oscillators, second the evolution of intersegmental coupling for making a body CPG, and third, the evolution of the limb CPG and its connections to the body CPG. A controller is developed which can produce a neural activity and locomotion gaits very similar to those observed in the real salamander. By varying the tonic excitation applied to the network, the speed, direction and type of gait can be varied. Movies of the simulations can be found at http://rana.usc.edu:8376/~ijspeert/ .

1 Introduction

Locomotion is a fundamental skill for animals, which need it for a variety of actions such as finding food, encountering a mate for reproduction, escaping predators, and moving to a more friendly environment. Similarly, efficient locomotion is essential in mobile robotics if we want robots to carry out useful tasks. As wheeled robots are limited in the type of environments in which they can move, there is an increasing interest to develop robots which use more animal-like types of gaits. This usually means that more complex means of locomotion than powered wheels are needed, involving a greater number of actuators generally used in a rhythmic way. Very quickly, the engineer is then faced with the same control problems faced by biological systems, namely the control of multiple actuators which only produce the desired behavior when appropriately coordinated. The problem is to find the right control mechanism which can translate commands concerning the speed and direction of motion into the set of rhythmic signals sent to the multiple actuators. Biologically inspired robotics may therefore not only gain from inspiration from biology for the structure of the robot (e.g. legged robots) but also for its control system (e.g. neural based central pattern generators). Examples of such an approach include [20, 2, 19].

In this work, we investigate control of locomotion in vertebrates using biomechanical and neuronal simulations. We are, in particular, interested in the locomotion of the salamander, an animal capable of both aquatic and terrestrial locomotion. The salamander makes axial movements during locomotion. It swims using an anguiliform swimming gait, in which the whole body participates to movement creation, and in which a wave of neural activity is propagated from head to tail, with an approximately constant wavelength along the spinal cord [9, 3]. On ground, the salamander switches to a trotting gait, in which the body forms an S-shaped standing wave with the nodes at the girdles, which is coordinated with the movements of the limbs such as to increase their reach during the swing phase. EMG recordings have shown that two

different motor programs underly these typical gaits, with a traveling of neural activity along the body for swimming and a mainly standing wave during trotting [9, 3]. The locomotor circuitry responsible for these motor programs has, however, not been decoded for the moment.

This article presents a potential control circuit capable of producing these two types of gaits in a biomechanical simulation of the salamander. The control circuit is a central pattern generator (CPG) whose circuitry is based on a lamprey-like organization, with a lamprey-like CPG for the body segments extended by a limb CPG for controlling the limbs as hypothesized in [1, 3]. Similarly to other works which have investigated biological locomotion control using neuromechanical simulations [21, 5, 6], a simple 3D mechanical simulation of the salamander's body in interaction with water or ground is developed whose muscular activity is determined by the locomotor circuit simulated as a leaky-integrator neural network. The work presented here follows preliminary experiments on the control of a 2D salamander simulation [17, 13, 15], and uses the same methodology as that used to develop potential swimming controllers for the lamprey [18]. This article presents, in particular, how the locomotor circuit for the 2D simulation can be extended to control a 3D salamander with more realistic limbs.

2 Mechanical simulation

The 3D mechanical simulation is composed of ten rigid links representing the trunk and the tail, and eight links representing the limbs (Figure 2). The tail and trunk links are connected by one degree-of-freedom (DOF) joints, while the limb joints have 2 DOF at the shoulder/pelvis and 1 DOF at the knee. The torques on each joint are determined by pairs of muscles simulated as springs and dampers, whose spring constant are modified by the signals sent from the motoneurons.

The simulation is implemented in a dynamical simulation package from Mathengine,[1] which handles the internal forces necessary for keeping the links connected, as well as the contacts of the body with the ground. During terrestrial locomotion, friction forces are applied to all links in contact with the ground (e.g. the trunk and tail links slide on the ground while the salamander is trotting), and in water, it is assumed that each link (limbs included) is subjected to inertial forces due to the water (with forces proportional to the square of the speed of the links relative to the water). A more detailed description of the biomechanical simulation can be found in [14]. The simulation is only a first approximation of a salamander, and does not attempt to reproduce in detail the biomechanical properties of any specific salamander species.

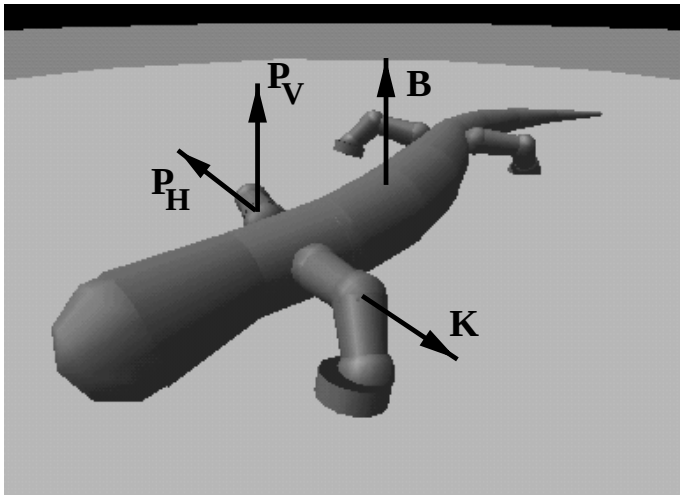

Figure 1: Mechanical simulation. The body is composed of 18 rigid links. Body (trunk and tail) links are connected by one-DOF hinge-joints, with vector B as axis of rotation. Limbs are attached to the body by two-DOF joints with one vertical axis of rotation P_V and one horizontal P_H. Finally, knee joints have one DOF and they rotate around axis K.

[1] MathEngine PLC, Oxford, UK, www.mathengine.com

3 Neuronal simulation

The locomotion controller is simulated as a leaky integrator neural network. It is composed of a body CPG and a limb CPG (Figure 2). The body CPG is lamprey-like with an interconnection of 40 segmental networks for the generation of traveling waves of neural activity. The limb CPG is made of two interconnected oscillators projecting to the limb motoneurons and to the body CPG segments, creating a unilateral coupling between the two CPGs. While the general organization of the controller is set by hand, the time parameters, biases and synaptic weights of the neurons are instantiated using a genetic algorithm. This is done in three stages, with first the evolution of segmental oscillators, second, the evolution of intersegmental coupling for the body CPG, and finally the evolution of the limb CPG connectivity.

In this article, only a summary of the different design stages will be given. For a detailed description of the design of neural controllers for a 2D simulation of the salamander, see [17, 13, 15]. This paper mainly investigates how the 2D neural controller developed in [15] can be extended to control the locomotion of a 3D body.

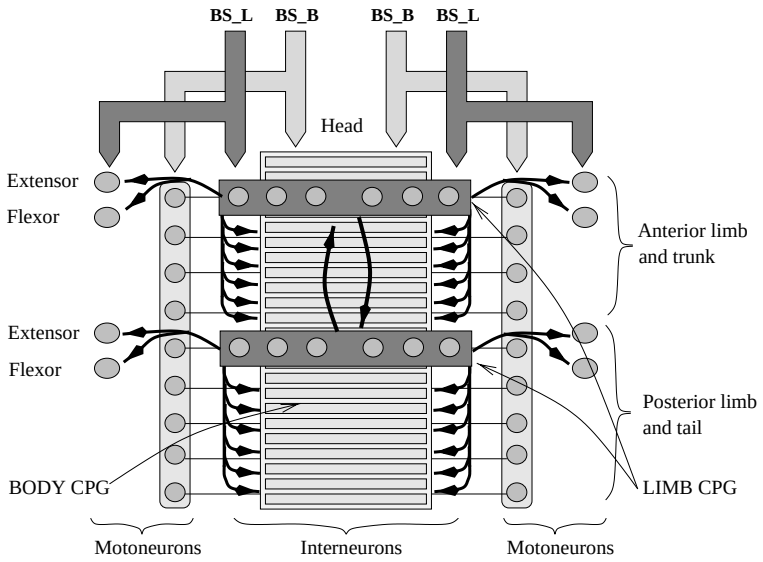

Figure 2: Proposed organization of the salamander's locomotor circuitry. The circuitry is composed of a body CPG and a limb CPG which can be activated by four pathways from the brainstem (BS). Each limb is activated by 3 pairs of flexor-extensor neurons (only one pair per limb shown here).

3.1 Neuron model

Leaky-integrator neurons, i.e. neurons of intermediate complexity between abstract binary neurons used traditionally in artificial neural networks and detailed compartmental models used in computational neuroscience, are used for implementing the neural controllers. Instead of simulating each activity spike of a real neuron, a neuron unit computes its average firing frequency [12]. According to this model, the mean membrane potential m_i of a neuron N_i is governed by the equation:

$$\tau_i \cdot dm_i/dt = -m_i + \sum w_{i,j} x_j$$

where $x_j = (1 + e^{(m_j + b_j)})^{-1}$ represents the neuron's short-term average firing frequency, b_j is the neuron's bias, τ_i is a time constant associated with the passive properties of the neuron's membrane, and $w_{i,j}$ is the synaptic weight of a connection from neuron N_j to neuron N_i.

4 Staged evolution of the central pattern generator

4.1 Segmental oscillators

In the first design stage, segmental oscillators are developed by using the genetic algorithm (GA) to instantiate neural (b_i,τ_i) and network parameters (the synaptic weights $w_{i,j}$) in a network composed of 8 neurons. For this stage, the fitness function of the GA is defined to reward networks which can produce stable oscillations and whose frequency of oscillation can be modulated by the level of tonic (i.e. non-oscillating) input applied to the network.

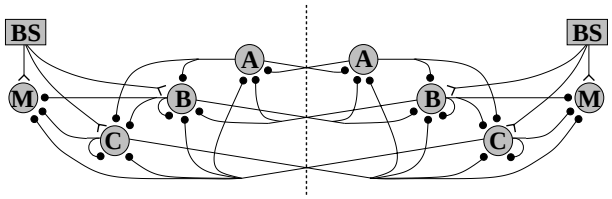

Figure 3: Connectivity of the segmental oscillator. The oscillator is composed of three types of inhibitory interneurons (A, B, and C) and of excitatory motoneurons (M). The neurons receive tonic input coming from the brainstem (BS).

Figure 3 illustrates one of these evolved networks. This network produces stable oscillations over a large range of frequencies (from 0.75 to 8.75Hz). It starts to oscillate when it receives sufficient tonic input (which can be viewed as the descending signals coming from the brainstem), with the frequency of oscillation increasing with the level of input. Note that the oscillations are due to the connectivity and the time-delayed reaction of the neurons to their synaptic input rather than to intrinsic oscillatory properties of the neurons (i.e. the circuit has no pacemaker cells).[2]

4.2 Intersegmental coupling

The aim of this stage is to develop a complete body CPG which can propagate a traveling rostro-caudal wave for swimming. The body CPG is made of 40 segments like the number of segments found in salamanders (instead of the 100 segments of lampreys). One of the best oscillators of the previous stage is chosen as template segmental oscillator. The coupling between segments is obtained using *synaptic spreading* [22], in which a connection between two neurons in a segmental oscillator is projected to corresponding neurons in neighboring segments. The extent of the projections in both rostral and caudal directions are instantiated using the GA, with a fitness function rewarding networks which produce regular oscillations in all segments, and which propagate a traveling wave from head to tail with a constant phase lag along the spinal cord.

Successful swimming controllers are thus created which, when connected to the mechanical simulation, produce the typical anguiliform swimming observed in salamanders and lampreys (Figure 4). Note that during swimming, tonic signals are also sent to the horizontal flexors of the limbs in order to keep the limbs against the body. The phase lag between neighboring segments is almost constant, leading to a neural wave of constant wavelength along the spinal cord (Figure 5, left). The speed of swimming can be modulated by varying the level of tonic input applied the whole body CPG, with the frequency of oscillation and therefore the speed of swimming increasing with the level of input. Interestingly, while the frequency of oscillation depends significantly on the level of tonic input, the wavelength of the neural wave remains more or less constant for any level of input, similarly to what is observed in the lamprey [10]. Finally, this body CPG has also the interesting property of being able to induce turning when asymmetrical input is applied between left and right sides of the spinal cord. If the asymmetry is permanent, the salamander swims in a circle, and if it is temporary it can be used to change the heading of swimming.

[2] In the lamprey, several mechanisms of rhythmogenesis have been found, with cellular properties playing an important role for low frequencies of oscillation, while higher frequencies are mainly generated by network properties [11, 10].

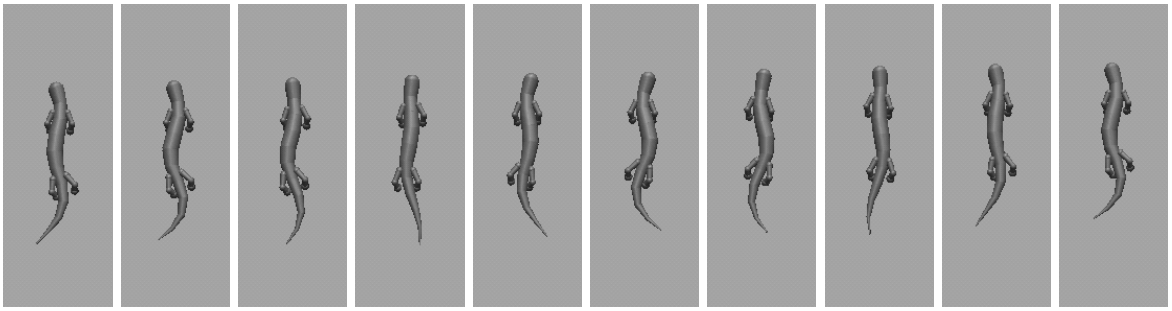

Figure 4: Swimming.

4.3 Complete CPG

The aim of this last stage is to develop a complete CPG able of producing both the swimming and the trotting gaits of the salamander. A limb CPG is therefore developed on top of the body CPG. The limb CPG is composed of two oscillators which are copies of the segmental oscillator. The GA is used to instantiate the synaptic weights of all connections represented as thick arrows on Figure 2, that is, the coupling connections between the limb oscillators, the connections from the limb oscillators to the limb motoneurons, and the connections from the limb oscillators to the segmental oscillators of the body CPG. The GA is also used to instantiate the neural parameters for the flexor and extensor limb motoneurons. The aim is to be able to switch between the swimming and the trotting gaits, by either applying tonic input only to the body CPG for swimming (by the left and right *BS_B* pathways in Figure 2), or applying tonic input to *both* the body and the limb CPGs for trotting (i.e. by both the *BS_B* and *BS_L* pathways). For this stage, the fitness function is defined to reward complete CPGs which have their limb oscillators oscillating out-of-phase and which can produce a trotting gait whose speed can be modulated by the level of tonic input applied to both the body and the limb CPGs.

Figure 6 illustrates the trotting gait of one of the evolved complete CPGs. Interestingly, the evolved coupling from the limb CPG to the body CPG induces a body-limb coordination very similar to that observed in the real salamander. The body makes an S-shaped movement which is coordinated with the movements of the limbs to increase their reach when they are in the swing phase. The effect of the coupling can be observed in Figure 5 (right). The unilateral coupling from the limb oscillators forces the chain of segmental oscillators of the body CPG (which would normally propagate a traveling wave) to be in perfect synchrony in the upper part of the body and in the tail, with an abrupt change of phase at the level of the posterior girdle (i.e. where the influence of the anterior limb oscillator stops and that of the posterior limb oscillator begins).

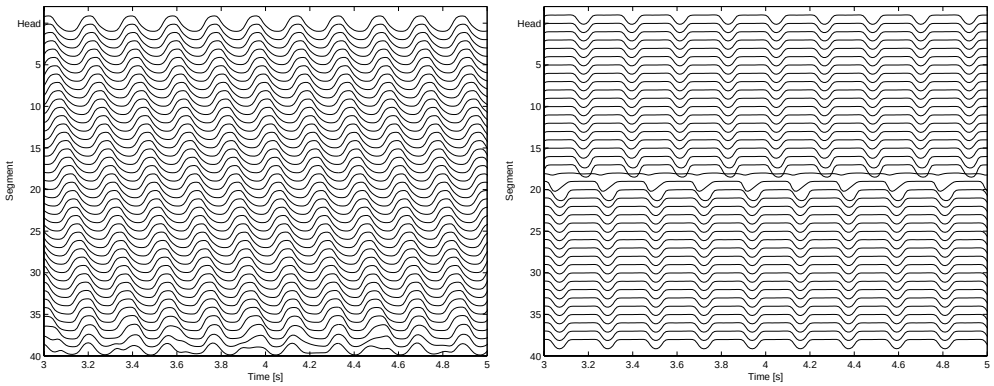

Figure 5: Neural activity in left motoneurons of the body CPG during swimming (*left*) and trotting (*right*).

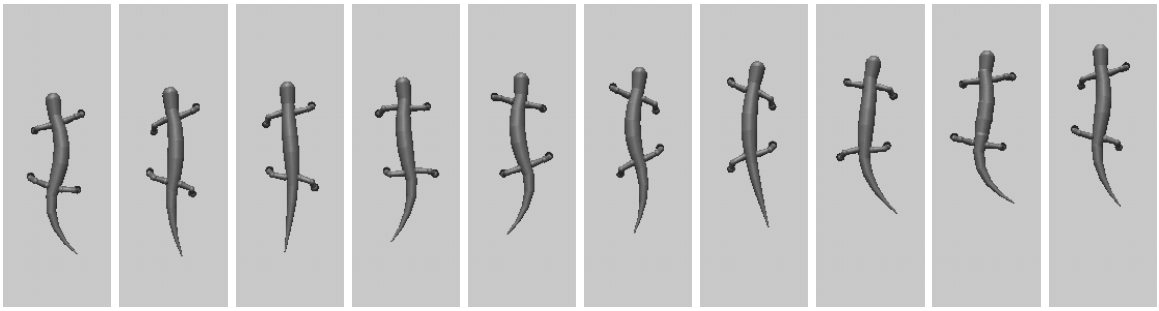

Figure 6: Trotting.

The activity of the limb CPG is shown in Figure 7. Note that this limb CPG was initially developed for a 2D simulation of the salamander. Two motoneurons F_V and E_V, for the vertical flexor and extensor muscles at the shoulder/pelvis, were added by hand to the network. These motoneurons oscillate with a phase of approximately 90 degrees compared to the horizontal motoneurons, so that the limbs perform approximate circles. Also the signals from the F_H and E_H motoneurons are sent to both the horizontal muscles at the shoulder/pelvis and to the knee muscles. Turning during trotting can be induced by applying asymmetrical input to both the limb and the body CPGs. Turning is then mainly due to the extra bending of the body which enables the simulated salamander to make relatively sharp turns.

Interestingly, the simulated trotting salamander did not present rolling problems in this 3D simulation. This is partly due to the fact that, in this first approximation of a salamander, joints connecting body links have been simulated as hinges (i.e. with only 1 DOF) therefore preventing torsion, but also to the intrinsic property of the salamander's trotting gait in which the whole body slides on the ground with a stabilizing S-shape, therefore significantly reducing postural instability compared to other, supported, quadrupedal gaits.

5 Discussion and conclusion

This article presented a potential locomotor circuit for salamander locomotion, based on a lamprey-like body CPG extended by a limb CPG. The limb CPG is based on two oscillators which are copies of the segmental oscillators of the body CPG. This could be seen as being the result of the evolution from a lamprey-like ancestor with two body oscillators having gradually specialized to control fins and then limbs. As the salamander has kept a partially aquatic habitat, it has kept the control circuitry for aquatic locomotion and developed a new motor program for terrestrial locomotion. In our model, we hypothesize that the salamander is able to switch between gaits by varying how tonic (i.e. non-oscillating) input is applied to the locomotor circuit through four different pathways from the brainstem.

The coupling from the limb CPG to the body CPG explains the capacity of the locomotor circuit to produce two different types of waves: when activated, the body CPG tends to produce traveling waves for swimming, unless it is forced by the unilateral coupling from the activated limb CPG to produce a standing wave for trotting. In agreement with the first assumption, it has recently been found out that the completely isolated spinal circuit of the salamander tends to spontaneously propagate traveling waves when submitted to an excitatory bath [4]. Further anatomical and physiological studies may test the validity of the model by investigating whether two distinct limb oscillatory circuits exist, and whether these circuits project through relatively long range projections to each other and to the body segments.

The mechanical simulation, even if it was just a first approximation, allowed an investigation of what phases and shapes the signals sent to the muscles should have for efficient locomotion. As biomechanical systems have complex nonlinear dynamics, including models of the body is important to fully understand the neural mechanisms underlying locomotion. Furthermore, having a representation of the body becomes necessary if one wants to investigate the effect of sensory feedback on the pattern generation. The controller presented in this article works in an open loop, i.e. without proprioceptive feedback. In future work, we intend to integrate such a feedback, as it is important for "shaping" the neural signals and coordinating

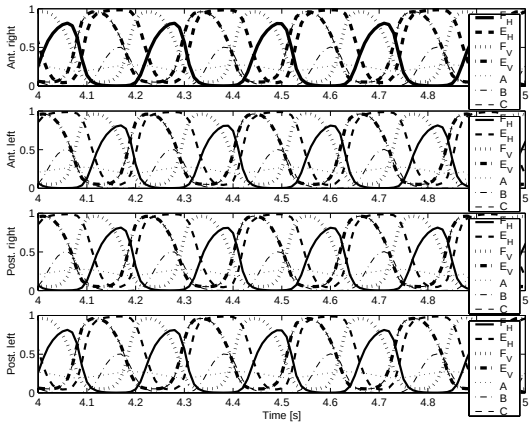

Figure 7: Neural activity in the limb CPG during trotting.

them with the actual mechanical activity. In models of lamprey swimming, for instance, it has been shown that sensory feedback enables the crossing of zones of non-stationary water which would be impossible to cross without [6, 18].

We are currently investigating how the locomotor circuit presented in this article can be integrated into a more comprehensive model of the salamander's central nervous system. Several models of the salamander's visual system have, for instance, been designed [7, 8], but a comprehensive model which interconnects sensory and motor systems remains to be developed. In [16], we present a first experiment in that direction in which a simple control circuit is designed to implement a tracking behavior based on two simple retinas and a "water" sensor. It is found 1) that the pattern generation of the locomotor circuit is robust against constantly varying inputs, 2) that the simulated salamander can robustly switch between swimming and trotting, and 3) that it can successfully track a randomly moving target.

To conclude, biologically inspired CPGs may be interesting for controlling robots using animal-like type of gaits, that is, machines which require control mechanisms for efficiently coordinating multiple actuators for locomotion. The CPG presented in this paper has the interesting property that the generated gait can be modulated by simple input signals. By simply varying how tonic input is applied to the different parts of the network, the speed, direction, and type of gait can be modulated.

Acknowledgments Facilities were provided by the University of Southern California. Many thanks to Michael Arbib for his insightful comments on this project. This work was supported by a grant for young researcher from the Swiss National Science Foundation.

References

[1] A.H. Cohen. Evolution of the vertebrate central pattern generator for locomotion. In A. H. Cohen, S. Rossignol, and S. Grillner, editors, *Neural control of rhythmic movements in vertebrates*. Jon Wiley & Sons, 1988.

[2] H. Cruse, D.E. Brunn, Ch. Bartling, J. Dean, M. Dreifert, T. Kindermann, and J. Schmitz. Walking: A complex behavior controlled by simple networks. *Adaptive Behavior*, 3(4):385–418, 1995.

[3] I. Delvolvé, T. Bem, and J.-M. Cabelguen. Epaxial and limb muscle activity during swimming and terrestrial stepping in the adult newt, *pleurodeles waltl*. *Journal of Neurophysiology*, 78:638–650, 1997.

[4] I. Delvolvé, P. Branchereau, R. Dubuc, and J.-M. Cabelguen. Fictive rhythmic motor patterns induced by NMDA in an in vitro brain stem-spinal cord preparation from an adult urodele. *Journal of Neurophysiology*, 82:1074–1077, 1999.

[5] Ö. Ekeberg. A combined neuronal and mechanical model of fish swimming. *Biological Cybernetics*, 69:363–374, 1993.

[6] Ö. Ekeberg, A. Lansner, and S. Grillner. The neural control of fish swimming studied through numerical simulations. *Adaptive Behavior*, 3(4):363–384, 1995.

[7] W.C. Eurich, G. Roth, H. Schwegler, and W. Wiggers. Simulander: a neural network model for the orientation movement of salamanders. *Journal of comparative physiology*, 176:379–389, 1995.

[8] W.C. Eurich, H. Schwegler, and R. Woesler. Coarse coding: applications to the visual system of salamanders. *Biological Cybernetics*, 77:41–47, 1997.

[9] L.M. Frolich and A.A. Biewener. Kinematic and electromyographic analysis of the functional role of the body axis during terrestrial and aquatic locomotion in the salamander *ambystoma tigrinum*. *Journal of Experimental Biology*, 62:107–130, 1992.

[10] S. Grillner, T. Degliana, Ö. Ekeberg, A. El Marina, A. Lansner, G.N. Orlovsky, and P. Wallén. Neural networks that co-ordinate locomotion and body orientation in lamprey. *Trends in Neuroscience*, 18(6):270–279, 1995.

[11] S. Grillner, P. Wallén, and L. Brodin. Neuronal network generating locomotor behavior in lamprey: Circuitry, transmitters, membrane properties, and simulation. *Annu. Rev. Neurosci.*, 14:169–199, 1991.

[12] J.J Hopfield. Neurons with graded response properties have collective computational properties like those of two-state neurons. In *Proceedings of the National Academy of Sciences*, volume 81, pages 3088–3092. Washington : The Academy, 1984.

[13] A.J. Ijspeert. Synthetic approaches to neurobiology: review and case study in the control of anguiliform locomotion. In D. Floreano, F. Mondada, and J.-D. Nicoud, editors, *Proceedings of the Fifth European Conference on Artificial Life, ECAL99*, pages 195–204. Springer Verlag, 1999.

[14] A.J. Ijspeert. A 3-D biomechanical model of the salamander. In J.C. Heudin, editor, *Proceedings of the Second International Conference on Virtual Worlds , Paris, France, 5-7 July*. Springer Verlag, 2000. To appear.

[15] A.J. Ijspeert. A connectionist central pattern generator for the swimming and trotting of a simulated salamander. *Submitted to Biological Cybernetics*, 2000.

[16] A.J. Ijspeert and M. Arbib. Visual tracking in simulated salamander locomotion. 2000. Submitted to the Sixth International Conference of The Society for Adaptive Behavior (SAB2000), Paris, France, 11-15 September 2000.

[17] A.J. Ijspeert, J. Hallam, and D. Willshaw. From lampreys to salamanders: evolving neural controllers for swimming and walking. In R. Pfeifer, B. Blumberg, J.-A. Meyer, and S.W. Wilson, editors, *From Animals to Animats, Proceedings of the Fifth International Conference of The Society for Adaptive Behavior (SAB98)*, pages 390–399. MIT Press, 1998.

[18] A.J. Ijspeert, J. Hallam, and D. Willshaw. Evolving swimming controllers for a simulated lamprey with inspiration from neurobiology. *Adaptive Behavior*, 7(2):151–172, 1999.

[19] H. Kimura, S. Akiyama, and K. Sakurama. Realization of dynamic walking and running of the quadruped using neural oscillators. *Autonomous Robots*, 7(3):247–258, 1999.

[20] R.D. Quinn and K.S. Espenschied. Control of a hexapod robot using a biologically inspired neural network. In R.D. Beer, R.E. Ritzmann, and T.M. McKenna, editors, *Biological neural networks in invertebrate neuroethology and robotics*. Academic Press, 1993.

[21] G. Taga, Y. Yamaguchi, and H. Shimizu. Self-organized control of bipedal locomotion by neural oscillators in unpredictable environment. *Biological Cybernetics*, 65:147–159, 1991.

[22] T.L Williams. Phase coupling by synaptic spread in chains of coupled neuronal oscillators. *Science*, 258:662–665, 1992.

Proceedings of the International Symposium on
Adaptive Motion of Animals and Machines,
Montreal, Aug.8-12, 2000

Evolutionary Creation of an Adaptive Controller for a Legged-Robot: A Dynamically-Rearranging Neural Network Approach

Akinobu Fujii[1] Akio Ishiguro[1] Kei Otsu[1] Yoshiki Uchikawa[1]
Takesi Aoki[2] Peter Eggenberger[3]

[1]Dept. of Computational Science and Engineering, Nagoya University
Nagoya 464-8603, Japan, {akinobu, ishiguro, kei, uchikawa}@cmplx.cse.nagoya-u.ac.jp
[2]Nagoya Municipal Industrial Research Institute, Nagoya 456-0058, Japan, aoki@nmiri.city.nagoya.jp
[3]ATR Human Information Processing Research Laboratories, Kyoto 619-0288, Japan, eggen@hip.atr.co.jp

Abstract

As there exists highly complicated interaction dynamics, it is in general extremely difficult to design controllers for legged robots. Therefore, the Evolutionary Robotics is one of the most promising approaches since it can automatically construct controllers by taking embodiment and the interaction dynamics with the environment into account. Although this approach has such advantages, there still exists several problems that have to be solved. One of the critical problems is known as the gap problem; the controller evolved in the simulator show not the same fitness as those in the real world due to unforeseen perturbation. Therefore, it is highly necessary to establish a method enables to efficiently construct adaptive controllers that can cope with different situation. For this purpose we introduce the concept of neuromodulators, allowing to evolve neural networks which can adjust not only the synaptic weights, but also the structure of the neural network by blocking and/or activating synapses or neurons. We apply this concept to create an adaptive legged–robot controller which realizes not only follow the desired walking velocity but also regulate the amount of the torque output applied to each joint for energy efficiency according to the current situation.

1. Introduction

egged o ots s o sigini cant ad antages o e ee ed o ots since t e can t a e se in ne en and nst ct ed en i onments is ig mo i it stems om t e act t at in cont ast to ee ed o t acked o ots egged o ots *discretely* contact it t ei en i onments ia t ei egs is o e e ine ita ca ses ig com icated d nam ics et een t e o ots and t ei en i onments s it is in gene a ext eme di c t to design cont o e s o egged o ots

o a a io s met ods a e een o osed to const ct egged o ot cont o e s i st e e st dies a e in estigated t e design o cont o e s conside ing t e inte action d namics it t e en i onments [1 4 1 18] o e e since t e a o e a oac es a e ased on a and c a ted manne it is estiona e et e o not t ese a oac es i e sti easi e (i e easi im emented) as t e com exit o t e desi ed task and t e inte action d namics inc eases

n t e ot e and ecent t e *Evolutionary Robotics* ( ) a oac as een att acting a ot o conce n in t e e d o o otics and a ti cia i e [6 16] n cont ast to t e con entiona a oac es e e designe s a e to const ct cont o e s in a to do n manne t e met ods in t e a oac a e signi cant ad antages since t e can a tonomo s and e cient const ct cont o e s taking *embodiment* (e g sica si e and s a e o o ots senso moto o e ties and dis osition etc) and t e *interaction dynamics* et een t e o ot and its en i onment into acco nt

n t is a e an e o tiona c eation o an *adaptive* ne o conto e o a egged o ot is in estigated n o de to const ct ada ti e con t o e s e oc s on c eation o eed ack oo s et een t e o ot and its en i onment ased on its em odiment and t ei eg ation mec anisms as t e ta gets to e e o ed instead o e o ing s na tic eig ts as in t e con entiona a oac es o t is end e int od ce t e con ce t o *neuromodulators* a o ing to e o e ne a net o ks ic can ad st not on t e s na tic

eig ts t a so t e st ct e o t e ne a net o k ocking and o acti ating s na ses o ne ons acco ding to t e c ent sit ation

e e as t e initia ste o t e in estigation e attem t to c eate a sing e eg cont o e ic e a i es not on o o t e desi ed a king e oc it t a so eg ate t e amo nt o t e to e o t t a ied to eac oint o ene g e cienc nde a io s od eig ts s t e e exists no t eo a o t o s c d namic ne a net o k can e const cted t e e o tiona a oac is t e met od o c oice to ex o e t e inte actions et een t e ne omod ato s ece to s s na ses and ne ons im ations a e ca ied o t to e i t e easa i it o t e o osed met od

2. Issues in the Evolutionary Robotics Approach

n t e a oac es a ti cia ne a net o ks a e ide sed to const ct cont o e s o a tonomo s mo i e agents eca se t e can gen e a i e a e non inea and noise to e ant n ot e ad antage o ne a net o k d i en o ots is t at a ne a net o k is *low level description* o a cont o e o e ecise it di ect ma s sen so eadings onto moto o t ts e to t is ic eme gent o e ties can e ex ected

t o g t e a oac as t e a o e ad antages t e o o ing d a acks sti exist

i st as t e com exit o t e desi ed task in c eases it ecomes signi cant di c t to e o e t e o e cont o e in one go is o em is sometimes e e ed as t e *bootstrap problem* [16]

s it is demanded to de e o a met odo og ic can a tomatica s nt esi e mo e com ex e a io t an t ose designed and n o de to a e iate t is o em se e a a t o s int od ced t e conce t o *shaping* [3] *canalization* [16] *incremental evolution* [2] and so o t

econd as t e e o tion in t e ea o d is time cons ming sim ations a e sed instead to e o e t e cont o e in sim ated en i onments and t e est indi id a s a e tested in t e ea o d e a o t is com ined a oac is t at e o ed agents in sim ated en i onments o ten s o a sigini cant di e ent e a io in t e ea o d d e to n o eseen e t ations since t e tend to o e ada t to t e gi en en i onments t o g t e e o tiona ocess n ot e o ds a *gap* et een t e sim ated and ea en i onments exists e e o e it is indis ensa e to esta is a met od ic ena es t e e o ed cont o e s ada t not on to se eci c en i onments t a so to en i onmetna e t ations

n t e o o ing e a tic a dea it t e second o em No t e t e o o ing estion a ises o can o ots ecogni e t ei c ent sit ation and eg ate t ei e a io a o iate

a t o t e ans e ma e t at in t e st dies so a e made in no attem t as made to se ect di ect o ada tation c anging t e settings o t e ex e iments s e en a sim e t e mostat needs senso eed ack to e a e to cont o t e tem e at e an essentia ing edient to an ada ti e cont o e a e cont o ing senso s to gi e t e ne a cont o e data o to c ange its c ent state to a ds t e good one

o const ct o st cont o e s against en i on menta c anges in t is st d e oc s on c eation o eed ack oo s and t ei eg ation mec anisms as t e ta get to e e o ed instead o e o ing t e s na tic eig ts(see ig e 1) e can s ccess e o et e a o iate eg ation mec anism e can ex ect ig ada ta i it against en i on menta e t ations

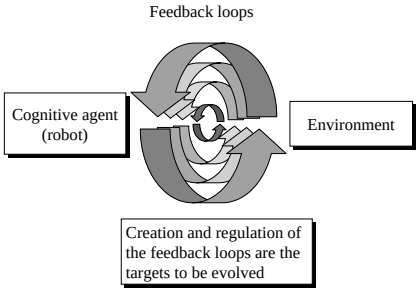

Figure 1: Feedback loops between the robot and its environment.

n inci e t e in o mation ca ied t e eed ack oo s can a e t e o o ing t o e ects i t e one c anges t e eig ts o t e s na ses and t e ne ons t es o ds o one a te s d namica t e st ct e o t e ne a net o k itse e estion is o can t is e done and can s c met ods e sed to so e t e a o e o em

nte esting ne oscienti c es ts s ggest t at io ogica net o ks not on ad st t e s na tic eig ts t a so t e ne a st ct e ock ing o acti ating s na ses o ne ons t e se o signa ing mo ec es so ca ed *neuromodulators* [13] ese ndings stem om in estigations made it t e o ste s stomatogast ic ne o s s stem in ic ce tain acti e ne ons di se ne omod

ato s ic t en ea ange t e net o ks Note t at t e e ect o a ne omod ato de ends not on on t eses s stances t a so on t e s eci c ece to s ic a e di e ent ex essed in di e ent ce s

e e ease o t e ne omod ato s de ends on t e acti it o t e ne ons and t e e o e di e ent senso in ts ma ca se di e ent atte ns o e eased ne omod ato s s s c d namic mec anisms ie d ema ka e ada tation in i ing o ganisms t e o osed a oac not on ca ies omise o a ette nde standing o ada ti e net o ks t t e can e a so a ied to ea o d o ems as e a ead s o ed in t e e io s o k [5 11]

3. Lessons from the Biological Findings

3.1. Dynamic rearrangement in the biological nervous system

n estigations ca ied o t on t e o ste s stom atogast ic ne o s s stem s ggest t at io ogica ne o s s stems a e a e to d namica c ange t ei st ct e as e as t ei s na tic eig ts [13]

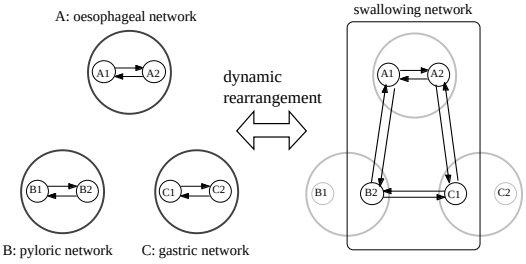

Figure 2: Dynamically–rearrangement of a lobster's stomatogastric nervous system.

is stomatogast ic ne o s s stem main con sists o an *oesophageal* a *pyloric* and a *gastric* net o k No ma t ese t ee indi id a net o ks s o t ei o n inde endent osci ato e a io s t in t e moment a o ste is eating t e net o ks a e integ ated and econst cted to a ne one t e s a o ing net o k in ic ce tain ne ons and connections a e exc ded and o me inac ti e connections a e acti ated (see ig e 2)

ecent st dies in ne o sio og s o ed ne omod ato s (e ea te N s) a a c cia o e to eg ate t is ema ka e enomenon (e g c anging o e ties o s na ses as e as ne ons)

3.2. Neuromodulators

N s a e s stances t at can d namica in ence se e a o e ties o s na ses as e as ne ons and t e e o e t e nction o a ne a net o k n cont ast to *neurotransmitters* (N s) t e e ect o N s s eads s o e and asts onge N s c ange t e ocessing c a acte istics o ne a net o ks a ecting t e mem ane otentia t e ate o c anging t e s na ses (i e in ence on ea ning mec anisms) and ot e a amete s ica N s a e *acetylcholine norepinephrine serotonin dopamin* (a a e a so sed as N s) *somatostatine* and *cholecystokinine* (ot a so sed as o mones in t e man od) and man sma oteins t o g t ese s stances a e e eased in a ess oca manne t an N s t e e ects can e ite s eci c is s eci cit comes om s eci c ece to s on t e ne ons and t ei s na ses

ese N s stem eit e oca om t e ne a net o k itse o om s eci c s co tica n c ei e oca e ease o N s de ends on t e acti it o t e oca ne a net o k itse n t e ot e and s co tica n c ei as t e oc s coe e s (*noradrenergic innervation*) t e ent a tegmenta a ea (*dopaminergic innervation*) o t e asa o e ain n c ei (*cholinergic innervation*) send ne o mod ato axons to co tica st ct es to e ease N s om axona a icosities ic is ca ed o me t ansmission an ications in ne o science s o t e im o tance o N s o d namic ea angement o ne ona mod es [13] o o ea ning and memo (s itc ing et een ea ning and eca mode) [8]

n t is st d e im emented t e o o ing o e ties

- d namic c ange o a ne on s t es o d
- d namic ocking o s na ses (ossi ne ons)
- d namic c ange o t e in i ito o excita to o e ties o a s na se
- d namic mod ation o s na tic eig ts (i e ea ning)

4. Proposed Method

4.1. Basic concept

e asic conce t o o o osed d namica ea anging ne a net o ks (e ea te NN) is sc ematica de icted in ig e 3 s in t e g e n ike t e con entiona ne a net o ks e ass me t at eac ne on can otentia di se its s eci c (i e genetica dete mined) N s ac co ding to its acti it and eac s na se as e ce to s o t e di sed N s e a so ass me t at eac s na se inde endent inte ets t e ecei ed N s and c anges its o e ties (e g s na tic eig t) e a o t ese c anges exe ted on t e s na ses is a so genetica dete mined

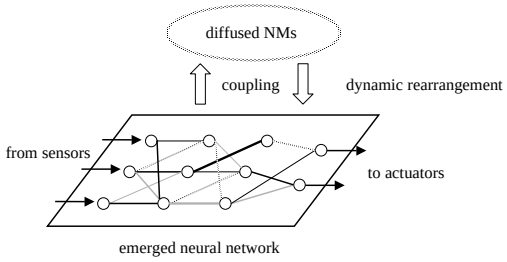

Figure 3: Basic concept of the DRNN.

se ecting o eg ato eed ack oo s (c c i ca inte action et een t e di sion and eaction o N s) e ex ect to e a e to e o e ada ti e ne a net o ks ic s o not on a seam ess t ans e om sim ations to t e ea o d t a so o stness against en i onmenta e t a tions (in t e g e t e t ick and t in ines denote t e connections eing st engt ened and eakened N s es ecti e)

n s mma in cont ast to t e con entiona a oac t at e o es s na tic eig ts and ne on s ias o ne o cont o e s in t is a oac e e o e t e o o ing mec anisms

- i sion o N s (en ic t e o N s a e di sed om eac ne on)
- eaction to N s (o do t e ece to s on eac s na se inte et t e ecei ed N s and modi t e s na tic o e t)
- Net o k a c itect e (t e n m e o in te ne ons and o to connect among t e senso inte and moto ne ons)

o dete mine t e a o e a amete s e se a e netic go it m ( ) etai ed ex anation on o a is im emented is gi en ate

4.2. Application problem

4.2.1. Task

aim is to c eate an ada ti e cont o e o a m ti egged o ot t at can a o iate co e it di e ent sit ation o e e in gene a it is ext eme di c t to e o e t e o e cont o e in one go

s in o de to in estigate t e easi i it o t e NN a oac in t is st d e attem t to const ct an ada ti e cont o e o a sing e egged o ot as t e initia ste o t e in estigation e e t e task o t e o ot is to not on o o t e de si ed a king e ocit t a so eg ate t e amo nt o t e to e o t t a ied to eac oint o en e g e cienc nde a io s od eig ts

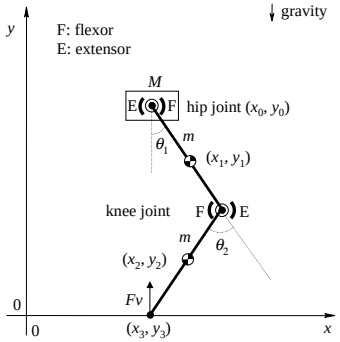

Figure 4: Model of the single-legged robot.

4.2.2. Single–legged robot model

e mode o t e sing e egged o ot is sc emat ica i st ated in ig e 4 e o ot consists o a od and t o sica inks (i e t ig and s ank) it t o oints (i e i oint and knee oint) ese oints a e a inde endent d i en ai s o antagonistic act ato s (i e *flexor* and *extensor*) in o de to take not on static to e t a so t e sti ness o t e oints (o ene g e cienc) into acco nt

e i ang e (θ_1) is meas ed acco ding to t e de iation om t e e tica ine e ass me t at t e i oint can otate et een an ang e o $-60°$ (extension) and $60°$ (exion) n t e ot e and t e knee ang e (θ_2) is meas ed it e e ence to t e t ig osition e e t e knee extension is an ang e o $0°$ and knee exion $-120°$

e ass me t at eac oint is e i ed it a ai o (ante io ext eme osition) and (oste io ext eme osition) senso s ic in o m

t e c ent i and knee ang es and a so e i ed it a to e senso to meas e t e a ied static to e n addition t e e exist a oad senso at t e ti o t e eg to detect t e amo nt o t e e tica o ce om t e g o nd (F_v in t e g e)

4.2.3. DRNN controller

ig e 5 sc ematica e esents t e st ct e o t e NN cont o e o t e sing e egged o ot n t e g e t e ne ons it S and M denote t e senso and moto ne ons es ecti e e ne on S_8 is a ne on ic is a a s acti ated (i e o t t a e o 1 0) to enco age an moto acti it e en nde no senso in ts e est o t e ne ons a e inte ne ons etai ed ex ana tion on o to c eate t e cont o e i e gi en in t e next section

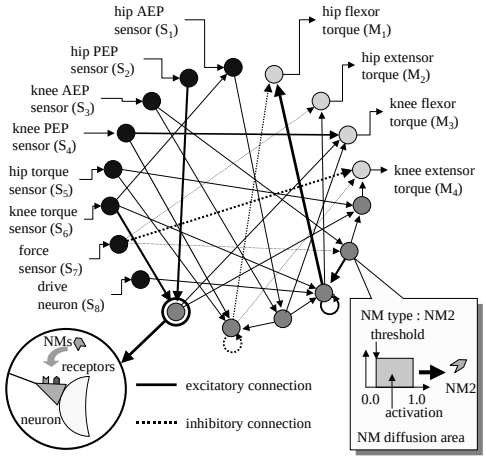

Figure 5: Controller for the single-legged robot.

s o t e ne a d namics e se a *leaky integrator* mode ic is ex essed as

$$\tau_i \frac{du_i}{dt} = -u_i + \sum_j w_{ij} \cdot a_j - \theta_i \quad (1)$$

$$a_i = \frac{1}{1 + \exp(-0.5u_i)} \quad (2)$$

e e a_i is t e acti it o ne on i and w_{ij} e esents t e s na tic eig t o a connection om ne on j to ne on i u_i is t e mem ane oten tia o ne on i and τ_i denotes t e time constant o t e mem ane otentia θ_i is t e t es o d o t e ne on s acti it e se a standa d sigmoida nction to imit t e ne on s acti it

4.3. Encoding scheme for the DRNN

ot t e net o k a c itect e and t e a o di sion and eaction to N s in t e NN a e c ose e ated to not on t e gi en task t a so t e em odiment and t e inte action d nam ics it t e en i onment s it is e e a e to a tomatica dete mine t ese a amete s t o g t e e o tiona ocess n o de to exc de os si e es osition on t ese a amete s e int o d ce t e conce t o t e *developmental process*

4.3.1. Structure of the Genotype

e genot e o t e NN (e ea te net o k genot e) is ex essed as a ina it st ing and is com osed o a set o ocks eac ock co e s onding to t e genot e o a sing e ne on (ne on genot e) o t e ease o nde standing e st ex ain t e st ct e o t e ne on genot e in detai

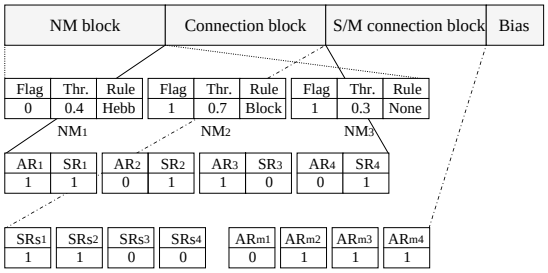

Figure 6: Structure of the neuron genotype.

ig e 6 s o s an exam e o t e ne on geno t e s in t e g eac ne on genot e con sists o t e ias gene and t ee ocks *NM block connection block* and *S/M connection block* e ias gene e esents t e t es o d o t e ne on N connection and connection ocks con tain genetic in o mation ic s eci t e o o ing o e ties o t e co es onding ne ons e s ecti e

(a) *NM block*

e genes contained in t is ock dete mine t e a o di sion and eaction to t e N s s in t e g e t is ock is com osed o a se ies o t e a amete set (*flag threshold rule*) and eac set is es onsi e o one s eci c t e o t e N s s in t is exam e at most t ee t es o N s can e di sed om t e ne on conce ned

e a amete s *flag* and *threshold* dete mine n de ic condition t e co es onding t e o N is di sed om t e ne on conce ned t e ne on s acti it exceeds t e genetica dete mined t es o d a e and a so t e *flag* is acti e t e co es onding N i e immediate di sed e e e ass me t at t e concent ation o t e di

sed N (denoted as $c(NM_k)$) is o o tiona to t e a ti ation a e o t e ne on conce ned (a_i) it in t e di si e a ea

n t e ot e and t e a amete *rule* dete mines o t e ece to on t e s na ses ic o t g o om t e ne on conce ned inte ets t e co es onding t e o N and modi es t e s na tic o e ties n o de to ed ce t e genetic in o mation e e e ass me t at a t e s na ses o t g o ing om a gi en ne on a e t e same set o t e ece to s

ac a amete *rule* can take one o t e o o ing o t es o mod ation *Hebbian learning* *anti–Hebbian learning* *non–learning* and *blocking* (i e exc ding t e s na se) es ecti e

ose t at t e e exists k t es o ece to s on a gi en s na se t e o o ing e ation is sed o t e d namic mod ation o t e s na tic eig ts as

$$c_{total}(NM_k) = \sum_N c(NM_k) \quad (3)$$

$$s = \sum_k R_{ij}(NM_k) \cdot c_{total}(NM_k) \quad (4)$$

$$w_{ij}^{t+1} = \begin{cases} w_{ij}^t + \eta|s|(-1 - w_{ij}^t)a_i a_j & \text{for } s < 0 \\ w_{ij}^t & \text{for } s = 0 \\ w_{ij}^t + \eta|s|(1 - w_{ij}^t)a_i a_j & \text{for } s > 0 \end{cases} \quad (5)$$

e e $c_{total}(NM_k)$ e esents t e tota concent a tion o t e di sed N o t e k in t e net o k at a gi en time and N is t e n m e o t e ne ons η is t e eaning ate and $R_{ij}(NM_k)$ denotes t e a amete ic dete mines o t e s na se con ce ned modi es its o e t en t e N o t e k is com ined it t e ece to on it o t is e se +1 1 and 0 to ex ess *Hebbian learning* *anti–Hebbian learning* and *non–learning* es ec ti e

e ass me t at t e *blocking* mod ation as t e ig est io it among t e o t es o mod a tion s i a ece to ic ex esses ocking is acti ated t e co es onding s na tic eig ts i e o ci set to e o not it standing ot e ece to s states

( ) *Connection block*

is ock is es onsi e o t e connection es ta is ment among t e ne ons s in g 6 t is ock ossesses a se ies o t e a amete set (AR_i SR_i) e e AR_i and SR_i stand o an axona and s na tic ece to s es ecti e t e a amete AR_i is acti ated t e ne on conce ned o tg o s axons ac AR (SR) as its o n ID n m e and t e AR can make connections on it t e SR it t e same ID n m e

(c) *S/M connection block*

is ock dete mines t e connection esta is ment et een t e co es onding ne on and t e senso and o moto s e i ed it t e o ot e ass me t at eac senso (moto) as its s e cia dedicated axona (s na tic) ece to ARs_i (SRm_i) and t is ece to is a a s acti e t e ne on conce ned acti ates t e gene SRs_i (ARm_i) t en t is ne on can connect it t e senso it ARs_i (t e moto it SRm_i)

4.3.2. Genetic operators

ac gene in t e ne on genot e is andom c anged it t e es eci ed o a i it n ad dition to t is as o t e N ock and connection ock in eac ne on genot e e se s ecia dedicated m tation o e ato s andom *insertion* and o *deletion* o t e a amete set (i e (*flag threshold rule*) o t e N ock (AR_i SR_i) o t e connection ock) is a ied in o de to ex o e t e a o iate n m e o N t es and connec tions it ot e ne ons

e to t e a o e inse tion and de etion o e ato s eac ne on genot e can a e di e ent engt onse ent t e engt o a net o k genot e can di e om one to anot e s in t is st d e se a *mixing pot method* [15] as a c osso e o e ato es ite o its sim icit t is o e ato can e cient dea it t e n m e o ne ons as t e ta get to e e o ed (detai ed de sc i tion o t is met od see [15])

5. Results

s mentioned e o e it ecomes signi cant di c t to e o e t e o e cont o e in one go as t e com exit o t e desi ed task inc eases o a e iate t is e int od ce t e conce t o an in c ementa e o tion n t is st d e st e o e t e cont o e nde t e o o ing e a ation c ite ion

$$fitness_1 = \frac{1.0}{D^* - D} \times \sum_{i=1}^{2} \int_0^{T_{max}} |\dot{\theta}_i| dt \quad (6)$$

e e D^* and D denote t e desi ed and es tant a king distance es ecti e $\dot{\theta}_i$ is t e ang a e ocit o oint i and T_{max} e esents t e d ation o t e e a ation ocess e second te m o t e ig t and side o t e e ation is o enco aging an osci ato e a io

te e o ing d ing 200 gene ations nde t is ttness nction t e o ation o tained in t e ast gene ation is sed o t e second stage o t e e o tion as t e initia o ation e tness nction sed in t e second stage is ex essed as

$$fitness_2 = \frac{fitness_1}{E_{con}} \tag{7}$$

$$E_{con} = \sum_{i=1}^{2} \int_0^{T_{max}} \{\delta(T_i\dot{\theta}_i) + {T_{fi}}^2 + {T_{ei}}^2\} dt \tag{8}$$

$$T_i = T_{fi} - T_{ei} \tag{9}$$

$$\delta(x) = \begin{cases} x & \text{for } x \geq 0 \\ 0 & \text{for otherwise} \end{cases} \tag{10}$$

e e E_{con} is t e amo nt o t e ene g con s med d ing t e e o tiona ocess T_{fi} and T_{ei} denote t e exo and extenso to e a ied to oint i es ecti e e od a amete s sed in t e o o ing sim ations a e isted on a e 1[1]

o e i t e ada ta i it o t e NN in t e sim ations eac indi id a is tested nde a io s od mass (M=1 8kg 2 8kg) and t e a e aged t ness a e is sed o t e e a ation

Table 1: Body parameters of the single–legged robot.

a t	engt	mass
od		1 80 2 80[kg]
t ig	0 1[m]	0 15[kg]
s ank	0 1[m]	0 15[kg]

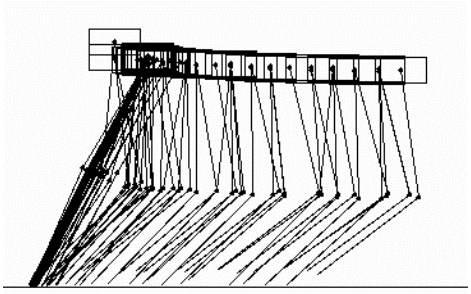

Figure 7: Resultant trajectory of the best evolved agent in the case of M=1.8kg.

ig e and 8 e esent t e es tant t a ecto o t e est e o ed agent nde t e ad mass o M=1 8kg and 2 8kg es ecti e ig e and 10 a e t e t ansition o t e to e o t ts at t e aist oint nde t e same condition om t e

[1]For simplicity, the body is represented as a material particle (i.e. no physical entity) with mass.

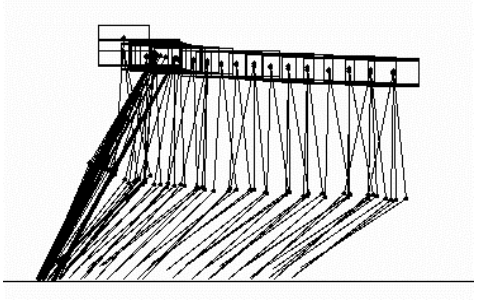

Figure 8: Resultant trajectory of the best evolved agent in the case of M=2.8kg.

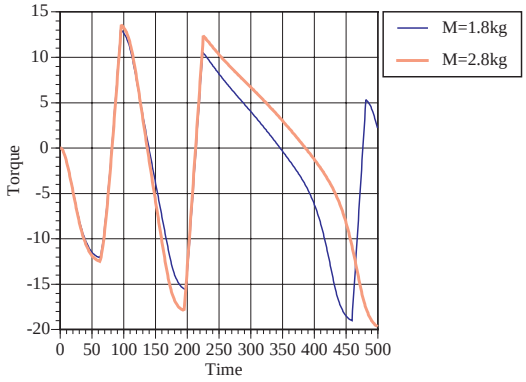

Figure 9: Transition of the torque output at the beginning of walking.

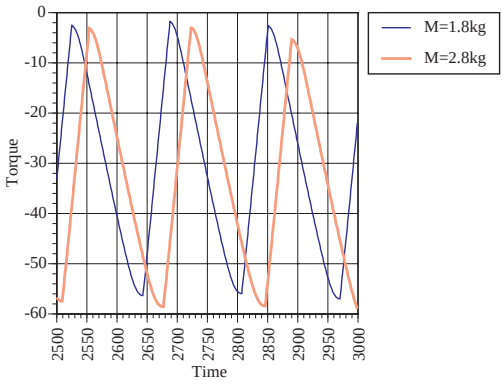

Figure 10: Transition of the torque output under the steady–state walking.

g es it is nde stood t at i es ecti e o t e di e ent od mass t e o ot can s ccess co e a most t e same distance ad sting t e amo nt o t e to e o t t at t e oints e o se ed t at di e ent t es o t e N s e e di sed ac co ding to t e senso in ts in o de to eg ate t e to e o t ts a ied to eac oint

6. Conclusions

n t is st d e o tiona c eation o an ada ti e cont o e o a sing e egged o ot as in es tigated o t is end e int od ced t e conce t o t e d namica ea anging nction in t e i o ogica ne o s s stems e e imina sim ation es ts e e enco aging e ex ect t is conce t i o ide a met odo og o not on seam ess t ans e om t e sim ated to t e ea en i onments t a so e o tiona c eation o con t o e s it ig ada ta i it etai ed ana sis o t e e o ed NN is c ent nde in esti gation e i a so antitati e in estigate t e ada ta i it o t e e o ed cont o e s com a ed it t e ones o t e con entiona a oac e e t e s ana tic eig ts a e t e ta gets to e e o ed n t e t e e i a t is conce t to i ed and ad ed o ots o t is ose e a e c ent de e o ing a 3 sim ato it t e se o a gene a ose d namics sim ato (namic na sis and esign stem)

References

[1] R. Beer, J. Chiel, and L. Sterling. Evolution of plastic neurocontrollers for situated agents. *An artificial insect, American Scientist,* **79***, 444–452,* 1989.

[2] D. Cliff, I. Harvey, and P. Husbands. Incremental evolution of neural network architectures for adaptive behaviour. *Proc. of the First European Symposium on Artificial Neural Networks (ESANN93), 39–44*, 1993.

[3] M. Colombetti and M. Dorigo. Training agents to perform sequential behavior. *Adaptive Behavior,* **2(3)***, 247–276*, 1994.

[4] H. Cruse, C. Bartling, J. Dean, M. Dreifert, T. Kindermann, and J. Schmitz. Walking: a complex behavior controlled by simple networks. *Adaptive Behavior,* **3***, 385–418*, 1995.

[5] P. Eggenberger, A. Ishiguro, S. Tokura, T. Kondo, T. Kawashima, and T. Aoki. Toward seamless transfer from simulated to real worlds: A dynamically–rearranging neural network approach. *Proc. of the Eighth European Workshop on Learning Robot (EWLR-8), 4–13*, 1999.

[6] D. Floreano and F. Mondada. Automatic creation of an autonomous agent: Genetic evolution of a neural-network driven robot. *Proc. of the 3rd International Conference on Simulation of Adaptive Behavior, MIT Press, 421–430*, 1994.

[7] Floreano, D. and Mondada, F. (1996). Evolution of plastic neurocontrollers for situated agents. *From animals to animats 4: Proc. of the 4rd International Conference on Simulation of Adaptive Behavior, MIT Press, 401–411.*

[8] M. Hasselmo. Neuromodulation and cortical function: modeling the physiological basis of behavior. *Behavioral Brain Research,* **67***, Elsevier Science B.V., 1–27*, 1995.

[9] S.L. Hooper and M. Moulins. Switching of a neuron from one network to another by sensory–induced changes in membrane properties. *SCIENCE,* **244***, 1587–1589*, 1989.

[10] Husbands, P., Smith, T., O'Shea, M., Jakobi, N., Anderson, J., and Philippides, A. (1998). Brains, gases and robots. *In Proc. ICANN98, Springer–Verlag, 51–63.*

[11] A. Ishiguro, T. Kondo, Y. Uchikawa, and P. Eggenberger. Autonomous robot control by a neural network with dynamically–rearranging function. *Proc. of the 11th SICE Symposium on Decentralized Autonomous Systems, 213–218 (in Japanese)*, 1999.

[12] Jacobi, N., Husbands, P., and Hervey, I. (1995). Noise and the reality gap: The use of simulation in evolutionary robotics. *Third European Conf. on Artificial Life (ECAL95), Advances in Artificial Life, Springer, 704–720.*

[13] P. Meyrand, J. Simmers, and M. Moulins. Construction of a pattern–generating circuit with neurons of different networks. *NATURE,* **351***-2MAY, 60–63*, 1991.

[14] Miglino, O., Lund, H., and Nolfi, S. (1995). Evolving mobile robots in simulated and real environments. *Artificial Life 2, 417–434.*

[15] K. Nakano, H. Hiraki, and S. Ikeda. A learning machine that evolves. *Proc. of International Conference on Evolutionary Computation (ICEC95), 808–813*, 1995.

[16] S. Nolfi. Evolving non–trivial behaviors on real robots: A garbage collecting robot. *Robotics and Autonomous System,* **22***, 187–198*, 1997.

[17] G. Taga, Y. Yamaguchi, and H. Shimizu. Self-organized control of bipedal locomotion by neural oscillators in unpredictable environment. *Biological Cybernetics,* **65***, 147–159*, 1991.

[18] T. Wadden and Ö. Ekeberg. A neuro-mechanical model of legged locomotion: single leg control. *Biological Cybernetics,* **79***, 161–173*, 1998.

Proceedings of the International Symposium on
Adaptive Motion of Animals and Machines,
Montreal, Aug.8-12, 2000

On Nonlinear Dynamics that Generates Rhythmic Motion with Specific Accuracy

Kei SENDA[1] **and Tsuyoshi TANAKA**[2]

[1]Dept. of Aerospace Eng., Osaka Prefecture Univ., Sakai, Osaka 599-8531, Japan, senda@aero.osakafu-u.ac.jp
[2]Graduate School of Eng., Osaka Prefecture Univ.

Abstract

This paper presents a method to generate rhythmic and cyclic motions observed in locomotion of animals or insects by using nonlinear dynamics, e.g., recurrent neural network (RNN). The proposed method enables to specify the approximation accuracy of the generated trajectory to the target trajectory though RNNs cannot easy to specify it. The method is based on a nonlinear oscillator generating cyclic motion and a the Fourier series. The realized dynamics has the desired trajectory as a limit cycle. A realization using neural networks is also shown. Effectiveness of the proposed method is examined by a numerical simulation where a space robot changes its orientation by the cyclic motion of the manipulator.

1. Introduction

Rhythmic and cyclic motions observed in locomotion, fluttering, and swimming of animals and insects are memorized in their brains or nervous networks. Those motion memories would not be stored as time histories but as limit cycles in nonlinear dynamical systems. For the stable generation of the motion, the cyclic trajectory is requested to be a steady attractor, which is called a dynamic associative memory (DAM). This study discusses the methodology to generate the rhythmic and cyclic motions of animals or robots using the DAMs.

Recurrent neural networks (RNNs) have been used generally to realize the DAMs and a back-propagation (BP)[1, 2] was proposed for the RNN. A multi-layered NN, e.g., multi-layered perceptron, can approximates any piecewise continuous function within a specific accuracy if the neural network (NN) has hidden units as many as necessary[3]. On the other hand, RNNs are not sure to express the desired dynamics nor to guarantee their learning convergence.

Consequently, this study proposes a methodology to realize the DAM that generates the desired rhythmic motion. The proposed method realizes a DAM based on a Fourier series and a standard oscillator with nonlinear units generating sinusoidal motion. The achieved DAM can generate any continuous cyclic trajectory, which is steady and multivariable vector function. It also makes the desired rhythmic motion be a limit cycle and attracts the trajectories started from almost all initial states to the desired. Moreover, the design procedure is established that ensures the DAM within the specific approximation accuracy evaluated by the mean squared error. Further, the DAM can be realized by using RNNs and LNNs.

The rest of this paper is organized as follows. Section 2 defines the desired dynamics that should be realized by DAMs and shows problems of the existing RNN, which is designed as in references[1, 2]. Section 3 represents the proposed DAM and illustrates its feasibility through a numerical simulation of a 1-degree-of-freedom (DOF) system. In the same section, a realization of the DAM using NNs is also mentioned. In section 4, effectiveness of the proposed method is examined by a numerical simulation where a space robot changes its orientation by the cyclic motion of the manipulator. Finally, concluding remarks are given by section 5.

2. Desired DAM and Problems in RNN

2.1. Specifications of desired DAM

This study uses DAMs to store the rhythmic and cyclic motions observed in locomotion, fluttering, and swimming of animals and insects. The followings are the specifications of the DAMs.

The desired cyclic trajectory is desired to be an attractor so as to start the trajectory from any initial state. It is also to be steady so as not to change its path. Hence, the desired cyclic trajectory is requested to be

a steady limit cycle.

For a desired trajectory $\psi(t)$ with a period T, an allowable trajectory $\theta(t)$ is

$$\theta(t) = \psi(\tau) \tag{1}$$

where $\tau = \alpha(t)t + \Delta t$ must be a monotone increase function of t, $\alpha(t) \simeq 1$, and the phase angle $\phi \stackrel{\triangle}{=} \Delta t/T$ is in $0 \leq \phi < 2\pi$. This requests the generated cyclic trajectory has an almost constant period and any phase angle to the desired trajectory.

Multivariable vector trajectories should be generated by the DAM for locomotion and so on where many joints are moved. For the purpose, independent limit cycle for each joint is not good enough, but they must be synchronized.

It is better to specify the approximation accuracy of the generated trajectory to the desired. The DAM must be able to learn the desired trajectory by using some learning method. In addition, an assurance of the learning convergence is desirable.

One would like to start motion from almost any state because initial joint states are various in locomotion. For the purpose, the desired trajectory is to be a limit cycle with a large convergence region in state space.

The DAM realized by nonlinear differential equations is good for a robot control. However, the neural network realization is desired to understand the brains and the nervous systems, where the NN uses only neuron units observed in living bodies.

2.2. Problems in RNN realization

Recurrent neural networks (RNNs) have been generally studied to realize the DAMs. The RNNs are used to construct dynamical systems and a recurrent backpropagation (RBP)[1, 2] was proposed for learning. A multi-layered NN, e.g., multi-layered perceptron, can approximates any piecewise continuous function within a specific accuracy if it has hidden units as many as necessary[3]. On the other hand, RNNs are not sure to express the desired dynamics nor to guarantee their learning convergence.

Following references [1, 2], Figure 1 shows a numerical simulation, where a RNN has 20 neural units connected by each other, it has studied the desired trajectory 15,000 times by the RBP, and the trajectory is a constant rate circle with (0.5 0.5) in center and 0.4 in radius. The RNN has formed a limit cycle that attracts the generated trajectories to the desired, where no teaching signals for studying are given to the RNN for the first 5 s. But, the learned trajectory is not the right circle. Consequently, one must discuss if the RNN enable to express the desired dynamics before discussing convergence of learning.

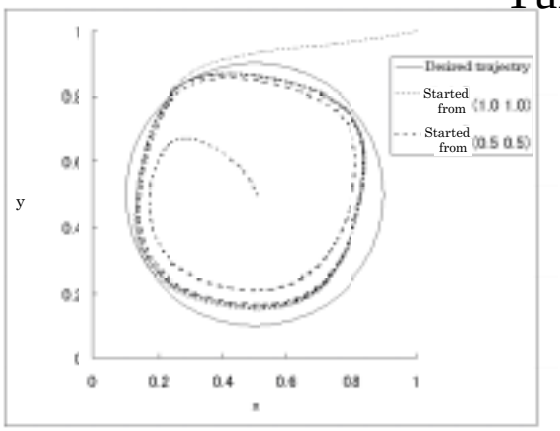

Figure 1: Learned trajectory by RBP following circular trajectory

3. DAM for Any Rhythmic Motion

3.1. Outline of DAM construction

The following outlines the design method of the DAM satisfying the specifications. Firstly, a standard oscillator is equipped to generate a sinusoidal oscillation with the desired period. Higher harmonic oscillators are constructed from the standard oscillator as many as necessary. The desired cyclic trajectory of time is then approximated by a Fourier series and its Fourier coefficients are obtained. The desired cyclic trajectory is generated by multiplying the harmonic oscillations to the Fourier coefficients and summing them up.

3.2. Fourier series approximation

A cyclic function of time t with a period $2L$ is approximated here by using a Fourier series. Assume that the trigonometric function system

$$1,\ \cos\frac{\pi}{L}t,\ \sin\frac{\pi}{L}t,\ \cos\frac{2\pi}{L}t,\ \sin\frac{2\pi}{L}t,\ \ldots \tag{2}$$

of t can be generated by dynamical systems, e.g., oscillators. If the function $f(t)$ with period $2L$ is piecewise smooth on a closed domain $[-L,\ L]$, then a Fourier series is generated from $f(t)$ as:

$$f(t) \sim \frac{a_0}{2} + \sum_{i=1}^{\infty}(a_i \cos\frac{i\pi}{L}t + b_i \sin\frac{i\pi}{L}t) \tag{3}$$

$$\left\{ \begin{array}{rcl} a_0 &=& \dfrac{1}{L}\displaystyle\int_{-L}^{L} f(t)dt \\ a_i &=& \dfrac{1}{L}\displaystyle\int_{-L}^{L} f(t)\cos\dfrac{i\pi}{L}tdt \\ b_i &=& \dfrac{1}{L}\displaystyle\int_{-L}^{L} f(t)\sin\dfrac{i\pi}{L}tdt \end{array} \right. \quad (4)$$

where $a_0,\ a_1,\ a_2, \cdots$ and $b_1,\ b_2,\ \cdots$ are called Fourier coefficients of $f(t)$. One can consider that the function $f(t)$ with period $2L$ is piecewise smooth and continuous because it describes a motion. The Fourier series then converges to $f(t)$ absolutely and uniformly.

The trigonometrical polynomial using finite number of trigonometric functions

$$\begin{aligned} S_n(t) = \quad & \frac{a_0}{2} + a_1\cos\frac{\pi}{L}t + \cdots + a_n\cos\frac{n\pi}{L}t \\ & + b_1\sin\frac{\pi}{L}t + \cdots + b_n\sin\frac{n\pi}{L}t \end{aligned} \quad (5)$$

approximates $f(t)$ with the minimum mean squared error

$$E(f - S_n) = \frac{1}{2L}\int_{-L}^{L}(f(t) - S_n(t))^2 dt \quad (6)$$

when the Fourier coefficients are used as $a_0,\ a_1,\ a_2,\ \cdots,\ a_n$ and $b_1,\ b_2,\ \cdots,\ b_n$. Therefore, one can specify the approximation accuracy of S_n by selecting the number n that makes the mean squared error $E(f - S_n)$ of Eq. (6) less than the specific value.

3.3. Standard oscillator and higher harmonic oscillations

In the previous subsection, one assumes that the trigonometric function system, Eq. (2), is generated by dynamical systems. This subsection presents a method to generate it. A standard oscillator is firstly equipped by von der Pol's equation. Higher harmonic oscillators are then constructed from the standard oscillator as many as necessary.

3.3.1. von der Pol's oscillator

A nonlinear dynamics is realized by von der Pol's oscillator, where the dynamics has a limit cycle with a constant rate trajectory on an unit circle:

$$\frac{d\boldsymbol{x}}{dt} = \left[\begin{array}{c} \dot{x} \\ \epsilon(\omega^2 - \omega^2 x^2 - \dot{x}^2)\dot{x} - \omega^2 x \end{array} \right] \quad (7)$$

$$\boldsymbol{y} = \boldsymbol{\Omega x} \quad (8)$$

where $\boldsymbol{x} = [x\ \ \dot{x}]^T$, $\boldsymbol{x} = [y_1\ \ y_2]^T$ and $\boldsymbol{\Omega} = \mathrm{diag}[1,\ 1/\omega]$, $\epsilon > 0$. To discuss the stability of the oscillator, let a Lyapunov function be

$$V(x, \dot{x}) = \frac{1}{2}(\omega^2 x^2 + \dot{x}^2) \quad (9)$$

then $V(0,0) = 0$ and $V(x, \dot{x}) > 0$ is satisfied when $\boldsymbol{x} \neq \boldsymbol{0}$ or $\dot{\boldsymbol{x}} \neq \boldsymbol{0}$. Since the time derivative is

$$\begin{aligned} \dot{V} &= \omega^2 x\dot{x} + \dot{x}\ddot{x} \\ &= \omega^2 x\dot{x} + \dot{x}(\epsilon(\omega^2 - \omega^2 x^2 - \dot{x}^2)\dot{x} - \omega^2 x) \\ &= \epsilon(\omega^2 - \omega^2 x^2 - \dot{x}^2)\dot{x}^2 \\ &= \epsilon(\omega^2 - 2V)\dot{x}^2 \end{aligned} \quad (10)$$

sign of $\dot{V}$ changes beyond $V = \dfrac{\omega^2}{2}$. Hence V increases in $0 < V < \dfrac{\omega^2}{2}$ with $\dot{V} > 0$ and V decreases in $\dfrac{\omega^2}{2} < V$ with $\dot{V} < 0$. Therefore $V \to \dfrac{\omega^2}{2}$ as $t \to \infty$. It means that the solution would be constrained on the ellipse $\omega^2 x^2 + \dot{x}^2 = \omega^2$. The ellipse is a limit cycle because no singular point exists on the ellipse and the state vector travels with nonzero rate. The parameter ϵ gives the speed of convergence to the ellipse and the convergence becomes quicker the larger ϵ is.

Because the steady state solution is $\omega^2 x^2 + \dot{x}^2 = \omega^2$, substituting it into Eq. (7) yields

$$\dot{\boldsymbol{x}} = \left[\begin{array}{cc} 0 & 1 \\ -\omega^2 & 0 \end{array} \right] \boldsymbol{x} \quad (11)$$

The solution becomes $x(t) = \sin\omega t$ if the initial state is $\boldsymbol{x}(0) = [0\ \ \omega]^T$ at $t = 0$ and one obtains $\dot{x}(t) = \omega\cos\omega t$. Hence the output becomes

$$\boldsymbol{y} = \left[\begin{array}{c} \sin\omega t \\ \cos\omega t \end{array} \right] \quad (12)$$

Because Eq. (7) generates the limit cycle, a solution started from another initial state converges to

$$\boldsymbol{y} = \left[\begin{array}{c} \sin(\omega t + \phi) \\ \cos(\omega t + \phi) \end{array} \right] \quad (13)$$

where a phase ϕ in $0 \leq \phi < 2\pi$ depends on the initial state. Eq. (12) can be considered as the steady state output when $t + \phi/\omega$ is redefined as t.

3.3.2. Higher harmonic oscillators

Higher harmonic oscillators are needed for the Fourier series approximation. For the purpose, a standard oscillator $g(x, \dot{x})$ is firstly equipped by the von der Pol's equation with a frequency $\omega = \pi/L$ and the output $\boldsymbol{y} = [y_1\ y_2]^T = [\sin\omega t\ \ \cos\omega t]^T$ is obtained. A higher

harmonic oscillation with a frequency $j\omega$ is generated by

$$\sin j\omega t = \sum_{i=0}^{(j-1)/2} \left(\begin{array}{c} j \\ 2i+1 \end{array} \right) (-1)^i y_1^{2i+1} y_2^{j-(2i+1)}$$
$$\cos j\omega t = \sum_{i=0}^{j/2} \left(\begin{array}{c} j \\ 2i \end{array} \right) (-1)^i y_1^{2i} y_2^{j-2i} \quad (14)$$

As a result, all the higher harmonic oscillations can be generated by the standard oscillator $g(x, \dot{x})$.

3.4. Generation of rhythmic motion

The cyclic function $f(t)$ with a period $2L$ is approximated by the following procedure.

(i) Evaluate the approximation accuracy of Eq. (5) to $f(t)$ by the mean squared error of Eq. (6) and select the number n. Calculate Fourier coefficients by Eq. (4) and define $\boldsymbol{w}$ as:

$$\boldsymbol{w}^T = \left[\begin{array}{ccccccc} \frac{1}{2}a_0 & b_1 & a_1 & \cdots & b_n & a_n \end{array} \right] \quad (15)$$

(ii) Equip the standard oscillator with the frequency $\omega = \pi/L$ and the amplitude 1 by Eqs. (7) and (8). Any initial state of $\boldsymbol{x} \neq \boldsymbol{0}$ can be selected because the output $\boldsymbol{y}_1 = [y_{11}\ y_{12}]^T$ converges to the standard oscillation from any initial state other than $\boldsymbol{x} = \boldsymbol{0}$. Select $\boldsymbol{x}(0) = [0\ \omega]^T$ as the initial condition when the standard oscillation should follow just after the initial time. Initial condition setting will be discussed later.

(iii) Define new output $\boldsymbol{\eta}$ including the higher harmonic oscillations as:

$$\boldsymbol{\eta} \stackrel{\triangle}{=} \left[1\ \ \boldsymbol{y}_1^T\ \ \boldsymbol{y}_2^T\ \ \cdots\ \boldsymbol{y}_n^T\right]^T \quad (16)$$

Generate $\boldsymbol{y}_1$, $\boldsymbol{y}_2, \ldots$, and $\boldsymbol{y}_n$ by Eq. (14).

(iv) Finally, generate the motion $z \simeq f(t)$ as:

$$z = \boldsymbol{w}^T \boldsymbol{\eta} \quad (17)$$

One often would like to start the trajectory from any initial condition $(z(0),\ \dot{z}(0))$ because the generated $z(t)$ is the motion of animals or robots. In this case, solve $\boldsymbol{y}_1$ from Eq. (17) as an independent variable and determine $\boldsymbol{y}_1(0)$. Calculate $\boldsymbol{x}(0)$ satisfying Eq. (12) with $\boldsymbol{y}_1(0)$ and give it to Eq. (7) as the initial condition. One can then start the motion from the specific initial condition $(z(0),\ \dot{z}(0))$ and attract it to the desired cyclic trajectory.

3.5. Extension to multivariable vector function

Multivariable vector function $\boldsymbol{f}(t)$ would be approximated by the following equations for the motion of animals and robots though the scalar function $f(t)$ has been discussed:

$$\begin{aligned} \boldsymbol{f}(t) &\stackrel{\triangle}{=} [f_1(t)\ \ f_2(t)\ \cdots\ f_m(t)]^T \\ &\simeq [z_1(t)\ \ z_2(t)\ \cdots\ z_m(t)]^T \stackrel{\triangle}{=} \boldsymbol{z}(t) \end{aligned} \quad (18)$$

where each z_i is obtained as

$$z_i = \boldsymbol{w}_i^T \boldsymbol{\eta}_i \quad (19)$$

by using Eq. (17). All $\boldsymbol{\eta}_i$s, i.e., $\boldsymbol{x}_i$s, must become equal since z_is are to be synchronized. In other words, phase angle ϕ_is must be equivalent for all is. An approach is to use only one common standard oscillator for all z_is but one cannot set the independent initial condition for each z_i. Accordingly, a standard oscillator of Eqs. (7) and (8) is equipped to each i and their phase angles are synchronized by the following equation. In order to catch up the oscillator j with the maximum phase angle ϕ_j, frequency ω_i $(i \neq j)$ of other oscillators are modulated as:

$$\omega_i = \omega + \varepsilon \left(1 - \frac{\boldsymbol{x}_i \cdot \boldsymbol{x}_j}{|\boldsymbol{x}_i| \cdot |\boldsymbol{x}_j|} \right) \quad (20)$$

where parameter ε gives speed of the synchronization.

3.6. NN realization

Discussed here is the realization of the DAM with NNs. Figure 2 shows a schematic diagram of the DAM, where the oscillator part is a RNN and the Fourier series part is a layered NN (LNN). It is known that the oscillators are realized by the RNNs composed of nonlinear neuron units [4, 5]. The Fourier series part is obviously achieved by a LNN if the Fourier coefficients are considered as the LNN's connecting weights. Therefore, the proposed DAM can be realized by the NN composed of the RNN and the LNN.

3.7. Numerical example

Figure 3 is a phase portrait of the desired trajectory and the trajectory generated by the proposed DAM. The generated trajectory asymptotically converges to the desired trajectory from the initial state that is not on the desired trajectory. The generated trajectory tracks the desired with almost no error after the convergence. The DAM successfully makes the desired trajectory be a limit cycle by using the von der Pol's oscillators.

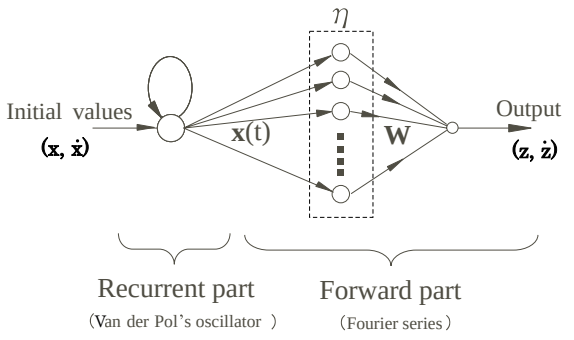

Figure 2: Construction of NN for proposed dynamic associative memory

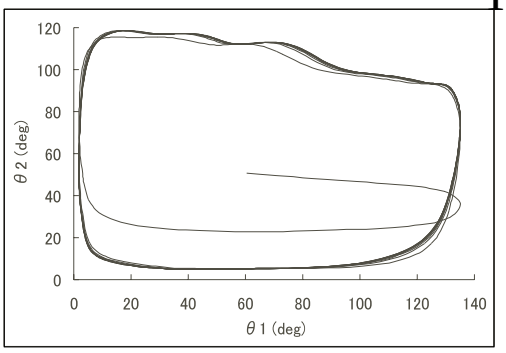

Figure 4: Generated trajectory in configuration space

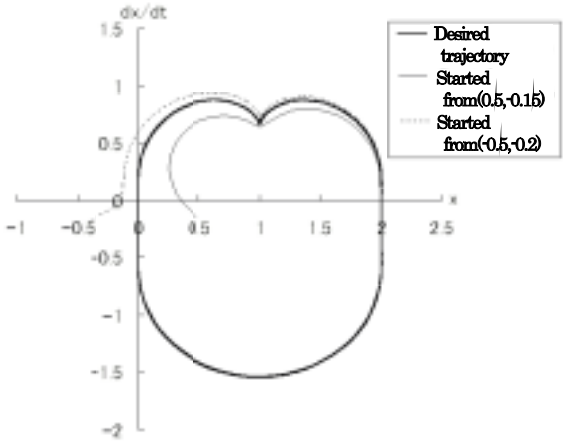

Figure 3: Phase portrait of generated and desired trajectories

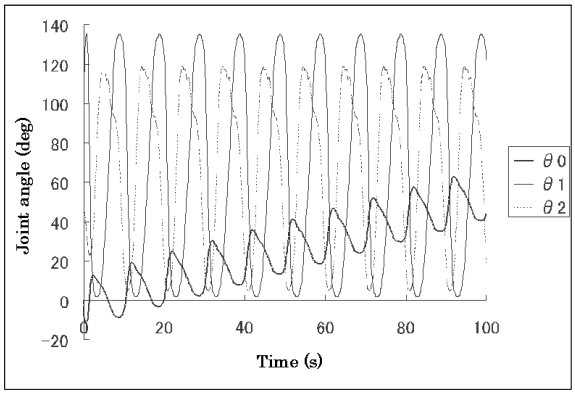

Figure 5: Time history of joint and attitude angles

4. Application to Space Robot Reorientation

A free-floating space robot is subjected to the nonholonomic constraint due to the angular momentum conservation. The attitude of the satellite vehicle may be changed during the manipulator operation. The system's orientation in the final state is not determined uniquely by the specific configuration of the manipulator since the final attitude of the satellite vehicle is dependent on the trajectory of the manipulator. Using the characteristics, the satellite attitude can be controlled. Shown here is a numerical simulation, where a space robot changes its orientation by the cyclic motion of the manipulator that is generated by the proposed DAM.

The mathematical model corresponds to the experimental system[6] simulating a space robot where the robot model composed of two SCARA type manipulators and a satellite vehicle can move freely on a two-dimensional planar table without friction by using air-bearings. For the reorientation, the robot drives only the shoulder and the elbow joints of one arm. The desired trajectory is based on the trajectory planned in references[7, 8]. Figure 4 illustrates the generated trajectory and the desired trajectory in the configuration space of the the shoulder angle θ_1 and the elbow θ_2. The generated trajectory converges to the desired as time passes. Figure 5 is the time history of the joint angles and satellite attitude angle θ_0. Figure 6 shows the motion of the space robot. The satellite attitude changes gradually.

5. Concluding Remarks

This study has proposed the methodology to realize the dynamic associative memory (DAM) that generates rhythmic and cyclic motions of animals and insects. The proposed DAM is based on the nonlinear oscillator and a Fourier series. It has the following characteristics.

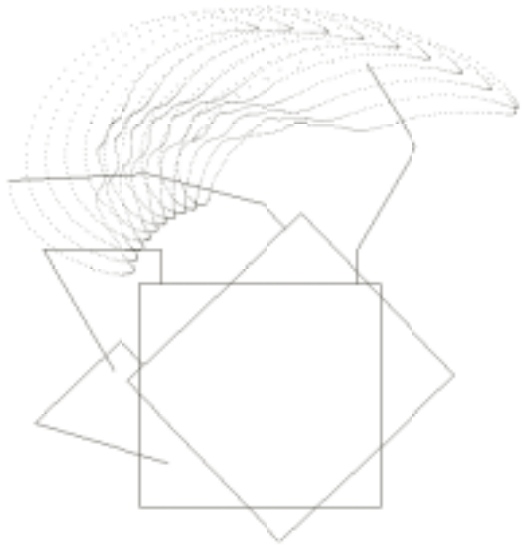

Figure 6: Motion of space robot through cyclic motion

(a) The desired cyclic trajectory can be a steady attractor, which does not change as time passes. Hence the generated trajectory is attracted to the desired trajectory.

(b) The DAM can generate multivariable vector functions.

(c) The DAM can generate the trajectory with the specific approximation accuracy evaluated by the mean squared error to the desired. The Fourier coefficients give the best approximation to the desired trajectory.

(d) The motion can start from almost any initial state because the von der Pol's oscillator is a limit cycle that attracts all trajectories started form points other than the origin.

(e) The proposed DAM can be realized by the NN composed of the RNN and the LNN.

Effectiveness of the proposed method has been examined by the numerical simulation of the space robot reorientation by the cyclic motion of the manipulator.

References

[1] Pearlmutter, B. A., "Learning State Space Trajectories in Recurrent Neural Networks," *Neural Computation*, Vol. 1, No. 2, 1989, pp. 263–269.

[2] Pineda, F. J., "Generalization of Backpropagation to Recurrent Neural Networks," *Physical Review Letters*, Vol. 59, No. 19, 1987, pp. 2229–2232.

[3] Funahashi, K. I., "On the Approximate Realization of Continuous Mapping by Neural Networks," *Neural Networks*, Vol. 2, 1989, pp. 183–192.

[4] Nakano, K., *An Introduction to Neurocomputing*, Corona Publishing, 1990. (in Japanese)

[5] Sawada, M. and Okabe, Y., "Generation of Rhythmic Motions of Multi-Joint Robots with Autonomic Distributed Neural Network Which Have Learning Systems," Proc. of 12th SICE Symposium on Decentralized Autonomous Systems, 2000, pp. 471–474

[6] Senda, K. et al., "A Hardware Experiment of Space Truss Assembly by Using Space Robot Simulator," *Proc. of 9th Workshop on Astrodynamics and Flight Mechanics*, Sagamihara, ISAS, July 22–23, 1999, B-16.

[7] Senda, K., Murotsu, Y., and Ozaki, M., "A Method of Attitude Control for Space Robots," *Trans. Japan Society of Mechanical Engineers*, Ser. C, Vol. 57, No. 539, 1991, pp. 2356–2362. (in Japanese)

[8] Senda, K., "Dynamics and Control of Rigid/ Flexible Space Manipulators", *Ph. D. Thesis, Osaka Prefecture University*, Osaka, Japan, 1993.

Keynote Speech IV

Proceedings of the International Symposium on
Adaptive Motion of Animals and Machines,
Montreal, Aug.8-12, 2000

Sensorimotor Integration in Lampreys and Robot I: CPG Principles

Avis H. Cohen* and M. Anthony Lewis**
***Department of Biology**
University of Maryland, College Park, MD 20742
****Iguana Robotics, Inc., Mahomet, IL 61853**

Movement through the world requires that the environment be fully integrated and understood. Biological systems are well known to be superb at integrating sensory and motor information during the production of movement. In our daily interactions with the world we are all familiar with the seamless way in which our nervous system combines sensory and motor information. The optimization of this integration has evolved over millions of years of natural selection. We suggest that a useful strategy for designing artificial organisms, that is robots, may be to copy the methods seen in such evolved systems. In this presentation, we will present first some biological observations and then some conclusions that seem most relevant to robotic systems. Finally, we will briefly illustrate how we have used the observations to implement efficient control of a robotic limb. In the paper by Lewis et al., this proceeding, these results are presented in more detail.

In the presentation by Trevor Drew (this proceedings), the concept of a central pattern generator (CPG) is introduced. Here we summarize the basic notion. In biological systems, it is well known that the motor output from all studied rhythmic movements is generated in part by neural circuits that are capable of operating in the absence of sensory feedback or external control (Delcomyn, 1980). This holds, for example, for locomotion (Grillner ref). These neural circuits generate a rhythmic output that provides periodic forcing of the required musculature. The neural circuits while not requiring external control for their basic operation, are highly sensitive to both sensory feedback and external control from such structures as the brain. The lamprey, a primitive fish-like organism, like all other vertebrates studied to date, has a CPG that provides periodic neural activity to drive locomotion (Cohen chapt). Such periodic forcing from spinal cord circuits can be produced in the absence of sensory feedback or brain input (Cohen and Wallén, 1980). However, sensory feedback from stretch receptive inputs along the spinal cord is extremely effective in entraining the rhythm (McClellan and Sigvardt, 1988).

The CPG in the lamprey and other organisms, appears to be a distributed system of coupled non-linear oscillators (Cohen, in press) that have been modeled using dynamical systems of non-linear differential equations (Cohen et al., 1980; 1992). Each neural oscillator is considered, on the basis of some experimental evidence (Cohen and Wallén, 1980) to be a single segment of the spinal cord with its own preferred frequency. The coupling, that maintains the whole ensemble at a single frequency, is known to be bi-directional and quite strong (Mellen et al., 1995)

It is clearly evident that sensory feedback is required to provide information regarding the status and position of an organism in its environment, and the nature of that environment. Feedback provides both a cycle by cycle regulation of the rhythm and phase dependent corrections elicited by perturbations. The traditional view of sensory feedback to the spinal cord has been that the feedback provides information regarding the position of the organism in space. Appropriate to this role, the feedback may correct a CPG on a cycle by cycle basis to maintain the organism in a proper relationship to the environment (Rossignol, et. al. 1988). For example, the hip joint angle of the cat can trigger a new step cycle as the body is propelled over its respective limb on the ground (Andersson and Grillner, 1983). Pearson and is colleagues have also recently found that stretch of muscle spindles can trigger a new step cycle through contractions of appropriate muscles. In these ways, the cycle periods will accommodate changes in the velocity of the animal (Pearson, 1995; Hiebert et al., 1996). Similarly, the

bending of the tail fin in dogfish or lamprey entrains the swimming so that swim cycle are appropriate lengths for the environmental conditions (Grillner and Wallén, 1982). Thus, if the body is not able to adequately bend against a strong current, this will be compensated for by a longer cycle. This type of sensory regulation is accomplished at the level of the spinal cord and requires no descending input although descending input is likely to influence the responses if present (Forssberg, 1979). All CPGs must have some stimulus that can trigger or prolong a new cycle as necessary in order to guarantee the CPG's movements are adaptive.

Another well documented role for sensory feedback is to elicit reflexive responses to environmental perturbations. This is also accomplished at the spinal level where sensory inputs are gated through the CPG during ongoing activity (Rossignol, et. al., 1988). A sensory stimulus can elicit phase dependent responses that are quite unlike the reflex responses that such stimuli would induce in the absence of CPG activity. For example, an obstacle encountered by the paw dorsum will produce an enhanced flexion during the flexion phase of the step cycle, but it will produce an enhanced extension during the extension phase (Forssberg, 1979). This guarantees that the limb is properly supported at the moment that it is raised to avoid the obstacle. The contralateral limb is also integrated with such responses. That is, the limb opposite the stimulus must be positioned to support the responsive limb before it will flex over such an obstacle (Hiebert et al., 1994). Such phase dependent responses to perturbations are very common across CPGs. For each rhythmic movement there are classes of stimuli that elicit such responses (Rossignol et al., 1988). In the case of locomotion the response requires no input from descending systems and is seen in spinal animals as well as intact animals (Forssberg, 1979).

Both cycle by cycle and phase dependent corrections are required for adaptive locomotion. The interaction between the CPG and sensory feedback can be shown to be complex than these examples suggest (review, Cohen and Boothe, 1999). For example, the CPG feedforwards to the sensory receptor input to provide a filtering mechanism. This type of feedforward combined with feedback is ubiquitous throughout motor control systems.

Another role for sensory feedback has been suggested by Cruse and his colleagues (1995) . They suggest that sensory feedback can provide a gain setting mechanism. We have recently found evidence that, indeed, in the lamprey this is true (Kiemel and Cohen unpublished).

To perform these experiments, we dissect the spinal cord free from the brain, the musculature and viscera. We then induce activity in the isolated spinal cord of the lamprey by bath application of an excitatory amino acid, D-glutamate. The resultant motor output pattern is termed "fictive swimming" because it is so similar to the motor pattern seen during the normal swimming of fully intact lampreys (Wallén and Williams, 1984). Fictive swimming in lampreys is typically highly stable and periodic, and lasts continuously during the exposure to excitatory amino acids.

When one bends the spinal cord during fictive swimming, the rhythm can be entrained by intrinsic stretch receptive mechanoreceptors as noted by others (McClellan and Sigvardt, 1988). In addition to this cycle by cycle entrainment effect, Kiemel and Cohen report that the baseline frequency of the locomotor rhythm is increased following the termination of the bending, with the frequency increase decaying only over one or more cycles. This slowly decaying excitation (SDE) can be so strong as to prevent entrainment by a bending at a frequency slower than the baseline.

The bending required to elicit SDE is very small, and the effect is seen with even one cycle of bending. The SDE is also impacted by the amplitude of the bending. Given the small amplitude of bending that can induce the effect, it seems highly likely that natural swimming in the intact animal will induce just such an increase in frequency of the CPG. *Thus, it appears that the gain of the system is increased by the movement of the animal*. Moreover, the gain will be increased whenever the animal begins movement. This type of slowly decaying excitation seen in lamprey seems to be an example of positive feedback. That is, the CPG generates movement that in turn causes the CPG to go faster. This phenomenon would also appear to guarantee that movement persists until actively terminated. There is also the implication that the gain remains less than 1, as the system is

highly stable even with the bending (Prochazka et al., 1997).

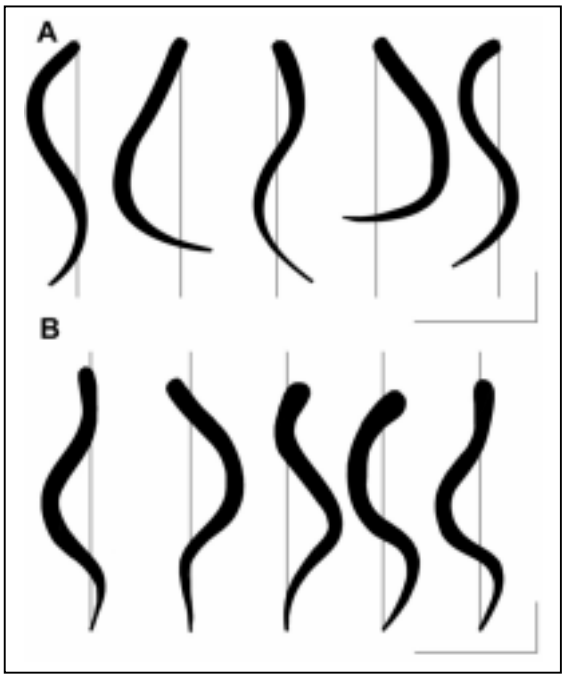

We have recently begun to use a semi-reduced lamprey preparation. This preparation is essentially the lamprey body in the absence of the brain or tail, with the spinal cord exposed to the bathing solution. Thus, the body is induced to swim with the mechanical properties and sensory feedback almost intact, and uninfluenced by the brain. This preparation, therefore, allows us to gain some insight into the roles of both mechanical aspects of the body, and the sensory feedback when interacting with the CPG, but without the brain to filter it.

In this reduced preparation, we show that the increased frequency caused by movement is indeed a factor when the body is driven by the CPG. In figure 1, above, we present two sets of images to illustrate this. In the upper set of images, the body is loosely pinned at the rostral or head end of the body. In the lower set of images, the body is pinned at the caudal or tail end. The calibration bars indicate one centimeter (vertical bar) and 0.33 seconds for the head end pinned, and 0.66 seconds for the tail end pinned. (horizontal bar). Note, that with the head pinned there is more movement at the free end of the body, than there is when the tail is pinned. Presumably, this is because the tail is thinner and provides less damping than does the head end. It seems reasonable to propose that the greater degree of bending at the tail end will create a greater degree of frequency increase than will the lesser movement of the head end.

Indeed, we find that the mechanical properties of the body apparently do have an impact on the degree of this increased frequency. Thus, the increased amplitude of tail end movement, while expected, causes an unexpected alteration in the motor pattern as the movement interacts with the spinal mechanism for increasing the frequency of swimming. What we see is that the head-end segments are not as speeded up as the tail-end segments. If we weaken the intersegmental coupling among the segments with some acute lesions, we see, with the head end pinned, that the alterations in the frequency in the tail end segments can be so great that it causes the head and tail segments to lose their 1:1 phase locking. This is shown in figure 2, below. The upper traces are with the head end pinned; the lower traces are with the tail end pinned. Notice, the head end pinned produces bursting that is 2:1, with the tail twice the frequency of the head. What impact this would have on the intact animal is not yet clear, but it seems likely to have an impact on the phase lags between segments (cf. Cohen et al., 1982).

From the insights into rhythmic movements described above, we take several principles that will be applied to the control of a robot limb. The first is that locomotion is best driven by a periodic feedforward forcing mechanism that is similar to that of a non-linear

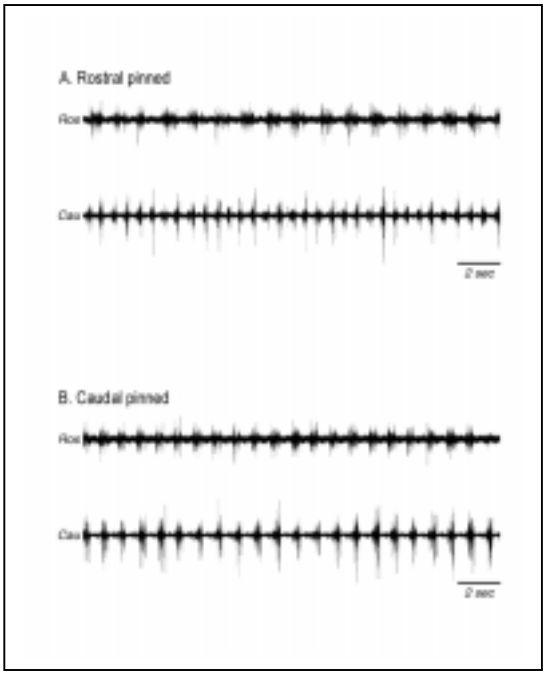

oscillator. Furthermore, sensory feedback will be essential in stabilizing the pattern on a cycle by cycle basis, and finally, that there will be a gain control initiated by movement that will cause the pattern to be increased in its frequency and requiring an active termination mechanism. All of these factors appear to improve the control of a robot limb. These principles are demonstrated in the accompanying contribution by Lewis et al., this proceeding. Another example of similar use of these principles successfully controlling a limb is found the work of Kimura and his colleagues (this proceeding).

References

Andersson, O., Grillner, S. (1983) Peripheral control of the cat's step cycle. II. Entrainment of the central pattern generators for locomotion by sinusoidal hip movements during "fictive locomotion.". Acta Physiol. Scand. 118:229-239, Scand. 474:3-43.

Cohen, A.H. and Boothe, D.L. (to appear) Sensorimotor interactions: Principles derived from central pattern generators, in M. Arbib (ed.) The Handbook of Brain Theory and Neural Networks, MIT Press., second edition.

Cohen, A. H. and Wallén, P. (1980). The neuronal correlate to locomotion in fish: "Fictive swimming" induced in an in vitro preparation of the lamprey spinal cord. Exp. Brain Res. 41: 11-18.

Cohen, A. H., Holmes, P. J. and Rand, R. H. 1982. The nature of the coupling between segmental oscillators of the lamprey spinal generator for locomotion: A mathematical model. J. Math. Biol. 13: 345-369.

Cohen, A.H., Ermentrout, G. B., Kiemel, T., Kopell, N., Sigvardt, K. and Williams, T. (1992) Modelling of intersegmental coordination in the lamprey central pattern or for locomotion. TINS 15:434-438.

Cohen, A.H. Control of movement is distributed and heterarchical. In: *Prerational Intelligence in Tactics and Low-Level Processes*. Eds. J. Dean, H. Cruse, and H. Ritter. Kluwer Academic Press. (in press).

Cruse, H., Bartling, Ch. and Kindermann, T. (1995) High-pass filtered positive feedback for decentralized control of cooperation, in F. Moran, A. Moreno, J.J. Merelo and P. Chacon (eds.), *Advances in Artificial Life,* Springer-Verlag, pp. 668-678.

Delcomyn, F. (1980) Neural basis of rhythmic behavior in animals. Science 210:492-8

Forssberg, H. (1979) On integrative motor functions in the cat,s spinal cord. Acta Physiol.

Grillner, S., Wallén, (1982) P. On peripheral control mechanisms acting on the central pattern generators for swimming in the dogfish. J Exp Biol 98:1-22

Hiebert, G., Gorassini, M., Jiang, W., Prochazka, A., and Pearson, K. (1994) Corrective responses to loss of ground support during walking II, comparison of intact and chronic spinal cats. J. Neurophys. 71:611-622.

Hiebert, G.W., Whelan, P.J., Prochazka, A., Pearson, K.G. Contribution of hind limb flexor muscle afferents to the timing of phase transitions in the cat step cycle. J. Neurophysiol. 75:1126-37, 1996.

Lewis, M.A. and Cohen, A. H.(this proceeding) Sensorimotor integration in lampreys and Robot II: CPG Hardware Circuit Realization

McClellan, A.D. and Sigvardt, K.A. (1988) Features of entrainment of spinal pattern generators for locomotor activity in the lamprey spinal cord. J. Neurosci. 8:133-45

Mellen, N., Kiemel, T., Cohen, A.H. Correlational analysis of fictive swimming in the lamprey reveals strong functional intersegmental coupling. J. Neurophysiol. 73: 1020-1030, 1995.

Pearson, K. G. (1995) Proprioceptive regulation of locomotion. Curr. Opin. Neurobiol. 5:786-91

Prochazka, A., Gillard, D., and Bennett, D.J. (1997) Implications of positive feedback in the control of movement. J Neurophysiol 77:3237-51

Rossignol, S., Lund, J.P. and Drew, T. (1988) The role of sensory inputs in reguating patterns of rhythmical movements in higher vertebrates: A comparison between locomotion, respiration

and mastication. In Neural Control of Rhythmic Movement in Vertebrates,, A. H. Cohen, S. Rossignol and S. Grillner(eds.), John Wiley and Sons, Inc., New York, pp. 201-284.

Wallén, P., Williams, T.L. Fictive locomotion in the lamprey spinal cord in vitro compared with swimming in the intact and spinal animal. J. Physiol. (Lond.) 347:225-39, 1984.

Session

Adaptive Locomotion

Proceedings of the International Symposium on
Adaptive Motion of Animals and Machines,
Montreal, Aug.8-12, 2000

Sensorimotor Integration in Lampreys and Robots II: CPG Hardware Circuit for Controlling a Running Robotic Leg

M. Anthony Lewis
Iguana Robotics, Inc.
P.O. Box 628
Mahomet, IL 61853
tlewis@iguana-robotics.com

Ralph Etienne-Cummings
Dept. of Electrical and Computer Engineering
Johns Hopkins University
Baltimore, MD 21218
etienne@ece.jhu.edu

Mitra Hartmann
Division of Biology
California Institute of Technology
Pasadena, CA 91125
hartmann@bbb.caltech.edu

Avis H. Cohen
Dept. of Biology, Neuroscience and Cognitive Science
University of Maryland
College Park MD 20742
ac61@umail.umd.edu

Abstract- *We present a silicon chip realization of a basic unit of locomotor control: the Central Pattern Generator(CPG). This chip is very low power, uses a minimum of chip space, and can be manufactured inexpensively. Although the control systems of robots and animals were designed by different agents, it appears that a common computational paradigm, adaptive non-linear dynamical systems, yields efficient implementations in both natural an artificial systems. Here we give an overview of a chip that implements this emerging computational paradigm.*

The chip uses 3 adaptive mechanism: (1) Firing rate adaptation— In the absence of sensory input the output motoneurons have a stable firing rate; (2) Phase resetting— 'stretch receptor' feedback can entrain the CPG's oscillator; (3) Interspike interval adjustment— compensates for dynamic variations in the mechanical system.

1.0 Introduction

Both roboticists and biologist have an interest in understanding the principles of locomotor control. Although natural agents and synthetic agents are studied under different disciplines in the artifice of human organization, they both must adhere to the same strict physical principles dictated by nature.

Evolutionary pressures largely dictate the design of the internal control systems of natural agents. The designer chooses the control systems of robots.

Walking machines and locomotory animals encounter the same fundamental problems such as postural control, coordination of contact points (limbs or body surface), coordination with the environment using distal sense (e.g. visuomotor coordination). Both systems would benefit from compact, efficient controllers that minimize energy usage and volume.

Even though these systems have different designers, a common level of abstraction for both the study of locomotion and its control may certainly be possible.

In this paper we present a recent work in creating a synthetic control element— a central pattern generator (CPG) chip— that mimics some properties of the basic functional unit of natural control system, yet has the potential for being the most efficient control system for synthetic agents yet proposed.

It is well recognized that the physics of silicon is in many ways analogous to the biophysics of the nervous system [1]. Therefore, neuromorphic systems are often implemented in silicon using as much of the properties of device physics as possible.

We show that the circuit, consuming less than one microwatt of power and occupying less than 0.4 square millimeters of chip area (using 1.2 micron technology), can generate the basic competence needed to control a robotic leg running on a circular treadmill. Furthermore, the circuit can use sensory feedback to stabilize the rhythmic movements of the leg.

Potentially, this technology could provide inexpensive circuits that are adaptable, controllable and able to generate complex, coordinated movements. Such circuits could be used in miniature systems to modulate repetitive cyclical movements based on appropriate sensory feedback. These systems could include miniature walking, running, flapping and swimming machines.

The following is largely a synopsis based on [2]. The reader is referred to the companion article for a review of the principles of locomotor control in vertebrates.

1.1 Modeling CPGs on a Neuromorphic Chip

CPGs are most often modeled as distributed systems of non-linear oscillators. In our implementation the basic coordination in the leg is achieved by phasically coupling two neurons together to achieve oscillations. When coupled together they are alternatively active. This alternating activity is the basic coordination needed to drive the hip of the robot. A phase control circuit governs the phase difference between the neurons. These oscillator neurons drive two integrate-and-fire motoneurons.

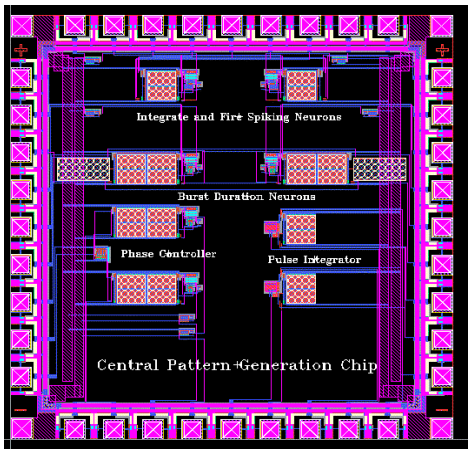

Figure 1. Layout of the CPG chip. Each component is wired to pins to facilitate the prototyping of oscillator circuits.

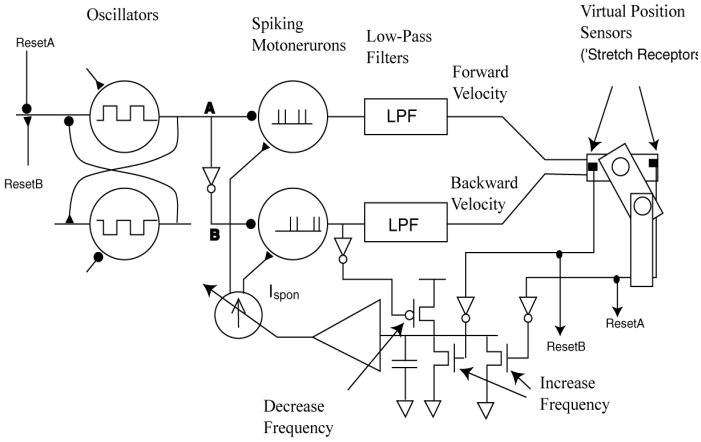

Figure 2. Adaptive control of a limb's dynamics using a neural CPG with learning capabilities.

In our experimental setup, the robot under control uses servomotors. To be compatible with this technology, it was necessary to low-pass filter the spiking neurons and then integrate the resulting smooth graded velocity signal.

We will show the circuit in autonomous operation and with sensory feedback from 'stretch receptors' used to reset the CPG. We also demonstrate a property of our biomorphic leg: we show that our limb and its control circuit not only produce stable rhythmic motion, but can also compensate for intentional chip biases, environment disturbances, as well as mechanical complexity of an active hip and passive knee.

2.0 The CPG Chip

The CPG chip is designed to provide biologically plausible circuits for controlling motor systems. The chip contains electronic analogues of biological neurons, synapses and time-constants. In addition, the chip also contains dynamic analog memories, and phase modulators. Using these components, non-linear oscillators, based on the central pattern generators of biological organisms, can be constructed.

The dynamical properties of the neural circuits can also be adapted using direct sensory information. In this first version of the chip, shown in Fig. 1, all the components are individually accessible such that they can be connected with off-chip wiring to realize any desired circuit. In future versions, tested neural CPG circuits will be integrated with completely hardwired or programmable circuits.

2.1 The Hardware Components

In this section we describe the basic elements of the CPG chip: the spiking motoneuron, the graded response neuron and the (CPG) oscillator.

2.1.1 The Spiking Motoneuron

Our neurons use an integrate-and-fire model. A capacitor, representing the membrane capacitance of biological neurons, integrates impinging charge. When the "membrane-potential" exceeds the threshold of a hysteretic comparator, the neuron outputs high. This logic high triggers a strong discharge current that resets the membrane potential to below the threshold of the comparator, thus causing the neuron's output to reset. This circuit therefore emulates the slow phase and fast phase dynamics of real neurons. The process then starts anew.

2.1.2 Graded Response Neuron

In addition to spiking neurons, we make use of neurons with graded response. These neurons are essentially the same as the spiking neuron except that the hysteretic comparator is replaced with a linear amplifier stage and no feedback signal is used.

2.1.3 The Oscillator

The neural circuits for creating the CPG are constructed using cross-coupled square-wave oscillators. The output of these oscillators drives the bursting motoneurons. A master-slave configuration of the neurons allows us to construct an oscillator with a constant phase relationship. By setting the excitatory and inhibitory weights to equal values, a square-wave with a duty-cycle of 50% is obtained. The phase relationship between the two sides can be varied. The frequency of oscillation is set by the magnitude of the weights. This asymmetrically cross-coupled oscillator serves as the basic CPG unit that can be

modified according to the application. By injecting or removing charge from the membrane capacitors of the oscillator neurons, the properties of the CPG can be altered.

For the experiments described here, a 180 degrees phase relationship is required. Hence an inverted version of one of the oscillators is used, as shown in Fig. 2.

2.1.4 The Neural Circuit

The complete neural circuit is given in Fig. 2. The output of the basic oscillator unit is used to inhibit the firing of the spiking motoneuron. When the oscillator output is high, the motoneuron is not allowed to fire. This produces two streams of 180 degrees out of phase spike trains. These trains can be low-pass filtered to get a voltage which can be interpreted as a motor velocity. Consequently, the oscillator controls the length of the motor spike train, while the spike frequency indicates the motor velocity.

The spike frequency is regulated by a feedback loop. Spiking places charges on the neuron membrane capacitor seen in the lower part of Fig. 2. The integrated charges are buffered and then used to down-regulate spike frequency. In this way spike frequency is less sensitive to component variations.

In the next section we describe two additional sensory mediated loops that adapt the oscillator and the motoneuron spiking.

2.2 Sensory Adaptation and Learning

2.2.1 Adaptation based on a 'stretch receptor'

As shown in Fig. 2, the oscillator neurons can be stopped or started with direct inhibitory and excitatory sensory inputs, respectively. When the inputs are received as strong inhibition, the membrane capacitor will be shunted and discharged completely. It will remain in this state until the inhibition is released, then the normal dynamics of the oscillator will continue from the inactive state.

Alternatively, if the sensory input is received as a strong excitation, the oscillator will be driven into an active state. When the excitation is released, the oscillator will continue from the active state. Clearly, the charge-up or discharge of the membrane capacitor will be influenced by any direct sensory input. If the sensory inputs are periodic, the oscillator outputs can be driven such that they are phase locked to the inputs.

We use this property to mimic the effect of the stretch reflex in animals. When the leg of an animal is moved to an extreme position, a special sensor called a stretch receptor sends a signal to the animal's CPG causing a phase resetting. This is mimicked in the circuit presented here. Referring to Fig. 2, the leg may reach an extreme position while still being driven by the oscillator. In this case, a virtual position sensor, which mimics a stretch receptor, sends a signal to *ResetA* or *ResetB* to cause a resetting of the oscillator circuit as is appropriate to cause a hip joint velocity reversal.

2.2.2 Spike Frequency Adaptation

The chip provides a short-term (on the order of seconds) analog memory to store a learned weight. Clearly, this architecture favors a continuous learning rule. Spikes from the motoneurons are used to increase or decrease a voltage on the capacitor of a graded response neuron. In the absence of the training inputs, the stored weights decay at approximately 0.1V/s. Figure 2 shows a schematic for adapting the spiking frequency of the motoneurons based on the swing amplitude of the limb.

3.0 Experimental Setup

The experimental setup consists of a small robotic leg, the CPG chip, necessary components to interface the chip to the robotic leg, a rotating drum treadmill and data collection facility.

The robotic leg is a small (10-cm height) two-joint mechanism. In our setup, only the "hip" is driven. The "knee" is completely passive. The knee swings freely, rotating on a low friction ball-bearing joint. A hard mechanical stop prevents the knee from hyperextending.

The leg runs on a drum that is free to rotate under the contact forces of the leg. As the leg pushed backward on the drum it sets the drum spinning

The robotic leg has three sensors on it. These sensors measure the angle of the hip and knee joints as well as force loading on the foot. The hip sensor is also processed to produced a 'stretch receptor' type of signal. The chip is integrated into the system as shown in Fig. 2.

4.0 Experiments

4.1 Running with a passive knee

In this experimental setup, the CPG circuit drives the actuator in the hip joint. The knee joint is passive and rotates with very little friction. The assembly is suspended above a rotating drum. The CPG circuit is started.

Data is collected from three sensors: Foot pressure, knee and hip. 'Stretch receptor' sensory feedback from the hip is used as feedback to the CPG.

4.2 Sensory feedback lesioning

This experimental setup is similar to the first experiment. The difference is that sensory feedback is lesioned (turned off) periodically. We collect data as before.

5.0 Results

5.1 Running Results with a Passive Knee

A remarkable feature of this system is that the knee joint adapts the correct dynamics to enable running (!). The natural dynamics of this particular system allow the lower

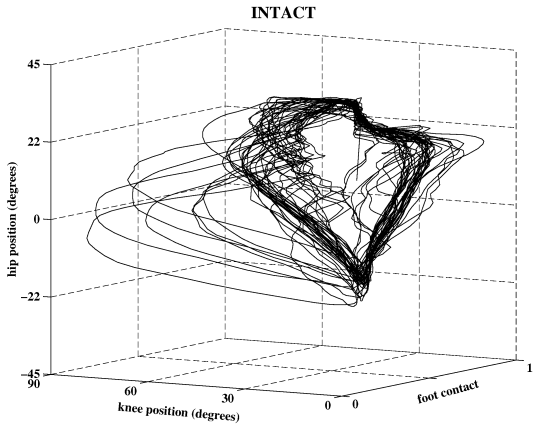

Figure 3. Hip, knee and foot-contact phase diagram. Most of the trajectory is in a tight bundle, while the outlying trajectories represent perturbations.

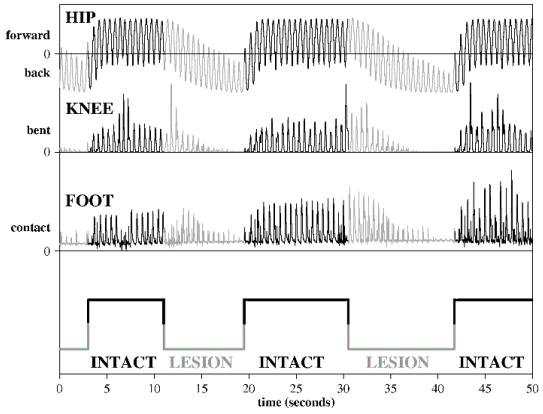

Figure 4. This figure shows the effect of lesioning sensory feedback. When the feedback is lesioned (Time 11-19 seconds and 31-42 seconds), the hip drives backward significantly. As it does the foot begins to lose contact with surface and the knee stops moving. When the lesion is reversed at 19 and 42 seconds, the regularity of the gait is restored.

limb to be driven in coordination with the higher limb, even though the knee is passive.

A phase plot of the knee, foot and hip position and foot contact is shown in Fig. 3. The bulk of the trajectory describes a tight 'spinning top' shaped trajectory while the few outlying trajectories are caused by disturbances. After a disturbance the trajectory quickly returns to its nominal orbit and we can infer that the system is stable.

5.2 Lesion Results

Next we lesioned the sensory feedback to the leg periodically. Figure 4 shows the effect of lesioning on the position of the hip and knee joints as well as the tactile input to the foot. After lesioning the leg drifts backward significantly due to a bias built into the chip. When the sensory input is restored, the leg returns to a stable gait.

5.3 Gait Stability

Perturbations to the leg cause momentary disturbances. As seen above in Fig. 3, several of the trajectories are clear "outlyers" to the typical orbit, and result from environmental disturbances.

We found that sensory feedback could compensate for both the bias of the chip and environmental perturbations.

6.0 Conclusions

In this paper we present a hardware implementation of a CPG model. Our custom aVLSI chip, having only 4 neurons and occupying less than 0.4 square mm, has the basic features needed to control a leg running on a treadmill.

We conclude that the control of a running leg using an aVLSI CPG chip is possible. We demonstrate that, at least in this experimental setup, running is possible using an under-actuated leg. Finally, we demonstrate a basic adaptive property of phase resetting using a stretch receptor.

It should be emphasized that the system being controlled is non-linear and the chip itself uses non-linear elements to control it. We have a coupled system of non-linear elements. We make no attempt to linearize the system. Instead we take advantage of the non-linearities.

Because (1) we do not make use of models, or linearization, (2) we adapt principles from biological systems, and (3) these principles can easily be implemented with low-power integrated circuits, we are able to achieve a very compact solution. Further experimentation with this system will allow us to determine if a robot can be made to walk by coupling together multiple circuits of the type presented here. The current results, however, are promising.

Acknowledgements

The authors acknowledge support of Grant No. N00014-99-0984 from ONR to Lewis & Etienne-Cummings, NSF Career Grant #9896362 to Etienne-Cummings and NIH grant MH44809 to Cohen.

[1] C. Mead, *Analog VLSI and Neural Systems*. Reading, MA: Addison-Wesley, 1989.

[2] M. A. Lewis, R. Etienne-Cummings, A. H. Cohen, and M. Hartmann, "Toward Biomorphic Control Using Custom aVLSI CPG Chips," presented at 2000 IEEE Inter Conf on Robotics and Automation, San Francisco, 2000.

Proceedings of the International Symposium on
Adaptive Motion of Animals and Machines,
Montreal, Aug.8-12, 2000

Decentralized Autonomous Control of a Quadruped Locomotion Robot

Katsuyoshi Tsujita[1], Kazuo Tsuchiya[2] and Ahmet Onat[3]

Dept. of Aeronautics and Astronautics, Graduate School of Engineering, Kyoto University,
Yoshida Hon-machi, Sakyo-ku, Kyoto 606-8501

[1]tsujita@space.kuaero.kyoto-u.ac.jp

[2]tsuchiya@space.kuaero.kyoto-u.ac.jp

[3]onat@space.kuaero.kyoto-u.ac.jp

Abstract

This paper deals with the design method of a control system for a quadruped locomotion robot. The proposed control system has a hierarchical architecture. It is composed of a leg controller and a gait pattern controller. The leg controller drives the actuators of the legs by using local feedback control. The gait pattern controller involves non linear oscillators. Various gait patterns emerge through the mutual entrainment of these oscillators. The performance of the proposed control system is verified by numerical simulations and hardware experiments.

As a result, the system locomotes stably in a wider velocity range by changing its gait patterns and the amount of power required for locomotion is decreased.

1. Introduction

Locomotion is one of the basic functions of a mobile robot. Using legs is one of the strategies for accomplishing locomotion. Using legs for locomotion allows the robot to move on rough terrain. Therefore, a considerable amount of research has been done on motion control of legged locomotion robots. This paper deals with the motion control of a quadruped locomotion robot.

The motion control of a walking robot has generally been achieved using a model-based approach[1][2] in which the inverse kinematics and the inverse dynamics of the robot are preprogrammed and when the desired motion is given, the motion of each link is controlled on the basis of the inverse models.

In the future, a walking robot which can carry out tasks in the real world, where the geometric and kinematic conditions of the environment are not specially structured, will be required. However, it is difficult for the model-based control system to carry out various tasks or to adapt to variations of the environment.

It is necessary to overcome the following difficulties in order to develop a walking robot which can carry out tasks in the real world: One is motion control of a large number of elements with nonlinear interactions. The other is evolution of a task specific motion pattern for many elements.

A considerable amount of study has been done on the motion of animals from the viewpoint of the dynamical systems theory [3] $\sim$ [6]. These studies reveal that the body of an animal is composed of a lot of joints and muscles, but during motion many of such elements are organized into a collective unit to be controlled as if it had fewer degrees of freedom and yet retain the necessary flexibility for changing internal and external contexts.

Recently, mechanisms of motion of animals have been studied in the field of ethology. Cruse et al.[7] have studied the locomotion mechanisms of insects from the viewpoint of ethology. According to their research, each leg autonomously repeats a forward and backward motion periodically when the leg has no mechanical interaction with the ground. Each leg has a touch sensor at its tip and motions of the legs interact with each other through the input signals from the touch sensors. As a result, a gait pattern that can satisfy the requirements of the locomotion velocity of the properties of the environment emerges. Kelso et al.[8] have investigated motions of animals from the viewpoint of synergetics. Motion of animals result from the processes of self-organization and a task-specific motion appears when a certain control parameter is scaled to be larger than some critical threshold. Knowledge of motion patterns of animals teaches

us some solutions to the problem of controlling a lot of elements and the problem of forming a task specific gait, walking pattern.

Based on the latest achievements of neurobiology and ethology, a new approach to robotics has been developed. Brooks [9], [10] has proposed the subsumption architecture as a principle of design of an autonomous mobile robot which can carry out tasks in the real world. The control system is composed of behavior-generating units. Each unit responds to the changes in the environment and generates a stereotyped action. Responses from all units compete with each other and one of them determines the action of the robot. Using the subsumption architecture, Brooks developed a six-legged robot, Genghis to walk over a rough terrain. Although the trajectory of the body was not specified, the robot successfully navigated on a rough terrain.

This paper deals with the design method of the control system of a quadruped locomotion robot based on decentralized autonomous control. In this method, a non-linear oscillator is assigned to each leg. The nominal trajectory of the leg is determined as a function of phase of its oscillator. We design the local feedback controller for each joint of the legs using the nominal trajectories as the reference. Touch sensors at the tips of the legs are used as triggers on which the dynamic interactions of the legs are based. The mutual entrainment of the oscillators with each other generate a certain combination of phase differences, which leads to the gait pattern. As a result, a gait pattern that can satisfy the requirements of the state of the system or the properties of the terrain emerges and the robot establishes a stable locomotion.

The performance of the proposed control system is verified by numerical simulations and hardware experiments.

2. Equations of Motion

Consider the quadruped locomotion robot shown in figure 1, which has four legs and a main body. Each leg is composed of two links which are connected to each other through a one degree of freedom (DOF) rotational joint. Each leg is connected to the main body through a one DOF rotational joint. The inertial and main body fixed coordinate systems are defined as $[\boldsymbol{a}^{(-1)}] = [\boldsymbol{a}_1^{(-1)},\ \boldsymbol{a}_2^{(-1)},\ \boldsymbol{a}_3^{(-1)}]$ and $[\boldsymbol{a}^{(0)}] = [\boldsymbol{a}_1^{(0)},\ \boldsymbol{a}_2^{(0)},\ \boldsymbol{a}_3^{(0)}]$, respectively. $\boldsymbol{a}_1^{(-1)}$ and $\boldsymbol{a}_3^{(-1)}$ coincide with the nominal direction of locomotion and vertically upward direction, respectively. Legs are enumerated from leg 1 to 4, as shown in figure 1. The joints of each leg are numbered as joint 1 and 2 from the main body toward the tip of the leg. The position vector from the origin of $[\boldsymbol{a}^{(-1)}]$ to the origin of $[\boldsymbol{a}^{(0)}]$ is denoted by $\boldsymbol{r}^{(0)} = [\boldsymbol{a}^{(-1)}]r^{(0)}$. The angular velocity vector of $[\boldsymbol{a}^{(0)}]$ to $[\boldsymbol{a}^{(-1)}]$ is denoted by $\boldsymbol{\omega}^{(0)} = [\boldsymbol{a}^{(0)}]\omega^{(0)}$. We define $\theta_i^{(0)}$ $(i = 1,\ 2,\ 3)$ as the components of Euler angle from $[\boldsymbol{a}^{(-1)}]$ to $[\boldsymbol{a}^{(0)}]$. We also define $\theta_j^{(i)}$ as the joint angle of link j of leg i. The rotational axis of joint j of leg i is parallel to the $\boldsymbol{a}_2^{(0)}$ axis.

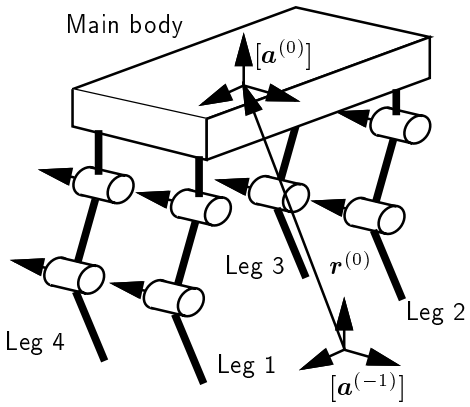

Figure 1: Schematic model of a quadruped locomotion robot

The state variable is defined as follows;

$$q^T = \left[\ \dot{r}_k^{(0)} \quad \omega_k^{(0)} \quad \dot{\theta}_j^{(i)}\ \right] \qquad (1)$$
$$(i = 1, \cdots, 4, \quad j = 1, 2, \quad k = 1, 2, 3)$$

Equations of motion for state variable q are derived using Lagrangian formulation as follows;

$$M\ddot{q} + H(q,\ \dot{q}) = G + \sum(\tau_j^{(i)}) + \Lambda \qquad (2)$$

where M is the generalized mass matrix and the term $M\ddot{q}$ expresses the inertia. $H(q,\ \dot{q})$ is the nonlinear term which includes Coriolis forces and centrifugal forces. G is the gravity term. $\sum(\tau_j^{(i)})$ is the input torque of the actuator at joint j of leg i. Λ is the reaction force from the ground at the point where the tip of the leg makes contact. We assume that there is no slip between the tips of the legs and the ground.

3. Gait pattern control

The architecture of the proposed control system is shown in figure 2. The control system is composed of leg controllers and a pattern controller. The leg controllers drive all the joint actuators of the legs so as to realize the desired motions that are generated by the pattern controller. The pattern controller involves non linear oscillators corresponding to each leg. The pattern controller receives the commanded signal of the nominal gait pattern as the reference. It also receives the feedback signals from the touch sensors at the tips of the legs. The generated gait pattern is determined by the phase differences between the non linear oscillators. A modified gait pattern is generated from the nominal gait pattern through the mutual entrainment of the oscillators with the feedback signals of the touch sensors. The generated gait pattern is given to the leg controller as the commanded signal of the locomotion pattern of the legs.

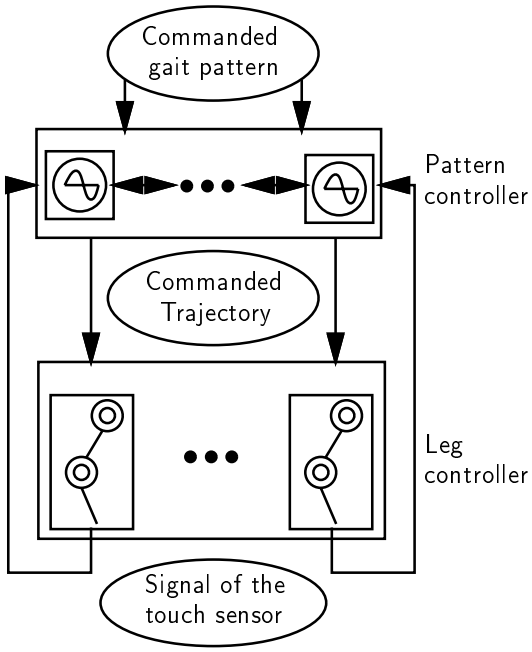

Figure 2: Architecture of the proposed controller

3.1. Design of the gait

3.1.1. *Design of the trajectories of the legs*

The position of the tip of the leg where the transition from the swinging stage to the supporting stage occurs is called the anterior extreme position (AEP). Similarly, the position where the transition from the supporting stage to the swinging stage occurs is called the posterior extreme position (PEP). We determine the nominal trajectories which are expressed in the coordinate system $[\boldsymbol{a}^{(0)}]$ in the following way: First, we define the nominal PEP $\hat{r}_{eP}^{(i)}$ and the nominal AEP $\hat{r}_{eA}^{(i)}$. The index $\hat{*}$ indicates the nominal value.

The trajectory for the swinging stage is a closed curve given as the nominal trajectory $\hat{r}_{eF}^{(i)}$. This curve involves the points $\hat{r}_{eA}^{(i)}$ and $\hat{r}_{eP}^{(i)}$. On the other hand, the trajectory for the supporting stage is a linear trajectory given as $\hat{r}_{eS}^{(i)}$. This linear trajectory also involves the points $\hat{r}_{eA}^{(i)}$ and $\hat{r}_{eP}^{(i)}$. The position of each leg on these trajectories is given as functions of the phase of the corresponding oscillator. The state of the oscillator for leg i is expressed as follows;

$$z^{(i)} = \exp(j\ \phi^{(i)}) \tag{3}$$

where $z^{(i)}$ is a complex number representing the state of the oscillator, $\phi^{(i)}$ is the phase of the oscillator and j is the imaginary unit.

The nominal phase dynamics of the oscillator is defined as follows;

$$\dot{\hat{\phi}}^{(i)} = \omega \tag{4}$$

The nominal trajectories $\hat{r}_{eF}^{(i)}$ and $\hat{r}_{eS}^{(i)}$ are given as functions of the phase $\hat{\phi}^{(i)}$ of the oscillator.

$$\hat{r}_{eF}^{(i)} = \hat{r}_{eF}^{(i)}(\hat{\phi}^{(i)}) \tag{5}$$
$$\hat{r}_{eS}^{(i)} = \hat{r}_{eS}^{(i)}(\hat{\phi}^{(i)}) \tag{6}$$

The nominal phases at AEP and PEP are determined as follows;

$$\hat{\phi}^{(i)} = \hat{\phi}_A^{(i)} \quad \text{at AEP}, \qquad \hat{\phi}^{(i)} = \hat{0} \quad \text{at PEP} \tag{7}$$

We use one of these two trajectories alternatively at every step of AEP and PEP to generate the desired trajectory of the tip of the leg $\hat{r}_e^{(i)}(\hat{\phi}^{(i)})$.

$$\hat{r}_e^{(i)}(\hat{\phi}^{(i)}) = \begin{cases} \hat{r}_{eF}^{(i)}(\hat{\phi}^{(i)}) & 0 \le \hat{\phi}^{(i)} < \hat{\phi}_A^{(i)} \\ \hat{r}_{eS}^{(i)}(\hat{\phi}^{(i)}) & \hat{\phi}_A^{(i)} \le \hat{\phi}^{(i)} < 2\pi \end{cases} \tag{8}$$

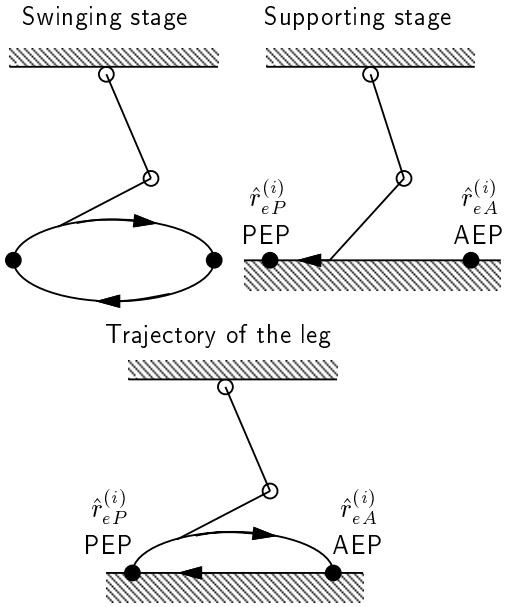

Figure 3: Trajectory of the leg

The nominal duty ratio $\hat{\beta}^{(i)}$ for leg i is defined to represent the ratio between the nominal time for the supporting stage and the period of one cycle of the nominal locomotion.

$$\hat{\beta}^{(i)} = 1 - \frac{\hat{\phi}_A^{(i)}}{2\pi} \tag{9}$$

The nominal stride$\hat{S}^{(i)}$ of leg i and the nominal locomotion velocity $\hat{v}$ are given as follows;

$$\hat{S}^{(i)} = \hat{r}_{eA}^{(i)} - \hat{r}_{eP}^{(i)} , \qquad \hat{v} = \frac{\hat{S}^{(i)}}{\hat{\beta}^{(i)}\hat{T}} \tag{10}$$

where, $\hat{T}$ is the nominal time period for a locomotion cycle.

3.1.2. *Design of the gait pattern*

The gait patterns, which are the relationships between motions of the legs, are designed. There are three gait patterns in which two legs support the main body at any instant during locomotion: In the trot pattern legs 1 and 3 form one pair and legs 2 and 4 form the other pair, in the pace pattern legs 1 and 2 form one pair and legs 3 and 4 form the other pair, finally in the bounce pattern legs 1 and 4 form one pair and legs 2 and 3 form the other pair. In such patterns, phases of the pairs of oscillators are coupled and the phase difference between them are zero.

A shift of the phase differences between the coupled oscillators by $\frac{\pi}{2}$ causes the gait pattern to change from those explained above to the walk pattern (Figure 4: The thick solid lines represent supporting stages). In walk pattern, tree legs support the main body at any instant during locomotion. Walk pattern has two types; One is transverse walk in which the legs 1,3,2 and 4 touch on the ground in this order. The other is rotary walk in which legs 1,2,3 and 4 touch on the ground in this order.

Each pattern is represented by a matrix of phase differences $\Gamma_{ij}^{(m)}$ as follows;

$$\phi^{(j)} = \phi^{(i)} + \Gamma_{ij}^{(m)} \tag{11}$$

where, $m = 1, 2$ represent transverse walk pattern and rotary walk pattern, respectively. $m = 3, 4, 5$ represent trot pattern, pace pattern and bounce pattern, respectively.

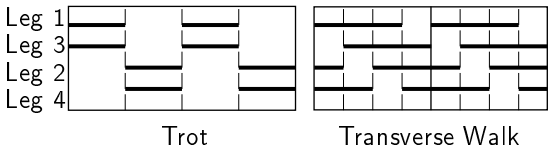

Figure 4: The trot and the transverse walk patterns

3.2. Locomotion control

3.2.1. *Trajectory controller of legs*

The angle of joint j of leg i is derived from the geometrical relationship between the trajectory $\hat{r}_e^{(i)}(\hat{\phi}^{(i)})$ and the joint angle. $\hat{\theta}_j^{(i)}$ is written as a function of phase $\hat{\phi}^{(i)}$ as follows;

$$\hat{\theta}_j^{(i)} = \hat{\theta}_j^{(i)}(\hat{\phi}^{(i)}) \tag{12}$$

The commanded torque at each joint of the leg is obtained by using local PD feedback control as follows;

$$\tau_j^{(i)} = K_{Pj}(\hat{\theta}_j^{(i)} - \theta_j^{(i)}) + K_{Dj}(\dot{\hat{\theta}}_j^{(i)} - \dot{\theta}_j^{(i)}) \quad (i = 1, \cdots, 4, j = 1, 2) \tag{13}$$

where $\tau_j^{(i)}$ is the actuator torque at joint j of leg i, and K_{Pj}, K_{Dj} are the feedback gains, the values of which are common to all joints in all legs.

3.2.2. Gait pattern controller

We design the phase dynamics of the oscillators corresponding to each leg as follows;

$$\dot{\phi}^{(i)} = \omega + g_1^{(i)} + g_2^{(2)} \qquad (i = 1, \cdots, 4) \quad (14)$$

where $g_1^{(i)}$ is the term which is derived from the nominal gait pattern and $g_2^{(i)}$ is the term caused by the feedback signal of the touch sensors of the legs.

Function $g_1^{(i)}$ is designed in the following way: We first define the following potential function.

$$V(\phi^{(i)},\ \Gamma^{(m)}) = \frac{1}{2}K \sum_i \left(\phi^{(i)} - \phi^{(j)} - \Gamma_{ij}^{(m)}\right)^2 \quad (15)$$

where matrix of phase differences $\Gamma_{ij}^{(m)}$ represents the commanded gait pattern defined in Eq.(11).

Function $g_1^{(i)}$ is then derived from the potential function V as follows;

$$g_1^{(i)} = -K\left(\phi^{(i)} - \phi^{(j)} - \Gamma_{ij}^{(m)}\right) \quad (16)$$

Function $g_2^{(i)}$ is designed in the following way: Suppose that $\phi_A^{(i)}$ is the phase of leg i at the instant when leg i touches on the ground. Similarly, $r_{eA}^{(i)}$ is the position of leg i at that instance. When leg i touches the ground, the following procedure is undertaken.

1. Change the phase of the oscillator for leg i from $\phi_A^{(i)}$ to $\hat{\phi}_A^{(i)}$.
2. Alter the nominal trajectory of the tip of leg i from the swinging trajectory $\hat{r}_{eF}^{(i)}$ to the supporting trajectory $\hat{r}_{eS}^{(i)}$.
3. Replace parameter $\hat{r}_{eA}^{(i)}$, that is one of the parameters of the nominal trajectory $\hat{r}_{eS}^{(i)}$, with $r_{eA}^{(i)}$.

Function $g_2^{(i)}$ is given as follows:

$$g_2^{(i)} = \hat{\phi}_A^{(i)} - \phi_A^{(i)} \quad (17)$$
at the instant leg i touches the ground

The pair of oscillators form a dynamic system that affect each other through two types of interactions. One is continuous interactions derived from the potential function V which depends on the nominal gait pattern. The other is the pulse-like interactions caused by the feedback signals from the touch sensor. Through these interactions, the oscillators generate gait patterns that satisfy the requirements of the environment.

4. Stability analysis of motion

The steady locomotion of the quadruped locomotion robot is strictly periodic and is characterized by a limit cycle in the state space.

The stability of the limit cycle is examined in the following way: First, four variables are selected as state variables.

$$X \in R^4, \quad X = \left[\ \theta_1^{(0)} \quad \theta_2^{(0)} \quad \dot{\theta}_1^{(0)} \quad \dot{\theta}_2^{(0)}\ \right] \quad (18)$$

When the robot starts the locomotion under a certain initial condition, the variable set X moves on a certain trajectory in the four-dimensional state space. If we choose a Poincaré section using the timing when the tip of a leg touches the ground, the first intersection of the trajectory of X with the Poincare section is mapped as X_0, and for every intersection, the corresponding values of X lead to a sequence of iterates in the state space.

$$X_1 \quad X_2 \quad \cdots \quad X_n \quad \cdots$$

The Poincaré map from X_n to X_{n+1} is expressed as follows;

$$X_{n+1} = F(X_n) \quad (19)$$

The fixed point $\bar{X}$ is defined such that $\bar{X}$ satisfies the following equation on the Poincaré section.

$$\bar{X} = F(\bar{X}) \quad (20)$$

This Poincaré map is approximated by use of linearization around the fixed point.

$$X_{n+1} - \bar{X} = M(X_n - \bar{X}) \quad (21)$$

Stability of the sequence of points $\{X_n\}$ is examined by checking the eigen values λ_k $(k = 1, \cdots, 4)$ of matrix M.

5. Numerical simulation

Table 1 shows the physical parameters of the robot which are used in numerical simulations.

Table 1

Main body		
Width	0.182	[m]
Length	0.338	[m]
Height	0.05	[m]
Total Mass	9.67	[kg]
Legs		
Length of link 1	0.188	[m]
Length of link 2	0.193	[m]
Mass of link 1	0.918	[kg]
Mass of link 2	0.595	[kg]

Numerical simulations are implemented under the condition that the nominal stride $\hat{S}$ and the nominal gait pattern $\Gamma^{(m)}$ are fixed. The nominal duty ratio $\hat{\beta}$ is selected as a parameter.

The nominal time period of the swinging stage is chosen as 0.20 [sec]. The frequency band width of joints 1, 2 are given as 5.5 [Hz] and 9.5 [Hz] for feedback gains of the joints, respectively.

We investigated the performance of the model-based control system through numerical simulation as a comparison with the performance of our system. The model-based control system is designed in the following way: The trajectories of the legs are given as functions of time. The actuators of the joints are controlled by using feedback control with the desired joint angles as the reference signals.

First, we investigated stability of the proposed control system, selecting duty ratio $\hat{\beta}$ as a parameter. The result is shown in figure 5. CASE 1 represents the model-based control system, and CASE 2 represents the proposed control system. From these figures, we can find that the proposed control system established stable locomotion of the robot with a wide parameter variance for duty ratio $\hat{\beta}$.

Variance of energy consumption of actuators E_c is investigated, selecting duty ratio $\hat{\beta}$ as a parameter. The results are shown in figure 6. Energy consumption of actuators E_c is defined as follows;

$$E_c = \frac{< \sum_{i,j} \tau_j^{(i)} \theta_j^{(i)} >}{< v >} \tag{22}$$

where, $< * >$ expresses the time averaged value of $*$.

From figure 6, we can see that the values of E_c of the proposed control system and also their variance with respect to the variance of the duty ratio is smaller than those of the model-based control system.

In order to clarify the adaptability of the proposed control system, we investigated variance of the gait patterns, selecting duty ratio $\hat{\beta}$ as a parameter. We investigated the variance of the gait pattern according to duty ratio in the following way: The states of leg i are represented by introducing the variable $\zeta^{(i)}$ as follows;

$$\zeta^{(i)} = \begin{cases} \dfrac{1}{1-\beta} & \text{Swinging stage} \\ -\dfrac{1}{\beta} & \text{Supporting stage} \end{cases} \tag{23}$$

Correlation between the swinging or supporting states of leg i and those of leg j is defined as follows;

$$W_{ij} = < \zeta^{(i)} \zeta^{(j)} > \tag{24}$$

Each gait pattern is characterized by correlation matrix W_{ij}. $\hat{W}^{(m)}$ and W are the correlation matrices according to the nominal gait pattern and the actually obtained gait pattern, respectively. The similarity between these two gait patterns is defined as follows;

$$D^{(m)} = \frac{1}{4} trace(\hat{W}^{(m)T} W) \tag{25}$$

Figures 7 and 8 show the similarity of gait patterns $D^{(m)}$ with respect to duty ratio $\hat{\beta}$ when we used the proposed control system and a model-based control system, respectively. From figure 7, we can find that although trot pattern is given as the nominal gait pattern, similarity between the obtained gait pattern and transverse walk pattern increases as duty ratio $\hat{\beta}$ increases. To the contrary, from figure 8, we can see that the gait pattern does not change from the given gait pattern when we use a model-based control system.

Gait pattern diagrams for $\hat{\beta} = 0.5$ and $\hat{\beta} = 0.75$ are shown in figures 9 and 10.

From these results, it is clear that the robot using the proposed control system adapts to variance of duty ratio $\hat{\beta}$ by changing the gait patterns, it keeps the stability of locomotion in a wide parameter area, and suppresses the energy consumption.

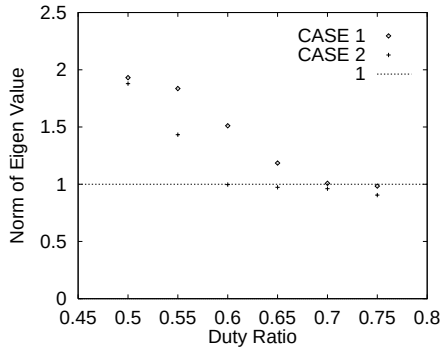

Figure 5: Stability
Commanded pattern: transverse walk

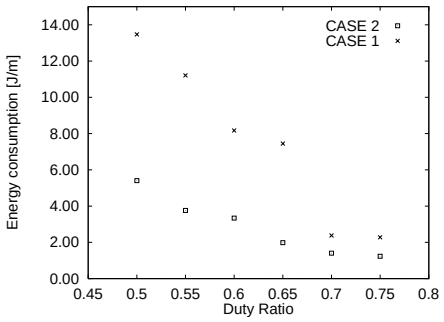

Figure 6: Energy consumption
Commanded pattern: transverse walk

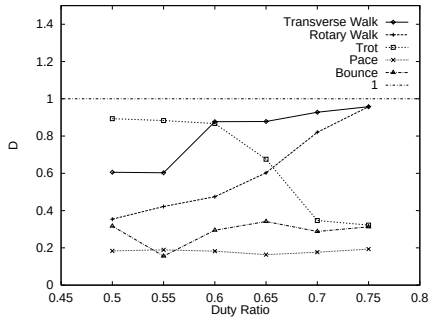

Figure 7: Similarity of gait pattern $D^{(m)}$
Commanded pattern: Trot
(proposed controller)

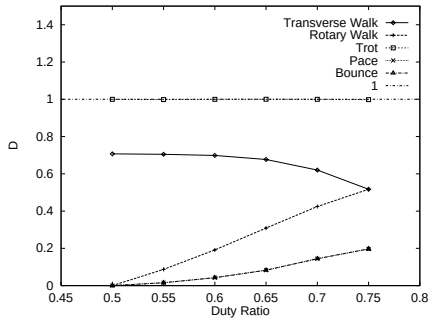

Figure 8: Similarity of gait pattern $D^{(m)}$
Commanded pattern: Trot
(model-based controller)

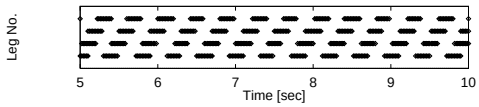

(a) $\hat{\beta} = 0.50$

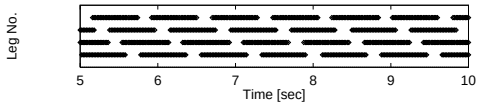

(b) $\hat{\beta} = 0.75$

Figure 9: Gait pattern diagram
Commanded pattern: Transverse walk
(proposed controller)

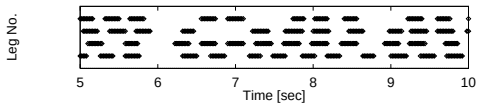

(a) $\hat{\beta} = 0.50$

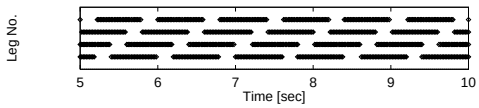

(b) $\hat{\beta} = 0.75$

Figure 10: Gait pattern diagram
Commanded pattern: Transverse walk
(model-based controller)

6. Hardware Experiments

The hardware equipment is shown in figure 11. The architecture of the hardware equipment is shown in figure 12.

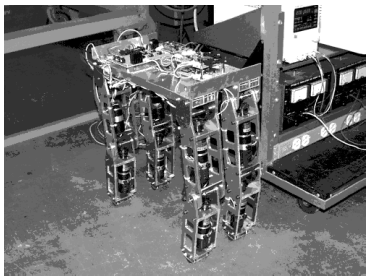

Figure 11: The hardware model

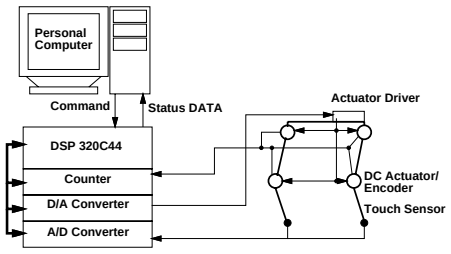

Figure 12: The architecture of the hardware equipment

The performance of the proposed control system was verified by hardware experiments. Figures 13.a and 13.b show the effects of duty ratio $\hat{\beta}$ when the trot walk pattern is commanded. From these figures, we can see that the proposed control system works well on the hardware equipment and realizes stable locomotion adaptively generating the appropriate gait patterns according to the variance of duty ratio $\hat{\beta}$.

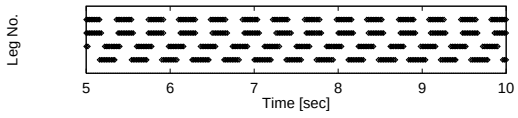

(a) $\hat{\beta} = 0.50$

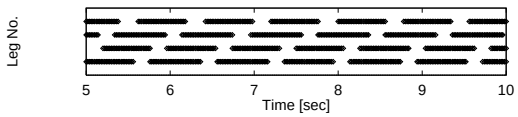

(b) $\hat{\beta} = 0.75$

Figure 13: Gait pattern diagram
Commanded pattern: Trot

7. Conclusions

We proposed a control system for a walking robot with a hierarchical architecture which is composed of leg controllers and a gait pattern controller. The leg controller drives the actuators at the joints of the legs by use of high-gain local feedback based on the commanded signal from the gait pattern controller. Whereas the gait pattern controller alternates the motion primitives by synchronizing with the signals from the touch sensors at the tips of the legs, and stabilizes the phase differences among the motions of the legs adaptively. In this paper, the nominal gait pattern is given as the command. In the future, we are planning to design the control system in which the nominal gait pattern is selected or generated according to the state of the robot. Using such a control system, it is expected that adaptability of the robot to variations of the environment will be highly improved.

Acknowledgments

The authors were funded by grants from the The Japan Society for the Promotion of Science (JSPS) as the Research for the Future program (RFTF) and from the Japan Science and Technology Corporation (JST) as the Core Research for Evolutional Science and Technology program (CREST).

References

[1] T. Mita and T. Ikeda, 1999, "Proposal of a Variable Constraint Control for SMS with Application to a Running and Quadruped," *Proc. of the 1999 IEEE International Conference on System, Man and Cybernetics*, Vol. III, pp. 140-145

[2] M. J. Coleman, M. Garcia, A. L. Ruina et al., 1997, "Stability and Chaos in Passsive-Dynamic Locomotion," *Solid Mechanics and its Applications*, Vol. 63, pp. 407-416

[3] G. M. Nelson, R. D. Quinn, R. J. Bachmann et al., 1997, "Design and Simulation of a Cockroach-like Hexapod Robot," *Proc. of the 1997 IEEE International Conference on Robotics and Automation*, Vol. 2, pp. 1106-1111

[4] G. M. Nelson and R. D. Quinn, 1998, "Posture Control of a Cockroach-like Robot," *Proc. of the 1998 IEEE International Conference on Robotics and Automation*, Vol. 1, pp. 157-162

[5] K. Akimoto, S. Watanabe and M. Yano, 1999, "A insect robot controlled by emergence of gait patterns," *Proc. of International Symposium on Artificial Life and Robotics*, Vol. 3, No. 2, pp. 102-105

[6] H. Kimura, K. Sakaura and S. Akiyama, 1998, "Dynamic Walking and Running of the Quadruped Using Neural Oscillator," *Proc. of IROS*, Vol. 1, pp. 50-57

[7] H. Cruse, C. Bartling, J. Dean, et al., 1996, "Coordination in a six-legged walking system. Simple solutions to complex problems by exploitation of physical properties," *From Animals to Animats 4*, Cambridge, MA, MIT Press, pp. 84-93,

[8] J. A. S. Kelso, 1995, "Dynamic Patterns: The self-organization of brain behavior," Boston, MIT Press

[9] R. A. Brooks, 1985, "A Robust Layered Control System for a Mobile Robot," *IEEE Journal of Robotics and Automation*, Vol. 2, No. 1, pp. 14-23

[10] R. A. Brooks, 1989, "A Robot that walks; Emergent Behavior from Carefully Evolved Network," *Neural computation*, Vol. 1, No. 2, pp. 253-262

[11] K. Tsuchiya and K. Tsujita, 1999, "A principle of design of an Autonomous Mobile Robot," *Proc. of the 4th International Symposium on Artificial Life and Robotics*, Vol. 1, pp. 320-323

[12] K. Tsujita, A. Onat, K. Tsuchiya et al, 2000, "Autonomous Decentralized Control of a Quadruped Locomotion Robot using Oscillators," *Proc. of the 5th International Symposium on Artificial Life and Robotics*, Vol. 2, pp. 703-710

Proceedings of the International Symposium on
Adaptive Motion of Animals and Machines,
Montreal, Aug.8-12, 2000

Controlling one-legged three-dimensional Hopping Movement

Klaus D. Maier[1]; Volkmar Glauche[2], Reinhard Blickhan[3] and Clemens Beckstein[2]

[1] Friedrich-Schiller-University, Institute of Sports Science, D-07740 Jena, k.maier@ieee.org
[2] Friedrich-Schiller-University, Institute of Computer Science, D-07740 Jena
[3] Friedrich-Schiller-University, Institute of Sports Science, D-07740 Jena

Abstract

Controlling the model of a movement system based on the dynamics of biological hopping and running is investigated. This movement system consists merely of a massless spring attached to a point mass. It is describing fast three-dimensional legged locomotion on even grounds. Rapidly moving legged autonomous systems require different hardware layouts and control approaches in contrast to slow moving ones. The spring mass system is a model that describes this principle movement as well as the principle control task. Multi-layer-perceptrons (MLPs) were used to implement neurocontrollers suitable for such a movement system. They prove to be suitable for exact control of the movement with a relatively small number of neurons. This is also shown by an experiment where the environment of the spring-mass system has been changed from even to uneven ground. The neurocontroller is performing well with this additional complexity without being trained for it.

1. Introduction

Control of movement is an issue for robotics and autonomous systems. For movement over ground, wheels as well as legs can be used. Most artificial movement systems use wheels while natural movement systems employ legged locomotion. Wheeled systems have some limitations like limited mobility or immobility on irregular ground surfaces. For this reason only about 50 percent of the worlds landmass can be entered by wheeled systems [1]. Legged systems have potential to overcome such limits: only discrete surface points are needed for leg placement, not continuos surfaces. The movement of the body is decoupled from the movement of the feet: This is a form of active suspension. For legged systems high movement velocities are desirable. To achieve this ballistic movement, i.e. flight phases are necessary. This results in landing impacts introduced into the systems. Legged systems must be able to cope with such impacts. This could be achieved by dimensioning bearings in a way that impact stress can be managed. Such a design would result in relatively heavy and large bearings. Also repeatedly introduced impact shocks reduce stand times.

Results from research on natural fast moving systems indicate that visco-elastic elements are used to effectively handle impact energy [2]. These are able to store and absorb impact energy. Using such elastic elements is an intelligent principle of construction that can be transferred to technical systems. Unfortunately elastic elements combined with ballistic movement phases make systems nonlinear and hard to control. This requires high computational efforts which complicates real time control. We therefore investigated in the suitability of multi-layer perceptrons (MLPs) [3] for implementing the control of dynamic movement systems. Characteristic properties of neural networks like fault tolerance, robustness and especially the ability to generalize make them a good choice for controller designs. They can be trained using available learning algorithms. Once trained they offer fast response. This allows to build control structures that provide online control which is essential for fast locomotion.

2. The Movement System

The movement system to be controlled is derived from a model that describes human and animal running and hopping [4]. It consists of a mass-less spring attached to a point mass that is jumping across even ground in three-dimensional space (Figure 1). The mass represents the body of the system and the spring its single leg. The motion of this system is divided into two phases: The 'flight phase' where the mass' trajectory is determined by gravity only and the 'ground phase' where the movement is determined by

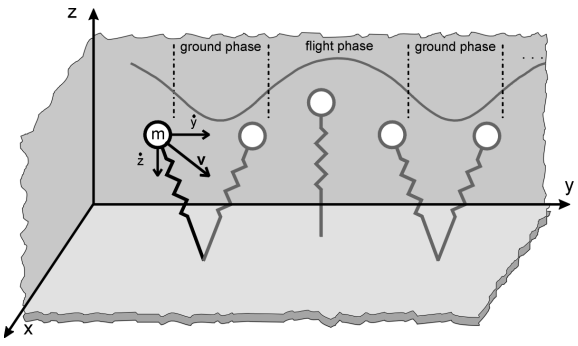

Figure 1: The spring mass movement system jumping across even ground in three dimensional space. (The figure shows the system hopping in a plane with x = constant).

the properties of the spring as well as gravity. The system is passive, i.e. mass, stiffness and length of the uncompressed spring remain constant (see appendix A).

The equations of motion during the ground contact phase are:

$$\ddot{x} = x\frac{k}{m}\left(\frac{l}{\sqrt{x^2+y^2+z^2}}-1\right) \quad (1)$$

$$\ddot{y} = y\frac{k}{m}\left(\frac{l}{\sqrt{x^2+y^2+z^2}}-1\right) \quad (2)$$

$$\ddot{z} = z\frac{k}{m}\left(\frac{l}{\sqrt{x^2+y^2+z^2}}-1\right)-g \quad (3)$$

where *x*, *y*: horizontal deflections, *z*: vertical deflection of the spring, g: gravitational acceleration, *k*: spring stiffness, *m*: mass and *l*: uncompressed length of the spring.

During the flight phase the equations of motion become:

$$\ddot{x} = 0 \quad (4)$$

$$\ddot{y} = 0 \quad (5)$$

$$\ddot{z} = -g \quad (6)$$

This dynamic system can be kept in motion (that is preventing ground contact of the mass) by active control only. The system has characteristic properties similar to hopping machines developed by Raibert [5]. It allows to reduce some of the complexity of the real world system by maintaining the principle of locomotion and the control task.

3. The Neurocontroller

A feedback structure is used to implement the neurocontroller. The multi-layer perceptron has two classes of input signals: control parameters from a higher center (like desired speed or directions) and sensed information on the observable system states. Output signals are motor control data to drive the controllable states of the movement system. The movement system is situated in its environment (the world) and is experiencing the immediate feedback of the environment (situatedness and embodiment [6]).

3.1 Fixed and changing coordinates

The number of input parameters to the controller can be reduced by using a designated Cartesian coordinate system *(a, b, c)* for each ground contact phase (Figure 2). The direction of the *a*-axis is set so that it coincides with the direction of the horizontal velocity $(\dot{x}, \dot{y})$ during the preceding flight phase. The origin of the *(a, b, c)* coordinate system is placed in the projection of the mass onto the *(x, y)*-plane at touchdown. With respect to this coordinate system the horizontal velocity b_{td} is always zero. For touch down the coordinates become

$$\dot{a}_{td} = \sqrt{(\dot{x}_{td})^2 + (\dot{y}_{td})^2} \quad (7)$$

$$\dot{b}_{td} = 0 \quad (8)$$

$$\dot{c}_{td} = \dot{z}_{td} \quad (9)$$

expressed in *(x, y, z)*-coordinates (index *td* indicates the values of the parameters at touch down).

The variables perceived are the legs' angle of attack $(\Delta a_{to}, \Delta b_{to})$ as well as the velocities $(\dot{a}_{to}, \dot{c}_{to})$ of the mass at the point where the spring lifts off the ground, i.e. the transitions between ground phase and flight phase (index *td* indicates the values of the parameters at take off / lift off). The parameter to be controlled is the angle of attack expressed as $(\Delta a_{td}, \Delta b_{td})$ at 'touch down' that has to be set in a way that the desired horizontal velocity $(\dot{a}_d, \dot{b}_d)$ for the flight phase is reached (index *d* indicates the desired velocity values; Figure 3).

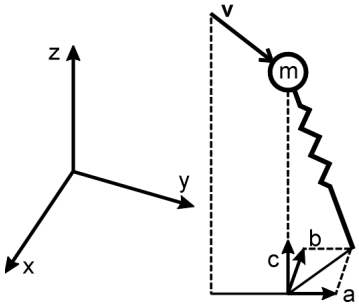

Figure 2: The fixed and changing coordinates.

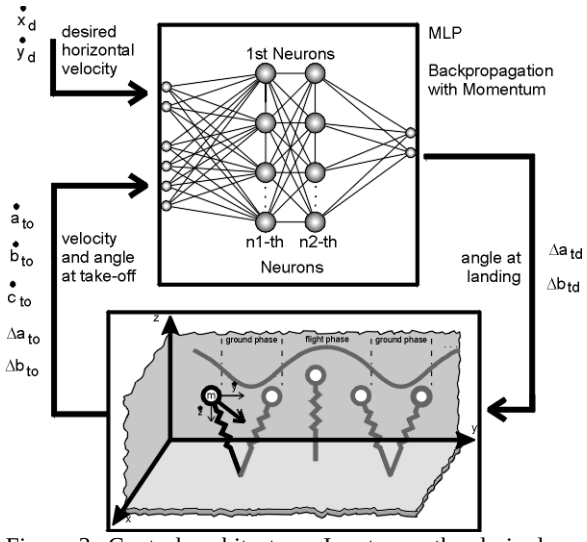

Figure 3: Control architecture: Inputs are the desired velocities, Outputs of the MLP are the landing angles of the leg and the observed states of the movement system are the velocities and angles at take-off.

The control task can be solved using numerical methods. A supervised learning approach is therefore appropriate to train the MLP. Training patterns for the control of the movement system have to be generated.

3.2 Generating training patterns

The spring-mass systems' equations of motion have been solved numerically for representative values covering the whole parameter space (see appendix B) using a fifth order Runge-Kutta-Gill method. The center of gravity trajectories have been numerically determined for all combinations of parameter values at touch down.
The initial and final states of a ground phase have to guarantee that the hopping height before landing and after take-off will be sufficient to move the leg into its new position during flight phase without hitting the ground. Data from center of gravity trajectories meeting these conditions have been used to compute the data patterns for the training set - based on the initial state, possible final states of the preceding ground phase were included as well as patterns for negative horizontal velocities.
To ensure good control of the system MLPs have to be trained with patterns that are representative for the movement. For the spring-mass system, training patterns have to cover the whole variety of possible movement patterns - hopping in place, acceleration, hopping at constant speed, deceleration and change of direction. If these characteristic movements are not sufficiently represented by the training patterns, the trained MLPs will not be able to control the movement of the system: the desired horizontal velocity will not be reached. This may lead to undesired behavior of the system (e.g. unnecessary change of direction, too fast or too slow movement, falling down). Inadequate selection of training patterns has not only an impact on the control abilities of trained MLPs, but also on the number of training cycles needed to learn the patterns. We selected representative data that covered the desired range of horizontal velocities. This is underlined by simulations that were made with desired horizontal velocities much higher than those used during training. In this case - as expected - the MLPs were not able to control the movement of the system. In order to reduce the number of training patterns, MLPs were trained only with patterns for selected horizontal velocities at touch down.

3.3 MLP - design

We have examined several different MLP architectures with one or more hidden layers using sigmoid activation functions [3]. Each hidden layer consisted of between 5 and 10 neurons. The learning algorithm used was back-propagation with momentum [7]. After reaching the error goal, the MLPs were tested on the quality of generalization using the samples that were not used for training. The movement system was left running with randomly changing velocities for more than 10000 steps to ensure stability of the controller.
One layer of hidden neurons was not sufficient to accomplish stable control of the spring mass system. We had good results for most of the setups with two layers of hidden neurons.

4. Results

For evaluating the trained networks test scenarios were developed. The neurocontroller has been tested under the following scenarios to gain information on it's capabilities: hopping in place, hopping a spiral, hopping an eight and hopping a square.
In order to further evaluate the quality of the control provided by the neurocontroller we tested our trained MLP in an environment with uneven ground. We introduced a stepwise changing surface describing the surface height at the point of touchdown. For simulation purposes this has the same effect as a continuously changing ground, since only the height of the ground at the position of touch-down is relevant for the behavior. Still, the leg has to be brought forward into the direction of the touch down point. The system is of course limited in its movement by energy constraints. It has no means to change its total energy during hopping. Therefore it is not able to hop over unconstrained rough ground.

4.1.1 Hopping in place

Hopping in place is a difficult task compared to hopping at high speeds. Even small deviations from the vertical position of the spring result in a substantial horizontal component of the take-off velocity. For the typical human parameters of mass and spring constant a deviation of 1° can result in horizontal velocities or more than 0.5 m/s. Ideal hopping in place is therefore not achievable in practice.
The neurocontroller is able to keep the system close to the place the system should ideally be for hopping in place. Figure 4 shows the behavior of the system using a MLP with 7 neurons in the first and 9 neurons in the second hidden layer for hopping on even ground. The cyclic movement of the spring mass system around a stationary point is due to a small constant deviation in control output from the ideal output. This cyclic effect originates from to the turn-

ing of the *(a,b,c)* coordinate system in the way that the *b* component is set to zero.

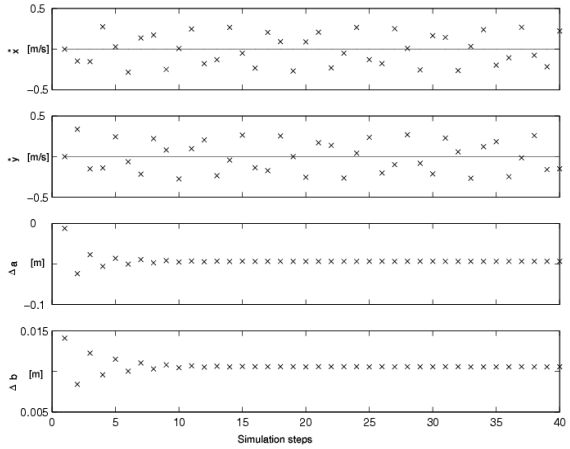

Figure 4a: Movement course for hopping in place.

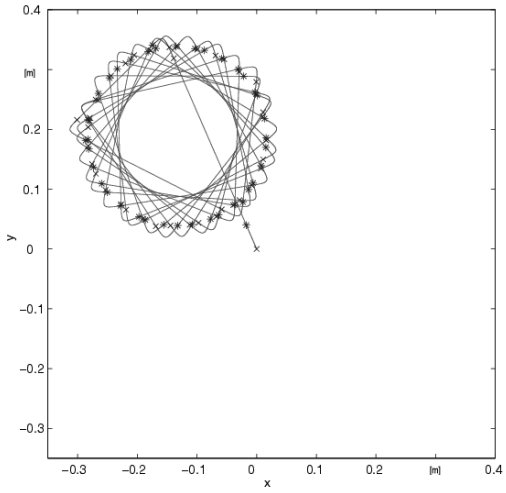

Figure 4b: Movement in the x-y plane for hopping in place.

4.1.2 Spiral

A combination of change of direction as well as change of speed hopping along a spiral shaped course on even ground has been chosen. Figure 5a shows that the controller is able to direct the movement along the desired velocity course and Figure 5b shows the spiral movement plotted over the *x-y*-plane.

4.1.3 Eight

Another complex movement task can be found in Figure 6a. The movement system is controlled to follow the shape of the number eight by hopping over uneven ground. The figure shows that the controller is clearly able to make the system follow the prescribed velocity curve. The influence of the uneven ground is disturbing the movement of the system but it is still capable of re-adjusting the movement of the spring mass system. Figure 6b shows the movement plotted over the *x-y*-plane. Even with the disturbances from the uneven ground, the figure eight can be clearly identified. The controller is performing well enough with its control of the time-velocity course, that its derivation, the time-place course remains in the desired shape.

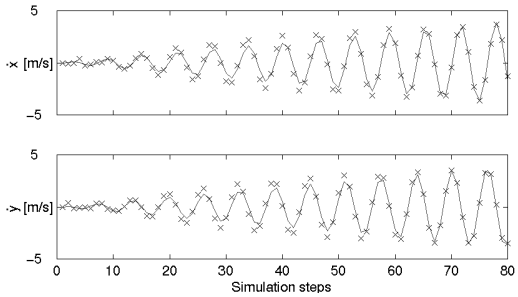

Figure 5a: Movement course for hopping a spiral.

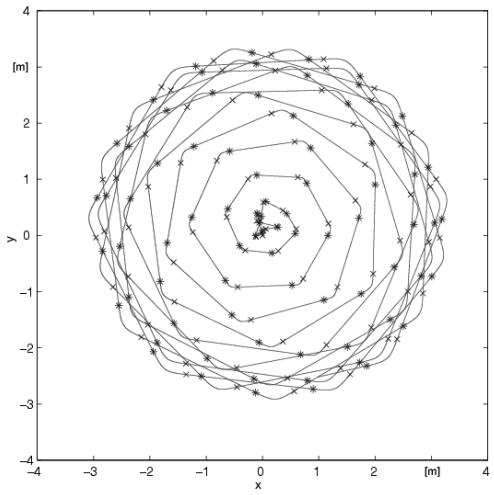

Figure 5b: Spiral hopping in the x-y-plane

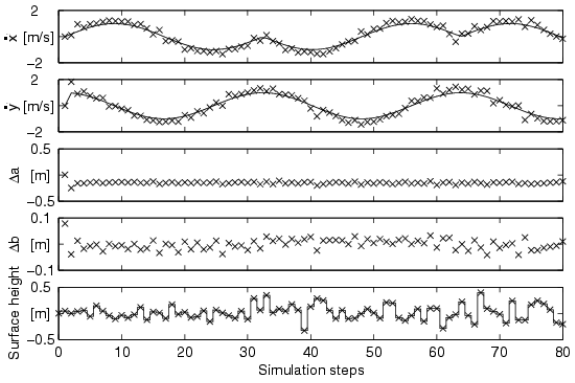

Figure 6a: Movement course for hopping of the figure eight over uneven ground.

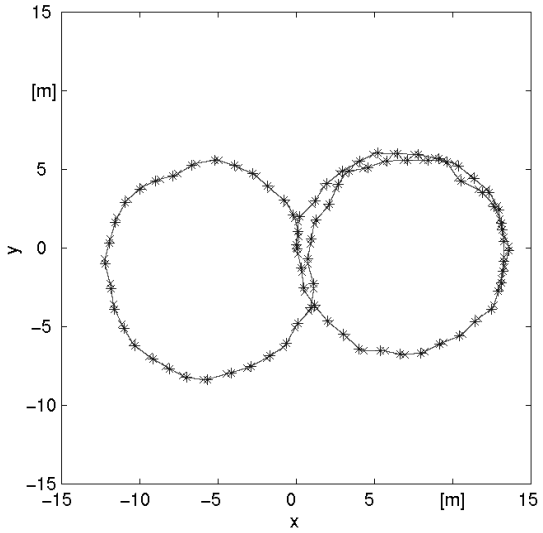

Figure 6b: Hopping an eight figure over uneven ground plotted in the x-y-plane.

4.1.4 Square

A movement course following a squared figure is giving information on the capability of the controller to keep certain directions. Figure 7a shows the time velocity course for several square figure across uneven ground. The disturbances to the movement introduced through the changes in the ground height can be clearly perceived. Changes from the prescribed movement course are regulated by the MLP to the desired values. The movement over the *x*-*y*-plane is shown in Figure 7b. The square figures are visible. Deviations from the ideal figure are due to the influence of the uneven ground. The system can not sense these deviations. This would be a task for a higher hierarchy controller: It can adjust the desired velocity that deviations can be compensated.
The neurocontroller is managing the untrained environment introduced through the uneven ground very well and allows for an exact control of the horizontal speed. The actual velocity follows the desired velocity by regulating the influence of the uneven ground within a few steps. Even extreme changes in the desired velocity are handled well - the MLP adjusts the system in a few steps.

5. Related Work

Using neural networks for the control of legged movement systems has been addressed by Beer et al. [8] for hexapod autonomous systems as well as by Berns et al. [9] for a six-legged robot modeled after the stick insect. Other groups are also working on

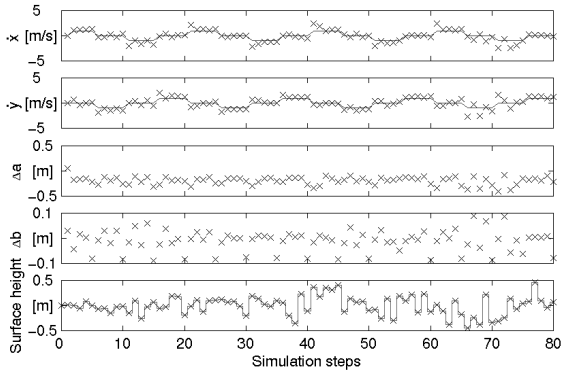

Figure 7a: Hopping squares over uneven ground.

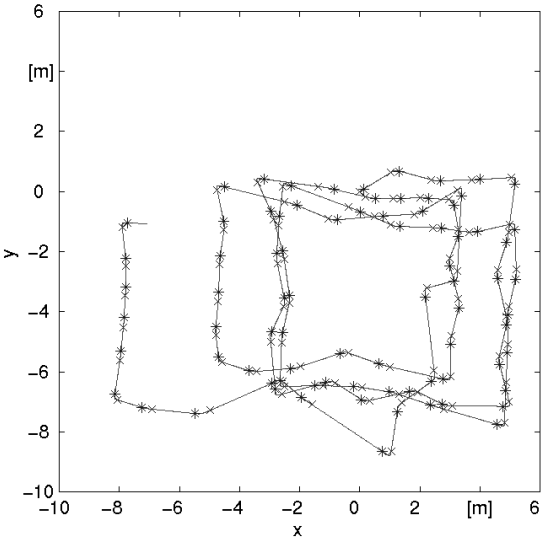

Figure 7b: Hopping square figures over uneven ground plotted in the x-y-plane.

control of legged systems with little or no elastic elements included. These systems are moving only slowly due to this construction principle. They control leg trajectories – when using elastic elements the trajectory is determined by material laws and only initial conditions are set by the controller. Exploiting ballistic movement for locomotion in the walking robots mentioned above is not desired nor possible. It would lead to very complex control problems. The approaches that demand static stability are another reason for the slow movement.
Simple dynamic movement has already been under investigation in many projects mostly in the form of the pole-balancing control task (e.g. like Anderson [1], Ritter [10], Widrow [12]). There are no applications for the design of walking machines though. Control of a dynamic movement system like the 3D-Hopper [5] has been partly addressed by Atkeson et

al. [13] using neural networks to improve the original look-up table control.
We have investigated on MLPs for the control of two dimensional spring mass systems [14]. They have proven to be successful for effective and exact control. Our investigation in Radial-Basis-Function Neural Networks for the control of such two dimensional spring-mass movement system has shown to give controllers of comparable performance but at the price of higher computational cost [15]. Experiments with controllers based on Self-Organising Motoric Maps (Ritter et al. [10]) have yielded unsatisfactory results [16].

6. Conclusion and Outlook

The implemented neurocontroller based on MLPs is capable of exactly controlling the hopping and running system in three dimensional space. The neurocontroller learned from the given examples to generalise untrained input/output values, i.e. to run at untrained speeds. It did not only perform well on the trained flat surface but also on uneven terrain. MLPs are a suitable way to implement a control task that has been solved separately. Using this approach permits building fast controllers that can provide real time control This is essential for dynamic movement systems.
Where modeling the control task explicitly is not possible or too expensive reinforcement approaches might prove successful. We are currently investigating in reinforcement based learning algorithms for the control of movement systems: an approach using MLP based reinforcement learning like TD(λ)- [17] or Q-learning [18] seems to be promising for future work on non-supervised control of dynamic movement systems.
High speed of locomotion is an issue for future artificial walking machines and elastic elements seem to be promising for implementation.

Appendix A

The constants of the spring mass system where set to physiological relevant values (Table A) taken from [4].

Table A: System constants

Constant	M	k	l
Value	60 kg	10 kN/m	1 m

Appendix B

Polar coordinates were used to solve the equations of motion of the spring mass system (Table B). This is done in order to achieve an even spread of initial states. φ_{td} is the direction of the spring at the point of touch down in the x-y-plane, ϑ_{td} is the angle of attack of the leg with respect to the *x-y*-plane and $(\dot{a}_{td}, \dot{b}_{td}, \dot{c}_{td})$ are the velocity components at touch down.

Table B: Initial states for numerical solution

Parameter	Range	In steps of
φ_{td}	$0 \le \varphi_{td} < 2\pi$	π/90
ϑ_{td}	$-\pi/2 \le \vartheta_{td} \le \pi/2$	π/90
$\dot{a}_{td}$	$-9 \le \dot{a}_{td} \le 9$	1m/s
$\dot{b}_{td}$	0	
$\dot{c}_{td}$	$0 \le \dot{c}_{td} \le 4$	1m/s

References

[1] Raibert, M. H., 1990, "Legged Robots." In Artificial Intelligence at MIT – Expanding Frontiers, P.H. Winston, S.A. Shellard, (Eds.), Cambridge, Mass.: MIT Press, Vol. 2, pp. 149-179.

[2] Blickhan, R., Full, R.J., 1993, "Similarity in multilegged locomotion: Bouncing like a monopode." *Journal of Comparative Physiology A*, pp. 509-517.

[3] Haykin, S., 1994, *Neural Networks*, New York: Macmillan Publishing Company.

[4] Blickhan, R., 1989, "The spring-mass model for running and hopping.", *Journal of Biomechanics*, Vol. 22, No. 11/12, pp. 1217-1227.

[5] Raibert, M.H. et al., 1984, "Experiments in balance with a 3D one-legged hopping machine.", *International Journal of Robotics Research*, 3, pp. 75-92.

[6] Brooks, R.A., 1991, "New Approaches to Robotics", *Science*, Vol. 256, 1227-1232.

[7] Rummelhart, D.E., et al., 1986, "Learning representations by back-propagating errors.", *Nature* (London), 323, pp. 533-536.

[8] Beer, R.D., et al., 1992, "A distributed neural network architecture for hexapod robot locomotion.", *Neural Computation*, No. 4, pp. 356-365.

[9] Berns, U. et al., 1994, "Learning control of a six-legged walking machine." In M. Jamashidi, et al. (Eds.), *Proceedings of the 5th International Symposium on Robotics & Manufacturing*, Vol. 5, New York: ASME Press.

[10] Anderson, C.W., 1989, "Learning to control an inverted pendulum using Neural Networks".

IEEE Control Systems Magazine, Vol. 9, 3, pp. 31-37.

[11] Ritter, H., Schulten, K., 1987, "Extending Kohonen's Self-Organizing Mapping Algorithm to Learn Ballistic Movements." *Neural Computers* (Eds. R. Eckmiller, and C. von der Malsburg), Heidelberg: Springer, pp. 393 – 406.

[12] Widrow, B., 1987, "The original adaptive neural network broom balancer." In *International Symposium on Circuits and Systems*, pp. 351-357.

[13] Atkeson, C.G. et al., 1990, "Using associative content addressable memories to control robots". In Miller,T.W. III et al. (Eds.): *Neural Networks for Control*, Cambridge, Mass.: MIT Press, pp. 255-286.

[14] Maier, K.D., Glauche, V., Beckstein, C., Blickhan R., 1998, "Controlling one-legged dynamic Movement with MLPs", *International ICSC / IFAC Symposium on Neural Computation (NC'98)*, Technical University in Vienna, Austria, pp. 784-790.

[15] Maier, K.D., Glauche, V., Beckstein, C., Blickhan R., 1999, "Control of Legged Planar Hopping with Radial Basis Function Neural Networks", *Proceedings of the Second International Conference on Climbing and Walking Robots (CLAWAR 99)*, University of Portsmouth, Professional Engineering Publishing Ltd., Bury St Edmunds, pp. 133-141.

[16] Maier, K.D., Glauche, V., Beckstein, C., Blickhan R., 1998, "Control of a one-legged Movement System: Artificial Neural Network Approach with Radial Basis Functions and Self-Organising Motoric Maps.", *Proceedings of the Euromech Colloquium 375, Biology and Technology of Walking*, pp. 82-89.

[17] Sutton, R.S., 1988, "Learning to predict by the methods of temporal differences.", *Journal of Machine Learning* 3, pp. 9-44.

[18] Watkins, C.J.C.H., 1989, "Learning from delayed rewards", Ph.D. Thesis, University of Cambridge, UK.

Proceedings of the International Symposium on
Adaptive Motion of Animals and Machines,
Montreal, Aug.8-12, 2000

Control of Walking Machines With Artificial Reflexes

M. Guddat[1] **and M. Frik**[2]

[1] Gerhard–Mercator Univ. Duisburg, Dept. of Engineering Mechanics, guddat@mechanik.uni-duisburg.de

[2] Gerhard–Mercator Univ. Duisburg, Dept. of Engineering Mechanics, frik@mechanik.uni-duisburg.de

Abstract

This paper describes the augmentation of our concept for the locomotion control of multi-legged walking machines. The concept is based on a neural control with artificial reflexes to react on sensor input. It is improved with the help of new sensorics as well as an internal ground map, build up with sensor information. Parts of the general concept together with the used sensorics are introduced. The ground map and its generation as well as the collaboration between the different reflexes are shown. The presented methods are applied to the six-legged TARRY I and TARRY II, but they are applicable to many other types of walking machines.

1. Introduction

The aim of the TARRY project is to realize autonomous walking in unknown and rough terrain. TARRY I and TARRY II, the machines we use to verify our software in the real world, were designed and manufactured in 1992[1] and 1999[2]. They are modeled according to the walking stick insect *carausius morosus*, where TARRY II has undergone many subtle changes that were derived from our experience with its predecessor TARRY I.

Both TARRY robots have six legs with three rotational joints each. The joints are modeled with servomotors used in airplane modeling normally. The whole structure is built to be as light as possible to allow a relatively high payload or a larger area of feasible motions. The machines are equipped with several sensors that are discussed below. Most important are to contact sensors in the feet to detect ground contact and the current measurement in the hip servos the recognize leg collisions.

To enable locomotion in different kinds of terrain we use a combination of several techniques. As a basis for walking in standard gaits we generate and optimize a set of walking patterns. These patterns are based on the machine's kinematics and a set of sixteen walking parameters (see table 1). Some of them are obvious as velocities in x- and y- direction and angular velocity around the z-axis. They are supplemented by values for roll and pitch angle as well as superimposed oscillations etc. These parameters together with the kinematical model of the machine are fed into the software library WALKINGLIB[3] creating the needed walking patterns. The WALKINGLIB creates the foot trajectories in cartesian coordinates or derives the joint angles via inverse kinematics.

These generated walking patterns are used to train a set of six neural networks (see figure 3), one for each leg, with the basic gaits. Their input values are also tied to a pacemaker to secure synchronization of the legs. The networks are feed forward networks that are trained by standard backpropagation algorithms[4].

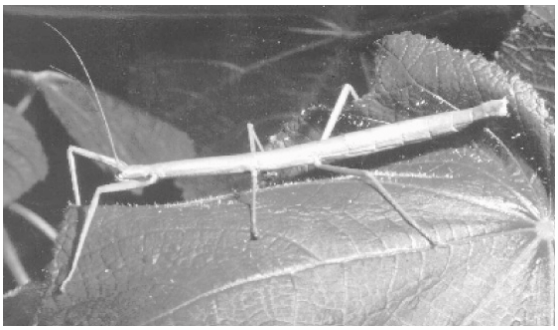

Figure 1: Walking stick insect *carausius morosus*

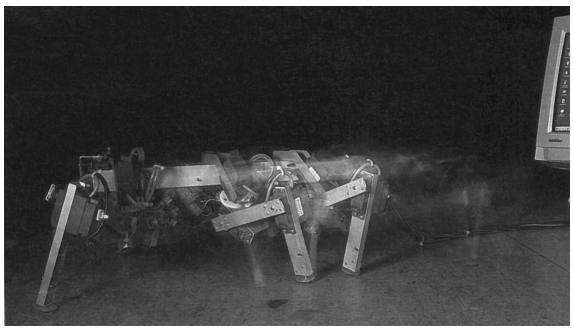

Figure 2: Walking machine TARRY II in motion

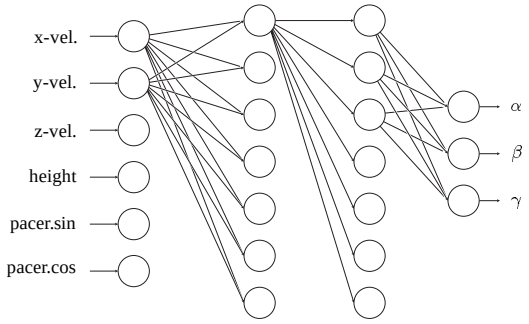

Figure 3: Neural Network

Table 1: Parameters of gait generation

Name	Meaning
XDot	Velocity in x-direction
YDot	Velocity in y-direction
OmegaZ	Angular velocity around z-axis
StepWidth[ ]	Step width per pair of legs
StepHeight	Step heigth
StepDuration	Step duration
RollAngle	Angle of rotation around y-axis
PitchAngle	Angle of rotation around x-axis
DutyFactor	Duty factor
BodyHeight	Height of body above ground
StanceCenter[ ]	Stance center per pair of legs
Phase[ ]	Phase difference per pair of legs
AmplitudeX	Ampl. superimp. osc. (x-dir.)
PhaseX	Phase superimp. osc. (x-dir.)
AmplitudeY	Ampl. superimp. osc. (y-dir.)
PhaseY	Phase superimp. osc. (y-dir.)

To train the neural networks a simplified set of input parameters together with the joint angles of the respective leg as outputs are used. Each of the six networks has six input neurons that are velocity in x- and y-direction, angular velocity around the z-axis as well as the body height for the individual leg. As already mentioned a pacemaker, giving two additional inputs, synchronizes all networks.

All sets of walking patterns as they have been created are only suitable for walking on even terrain. None of them is able to facilitate walking in rough terrain in the original combination.

To provide useful propulsion in rough terrain the given trajectories have to be adapted to meet the real environment. To do this, a set of sensors is used to observe the state and the properties of certain elements of the walking machine and to react in convenient ways.

These reactions, also called reflexes in the following, are able to initiate an adaptation of the input values of each neural network. On the one hand they can cause local reactions, which provide only changes to one leg. This method is used for small corrections. On the other hand they are able to manipulate the input values of all legs. This behavior is called a global action and is taken for large corrections or changes that demand cooperation between all legs, such as changes of direction of locomotion or the orientation.

With these coded reflexes the machine is able to climb or avoid obstacles, to walk over bumps and small holes as well as balancing slopes just by rearranging the input of the networks trained with basic gaits.

2. Sensorics

The robots have several types of sensors. As already mentioned, the most important part are the ground contact sensors mounted in each foot. They enable the machine to detect whether a foot has ground contact or not. They are simple switches just delivering binary information. Another important element, needed for proper locomotion is the measurement of the servo motors' current to detect collisions with obstacles. These sensors deliver sufficient information to initiate the so called Levator-Reflex, also observed at the walking stick insect. In addition the servomotors are able to measure their own angular position.

These two sets of main sensors are completed by several other input sources. To get the information about the load the middle segment of each leg has been equipped with four strain measurement gauges. This enables the robot to improve the ability to detect obstacles that do not come up in the longitudinal axis of the walking machine. To give the machine the ability to level its own orientation as well as to enable the internal model to identify its relation to the environment an inclinometer with two axes has been installed.

Most of the data the sensors deliver is smoothed and filtered to get reasonable information, suited for further processing.

3. Artificial reflexes

To meet the current environmental conditions several different modules are working to propel the machine in a useful way. This cooperation is done by reflexes of different levels where some of them have to rely on the information others have gathered or even have to delegate some tasks to them.

The most important of the implemented reflexes are the reflexes to overcome obstacles and to secure proper standing. They are followed by a reflex to correct the

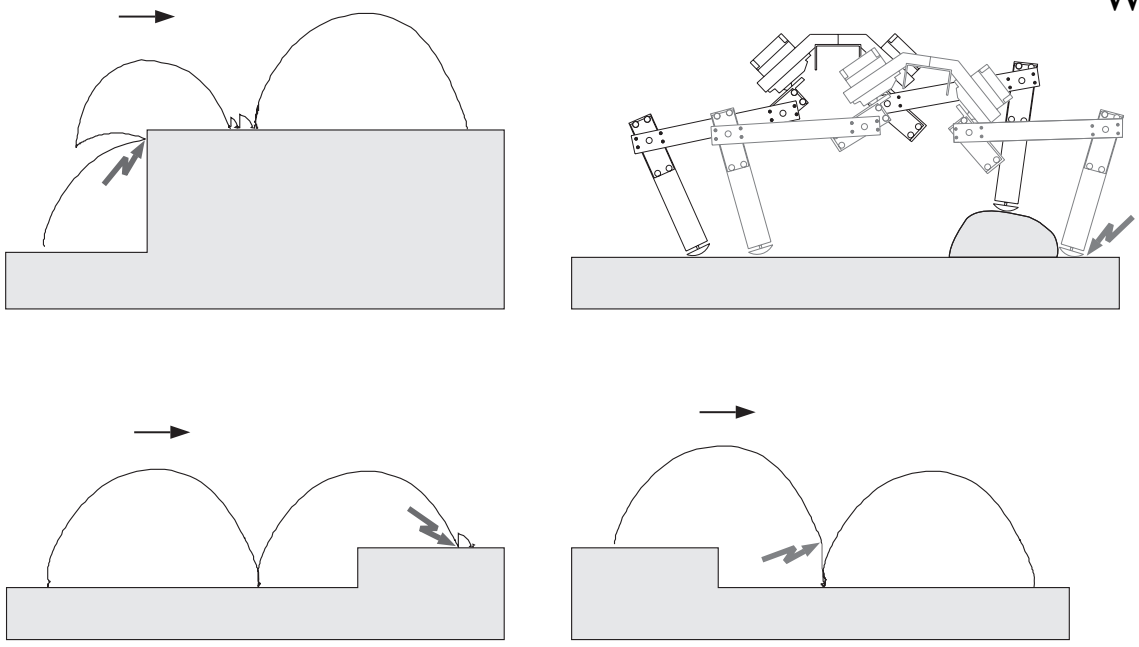

Figure 4: Schematic view of some reflex actions

machine after slipping from an obstacle, to lift or lower the body to a reasonable body height and body orientation. The lowest level is formed by reflex actions to navigate the machine, such as the ultrasonic module. An ultrasonic sensor scans the environment in front of the machine for large obstacles. If an obstacle in the current walking direction is detected the course is changed to pass by. The lower levels are only able to change values if they do not interfere with other reactions as they are supposed not to disturb critical events that demand instant reaction.

3.1. Securing ground contact

To secure proper ground contact the former pattern based approach[1] has been replaced by a neural network based method. Although the simple usage of the pattern-based approach is appealing it has two major drawbacks. It just works with selected gaits just as tripod gait and it does not take the inaccuracies and elasticity of the machine into account, as it just compares the current stance pattern with two fixed stance patterns.

The chosen neural approach relies on the real machine as model for itself. The machine walks on a plane with its basic gaits and the arising stance patterns combined with the belonging pacemaker information are recorded. This information is taken to train a neural network with the pacemaker as input and the stance pattern as output values. This method has the additional advantage, that leaps in the pattern on hitting the ground get smoothed in the output. During normal walk the current stance pattern is compared with the response of the network to the current pacemaker position, creating a correction if some values are not met.

3.2. Leveling the machine

To be able to fully level the machine, a sensor to detect the inclination of the robot has to be used. Before this sensor had been mounted the machine tried to achieve horizontal alignment by using information about the leg angles as well as the assumption of a plane ground. This method has been comparatively successful although it was not able to detect slopes e.g.

With the addition of the Analog Devices ADXL 202 accelerometer[5] the machine gained the ability to measure its angle in relation to the gravitation. The strategy to level out the measured angle relies partly on the other implemented reflex actions. To put the robot into horizontal orientation the geometric characteristics of the machine are used. Although the WALKINGLIB provides some parameters for the creation of walking patterns with roll and pitch angles (see table 1) another approach has been taken. To use the roll and pitch angles inside the neural control it would have been necessary to extend the number of input neu-

rons. To avoid this and keep the simple structure of the neural control a pure geometrical approach has been taken to change the inclination of the robot. In principle the geometric properties of the machine are changing periodically during a walking cycle, as shown in figure 5. Under normal conditions this effect only occurs in longitudinal direction, as the relative contact points change during the support phase of the feet, but depending on the situation even the traversal geometry could change.

The main part of the control strategy to align the machine to a horizontal state is based on a simple p-control changing the height of the body for the individual legs. With values that have been determined experimentally before, raise and lower commands for each leg are generated. Due to the geometric problems described above, this can cause a leg to take off the ground. The reflex to level out the machine does not take this into account but instead relies on a collaborating reflex. As a leg looses contact the respective reflex takes place automatically. It forces the leg lifting too early, to move back towards the ground, thus guaranteeing a secure standing.

The necessary parameters as the amplification of the controller have been derived experimentally to secure fast as well as stable control of the inclination. The control mechanism is able to deal with small changes as they occur in normal walking as well as with seesaw like situations.

If large changes in inclination occur over a short period of time the machine stops walking to adjust to the new situation. By this mechanism it is also possible to deal with the large changes that occur if the machine has climbed an obstacle and slips down.

4. Ground map

The coordination of the walking stick insect *carausius morosus* is built in an extremely decentralized

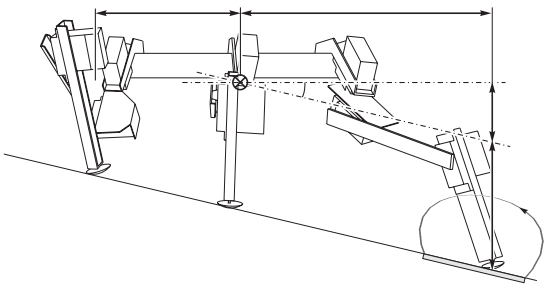

Figure 5: Geometric proportions of TARRY II

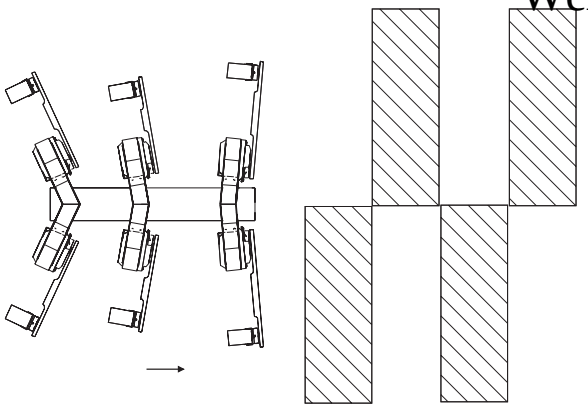

Figure 6: Alternating beams as obstacles

manner[6], working with stimulating and repressive excitements. The system does not seem to affect the feet height of lateral neighboring legs. Due to this the subsequent legs also collide with an obstacle, even if it has been hit before.

This was the same with the walking machine TARRY. But as we use a more centralized approach we are able to create a global repository for information the machine gathers. To take the inaccuracy of the robot and its relatively poor repetitive accuracy into account, we just memorize the small area directly below the machine enlarged by a reasonable border.

Due to the machines knowledge about its current angular servo positions and the feet with ground contact it is able to determine the position of the feet in a body fixed frame. Together with the orientation of the body the information about the relative height of the ground can be achieved. With this information a local map is constructed. As the machine itself has no idea about its geometry it is not able to compute the cartesian position of the feet with the known joint angles without help. To get this information, the WALKINGLIB provides an internal model for the machine that is updated permanently. The current joint and inclination angles are given and the model calculates the feet positions that can be used to update the internal map. The mapped area is moving with the machine. With an enlargement of these foot contact points to areas the machine is able to adapt the height of the successional feet before a collision takes place. As a result the machine bears recently detected obstacles in mind to pass by fluently and without interruption after the first collision has taken place.

An example for an obstacle configuration is given in figure 6. The machine approaches a set of alternating obstacles. At this point the map looks like in figure 7a. As there has been no disturbance the map con-

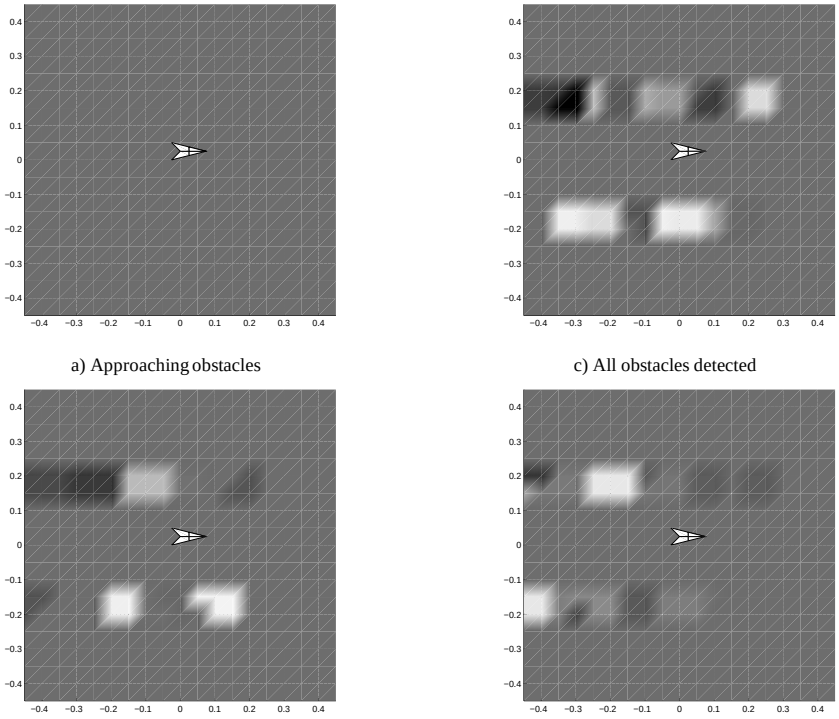

a) Approaching obstacles

c) All obstacles detected

b) Between the obstacles

d) Crossing completed

Figure 7: Graphical representation of an evolving ground map

sist just of one level, indicated by the plain gray color. In fig. 7b the machine has taken the first three obstacles, that are now marked as light spots, denoting the elevated ground. Due to inaccuracies the dark trail in the upper left area has been created. As reaction to lost ground contact detected by the respective reflex the last left leg had to be lowered to reconstitute the contact. In fig. 7c TARRY II has passed all obstacles with at least one leg as they are marked in the map. Some more areas have been marked as lower-leveled, as described above. Finally in fig. 7d all obstacles have been passed completely. The inexactness of the detected ground begins to converge to the real, even ground, now.

As one can see in the video belonging to this example[7], the machine has been able to pass this configuration much faster and without unnecessary interruptions.

5. Conclusions

The control strategy of the TARRY walking machines utilizes a set of basic gaits learned beforehand to achieve movement. These basic gaits are created with a kinematical model and a set of parameters with the help of the WALKINGLIB. They are adapted due to sensor input by different kinds of reflex actions to create a proper leg motion. The different reflex actions are initiated by different kinds of sensor signals. Some of them work completely local with their own data, others rely on an internal model of the machine or on data that has been stored in a central repository. With these methods the machines are able to walk through different kinds of rough terrain. They are able to memorize the explored environment for a short time and to react according to this knowledge. In addition they are able to adapt their orientation according to the information of the inclinometer.

In future applications the robot should be able to adapt some of the internal parameters online as a reaction on recent explorations.

Acknowledgments

The TARRY project is supported by the German Research Council (DFG) within the scope of the special research program ”Autonomous walking”.

References

[1] Amendt, Oliver: *Neuronale Steuerung eines insektenartigen Schreitroboters*. Düsseldorf : VDI-Verlag, 1995 (Fortschritt-Berichte VDI Reihe 8 Nr. 483, Dissertation, Universität – GH Duisburg)

[2] Frik, Martin; Guddat, Martin; Karataş, Michael; Losch, Dirk C.: A novel approach to autonomous control of walking machines. In: Virk, G. S. (Editor); Randall, M. (Editor); Howard, D.(Editor): *Proceedings of the 2nd International Conference on Climbing and Walking Robots CLAWAR 99, 13–15 September, Portsmouth, UK*. Bury St. Edmunds : Professional Engineering Publishing Limited, 1999, p. 333–342

[3] Karataş, Michael; Losch, Dirk C.: WALKINGLIB, *Referenzhandbuch zur Programmbibliothek für die Gangmustergenerierung, Entwicklerversion*. Stand: Datum der vorliegenden Dokumentation / no. Fachbereich Maschinenbau, Fachgebiet Mechanik: Gerhard-Mercator-Universität – GH Duisburg, 2000

[4] Frik, Martin; Guddat, Martin; Karataş, Michael; Losch, Dirk C.: Terrain Adaptive Control of the Walking Machine TARRY II In: Proc. European Mechanics Colloquium, Euromech 375 – Biology and Technology of Walking, Munich, Germany, 1998, p. 108–115

[5] Analog Devices, Corporate Headquarters, Norwood, MA 02062-9106, `http://www.analog.com`

[6] Cruse, Holk; Bartling, Christian; Dreifert, et. al.; Walking: A Complex Behavior Controlled by Simple Networks. In: *Adaptive Behavior* 3, No. 4 (1995), S. 385–418

[7] TARRY walking machines homepage, Video examples, `http://www.tarry.de/videos_us.html`

Proceedings of the International Symposium on
Adaptive Motion of Animals and Machines,
Montreal, Aug.8-12, 2000

Novel Gaits for a Novel Crawling/Grasping Mechanism

Richard M. Voyles

Dept. of Computer Science and Engineering
University of Minnesota
Minneapolis, MN 55455
voyles@cs.umn.edu

Abstract

A novel, miniature robot designed to use its two arms for both manipulation and locomotion is described. Intended for military and civilian surveillance and search-and-rescue applications, the robot must be small, rugged, and lightweight, hence the desire for dual-use. The robot consists of two, three-degree-of-freedom arms that can stow completely inside the 75 mm diameter cylindrical body for ballistic deployment. Its design is loosely biologically inspired, but heavily constrained by sponsor demands. This paper describes the mechanism and design motivation as well as three novel locomotion gaits and a fourth conventional gait.

1 Introduction

The design of this small robot was biologically inspired in the sense of vague resemblance to biological organisms [1]. This is in contrast to the work of Beer et al [2], for example, in which biological organisms are rigorously studied and relevant lessons are adapted to mechanisms, or Pratt et al [7], for example, in which biological mechanisms are emulated. Rather, I took inspiration from mice, raccoons, and insects and melded them with the decidedly non-biological constraints of my DoD (U.S. Department of Defense) sponsors -- the desire for gun-launchability being a prime example of a non-biological constraint.

The project is aimed at investigating adaptation of very small, rugged, highly resource constrained robots with novel locomotion modes. The target applications are stealthy surveillance and reconnaissance (civilian SWAT teams and the military) and search and rescue after cataclysmic events (natural disasters or major military engagements).

Our primary design is a 40 mm diameter cylindrical robot that is 110 mm long. This robot [15], shown in Figure 1, uses two modes of locomotion: rolling and hopping. Unfortunately, it possesses no ability to manipulate (other than pushing). While manipulation is not required for surveillance, it could aid in "active camouflage" for improved stealth and in active path clearing for search-and-rescue. It also opens up many possibilities for additional missions.

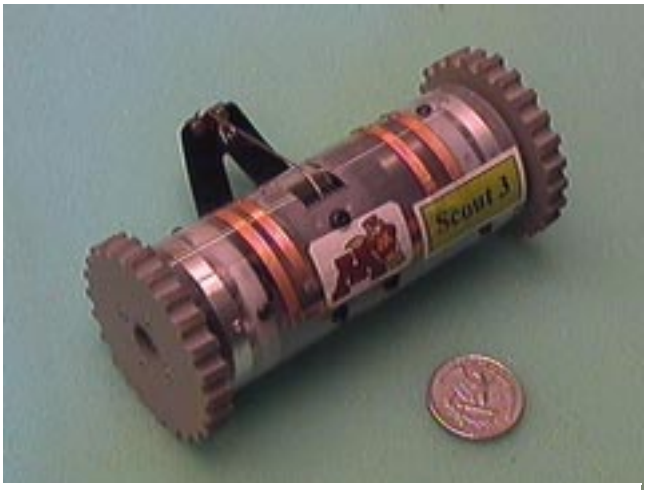

Figure 1: An example of the primary "Scout" mobile surveillance robot.

The resource constraints prevent merely adding arms to the existing "Scout" robot. Every cubic centimeter of mechanism would displace approximately 420 mW-hr of battery power. (For comparison, the CPUs consume around 40 mW while wheeled locomotion consumes from 180 - 600 mW, depending on terrain.) Instead, I chose to design a new robot based on dual-use: arms that serve as both manipulators and locomotors.

The dual-use concept was inspired by raccoons and some insects that use their legs as manipulators. This makes for efficient use of mechanisms, but dual-use generally implies sub-optimality for either use. Due to our space and power constraints, "mechanism efficiency" is of greater concern. Although I'm not aware of any biological creatures that normally possess only two limbs and drag their bodies along the ground, as in the robot described here, insects have been demonstrated to adapt to the loss of limbs.

This paper focuses on the design of the "TerminatorBot" mechanism and the novel (and conventional) gaits that it uses for locomotion. The aspects of adaptation of those gaits to varying terrain are currently under investigation and will be presented when comparative results are available.

2 Prior Work

Mobile manipulation is an area of research that has not been extensively addressed in the robotics community. Manipulators have been placed on mobile robots before (in fact, commercial offerings from Nomadic Technologies and RWI include various "manipulators" as options, including PUMA robots), but they have generally been treated disjointly. Sandia, for example, has put Schilling arms on a variety of platforms for teleoperation in hazardous environments (e.g. [8]). Carriker, et al integrated the path planning of low-DoF subsystems, but motion operations and design for each were treated separately [3]. Khatib has done significant work in integrating the motion control of arms and mobile bases through the Operational Space formulation [6], but has not performed visual servoing nor are the mechanisms dual-use. Brachiation robots, which use arms for locomotion by swinging like a gibbon, have also received some study (e.g. [9]), but current mechanisms are incapable of manipulation.

A few robots have been considered with dual use design. SM^2 and DM^2 at Carnegie Mellon ([12] and [13], respectively) and PolyPod/PolyBot at Stanford/Xerox ([16]) are notable examples. SM^2 and DM^2 are symmetric, biologically inspired inch-worm-like robots with grippers at each end. The robots are designed to walk around the outside of the space station to perform repair and inspection tasks. PolyPod is a modular serpentine manipulator of many similar joint modules designed with both manipulation and locomotion in mind.

Hirose's snake-like robots [4] have been investigated for both locomotion and manipulation with great success (and complexity). These are also clearly biologically inspired, as well. Several additional summaries of work on biologically inspired robotics (such as [1]) are well known to AMAM conference attendees.

3 Target Applications

With its reconfigurable payloads and dual locomotion modes, the Scout robot pictured in Figure 1 is quite capable. Rolling is fairly power efficient and hopping enables it to overcome obstacles, which are common for a robot only 40 mm tall. Unfortunately, while the hopping is required for practical mobility, it is rather time and power inefficient due to the inefficiency of the winch mechanism. Navigational certainty is also very low for hopping. The distance and direction of travel is poorly known and orientation in the plane upon landing is completely random.

Its small size and stealth are useful for military and civilian uses. As mentioned, equipped with a camera or microphone Scouts could be used in search-and-rescue operations following natural disasters (e.g. earthquakes) or terrorist actions (e.g. Oklahoma City bombing). There is also potential interest from civilian SWAT teams in hostage situations and police standoffs. These are natural military uses, as well, particularly in urban warfare environments that involve civilians. Surveillance robots of this size could be carried and deployed by warfighters, keeping the warfighters out of the line of fire and minimizing the risk of civilian casualties in the "heat of the moment."

With vibration detecting payloads, Scouts can be deployed along a roadside to discretely monitor traffic for unique vibration signatures indicating heavy equipment or large troop movements. Finally, it has been suggested they could be used to carry small distributed explosive charges that can be amassed to sufficient volumes through their numerosity. This can serve for demolition of specific targets or detonation of land mines or other unexploded ordnance.

While the Scouts' dual locomotion modes are necessary to achieve many of these missions in real environments, there are concerns they may be inadequate for particular scenarios, hence the investigation of alternate designs. For example, the Scouts would be most useful in search-and-rescue operations in which the damage is too severe and constricting to send in dogs (which arguably will be superior to robots in sensing for the near future). But large amounts of rubble within extremely cramped spaces may thwart both locomotion modes of the Scouts (too much rubble to roll, too little headroom to hop). A crawling robot such as TerminatorBot could fill this niche in which available headroom is, on average, just a few times the rubble size.

In surveillance tasks, it is desirable for the robot to conceal itself. The Scouts will only be able to make use of existing open spaces such as underneath furniture. A robot with manipulators could actually pull objects over itself, creating its own cover and enhancing its stealth. A miniature, telescoping pan/tilt unit has been developed to facilitate such stealthy surveillance, too [14].

The idea of many small robots amassing a useful charge from small, insignificant explosives has been suggested by researchers in a number of scenarios. The main problem with this idea is that the efficiency of explosives is highly dependent on their placement. A bunch of mobile robots with no ability to manipulate would amass a rather inefficient bomb. Just one or two robots with the ability to locomote *and* manipulate could carefully place the charges, demanding many fewer trips to achieve a given objective.

Finally, in many of these scenarios, the ability to dig or burrow in light soils is be beneficial. This could provide camouflage during surveillance, additional access during search-and-rescue, and an alternate detonation means during de-mining.

4 Mechanism Design

The robot consists of a cylindrical body with two 3-degree-of-freedom (DoF) arms that can fully stow inside the

Figure 2: CAD rendering of TerminatorBot in the stowed configuration.

body (Figure 2). The ultimate goal is to fit the 40mm diameter form factor of a launchable grenade, but the current prototype is approximately two times oversize with a diameter of 75 mm and maximum reach of each arm of 170 mm.

Two gearmotors within the body drive a 2-DoF shoulder joint through a differential. This arrangement couples the torque of both motors through the same axis of rotation for pure motions around the principal axes. Encoders on each motor provide position feedback for positioning link 1. The gearmotors have a relatively low ratio of 17:1, but an additional reduction stage in the form of a 15:1 worm gear boosts the total gear ratio to 255:1 and prevents back-driving the motors. Back-drivability is bad for power conservation in this case.

The first link is 100 mm in length and 23 mm in width, allowing the inclusion of the gearmotor and encoder for the third joint within. A right-angle gear arrangement transfers torque to a traditional 1-DoF elbow joint that drives the 70mm second link. Incorporated into the joint are torque sensors for direct measurement of joint torque at the point of application. Force/torque sensing is incorporated for use during manipulation of objects and also to enable servoed back-drivability of the gear train.

The torque sensors include a number of important design features to increase their utility. Each sensor wheel (see Figure 4) is designed to provide two axes of force/torque. A traditional torque sensor (see cross-section in Figure 5) consists of four to eight radial flexures arranged with regular spacing about the center point [10]. By biasing the distribution of flexures toward a single diameter, as in Figure 5, the sensor is made more sensitive to forces along **F**. As in a multi-axis wrist force/torque sensor, the flexures can be used to sense multiple components. But a common problem with multi-axis sensors is maximum load capacity is dominated by torques, which multiply quickly. To combat

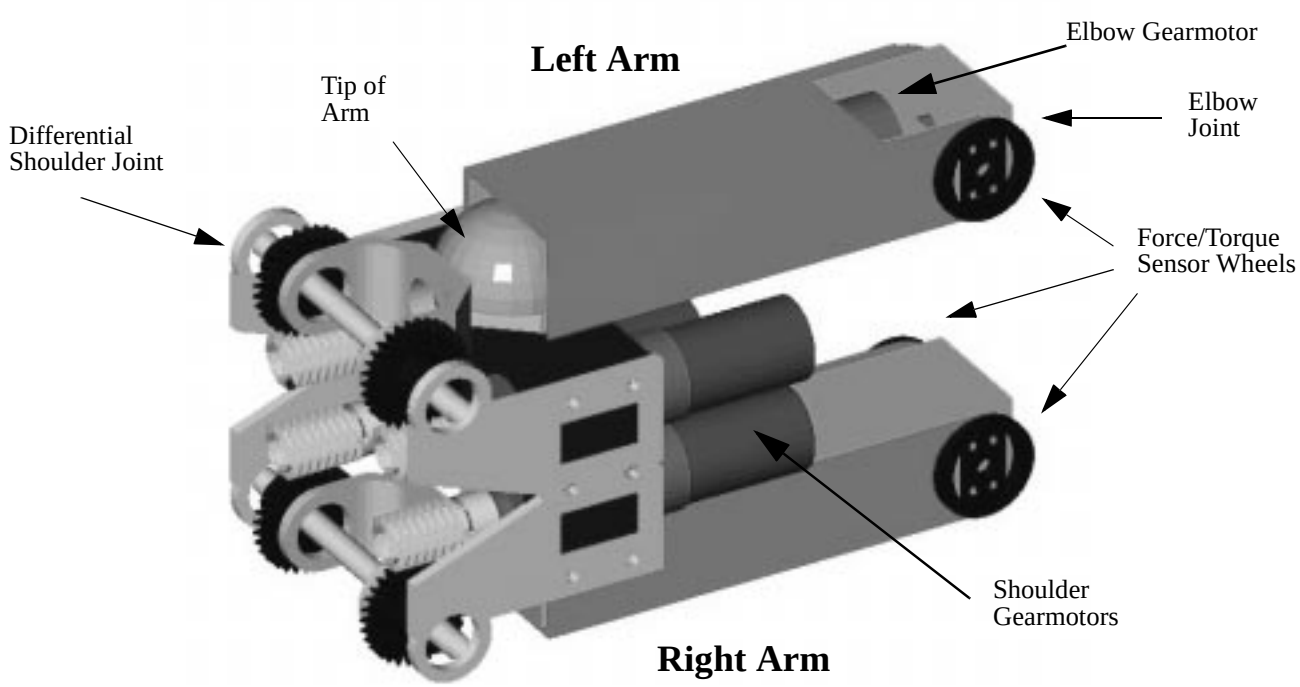

Figure 3: Internal parts of the TerminatorBot in the stowed configuration. Bearings and some other parts are not illustrated.

Figure 4: 2-DoF force/torque sensor wheel for elbow joint.

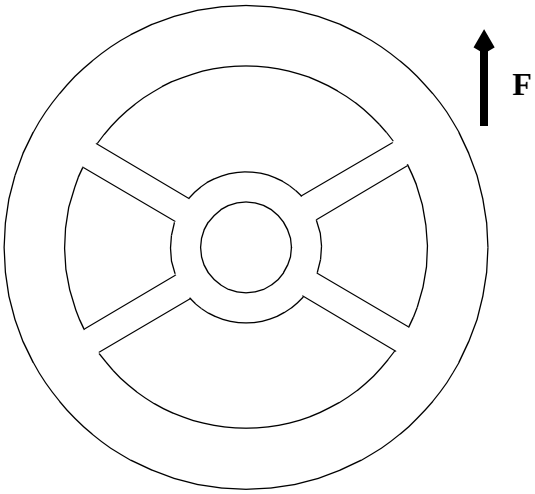

Figure 5: Cross-section of "traditional" torque sensor with radial flexures (although irregular flexure spacing is "non-traditional" - see text).

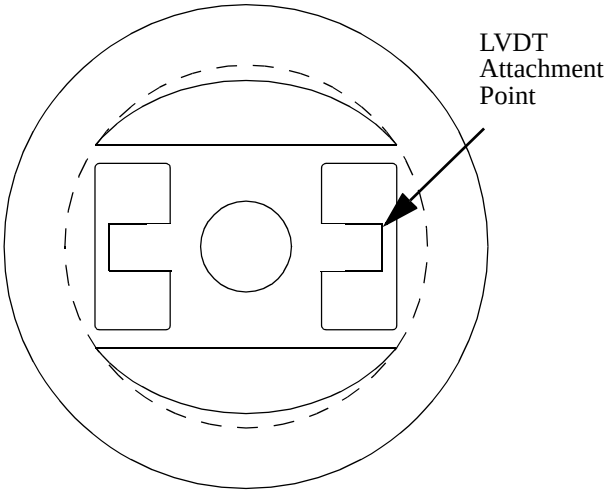

Figure 6: Cross-section of the force/torque sensor wheels used on TerminatorBot.

this problem, the flexures are placed off the radii and perpendicular to the force (Figure 6). For a given flexure dimension, this diminishes the torque sensitivity and increases the force sensitivity, making the response more isotropic.

The use of strain gages on such a small device (The flexures are only 2 mm wide and 2.5 mm long) would present manufacturing problems and the compressive strains introduced by the off-radii flexures would inject noise. Instead, LVDTs (linear variable differential transformers) are mounted between the hub and the link to sense pure deflection as in [5]. LVDTs are insensitive to the noise strains experienced by the flexures and, due to their high frequency carrier wave excitation, are more immune to electrical noise produced by the motors and other sources.

Finally, two sensor wheels are employed on each joint, one on each side. This allows the measurement of a third axis of force at the manipulator tip, complementary to the other two components. This is somewhat problematic because the sensors are not collocated and it is impossible to disambiguate a force at the tip from a transverse torque. Nonetheless, the additional force axis will be valuable during manipulation as the manipulators do possess the ability to move out of plane and it is unlikely that transverse torques will come into play during manipulation of objects (which is the only time precise measurements are required).

The tips of the arms are hemispherical shells that serve a dual purpose. The concave side is claw-like and is useful for traction during locomotion and even for digging in very light soils, such as sand. When manipulating objects, the arms will flip 180 degrees, exposing the convex sides to one another. These surfaces are like fingertips and provide a fixed center of rotation for objects moving across the spherical surface. Coupled with the force/torque sensors, this can be modeled as a passive, but sensable, fourth joint on each arm during manipulation.

The assembled prototype is shown in figures 7 and 8. The arms of the prototype are 105 grams each and the body is 440 grams excluding batteries and CPU, for a total of 650 grams in mechanism alone.

5 Locomotion Gaits

Novel mechanisms often suggest novel and mechanism-specific gaits, as was the case with PolyPod [16]. There are four proposed classes of locomotion gaits for use on TerminatorBot: swimming gaits, narrow-passage gaits, bumpy-wheel gaits, and a dynamic rolling gait. All the gaits are used on dry land, but the "swimming gaits" are so named because of their similarity to two-armed swimming strokes. These are the "conventional" gaits, characterized by stances with the arms slightly splayed out to the sides and a full stride through much of the range of motion of the shoulder joints (Figure 9). To clarify operation on the target mechanism. Figure 10 contains a sequence of images of the TerminatorBot "swimming."

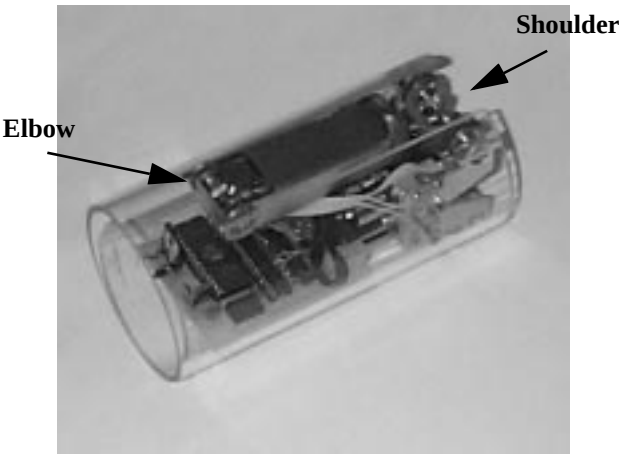

Figure 7: Assembled TerminatorBot in stowed configuration.

Figure 8: Assembled prototype with microcontroller for joint control in deployed configuration.

The narrow-passage gait is a novel gait that makes profitable use of the differential shoulder joint and unique ability of the first link to rotate around its principal axis. Motivated by the ability of mice, which can penetrate any opening through which they can pass their head, the robot can gain passage through openings that are no wider than the body itself (provided navigational capability is sufficiently precise). The motions of the limbs require zero lateral clearance. (Although required vertical clearance is slightly

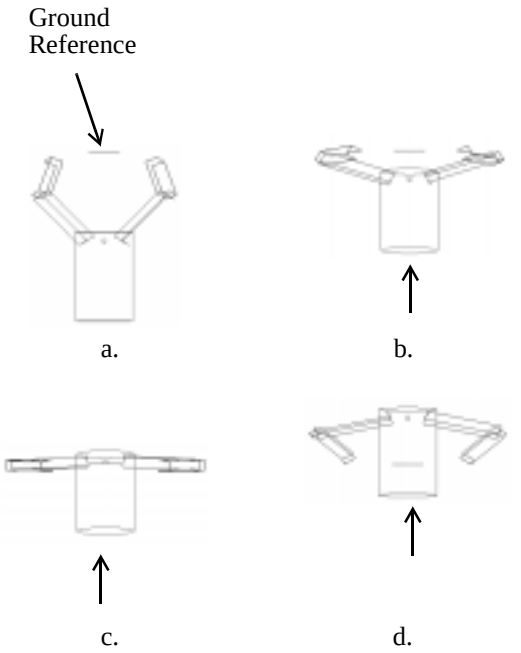

Figure 9: Simulation of an example swimming gait. (top view)

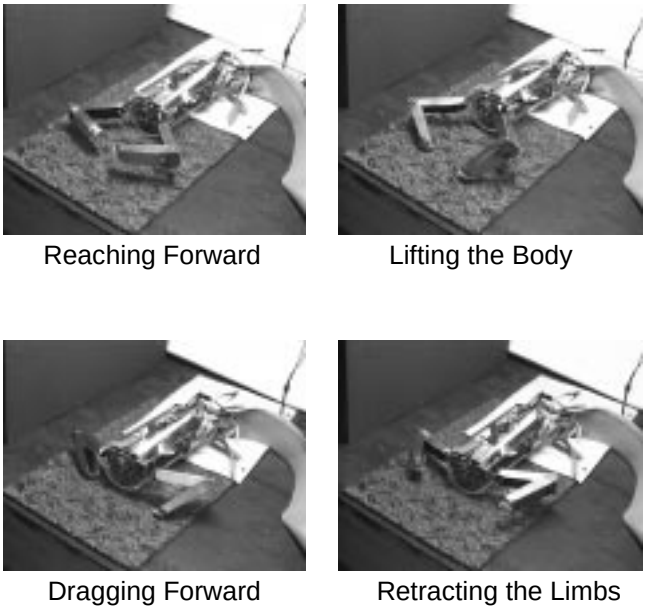

Figure 10: Implementation of a swimming gait on the prototype robot.

larger than one body diameter.) Illustrated in Figure 11 with both top and side views, motion is effected entirely forward of the robot's body as it pulls itself along. Again, Figure 12 illustrates the narrow-passage gait on the prototype.

The bumpy wheel gait is another novel gait that makes use of the ability of the differential shoulder to rotate 360 degrees. As Figure 13 indicates, the arms "roll" like broken

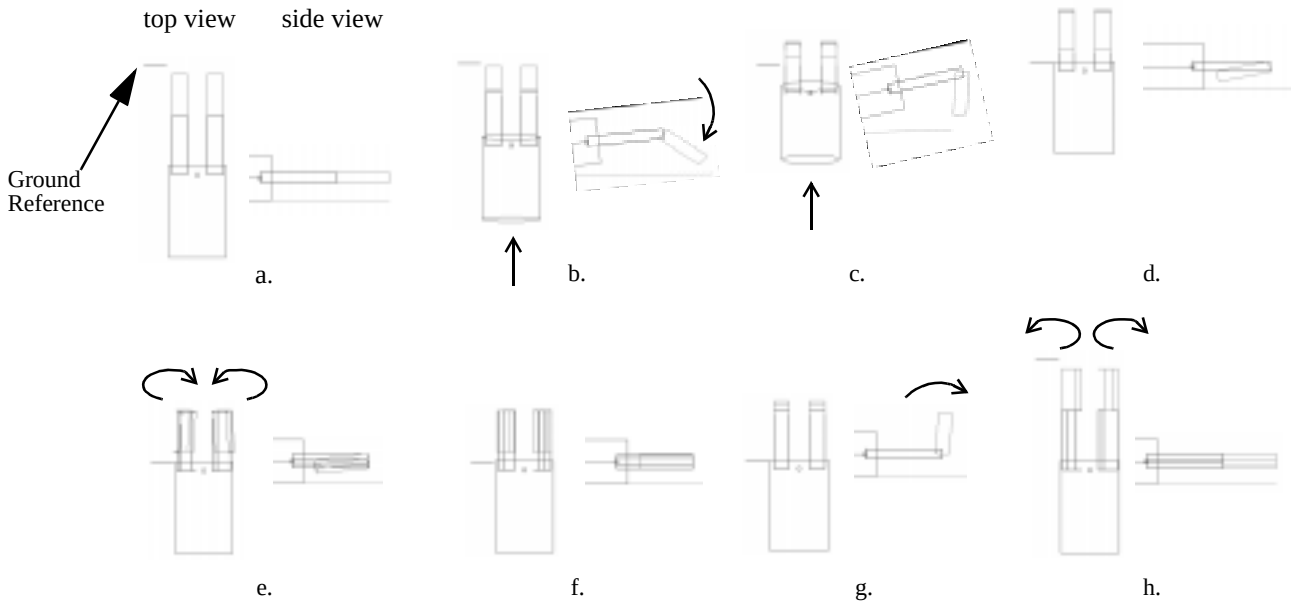

Figure 11: A narrow-passage gait. The robot's arms start a stride outstretched in front of it. In a. through d. it pulls itself forward with the elbow joints, while in e. through d. it rotates the arms back into position to begin another stride. The end effector (claw) is not drawn, hence the space between the robot and the ground line.

wheels to move the body forward. This is the most powerful gait as all four shoulder motors are coupled to drive the body forward and forces on the elbow joint are absorbed by the structure. In fact, the current prototype does not have slip-ring electrical contacts, so continuous rolling of joint two is not permitted. Still, the bumpy wheel gait can be implemented by rolling 180 degrees, straightening the elbow, and rotating back to the start position.

The body-roll gait is quite different from the others. Rather than being a kinematic approach to dragging the robot to its destination, this proposed locomotion gait uses dynamics and an assumption of a smooth, level surface. Since the arms can tuck inside the cylindrical form of the body, the "can" is able roll, once it gets going. The body-roll uses a single arm to build angular momentum by swinging it perpendicular to the roll axis. The other arm tries to prevent

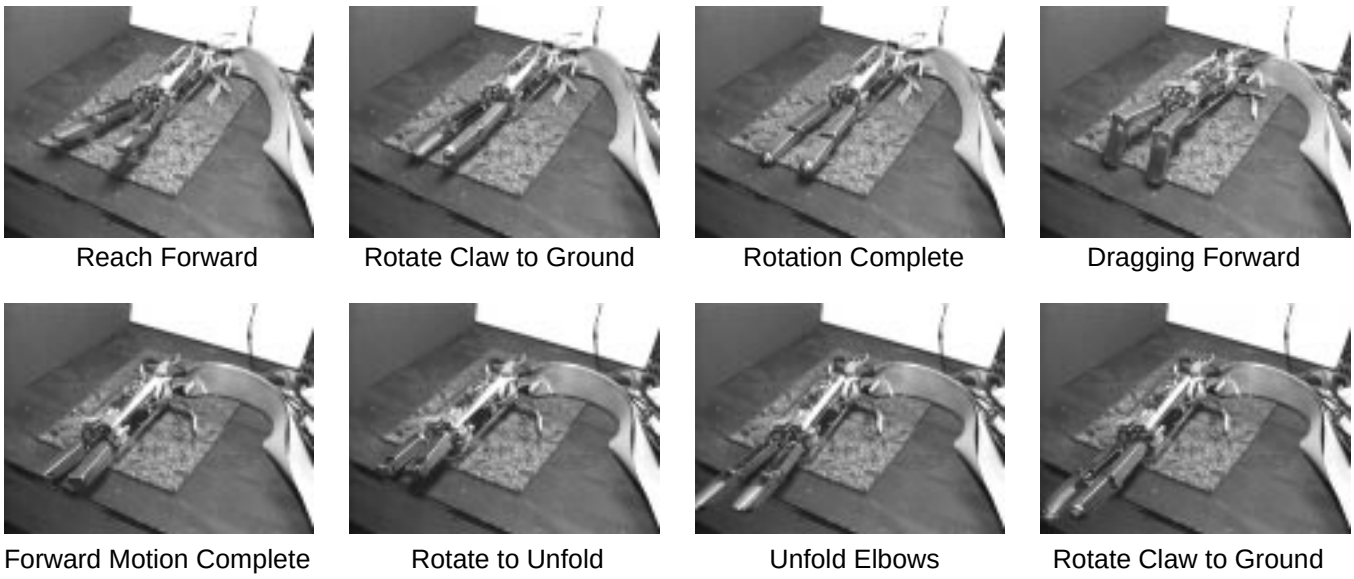

Figure 12: Implementation of the narrow-passage gait on the protptype robot.

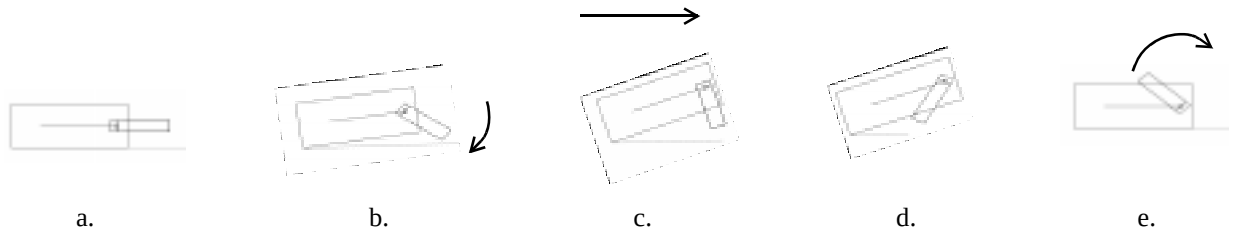

Figure 13: A bumpy wheel gait (side view). The torque of all four shoulder motors is coupled to produce forward motion (toward the right). Again, the claw is not drawn.

kick-back during the swinging motion. The swinging arm then folds up, into the body, causing a reactionary torque that rolls the body forward or backward. In order to effect turns, a swimming gait would most likely be used to reposition the body. The use of an accelerometer for gravity sensing would provide odometry.

The body-roll gait can be achieved using one arm, but one-arm gaits, in general, are another category that could be based on variations of the other four gaits. These can be implemented as emergency homing measures in the event of an arm failure.

It can be argued that these gaits are inefficient compared to wheels or even legs that are optimized for locomotion. This may be true. Dual-use generally implies non-optimal for both uses. The motivation behind this design is that both locomotion and manipulation are required to maximize utility of the robot as a whole, but size and ruggedness constraints prohibit redundant systems optimized for their specific purposes. In this sense, we are trying to optimize the robot as a whole, rather than specific parts.

6 Acknowledgments

This material is based upon work supported by the Defense Advanced Research Projects Agency, Electronics Technology Office ("Distributed Robotics" Program), ARPA Order No. G155, Program Code No. 8H20, Issued by DARPA/CMD under contract #MDA972-98-C-0008 and by the Air Force Research Laboratory under Contract Number F30602-96-2-0240. Any opinions, findings, conclusions or recommendations expressed herein are those of the author and do not reflect the views of the Air Force Research Lab, DARPA, Carnegie Mellon or the University of Minnesota.

7 References

[1] Beer, R.D., H.J. Chiel, R.D. Quinn, and R.E. Ritzmann, 1998, "Biorobotic Approaches to the Study of Motor Systems," in *Current Opinion in Neurobiology*, v. 8, pp. 777-782.

[2] Beer, R.D., R.D. Quinn, H.J. Chiel, and R.E. Ritzmann, 1997, "Biologically Inspired Approaches to Robotics," in *Communications of the ACM*, v. 40, pp. 30-38.

[3] Carriker, W.F., P.K. Khosla, B.H. Krogh, 1991, "Path Planning for Mobile Manipulators for Multiple Task Execution," in *IEEE Transactions on Robotics & Automation*, v. 7, n. 3, June, pp. 403-408.

[4] Hirose, S., 1993, *Biologically Inspired Robots*, Oxford University Press, New York.

[5] Holmberg, R., S. Dickert, and O. Khatib, 1992, "A New Actuation System for High-Performance Torque-Controlled Manipulators," in *Proc. of the Ninth CISM-IFToMM Symp. on the Theory and Practice of Robots and Manipulators*, Udine, Italy, pp. 285-292.

[6] Khatib, O., 1999, "Mobile Manipulation: The Robotic Assistant," in *Robotics & Autonomous Systems*, v 26, n. 2-3, Feb. pp. 175-183.

[7] Pratt, J., P. Dilworth, and G. Pratt, 1997, "Virtual Model control of a Bipedal Walking Robot," *Proc. of the IEEE International Conf. on Robotics and Automation*, v 1, pp. 193-198.

[8] Morse, W.D., D.R. Hayward, D.P. Jones, A. Sanchez, D.L. Shirey, 1994, "Overview of the Accident Response Mobile Manipulation System (ARMMS)," in *Proceedings of the ASCE Specialty Conference on Robotics for Challenging Environments*, Albuquerque, NM., pp. 304-310.

[9] Saito, F., T. Fukuda, F. Arai, "Swing and Locomotion Control for a Two-Link Brachiation Robot," in *IEEE Control Systems Magazine*, v. 14, n. 1, Feb. pp. 5-11.

[10] Vischer, D. and O. Khatib, 1995, "Design and Development of High-Performance Torque-Controlled Joints," *IEEE Transactions on Robotics & Automation*. v 11, n 4, pp. 537-544.

[11] Voyles, R.M., G. Fedder and P.K. Khosla, 1996, "A Modular Tactile Sensor and Actuator Based on an Electrorheological Gel," *Proceedings of the IEEE International Conference on Robotics and Automation*, v1, pp. 13-17.

[12] Xu, Y., H.B. Brown, Jr., M. Friedman, and T. Kanade, 1994, "Control Systems of Self-Mobile Space Manipulator," in *IEEE Trans. on Control Systems Technology*, v. 2, n. 3, pp. 207-219.

[13] Xu, Y., C. Lee, and H.B. Brown, Jr., 1996, "A Separable Combination of Wheeled Rover and Arm Mechanism: (DM)2," in *Proceedings of the IEEE International Conference on Robotics and Automation*, v. 3, pp. 2383-2388.

[14] Yesin,K.B., B.J. Nelson, N.P. Papanikolopoulos, R.M. Voyles, and D. Krantz, 1999, "Active Video Modules for Launchable Reconnaissance Robots," in *Proc. of the 2nd International Conf on Recent Advances in Mechatronics*, May, Istanbul.

[15] Hougen,D.F., S. Benjaafar, J. C. Bonney, J. R. Budenske, M. Dvorak, M. Gini, H. French, D. G. Krantz, P. Y. Li, F. Malver, B. Nelson, N. Papanikolopoulos, P. E. Rybski, S. A. Stoeter, R. Voyles and K. B. Yesin, 2000, "A Miniature Robotic System for Reconnaissance and Surveillance," in *Proceedings of the 2000 IEEE International Conf. on Robotics and Automation*.

[16] Yim, M., 1994, "New Locomotion Gaits" in *Proc. of IEEE Int. Conf. on Robotics and Automation*, San Diego, CA.

Session

Modeling and Analysis of Motion

Proceedings of the International Symposium on
Adaptive Motion of Animals and Machines,
Montreal, Aug.8-12, 2000

Damping And Size: Insights And Biological Inspiration

Mariano Garcia[1], Arthur Kuo[2], Anne Peattie[3], Paul Wang[4], and Robert Full[5]

[1]Dept. of Integrative Biology, University Of California, Berkeley, CA 94720, garcia@socrates.berkeley.edu

[2]Dept. of Mech. Eng. And Appl. Mech., University of Michigan, Ann Arbor, MI 48109, artkuo@umich.edu

[3]Dept. Of Biology, Lewis & Clark College, Portland, OR 97219, peattie@lclark.edu

[4]Dept. of Integrative Biology, University Of California, Berkeley, CA 94720, palwag@uclink4.berkeley.edu

[5]Dept. of Integrative Biology, University Of California, Berkeley, CA 94720, rjfull@socrates.berkeley.edu

Abstract

We present scaling arguments verifying that as an animal's size decreases, the relative friction and viscosity (damping ratio) of their limbs increases. These intuitive predictions are supported by data from other studies, our experiments on the death head cockroach (Blaberus Discoidalis), and our modeling results, all of which we briefly describe. High damping has implications for control, favoring the use of simple feedforward strategies; we show evidence that this is actual control mechanism which cockroaches use. Additionally, high damping ratios and the presence of Coulomb friction lead to a preference for running over walking, which is also observed. For the joints we studied, the majority of the damping was apparently due to the mechanics of the joint itself, and not to the soft tissues.

1. Introduction

Relative to their size, cockroaches are among the fastest land animals [1]. In addition, there is a growing body of knowledge regarding their kinematics and biomechanics. Thus, they are attractive design targets for biomimetic locomotive robots [2].

Most biomimetic walking and running robots fall far short of the dynamic capabilities of their biological relatives. One reason is that the robots are typically built on larger length scales than the animals that inspire their design, and the dynamical characteristics and control strategies of the animals are not preserved.

In this paper, we propose a particular model for the scaling of damping in small insects, summarize our results of ongoing laboratory damping measurements in cockroaches, suggest how these phenomena are relevant to control, and briefly test some of our hypotheses with observations and data from the animals.

2. Scaling Theory

During legged locomotion, a leg can be in one of two phases: swing phase or stance phase. During swing phase, the leg moves forward relative to the body, and is commonly thought to act like a pendulum [3]. During stance phase, the leg is thought to behave more or less like an inverted pendulum as it supports the body. (We say "more or less" because for running gaits, a pogo stick is a more appropriate analogy than a pendulum, but the pogo stick is a combination of an inverted pendulum and a spring.) The dynamic behaviors of these two cases will be different because in stance phase, the body is considered to be part of the pendulum, while in swing phase, the body is not considered to be part of the pendulum. In a sense, we will test the extent to which these pendulum assumptions are valid.

Using pendulum-like models, studies over the past thirty or so years have established scaling rules which have mostly dealt with the effects of animal size on limb shape and gait characteristics [4, 5]. In humans and large animals, we are accustomed to the notion that the limbs are underdamped when they move as pendula; that is, friction and viscous effects (which we refer to collectively as "damping") play a minor role in the limb dynamics during one step, both in swing and stance phases. In cockroaches and smaller animals, however, damping may not be negligible, especially during the swing phase.

We use a simple second-order mechanical model, shown in Figure 1, to quantify how damping should increase as length scales decrease. Consider a system with a single cylindrical limb connected to the body at a hinge joint. The limb has mass m, density ρ, length L, diameter d, and angular position θ (positive counterclockwise), and we could include the effects of gravity g, depending on how the joint is oriented with respect to gravity (neglect g for sprawled postures, include g for upright postures). A single muscle actuates the

limb; this muscle is modeled as an ideal force generator which produces a force $f(t)$. This muscle and its (presumably relaxed) component on the opposite side of the joint have some stiffness and viscosity which can be collected into a spring and damper acting in parallel. Because muscle tissue consists of sarcomeres in series and in parallel, the spring and damper are assumed to have stiffness and viscosity proportional to the limb cross-sectional area A and inversely proportional to the limb length. The net stiffness will be proportional to the muscle elastic modulus E, and the damping will be proportional to the viscosity γ; E and γ are material constants which are invariant to length scale. We may include the damping torque of the joint itself, which we assume is equal to the product $C\dot{\theta}$, where C is proportional to the amount of surface area contact at the joint $C = \hat{C}A$ (assuming that the joint surface area scales with A). When considering the limb as an inverted pendulum, we also need to know the effective mass M of the body, which for simplicity will be concentrated at the body center of mass.

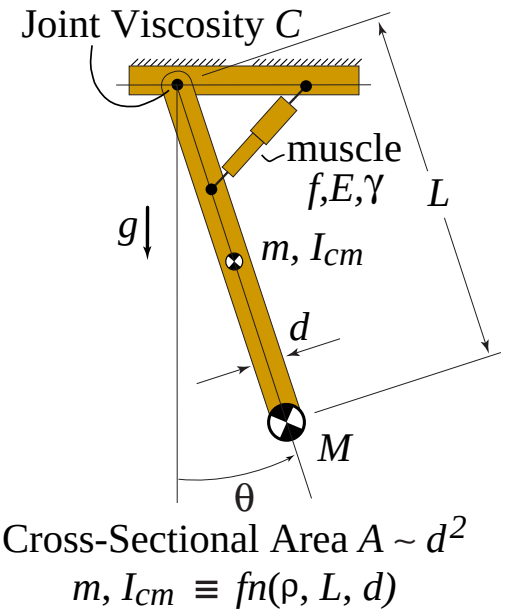

Figure 1: Theoretical pendulum model used to predict scaling of damping ratio. For the stance phase, it would be more correct to present an inverted pendulum, but for consistency and familiarity we only use one orientation. Moreover, the scaling of the damping ratio does not change with the pendulum orientation.

The general dynamics of the system (both swing and stance phase) are described by an equation of the form

$$J\ddot{\theta} + B\dot{\theta} + K\theta = rf(t), \tag{1}$$

where J is an inertia term, K is a stiffness term, and B is a damping term. The actual scaling relationship will depend on whether it is the swing phase or stance phase under consideration, as well as several other assumptions, the most important of which is the relative scaling of lengths and diameters. These assumptions affect the constants J, K, and B (which in turn are functions of m, ρ, L, d, $\hat{C}$, A, etc.) in Equation 1, and hence the damping. The details of the calculations can be found in a full-length paper in preparation [6].

We are interested in the damping ratio ζ,

$$\zeta = \frac{B}{2\sqrt{JK}}, \tag{2}$$

which describes the significance of the damping over short time scales. If $\zeta > 1$, the damping dominates the dynamics and the system is said to be *overdamped*, whereas if $\zeta < 1$, the damping is negligible and the system is said to be *underdamped*. If $\zeta \approx 1$, the system is *critically damped*; critical damping is associated with fast return to equilibrium. In general, higher ζ suggests that more energy is lost during voluntary motions, while if $\zeta = 0$, no energy is lost. The value of ζ also has implications for control, as we will address below.

2.1. Swing Leg

We first restrict our attention to the behavior of the swing leg. Independent of the assumptions, we find the general rule that damping ratio increases as leg length (or length scale) decreases. The leading terms in the series expansions for ζ as a function of L about $L = 0$ are shown in Table 1, for a number of different scaling laws. These include isometric scaling ($d \sim L$) and elastic similarity ($d \sim L^{3/2}$) [7], with and without joint viscosity C.

2.2. Stance Leg

Now we consider the behavior of the stance leg, during which the body is considered to be part of the pendulum, now inverted and hinged at the ground (we neglect the limb mass m and assume that the body mass M is attached at the top end of the pendulum). Since damping is assumed to be insensitive to limb orientation, Equation 1 and Figure 1 still apply if we fix the foot on the ground and swing the leg upside down (in order to simplify the experiments described later). In the stance phase, the scaling predictions differ more, depending on the assumptions used. For most of the assumptions, damping ratio increases as leg length decreases, as shown in Table 2.

Assume	$g \neq 0$	$g = 0$
$d \sim L, C = 0$	$\zeta \sim L^{-1}$	$\zeta \sim L^{-1}$
$d \sim L^{3/2}, C = 0$	$\zeta \sim L^{-1/2}$	$\zeta \sim L^{-1/2}$
$d \sim L, C \neq 0$	$\zeta \sim L^{-2}$	$\zeta \sim L^{-2}$
$d \sim L^{3/2}, C \neq 0$	$\zeta \sim L^{-5/2}$	$\zeta \sim L^{-5/2}$

Table 1: Leading-term scaling results for the damping ratio ζ during swing phase as a function of limb length L as $L \to 0$. Assumptions are as follows: $g \neq 0$ represents upright posture, while $g = 0$ if gravity is neglected (sprawled posture). $C = 0$ neglects joint viscosity, while $C \neq 0$ includes a joint viscosity term proportional to surface area and joint angular velocity. $d \sim L$ assumes geometric scaling of limb thickness, while $d \sim L^{3/2}$ assumes elastic similarity as proposed by McMahon [7]. Regardless of the assumptions used, ζ increases with decreasing L, suggesting that damping is more dominant at smaller length scales.

Assume	$g \neq 0$	$g = 0$
$d \sim L, C = 0$	$\zeta \sim L^{-1}$	$\zeta \sim L^{-1}$
$d \sim L^{3/2}, C = 0$	$\zeta \sim L^{1/2}$	$\zeta \sim Const.$
$d \sim L, C \neq 0$	$\zeta \sim L^{-2}$	$\zeta \sim L^{-2}$
$d \sim L^{3/2}, C \neq 0$	$\zeta \sim L^{-3/2}$	$\zeta \sim L^{-2}$

Table 2: Leading-term scaling results for the damping ratio ζ during stance phase as a function of limb length L as $L \to 0$. See the caption of Table 1 for an explanation of the assumptions. For most of the assumptions, and for the most reasonable assumption of joint viscosity and elastic similarity, stance phase ζ increases with decreasing L.

2.3. Comments On Scaling Results

The scaling results shown in Tables 1 and 2 demonstrate that, for both isometric and elastic scaling assumptions, the length scale decreases as the damping ratio increases. Insects operate at much smaller length scales than humans, and so the higher damping ratio should be evident. It is of course expected that at very small length scales, other forces which are not modeled in Equation 1 might become relevant, such as more complicated viscoelasticity, plastic-like bulk deformation effects, sliding friction, etc. It is also important to note that comparing scaling as $L \to 0$ is not the same as comparing actual scaling exponents for small but finite L. In the former case, the leading term dominates the scaling, but in the latter case, the relative contributions of the terms in the series depend on the particular values of the length-independent constants ($\hat{C}$, E, and γ, for instance). By themseles, our results should not be used to compare assumptions about scaling as much as to indicate that at small length scales, damping plays an increasingly dominant role in the dynamics of small animals.

3. Measurements From Cockroach Legs

There are little data on how damping scales with size, in part because controlled (e.g., muscle activation) and uncontrolled (e.g., viscous) effects are usually not separated in the motor control literature. In humans, Reiner and Edrich [8] estimated the passive joint moments of the lower extremities and found that damping was negligible for most purposes. At the smaller scale of the human finger, Hajian and Howe [9] found damping ratios at the human finger joint to be of order(1); they also found that the ratios differed by a factor of about 2, depending on whether or not the joint was extending or flexing. Esteki and Mansour [10] also studied the properties of a finger joint and applied a nonlinear viscoelastic model to characterize the passive joint moment. They claimed that joint friction is relatively insensitive to joint speed in human fingers. We estimated the passive damping properties of cockroach legs, with the expectation that they would exhibit greater damping than seen in human limbs. We also wanted to determine the accuracy of a damping model of the form of Equation 1.

3.1. Method

To estimate passive damping parameters of cockroach muscles and joints (for eventual use in dynamic simulations), we performed some simple pendular experiments. We separated the femur-tibia segments from the rest of the body and fixed the femur. In some experiments, we removed relevant muscles and internal tissue in order to isolate the effects of the joint itself, as opposed to the effects of the muscles and apodemes. We then applied perturbations to the tibia and filmed the time response as it returned to a resting position, mainly due to gravity. We added different masses (between one-tenth of body mass and body mass) to the tibia and repeated the procedure several times. Results were compared with numerical simulations having different dissipation laws. More sophisticated experiments are planned, and more complete details will be given in a full-length paper [6].

3.2. Results

Motivated by the familiar damped oscillator model (Equation 1 with $f(t) = 0$), and similar studies, we attempted to fit our results to this model (assuming a viscous torque proportional to $\dot{\theta}$.

Poor Model Fit For Swing Phase

For the unloaded trials (which represent swing phase) there appear to be some effects which are difficult to model if $M = 0$ but negligible if $M > 0.1\times$(body mass). The effects appear in trials with and without muscle and seem to dependent on the direction of the initial perturbation. Possible explanations for these complicating effects are: (1) effects of the joint membrane itself, or (2) residual effects of the elastic apodeme (which is not removed when the muscle is removed). Figure 2 shows an example data set from a swing-phase experiment with muscles removed.

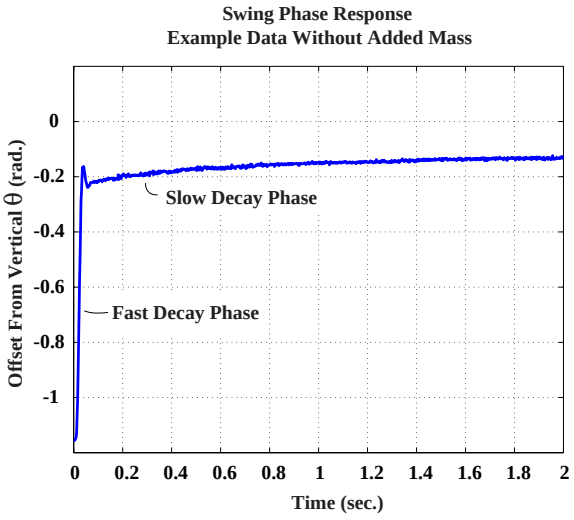

Figure 2: Example results from a perturbation experiment with no added mass and muscles removed. The plot has a fast-response phase and a slow-response phase, and is not well-characterized by a simple spring-dashpot model. However, the model can be used to characterize each phase independently, and the model results from the slow-response phase only are consistent with the results from the experiments with added mass. The fast response may be caused by some residual elasticity in the joint membrane or possibly the elastic apodeme, which remains in the joint after the muscle tissue is removed. This effect becomes negligible when we add mass to the swing limb; the smallest increment of added mass was about one-tenth of body mass.

Model Works Well For Stance Phase

For trials with added mass, a linear damping component models the passive limb motions reasonably well (RMS errors of less than 5%, see Table 3) Adding a Coulomb or quasi-Coulomb component (so that frictional torque is approximately proportional to $B_1\dot{\theta} \pm B_2$) would give an even better fit, although the constant term is not considered in the scaling law derivation for ζ in Section 2.. We say "quasi-Coulomb" and "approximately proportional" because a true Coulomb term is discontinuous at $\dot{\theta} = 0$ and can be problematic for numerical simulations. High-order roots or arctangent functions are smooth Coulomb-like functions that are more practical from a numerical standpoint [24].

Although we could include Coulomb-like terms in our model, we still discuss the damping ratio as if the damping were linear because the linear term accounts reasonably well for the majority of the damping, and because the damping ratio is a convenient concept. The values of B (i.e. B_1 with $B_2 = 0$) which yielded good agreement with the experiments were between $1e-7$ and $5e-7$ kg-m^2/s. Figure 3 shows example simulations, overlayed on top of data for cases with and without added mass.

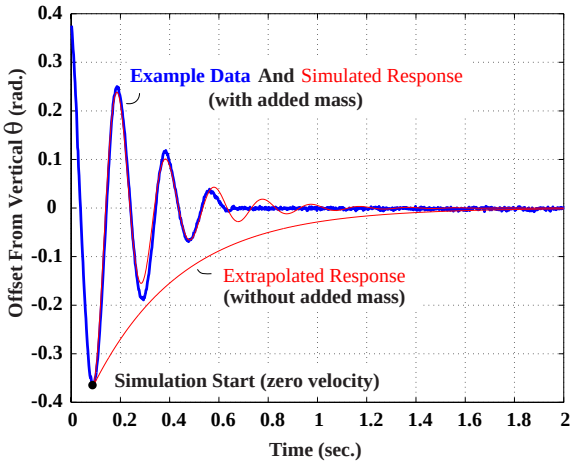

Figure 3: Example results from a perturbation experiment with added mass. Damping was assumed to be proportional to angular velocity; we chose a damping constant B which minimized the total RMS error between simulation and experiment. The extrapolated response results from a simulation with the same damping constant but no extra mass, intending to simulate the unloaded swing-phase response shown in Figure 2. The extrapolated response suggests that the leg is overdamped during swing phase, but there are complicating factors implied by Figure 2. The parameters from the simulations are as follows: $m = 1.3e-5$kg, $L = 0.0113$m, $I_{cm} = 2.0e-10$kg-m^2, $M = 0$ or $2.71e-4$kg, $g = 9.81$m/s^2, $B = 2.17e-7$kg-m^2/s, $\theta_0 = -0.367$rad.

Damping Ratios For Swing And Stance

Preliminary results from a best-fit B with no Coulomb-like terms are shown in Table 3. Although we could not directly model the swing phase, we extrapolated the damping ratio by assuming that the damping co-

efficient B was independent of added mass. We then simulated the limb response with no added mass using the same B, as shown in Figure 3. The no-mass simulations were consistent with the slow decay phase of the no-mass experiments (see Figure 2).

Case	ζ	RMSE, %
Stance w/ muscle	0.19 ± 0.01	1.6 ± 0.5
Stance w/o muscle	0.13 ± 0.01	3.6 ± 0.6
Swing w/ muscle	6.53 ± 0.11	NA
Swing w/o muscle	5.92 ± 0.41	NA

Table 3: Best-fit results for damping assumed proportional to $\dot{\theta}$ with and without muscles. RMS error is expressed as percentage of maximum angular displacement per trial. For each case, we performed 2-4 experiments. The added masses during stance phase produce leg forces comparable to individual leg forces measured during the stance phase of running. The swing phase damping ratios are extrapolated from the results of the stance phase, assuming similar frictional characteristics with no added mass. Because an accurate model for the swing phase would probably need to include extra springs, dampers, etc., we were not able to effectively model the swinging limb response using Equation 1.

Effect Of Muscle Tissue Removal

Removal of muscle tissue (but not the apodeme) lowered the damping ratio by about 30 % for the stance (weighted) case and by about 10% for the swing (unweighted) case.

4. Discussion

Our preliminary results support the theoretical and intuitive predictions of higher damping in cockroach limbs than in larger mammals. During stance phase, cockroach limbs are underdamped, while during swing phase, they are overdamped. Because removal of the muscle tissues did not dramatically decrease the damping ratio, we conclude that joint damping is primarily due to the internal friction and viscosity associated with the joint, and secondarily to the viscosity of the muscles and surrounding tissues.

4.1. Implications For Control

Higher damping ratios are associated with decreased energetic efficiency, and thus might be deemed undesirable. However, higher damping ratios have several potentially-interesting control implications.

- **Preference For Running Over Walking**
  As relative damping increases, walking motions become less "free." This is because the exchange between potential and kinetic energy (which characterizes walking) has a cost proportional to the amount of joint friction (and is further reduced by the horizontal orientation of the limbs). As the damping increases, the effectiveness of the pendular mechanism is compromised, and a new locomotion strategy (running) emerges. The transition between walking and running appears to be modulated by their relative energetic costs [11]. Insects and other animals with relatively high damping and sprawled postures should have a walk-to-run transition that occurs at a lower speed. (A rough analogy is the observation that people have a lower transition speed when moving in deep water, although this analogy will break down under careful scrutiny [24].) Likewise, insects should prefer lower stride frequencies than might be predicted from size-related scaling arguments, due to the high-swing-velocity penalty. Lastly, the presence of speed-independent damping (Coulomb friction) mentioned in Section 3 implies a preference for short, quick bursts of force to minimize frictional energy loss [24].

- **Motor Command Is A Velocity Command**
  In an underdamped environment, muscle activation is like a force or torque command; the limb exhibits poor stability and requires additional (feedback) control to return to equilibrium and minimize oscillation following a perturbation [12, 13]. An overdamped or critically damped environment is like a first-order system, since there is no overshoot when returning to equilibrium. Applied forces or torques are analogous to constant limb velocities which quickly decay to zero if removed. When coupled with some sensing of time or position, velocity control is analogous to position control. This implies that small animals should be able to successfully locomote in a dynamically stable fashion using feedforward commands with relatively little feedback. Larger animals, however, would exhibit greater sensitivity to perturbations and therefore presumably require some feedback to minimize leg oscillations that might upset the dynamic stability of gait.

4.2. Observations From Cockroaches

- **Preference For Running Over Walking**
  Cockroach data from Full and Tu [14] support this hypothesis. Energy traces of kinetic and po-

tential energy are nearly in phase, in contrast to the out-of-phase patterns which are seen in walking. They were unable to find evidence of walking gaits at any speed. Cockroaches and other small animals prefer to run intermittently than to walk [15]. Although Alexander [16] suggests that gait transitions occur at equivalent Froude numbers (squared nondimensional velocities), cockroaches do not follow this trend. Specifically, walk-run transitions in humans and similarly sized animals occur at Froude numbers of about 0.5 [16]. Although the walk-run transition was not measured in cockroaches, they are observed to use running gaits down to Froude numbers of 0.027 (0.08 m/s). One possible reason for the discrepancy with the Alexander study is that Alexander's conclusions may not apply to animals with overdamped swing limbs.

- **Motor Command Is A Velocity Command**
  There is some reason to believe that cockroaches rely primarily on feedforward strategies. Unpublished experiments on cockroaches with a "Rapid Impulsive Perturbation" system [17] suggest that limb angles in cockroaches do not change significantly in response to impulsive perturbations, even relatively large ones which noticeably disrupt the animal's posture and velocity while it is running. Other researchers have also found evidence that insect limbs appear to follow a predetermined kinematic pattern [18], possibly using position control [19] or velocity control [20]. Moreover, hindlimb muscle EMG measurements during steady state cockroach running are nearly identical as compared to those taken while maneuvering over large obstacles [21]. Lastly, simple horizontal-plane models by Schmitt and Holmes [22] and Kubow and Full [23] demonstrate the plausibility of passive and/or feedforward strategies producing dynamically-stable planar gaits with no feedback.

4.3. Generalizability Of Scaling Ideas

The scaling results presented here may be roughly interpreted in a larger, less specific context that is "part of the common folklore of physics and engineering" [24]. Many processes can be approximately modeled by the damped oscillator of Equation 1. In these processes, the damping component B is often assumed to be proportional to some characteristic surface area, while the inertia term J might be proportional to a characteristic mass. In this case, the importance of the damping (as compared to the inertia) at different length scales would follow a surface area to volume power law (length$^{-1/3}$) [25]. Generally speaking then, for many phenomena, one would expect the relevance of damping to increase in any observations or applications at very small length scales.

This argument extends across various disciplines; for instance, in fluid dynamics, the Reynolds number (Re) is a well-known measure of the relative importance of dynamic forces as compared to viscous forces (low Re signifies relatively higher viscous forces). Re is proportional to (length) $\times$ (velocity). Thus, it is common knowledge in fluid mechanics that as length scale decreases, Re decreases, and viscous forces tend to dominate.

Acknowledgments

The initial ideas in this work were originally born out of discussions between Anna Ahn, Devin Jindrich, and the authors. Kenneth Meijer and Thang Lian assisted in the first set of damping experiments. Andy Ruina, Anindya Chatterjee, Dan Koditschek, Devin Jindrich, Rob Howe, and Phil Holmes provided many helpful insights and suggestions.

References

[1] R. J. Full and M. S. Tu, "The mechanics of rapid-running insects: Two, four, and six-legged locomotion," *Journal of Experimental Biology*, vol. 156, pp. 215–231, 1991.

[2] R. J. Full, "Biological inspiration: Lessons from many-legged locomotors," in *Robotics Research: The Ninth International Symposium*, J. Hollerbach and D. Koditschek, Eds. Springer-Verlag, 2000.

[3] W. Weber and E. Weber, *Mechanics of the Human Walking Apparatus*, Springer-Verlag, New York, 1992, translation from the original 1836 German text by P. Maquet and R. Furlong.

[4] R. McN. Alexander, *Size And Shape*, Edward Arnold, London, 1971.

[5] T. A. McMahon and J. T. Bonner, *On Size And Life*, Scientific American Library, New York, 1983.

[6] M. S. Garcia, A. D. Kuo, R. J. Full, A. M. Peattie, and P. Wang, "Joint friction in insects: Implications for hexapedal robots," Full-length version of these proceedings, in preparation, 2000.

[7] T. A. McMahon, *Muscles, Reflexes, and Locomotion*, Princeton University Press, 1984.

[8] R. Riener and T. Edrich, "Identification of passive elastic joint moments in the lower extremities," *Journal of Biomechanics*, vol. 32, pp. 539–544, 1999.

[9] A. Z. Hajian and R. D. Howe, "Identification of the mechanical impedance at the human fingertip," *ASME Journal of Biomechanical Engineering*, vol. 119, pp. 109–114, 1997.

[10] A. Esteki and J. M. Mansour, "An experimentally-based nonlinear viscoelastic model of joint moment," *Journal of Biomechanics*, vol. 29, no. 4, pp. 443–450, 1996.

[11] F. J. Diedrich and W. H. Warren Jr., "Why change gaits? dynamics of the walk-run transition," *Journal of Experimental Psychology*, vol. 21, no. 1, pp. 183–202, 1995.

[12] N. Hogan, "The mechanics of multi-joint posture and movement control," *Biological Cybernetics*, vol. 52, pp. 315–331, 1985.

[13] F. A. Mussa-Ivaldi, N. Hogan, and E. Bizzi, "Neural, mechanical, and geometric factors subserving arm posture in humans," *The Journal Of Neuroscience*, vol. 5, no. 10, pp. 2731–2743, 1985.

[14] R. J. Full and M. S. Tu, "The mechanics of six-legged runners," *Journal of Experimental Biology*, vol. 148, pp. 129–146, 1990.

[15] N. C. Heglund and C. R. Taylor, "Speed, stride frequency, and energy cost per stride: How do they change with body size and gait?," *Journal of Experimental Biology*, vol. 138, pp. 301–318, 1988.

[16] R. McN. Alexander, "The gaits of bipedal and quadrupedal animals," *The International Journal Of Robotics Research*, vol. 3, no. 2, pp. 49–59, 1984.

[17] D. Jindrich, 1999, Personal Communication.

[18] J. T. Watson and R. E. Ritzmann, "Leg kinematics and muscle activity during running in the cockroach, *Blaberus discoidalis*," *J. Comp. Physiol. A*, vol. 182, pp. 11–33, 1998.

[19] H. Cruse, "Is the position of the femur-tibia joint under feedback control in the walking stick insect?," *Journal of Experimental Biology*, vol. 92, pp. 87–95, 1981.

[20] J. Dean, "Control of leg protraction in the stick insect: A targeted movement showing compensation for externally applied forces," *J. Comp. Physiol. A*, vol. 155, pp. 771–781, 1984.

[21] R. J. Full, K. Autumn, J. I. Chung, and A. Ahn, "Rapid negotiation of rough terrain by the deathhead cockroach," *American Zoologist*, vol. 38, pp. 81A, 1998.

[22] J. Schmitt and P. Holmes, "Mechanical models of insect locomotion i: Dynamics and stability in the horizontal plane," in preparation, 1999.

[23] T. M. Kubow and R. J. Full, "The role of the mechanical system in control: A hypothesis of self-stabilization in hexapedal runners," *Phil. Trans. R. Soc. Lond. B*, vol. 354, pp. 849–861, 1999.

[24] A. Ruina, 2000, Personal Communication.

[25] R. Howe, 1999, Personal Communication.

Proceedings of the International Symposium on
Adaptive Motion of Animals and Machines,
Montreal, Aug.8-12, 2000

Approximate Solutions for Gait Simulation and Control.

Paul Bourassa(1), Margrit-R. Meier(1), Philippe Micheau(2), Paulin Buaka(2)

Université de Sherbrooke, Qué, Canada

(1) IUGG, centre de recherches.

(2) Faculté de génie

A biped model is analysed and its relevant second order differential equation of motion are obtained using the Lagrange or the Kane formalism. Previous studies by McGeer [1], Goswani & al. [2], Garcia & al. [3], and others have been very helpful in the understanding of bipedal passive locomotion under gravity alone. This is an attempt to go somewhat further in the same direction: a biped moving on a level surface under the influence of impulsive forces. A four d.o.f. model is studied in the sagittal plane over a visco-elastic medium. A two d.o.f. model with one foot fixed to a rigid floor is also investigated in order to get closed form results. With proper initial conditions, impulses and torques, the programme is able to numerically provide a solution, which lasts for many consecutive steps, leading to steady and stable limit cycles in angular velocities. An animation programme has been proven useful in showing such sequences. The problem addressed here is how to compute the value of the feet impulses and the corresponding torque amplitude in order to attain a given gait velocity and maintain a repeatable gait pattern.

Model description: The model is shown in Figure 1. It consists of two rigid segments representing the left and the right leg with mass M_A located at mid length and a central moment of inertia I_A. The trunk is assumed as a point mass M_e located at E. Figure 1 shows the right leg resting on the floor while the left is subject to a short impulse directed along the segment. Afterward, an internal torque T_{BA} is applied to the left leg. A similar reversed scenario occurs on the following step, with a torque Tab applied to left leg The Lagrange equations for the two d.o.f model walking on a rigid surface are represented in Equation (1):

$$[A(q_i)]\begin{Bmatrix} U_1 \\ U_2 \end{Bmatrix} = \begin{Bmatrix} f_1(q_i,U_i) \\ f_2(q_i,U_i) \end{Bmatrix} + \begin{Bmatrix} c_1 F_{i1} \\ c_2 F_{i2} \end{Bmatrix} \qquad (1)$$

where A is a 2x2 matrix; q_i and U_i, are the state variables; (i = 1,2), F_{i1}, and F_{i2} are the required impulses for either leg; U_1 and U_2 are the time derivatives of q_1 and q_2. The matrix A consists of four elements a_{ij} with

$a_{11} = (I / ML^2 + ¼)$ $\quad a_{12} = -\cos(q_1-q_2) / 2$

$a_{21} = a_{12}$ $\quad a_{22} = (I/ML^2 + 5/4 + M_e/M)$

$f_1(q_i,U_i) = 0.5 \sin(q_1-q_2)U_2^2 + 0.5\, G/L \cos(q_1) + T_{ba}/ML^2$

$f_2(q_i,U_i) = -0.5 \sin(q_1-q_2)U_1^2 + (M_e/M + 3/2)\, G/L \cos(q_2) - T_{ba}/ML^2$

$c_1 = \sin(q_1-q_2)/ML$ or 0 $\quad c_2 = \sin(q_1-q_2)/ML$ or 0

The determinant. $\det(A) = a_{11}a_{22}-a_{12}a_{21}$ and $a_{12} = a_{21}$ has one term a_{12} which is very slightly co-ordinate dependant.

G is the constant of gravity, assumed to be $10 m.s^{-2}$. Similar expressions are obtained when interchanging the angular leg generalised co-ordinates q_1 and q_2, and using T_{ab} in place of T_{ba}, when the left leg is in the support mode and the right leg is in the swinging mode. These equations are used to derive some basic relationships between the torque, the impulse and the kinematics of the walking gait pattern. The system is solved numerically using Runge-Kutta algorithm. The code is provided with branching in order to generate a set of multi-step sequences. Ground interference with the swinging leg is ignored except at contact time where ground reaction forces are evaluated. Such a system has the advantages of producing continuous motion from one step to another by simple branching and constants resetting, as the model goes from one configuration to the next.

Impulse: During the push-off phase in human gait, the foot reacts against the ground to produce a reaction force. Its integral over time is known as an impulse. During that phase, the legs are changing angular velocities and the body is rising. The simplest form of an impulse is a force amplitude F_{imp} applied over a single time step. The integration of (1) over a short impulse time results in a sudden increase in the angular velocities of all the generalized velocities of the system. For the present model the relationship is given in Equation (2).

$$\Delta U_1 = f_3(q_i, U_i)\Delta t + f_4 \Delta U2 \qquad (2)$$
$$\Delta U_2 = f_5(q_i, U_i)\Delta t + f_6(F_{i2}\Delta t)$$

The angular velocity increments are seen to be function of the impulse value. Thereafter, a properly selected torque T_{ba} will accelerate and bring the swinging leg to an eventual maximum velocity v_m and in phase with the support leg at mid-stance. To this end, we investigate the equations [1] with a null value for the impulse and find out that f_1 in the second equation is relatively small. Considering furthermore small angles approximations, the expression for the derivative dU_2/dt becomes

$$dU_2/dt = a (q_1 - q_2) U_1^2 + b(\pi/2 - q_2) + cT_{BA} \qquad (3)$$

U_1 can be shown to be increasing in a nearly linear manner with time and to be proportional to T_{BA}. Therefore the above equation takes the form

$$d^2q_2/dt^2 = c_1 + c_2 q_2 + g(t) + c_3 t^2 q_2 \qquad (4)$$

This equation is linear and a power solution for q_2 may be found by the method of variable coefficients. From this solution, the time t_{MS} required to reach mid-stance ($q_2=\pi/2$) and the velocity at mid-stance $U_2(t_{MS})$ may be obtained. These values are functions of T_{ba} and of the values U_{1+} and U_{2+} immediately following the impulse. These U_i values have just been given angular velocities increments which are fonction of the impulse intensity. Therefore it is possible to establish a required initial impulse and a proper torque amplitude that will yield a synchronised stance for a given velocity at mid-stance. Examples of such solutions and corresponding animations will be shown in the presentation. After applying the initial impulse, F_{img} is taken as zero until the next step occurs and equation (1) is than easily inverted. The synchronised mid-stance angles and velocity objectives may also be expressed by algebraic equations which may be solved numerically by Newton Raphson algorithm and also by repeated integration.

Polynomial solution: The angles q_1 and q_2 range from 70 to 110 degrees approximately and approximations may be taken for linearization purposes. Replacing in equation (1) sin(q1-q2) by (q1-q2) , cos(q1-q2) by 1, det(A) becomes a constant and the expressions on the right hand side take the following form:

$$f_1 = 0.5(q_1-q_2)\, U_2^2 + G/2L + T_{ba}/ML^2$$
$$f_2 = -.5(q_1-q_2)\, U_1^2 - (M_e/M+3/2)\, G/2L - T_{ba}/ML^2 \qquad (6)$$

The torque T_{ba} will be taken as a constant during the first part of the walking step until mid-stance. After mid-stance, a change of sign for T_{ba} will be introduced in the simulation that will slow down the fast moving leg. We may rewrite the system as

$$dU1/dt = [(a11.f1g - a12.f2g) + (a22+a12)T'_{ab}]/detA$$
$$dU2/dt = [(-a12f1g+a11f2g) - (a11+a12)T'_{ab}]/detA \qquad (7)$$

Figure 1: Polynomial Solution q2p(t) vs integrated solution q2(t)

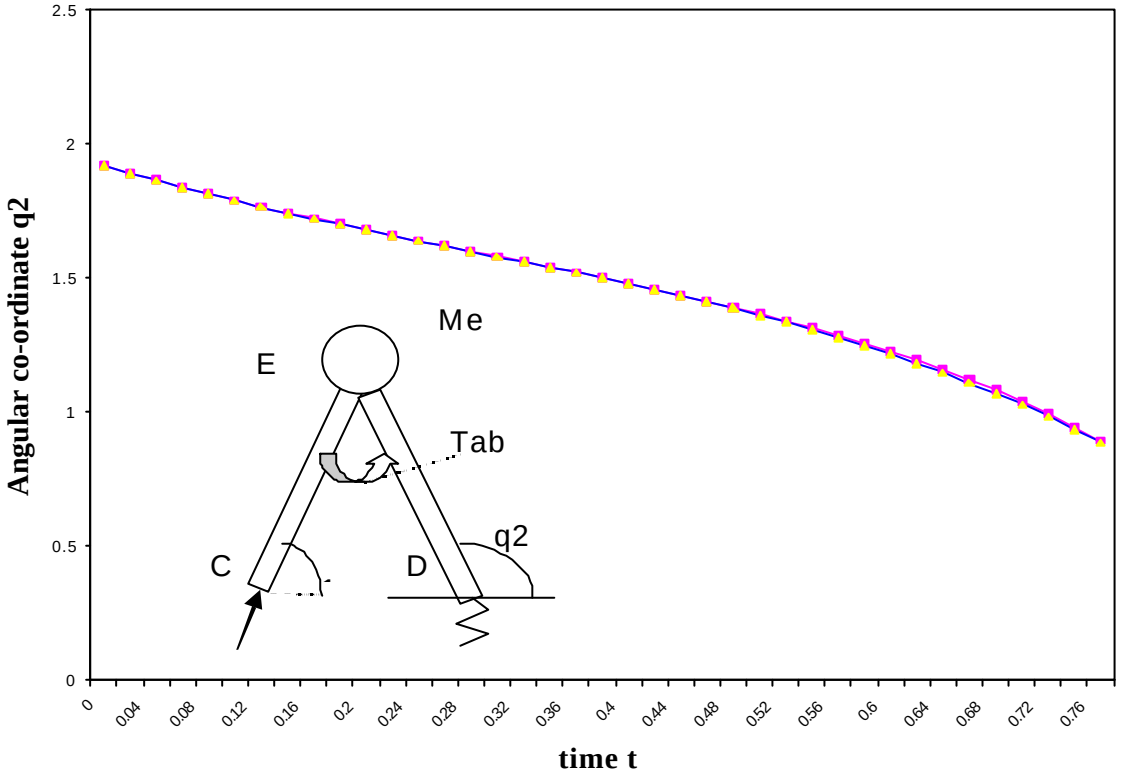

The equations may be uncoupled when observing during simulation that the term including the torque T_{ba} in the first differential equation is dominant. This results into $dU_1/dt = T_{ba}/I_e$ where $I_e = I_a + M L^2$ and represents the leg moment of inertia around the hip pivot point. Therefore $U_1(t) = U_1(0) + (T_{ba}/I_e)t$ and $q_1(t) = q_1(0) + U_1(0)t + 0.5(T_{ba}/I_e)t^2$. This simple solution has been verified with sufficient accuracy for the cases at hand. The quadratic form may be solved to find out the time t_{1ms} at which the swinging leg will reach a vertical position.

$$t_{1ms} = -b + \sqrt{(b^2-c)} \quad \text{where } b=(I_e/T_{ba})U_1(0) \text{ and } c = [(2q_1(0) - \pi/2]\, I_e/T_{ba} \qquad (8)$$

where the plus sign must be assumed in front of the square root. In the second differential equation, the term $a_{12}f_{1g}$ is small compared to the others terms and the replacement of $U_1(t)$ produces a time dependent linearized equation of the form

$$d^2q_2/dt^2 = dU_2/dt=e_0+e_1t+e_2t^2 + e_3t^3 +e_4t^4 + (e_5 +e_6t +e_7t^2)q_2 \qquad (9)$$

where the expressions for e_0 to e_7 are given in the appendix. This linearized, time-dependant differential equation may be solved using a polynomial solution for q_2 in powers of t.

$$\begin{aligned} q_2 &= b_0 + b_1t + b_2t^2 +\ldots\ldots+b_nt^n \quad \text{and} \\ U_2 &= b_1 + 2b_2t + 3b_3t^2 +\ldots..+(n+1)b_{n+1}t^n \\ dU_2/dt^2 &= 1®2b_2 + 2®3b_3t + 3®4b_4t^2 +\ldots..(n+1)*(n+2)b_{n+2}t^n \end{aligned} \qquad (10)$$

The replacement of these polynomial into the differential equation yields a polynomial in t^i. Each coefficient must be zero to give the recurrent expressions for the b_i coefficients in terms of the initial conditions and in terms of the known e_i coefficients. These are as follows:

$$\begin{aligned} &b_o = q_2(0) \quad b_1 = U_2(0) \quad b_2 = (e_0 + e_5b_o)/2 \quad b_3 = (e_1 + e_6b_o + e_5b_1)/2®3 \\ &b_4 = (e_2 +e_7b_o + e_6b_1 + e_5b_2)/3®4 \quad b_5 = (e_3 + e_7b_1 + e_6b_2 + e_5b_3)/4®5 \\ &b_6 = (e_4 + e_7b_2 + e_6b_3 + e_5b_4)/5®6 \quad b_7 = (e_7b_3 + e_6b_4 + e_5b_5)/6®7 \\ &b_{n+2} = (e_7b_{n-2} + e_6b_{n-1} +e_5b_n)/(n+1)®(n+2) \end{aligned} \qquad (11)$$

This polynomial solution for the leg angular co-ordinate and for its angular velocity has shown to be a very good approximation for the integrated numerical solution using Runge-Kutta algorithm, for cases where the balancing leg is reaching a vertical position at approximately the same time as the supporting leg Figure 2).

Discussion and conclusion: The generated gait cycles comprise a multitude of continuous steps accompanied by steady and stable limit cycles in angular velocities. The relationships between the impulse, the torque, the model parameters and initial conditions pave the way to a better understanding and simulation. Animation is found to be a very useful tool in order to assess the progress made during the whole development. Further refinements are required in order to broaden the stability range of successful gait solutions. An approximate solution to the linearized set of differential equations provide some important relationships between the model variables at impulse time, its parameters and the values of the impulse and of the constant torque in order to achieve a continuous and repeatable gait cycle with a desired mid-stance velocity.

Acknowledgements: This investigation was carried out with the financial support of the National Science and Engineering Research Council of Canada (NSERC).

References:

1 McGeer, T (1990). Passive dynamic walking. *Int J Robotic Res* 9:62-82.
2 Goswani A, Thuilot B and Espiau B (1998). A study of the passive gait of a compass-like biped robot: symmetry and chaos. *Int J Robotic Res* 17(12): 1282-1301.
3 Garcia M, Chatterjee A, Ruina A, Coleman M (1998) The simplest walking model: stability, complexity, and ccaling" *J Biomech Eng* 120: 281-287.
4 Bourassa P et al. Gait Modelling, Animation and Limit Cycle, 7th ISCSB, Calgary 1999

Proceedings of the International Symposium on
Adaptive Motion of Animals and Machines,
Montreal, Aug.8-12, 2000

Energy Optimal Trajectory Planning of Biped Walking Motion

Rongqiang Liu[1] and Kyosuke Ono[2]

[1,2]Dept. of Mechanical Science and Engineering, Tokyo Institute of Technology
2-12-1 Ohokayama Meguro-ku Tokyo,152-8552 Japan
[1]E-mail: liurq@stu.mech.titech.ac.jp, [2]E-mail: ono@mech.titech.ac.jp

Abstract

This paper describes an optimal trajectory planning of walking locomotion for a biped mechanism system which has thighs, shanks and small feet. We model the mechanism to be a 3-DOF link system composed of an inverted pendulum and a 2-DOF swing leg. The locomotion of the swing and supported legs is solved by the optimal trajectory planning method based on the function approximation method. It was found that the lowest energy walking motion can be obtained at the one step period of 0.586s similar to the human walking when the ankle is a passive joint.

1 Introduction

Many studies have been published on dynamic biped locomotion mechanism, in which there are many successful examples to realize dynamic walking of biped robots. Mita et al. built a seven-link biped walker and realized dynamic biped walking by using linear optimal state regulator theory[1]. As a result, one step took one second when the step length was shorter than 20cm. Furusho et al. proposed a hierarchical control strategy for their biped robot and realized high speed movement[2]. The local feedback which makes the total system robust was implemented at the low level. The stability of steady walking was examined by using the reduced order model. Shih studied dynamics of a 7-DOF biped walking robot which included variable length legs and a translational balance weight in the body[3]. He presented a piecewise cubic polynomials method to generate a trajectory by constraining the location of the ZMP and showed an experimental result of dynamic walking with a speed of 16cm/s.

However, most of the previous control algorithms are very complicated, and the walking stability and speed are not as good as expected. On the other hand, human biped walking has been considered to be robust and efficient. The human walking pattern can be described similarly by the simplest inverted pendulum model in gravitational field[4]. Therefore, human utilizes its gravity skillfully to achieve efficient walking. Miura and Shimoyama developed biped robots named BIPER-3 and BIPER-4, and proposed a control method based on the inverted pendulum principle to realize dynamic walking[5] . McGeer demonstrated a passive biped walking mechanism which walked down along a ramp and utilized its gravitational potential energy as input power of walking[6] . It is indicated that the biped walking under gravitational field has a natural gait and the walking is generated as a limit cycle of non-linear system. Based on natural dynamics concept of a biped system, Pratt et al. studied a planar biped walking control by the virtual model method. They exploited the natural dynamics of human legs to simplify the control algorithm greatly[7] .

Ono and Okada proposed self-excitation of natural mode of vibration system and demonstrated an insect wing driven by the Van Der Pole self-excitation [8][9]. They also proposed a biped mechanism which walked on a level ground with two single-link legs. The biped walking motion was realized by the swing roll motion of the upper body driven by a self-excited vibration system with asymmetric stiffness matrix[10] . Moreover, Ono et al. described a self-excited biped mechanism with one actuator only at the hip and realized the natural dynamic walking motion with a speed of about 3km/h on a level ground[11] .

Since a natural walking locomotion means such an efficient motion that the energy consumption is the lowest, it is thought that the natural walking locomotion can be obtained as a motion of a biped mechanism that consumes the lowest possible energy. Thus, our main concern in this study is whether we can get a stable, efficient and natural walking motion and the lowest input torque at all joints, by means of an optimal trajectory planning method based on energy consumption mini-

1 Visiting Researcher, Associate Professor.
Harbin Institute of Technology, Harbin, China.

mization. Another concern is whether we can also obtain ideal walking motion even if we assume the ankle or knee joint to be a passive joint. In addition, we are interested in the similarity between the optimal walking motion solutions and actual human walking motion.

The trajectory planning problem can be solved by the variational method, the maximum principle or the dynamic programming method, but the state equations are very complicated and the convergence is difficult. Thus, we approximate the joint motion trajectory by a set of Hermite polynomials functions [12], and convert the optimal trajectory planning problem into the boundary parameter optimization problem.

2 Analytical Method

In this section, we model a planar biped walking mechanism with thighs, shanks and small feet as shown in Figure 1 to be a 3-DOF link system, We disregard upper body above waist, because it has little effect on walking motion. Thus, the two legs are assumed to be directly connected each other through an actuator. We assume that both knee and ankle joints can be driven by individual actuators.

2.1 Model of a Biped Mechanism and Walking Motion

For the biped mechanism as shown in Figure 1, we assume that the knee joint of the supported leg is passively locked by means of a stopper mechanism to prevent the mechanism from collapse. The ankle of the supported leg is modeled as a rotating joint fixed on the ground, while the foot of the swing leg is neglected. The mechanism is modeled as a 3-DOF link system as shown in Figure 2, which consists an inverted pendulum and a 2-DOF swing leg.

The one step walking locomotion is divided into three sections which have different phases of the walking mechanism as shown in Figure 3. In the first section from the posture 1 to 2, the swing leg swings from left to right as a 2-DOF pendulum until the swing leg becomes straight, avoiding collision with the ground, while the supported leg moves from left to right as a 1-DOF inverted pendulum. In the second section, it is assumed that the straight two legs move freely during the period t_2 from posture 2 to 3 until the swing leg touches the ground. In the third section, only the foot exchange is performed from posture 3 to 4 at the instant of collision of the swing leg. An efficient and natural walking motion of a 3-DOF walking

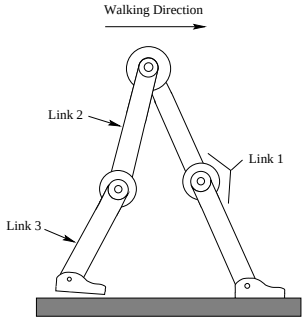

Figure 1: Biped walking mechanism

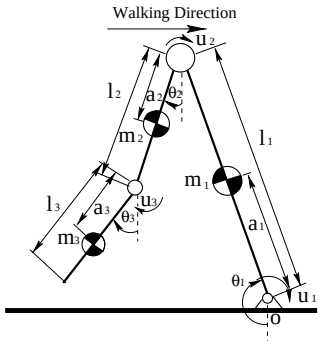

Figure 2: The model of biped walking mechanism

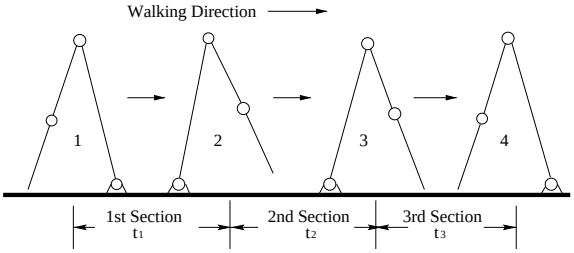

Figure 3: Sections of one step walking

mechanism in the first section is solved by the optimal trajectory planning method.

2.2 Basic Equations and Cyclic Walking Locomotion Condition

The equation of motion of the 3-DOF link system as shown in Figure 2 is written as follows:

$$[\boldsymbol{M}]\{\ddot{\boldsymbol{\theta}}\} + [\boldsymbol{c}]\{\dot{\boldsymbol{\theta}}^2\} + \{\boldsymbol{k}\} = \{\boldsymbol{u}\} \qquad (1)$$

where $[\boldsymbol{M}]$, $[\boldsymbol{c}]$ and $\{\boldsymbol{k}\}$ are calculated by the parameter values of the mechanism and the angular positions of the links, and $\{\boldsymbol{u}\}$ is the input torque vector.

We assume that the foot exchange takes place instantly for the sake of analytical simplicity and the collision between the swing leg and the ground is perfect non-elastic collision. By using the impulse-momentum equations for translation and rotation,

the relationship of the link angular speeds between right before and after collision is obtained as follows.

$$[\boldsymbol{H}]\{\dot{\boldsymbol{\theta}}^-\} = [\boldsymbol{M}]\{\dot{\boldsymbol{\theta}}^+\} \tag{2}$$

where $[\boldsymbol{H}]$ is calculated by the parameter values of the mechanism and the angular positions of the links. In order to realize the cyclic walking locomotion, the angular speed $\dot{\boldsymbol{\theta}}^+$ right after the foot exchange must be the same as that at the beginning of the first section which is given as the initial condition. So the angular speed $\dot{\boldsymbol{\theta}}^-$ right before the foot exchange is solved by Eq. (2).

From Eq. (1), the equation of motion of 2-DOF link system in the second section is written in following.

$$\ddot{\boldsymbol{\theta}} = \boldsymbol{f}(\boldsymbol{\theta}, \dot{\boldsymbol{\theta}}) \tag{3}$$

To determine the end boundary condition of the first section, we adopt a backward time integration method. By integrating Eq. (3) from posture 3 to 2 during the second section and using Eq. (2), we have the relationship between the beginning and end boundary conditions.

2.3 Optimal Trajectory Planning Based on Function Approximation

In the first section, the walking motion of 3-DOF link system is solved by the optimal trajectory planning method[12] . To minimize the energy consumption in the first section, we define the performance index function as follows.

$$J = \sum_{i=1}^{3} k_{p_i} \int_0^{t_1} u_i^2(t)dt \tag{4}$$

where k_{p_i} is the weighting factor corresponding to joint i, and u_i is the input torque at joint i. Arranging Eq. (1), u_i is expressed as:

$$u_i = \Gamma_i(\boldsymbol{\theta}, \dot{\boldsymbol{\theta}}, \ddot{\boldsymbol{\theta}}) \quad (i = 1, 2, 3) \tag{5}$$

In order to compare the full-actuated and under-actuated systems, we solve this trajectory planning problem under three input conditions as follows.

1. No input at the ankle joint: $k_{p_1} = 0$ in (7); the constraint condition $u_1 = 0$.

2. No input at the knee joint: $k_{p_3} = 0$ in (7); the constraint condition $u_3 = 0$.

3. Input at all the joints: no constraint condition.

If the first section is divided into m subsections, then the joint motion trajectory in the j-th subsection is expressed as

Table 1: Link parameters

	1st link	2nd link	3rd link
Mass m_i [kg]	5.0	3.5	1.5
Link length l_i[m]	0.8	0.4	0.4
Inetia moment I_i [kgm^2]	0.35	0.054	0.02
Offset of mass center a_i [m]	0.56	0.09	0.20

$$\boldsymbol{\theta}_j(\boldsymbol{p}, t) = \boldsymbol{h}(t)^T \boldsymbol{p}_j \quad (j=1,\ldots,m) \tag{6}$$

where $\boldsymbol{h}(t)$ is the Hermite base function vector of n_h order. In this paper, we take $n_h = 7$ and $m = 2$. $\boldsymbol{p}_j$ is the boundary state variable vector. Therefore,

$$\boldsymbol{p}_j = \{\boldsymbol{\theta}_{j-1}^T, \boldsymbol{\theta}_j^T, \dot{\boldsymbol{\theta}}_{j-1}^T, \dot{\boldsymbol{\theta}}_j^T, \ddot{\boldsymbol{\theta}}_{j-1}^T, \ddot{\boldsymbol{\theta}}_j^T, \boldsymbol{\theta}_{j-1}^{(3)T}, \boldsymbol{\theta}_j^{(3)T}\}^T \tag{7}$$

where the number in the () is the derivative order number, $\boldsymbol{\theta}_{j-1}$, $\dot{\boldsymbol{\theta}}_{j-1}$ etc are the beginning boundary state variables of the j-th subsection, while $\boldsymbol{\theta}_j$, $\dot{\boldsymbol{\theta}}_j$ etc are the end boundary state variables of the j-th subsection. To satisfy the dynamic constraint condition of the passive joint, the input torque $u_k(t, \boldsymbol{p})$ of this joint must satisfy the condition that the projection of the $u_k(t, \boldsymbol{p})$ in the Hermite base functional space is zero. That is,

$$\boldsymbol{c}(\boldsymbol{p}) = \int_0^{t_1} u_k(t, \boldsymbol{p}) h_i(t) dt = 0 \quad (i = 1, \ldots, n_h). \tag{8}$$

The constrainted optimization problem as shown in (4) and (8) is solved iteratively until the ratio of difference of the successive value of $\boldsymbol{p}$ becomes small enough.

3 Results and Discussions

We solve the optimal walking locomotion trajectory for the 3-DOF link system as shown in Figure 2 for various values of the second period t_2 under three input conditions, using the calculation method stated above. The parameter values of the mechanism are shown in Table 1, which are close to an adult human's data. In the iteration calculation, the convergence accuracy ε is chosen to be 1.0×10^{-10}.

First, we show the optimal solutions of walking motion under the constraint condition $u_1 = 0$. Figures 4, 5 and 6 show the stick figures and joint torque in the cases of t_2=0.10s, 0.12s and 0.13s, respectively. Note that, the teo track of the swing leg is like a straight line which parallels the ground when $t_2 = 0.1s$, as shown in Figure 4(a). When the

t_2 is less than 0.09s, the teo track comes to collide with the ground, so the result could not be obtained. From the comparison of Figures 4, 5 and 6, it is clear that the larger the t_2 is, the higher the peak of the teo track. The calculation at $t_2 > 0.13$s is unnecessary, because the higher the peak of the teo track, the larger the energy consumption value is. The joint input torque in Figure 4(b) is obviously smaller than that in Figures 5(b) and 6(b). In Figures 4(b), 5(b) and 6(b), we note that the u_1 is not zero. However, since the u_1 is orthogonal with the Hermite polynomial base functional space, the u_1 has no influence on the $\boldsymbol{\theta}(\boldsymbol{p}, t)$. Because the u_1 satisfies Eq. (11). We confirmed that the same walking motion as in Figures 4(a), 5(a) and 6(a) can be obtained from forward dynamic simulation by using u_1=0 and the same u_2 and u_3 as in Figures 4(b), 5(b) and 6(b), respectively.

Next, we calculate optimal trajectory under the constraint condition $u_3 = 0$. Figure 7 shows the stick figure and input torque in the case of $t_2 = 0.10s$. During the iteration, the final constraint condition error is 1.0×10^{-4}, which is much worse than the required convergence accuracy of 1.0×10^{-10}. Sharp peak on the u_3 curve near the end of the first section is observed in Figure 7(b). Therefore, under no input torque at joint 3, the optimum joint motion trajectory which satisfies the required boundary condition could not be found. This indicates that some input torque at the knee is very important to generate an efficient walking motion.

Finally, we calculate the optimal trajectories when the torque is input at all three joint. The stick figures for $t_2 = 0.10$ and 0.13s are shown in Figure 8. The stick figures are very smooth in both two cases and are very similar to each other as shown in Figure 8. It is understood that the trajectory pattern and energy consumption are insensitive to the boundary condition in the full-actuated control system.

The value of the performance index in the 12 cases is shown in Figure 9. The energy consumption value in the full-actuated control system increases slowly with the increase in t_2. When joint 1 is a passive joint, the energy consumption value increases quickly with an increase in t_2. However the energy consumption shows the lowest value in all 12 cases when $u_1 = 0$ and $t_2 = 0.10s$, as seen in Figure 9. Therefore, this motion trajectory is considered to be the most optimal walking motion. It is interesting to note that a cyclic walking motion with the lowest energy consumption can be realized in an under-actuated control system as a kind of natural motion of a multi-link system, if a suitable boundary condition is adopted.

Of all the 12 examples, the period t_1 of the first

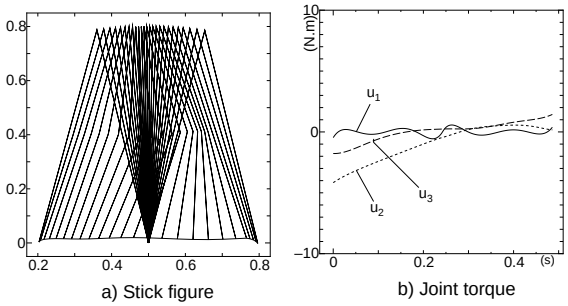

Figure 4: Computation results on $u_1 = 0$ and $t_2 = 0.10s$

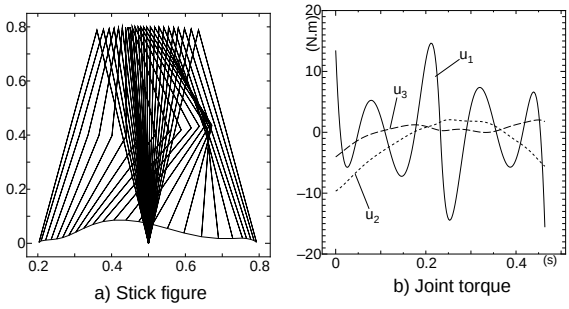

Figure 5: Computation results on $u_1 = 0$ and $t_2 = 0.12s$

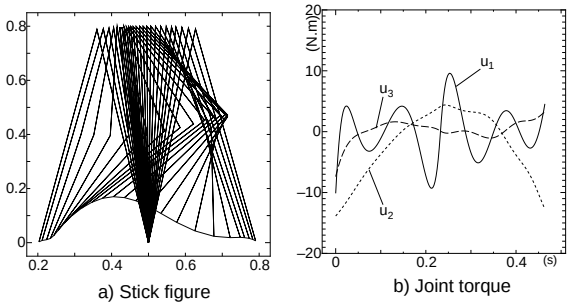

Figure 6: Computation results on $u_1 = 0$ and $t_2 = 0.13s$

section is within $0.462s \sim 0.486s$, while the one step walking period $(t_1 + t_2)$ is within $0.582s \sim 0.596s$. This value is very close to the human walking period. Accordingly, it can be said that the optimal solution solved by the trajectory planning method described above is close to human walking locomotion.

4 Conclusions

In this paper, we computed the optimal joint motion trajectory for the 3-DOF biped walking mechanism, using the optimal trajectory planning method. From comparison of the computation results, the main conclusions are summarized as follows.

(1) The computation results prove that the op-

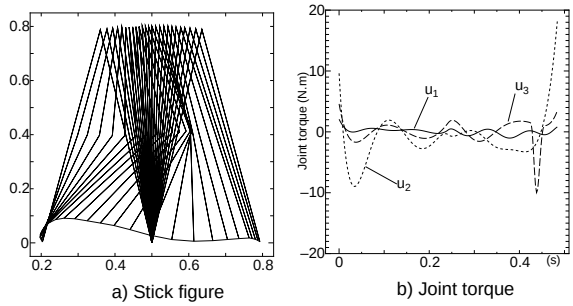

Figure 7: Computation results on $u_3 = 0$ and t_2=0.10s

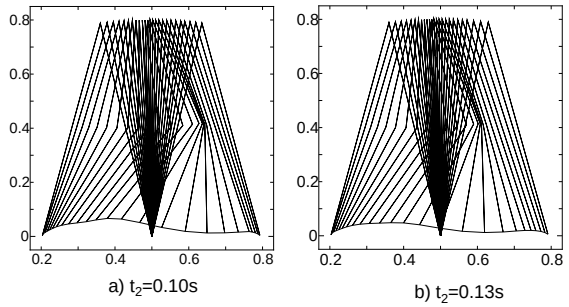

Figure 8: Stick figures (no constraint)

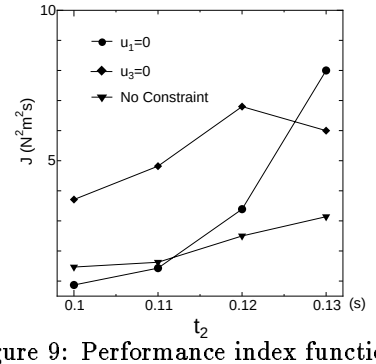

Figure 9: Performance index function value

timal trajectory planning method adopted in this paper is an effective tool to solve the walking motion and joint control torque for a 3-DOF biped walking mechanism.

(2) Under the constraint condition $u_1 = 0$, the period t_2 in the second section has a great influence on the results. When $t_2 = 0.10s$, the energy consumption is the lowest among all examples. In this case, the one step period $t_1 + t_2 = 0.586s$. It is very close to the human walking period, which is about 0.6s. Therefore the corresponding joint motion trajectory is considered to be close to human walking locomotion. This confirms the validity of the inverted pendulum model of human leg system, in which the ankle is a passive joint.

(3) The under-actuated control system is more sensitive to the boundary condition than the full-actuated system. If the suitable boundary condition is adopted, the natural cyclic motion with the lowest energy consumption can be realized in the under-actuated control system.

References

[1] T. Mita et al., Realization of a High Speed Biped Using Modern Control Theory, *Int. J. Control*, **40**-1(1984),107-119.

[2] J. Furusho and M. Masubuchi, Control of a Dynamical Biped Locomotion System for Steady Walking, *J. of Dynamic System, Measurement and Control, Trans. of ASME* , **108**-June(1986),111-118.

[3] C. Shin, Analysis of the Dynamics of a Biped Robot with Seven Degrees of Freedom, *Proc. of the 1996 IEEE Int. Con. on Robotics and Automation*, Minneapolis, Minnesota-April(1996), 3008-3013.

[4] A. Sano, Dynamic Biped Walking by Using Skillfully a Gravity Field (Challenge to a Human Walking), *J. of the Robotics Society of Japan*, **11**-3(1993), 354-359.

[5] H. Miura et al., Dynamic Walk of a Biped, *Int. J. of Robotics Research*, **3**-2(1984), 60-74.

[6] Jerry Pratt and Gill Pratt, Exploiting Natural Dynamics in the Control of a Planar Bipedal Walking Robot, *Proc. of the 36th IEEE Annual Allerton Conf. on Communication, Control and Computing*, Monticello, Illinois, Sept. 1998.

[7] Tad McGeer, Passive Dynamic Walking, *Int. J. of Robotics Research*, **9**-2(1990), 62-82.

[8] K. Ono and T. Okada, Self-Excited Vibratory Actuator (1st Report, Analysis of Two-Degree-of-Freedom Self-Excited System), *Trans. of the JSME*, **60**-577, C(1994a), 92-99.

[9] K. Ono and T. Okada, Self-Excited Vibratory Actuator (2nd Report, Self-Excitation of Insect Wing Model) *Trans. of the JSME*, **60**-579, C(1994b),117-124.

[10] K. Ono and T. Okada, Self-Excited Vibratory Actuator (3rd Report, Biped Walking Mechanism by Self-Excitation) *Trans. of the JSME*, **60**-579, C(1994c),125-132.

[11] K. Ono et al., Self-Excitation of Biped Locomotion Mechanism, *Proc. of the 1999 JSME Con. on Robotics and Mechatronics*(CDROM 2P1-41-093), Tokyo, 1999.

[12] A. Imadu and K. Ono, Optimal Trajectory Planning Method for a System That Includes Passive Joints (1st Report, Proposal of a Function Approximation Method), *Trans. of the JSME*, **64**-618, C(1998),516-522.

Biped Humanoid Robots in Human Environments: Adaptability and Emotion

*† *†
*
⋆
†

Abstract

To explore issue of human-like motion, we have constructed a human-like biped robot called WABIAN-RII (WAseda BIped humANoid robot-Revised II) that has a total of forty-three mechanical degrees of freedom (DOF); two six DOF legs, two ten DOF arms, a four DOF neck, four DOF in the eyes and a torso with a three DOF waist. We present a follow-walking control with a switching pattern technique for the biped robot to follow human motion. Also, emotional walking of the biped robot is described, which expresses emotions by parameterizing its motion. The follow walking and emotion expression can be realized by the compensation of moment by the combined motion of the waist and trunk.

1. Introduction

o date t e iss e o sta e i ed a king as een add essed man esea c e s [1 2 3 4 5] aseda s i ed o ot g o as een engaged in st d ies o i ed o ots it man con g ation om t o ie oints ne is an enginee ing ie oint to e cidate t e a king mec anism o mans e ot e ie oint is t e de e o ment o ant o omo ic o ots t at ecome man a tne s in t e next cent

e aseda g o s cceeded in ac ie ing a d namic i ed a king it a d a ic i ed o ot 10 in 1 84 [6] d a ic i ed o ot 12 a ing an e od and a t o deg ees o eedom aist as const cted to ea i e mo e man ike mo tion in 1 86 so t e ne cont o a go it m as de e o ed to im o e a king sta i it ic com ensates o moment gene ated t e motion o t e o e im s sing t e t nk motion e d namic i ed a king as ea i ed nde exte na o ces o n kno n en i onment and on nkno n a king s aces [8] o ada t to man s i ing en i onments t e cont o met od ased on a i t a s ace as int o d ced ic co d dea it e en and ne en te ain [ ]

n 1 2 t e ne o ect manoid as o nded t e ate c i o ato at (manoid e sea c a o ato) d anced esea c nstit te o cience and nginee ing aseda ni e sit is o ect aims at t e de e o ment o an ant o omo ic o ot t at can s a e t e same a king s ace it mans n de e o ing a i ed manoid o ot e t ings a e conside ed as o o (1) t e si e o t e i ed o ot s o d e t e a e age si e o an ad t a anese oman to do a co a o ati e o k it mans (2) t e o ot co d a k at a oximate man s eed (3) t e o ot s o d a e 3 t nk and 6 a m (4) t e oints o t e o ot s o d se e ec t ic se omoto s (5) a cont o com te and moto d i es exce t o e s s o d e insta ed

n t is a e e desc i e a i ed manoid o ot N to ea i e man ike motion t at as o t t ee mec anica deg ees o eedom and cont o s stems ict e o t e N is s o n in ig e 1 e desc i e a man o o a king to co o e ate it a man e o o a king is ac ie ed sing a atte n s itc ing met od so e de sc i e a matte o emotion ex essed t e a king and t e od motion e a king o emotion is c e ated a set o motion a amete s t at consists o t e o e im e im aist t nk and ead a am ete s

2. Development of WABIAN-RII

n t is section t e a d a e and so t a e o t e N a e desc i ed

2.1 Hardware

a min (o o ation) and (a on i e ein o ced astic) a e main em o ed as st ct a mate ia s o t e N e eig t o t e N is a o t 1 84[m] and its tota eig t is 12 [kg] e od and egs a e d i en se omoto s it ed ction gea s e neck ands and a ms a e act ated se omoto s it ed ction gea s t t e e es se o moto s

Proceedings of the International Symposium on Adaptive Motion of Animals and Machines, Montreal, Aug.8-12, 2000

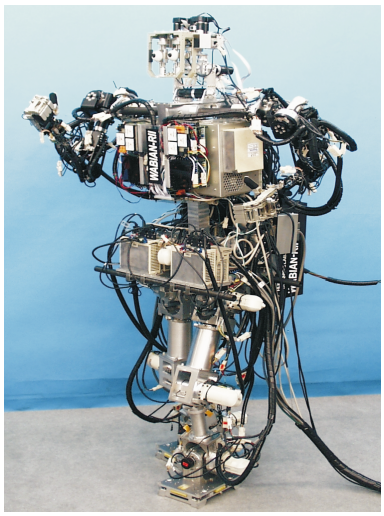

ig e 1 e oto o N

it o t ed ction gea s e t nk a ing t ee de g ees o eedom can end ont to ack (40 deg ees) and side to side (50 deg ees) and t ist e t to ig t (0 deg ees) e neck a ing o deg ees o eedom can ti t ont to ack t o itc axes (0 deg ees eac) ti t side to side (0 deg ees) and t ist e t to ig t (0 deg ees) e e es a ing o deg ees o eedom can ook to do n (100 deg ees) and o tate ig t to e t (0 deg ees) man ike ange o motion is gi en mec anica sto e s and so t a e on t e aist and on so t a e on t e neck and e es e a ms and egs a e e i ed it mec an ica sto e s inc ding so t a e to ea i e man ike ange o motion (knee end is 0 deg ees i t ist 180 deg ees i and ank e o s 40 deg ees i itc 80 deg ees ank e itc 5 deg ees)

2.2 Software

e N is cont o ed a com ati e com te 530 (an nte enti m 200[ ] ocesso) ic a e go e n a 6 2 (16 it) N xtende (e 6 1) is em o ed to extend t e to a 32 it t as t ee co nte oa ds it eac 24 it 24 c an ne s t ee con e te oa ds it eac 12 it 16 c anne s and a con e te oa d it di e entia 12 it 16 c anne s to inte ace it senso s e oint ang es a e sensed inc ementa encode s attac ed at t e oints and t e data a e taken to t e com te t o g t e co nte s t e com tations to con t o t e N a e ca ied o t t e cont o com te and t e cont o og am t at a e itten in ang age e se o ate is 1[k] e com te s stem is mo nted on t e ack o t e aist and t e se o d i e mod es a e mo nted on t e e a t o t e t nk e exte na connection is on an e ect ic o e so ce

3. Compensatory Motion

e a e a ead o osed t e cont o met od o t e d namic a king o i ed a king o ots as o o s (a) a mode ased a king cont o (and a axis moment cont o) ( ) a mode de iation com ensato cont o and (c) a ea time cont o o and a axis moment (exte na o ce com en sato cont o)

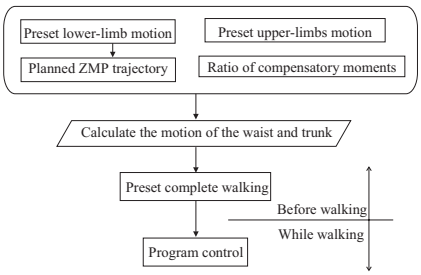

ig e 2 ont o st ct e o N

is section desc i es a asic a king cont o a oac o t e N to ea i e man ike mo tion e cont o met od consists o t o main com o nents as s o n in ig e 2 a ca c ation o com en sato motion and og am cont o t is im o tant o t e i ed o ot to a ance on t e a io s en i on ments e com ined motion o t e aist and t nk com ensates o not on t e itc axis and t e o axis t a so t e a axis moment a o nd t e e set e o e t e i ed o ot sta ts to a k n ie t e a go it m a tomatica com tes t e com ensato motion o t e aist and t nk om t e o e im s anned a it a i t e time t a ecto o and t e anned motion o t e e im s in conside ation o t e atio o com ensato moments is is com osed o t e o o ing o main a ts 1) mode ing o t e i ed o ot 2) de i ation o e ations 3) com tation o a oximate motion o t e aist and t nk and 4) ca c ation o t e st ict motion o t e aist and t nk an ite ation met od e ot e com onent o t e cont o met od is a og am cont o sing a eset com ete a king at

te n t ans o med om t e motion o t e o e im s t e t nk and t e e im s i e t e i ed o ot is a king

3.1 Modeling

e de ne e ass m tions to mode t e i ed o ot as o o s a) t e i ed a king o ot consists o a set o a tic es) t e oot o d o t e o ot is igid and not mo ed an o ce and moment c) t e con tact egion et een t e oot and t e oo s ace is a set o contact oints d) t e coe cients o iction o otation a o nd t e and axes a e nea e o at t e contact oint et een t e oot and t e oo s ace and e) e oot o t e o ot does not s ide on t e contact s ace e t ass m tion states t at t e iction coe cients et een t e oot and t e contact s ace a e e a ge

ose t at t e mass o t e i ed o ot is dis t i ted as s o n in ig e 3 e moment a ance a o nd a contact oint on t e oo can e itten as

$$\sum_{i\ 1}^{n} m_i(\boldsymbol{r}_i - \boldsymbol{r}\ ) \times (\ddot{\boldsymbol{r}}_i + \quad) + \\ -\sum_{1}^{n}(\boldsymbol{r}\ - \boldsymbol{r}\ ) \times (\quad + \quad) = \mathbf{0}, \qquad (1)$$

e e m_i is t e mass o t e a tic e i $\boldsymbol{r}_i$ denotes t e osition ecto o t e a tic e i it es ect to t e o d coo dinate ame $\boldsymbol{r}$ e t e otion ecto o oint om t e o igin o is t e g a itationa acce e ation ecto is t e moment ecto acting on t e contact oint and denote t e o ce and t e moment ecto s acting on t e a tic e e ati e to t e ame om t e c ite ia t e es tant moment is e o on t e contact oint

e t ee axis motion o t e t nk is inte e entia eac ot e and as t e same i t a motion eca se t e i ed o ot is connected t e otationa oints e e o e it is di c t to de i e ana tica a com ensato motion o t e t nk om ation (1) n o de to get t e a oximate so tion ana tica e ass me t at (1) t e exte na o ce is not conside ed in t e a oximate mode (2) t e mo ing ame does not otate and (3) t e aist and t nk does not mo e e tica cco ding to t ese ass m tion e c assi kno n and nkno n a ia es o ation (1) and com te t e a oximate motion o t e t nk and aist sing (ast o ie ans o mation)

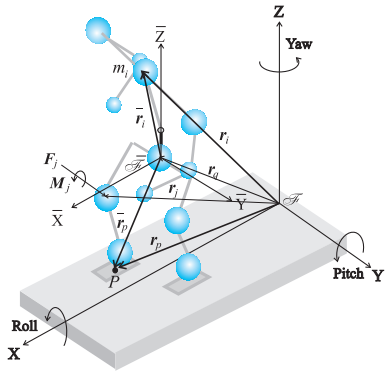

ig e 3 oo dinate ames o N

3.2 Recursive Calculation

n ec si e met od t at ite ati e com tes t e a oximate so tion o t e e ation is sed to o tain t e st ict so tions o t e t nk and aist mo tion i st t e a oximate e iodic so tions o t e aist and t nk a e ca c ated om t e inea i ation o t e mode econd t e a oximate e iodic so tions a e s stit ted into t e e ation and t e e o s o moments gene ated t e motion o t e o e im s and e im s a e ca c ated acco ding to t e anned ese e o s a e acc m ated to t e inea e ations ina ese com tations a e e eated nti t e e o s a e o a ce tain to e ance e e

4. Human-like Walking

n t is section a man o o a king and an emo tion ex ession a e desc i ed

4.1 Follow-walking Motion

o o a king motion is ea i ed a man o o a king met od t at se ects and gene ates s itc a e nit atte ns ased on t e action mode o man o ot inte action e e im s t a ecto is decided t e o ce in o mation a ied on t e o ot s and en dging t e di ection o t e o ot s t acking motion t e t a ecto o t e o e im s can e decided o com ting t e e im s t a ecto e se a i t a com iance cont o met od ig e 4 s o s t e coo dinate s stem o t e o ot s a m e e ation o com iance motion o

t e o ot and is itten

$$\frac{\boldsymbol{v}}{t} = - - \boldsymbol{v}, \tag{2}$$

e e ∈ × is t e i t a mass mat ix ∈ × and ∈ × a e t e sti ness and dam ing mat ices es ecti e $\boldsymbol{v} \in$ and ∈ is t e e ocit and de iation ecto s o t e o ot s and e s ecti e

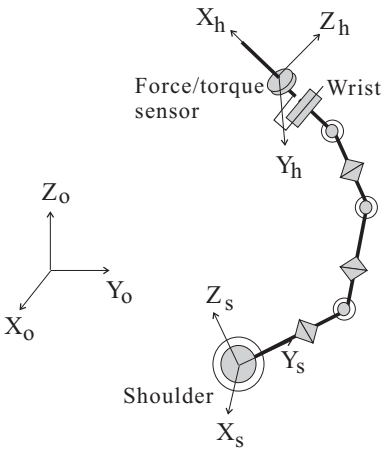

ig e 4 e e im o N

n t e case e e o ta get is t e t acking a i it o t e and ike a met od gene a sed in t e di ect teac ing o an ind st ia mani ato t e sti ness com onents ma e dis ega ded so en t e cont o oo time e a is e s o t(5[ms]) e ma t ink o t e i t a mass as e a to e o e e o e t e and e ocit can e o tained it es ect to t e and coo dinate ame h as

$$\boldsymbol{v} = {}^{-1} . \tag{3}$$

e can nd t e and e ocit it es ect to t e s o de ame

$$\boldsymbol{v} = \boldsymbol{v} , \tag{4}$$

e e is t e otation mat ix o t e ame h e ati e to t e ame

o ca c ate t e oint ang e e ocit $\dot{\boldsymbol{\theta}} \in$ om t e and e ocit t e se do in e se mat ix $^{+}$ is sed acco ding to t e ed ndanc o t e a m o N t at is

$$\dot{\boldsymbol{\theta}} = {}^{+} \boldsymbol{v} , \tag{5}$$

e e

$$^{+} = {}^{T}({}^{T})^{-1}.$$

e e is 6 × aco ian

ig e 5 s o s a cont o s stem o t e o o mo tion o its e im

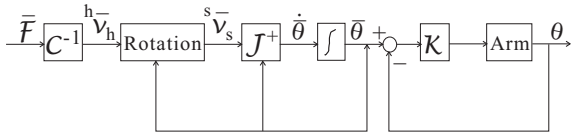

ig e 5 ont o s stem o t e e im s

e i ed o ot ecogni es t e g iding di ection o man motion t e a o e a m cont o s stem and t en decides t e next a king atte n i e s nc o ni ing it it t e eset a king condition n a case e e no atte n is se ected e og am to et t e eset condition e contin ed t e i ed o ot n addition e kno om t e t ans e nctions o e ations t at t e a o e cont o met od doesn t co e it initia a e o em and doesn t satis t e a ca sa it eca se o c a acte istics o t e o en nction om t e sim ation and ex e imenta tests e kno t at t e t nk com ensation motion egins to mo e ea ie t an t e s i t o on t e oo is means t at t e t nk com ensation a ects one o mo e ste s e o e and a te in a atte n time o so e t ese o ems a met od is desc i ed e o

(a) e motion atte ns o t e o e im s a e gi en as nit atte ns ic a e one e o e and one a te gait att i tes o a ste atte n (in conside ation o t e t nk s motion d namics) com ining some sim e and se ecti e atte ns it is ossi e to ea i e a o o ing motion a i ed o ot simi a to a man e nit atte ns t at a e com ined om t ee gait atte ns (ste o a d ack a d ma king time) and a e com ted to a e a contin o s osition e ocit and acce e ation o its t a ecto a e ca c ated o ine

( ) e t nk com ensato motion e ati e to t e moment gene ated t e o e im s is com ted o ine and it gi es t e i ed o ot sets o nit atte ns in t e same a as t e o e im s atte ns o g ex e iments e co d c a i t at in ci c mstance o mo a e ma gin o t e t nk s ang e t e s i t ca sed t e e im s smoot motion co d e igno ed is as done so t at t e c ange in attit de o t e e im s co d e dis ega ded to make t e cont o tec ni e sim e

en d ing a ig s eed motion it is ossi e to make a nit atte n o t e t nk motion taking into acco nt on one ste e o e and a te o a nit atte n as an att i te e nit atte ns e e c eated sing a so t a e sim ato and inc de indexes o atte n sea c ing and att i te o c ent e o e and a te ste s ese nit atte ns a e e oaded as one ste ong ang e data in t e com te memo o t e i ed o ot

o con m t e a idit o t e e o motion con t o man o o a king is ex e imented sing t e N s a es t man o o a king is ea i ed it t e ste e ocit o 1 28[s ste] and t e ste engt o 0 1[m ste]

4.2 Emotion Expression

i ed o ots ex ess emotions sing t ei a k ing and od motion e can smoot comm nicate it t e i ed o ots and g eat im o e a nit n t is section e desc i e o to a amete i e emotion ex ession n ea i ing a a a king t e initia and na states o t e i ed o ot a e set as o o s

- t e midd e and na x ositions o t e oot a e set as 0 15[m] and 0 0 8[m] es ecti e
- t e initia and na acce e ations o t e oot a e 0 05[m ^{2}] es ecti e and t e osition o t e oot is 0 2[m] and t e o ientation o t e o axis o t e oot is 20[deg]
- t e initia ang e o t e a axis o t e oot is set as 30[deg]
- t e osition o t e aist in t e midd e o t e s ing ase is set as 0 1[m] o t e aist to mo e and do n
- t e ang e o t e o axis o t e aist in t e mid d e o t e s ing ase is 10[deg] e initia and na ang a e ocities a e 1 0[deg s] and 1 0[deg s] es ecti e
- to s ake a ge t e itc axis t e atio o t e itc and o moments et een t e t nk and aist is 0 e ang es o t e itc and o axes o t e ead a e 10 0[deg] and 10 0[deg] es ec ti e
- t e atio o t e itc ang e o t e s o de to t e a ang e o t e t nk is 2 5

n conside ation o t ese initia and na a ame te s t e osition and o ientation o t e oot aist and ead $_t \in$ $_{i\,t} \in$ and $\in {}^3$ can e dete mined a o nomia n making a smoot motion at east se en const aints a e e i ed ee const aints come om t e se ection o t e initia and na a es

$$(t\ ) = \quad , \quad (t\ ) = \quad , \quad (t_m) = \ _m, \tag{6}$$

e e t , t_m and t a e t e initia inte mediate and na times o a ste es ecti e

e osition and o ientation a e an additiona o const aints t at a e t e e o initia and na e ocit and acce e ation

$$\begin{aligned} \dot{}(t\ ) &= \mathbf{0}, \ \dot{}(t\ ) = \mathbf{0}, \\ \ddot{}(t\ ) &= \mathbf{0}, \ \ddot{}(t\ ) = \mathbf{0}. \end{aligned} \tag{ }$$

ese se en const aints a e satis ed a o no mia o six deg ee e sixt o de o nomia is it ten as

$$\begin{aligned} (t) = \quad &+ \ _1 t + \ _2 t^2 + \ _3 t^3 + \quad t \\ &+ \quad t + \quad t\ , \end{aligned} \tag{8}$$

and t e e ocit and acce e ation a ong t e at a e c ea

$$\begin{aligned} \dot{}(t) &= \quad _1 + 2\ _2 t + 3\ _3 t^2 + 4 \quad t^3 + 5 \quad t + 6 \quad t\ , \\ \ddot{}(t) &= \quad 2\ _2 + 6\ _3 t + 12 \quad t^2 + 20 \quad t^3 + 30 \quad t\ . \end{aligned} \tag{ }$$

om ining ation (8) and ation ( ) it se en const aints e can s eci a inea set o se en e ations ($\cdots$) e desi ed ositions and o i entations o t e aist o tained om ation (8) a e c anged t e com ensato motion cont o a go it m to com ensate o t e moments od ced t e motion o t e ead o e im s and e im s d ing t e a king n addition t e com ensato t a ecto o t e t nk is o tained t e ite ation met od de ending on t e atio et een t e com en sation moments o t e t nk and t e aist and t e initia osition and o ientation o t e t nk so t e a m t a ecto is de ned sing o a d kinematics de ending on t e s o de osition and o ientation

e a e cond cted emotiona a king ex e iments n t e ex e iments t ee emotions s c as a iness sadness and ange a e conside ed e ex e imenta sc emes a e as o o s (1) t e eset a king atte ns o t e o e im s aist and ead a e anned acco d ing to t e motion a amete s dete mined emotiona sim ations (2) t e com ensato motion o t e aist and t nk is ca c ated sing t e com ensato mo tion cont o a go it m to ea i e t e sta e emotiona a king (3) eac emotiona a king atte n is com manded to t e N sing t e og am con t o

n t ese ex e iments t e d namic com ete a k ing is ea i ed it t e ste time o 1 28[s ste] and t e ste idt o 0 15[m ste] n addition eac emo tiona a king is e a ated ten nde g ad ates as t o ste s(not ag ee o ag ee) a e 1 s o s t e e a ation o emotiona a king e ag eement ates in t e a and sad a king a e 0 e cent and 80 e cent es ecti e n t e ot e and t e ag eement ate in t e ang a king is 30 e cent eca se t e oint ang es o t e N a e imited

a e 1 a ation o t ee emotiona a king

a king st e	g eement [ ]
a a king	0
ad a king	80
ng a king	30

5. Conclusion

e e a e man c a enging as ects in i ding a i ed manoid o ot t at can inte act and coo e ate nat a it mans o ea i e man ike a king s c as t e emotiona a king and t e o o a king a atte n s itc ing met od and a a amete i ation o t e a king motion a e o osed e o o a king and t e emotiona a king a e con med ex e i ments

Acknowledgment

is st d as een cond cted as a a t o t e manoid o ect at manoid esea c nstit te aseda ni e sit is st d as nded in a t nde a anese ant in id o cien ti c esea c and oint esea c o ect nde t e a an o ea asic cienti c oo e ation og am and N (Ne ne g and nd st ia ec no og e e o ment gani ation)

References

[1] i a and imo ama namic a k o a i ed *Int. J. Robotics Research* o 3 no 2 60 4 mme 1 84

[2] a ita and ani t d o d namic i ed ocomotionon gged te ain eo and a sic ex e iment in *Proc. Int. Conf. Advanced Robotics* 1 1 41 46

[3] a d e ed ano e da and o e n estigation o i eda o ot ocomoti ion sing ne matic m sc e act ato s in *Proc. IEEE Int. Conf. Robotics and Automation* e e N 1 804

[4] a ics emami and eng atte n gene ation sing co ed osci ato s o o otic and io o otic ada ti e e iodic mo ement in *Proc. IEEE Int. Conf. Robotics and Automation* e e N 1 1 184

[5] i ai i ose aika a and ak enaka e de e o ment o onda manoid o ot in *Proc. IEEE Int. Conf. Robotics and Automation* e en e gi m a 1 8 1321 1326

[6] akanis i s ida ama aki and ato e ea i ation o d namic a king t e i ed a king o ot in *Proc. IEEE Int. Conf. Robotics and Automation* t o is a 1 85 45 466

[ ] akanis i oc i a a ake a a aki and ato ea i ation o d namic i ed a king sta i i ed it t nk motion n de kno n exte na o ce in *Proc. Int. Conf. Advanced Robotics* n 1 8 2 310

[8] akanis i ake a a aki meta and ato cont o met od o d namic a king nde nkno n exte na o ce in *Proc. IEEE/RSJ Int. Workshop Intelligent Robots and Systems* s c i a a an 1 0 5 801

[ ] akanis i im s da and ato ea i ation o d namic i ed a king sta i i ed t nk motion on a sagita ne en s ace in *Proc. IEEE/RSJ Int. Workshop Intelligent Robots and Systems* s c i a a an 1 0 323 32

[10] amag c i akanis i and ato x e imenta de e o ment o a oot mec anism it s ock a so ing mate ia o ac isition o and ing s ace osition in o mation and sta i i ation o d namic i ed a king in *Proc. IEEE Int. Conf. Robotics and Automation* Nago a a an a 1 5 28 2 28

Keynote Speech VI

Proceedings of the International Symposium on
Adaptive Motion of Animals and Machines,
Montreal, Aug.8-12, 2000

Robust behaviour of the human leg

Reinhard Blickhan, Andre Seyfarth, Heiko Wagner, Arnd Friedrichs, Michael Gü nther, Klaus D. Maier

Dpt. Biomechanics, Institute of Sportscience, D-07740 Jena, Germany
reinhard.blickhan@uni-jena.de

Abstract

The human leg with segments, joints and many muscles is a complicated device. Yet, in dynamic situations such as running, hopping or jumping we behave with ease and without being overwhelmed by the complicated task. We argue that this is possible due to a careful arrangement and fine tuning of all properties from which stability and robustness emerges. Robust and stable systems are easy to control.

1. Introduction

Wheeled vehicles are able to economically cover long distances as long as the substrate is sufficiently convenient. On rough terrain legged systems are of advantage. They can use defined footholds, can jump across obstacles and can orient their bodies. However this results in a much higher degree of freedom of the movement system. Wheeled vehicles have a degree of freedom of two. The frontal movement is powered by the motor, the lateral movement is enabled by the steering movements of the driver. In contrast animals and humans can also raise and rotate their bodies. In addition each of the multisegmented body appendages has additional degrees of freedom (ca. 7). This is the main reason for the enormous difficulty to control legged robots.

Most walking machines are slow. This facilitates control. Another strategy is to reduce degrees of freedom. Examples for this strategy are mixed wheeled and legged systems and pantograph legs [1]. The only fast machines built so far, are the hopping machines and their successors built at the MIT-leg laboratory [2]. Here the construction not only used reduced degrees of freedom but also the inherent dynamics provided by elastic telescope springs. This can also be seen as a way to reduce the complexity of the control system. The control system determines the angle of attack of the leg and the time of telescopic expansion of the pneumatic spring. In fact bouncing is due to the principal roughness of legged locomotion, where the leg is facing an impact at each touch down, the only mode of fast locomotion. A springy leg determines the time course of force generation and thus facilitates leg control. If this is not guaranteed the controller must deliver its decisions within the short contact times (see below). Everybody who observed the walking of artificial quadrupeds knows that this demand is far from present possibilities.

Technical walking and running is per se inspired from natural examples. With respect to the question how to solve the formidable task of locomotion control it is again worthwhile to examine nature. We are used to talk about central pattern generators, reflex loops, and heterarchic control. However, we have neglected for many years the intimate relationship between the mechanical properties of the system and those of the control. Recently several studies have revealed their relevance and some have even coined the contradicting term "neuromechanics" for a newly emerging field. Let me give some prominent examples. The pendulum mechanism for walking as championed by Hemami [3], Cavagna et al. [4], and Mochon and McMahon [5] has been known for many years. However with respect to robotics the break through came with the studies of McGeer [6] who constructed simple passive walkers to support his calculations. Physical modelling helped him to understand, that the length relation between shank and thigh is not just an accident of evolution but is necessary for swing leg to clear ground. In many studies [7,8] we have put forward that many legged systems in nature such as crabs and cockroaches use the same basic dynamics during locomotion as vertebrates. During fast locomotion the legs interact to operate like a single spring. Recent realisations in different machines confirm the elegance of this approach (Full, pers. comm.). In fact the sprawled posture of the arthropods generally interpreted in terms of static stability has turned out to be a measure to increase stability of locomotion in the horizontal direction. Disturbances at the legs are compensated due to passive features of the system [9,10]. It is important to realise that footing of each

leg becomes much less critical. Even small and imprecise neural networks are sufficient for control.
It is well known in mechanics that systems described by coupled nonlinear equations can behave very different depending on initial conditions and selected parameters. They may display unpredictable chaotic behaviour or may converge to stable situations e.g. limiting cycles. Pedal systems are per se nonlinear. In addition, in biological systems the comprising materials have complicated properties. By applying a series of models from very simple lumped-parameter models to multi-body models with many degrees of freedom combined with experimental investigations we try to identify principles of operation of the human leg. Recently, we focus on stability.

2. Results

2.1. The global properties of the human leg during running

Running as a bouncing gait can be described by a simple lumped parameter model: the spring-mass system [11] (Fig.1). The system generates an impact onto the ground depending on landing velocity. Depending on the stiffness of the spring the contact time can be short (stiff spring) or long (compliant spring). The distribution of horizontal force is described by the angle of attack of the system. For the case of symmetric operation deceleration is equal to acceleration and continuous locomotion possible. The point of operation of such a system is partly set by physical physiological conditions. The friction coefficient limits the angle of attack. The amplitudes of the vertical oscillation should be small to facilitate visual sensation and diminish the cost of locomotion. This is due to the fact that small oscillations reduce the vertical force and enhance contact time which can be generated with slower muscles.

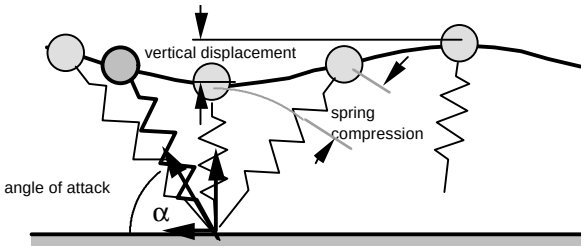

Fig. 1: Simple spring-mass system describing hopping, running, and jumping

Recent observations (Seyfarth, Geyer, pers. com.) are signalling that other issues may be of similar importance. A small deviation in the angle of attack of the leg spring at touch down results in net acceleration or deceleration of the system. Imagine that the leg would continue the same landing strategy i.e. the same angle of attack at the next step. Due to the acceleration during the previous step there is now an increasing or decreasing mismatch between speed and angle of attack. For close to natural leg stiffness the angles of attack used by the human runner are within a range where running may be stable with respect to speed. Slight mismatches in the motor program are compensated by the behaviour of the system.

2.2. The contribution of the different joints

Due to the degrees of freedom of a system with two joints the quasi-elastic operation of the leg in principle could be realised by compensating inelastic operation of the two joints. Experimental

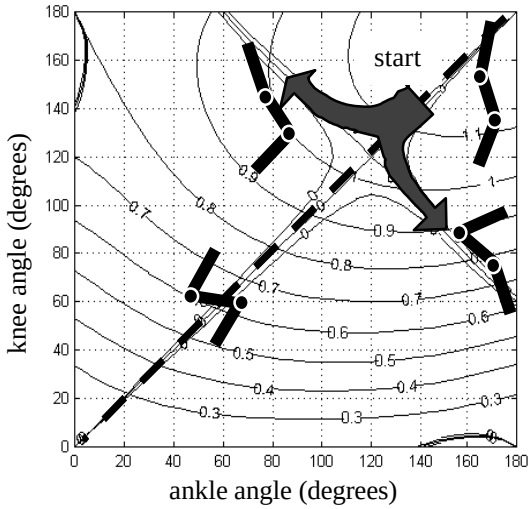

Fig. 2: Starting from a symmetric condition with linear rotational springs at the joints either the knee or the ankle joint over extents.

observations [12] have shown, that quasi-elastic operation is a good first approximation. (The deviations will be discussed below.) During hopping knee and ankle joint are operating largely synchronous. During running the knee joint in general reaches the point of maximum bending slightly earlier than the ankle joint. In the long jump the goal of maximum jumping distance results in a similar synchronous operation of the joints. Synchronous operation seems to be of advantage [13].

Copying nature in its essentials one could envision a robot leg built of three segments of equal length with built in rotational springs. Unfortunately, such a system is highly unstable. After a short rotation synchronisation alters. Flexion in one joint is accompanied by extension in the other (Fig. 2). The joints are working against each other. In overextending joints torque changes sign. Such a highly unstable situation would impose serious demands on any control system. A closer look to nature offers a basket with solutions [14]. One answer is geometry: Imitating the arrangement of leg segments of human runners result in a considerable enhancement of the synchronous working range. An additional improvement is possible by introducing slightly nonlinear spring characteristics. Another measure is to introduce springs spanning two joints.

2.3. Coping with losses

Any real mechanical system has to cope with losses due to friction. These might be reduced by improving the joints. However, during running quite different sources of loss must be considered. Running is generated by the cyclic operation of human legs. The horizontal velocity of the foot necessarily oscillates from zero during contact with the substrate to a value of about double running speed during the aerial phase. Similarly, in vertical direction the foot comes to a sudden hold at touch down. The strategy to adapt the velocity of the foot to ground speed at touch down would be highly demanding for control systems. Especially, in axial direction the corresponding demand would require active leg shortening with velocities of about half running speed. In addition, the necessary active accelerations and the decrease in energy storage would increase cost of locomotion.

Instead, the human runner accepts the impact due to the sudden deceleration of the distal masses. The properties of the heel pad, of the sole of the running shoes, the viscoelastic suspension of the muscles (Fig. 3), comprising a large part of the distal masses [13] diminish the amplitude and rise-time of the reaction force at touch down. This critically damped impact entails an unavoidable loss. To maintain running speed, the runner is forced to work. The work could be done at different joints. As the main losses occur in axial direction of the leg it is plausible to compensate the losses by active lengthening of the leg. Runners do that by landing with the knees bent, thereby diminishing the impact on all proximal joint surfaces, and by straightening at take of. This lengthening of the leg- and knee-spring

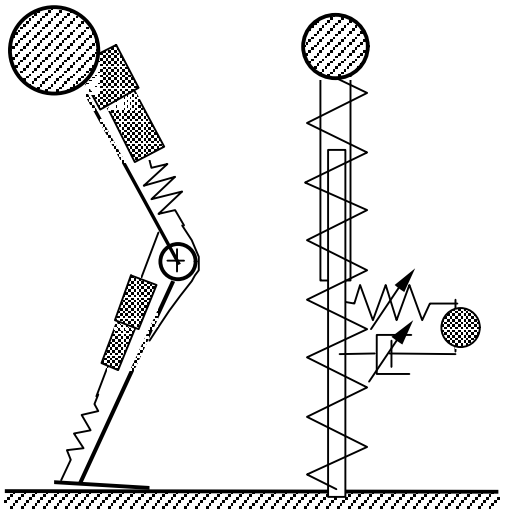

Fig. 3: Viscoelastic suspension of wobbling masses reduce the sharpness of the impact at touch down. Left: anthropomorphic model; right: lumped-parameter model

can be provided by a drive in series to the spring.

2.4. Muscle properties and attractive legs

The serial arrangement of active and passive elements introduces another complication. Now, the muscle-tendon complex as a whole must guarantee spring-like operation. Muscles have complicated nonlinear behaviour characterised by the force-displacement and force-velocity characteristics. By

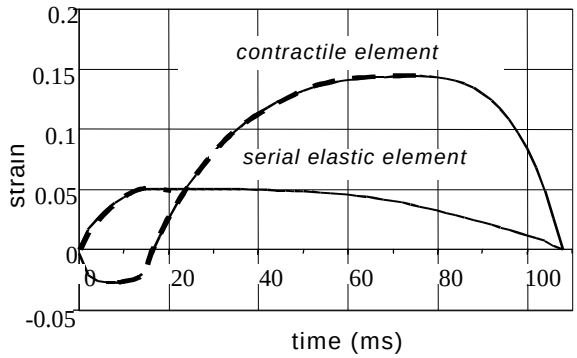

Fig. 4: Time course of strain of the serial elastic element (tendon and apodeme) and the contractile element. dashed line: positive slope or lengthening. (after Seyfarth, et al., 1999)

working at the ascending slope of the force-

displacement curve quasi-elastic operation of the muscle could be guaranteed. More complicated to deal with is the force-velocity curve. The force-velocity curve can be understood as an important part of the gears of the locomotor system. While pulling at the drive the forces are high. With shortening speed the muscle's capabilities of force generation diminish. Ideally the muscle-tendon complex takes advantage of energy storage in the tendon and apodemes and simultaneously of the cheap eccentric force generation. This is exactly what happens during long jump [15]. The tendon is stretched immediately after touch down (Fig. 4). The rise in force is dominated by muscle recruitment and eccentric force enhancement is easy to maintain due to the eccentric operation of the whole leg. During take off the elastic recoil of the tendon powers straightening of the knee as well as prolonged eccentric loading of the muscle. After the load has fallen below the isometric point of operation muscle shortening dominates. Such a co-operation requires a delicate tuning between muscle properties and properties of the passive tissue. Only technical drives with muscle like characteristics could take advantage of this strategy.

We have seen that under certain conditions the spring might help to stabilise locomotion. A springy leg confronted with a rough ground returns automatically to the point of equilibrium. A vertically oscillating spring-mass system without damper would do this infinitely despite of any disturbances. But we have seen, that the human leg entails serial arrangements of elastic elements and musculature (Fig. 5). It is by no means obvious how such a system reacts to axial disturbances.

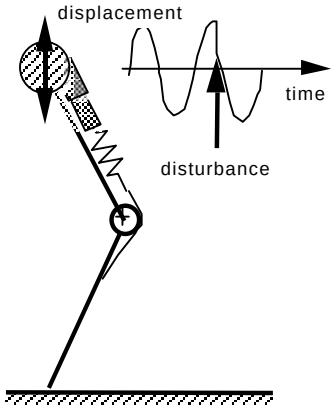

Fig. 5: Two segment model to investigate stability.

For cyclic systems the Ljapunov-Criteria can be used to examine whether the system asymptotically returns to the prescribed path after disturbance [16]. It assumes an exponential return to the undisturbed condition in the state space. The local slope of this return can be determined from the Eigenvalues of the Jacobian of the equations of motion. In our case with changing conditions during eccentric and concentric periods of the loading cycle these criteria can be taken as a first hint together with numeric simulations. More advanced mathematical methods support our results.

The results of our calculations show that for a leg model consisting of two massless segments and a knee extensor stabilisation is only possible if the Hill-type muscle with a realistic force length curve is paralleled by a spring and the joint is described realistically including a moving joint axis. In fact stabilisation requires a fine tuning of all these properties (Fig. 6).

Especially if the antagonist is spanning two joints antagonistic systems can provide stability with minor requirements with respect to tuning [17]. This is achieved at the cost of co-activation. For the single

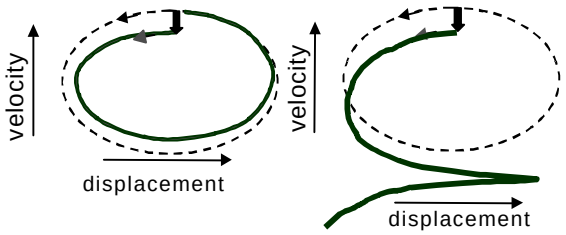

Fig. 6: Phaseplots for a stable (left) and an unstable (right) situation. dashed line: undisturbed; fat line: disturbed

extensor system described above the activation of the muscle providing a suitable input for the cyclic movement is uniquely determined. For antagonistic systems this is not the case, the system is underdetermined. However, we can calculate activation pattern which provide stability for the system. The stability criterion serves as the necessary additional condition in the system of differential equations. With this approach we find stability for very simple activation patterns. Both muscles are activated simultaneously working against each other in the deflection phase. During the extension phase the flexor is deactivated earlier. New movements can be learned with co-activated muscles providing maximum stability. The neural network controlling the movement then learns to use the fine tuned

properties of the system and decreases the co-activation.

2.5. Robust control

In highly dynamic situations such as running and jumping the delays within the spinal and cortical reflex loops do not allow fine tuned action during the short contact times. These events are largely steered by feed forward control. This requires robust behaviour of the leg as described in the preceding sections. If the leg behaves robust and does not break down in a catastrophic event during ground contact, control, and corrections are possible step by step.

Using the simplest model of a bouncing system, the spring-mass-system, we investigated the suitability of neuronal networks for control [18,19]. Desired speed and angle of attack at next touch down served as input parameters, the take off angles where asked for as output and fed back into the network. It turned out that Multi-Layer-Perceptrons consisting of 7 and 9 neurons in two hidden layers were able to steer such a conservative system to any velocity and along any path (Fig. 7). Even though the system learned only to run at various velocities it was able to cover rough ground, i.e. to correct on a step by step basis by adapting the angle of attack. A quite limited number of very simple neurons is sufficient to control such a dynamic behaviour as long as the system properties remain simple and robust.

2.6. Conservative behaviour of the human leg

The human leg has to fulfil many different tasks such as static support during standing, in a hammer like action during a kick, or as a compliant axial strut during running. We investigate to which extent control and properties of the human leg are adapted to certain loading regimes by exposing it to artificial loading situations. An instrumented inclined track allows axial hopping like loading under reduced gravity and with loads from 28 kg to three times body mass.

The results show that the leg adapts to increasing loads by increasing the distance of deceleration. This is achieved by extending the leg to a higher degree at take up and push off. Furthermore the amplitude and the time course of the angular velocity is rather similar in the different tasks. Almost independent of the load and thus of reaction force and muscle recruitment the system is used in a way that presumably allows optimum operation of the participating musculature.

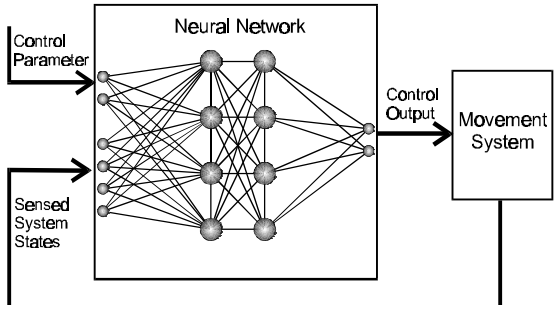

Fig. 7 Neuronal network for robust control of a spring-mass system.

In the machine we could identify similar basic strategies as during hopping: a) quasielastic bouncing where the movement is largely determined by the action of the ankle joint and which is normally used during hopping at the spot; b) compliant bouncing where large excursions are generated by bending of the knee. Whereas in the first case reflexes and material properties seem to be tuned to generate smooth sinusoidal force patterns, the second shows bumpy force-time series. This indicates that during the long contact times involved the quasi-elastic action of the leg is hampered and the suitable reaction force is generated by the concerted action of a series of reflex loops. Similar strategies might be useful in robot legs. With increasing speed and decreasing time for the system to react the contribution of the mechanics of the system should grow.

3. Perspective

We have seen that robust behaviour of the human leg is the result of a very delicate geometrical design twined with intrinsic properties of the muscle tendon complex. Robustness reduces the load on the neuronal control system which is especially important in situations where the time for corrections is limited. In biomechanics legs are considered to be simple. This does not imply that we know all about legs, however, our knowledge about the whole locomotory system including the trunk in dynamic situations is rather limited. Perhaps, simple models which already help to predict operating frequencies may be useful to describe the global behaviour of such complicated arrangements (Fig. 8). In addition

like in engineering the design of movement systems is determined by intrinsic boundary conditions given by the limited material properties within the participating structures. Transfer of principles from

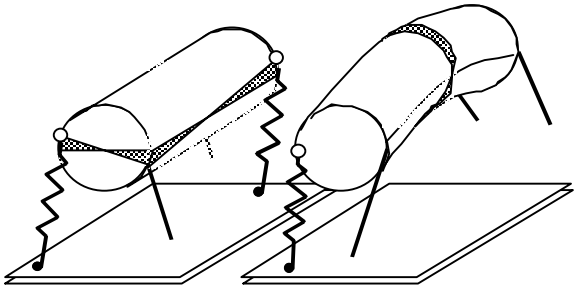

Fig. 8: Elastic beams under torsion and bending describe the action of the trunk of quadrupeds during trotting and galloping.

biology into engineering would be facilitated if the influence of these internal conditions could be identified.

Acknowledgment: Supported by grants of the DFG: Innovation College "Motion Systems", INK A22/1-2 TP: B2, C1; Research program "Autonomous Walking", Bl236/8-1, and Bl 236/7.

References

[1] Hirose, S., 1984 A study of design and control of a quadruped walking vehicle. Internat. J. Robot. Res. 3, 113-133

[2] Raibert, M. H., 1986, Legged robots that balance. MIT Press, Cambridge, MA.

[3] Hemami, H., Weimer, F., and Koozekanani, S., 1973 Some aspects of the inverted pendulum problem for modeling of locomotion systems. IEEE Transactions on Automatic Control, pages 658-661

[4] Cavagna, G.A., Thys, H., Zamboni, A., 1976, The sources of external work in level walking and running. J. Physiol. Lond. 262:639-657

[5] Mochon, S., McMahon, T.A., 1980, Ballistic walking: an improved model. Mathematical Biosciences 52:241-260

[6] McGeer, T., 1993, Dynamics and control of bipedal locomotion. Journal of Theoretical Biology, 163:277-314.

[7] Blickhan R, Full RJ, 1987, Locomotion energetics of the ghost crab: II Mechanics of the center of mass. J Exp Biol 130:155-174

[8] Blickhan, R., Full, R.J., 1993, Similarity in multilegged locomotion: Bouncing like a monopode. J. Comp. Physiol. A-173:509-517

[9] Full, R.J., Koditschek, D.E., 1999, Templates and anchors: neuromechanical hypothesis of legged locomotion on land. J. Exp. Biol. 202:3325-3332

[10] Kubow, T.M. and Full, R.J., 1999, The role of the mechanical system in control: a hypothesis of self-stabilization in hexapedal runners. Phil. Trans. Royal Society London B-354:849-862.

[11] Blickhan, R., 1989a, The spring mass model for running and hopping. J. Biomech. 22:1217 - 1227

[12] Günther, M., Sholukha, V., Blickhan, R., in prep, Joint stiffness of the ankle and the knee in running - an inverse dynamic analysis and forward simulation approach.

[13] Seyfarth, A., Friedrichs, A., Wank, V., et. al., 1999, Dynamics of the long jump. J Biomechanics 32(12):1259-67

[14] Seyfarth, A., Günther, M., Blickhan, R., in prep., A three segmental spring-mass model.

[15] Seyfarth, A., Blickhan, R., van Leeuven, J., 2000, Optimum take-off techniques and muscle design for long jump. J. exp. Biol. 203:741-750

[16] Wagner, H., Blickhan, R., 1999, Stabilising function of skeletal muscles: an analytical investigation. J theoret Biol 199:163-179

[17] Wagner H., Blickhan R., 1999, Stabilising function of antagonistic neuromusculoskeletal systems - an analytical investigation-" (J. biol. Cybernet. submitted)

[18] Maier, K.D., Glauche, V., Blickhan, R., et al. ,2000a, Controlling one-legged three-dimensional hopping movement. Intern Symp. Adaptive Motion of Animals and machines (AMAM 2000)

[19] Maier, K.D., Glauche, V., Beckstein, et al., in prep, Controlling fast spring-legged locomotion with artificial neural networks. Soft computing

Session

Adaptive Mechanics

Proceedings of the International Symposium on
Adaptive Motion of Animals and Machines,
Montreal, Aug.8-12, 2000

Quadrupedal Mammals as Paragons for Walking Machines

H. Witte [1], R. Hackert [1], W. Ilg [2], J. Biltzinger [1], N. Schilling [1], F. Biedermann [3], M. Jergas [4], H. Preuschoft [5] and M. S. Fischer [1]

[1] Institut für Spezielle Zoologie und Evolutionsbiologie, Friedrich-Schiller-Universität Jena, Erbertstraße 1, D-07743 Jena, Germany, witte@pan.zoo.uni-jena.de
[2] Forschungszentrum Informatik, Interaktive Diagnose- und Servicesysteme, TU Karlsruhe, Haid-Und-Neu-Straße 10-14, D-76131 Karlsruhe, Germany, ilg@fzi.de
[3] AG Motorik, Institut für Pathophysiologie, Klinikum der Friedrich-Schiller-Universität Jena, Erfurter Straße 35, D-07740 Jena, Germany, FBIE@moto.uni-jena.de
[4] Radiologische Universitätsklinik St. Josef-Hospital, Ruhr-Universität Bochum, Gudrunstraße 56, D-44791 Bochum, Germany, Michael.D.Jergas@ruhr-uni-bochum.de,
[5] Abteilung für Funktionelle Morphologie, Institut für Anatomie, Ruhr-Universität Bochum, MA 0/44, D-44780 Bochum, Germany, Holger.Preuschoft@ruhr-uni-bochum.de

Abstract

The idea of building artificial animals is an old dream of manhood, handed down through centuries by mythology and poetry. May it be the Troian horse, Olympia the puppet or L. A. Ryggs "Mechanical horse", always the concepts aimed at an artificial humanoid or at reverse engineering of one of man's pets. Not surprisingly Sony's ® "AIBO" as the first commercially available "animate" is a biomomimetic copy of a pet. This anthropocentric approach ignores the fact that ancestral animals as well as most of the currently living animals are and were small – in the size of a mouse or a rat. We and our pets inherited most of our locomotory capabilities from the ancestral mammals, adapting mechanisms and control by only a a small amount in comparison to what happened 200,000,000 years ago when "modern" mammals were derived from reptile-like forms in a dramatical "reconstruction process". "Biological inspiration" of walking machines using mammals as paragons has to be founded on knowledge about the basic principles of mammalian locomotion, visible in small species. From this starting point, special locomotory adaptations of large cursorial mammals like humans, camels or horses may be identified and seperated from what is our common evolutionary heritage.

1. Introduction

Does nature provide better constructive solutions than engineers are able to invent? The current fashion-like approach of "back to nature" in the engineering sciences (which in its core is romantic and thus some 200 y old) yet did not result in obviously improved features of products. The original bionic approach led to pure biomimikry, and with the lack of adapted materials the simple copying of natural constructions in most cases could not result in improved technology. But perhaps should "learning from nature" be understood as the systematic analysis and understanding of biological principles and its transfer into machines by technical means? To test this approach the transfer of a functions tested by evolution for several 100 My promises best results. Legged locomotion in this context is of highest interest for engineers constructing non- wheel-driven vehicles as well as for biologists.

Biological Inspiration of the building of a walking machine may choose its paragons from the whole variety of species described by zoology. Terrestrial legged animal locomotion is a principle which seems to be under high evolutionary pressure what concerns the mechanical needs and solutions, since the overall motion of cockroaches [cf. Garcia et al., this issue] and cursorial mammals like horses may be explained by the same simple equations describing spring-mass systems [1], even if the neural control structures of these only far-related animals are quite different. But on the other hand, the morphological differences between species, base of classical taxonomy, indicate that these functional solutions may be realised by several mechanisms.

Historically the ideas for realising animates mainly aimed at humanoids for service purposes, or at man's pets, if higher loads were planned to be carried. "The Mechanical Horse" [2] (fig. 1) nicely illustrates this anthropocentric approach by simply making copies of pets, which from a biological perspective is a very inefficient way to provide

engineers the informations they need for the construction of a technical walking machine.

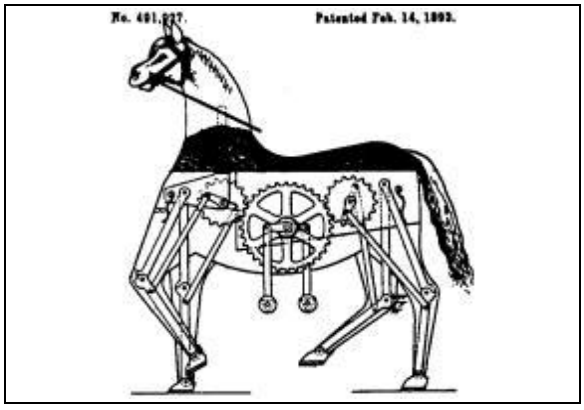

Figure 1: "The Mechanical Horse", patented for L. A. Rygg 1893. [2]

From an evolutionary point of view, man and his pets are cursorial specialists each, showing morphological adaptations to the mechanical needs of species-specific locomotion. This specialisation is derived from a complete chain of heritage without any gap, with only slight modifications from generation to generation. Thus today's structural, mechanical, neural needs in each animal have to interact with evolutionary "decisions" millions of years of age old. Once a switch was turned, and it directed development and the range of possible adaptations in an irreversible manner. All recent animals have to deal with the material properties of musculature, all are controlled by a central nervous system which with the same main locomotory control functions was available already 200 My ago. In reptiles, which seperated from mammals at least at that time, the motoneuron pools for the extremities have the same locations as in mammals [3]. A morphological and functional convergence to the current situation from different starting points has only a low probability.
Biomometic copying of the specialist "horse" into a walking machine without knowing about the functional and evolutionary background which led to this biological solution thus is programmed to fail. But how to uncover the share of evolutionary heritage in relation to that of adaptations to current needs? Surprisingly, most of the living mammals and the ancient representants of the mamalian "stem line" own a common property: they are and were small and light-weighted, with body masses less than 1 kg (fig. 2).

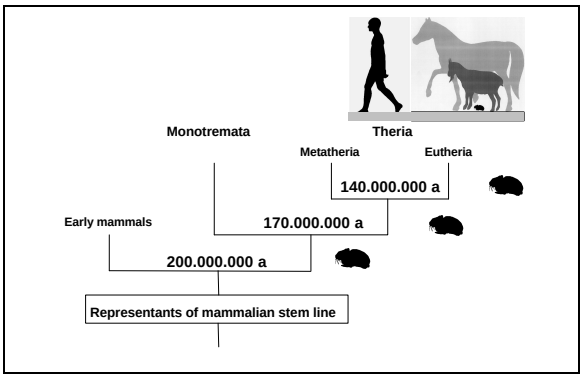

Figure 2: Most of the living mammalian species and the ancestors of modern mammals are and were small. [4]

They all look more or less alike (here demonstrated by the potograph of a pika *Ochotona rufescens*, fig. 3) – some species owning a tail, some not – and, what have shown our own studies of the recent years, move in quite comparable manner, as well as what concerns kinematics as dynamics [5-10]. This is the reason why we suppose that small mammals may teach us the basic principles of mamalian locomotion. On this basis we may derive the special adaptations of large mammals like horses, which are the traditional load carrying "walking machines" of man, to special environmental needs.

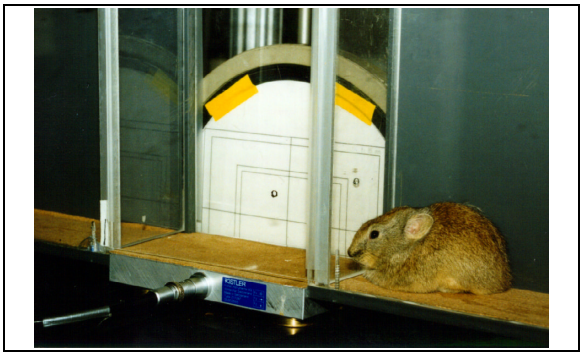

Figure 3: Pika (*Ochotona rufescens*) sitting near the amplifier of a cineradiographic apparatus (Philips®, 150 frames /sec).
In front of the device a Kistler® force plate (200 mm x 120 mm). [4]

To transfer these principles into a machine by technical means, thus extending the catalogue of possible technical solutions, not to substitute techniques by biology is the bionic strategy realised by the programm "Autonomous Walking", granted by the German Research Council DFG.

2. Small mammalian quadrupeds

Cineradiographies taken with the apparatus shown in fig. 3 show that 30 % or more of spatial gain during cyclic locomotion of small mammals is produced by sagittal bending of the trunk for more than 40° (fig. 4). The vertebral column and its driving musculature (paravetrebral and in the thoracic/abdominal wall) are the "main engines" of the animals.

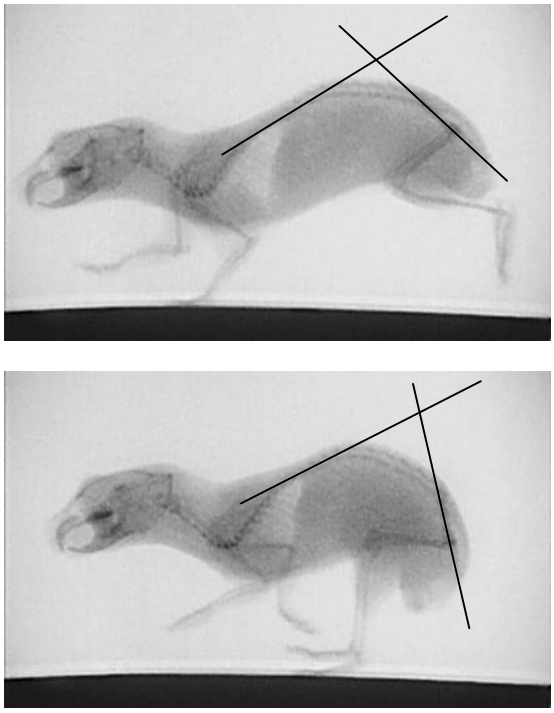

Figure 4: Crouching of the trunk and bending of the vertebral column of a pika (*Ochotona rufescens*) during cyclic locomotion (half-bound). The pelvis is coupled fix to the vertebral column and thus indicates its orientation.

Even between not nearly related species the configurations of the extremities during the locomotion cycle are quite comparable, rather independantly of the gait pattern chosen. This observation allows us to abstract leg movement into the stick figures of an idealized mammal (fig. 5).
A pantograph, which is more or less rectangular, during about 90° of rotation around the legs' bearings at the trunk in the stance phase is crouched to guide the animal's center of mass in a spring-mass system. The springs are muscles, the stiffer and faster ones mainly serving as bi-articular, tunable coupling elements, the compliant slower mono-articular ones mainly offering the possibility to elastically store energy (fig. 6).

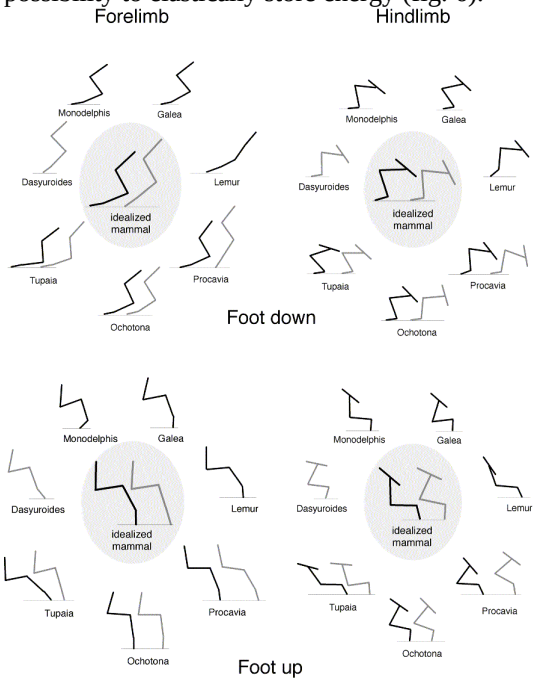

Figure 5: Stick figures of the legs of a variety of small mammals at the reversal points of a motion cycle (foot down, foot up).
The grey shaded ellipses contain the stick figures of an "idealized mammal". [11]

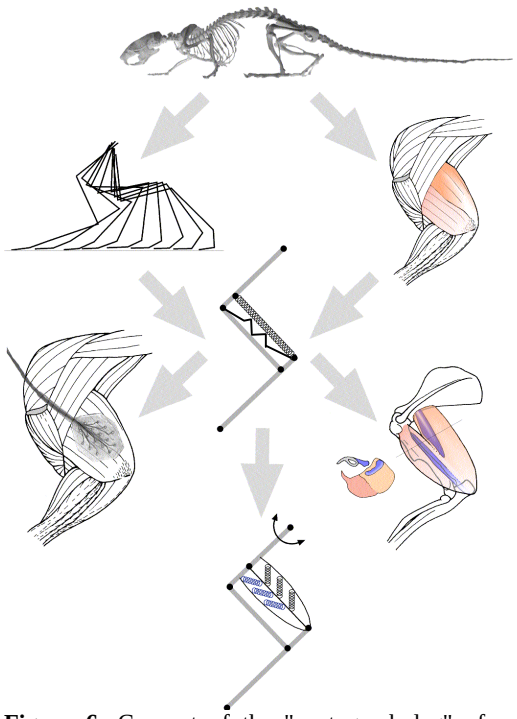

Figure 6: Concept of the "pantograph leg" of small mammals. This model is derived from cineradiography,

topographic typing of muscle fibres and electromyography, in a study on twelve species. [4]
Main elements of the springs are the muscle bellies, containing elastic proteins like titin and nebulin [12, 13]. Combining cineradiographic data with force data yields the results that joint torques in the extremities are rather uniform, independent of the species under study (fig. 7).

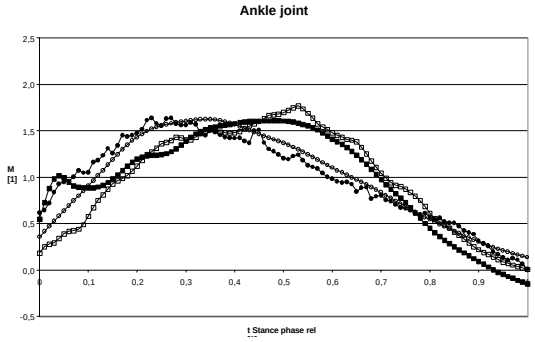

Figure 7: Comparison of the joint torques of four species of small mammals (two species owning a tail and two without a tail).

Interlimb coordination shows no distinct phase shift patterns allowing to identify "gaits", synchronous and symmetrical patterns are chosen in high variability and may be combined with one each other from one step to the next. Speed gain mainly is achieved by an increase of step frequency (decrease of step duration, fig. 8), in extreme keeping half-bound coordination schemes over a tenfold range of velocity.

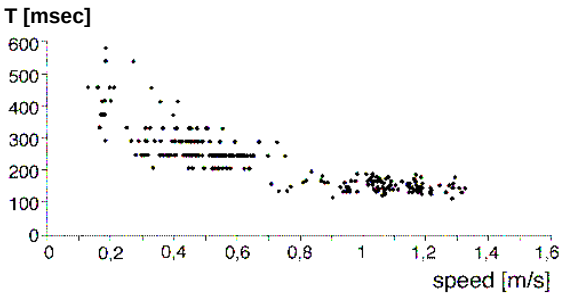

Figure 8: Cycle duration of the half-bound of a pika (*Ochotona rufescens*) as a function of speed. [11]

3. Large mammalian quadrupeds

On the basis of the above described principles of the functional morphology of small versatile mammals we are able to point onto the special adaptations of the evolutionary younger, large mammals, used by man as load-carrying pets.
Large cursorial mammals like horses use motions of their vertebral columns in notable, but much lower extents than small mammals do (fig. 9).

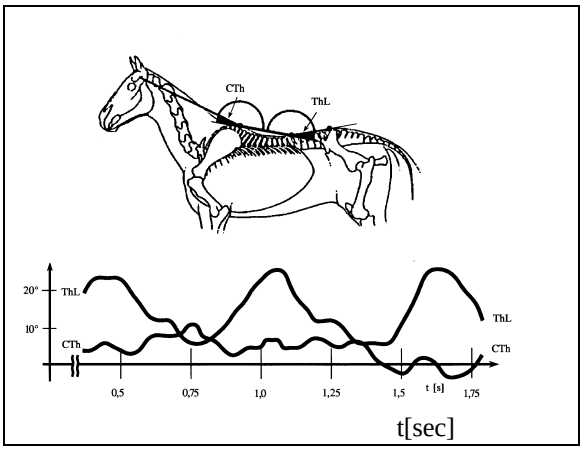

Figure 9: Bending excursion of the vertebral column of a horse during gallop. Data taken from high-speed films (200 frames/sec).

Due to the decreasing muscular capabilities with growing body mass (load is increasing by the third power of length, muscle forces are proportional to the cross sectional areas of muscles, which only increase by the square of length) the leg construction is extended, the long elements are of uneven length, the long tendons of the muscles serve as springs (fig. 10).

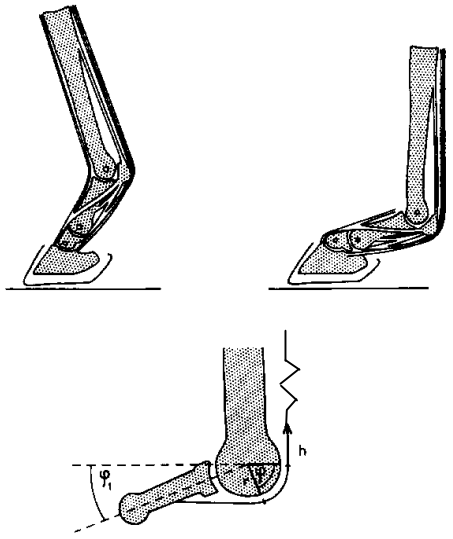

Figure 10: The spring construction formed by the tendon of the long finger flexor of a horse, acting around the fetlock joint. [14]

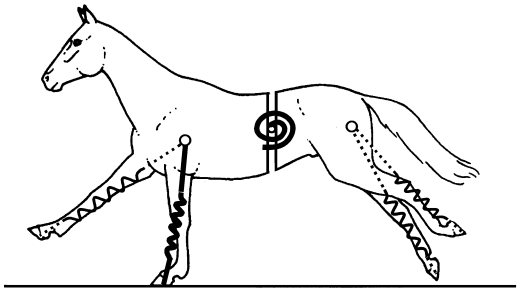

Figure 11: Simple model of a horse in gallop.

These springy legs interact with a bending beam in the trunk [15] (fig. 11). Collagenous tendons own fixed elastic properties, the spring-mass systems have rather fixed resonance frequencies. The consequence is that horses show the well-known phenomenon we call "gaits" (fig. 12).

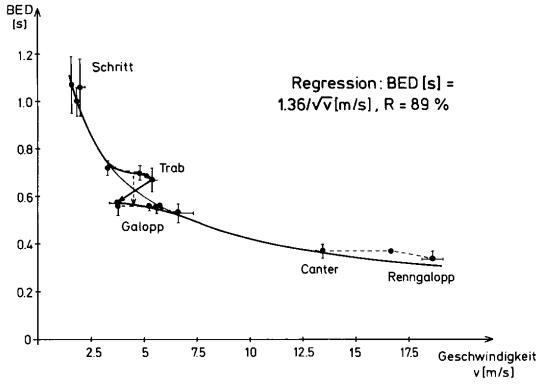

Fig 12: Cycle duration of a horse as a function of speed. Within one gait the frequency is kept rather constant. [16]

4. Principles to be transferred into a machine

The main influence factor on the extension of the legs and the reduction of sagittal spine bending in large mammals seems to be the limited range of adaptibility of structural properties of the materials of the locomotor apparatus (producable tension in muscles, sustainable tension in support tissues, Young's modulus). In our first "naive" approach of transferring principles of natural locomotion into a four-legged technical walking machine ["BISAM II", cf. Ilg et al., this issue] we assume that these limitations may be overcome by technical materials. Thus we construct the machine as an enlarged small mammal, hoping on small mammals' versatility in combination with large mammals' load carrying capacities. If our simulations and results of experiments identify limitations of currently available technical materials for these purposes, we shall follow the adaptive principles shown by large mammals. In detail this leads to the following rules for our basic construction:

1. Use rectangular pantograph legs with minimally three segments (what concerns proportions cf. Blickhan et al. this issue).
2. Guidance of parallized segment in the pantograph should be realized as a stiff coupling, the coupling of neighboured levers should be more compliant.
3. The leg drive should be located near to or on the trunk (proximal).
4. Tuning of the height guidance of the CoM should be realised by distal elements (near to the ground).
5. Fore- and hindlimbs may have the same construction.
6. Legs should use standard dynamics. Reactive control for needs of propulsion should mainly act on the hindlimbs.
7. In a first step, optimise the leg construction in interaction with a stiff trunk.
8. In the next step, allow sagittal bending of the trunk preferably to lateral bending or torsion.
9. The pivots of the legs may be shifted longitudinally (like in the scapula of a horse).
10. Follow Raibert's and Buehler's principles and do use resonance processes for quadrupedal walking machines!

5. Outlook

Biomechanics is not only humano-mechanics. Extension of our field of view to what is outside of our anthropocentric perspective yields high potential to derive principles from nature, which may enlarge and enrich the engineer's toolbox.

Acknowledgements
The studies were granted by the German Research Council DFG (INK-24 A1/B1 and Fi 410-4). Prof. Dr. Dr. H.-R. Duncker, University of Gießen, and Dr. Alain Puget, University of Toulouse made living animals for functional analyses accessible to us. Dr. L. Peichel, Max-Planck-Institut für Hirnforschung, Frankfurt/Main provided a dead animal for morphometrics. Dr. Haarhaus from IWF Göttingen sustained the realisation

of cineradiographies. Prof. Dr. W. Thonfeld and Dipl.-Ing. K. Urban (Fachhochschule Jena) realised the laser-scanning volumetry of animals.

References

[1] TA McMahon & GC Cheng (1990): The mechanics of running: how does stiffness couple with speed? – J Biomech 23 (Suppl. 1): 65 - 78.

[2] SM Song & KJ Waldron (1989): Machines that walk: the adaptive suspension vehicle. The MIT Press, Cambridge (Mass.).

[3] JM Ryan, J Cushman, B Jordan, A Samules, H Frazer & C Baier (1998): Topographic position of forelimb motoneuron pools is conserved in vertebrate evolution. – Brain Behav Evol 51: 90 – 99.

[4] H Witte, J Biltzinger, N Schilling, H Preuschoft & MS Fischer (1999): Was hat der Sportbiomechaniker von den Ergebnissen biomechanischer Analysen an Tieren? Edition Czwalina, Feldhaus Verlag, Hamburg.

[5] MS Fischer (1994): Crouched posture and high fulcrum. A principle in the locomotion of small mammals: the example of the rock hyrax (*Procavia capensis*) (Mammalia: Hyracoidea). – J Human Evol 26: 501 – 524.

[6] MS Fischer (1998): Die Lokomotion von *Procavia capensis* (Mammalia: Hyracoidea). Ein Beitrag zur Evolution des Bewegungssystems der Säugetiere. - Abh. Naturwiss. Verh. naturwiss. Vereins Hamburg (NF): 33: 1-188

[7] MS Fischer (1999): Kinematics, EMG, and inverse dynamics of the Therian forelimb – a synthetic approach. – Zool Anz 238: 41 – 54.

[8] MS Fischer & R Lehmann (1998): Application of cineradiography for the metric and kinematic study of in-phase gaits during locomotion of the pika (*Ochotona rufescens*, Mammalia: Lagomorpha). - Zoology 101: 12 - 37.

[9] N Schilling & MS Fischer (1999): Kinematic analysis of treadmill locomotion of tree shrews, *Tupaia glis* (Scandentia: Tupaiidae). – Z Saeugetierk 64: 129 – 153.

[10] M Schmidt & MS Fischer (2000): Cineradiographic study of forelimb movements during quadrupedal walking in the Brown Lemur (*Euleumur fulvus*, Primates: Lemuridae). – Amer. J. Phys. Anthropol. 111: 245 - 262.

[11] MS Fischer & H Witte (1998): The functional morphology of the three-segmented limb of mammals and its specialities in small and medium-sized mammals. – Proc Europ Mechanics Coll Euromech 375 Biology and Technology of Walking: 10 – 17.

[12] K Wang, R McCarter, J Wright, J Beverly & R Ramirez-Mitchell (1991): Regulation of skeletal muscle stiffness and elasticity by titin isoforms. – Proc Natl Acad Sci USA 88: 7101 – 7109.

[13] S Labeit & B Kolmerer (1995): Titins: giant proteins in charge of muscle ultrastructure and elasticity. – Science 270: 293 – 296.

[14] H Preuschoft, C Lesch, H Witte & C Loitsch (1995): Die biomechanischen Grundprinzipien der Gangarten, Insbesondere des Galopps. – In: PF Knesevic, Orthopädie bei Huf- und Klauentieren. Schattauer, Stuttgart: 355 – 370.

[15] RM Alexander, NJ Dimery & RF Ker (1985): Elastic structures in the back and their role in galloping in some mammals. – J Zool (Lond) A207: 467 – 482.

[16] H Witte, C Lesch, H Preuschoft & C Loitsch (1995): Die Gangarten der Pferde: sind Schwingungsmecha-nismen entscheidend? Federschwingungen bestimmen den Trab und den Galopp.– Pferdeheilkunde 11(4): 265 – 272.

Proceedings of the International Symposium on
Adaptive Motion of Animals and Machines,
Montreal, Aug.8-12, 2000

Some Issues in Creating 'Invertebrate' Robots

I.D. Walker

Clemson University, Dept. Electrical/Computer Engineering, Clemson SC 29634 USA, ianw@ces.clemson.edu

Abstract

In this paper, we discuss some of the key issues involved in the design, analysis, and implementation of 'invertebrate-like' robots. Using as case examples several novel 'trunk and tentacle' robot arms recently constructed at Clemson University, we discuss the design of 'continuous backbone' and 'snakelike' robots, and their motion planning. The potential of these types of robots for enhanced manipulation and locomotion is discussed.

1. Introduction

Traditional robot manipulators are based strongly on the human (vertebrate) model, with a (relatively small number of) rigid links connected by joints. Thus, like the human model, bending down the length of the structure is restricted to a small number of (fixed) points. While this works well in numerous cases, there are many examples in nature where a different design philosophy proves to be more advantageous.

For example, in invertebrate structures such as those in 'tongues, trunks, and tentacles', highly dextrous manipulation can be produced via compact structures in which bending can occur down along the length of the structure [14, 24]. Consider the examples of octopus tentacles or elephant's trunks, which can perform 'whole arm' manipulations in cluttered environments beyond the capability of conventional robots.

Snakes are vertebrates, but their ability to bend at essentially arbitrary points along their body allows them to maneuver effectively in terrain that is inaccessible to wheeled, tracked, or even legged machines [7].

The above types of examples provide inspiration to engineers seeking to recreate the abilities of creatures in the biological world [6]. However, engineers do not have analogs of many of the amazing actuation and sensory systems present in the animals.

At Clemson University, we are conducting extensive research in the area of biologically inspired robotics, concentrating on the development of robot 'tongues, trunks, and tentacles'. We are working with both discrete (figure 1) and continuous (figure 2) backboned devices, each type of which presents interesting and unique challenges. In this paper, we summarize the results of our efforts so far, concentrating on design and motion planning issues.

Figure 1: Discrete backboned elephant's trunk robot.

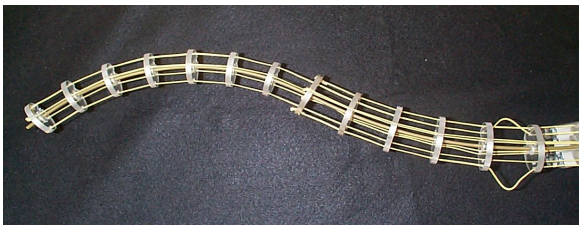

Figure 2: Continuous backbone tentacle robot.

2. Design Issues

Nature suggests two different strategies for constructing 'invertebrate' robot limbs; (1) an 'essentially invertebrate' (snake-like) approach, using a 'discrete backbone' comprised of (a large number of) small links; and (2) a 'fully invertebrate' continuous backbone. Each of these case presents unique issues.

In case (1) above, bending occurs at distinct and well-defined points of the mechanism, with the 'invertebrate' effect coming from the large number of joints and small intervening links. This can be considered a particular class of hyperredundant robot [2], or a nat-

ural extension of the traditional robot with the number of joints tending towards infinity and the link lengths towards zero. Physical examples of this type of robot include serpentine robots at NASA Jet Propulsion Laboratory [20], the EMMA manipulator [10] by GreyPilgrim, Inc., and the 'Elephant's Trunk' robot at Clemson [1, 26] (figure 1). Backboned robot 'snakes' are described in [4, 16, 19]. A series of novel 'snake' robots, which have inspired our own efforts, and indeed much of this field of research, are summarized in [12].

The 'discrete backbone' approach has the advantage of being (conceptually) a simple extension of traditional designs, and thus amenable to traditional kinematic analysis. However, as discussed in the following, the large number of joints and small links lead to difficulties in weight, actuation and complexity of analysis.

In case (2) (continuous backbone) above, bending can occur at any point along the structure (this is of course appealing from the perspective of 'whole arm manipulation). This type of robot is termed 'continuum' in [22]. Examples of manipulators of this general type are given in [5, 27]. The 'joint space' in thus infinite-dimensional. Practical considerations dictate that these devices must be actuated by a finite set of inputs. A key question therefore is how to constrain the backbone so that it can be effectively moved by a finite set of actuators.

The trunk robot in figure 1 has a 32 degree of freedom backbone, consisting of 16 two degree of freedom joints connected in series. The motion capabilities of the robot closely resemble that of a real elephant. For more details, see [26]. The tentacle robot in figure 2 features a continuous backbone, and bends in three dimensions. Both robots, along with similar variants, are under investigation in the robotics laboratories at Clemson University.

A key question is how best to actuate these types of devices. Two strategies present themselves: local and remote actuation. Local actuation, as featured in [4, 16, 19, 20], while conceptually simple, has several major disadvantages. Traditional electric motors are relatively bulky and heavy, and the prospect of having to package and move a large number of such actuators distributed through the robot is unattractive. The use of alternative types of actuators, such as new classes of artificial muscles [23] for local actuation (as is found in the biological equivalents) is an interesting possibility. However, at the present time, it seems, at least for macroscopic devices, that the strength of current artificial muscles is insufficient.

For the above reasons, in our robots we have chosen to follow the strategy of remote actuation for our devices. Tendons provide a simple way of transmitting power through the structure, and allow the devices to be fairly light, as the actuators themselves are remote. The trunk in figure 1 is actuated by 8 pairs of tendons, and the tentacle in figure 2 by 4 tendon pairs. Similar remote tendon drive approaches are used to actuate the EMMA robot [10] and the KSI tentacle robot [13].

An important factor in determining the capabilities of such remotely actuated devices is the physical routing of the tendons. Our group is conducting extensive analyses of the effects of tendon displacement (from the backbone), conduit selection, and termination points on robot workspace and strength. Initial results are reported in [15].

The key remaining design issue is how to endow the devices with structural stiffness. In the case of the tentacle robot in figure 2, the backbone itself (a rod of circular cross-section) provides the basic stiffness properties. Notice that robots of quite different characteristics can be obtained by changing backbone rods. The trunk robot in figure 1 is constrained by a series of springs running (segment to segment) down the exterior of the device. This provides the passive constraints that transform the actuation values (4 for the tentacle, 8 for the trunk) to the degrees of freedom (theoretically infinite for the tentacle, 32 for the trunk) of the device.

In each type of device, the resulting robot is relatively light, highly maneuverable, and very compliant, which together provide ideal testbeds for research in biologically inspired robot manipulation. However, in order to make use of the devices, the motions must be effectively planned and coordinated.

3. Motion Planning

In addition to the issues inherent in designing and constructing effective continuum robots, the issue of motion planning is a significant challenge. One immediate difficulty is the sheer complexity of the kinematics. Even for the 'discrete backbone' types of robots, where conventional kinematics can still sometimes be valid, the number and complexity of terms involved can be formidable.

The most commonly followed approach in the literature in this case has been to use concepts from differential geometry to analyze the kinematics of a continuous 'backbone curve', and then 'fit' the discrete robot backbone to that curve in some appropriate manner [2, 3, 17, 18]. However, a practical problem with this approach is that real robots have constraints that are not taken into account by traditional differential geometric methods [8]. Thus the real robots bend in

ways not possible for the theoretical curves, and vice versa! In addition, the existing methods provide little intuition.

However, significant progress can be made by observing common features that are inherent in these types of robots, such as locally constant curvature. This feature, common to all the robots described in this paper, is a natural result of actuating a stiff backbone (with stiffness provided by springs in the trunk robot example, and by the inherent stiffness of the backbone rod for the tentacle) with finite pairs of tendons terminated at discrete points along the structure. Between the tendon termination points, the natural behavior of the device is to assume a configuration of constant curvature.

For an example with a planar continuous backbone robot, see figure 3. (Here the 'backbone' is a spring steel bar, and the actuation is by a single pair of tendons routed through discrete discs, and terminated at the 'end effector'). A curve of constant curvature is overlaid on the figure, and it can be seen that the device assumes an almost constant curvature configuration. Similar behavior can be seen in the figures of the trunk manipulator (note: 4 constant curvature sections in the plane in this case) in figures 1, 4, and 5.

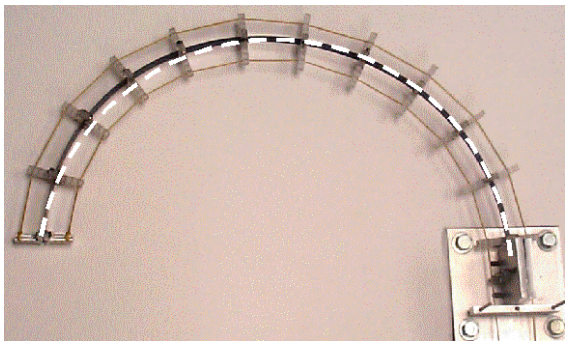

Figure 3: Continuous backbone planar robot.

In recent works, we have proposed several alternative methods for trunk and tentacle kinematics which exploit the constant curvature feature [8, 9, 11]. In [11], it is observed that a robot made up of constant curvature sections can be modeled as a series of prismatic/revolute joints (one pair per section) where the translation and rotation variables of each joint pair are coupled and determined by the curvature of the section. This fact is used to define the forward kinematics of the robot using the conventional Denavit-Hartenberg technique. This in turn yields a manipulator Jacobian (relating changes in *curvature* to task space velocities), the pseudoinverse of which can be used to plan *cur-*

Figure 4: Elephant's trunk robot - curved.

Figure 5: Elephant's trunk robot -outstretched.

vature space velocities using conventional redundancy resolution techniques. Details and examples are give in [11].

A key feature of the work in [11] is the replacement of the traditional joint angles in the kinematics by local curvatures. This allows us to reduce the problem of determining the shape of the robot (given task space requirements) from a large dimensional problem (32 axes for the trunk robot, and theoretically infinite for the tentacle) to a space of the dimension of the number of actuators (8 for the trunk, 4 for the tentacle). This is both computationally more tractable and significantly more intuitive.

A similar 'modal decomposition' approach has been proposed for abstract spatial 'fitting' curves in [3]. However, in [3] the modal functions were chosen to be the Fourier basis functions. In [8], we argue that other basis functions (such as the set of curvatures described above and in [11]) are more 'natural' and easy to use than the Fourier basis set (for example, a finite set always describes the robot configuration). In [9], an alternative basis set based on Wavelet decomposition is used to describe these continuum robots. In this case the 'joint angles' become a Wavelet basis set, the shape of which can intuitively be seen to define the shape of the overall robot. This approach is proving to be highly useful for motion planning for the devices.

However, effective performance of the devices is also dependent on the solution of other, lower level, problems. The overall kinematics for these types of robots involve issues not found in traditional robots. The kinematics must take into account the backbone stiffness profile, and external forces due to gravity or contact (note that a unique actuator position does not translate into a unique pose for the robot). In [8], a kinematic model taking into account the above issue is proposed. The model reveals some useful structure (including an appropriate mapping from changes in local curvatures to cable length changes, required for control). However, the resulting system of differential equations can be hard to solve. We are currently conducting active research in this area.

4. Discussion and Conclusions

The potential for the types of 'invertebrate' robots described in this paper is huge. The inherent maneuverability and compliance of the devices lend themselves to a number of arenas. For example, the ability of the structures to bend at essentially arbitrary points offers the opportunity for operation in cluttered and obstacle-filled environments, if sufficient actuation can be provided. Notice that a (biological) elephant's trunk can manuever very effectively in crowded spaces. This is also true for the class of robots described here.

The lack of rigid links, or 'bones' (at least of any significant size) is the key to the above maneuverability. It it also the key to the inherent compliance in the structures, which can bend around even quite complex shaped objects. This has obvious benefits for making 'soft' robots for hazardous environments or for interaction with humans, and also suggests strong potential for 'whole arm manipulation' (interaction with the world along a length of the structure, as opposed to simply the end effector), which is a key feature of the biological equivalents.

Motivated by our previous work in robot manipulation inspired by biology (specifically involving raccoons [25] and raptors [21]) we plan to investigate the potential of the trunk and tentacle manipulators for impulsive manipulation, where the dynamics of the interaction between the robot and the environment are actively exploited to achieve tasks. We believe that these 'trunk and tentacle' robots offer a novel and interesting vehicle with which to test new manipulation strategies. We are currently conducting whole arm manipulation experiments with the trunk manipulator, and in 2000 we plan to mount a tentacle arm (figure 6) to a mobile platform to conduct experiments in biologically inspired impulsive manipulation research. Results in this direction will be reported in future papers.

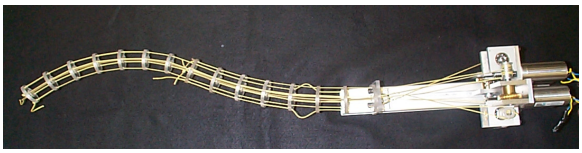

Figure 6: Continuous backbone spatial robot.

Longer term applications for the robot structures described in this paper include inspection and payload transport in complex environments, remote teleopera-

tion, medical applications, and locomotion. The latter case seems particularly interesting in the longer term, if current constraints on weight, power, and sensing can be resolved.

Acknowledgments

This work has been supported in part by NSF/EPSCoR grant EPS-9630167, NASA grant 98-HEDS-04-054, NSF grant CMS-9796328, and DOE contract DE-FG07-97ER14830.

References

[1] S. Braunhardt, T. League, T. McDowell, and G. Sohl. *Robotic Arm*. Rice University, Department of Mechanical Engineering, 1992.

[2] G.S. Chirikjian. *Theory and Applications of Hyperredundant Robotic Mechanisms*. Ph.D. thesis, Department of Applied Mechanics California Institute of Technology, 1992.

[3] G.S. Chirikjian and J.W. Burdick. Selected Applications and Intrinsic Kinematics of Hyper-Redundant Robots. In *Proceedings 4th American Nuclear Society Topical Meeting on Robotics and Remote Systems*, pages 61–70, 1991.

[4] G.S. Chirikjian and J.W. Burdick. Design and Experiments with a 30 DOF Robot. In *Proceedings 1993 IEEE Conference on Robotics and Automation*, pages 113–119, 1993.

[5] R. Cieslak and A. Morecki. Elephant Trunk Type Elastic Manipulator - A Tool for Bulk and Liquid Type Materials Transportation *Robotica*, Vol. 17, pp. 11-16, 1999.

[6] P. Dario, *Robots and Biological Systems: Towards a New Bionics?*, Springer-Verlag, 1986.

[7] C.H. Ernst and G.R. Zug, *Snakes in Question*, Smithsonian Institution Press, 1996.

[8] I.A. Gravagne and I.D. Walker. *On the Kinematics of Remotely-Actuated Continuum Robots*, to appear, IEEE International Conference on Robotics and Automation, San Francisco, April 2000.

[9] I.A. Gravagne and I.D. Walker. *Kinematic Transformations for Remotely-Actuated Planar Continuum Robots*, to appear, IEEE International Conference on Robotics and Automation, San Francisco, April 2000.

[10] GreyPilgrim Company, http:/www.greypilgrim.com

[11] M.A. Hannan and I.D. Walker, *Novel Kinematics for Continuum Robots*, to appear, 2000 Conference on Advances in Robot Kinematics (ARK2000), Piran, Slovenia, June 2000.

[12] S. Hirose, *Biologically Inspired Robots*, Oxford University Press, 1993.

[13] G. Immega and K. Antonelli. The KSI Tentacle Manipulator. In *Proceedings 1995 IEEE Conference on Robotics and Automation*, pages 3149–3154, 1995.

[14] W.M. Kier and K.K. Smith, "Tongues, tentacles and trunks: The biomechanics of movement in muscular-hydrostats", *Zoological Journal of the Linnean Society*, 83: 307-324, 1985.

[15] C. Li and C.D. Rahn. Nonlinear Kinematics for a Continuous Backbone, Cable-Driven Robot To appear, 20th Southeastern Conference on Theoretical and Applied Mechanics, 2000.

[16] G. Migadis and K.J. Kyriakopoulos, "Design and Forward Kinematic Analysis of A Robotic Snake", *IEEE International Conference on Robotics and Automation*, 3493-3498, 1997.

[17] H. Mochiyama, E. Shimemura, and H. Kobayashi. Direct Kinematics of Manipulators with Hyper Degrees of Freedom and Frenet-Serret Formula. In *Proceedings 1998 IEEE Conference on Robotics and Automation*, pages 1653–1658, 1998.

[18] H. Mochiyama, E. Shimemura, and H. Kobayashi. Shape Correspondence between a Spatial Curve and a Manipulator with Hyper Degrees of Freedom. In *Proceedings 1998 IEEE/RSJ Int. Conf. on Int. Robotics and Systems (IROS)*, pages 161-166, 1998.

[19] M. Nilsson, "Why Snake Robots Need Torsion-Free Joints and How to Design them", *IEEE International Conference on Robotics and Automation*, 412-417, 1998.

[20] E. Paljug, T. Ohm, and S. Hayati. The JPL Serpentine Robot: a 12 DOF System for Inspection. In *Proceedings 1995 IEEE Conference on Robotics and Automation*, 3143–3148, 1995.

[21] A.M. Ramos and I.D. Walker. Raptors: Inroads to Multifingered Grasping In *Proceedings of the IEEE/RSJ International Conference on Intelligent Robots and Systems*, pages 467–475, 1998.

[22] G. Robinson and J.B.C. Davies. Continuum Robots - A State of the Art In *Proceedings 1999 IEEE Conference on Robotics and Automation*, pages 2849–2854, 1998.

[23] M. Shahinpoor. Continuum Electromechanics of Ionic Polymeric Gels as Artificial Muscles for Robotic Applications, *Smart Materials and Structures*, Volume 3, pages 367-372, 1994.

[24] K.K. Smith and W.M. Kier, "Trunks, tongues, and tentacles: Moving with skeletons of muscle", *American Scientist*, 77: 28-35 1989.

[25] I.D. Walker. A Successful Multifingered Hand Design: The Case of the Raccoon. In *Proceedings of the IEEE/RSJ International Conference on Intelligent Robots and Systems*, pages 186–193, 1995.

[26] I.D. Walker and M.A. Hannan, "A Novel 'Elephant's Trunk' Robot," *Proceedings IEEE/ASME International Conference on Advanced Intelligent Mechatronics*, Atlanta, GA, 1999, pp. 410-415.

[27] J.F. Wilson and D. Li and Z. Chen and R.T. George. Flexible Robot Manipulators and Grippers: Relatives of Elephant Trunks and Squid Tentacles, In *Robots and Biological Systems: Towards a New Bionics?*, pages 474-494, 1993.

Proceedings of the International Symposium on
Adaptive Motion of Animals and Machines,
Montreal, Aug.8-12, 2000

An Adaptive Controller for Two Cooperating Flexible Manipulators

C. J. Damaren[1]

[1]University of Toronto, Institute for Aerospace Studies, 4925 Dufferin Street, Toronto, Ontario, M3H 5T6, CANADA
cjd@sdr.utias.utoronto.ca

Abstract

The control problem for two serial flexible multilink robots which carry a common rigid payload is considered. An adaptive controller with feedback and feedforward elements is presented which can track a prescribed trajectory for the payload with simultaneous vibration suppression when the manipulated payload is sufficiently large.

1. Introduction

The adaptive control of robot manipulators has been presented as a solution for dealing with uncertainty and variation of the mass properties. Although these systems are nonlinear, globally stable tracking has been demonstrated both analytically and supported through experiments [1]. The key to these results has been the linear dependence of the model on the unknown parameters and, in many cases, the passivity of an appropriate input-output mapping [2]. For instance, with rigid robots it is well known that the map from joint torques to joint rates is passive and this property can be used to explain the stabilization properties of many motion control strategies including the ubiquitous proportional-derivative position feedback.

Motivated by the utility of the passivity concept in rigid robot control and its occurrence in a single flexible link when the reflected tip rate is taken as the output [3], the present author introduced the μ-tip rate in [4] which generalized this output to open-chain flexible manipulators. Passivity using this output was demonstrated for $\mu < 1$ when the manipulated payload was much more massive than the manipulator and a feedforward which permitted its use in tracking problems was constructed in [5]. The adaptive counterpart of that controller was detailed in [6] and variations of both controllers were implemented experimentally with great success in [7].

The extension of the μ-tip rate idea to cooperating robot arms forming a closed chain was treated in [8] where detailed stability proofs and experimental results were presented. An interesting feature of this development was the occurrence of a free-loading sharing parameter which was used to distribute the control torques between the two arms and form the generalization of the μ-tip rate. Beyond this, the dynamics and control of cooperating flexible arms has received little attention but there has been some [9,10]. This paper represents the dénouement for the line of research pursued in [4-8]. A fusion of the previous techniques is brought to bear on the problem of adaptive control for cooperating flexible robot arms in the case where the payload is significantly larger than the manipulators but otherwise unknown.

Simulation results will be presented for a system of two planar arms each with three joints that manipulate a shared rigid payload. Each arm has two flexible links and a third rigid link which is cantilevered to the large rigid payload. Excellent tracking is demonstrated with simultaneous vibration suppression for the adaptive controller when the payload is sufficiently large for a variety of load-sharing parameters.

2. Cooperating Flexible Robots

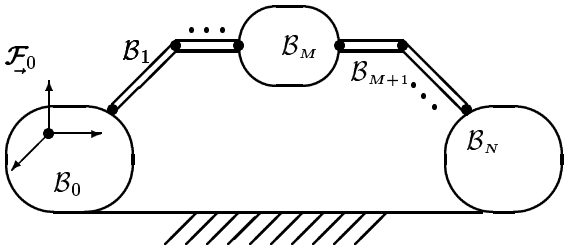

Figure 1: Closed-Loop Multibody System

This work deals with a chain of flexible and/or rigid bodies as shown in Figure 1. Bodies $\mathcal{B}_0$ and $\mathcal{B}_N$ are cantilevered in an inertial reference frame $\mathcal{F}_0$ so as to form a closed loop. The bodies are connected by revolute joints and $\boldsymbol{\theta} = \text{col}\{\theta_n\}$, $n = 1 \cdots N$, denotes the collection of joint angles and $\mathbf{q}_e = \text{col}\{\mathbf{q}_{en}\}$ is the collection of N_e elastic degrees of freedom.

The body $\mathcal{B}_M$, $1 \leq M \leq N$, is taken to be a rigid payload under manipulation and it is assumed that M

is equal to the number of rigid degrees of freedom after loop closure. The joint angles and elastic coordinates are further partitioned as

$$\begin{aligned}\boldsymbol{\theta}_1 &= \text{col}\{\theta_n\}, n = 1, \cdots, M, &(1)\\ \boldsymbol{\theta}_2 &= \text{col}\{\theta_n\}, n = M+1, \cdots, N, &(2)\\ \mathbf{q}_{1e} &= \text{col}\{\mathbf{q}_{en}\}, n = 1, \cdots, M, &(3)\\ \mathbf{q}_{2e} &= \text{col}\{\mathbf{q}_{en}\}, n = M+1, \cdots N. &(4)\end{aligned}$$

The payload position $\boldsymbol{\rho}$ is interpreted as a six-tuple whose top half contains the position of $\mathcal{B}_M$ with respect to $\boldsymbol{\mathcal{F}}_0$ and whose bottom half is an attitude parametrization such as Euler angles.

The payload position can be written as $\boldsymbol{\rho} = \boldsymbol{\mathcal{F}}_1(\boldsymbol{\theta}_1, \mathbf{q}_{e1}) = \boldsymbol{\mathcal{F}}_2(\boldsymbol{\theta}_2, \mathbf{q}_{e2})$ where $\boldsymbol{\mathcal{F}}_i$, $i = 1, 2$, are the forward kinematics maps. Its velocity is given by

$$\dot{\boldsymbol{\rho}} = \boldsymbol{J}_{i\theta}(\boldsymbol{\theta}_i, \mathbf{q}_{ie})\dot{\boldsymbol{\theta}}_i + \boldsymbol{J}_{ie}(\boldsymbol{\theta}_i, \mathbf{q}_{ie})\dot{\mathbf{q}}_{ie},\ i = 1, 2, \quad (5)$$

where $\boldsymbol{J}_{i\theta}$, $\boldsymbol{J}_{ie}$, $i = 1, 2$, are the corresponding Jacobian matrices. The μ-tip rate described in Sec. 1 is defined by

$$\begin{aligned}\dot{\boldsymbol{\rho}}_\mu &= \mu\dot{\boldsymbol{\rho}} + (1-\mu)[C_1\boldsymbol{J}_{1\theta}\dot{\boldsymbol{\theta}}_1 + C_2\boldsymbol{J}_{2\theta}\dot{\boldsymbol{\theta}}_2] &(6)\\ &= \dot{\boldsymbol{\rho}} - (1-\mu)[C_1\boldsymbol{J}_{1e}\dot{\mathbf{q}}_{1e} + C_2\boldsymbol{J}_{2e}\dot{\mathbf{q}}_{2e}] &(7)\end{aligned}$$

where C_1 with $0 < C_1 < 1$ and $C_2 = 1 - C_1$ will be termed *load-sharing parameters*. For $\mu = 1$, $\boldsymbol{\rho}_\mu = \boldsymbol{\rho}$, the true payload position, while for $\mu = 0$, $\boldsymbol{\rho}_\mu$ describes an output based on the joint motion alone. If the approximations $\boldsymbol{J}_{i\theta}(\boldsymbol{\theta}_i, \mathbf{q}_{ie}) \doteq \boldsymbol{J}_{i\theta}(\boldsymbol{\theta}_i, \mathbf{0})$, $i = 1, 2$, are made then the integral of (6) yields $\boldsymbol{\rho}_\mu(t) = \mu\boldsymbol{\rho}(t) + (1-\mu)[C_1\boldsymbol{\mathcal{F}}_1(\boldsymbol{\theta}_1, \mathbf{0}) + C_2\boldsymbol{\mathcal{F}}_2(\boldsymbol{\theta}_2, \mathbf{0})]$ where $\boldsymbol{\mathcal{F}}_i(\boldsymbol{\theta}_i, \mathbf{0})$ are the rigid forward kinematical maps. The control torques are assumed to be determined according to

$$\boldsymbol{\tau} = [\tau_1 \ \cdots \ \tau_N]^T = [C_1\boldsymbol{J}_{1\theta} \quad C_2\boldsymbol{J}_{2\theta}]^T\widehat{\boldsymbol{\tau}} \quad (8)$$

where $\widehat{\boldsymbol{\tau}}$ is a collection of M control inputs; hence the load-sharing description for the C_i. The paper establishes a control scheme for $\boldsymbol{\tau}(t)$ so that $\boldsymbol{\rho}(t)$ tracks a prescribed payload trajectory $\boldsymbol{\rho}_d(t)$.

3. Large Payload Dynamics

In [8], it was established that the dynamics of the closed-loop flexible robot under the assumption that $\mathcal{B}_M$ was large were described by

$$\begin{aligned}\boldsymbol{M}_{\rho\rho}\ddot{\boldsymbol{\rho}} + \boldsymbol{C}_\rho(\boldsymbol{\rho}, \dot{\boldsymbol{\rho}})\dot{\boldsymbol{\rho}} &= \widehat{\boldsymbol{\tau}}, &(9)\\ \boldsymbol{C}_\rho(\boldsymbol{\rho}, \dot{\boldsymbol{\rho}})\dot{\boldsymbol{\rho}} = \dot{\boldsymbol{M}}_{\rho\rho}\dot{\boldsymbol{\rho}} &- \tfrac{1}{2}\partial(\dot{\boldsymbol{\rho}}^T\boldsymbol{M}_{\rho\rho}\dot{\boldsymbol{\rho}})/\partial\boldsymbol{\rho}, &(10)\\ \widehat{\boldsymbol{M}}_{ee}\ddot{\mathbf{q}}_e + \mathbf{D}_{ee}\dot{\mathbf{q}}_e &+ \mathbf{K}_{ee}\mathbf{q}_e = \\ &- [C_1\boldsymbol{J}_{e1}\ C_2\boldsymbol{J}_{e2}]^T\widehat{\boldsymbol{\tau}}. &(11)\end{aligned}$$

In the first of these, $\boldsymbol{M}_{\rho\rho}$ is the task-space mass matrix of the equivalent rigid arm evaluated at $\boldsymbol{\theta}_i = \boldsymbol{\mathcal{F}}_{ri}^{-1}(\boldsymbol{\rho})$ where $\boldsymbol{\mathcal{F}}_{ri}^{-1}(\cdot)$, $i = 1, 2$, are the rigid inverse kinematics maps. Hence, (9) and (10) are equivalent to the rigid-body *task-space* motion equations. In the second equation, $\widehat{\boldsymbol{M}}_{ee} = \widehat{\boldsymbol{M}}_{ee}^T > \mathbf{O}$ is the mass matrix relative to $\mathbf{q}_e$ assuming that the large payload forms a clamping boundary condition ($\boldsymbol{\rho} = \mathbf{0}$) and $\boldsymbol{K}_{ee} = \boldsymbol{K}_{ee}^T > \mathbf{O}$ is the stiffness matrix. We have added a damping term $\boldsymbol{D}_{ee}\dot{\mathbf{q}}_e$ with $\boldsymbol{D}_{ee} = \boldsymbol{D}_{ee}^T > \mathbf{O}$ which is required in the stability proof in the adaptive case.

A further simplification is possible if one includes only the payload contributions to $\boldsymbol{M}_{\rho\rho}$. First, recognize that in this case (9) is equivalent to the motion equation for a single rigid body with kinetic energy $(1/2)\dot{\boldsymbol{\rho}}^T\boldsymbol{M}_{\rho\rho}\dot{\boldsymbol{\rho}} = (1/2)\boldsymbol{\nu}^T\boldsymbol{M}\boldsymbol{\nu}$ where

$$\boldsymbol{M} = \begin{bmatrix} m\mathbf{1} & -\mathbf{c}^\times \\ \mathbf{c}^\times & \mathbf{J} \end{bmatrix}, \ \boldsymbol{\nu} = \begin{bmatrix} \mathbf{v} \\ \boldsymbol{\omega} \end{bmatrix}.$$

Here, $\boldsymbol{\nu}$ is the generalized velocity of the payload body expressed in a body-fixed frame consisting of the translational velocity $\mathbf{v}$ in the top three-tuple and the angular velocity $\boldsymbol{\omega}$ in the bottom. $\boldsymbol{M}$ is the corresponding (constant) mass matrix containing the zeroth (m), first ($\mathbf{c}$), and second ($\mathbf{J}$) moments of mass. Note that $\boldsymbol{\nu} = \boldsymbol{P}(\boldsymbol{\rho})\dot{\boldsymbol{\rho}}$ where $\boldsymbol{P} = \text{diag}\{\mathbf{C}_{M0}(\boldsymbol{\rho}), \mathbf{S}_{M0}(\boldsymbol{\rho})\}$, $\mathbf{C}_{M0}$ is the rotation matrix describing the orientation of $\mathcal{B}_M$ with respect to $\boldsymbol{\mathcal{F}}_0$, and $\mathbf{S}_{M0}$ is the corresponding matrix transforming Euler rates into (body-frame) angular velocity. To facilitate the subsequent development, the six-dimensional extension of the cross-operator is defined by

$$\boldsymbol{\nu}^\otimes = \begin{bmatrix} \boldsymbol{\omega}^\times & \mathbf{O} \\ \mathbf{v}^\times & \boldsymbol{\omega}^\times \end{bmatrix}, \ \boldsymbol{\nu}^T\boldsymbol{\nu}^\otimes = \mathbf{0}.$$

The notation $(\cdot)^\times$ denotes the 3×3 skew-symmetric matrix used to implement the vector cross product. The motion equation (9) can now be written in the form

$$\boldsymbol{M}\dot{\boldsymbol{\nu}} + \boldsymbol{\nu}^\otimes\boldsymbol{M}\boldsymbol{\nu} = \boldsymbol{P}^{-T}(\boldsymbol{\rho})\widehat{\boldsymbol{\tau}}. \quad (12)$$

4. The Adaptive Controller

The desired trajectory is prescribed by $\{\boldsymbol{\rho}_d, \dot{\boldsymbol{\rho}}_d, \ddot{\boldsymbol{\rho}}_d\}$ and it is assumed that $\boldsymbol{\rho}_d \to \bar{\boldsymbol{\rho}}_d$ (constant) as $t \to \infty$. The following quantities play an essential role:

$$\begin{aligned}\boldsymbol{\nu}_d &= \boldsymbol{P}(\boldsymbol{\rho})\dot{\boldsymbol{\rho}}_d,\\ \widetilde{\boldsymbol{\nu}} &= \boldsymbol{\nu} - \boldsymbol{\nu}_d = \boldsymbol{P}(\boldsymbol{\rho})\dot{\widetilde{\boldsymbol{\rho}}}, \ \widetilde{\boldsymbol{\rho}} = \boldsymbol{\rho} - \boldsymbol{\rho}_d,\\ \boldsymbol{\nu}_r &= \boldsymbol{\nu}_d - \boldsymbol{P}(\boldsymbol{\rho})\boldsymbol{\Lambda}\widetilde{\boldsymbol{\rho}}_\mu = \boldsymbol{P}(\boldsymbol{\rho})[\dot{\boldsymbol{\rho}}_d - \boldsymbol{\Lambda}\widetilde{\boldsymbol{\rho}}_\mu],\\ \widetilde{\boldsymbol{\rho}}_\mu &= \boldsymbol{\rho}_\mu - \boldsymbol{\rho}_{\mu d}, &(13)\end{aligned}$$

$$\widetilde{\boldsymbol{\nu}}_r = \boldsymbol{\nu} - \boldsymbol{\nu}_r = \boldsymbol{P}(\boldsymbol{\rho})[\dot{\widetilde{\boldsymbol{\rho}}} + \boldsymbol{\Lambda}\widetilde{\boldsymbol{\rho}}_\mu], \quad (14)$$

$$\mathbf{s}_\mu = \dot{\widetilde{\boldsymbol{\rho}}}_\mu + \boldsymbol{\Lambda}\widetilde{\boldsymbol{\rho}}_\mu, \quad (15)$$

where $\boldsymbol{\Lambda} = \boldsymbol{\Lambda}^T > \mathbf{O}$ and $\boldsymbol{\rho}_{\mu d}$ is the desired form of $\boldsymbol{\rho}_\mu$ discussed below. Given the structure of the payload motion equation (12), our choice of feedforward torque can be written as

$$\boldsymbol{P}^{-T}\widehat{\boldsymbol{\tau}}_d = \boldsymbol{W}(\dot{\boldsymbol{\nu}}_r, \boldsymbol{\nu}_r, \boldsymbol{\nu})\mathbf{a} \triangleq \boldsymbol{M}\dot{\boldsymbol{\nu}}_r + \boldsymbol{\nu}_r^{\otimes}\boldsymbol{M}\boldsymbol{\nu} \quad (16)$$

where $\mathbf{a} = \mathrm{col}\{m, \mathbf{c}, \mathbf{j}\}$ ($\mathbf{j}$ is a column of the six independent moment of inertia elements) and $\boldsymbol{W}$ is termed the regressor matrix.

The desired behaviour for the elastic displacements, $\mathbf{q}_{ed}$, is defined by

$$\widehat{\boldsymbol{M}}_{ee}\ddot{\mathbf{q}}_{ed} + \mathbf{D}_{ee}\dot{\mathbf{q}}_{ed} + \mathbf{K}_{ee}\mathbf{q}_{ed} = - [C_1\boldsymbol{J}_{1e}\ C_2\boldsymbol{J}_{2e}]^T\widehat{\boldsymbol{\tau}}_d \quad (17)$$

and the desired form of $\boldsymbol{\rho}_\mu$ is defined by $\dot{\boldsymbol{\rho}}_{\mu d} = \dot{\boldsymbol{\rho}}_d - (1-\mu)[C_1\boldsymbol{J}_{1e}\dot{\mathbf{q}}_{1e,d} + C_2\boldsymbol{J}_{2e}\dot{\mathbf{q}}_{2e,d}]$. Subtracting (16) from (12) and (17) from (11) yields the following form of the error dynamics:

$$\boldsymbol{M}\dot{\widetilde{\boldsymbol{\nu}}}_r + \widetilde{\boldsymbol{\nu}}_r^{\otimes}\boldsymbol{M}\boldsymbol{\nu} = \boldsymbol{P}^{-T}(\boldsymbol{\rho})\widetilde{\boldsymbol{\tau}} \quad (18)$$

$$\widehat{\boldsymbol{M}}_{ee}\ddot{\widetilde{\mathbf{q}}}_e + \mathbf{D}_{ee}\dot{\widetilde{\mathbf{q}}}_e + \mathbf{K}_{ee}\widetilde{\mathbf{q}}_e = - [C_1\boldsymbol{J}_{1e}\ C_2\boldsymbol{J}_{2e}]^T\widetilde{\boldsymbol{\tau}} \quad (19)$$

where $\widetilde{\boldsymbol{\tau}} \triangleq \widehat{\boldsymbol{\tau}} - \widehat{\boldsymbol{\tau}}_d$ and $\widetilde{\mathbf{q}}_e = \mathrm{col}\{\widetilde{\mathbf{q}}_{1e}, \widetilde{\mathbf{q}}_{2e}\} \triangleq \mathbf{q}_e - \mathbf{q}_{ed}$.

Now consider the function

$$S_\mu = \tfrac{1}{2}\widetilde{\boldsymbol{\nu}}_r^T\boldsymbol{M}\widetilde{\boldsymbol{\nu}}_r + \tfrac{1}{2}(1-\mu)\left[\dot{\widetilde{\mathbf{q}}}_e^T\widehat{\boldsymbol{M}}_{ee}\dot{\widetilde{\mathbf{q}}}_e + \widetilde{\mathbf{q}}_e^T\boldsymbol{K}_{ee}\widetilde{\mathbf{q}}_e\right] \quad (20)$$

which is nonnegative if $\mu < 1$. Its time derivative yields, after substituting for the error dynamics,

$$\dot{S}_\mu = (\widehat{\boldsymbol{\tau}} - \widehat{\boldsymbol{\tau}}_d)^T\mathbf{s}_\mu - (1-\mu)\dot{\widetilde{\mathbf{q}}}_e^T\mathbf{D}_{ee}\dot{\widetilde{\mathbf{q}}}_e. \quad (21)$$

Integrating with respect to time from zero to $T > 0$ and taking $S_\mu(0) = 0$ yields $\int_0^T(\widehat{\boldsymbol{\tau}} - \widehat{\boldsymbol{\tau}}_d)^T\mathbf{s}_\mu\,dt = S_\mu(T) + (1-\mu)\int_0^T\dot{\widetilde{\mathbf{q}}}_e^T\mathbf{D}_{ee}\dot{\widetilde{\mathbf{q}}}_e\,dt$ which suggests that the mapping $\mathbf{s}_\mu = \boldsymbol{G}[\widehat{\boldsymbol{\tau}} - \widehat{\boldsymbol{\tau}}_d]$ embodied by (18), (19), (15), and $\dot{\widetilde{\boldsymbol{\rho}}}_\mu = \dot{\widetilde{\boldsymbol{\rho}}} - (1-\mu)[C_1\boldsymbol{J}_{1e}\dot{\widetilde{\mathbf{q}}}_{1e} + C_2\boldsymbol{J}_{2e}\dot{\widetilde{\mathbf{q}}}_{2e}$ is passive [11] if $\mu < 1$. On the basis of the passivity theorem [11], $\mathbf{s}_\mu \in \boldsymbol{L}_2$ if $\widehat{\boldsymbol{\tau}} - \widehat{\boldsymbol{\tau}}_d = -\boldsymbol{H}[\mathbf{s}_\mu]$ and $\boldsymbol{H}$ is a strictly passive operator, *i.e.*, $\int_0^T\mathbf{s}_\mu^T\boldsymbol{H}[\mathbf{s}_\mu]\,dt \geq \epsilon\int_0^T\mathbf{s}_\mu^T\mathbf{s}_\mu\,dt$, $\forall T > 0$, $\forall\mathbf{s}_\mu \in \boldsymbol{L}_{2e}$, and some $\epsilon > 0$. (If $\epsilon = 0$, $\boldsymbol{H}$ is a passive operator.)

Now, let us replace the parameters in the feedforward in (16) with estimates $\widehat{\mathbf{a}}(t)$ and motivated by the passivity theorem use a positive-definite feedback gain matrix $\mathbf{K}_d = \mathbf{K}_d^T > \mathbf{O}$ for $\boldsymbol{H}$:

$$\widehat{\boldsymbol{\tau}} = \boldsymbol{P}^T\boldsymbol{W}(\dot{\boldsymbol{\nu}}_r, \boldsymbol{\nu}_r, \boldsymbol{\nu})\widehat{\mathbf{a}}(t) - \mathbf{K}_d\mathbf{s}_\mu. \quad (22)$$

Hence,

$$-\int_0^T(\widehat{\boldsymbol{\tau}} - \widehat{\boldsymbol{\tau}}_d)^T\mathbf{s}_\mu\,dt = - \int_0^T\widetilde{\mathbf{a}}^T\boldsymbol{W}^T\boldsymbol{P}\mathbf{s}_\mu\,dt + \int_0^T\mathbf{s}_\mu^T\mathbf{K}_d\mathbf{s}_\mu\,dt.$$

The operator $\boldsymbol{H}$ will be strictly passive if $\widetilde{\mathbf{a}}$ is a passive function of $-\boldsymbol{W}^T\boldsymbol{P}\mathbf{s}_\mu$. The simplest such function if knowledge of the true parameters is to be avoided is an integrator. Therefore,

$$\dot{\widetilde{\mathbf{a}}} = \dot{\widehat{\mathbf{a}}} = -\boldsymbol{\Gamma}\boldsymbol{W}^T(\dot{\boldsymbol{\nu}}_r, \boldsymbol{\nu}_r, \boldsymbol{\nu})\boldsymbol{P}(\boldsymbol{\rho})\mathbf{s}_\mu, \quad (23)$$

$$\boldsymbol{\Gamma} = \boldsymbol{\Gamma}^T > \mathbf{O}$$

The final form of the controller gives us the following:

Theorem. The use of the controller given by (8), (22), (16), and (23) yields $\widetilde{\boldsymbol{\rho}}(t) \to \mathbf{0}$ as $t \to \infty$.

Proof. It has been noted that on the basis of the passivity theorem, $\mathbf{s}_\mu \in \boldsymbol{L}_2$. Now, consider the function

$$V = S_\mu + \tfrac{1}{2}\widetilde{\mathbf{a}}^T\boldsymbol{\Gamma}^{-1}\widetilde{\mathbf{a}} > 0 \ \ (\mu < 1).$$

Using (21), (22), and (23), its time derivative satisfies

$$\dot{V} = -\mathbf{s}_\mu^T\mathbf{K}_d\mathbf{s}_\mu - (1-\mu)\dot{\widetilde{\mathbf{q}}}_e^T\boldsymbol{D}_{ee}\dot{\widetilde{\mathbf{q}}}_e \leq 0.$$

Hence $\mathbf{s}_\mu \in \boldsymbol{L}_2 \cap \boldsymbol{L}_\infty$, $\dot{\widetilde{\mathbf{q}}}_e \in \boldsymbol{L}_2 \cap \boldsymbol{L}_\infty$, $\dot{\widetilde{\boldsymbol{\rho}}}_\mu \in \boldsymbol{L}_2$, $\widetilde{\boldsymbol{\rho}}_\mu \in \boldsymbol{L}_2 \cap \boldsymbol{L}_\infty$, and $\widetilde{\boldsymbol{\rho}}_\mu \to \mathbf{0}$ as $t \to \infty$. Since V is bounded, so are $\widetilde{\mathbf{a}}$ and $\widetilde{\boldsymbol{\nu}}_r$. Since $\mathbf{s}_\mu$, $\dot{\widetilde{\boldsymbol{\rho}}}_\mu$, $\widetilde{\boldsymbol{\rho}}_\mu$, $\dot{\boldsymbol{\rho}}_d$, $\ddot{\boldsymbol{\rho}}_d \to \mathbf{0}$ as $t \to \infty$, so do $\boldsymbol{\nu}_r$ and $\dot{\boldsymbol{\nu}}_r$. Therefore, $\widetilde{\boldsymbol{\tau}} = \widehat{\boldsymbol{\tau}} - \widehat{\boldsymbol{\tau}}_d \to \boldsymbol{P}^T\boldsymbol{W}(\dot{\boldsymbol{\nu}}_r, \boldsymbol{\nu}_r, \boldsymbol{\nu})\widetilde{\mathbf{a}} = \mathbf{0}$. Since $\widetilde{\mathbf{q}}_e$ is the solution of the stable system in (19) with $\widetilde{\boldsymbol{\tau}} \to \mathbf{0}$, then $\widetilde{\mathbf{q}}_e \to \mathbf{0}$. When this result is combined with $\widetilde{\boldsymbol{\rho}}_\mu \to \mathbf{0}$, then $\widetilde{\boldsymbol{\rho}} \to \mathbf{0}$. □

5. Numerical Example

Simulation results will now be presented for a system of two planar arms each with three joints that manipulate a shared object (Figure 2). Each arm has two flexible links and a third rigid link which is cantilevered to the large rigid payload. Bodies $\mathcal{B}_1$, $\mathcal{B}_2$, $\mathcal{B}_4$, and $\mathcal{B}_5$ are modelled as an inboard rigid body, a homogeneous, isotropic flexible beam exhibiting in-plane bending (with bending stiffness EI), and an outboard rigid body. The mass properties of each body are presented in Table 1 where m, c, and J are the zeroth, first,

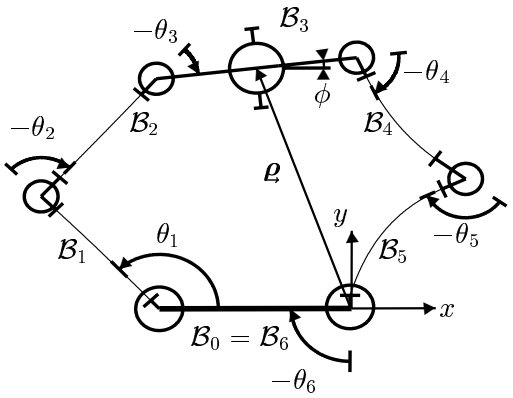

Figure 2: System for Simulation

and second moments of mass relative to the inboard attachment point of the sub-body and ℓ is its length. The geared actuators exhibit a lumped rotor inertia each of which is given in Table 2.

This is a mathematical model of an experimental testbed constructed in the Department of Mechanical Engineering at the University of Canterbury in Christchurch, New Zealand. An analysis of the system vibration modes and both experimental and simulation results for the nonadaptive form of the controller presented in this paper ($\widehat{\mathbf{a}} = \mathbf{a}$ in (22)) is presented in [8]. The close agreement demonstrated there suggests that the simulation results given here for the adaptive case are indicative of what would be achieved in experiment. Other details concerning the modelling procedure and the simulation of the *exact* motion equations (no large payload approximation) subject to the loop-closure constraint are discussed in [8].

The desired trajectory is a circle for the centre of the payload with constant orientation. The centre of the circle is given by $\boldsymbol{\rho}_c = [-0.3 \quad 0.75 \quad 0]^T$ m and its radius is $r_c = 0.15$ m. The payload position around the circle is measured with the angle $\psi(t)$ with $\psi = 0$ corresponding to the "3 o'clock" position. This angle is selected so that the first semicircle is an acceleration phase with $\psi(0) = \pi/2$ (roughly the position in Figure 2), $\dot{\psi}(0) = \ddot{\psi}(0) = 0$, $\dot{\psi}(T) = 2\pi/T$, and $\ddot{\psi}(T) = 0$ with $\psi(t) = (\pi/2) + (\pi t/T) - \sin(\pi t/T)$. The next three full circles are performed with constant angular velocity $\dot{\psi} = 2\pi/T$. The last semicircle is a deceleration phase terminating with $\psi(5T) = \pi/2$ and $\dot{\psi}(5T) = \ddot{\psi}(5T) = 0$, with $\psi(5T - t) = \pi - \psi(t)$, $0 \le t \le T$.

For the following study, $T = 4$ sec., $\mu = 0.8$, $\boldsymbol{\Lambda} = \Omega_c \mathbf{1}$ in (15), and $\mathbf{K}_d = \Omega_c \cdot \boldsymbol{P}(\boldsymbol{\rho}_c)^T \boldsymbol{M} \boldsymbol{P}(\boldsymbol{\rho}_c)$ in (22), where $\Omega_c = 4$ rad/s. The value of $\boldsymbol{\Gamma}$ in the adaptation law is selected to be diagonal with entries

Table 1: Robot Mass Properties

	ℓ (m)	m (kg)	c (g·m)	J (g·m^2)	EI (N·m^2)
Base ($\mathcal{B}_0 = \mathcal{B}_6$)	0.600				
Arm 1					
$\mathcal{B}_1$ rotor	0.037	2.66	1.84	0.23	
$\mathcal{B}_1$ link	0.406	0.20	40.4	10.9	39.3
$\mathcal{B}_1$ stator	0.062	1.92	112.	8.43	
$\mathcal{B}_2$ rotor	0.082	1.80	15.8	2.19	
$\mathcal{B}_2$ link	0.360	0.18	32.3	7.76	39.3
$\mathcal{B}_2$ stator	0.067	0.93	54.6	4.15	
Payload ($\mathcal{B}_3$)	0.598	15.7	4670	1950	
Arm 2					
$\mathcal{B}_4$ rotor	0.067	0.93	7.99	1.02	
$\mathcal{B}_4$ link	0.327	0.19	26.1	9.69	39.3
$\mathcal{B}_4$ stator	0.112	2.10	206.	24.3	
$\mathcal{B}_5$ rotor	0.077	2.23	10.2	3.26	
$\mathcal{B}_5$ link	0.390	0.16	37.3	5.69	39.3
$\mathcal{B}_5$ stator	0.037	2.53	92.5	131.	

Table 2: Rotor Inertias

joint	(g·m^2)	(g·m^2)
1, 6	128.	128.
2, 5	150.	307.
3, 4	16.1	16.1

given by $\Gamma_{mm} = 4\Omega_c T \widehat{\Gamma}_{mm}$ where

$$\begin{aligned} \widehat{\Gamma}_{mm} &= \left[\int_0^T \boldsymbol{W}(\dot{\boldsymbol{\nu}}_d, \boldsymbol{\nu}_d, \boldsymbol{\nu}_d) \mathbf{K}_d^{-1} \right. \\ &\times \left. \boldsymbol{W}(\dot{\boldsymbol{\nu}}_d, \boldsymbol{\nu}_d, \boldsymbol{\nu}_d)\, dt \right]_{mm} . \end{aligned}$$

Given the planar nature of the problem $\mathbf{a}$ effectively contains 4 parameters: m, c_x, c_y, and J_{zz}. For simplicity, we take $\boldsymbol{\rho}_{\mu d} \doteq \boldsymbol{\rho}_d$ so that (17) is not used.

Initially, the control law was implemented using only the feedback portion ($\widehat{\mathbf{a}} \equiv \mathbf{0}$) with balanced load-sharing ($C_1 = C_2 = 0.5$). The resulting tracking performance is illustrated in Figure 3 with large position and orientation errors in evidence. When the feedforward was implemented using the true known parameters ($\widehat{\mathbf{a}} \equiv \mathbf{a}$), the tracking performance illustrated in Figure 4 was obtained with corresponding errors and orientation given in Figure 5. There is considerable improvement over the results using PD feedback alone

with simultaneous vibration suppression.

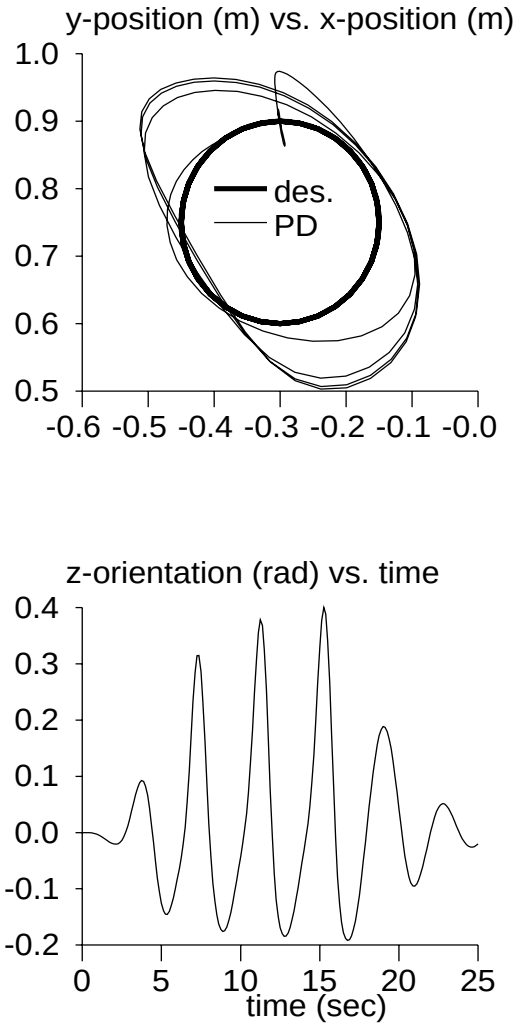

Figure 3: Simulation Results for PD Feedback Control

The results corresponding to the use of the adaptation law in (23) with $\hat{\mathbf{a}}(0) = \mathbf{0}$ are shown in Figure 5 for two different load-sharing scenarios. Interestingly, they are significantly better than the fixed (known) parameter case which occurs because the feedforward is based on the payload alone. The adaptive form evidently has the ability to account for the "missing" mass in the arms. The evolution of three of the four parameter estimates is shown in Figure 6. As might be expected, the parameters do not converge to the true payload values but larger values indicative of the entire robot.

6. Conclusions

A passivity-based adaptive controller has been developed for two flexible robot arms which manipulate a large rigid payload. The underlying passivity property depends only on the size of the payload and hence is robust with respect to the stiffness properties of the link and the number of modelled modes. A free load-sharing parameter permits the required joint torques to be shared between the arms in an arbitrary fashion.

The robotic system used in the numerical example exhibited significant departures from the assumed payload-dominated model: the payload mass is on the order of that of the two robot arms and the joints exhibit significant rotor inertias. In spite of these effects, the adaptive controller worked quite well.

References

[1] Slotine, J.–J.E. and Li, W., On the Adaptive Control of Robot Manipulators, *Int. J. Rob. Research* 6, 49–59, 1987.

[2] Ortega, R., Loría, A., Nicklasson, P. J., and Sira–Ramírez, H., *Passivity-Based Control of Euler-Lagrange Systems*, Springer–Verlag, London, 1998.

[3] Wang, D. and Vidyasagar, M., Passive Control of a Stiff Flexible Link, *Int. J. Rob. Research* 11, 572–578, 1992.

[4] Damaren, C. J., Passivity Analysis for Flexible Multilink Space Manipulators, *J. Guidance, Control, and Dynamics* 18, 272–279, 1995.

[5] Damaren, C. J., Approximate Inverse Dynamics and Passive Feedback for Flexible Manipulators with Large Payloads, *IEEE Trans. Robotics and Automation* 12, 131–138, 1996.

[6] Damaren, C. J., Adaptive Control of Flexible Manipulators Carrying Large Uncertain Payloads, *J. of Robotic Systems* 13, 219–228, 1996.

[7] Christoforou, E. G. and Damaren, C. J., The Control of Flexible-Link Robots Manipulating Large Payloads: Theory and Experiments, *J. of Robotic Systems*, To appear, 2000.

[8] Damaren, C. J., On the Dynamics and Control of Flexible Multibody Systems with Closed Loops, *Int. J. Rob. Research* 19, 238-253, 2000

[9] Krishnamurthy, K., and Yang, L., Dynamic Modeling and Simulation of Two Cooperating Structurally-Flexible Robotic Manipulators, *Robotica* 13, 375-384, 1995

[10] Matsuno, F. and Hatayama, M., Robust Cooperative Control of Two Two-Link Flexible Manipulators on the Basis of Quasi-Static Equations, *Int. J. Rob. Research* 18, 414–428, 1999.

[11] Desoer, C. A. and Vidysagar, M., *Feedback Systems: Input-Output Properties*, Academic Press, New York, 1975.

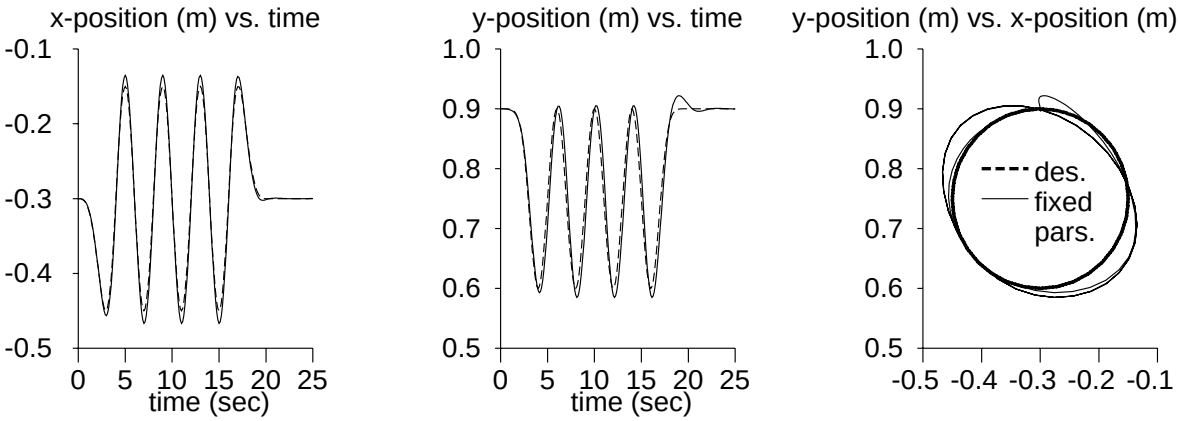

Figure 4: Fixed Parameter Results

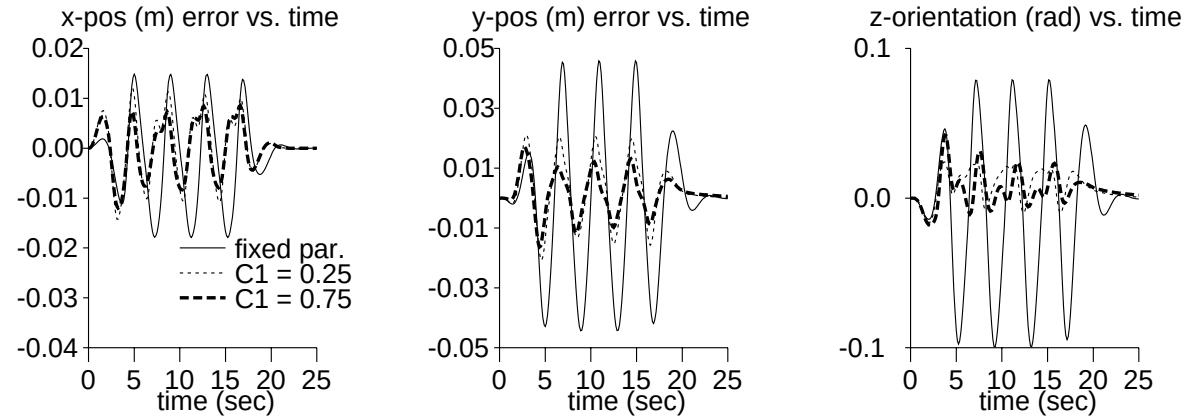

Figure 5: Tracking Errors

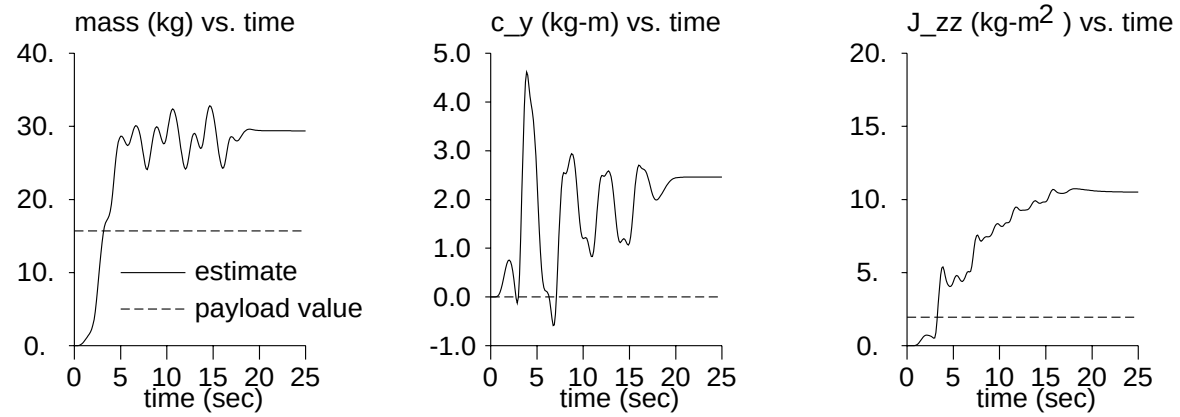

Figure 6: Parameter Estimates

Proceedings of the International Symposium on
Adaptive Motion of Animals and Machines,
Montreal, Aug.8-12, 2000

Spontaneous generation of anti-gravitational arm motion based on anatomical constraints of the human body

Naomichi Ogihara and Nobutoshi Yamazaki

Keio University, Dept. of Biomedical Eng., Yokohama 223-8522, Japan
{oginao,yamazaki}@mech.keio.ac.jp

Abstract

A neuro-musculo-skeletal model of human upper limb is constructed that can spontaneously generate natural reaching motion without prior formation of an optimal trajectory. Given a goal position, the model immediately generates muscular activation signals that tend to move the hand to the goal, utilizing the anatomical constraints of the body motion. The simulated motions agree with those of humans, suggesting that such mechanism may be incorporated in actual human motor control.

1. Introduction

It is generally accepted that human well-practiced movement is generated along a priorly planned trajectory that minimizes a certain objective function such as hand position jerk or rate of change of joint torque[1,2]. In order to generate appropriate muscle stimulation signals for an optimally planned hand trajectory, an inverse-dynamics problem of the musculoskeletal system should be solved in the brain[3]. Humans, however, can also generate reasonable motions, even for natural unconcerned gesture or inexperienced motion, in which we can not assume formation of an optimal trajectory based on an objective function.

Human motion seems to be generated not to resist against the anatomical constraints of the human body, such as limb kinematics, inertial properties of limbs, range of joint motion, muscle size and attachment and so on. Such body constraints may be utilized so as to spontaneously induce casual movement. Based on this hypothesis, in this study, we attempt to develop a neural network model that can spontaneously generate natural reaching motion toward a target. An inexperienced targeted reaching movement can be regarded as an example of natural, casual motion.

2. Model

2.1 Musculo-skeletal model

Human mimetic musculo-skeletal model is constructed as two-dimensional three rigid links representing upper arm, fore arm and hand in a sagittal plane as shown in Figure 1. The equations of motion of the three rigid-link system are derived as

$$\mathbf{M(q)}\ddot{\mathbf{q}} + \mathbf{h}(\dot{\mathbf{q}},\mathbf{q}) + \mathbf{g(q)} - \alpha\mathbf{(q)} + \beta(\dot{\mathbf{q}}) = \mathbf{T} \qquad (1)$$

where $\mathbf{q}$ is a (3 × 1) vector of joint angles, $\mathbf{T}$ is a (3 × 1) vector of joint torques caused by contraction of muscles, $\mathbf{M(q)}$ is a (3 × 3) inertia matrix, $\mathbf{h}(\dot{\mathbf{q}},\mathbf{q})$ is a (3 × 1) vector of torque component depending on Coriolis and centrifugal force, and $\mathbf{g(q)}$ is a (3 × 1) vector of torque component depending on the gravity respectively, elements of which are functions of parenthesized variables. $\alpha\mathbf{(q)}$ and $\beta(\dot{\mathbf{q}})$ are (3 × 1) vectors of the torques exerted by the joint elastic and viscous elements, which defines the passive resistive torques due to joint capsules and ligaments, restricting ranges of joint motions. The inertial parameters of each segment are determined so as to be equivalent to those of actual human. The joint elastic and viscous elements are represented by the following double-exponential function[4] and the linear viscous elements:

$$\alpha_j = k_1 \exp(-k_2(q_j - k_3)) - k_4 \exp(-k_5(k_6 - q_j)) \qquad (2)$$
$$\beta_j = c_j \dot{q}_j \qquad (3)$$

where α_j and β_j are the torques exerted by elastic and viscous elements around the j th joint (the j th element of $\alpha\mathbf{(q)}$ and $\beta(\dot{\mathbf{q}})$), q_j is the j th joint angle, and $k_{1\sim6}$ and c_j are coefficients (see Table 1), respectively.

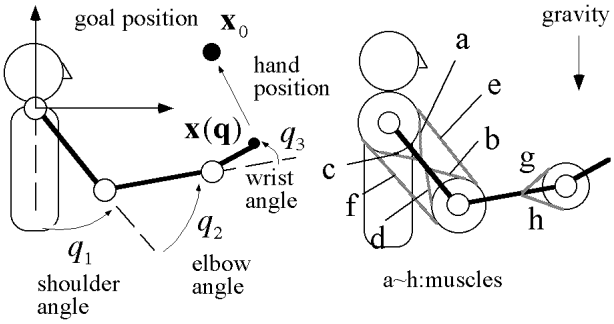

Figure 1. Musculo-skeletal model

Table1. Joint parameters

Joint	k_1	k_2	k_3	k_4	k_5	k_6	c
Shoulder	1.	2.16	-0.12	1.	3.35	2.02	1.6
Elbow	1.	3.96	0.70	1.	3.14	1.73	0.8
Wrist	1.	2.04	-0.76	1.	2.40	0.83	0.5

On each upper extremity, total of 8 muscles are considered including biarticular muscles as shown in Figure 1. Moment arms of the muscles are assumed to be constant irrespective of joint angles. The joint torque vector $\mathbf{T}$ can be expressed as

$$\mathbf{T} = -\mathbf{G}^T \cdot \mathbf{F} \tag{4}$$

where $\mathbf{F}$ is a (8 × 1) vector of muscle forces, and $\mathbf{G}$ is a (8 × 3) matrix of the moment arms. Each muscle generate force according to muscle activation a_m by the following muscle model[5]:

$$\begin{aligned} f_m &= \bar{f}_m \cdot k(\xi_m) \cdot h(\eta_m) \cdot a_m \\ k(\xi_m) &= 0.32 + 0.71\exp\{-1.11(\xi_m - 1)\}\sin\{3.72(\xi_m - 0.66)\} \\ h(\eta_m) &= \{1 + \tanh(3.0\eta_m)\} \end{aligned} \tag{5}$$

where m is muscle number, f_m is muscle force, $\bar{f}_m$ is the maximum muscle force, L_m is muscle length, $\bar{L}_m$ is the optimal muscle length, $\dot{L}_m$ is muscle shortening velocity (positive for stretching), $\bar{\dot{L}}_m$ is the maximum muscle velocity (=3.0m/s), ξ_m is the normalized muscle length $L_m / \bar{L}_m$, η_m is the normalized muscle velocity $\dot{L}_m / \bar{\dot{L}}_m$, $k(\xi_m)$ is the force-length relationship, and $h(\eta_m)$ is the force-velocity relationship, respectively. Muscle activation dynamics are modeled by the following equation:

$$\tau(da_m / dt) = -a_m + y_m \tag{6}$$

where y_m is a motor command to the muscle from the nervous system, τ is the muscle activation time constant (=0.07sec). Musculo-skeletal parameters, such as moment arms and maximum muscle forces are determined by literature so as to be equivalent to those of actual human.

2.2 Nervous model

2.2.1 Motion generating principle

In this study, motion is generated based on the following pseudo-potential P, the minimum point of which is the goal position, $\mathbf{x}_0$, represented in the spatial coordinate.

$$P = (\mathbf{q} - \mathbf{q}_0)^T \mathbf{W} (\mathbf{q} - \mathbf{q}_0) \tag{7}$$

where $\mathbf{q}_0$ is the joint angles of the limb when the goal position $\mathbf{x}_0$ is reached, $\mathbf{W}$ is a (3 × 3) positive definite weight matrix. In order to generate motion based on this potential, the muscles need to generate joint torques satisfying the following equation:

$$\mathbf{T} = \mathbf{W}(\mathbf{q}_0 - \mathbf{q}) - \alpha(\mathbf{q}) + g(\mathbf{q}) \tag{8}$$

It is theoretically confirmed that such system is stable because of the viscous property of the joints[6].

2.2.2 Recurrent neural network model

In order to generate joint torques by Equation (8), $\mathbf{q}_0$ has to be estimated from the goal position $\mathbf{x}_0$, which is represented in the spatial coordinate provided by the visual system. However, because the number of degrees of freedom of joint angles exceeds that of the two-dimensional spatial coordinate system, there are infinitely many combinations of joint angles to point the same position. Here we consider to utilize the dynamics of a recurrent neural network[7] to spontaneously transform spatial position into joint angles. In order to construct a recurrent neural network that can autonomously estimate the joint angles from present hand position, the following potential function $I_{\mathbf{u}}$ is defined:

$$\begin{aligned} I_{\mathbf{u}} &= \delta\Big(\sum_j \int_{\bar{q}_j}^{u_j} -\alpha_j(\theta)d\theta + \sum_i -m_i \bar{\mathbf{g}}^T \cdot \mathbf{r}_i^g(\mathbf{u})\Big) \\ &+ \frac{\kappa}{2}\{\mathbf{J}(\mathbf{u})(\mathbf{u}-\mathbf{q}) - (\mathbf{x}_0 - \mathbf{x})\}^T \{\mathbf{J}(\mathbf{u})(\mathbf{u}-\mathbf{q}) - (\mathbf{x}_0 - \mathbf{x})\} \end{aligned} \tag{9}$$

where $\mathbf{u}$ is the neural representation of joint angles, u_j is the j th element of $\mathbf{u}$, $\bar{q}_j$ is the angle when $\alpha_j = 0$ (neutral posture), m_i is the mass of the i th segment, $\mathbf{r}_i^g$ is a (2 × 1) vector of center of gravity of the i th segment, $\bar{\mathbf{g}}$ is the gravitational acceleration vector, $\mathbf{J}(\mathbf{u})$ is the Jacobian matrix at $\mathbf{u}$, and δ and κ are coefficients. The first and second terms represent total potential energy stored in the musculo-skeletal system of the upper limb. The third term denotes a penalty for not satisfying a constraint $\mathbf{J}(\mathbf{u})(\mathbf{u}-\mathbf{q}) - (\mathbf{x}_0 - \mathbf{x}) = \mathbf{0}$, which decreases as the hand position $\mathbf{x}(\mathbf{u})$ approaches to $\mathbf{x}_0$. The recurrent neural network which autonomously decrease the potential $I_{\mathbf{u}}$ can be expressed as

$$\begin{aligned} d\mathbf{u}/dt &= -\mu(\nabla_{\mathbf{u}} I_{\mathbf{u}}) \\ &= -\mu\{\delta(-\alpha(\mathbf{u}) + \mathbf{g}(\mathbf{u})) + \kappa \mathbf{J}^T \{\mathbf{J}(\mathbf{u})(\mathbf{u}-\mathbf{q}) - (\mathbf{x}_0 - \mathbf{x})\}\} \end{aligned} \tag{10}$$

where μ is a coefficient. According to the change in $\mathbf{u}$ represented in the nervous system, the nervous

system then calculates neural representation of joint torques, $\mathbf{N}$, according to Equation (8) as

$$\mathbf{N} = \mathbf{W}(\mathbf{u} - \mathbf{q}) - \alpha(\mathbf{q}) + \mathbf{g}(\mathbf{q}) \tag{11}$$

In this study, it is assumed $\mathbf{W} = w\mathbf{I}$, where $\mathbf{I}$ is a (3 × 3) unit matrix, and w is a coefficient.

Since number of muscles exceeds number of joint degrees of freedom, another layer of recurrent neural network is constructed for estimation of appropriate muscle activation signals from $\mathbf{N}$, assuming the following potential function:

$$I_{\mathbf{v}} = \xi \mathbf{v}^T \mathbf{v} + \frac{\kappa'}{2}(-\mathbf{G}^T\mathbf{F} - \mathbf{N})^T(-\mathbf{G}^T\mathbf{F} - \mathbf{N}) \tag{12}$$

where $\mathbf{v}$ is the (8 × 1) vector of the inner states of motoneurons, and ξ and κ' are coefficients. The first term represents the sum of square of v_m, and the second term denotes a constraint that $\mathbf{N}$ is equal to the summation of the muscular forces. The recurrent neural network which autonomously decrease the potential $I_{\mathbf{v}}$ can be expressed as

$$\begin{aligned} d\mathbf{v}/dt &= -\mu'(\nabla_{\mathbf{v}} I_{\mathbf{v}}) \\ &= -\mu'\left\{2\xi\mathbf{v} - \kappa'(\mathbf{G}^T\overline{\mathbf{F}})^T(-\mathbf{G}^T\mathbf{F} - \mathbf{N})\right\} \end{aligned} \tag{13}$$

$$y_m = \max(2/(1+\exp(-3v_m)) - 1, 0) \tag{14}$$

where $\overline{\mathbf{F}} = diag[\bar{f}_1, \bar{f}_2, \bar{f}_3, \bar{f}_4, \bar{f}_5, \bar{f}_6, \bar{f}_7, \bar{f}_8]$, y_m is the motor command to the mth muscle, value of which is restricted from 0 to 1 by the output function (14), and μ' is a coefficient.

By incorporating the potential described by Equation (12), Equation (10) can be rewritten as

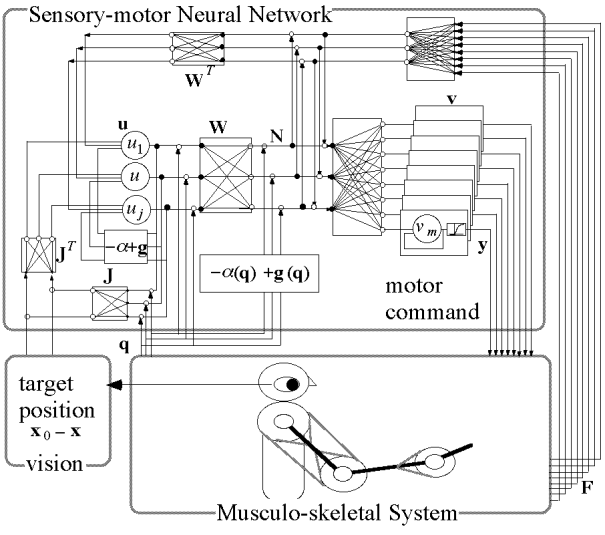

Figure 2 Nervous model

$$\begin{aligned} d\mathbf{u}/dt = -\mu\{&\delta(-\alpha(\mathbf{u}) + \mathbf{g}(\mathbf{u})) \\ &+\kappa\mathbf{J}^T\left\{\mathbf{J}(\mathbf{u})(\mathbf{u} - \mathbf{q}) - (\mathbf{x}_0 - \mathbf{x})\right\} - \lambda\mathbf{W}^T(-\mathbf{G}^T\mathbf{F} - \mathbf{N})\} \end{aligned} \tag{10*}$$

where λ is a coefficient.

Figure 2 shows a schematic diagram of the neural network model. Given the visual information regarding a goal position, $\mathbf{x}_0 - \mathbf{x}$, the neural network model produces muscle activation signals that tends to minimize the potential defined by Equation (9) and (12), and motion is generated. Then the resultant motion (joint angles $\mathbf{q}$ and muscle forces $\mathbf{F}$) is returned back continuously to the nervous system through proprioceptors. Thus the entire neuro-musculo-skeletal systems are mutually integrated, and motion that is naturally affected by the structure and properties of the musculo-skeletal system can be generated.

In this model, the joint torques due to the joint elasticity and the gravity seems to be compensated as Equation (11), but because of the time lag or delay in the neuro-dynamics, generated motions are actually affected by them passively.

3. Simulation Method

Motion towards a given goal position $\mathbf{x}_0$ from an initial posture at $t = 0$ can be calculated by numerically integrating Equations (1,6,10*,13), which are expressed as 25 simultaneous differential equations. In order to solve this initial-value problem, we use the fourth-order Runge-Kutta method for numerical integration, for a time interval of 0.005sec. All programs are written in C language on an engineering workstation (HP C160).

The coefficients, $\mu, \delta, \kappa, w, \mu', \gamma, \kappa', \lambda$, are determined as 0.01, $500/(t+1)^2$,$800(t+1)^2$,10 (4 for downward motion),0.02, 25, 5, and 100, respectively, so that the human-like motion can be generated. The values of δ and κ are represented as functions of time, because $d\mathbf{u}/dt$ (Equation(10*)) becomes zero before the hand reaches to the goal, especially when motion opposes the joint property and/or the gravity.

4. Results

Figure 3 shows the stick figures of the simulated reaching motions for two different combinations of initial and goal positions. A dot in each stick diagram represents a goal position, and an arrow indicates direction of motion. The generated trajectories are compared with the actually measured trajectories, represented by series of white circles in the figure. The attached graphs compare the joint angles (JA) and tangential speed of hand (tan sp) for each simulated and actually

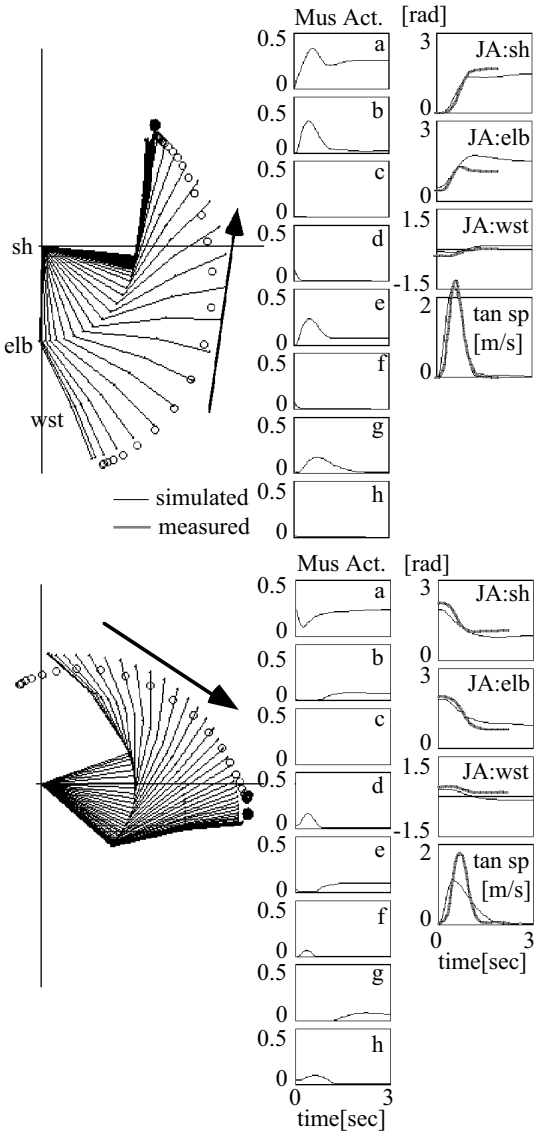

Figure 3. Generated anti-gravitational motions

measured motions. The muscle activations a_m (Mus Act) are also presented.

Figure 3 demonstrates that the proposed model can successfully generate anti-gravitational reaching motions similar to those of actual humans. The minimum hand jark model[1] predicts linear trajectories for these motions, but the proposed model could successfully generate curved paths, not going against structural restrictions of the body due to the passive joint properties and the gravitational effect. The tangential speed profile also becomes a bell-shaped curve. The muscle activation profiles are smooth and not contradicting to the motions, indicating that muscles are reasonably utilized.

5. Discussions

In this study, anatomical constraints of the musculoskeletal system are assumed to be represented as potential functions; by utilizing the neural dynamics of the proposed network, the redundancy problem in motor coordination is solved and structurally reasonable motions are spontaneously generated. Complex musculo-skeletal structure of the human body is often regarded as constraints or perturbations which must be technically compensated for intended motion control. This study implies that the anatomical constraints can be turned into advantage, and may be utilized for inducing structurally reasonable motion. Such structurally adapted motion may be energetically reasonable as well. Optimality of human movement seems to be collaterally emerged as a consequence of motion generation based on the body structure.

In this study, the structurally adapted motions are not generated by explicit control based on a priorly planned optimal trajectories, but continuously emerged due to attractor dynamics. Because of the mutual interactions among the entire neuro-musculo-skeletal systems, the integrated system becomes a gradient system, attractor of which is an equilibrium point defining a goal position and all state variables behave autonomously as if a ball slides down a valley to its bottom. Therefore, reasonable motion can be spontaneously generated without explicit optimization.

Synthesis of human motion generally requires massive computational power for solving an optimization problem. This model, however, can generate almost real time movement by using an engineering workstation, indicating its possible future application in motion synthesis of a computerized mannequin for evaluation of human interaction with system or environment.

Acknowledgments: This work was partly supported by fellowship of the Japan Society for the Promotion of Science and by a grant from The Kawakami Memorial Foundation.

References

[1] Flash, T. & Hogan, N., 1985, *J. Neurosci.*, **5**-7 1688-1703.
[2] Uno, Y., Kawato, M. and Suzuki, R., 1989, *Biol. Cybern.*, **61**, 89-101.
[3] Kawato, M. and Gomi, H., 1992, *Biol. Cybern.*, **68**, 95-103.
[4] Davy, D.T. and Audu, M.L., 1987, *J. Biomech.*, **20**, 187-201.
[5] Pierrynowski, M.R. and Morrison, J.B., 1985, *Math. Biosci.*, **75**, 65-101.
[6] Miyazaki, F. and Arimoto, S., 1985, *J. Rob. Syst.*, **2**-1, 53-71.
[7] Hopfield, J.J. and Tank, D.W., 1985, *Biol. Cybern.*, **52**, 141-152.

Proceedings of the International Symposium on
Adaptive Motion of Animals and Machines,
Montreal, Aug.8-12, 2000

Interaction between motions of the trunk and the limbs and the angle of attack during synchronous gaits of the pika (*Ochotona rufescens*)

R. Hackert, H. Witte and M. S. Fischer

Institut für Spezielle Zoologie und Evolutionsbiologie, Friedrich−Schiller−Universität Jena,
Erbertstraße 1, D−07743 Jena, Germany, hackert@zoo.uni−jena.de

Abstract

We analysed the trajectory of the body center of mass (CoM) of the pika during half−bound gaits redundantly using high−speed kinematics and integration of ground reaction forces. The relative motion of the CoM in the body is mainly determined by the bending and extension of the back. In relation to the forelimbs the CoM is aligned with the ulna of the trailing or the leading limb during the major part of the forelimbs‘ stance phase. The angle of attack is rather speed−independant in half−bound. Additionally we could observe a distinct handedness of trailing and leading limbs.

1. Introduction

Synchronous gaits, where the feet within a pair of fore− or hindlimbs touch ground with only slight time differences, gain growing interest in robotics. In comparison to the machines using symmetrical gaits (where feet are placed in diagonals − on the definition of gaits cf. [1],[2]) programming work is hoped to be simplified considerably by stronger coupling of DOFs. In extreme the Buehler hopper shows a pure bound, with no phase difference occuring within a pair of legs.
Animals are as well able to produce pure bounds (e. g. Bouncing artiodactyls like goats even move all four legs synchronously), but the common synchronous locomotor mode of small (and thus the ancestral) mammals is the half−bound. The hindlimbs are moved synchronously, while the forelimbs show fluctuating phase lags. The leg which touches the ground first is called „trailing forelimb", the other one which shows the greater cranial excursion thus is called the „leading limb" [3].

Material

We performed our analyses in this study with the pika (*Ochotona rufescens:* Lagomorpha), a small tailless mammal. It owns a body weight of 150−200 g, a crown−rump−length of 140 mm and a height of the CoM over ground 45 mm (for a picture of this animal cf. Witte et al., this issue). It lives in the steppes of central Asia. Its kinematic motion principles have been decovered by [4]. The half−bound is the gait currently used by the pika as it wants to escape rapidly (fig. 1).

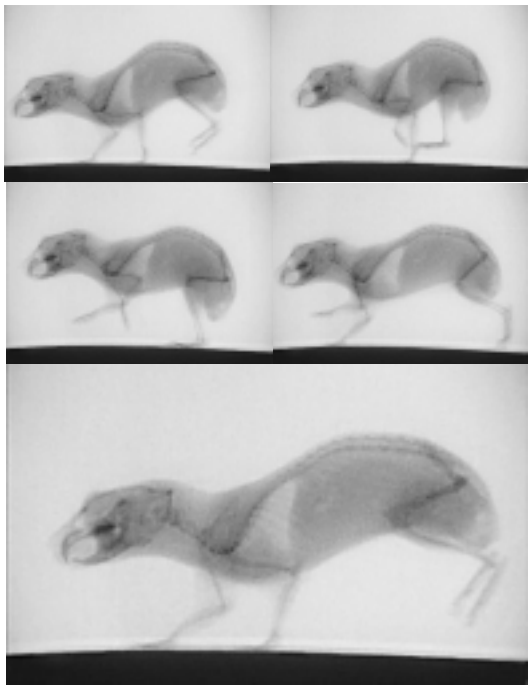

Figure 1: Pika (*Ochotona rufescens*) in half−bound. Cineradiography with 150 fps. Five events during one motion cycle in time intervals of 33 ms. The hindlimbs move synchronously, while the forelimb show a phase difference.

2. Handedness of the forelimbs during the pika‘s half−bound

Methods

Three pikas were filmed from the lateral side with one camera at a frequency of 1.000 fps, half−bounding on a treadmill at different speeds distributed in the following intervals [1.0;1.4[(slow), [1.4;1.8[(medium) and [1.8;2.2] (fast).

Results

Pikas show a preference in the choice of their trailing forelimbs (fig. 2). With increasing speed this preference becomes more evident.

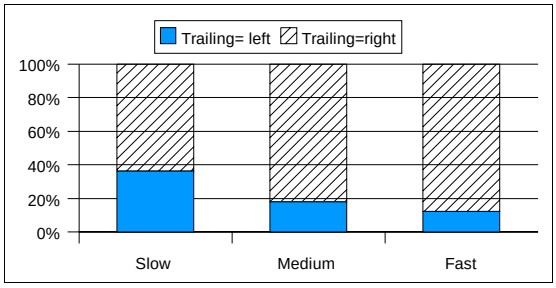

Figure 2: The individuals under study prefer one body side for the first touch down in a motion cycle of half−bound (trailing forelimb). Example for the frequency of side−different ground contact of one individual (N=517 step cycles) to illustrate the distinct handedness.

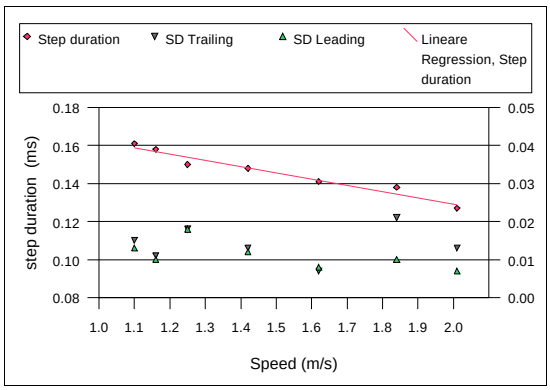

Figure 3: Step duration of the pika in half−bound. At speeds > 1.8 m/s, the SD (standart deviation) of the step duration is significantly higher ($p < 0.05$) for the leading limb than for the trailing limb. SD have to be read on the right scala. At each speed N = 20 motion cycles were analysed.

The step duration of a pika is described by a decreasing power like function of speed [4]. In half−bound, this function may be linearized (fig. 3). At high speeds (v > 1.8 m/s), in the three individuals under study we noted that the standard deviation of the cycle duration of the leading limb to the next touch down was significantly smaller than the standard deviation of the cycle duration of the trailing limb ($p < 0.05$).
These two observations may reflect a functional difference of the two forelimbs and initially motivated the following study on the side−different analysis of the interaction of the limbs with the trunk. At first, we were interested in the time−variant location of the CoM to precise its position relatively to the limbs, and to decover whether we could observe any effects of „handedness″ (which means kinematic asymmetry) on the guidance of the CoM.

3. The motion of the CoM in the body during half−bound

Methods

We filmed a pika as described in §2 running on the treadmill at a speed of 2m/s. This speed turned out to be the mean velocity of the pikas as they were escaping from unexpected dangers along our runway over a force plate. A second camera documented the front view, to ensure that the pika was running straight forward (the treadmill belt is twice as wide as the pika). At this speed, the step frequency is about 8 cycles per second. To control the permanence of speed, the lateral zoom−camera was adjusted in the way that the picture just covered the length of the pika as it was extended.
At a frequency of 1.000 fps the high speed cameras (Camsys®, optics: zoom Fujinon® 2.0/12.5−75.5 mm) provide a resolution of 256 x 64 pixels. To control the effects of optical distorsion, a reference grid (mesh width 10 ± 0.05 mm, steel balls of 1 ± 0.01 mm diameter) was filmed and served as a control for linearization means. The contour of the body was digitised in the global frame with 35 points alternately distributed on the vemtral and dorsal border of the sagittal projection of the animal. The limb segments were incorporated into the body shape proximally of the elbow and knee joints. 90% of the animal mass is included in this digitised area.
The distribution of the points on the body outline defined a series of triangles, the areas and centers of which were computed from the corner coordinates. To take account of the mass distribution, we weighed a series of 14 transversal slices of a pika frozen in its extended position (fig. 4).

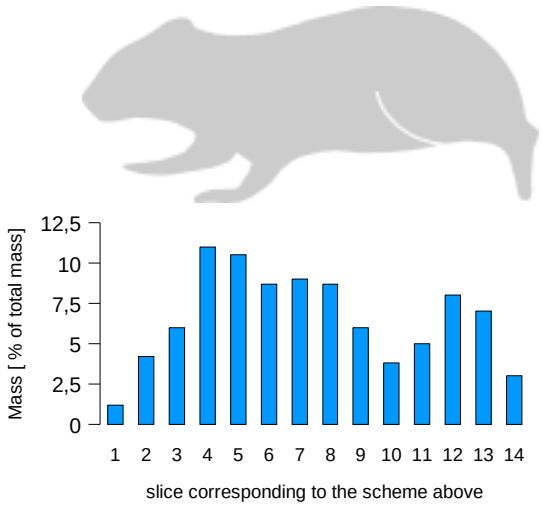

Figure 4: Mass distribution of the trunk of a Pika (*Ochotona rufescens*) including the upper arm (proximally of the elbow joint) and the thigh.

These values were the basis for the computational weight distribution onto the triangles. We thus implicitely neglected the effect of oscillating masses, or seen the other way round, since the thickness of the zone defined by the base of the triangle is about 1cm, this means that the masses have been considered to oscillate locallly in this volume.

Results

Motion of the center of mass in the body:

- The above described method leads to motion patterns which are comparable to the pattern issued from the two−fold integration of ground reaction forces.
- The CoM is located just underneath the lung base. It is closer to the ventral outline than to the dorsal one (40:60) (fig. 5).
- The relative position of the CoM relatively to the nose (which is a representative for the rather unaccelerated head) is not constant (fig. 6). The horizontal excursion of the CoM is in fixed phase coupling with the motion of the back. During spinal extension, which takes place during the stance phase of the hindlimbs, and at the beginning of the forelimbs‘ stance phase the CoM moves caudal. During spinal bending the CoM moves cranial. This excursion equals about 15 % of the animals‘ length (fig. 7)
- The amplitude of the vertical motion relative to the nose is about 10 mm (fig. 6).

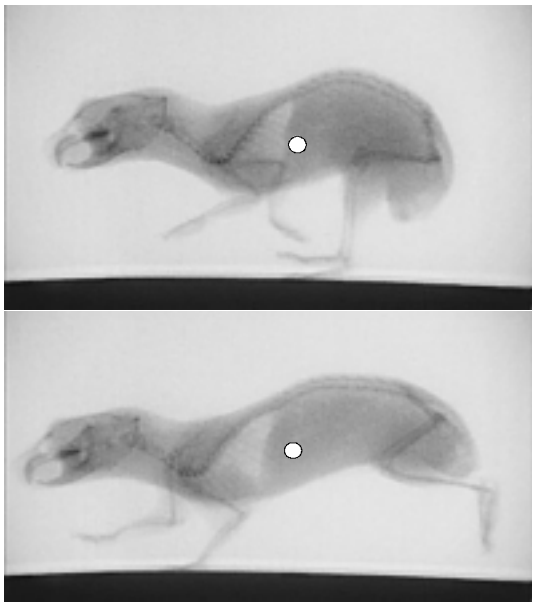

Figure 5: Location of the CoM during half−bound of a pika. For means of comparability, for this illustration the same cineradiographic pictures have been taken as in Witte et al., fig. 4 [this issue].

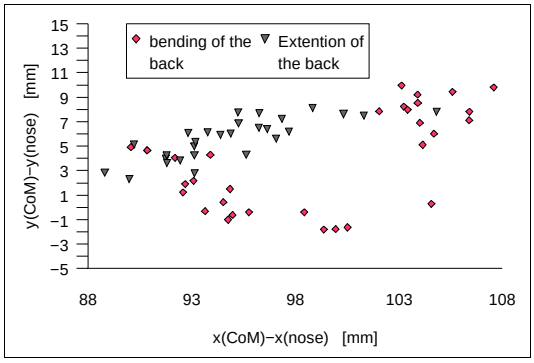

Figure 6: Motions of the CoM relative to the nose during half−bound of a pika.

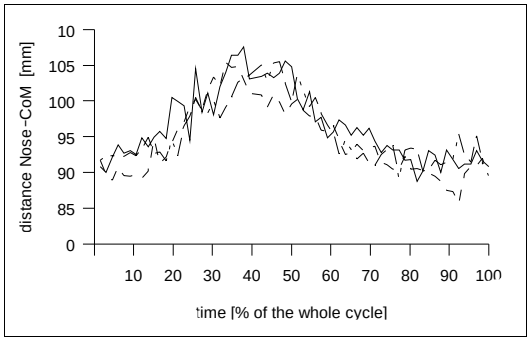

Figure 7: Horizontal distance between the CoM and the nose during the half−bound of a pika for a three steps serie. Footfall pattern are shown fig. 8.

Vertical motions of the CoM in the global frame:

- The amplitude of the motion of the CoM at 2 m/s accounts for about 6 mm (10% of the animal height of about 60 mm (fig. 8).
- The extension phase of the back is dominated by a downward movement of the CoM with a possible ascent at the end. In the flexion phase of the back after initial descent the CoM moves upward (fig. 8).
- The global vertical motion pattern may have one or two local extrema.

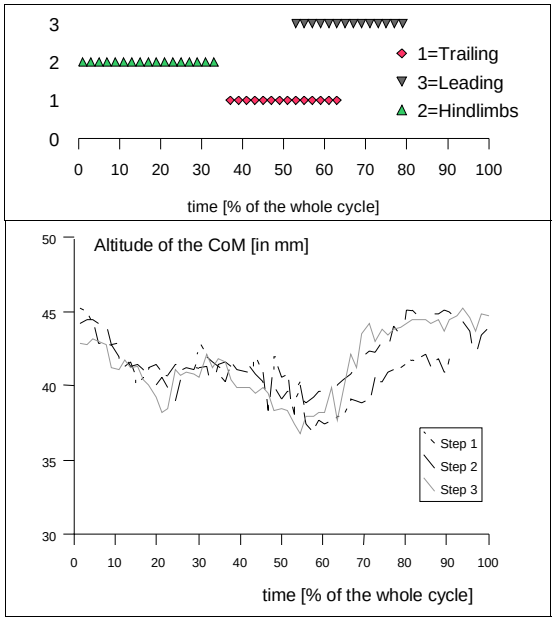

Figure 8: Vertical excursions of the CoM during half−bound of a pika and above the corresponding footfall pattern.

Position of the CoM relative to the forelimbs:

- The angle wrist−elbow−CoM of the trailing forelimb is about 180° during that part of its stance phase when no other ground contacts occur (fig. 10).
- After the leading forelimbs touches the ground, the weight is transferred to it: the alignement CoM−trailing ulna decreases while the alignement with the leading ulna becomes almost complete (fig. 10).

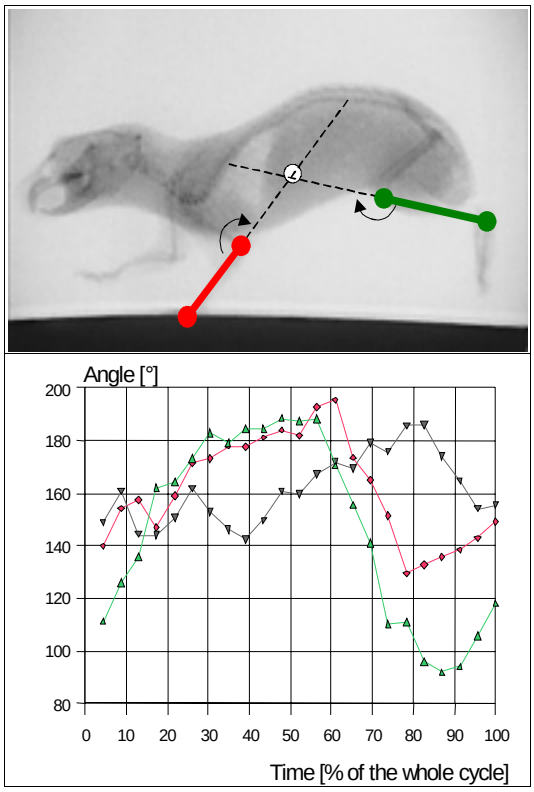

Figure 10: The angle wrist−elbow−CoM of the trailing forelimb is about 180° during that part of its stance phase when no other ground contacts exist. During late mid stance the leading forelimb takes over and its ulna points to the CoM. Alignement of the shank (kinematically eqivalent to the upper arm) mainly occurs during aerial phases. For the footfall pattern see fig 8.

4. Does the angle of attack couple with speed ?

The angle of attack is defined as the angle formed between the connection line of CoM and the ground contact point and the ground. To quantify the variation of the angle of attack with speed we take advantage of the above detailed experience that at touch down of the trailing limb the ulna points in the direction of the CoM. The orientation of the ulna does not coincide with the direction defined by the connection line of the ground contact point (underneath the metatarso−phalangial joint) and the CoM. The error we provoke is a systematic error of +5°.

Methods

The cineradiographic apparatus accessible to us provides 150 fps. This frame rate is insufficient to determine significant values for the angle of attack, since a pika may run up to 8 steps per second. Consecutively we shaved the forelimbs of a pika and filmed its half−bounding on the treadmill with the high speed video system (500 fps, resolution of 256x256 pixels).
The camera field was adjusted to cover one pika length. This enables a rigorous control of the pika speed.

Results

- The angle of attack does not strongly variate with increasing speed.
- The difference between the mean values are small but significant (t−Test $p<0.10$ for the four first values).
- The angle ulna/ground equals 50°, consequently the angle of attack is about 45°.

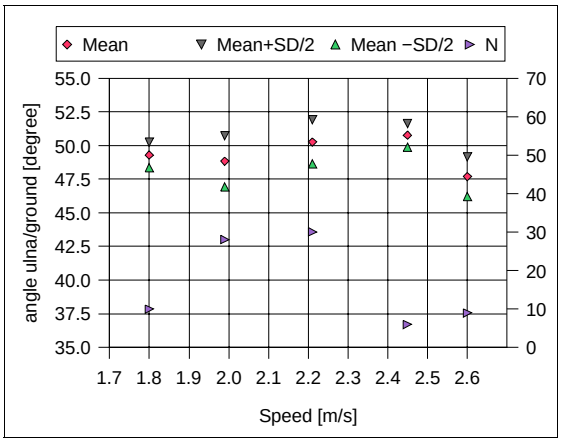

Fig 11. The variations of the angle ulna/ground with speed are small. The rigtht scale gives the number of steps N used to calculate the mean values.

5. Discussion

The small mammal‘s limb is a four segmented flexed structure, which may be compared to a pantograph [5]. It effectively allows compensation of small irregularities of the ground and also plays the role of a spring−damper system as the pika runs or trots. The occurance of elastic phenomena during legged locomotion is commonly accepted in biology (cf. [6], [7], [8] and succeeding publications). The movement of the human CoM during running may be described using spring−mass models [9], [10]. The vertical excursion of the CoM of the half−bounding pika (about 7 mm) relatively to the leg length (70 mm) is quite comparable to the excursion of the CoM in human running (about 10 %) (cf. [11]). From this point of view (in addition to many others), it also seems promising to extend these templates to quadrupedal locomotion [12]. In humans the spring−leg and the mass (CoM) are well aligned. The above described results indicate, that the common linear spring−point mass model may well be applied to the situation in the pika’s forelimbs. In the hindlimbs, the consideration of the mass extension of the trunk seems inevitable. [13] calculate how the angle of attack of a spring−mass system defined as the angle which minimized the maximum of the force during the stance phase variate as a function of the horizontal and vertical velocity. The variation of this angle with horizontal velocity was also small (about 7°).

6. Conclusion

Our study shows that the motion of the trunk is a determinant factor in the motion of the center of mass of a small mammal. The model of a rigid body that jumps from one limb to the other is not able to explain the variety of the pattern of the vertical motion of CoM by running locomotor modes. The bending of the back is not a passive bending due to the inertia of the back, since the deceleration in the forward direction by landing of the forelimbs is minimal (a few percent). For robotics the Raibert idea of minimizing dissipative energy flows in combination with the usage of intelligent“, self−stabilising mechanics with minimal neuronal/computational control effort is attractive. The understanding of motion systems evolutively tested for longer periods in this context may be a promising directive.

7. Acknowledgments

We thank Prof. R. Blickhan, who kindly provided us access to the high speed camera system. Dr. D. Haarhaus invested his experience in a multitude of cineradiographic experiments performed at the Institut fuer den wissenschaftlichen Film (IWF) in Goettingen, Germany.

References

[1] M Hildebrand (1965): Symmetrical gaits of horses. – Science **150**: 701−708.

[2] M Hildebrand (1977): Analysis of asymetrical gaits. – J Mamm **58(2)**: 131−156.

[3] FA Jenkins (1971): Limb posture and locomotion in the Virginia opossum (*Didelphis marsupialis*) and other non−cursorial mammals. J Zool (Lond) **165**: 303−315.

[4] MS Fischer & R Lehmann (1998): Application of cineradiography for the metric and kinematic study of in−phase gaits during locomotion of the pika (*Ochotona rufescens*, Mammalia: Lagomorpha). − Zoology **101**: 12−37.

[5] MS Fischer & H Witte (1998): The functional morphology of the three−segmented limb of mammals and its specialities in small and medium−sized mammals. Proc Europ Mechanics Coll Euromech **375** Biology and Technology of Walking: 10–17.

[6] GA Cavagna, FP Saibene &R margaria (1964) Mechanical work in running − J Appl Physiol **19(2)** 249−256.

[7] GA Cavagna, NC Heglund & CR Taylor (1977): Mechanical work in terrestrial locomotion: two basic mechanisms for minimizing energy expenditure. − Am J Physiol **233**: 243−2.

[8] TA McMahon (1985): The role of compliance in mammalian running gaits. − J exp Biol **115**: 263−282.

[9] NA Bernstein (1967): The coordination and regulation of movements. Pergamon, London.

[10] R Blickhan (1989): The spring−mass model for running and hopping. − J Biomech **22(11/12)**: 1217−1227.

[11] CR Lee & C Farley (1998): Determinant of the center of mass in human walking and running. − J exp Biol **201(pt 21)**: 2935−2944.

[12] RJ Full and DE Koditschek (1999): Templates and anchors: neuromechanical hypotheses of legged locomotion on land. – J exp Biol **202(Pt 23)**, 3325–3332.

[13] TA McMahon & GC Cheng (1990): The mechanics of running: how does stiffness couple with speed? – J Biomech 23 (Suppl. 1): 65−78.

Proceedings of the International Symposium on
Adaptive Motion of Animals and Machines,
Montreal, Aug.8-12, 2000

Optimal Attitude Control for Articulated Body Mobile Robots

Edwardo F. Fukushima *and* **Shigeo Hirose**

Tokyo Institute of Technology, Dept. of Mechano-Aerospace Engineering,
2-12-1 Ookayama, Meguro-ku, Tokyo 152-8552, Japan
fukusima@mes.titech.ac.jp *and* hirose@mes.titech.ac.jp

Abstract

Optimal force distribution has been active field of research for multifingered hand grasping, cooperative manipulators and walking machines. The articulated body mobile robot "KORYU" composed of cylindrical segments linked in series and equipped with many wheels have a different mechanical topology, but it forms many closed kinematic chains through the ground and presents similar characteristics as the above systems. This paper introduces an attitude control scheme for the actual mechanical model "Koryu-II (KR-II)", which consists of optimization of force distribution considering quadratic object functions, combined with attitude control based on computed torque method. The validity of the introduced method is verified by computer simulations and experiments using the actual mechanical model KR-II.

1. Introduction

The authors have been developing a new type of mobile robot configuration called an "Articulated Body Mobile Robot". This class of robot has a snake-like configuration and is composed of many segments linked in series. This configuration introduces advantageous characteristics such as high rough terrain adaptability and load capacity, among others. Two mechanical models of articulated body mobile robot called KORYU (KR for short) have been developed and constructed, so far. KORYU was mainly developed for use in fire-fighting reconnaissance and inspection tasks inside nuclear reactors. However, highly terrain adaptive motions can be achieved by KR: 1) stair climbing, 2) passing over obstacles without touching them, 3) passing through meandering and narrow paths, 4) running over uneven terrain, and 5) using the body's degrees of freedom not only for "locomotion", but also for "manipulation". Many other related studies have been reported [3]-[10], but very few practical mechanical implementations are available.

The fundamental control strategies necessary for KORYU to perform the many inherent motion capabilities are: 1) Attitude Control; 2) Steering Control [1]; and 3) Mobile Manipulator Control [2]. This paper in particular address the attitude control problem.

Figure 1: KR-II moving on uneven terrain.

1.1. Attitude control problem description

KR-II is composed of cylindrical units (**Fig.2**(a)(b)) linked in series by prismatic joints which generate vertical motion between adjacent segments. These prismatic joints are force controlled so that each segment vertical position automatically adapts to the terrain irregularities, as shown in **Fig.3**(a). The most simple implementation of force control is to make these joints free to slide. However, in this case the system acts like a system of wheeled inverted pendulum carts connected in series and is unstable by nature, as shown in **Fig.3**(b). Thus, an attitude control scheme to maintain the body in the vertical posture is demanded. This work introduces a new attitude control based in optimal force distribution calculation using quadratic programming for minimization of joint energy consumption. As pointed out in detail in this paper, this method shares similarities with force distribution for multifingered hands, multiple coordinated manipulators and legged walking robots.

This paper is organized as follows: In Section 2 the background on optimal force distribution problem is described. Section 3 introduces the optimal force dis-

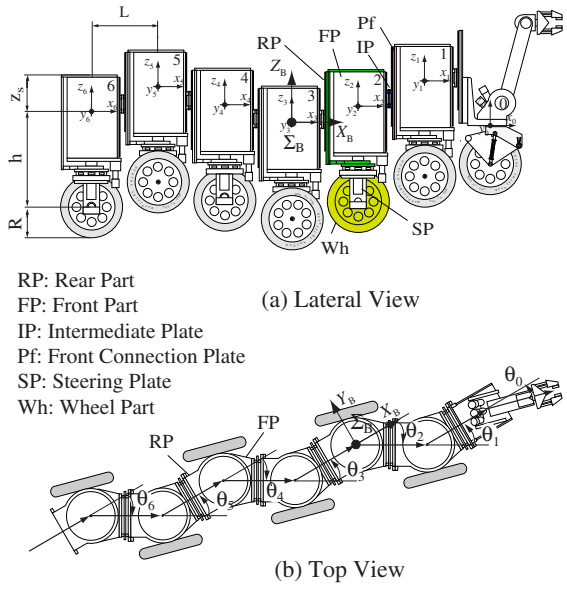

Figure 2: KR-II's mechanism and motion variables.

tribution formulation and shows an efficient algorithm to solve this problem. Section 4 presents the mechanical modeling of KR-II and introduces the feedback control law for attitude control. Finally in Section 5 the computer simulation and experimental results are shown to demonstrate the validity of the introduced method.

2. Background on Optimal Force Distribution Problem

Many types of force distribution problems have been formulated for multifingered hands, multiple coordinated manipulators and legged walking robots. A brief review of the fundamental concepts and similarities with formulation of balance equation and equations of motion of multibody systems are described.

2.1. Balance equations for the reference member

Multifingered hands, multiple coordinated manipulators and legged walking robots can be modeled as one *reference member* with k external contact points as shown in **Fig.4**(a). Consider the reference member parameters given by: mass m_0; linear and angular acceleration at the center of mass $\boldsymbol{\alpha}_0, \boldsymbol{\omega}_0 \in \boldsymbol{R}^3$; inertia tensor at the center of mass coordinate $\boldsymbol{H}_0 \in \boldsymbol{R}^{3\times 3}$; force $\boldsymbol{F}_i \in \boldsymbol{R}^3$and moment $\boldsymbol{M}_i \in \boldsymbol{R}^3$ acting on the ith contact point; position of the contact point with respect to the center of mass coordinate $\boldsymbol{p}_i = [\,p_{i1} \quad p_{i2} \quad p_{i3}\,]^T \in \boldsymbol{R}^3$. The resulting force and moment at the center of mass is given by $\boldsymbol{F}_0 = \sum_{i=1}^{k} \boldsymbol{F}_i \in \boldsymbol{R}^3$ and $\boldsymbol{M}_0 = \sum_{i=1}^{k} (\boldsymbol{M}_i + \boldsymbol{p}_i \times \boldsymbol{F}_i) \in \boldsymbol{R}^3$. The balance equations is given below, where the gravitational acceleration $\boldsymbol{g}$ which in principle is an external force, was included in the left term for simplicity of notation.

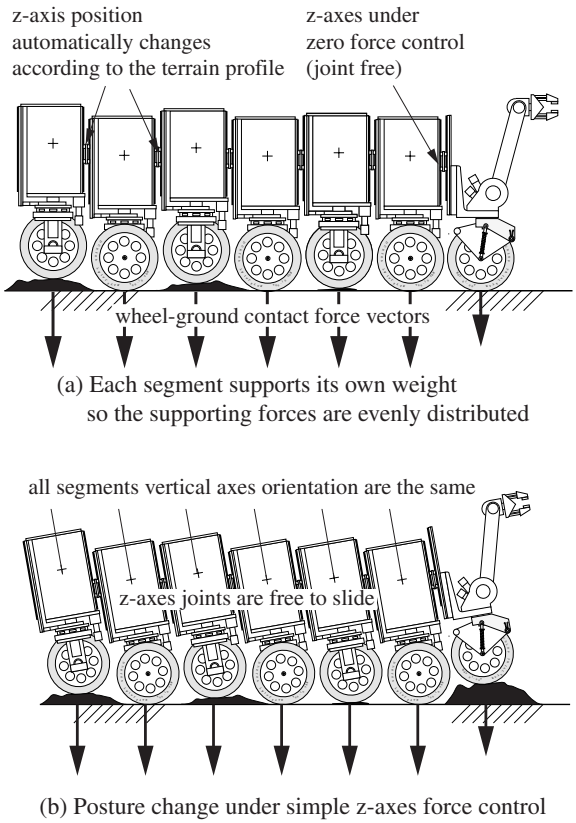

Figure 3: Effects of force control.

$$m_0\,(\boldsymbol{\alpha}_0 - \boldsymbol{g}) \;=\; \boldsymbol{F}_0 \qquad (1)$$

$$\boldsymbol{H}_0\,\dot{\boldsymbol{\omega}}_0 + \boldsymbol{\omega}_0 \times (\boldsymbol{H}_0\,\boldsymbol{\omega}_0) \;=\; \boldsymbol{M}_0 \qquad (2)$$

The inertial terms can be grouped as $\boldsymbol{Q} \in \boldsymbol{R}^6$, and the external force terms into the matrix $\boldsymbol{P}$ and vector of contact points $\boldsymbol{N}$,

$$\boldsymbol{P} \;=\; \begin{bmatrix} \boldsymbol{I}_3 & 0 & \cdots & \boldsymbol{I}_3 & 0 \\ \tilde{\boldsymbol{p}}_1 & \boldsymbol{I}_3 & \cdots & \tilde{\boldsymbol{p}}_k & \boldsymbol{I}_3 \end{bmatrix} \in \boldsymbol{R}^{6\times 6k} \qquad (3)$$

$$\tilde{\boldsymbol{p}}_i \;=\; \begin{bmatrix} 0 & -p_{i3} & p_{i2} \\ p_{i3} & 0 & -p_{i1} \\ -p_{i2} & p_{i1} & 0 \end{bmatrix} \in \boldsymbol{R}^{3\times 3}$$

$$\boldsymbol{I}_3 \;\in\; \boldsymbol{R}^{3\times 3} : \text{Identity Matrix}$$

$$\boldsymbol{N} = [\,\boldsymbol{F}_1^T \quad \boldsymbol{M}_1^T \quad \cdots \quad \boldsymbol{F}_k^T \quad \boldsymbol{M}_k^T\,]^T \in \boldsymbol{R}^{6k} \qquad (4)$$

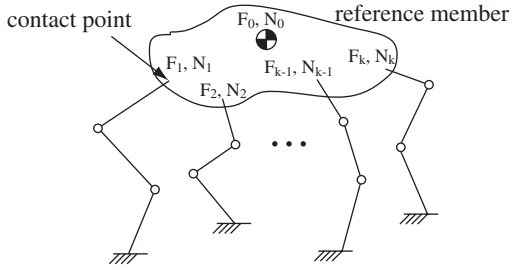

(a) Multifingered hands, multiple coordinated manipulators and legged walking robots

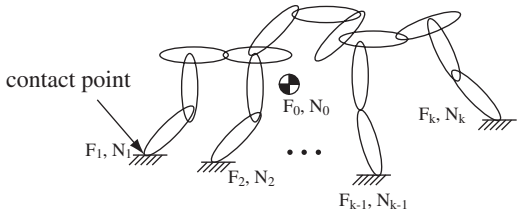

(b) A general multibody system (KR included)

Figure 4: Comparison of single and multibody systems.

Thus the balance equations are described by the following linear relation.

$$\boldsymbol{Q} = \boldsymbol{P}\,\boldsymbol{N} \tag{5}$$

2.1.1. General solution

The general solution of Equation (5) with respect to $\boldsymbol{N}$ is given by

$$\boldsymbol{N} = \boldsymbol{P}^{+}\boldsymbol{Q} + (\boldsymbol{I} - \boldsymbol{P}^{+}\boldsymbol{P})\boldsymbol{\lambda} \tag{6}$$

as described in reference [12], where $\boldsymbol{P}^{+}$ is a generalized pseudo-inverse matrix.

Basic formulation of force distribution and description about internal forces concepts were first addressed by Kerr and Roth [11]. The fundamental concepts are: i) the general solution can be divided in two orthogonal vectors $\boldsymbol{N} = \boldsymbol{N}_e + \boldsymbol{N}_i$; ii) the partial solution $\boldsymbol{N}_e$ can be solved by $\boldsymbol{N}_e = \boldsymbol{P}^{+}\boldsymbol{Q}$ using the pseudo-inverse matrix; iii) the partial solution $\boldsymbol{N}_i$ resides in the null-space of $\boldsymbol{P}$ and corresponds to the internal forces; iv) $(\boldsymbol{I} - \boldsymbol{P}^{+}\boldsymbol{P})$ is a matrix formed by orthonormal basis vectors which span the null space of $\boldsymbol{P}$, and $\boldsymbol{\lambda}$ corresponds to the magnitude of the internal forces. Kerr and Roth used these concepts to formulate a linear programming problem which took in account friction forces at contact points and also joint driving forces.

Force distribution problem for gripper and hands usually results in searching optimal values for $\boldsymbol{\lambda}$. Nakamura et al were the first to formulate a nonlinear problem using quadratic cost function $\|\boldsymbol{N}\|$ to solve the internal forces [13]. Efficient solutions using linear programming were also analyzed by other authors [14][16]. Nahon and Angeles [15] showed that minimization of internal forces and joint torques can both be formulated in an efficient quadratic programming method, and Goldfarb and Idnami method [19] can be used to solve this problem. Other efficient formulations are also been investigated [17][18].

2.2. Multibody systems

Multibody systems differ from multifingered hands as shown in **Fig.4**(a)(b) not only by the fact that in general they have no commom reference member, but also because that forces and moments $\boldsymbol{F}_i, \boldsymbol{M}_i$ acting in the contact points arises from different phisical natures. In system (a) the external forces are exerted from the fingers, manipulators or legs. However, system (b) can not have external forces exerted from the ground. Instead, the forces and moments at the contact points are originated from the gravitational acceleration and internal motion of the system itself. However, balance equations and equations of motion for these systems present similar characteristics as described next.

2.2.1. Balance equations

Let the variables k, $\boldsymbol{F}_i$, $\boldsymbol{M}_i$, $\boldsymbol{p}_i$ be defined the same in **Fig.4**(a)(b), the Equations (3)(4) are valid for both systems, but Equations (1)(2) due to inertial forces are not. However, the total force acting on the systems's center of mass can be derived as $\boldsymbol{Q}(\boldsymbol{q}, \dot{\boldsymbol{q}}, \ddot{\boldsymbol{q}})$, i.e., as function of generalized coordinate $\boldsymbol{q}, \dot{\boldsymbol{q}}, \ddot{\boldsymbol{q}}$. Hence, the balance equations can be described by

$$\boldsymbol{Q}(\boldsymbol{q},\ \dot{\boldsymbol{q}},\ \ddot{\boldsymbol{q}}) = \boldsymbol{P}\,\boldsymbol{N} \tag{7}$$

Equations (7) and (5) are mathematically equivalent, and therefore the fundamental theory discussed in section 2.1.1 can also be applied to multibody systems.

2.2.2. Equations of motion

For the system in **Fig.4**(a), the problem of finding optimal values for contact forces $\boldsymbol{N}$ and joint forces $\boldsymbol{\tau}$ can be independently formulated. However, the equations of motion can also be grouped as Equation (8) for optimization of joint forces of the entire system [12].

$$\boldsymbol{\tau} = \boldsymbol{H}\ddot{\boldsymbol{q}} + \boldsymbol{C} + \boldsymbol{G}_g + \boldsymbol{J}^{T}\boldsymbol{N} \tag{8}$$

It is well known that Equation (8) has the same structure for robot manipulators and multibody-systems where $\boldsymbol{H}$ is the inertial term, $\boldsymbol{C}$ the coriolis and cen-

trifugal term, $\boldsymbol{G}_g$ the gravitational term, and $\boldsymbol{J}$ is the Jacobian matrix. Therefore, the equations of motion for systems in **Fig.4**(a) and (b) are mathematically equivalent.

3. Efficient Algorithm for Solving Optimal Force Distribution Problem

3.1. Cost function

Electrical motor's energy consumption at low speed but high output torque operation can be estimated by the power loss in the armature resistance. Hence, the sum of squares of joint forces $\boldsymbol{\tau}$ can be used as the cost function to be minimized.

$$S(\boldsymbol{\tau}) \quad = \quad \boldsymbol{\tau}^T \boldsymbol{W} \boldsymbol{\tau} \tag{9}$$

Note that $\boldsymbol{W}$ is a symmetric positive definite matrix. Now let $\boldsymbol{H}_q = \boldsymbol{H}\ddot{\boldsymbol{q}} + \boldsymbol{C} + \boldsymbol{G}_g$, $\boldsymbol{G} = 2\boldsymbol{J}\boldsymbol{W}\boldsymbol{J}^T$ and $\boldsymbol{d} = 2\boldsymbol{J}\boldsymbol{W}\boldsymbol{H}_q$ be defined as auxiliary variables. Substituting Equation (8) into (9) results in

$$S(\boldsymbol{\tau}) \quad = \quad \boldsymbol{H}_q^T \boldsymbol{W} \boldsymbol{H}_q + \boldsymbol{d}^T \boldsymbol{N} + \frac{1}{2} \boldsymbol{N}^T \boldsymbol{G} \boldsymbol{N} \tag{10}$$

a new cost function depending on the variable $\boldsymbol{N}$.

3.2. Quadratic problem formulation

The first term in the right side of Equation (10) does not depend on $\boldsymbol{N}$, so the new const function can be described by Equation (11). A general quadratic programming problem can now be formulated as Equations (11)(12)

$$\underset{\boldsymbol{N}}{min.}: \quad S(\boldsymbol{N}) = \boldsymbol{d}^T \boldsymbol{N} + \frac{1}{2} \boldsymbol{N}^T \boldsymbol{G} \boldsymbol{N} \tag{11}$$

$$\text{subject to:} \left\{ \begin{array}{rcl} \boldsymbol{P}_e \boldsymbol{N} & = & \boldsymbol{Q}_e \\ \boldsymbol{P}_i \boldsymbol{N} & \geq & \boldsymbol{Q}_i \end{array} \right. \tag{12}$$

Equations (12) are linear constraint equations, with equality constraints given by Equations (5) or (7), and inequality constraints given by the system's friction, contact and joint force limitations. A positive definite matrix $\boldsymbol{W}$ guarantees this problem to be strictly convex, thus having efficient solution algorithms [19].

3.3. Solution considering equality constraints

The partial problem when considering only equality constraints can be solved as

$$\boldsymbol{N}_e = \boldsymbol{P}_e^+ \boldsymbol{Q}_e - \boldsymbol{H}_e \, \boldsymbol{d} \tag{13}$$

with generalized pseudo-inverse matrix $\boldsymbol{P}_e^+$ defined as

$$\boldsymbol{P}_e^+ = \boldsymbol{G}^{-1} \boldsymbol{P}_e^T (\boldsymbol{P}_e \boldsymbol{G}^{-1} \boldsymbol{P}_e^T)^{-1} \tag{14}$$

and auxiliary matrix $\boldsymbol{H}_e$ defined as

$$\boldsymbol{H}_e = (\boldsymbol{I} - \boldsymbol{P}_e^+ \boldsymbol{P}_e) \boldsymbol{G}^{-1} \tag{15}$$

From the observation that the first term of Equation (13) corresponds to the norm of $\boldsymbol{N}$, i.e., the solution which minimizes $\boldsymbol{N}^T \boldsymbol{G} \boldsymbol{N}$, the second term is the partial solution which minimizes the norm of $\boldsymbol{\tau}$. Note that although it resides in the null-space of $\boldsymbol{P}_e$ an analytic solution is available.

3.4. Solution considering inequality constraints

Problems with inequality constraints usually do not have analytical solutions but use some kind of search algorithms [13][15][19]. In order to achieve better real-time performance, only negative contact forces will be considered in this formulation. This is valid for hands, grippers, walking machines and mobile robots in general, that can exert positive forces, i.e., "push", but can not exert negative forces, i.e., "pull". The proposed method introduces a new equality constraints term $\boldsymbol{P}_d \boldsymbol{N} = \boldsymbol{Q}_d \in \boldsymbol{R}^d$ into the balance Equation $\boldsymbol{P}\boldsymbol{N} = \boldsymbol{Q}$,

$$\boldsymbol{P}_e \quad = \quad [\boldsymbol{P}^T \quad \boldsymbol{P}_d^T]^T \tag{16}$$

$$\boldsymbol{Q}_e \quad = \quad [\boldsymbol{Q}^T \quad \boldsymbol{Q}_d^T]^T \tag{17}$$

The basic idea is to transform the problem with inequality constraints into a problem with only equality constraints that can be solved efficiently by Equation (13). This is accomplished by the algorithm described below. Note that the variable d represents the number of contact points included in the equality constraints.

Step 0. Initialization: case $d_0 > 0$ make $d = d_0$ and include the contact forces $\boldsymbol{P}_d \boldsymbol{N} = \boldsymbol{Q}_d \in \boldsymbol{R}^{d_0}$ into Equations (16)(17). Case $d_0 = 0$, initialize $\boldsymbol{P}_e = \boldsymbol{P}$ and $\boldsymbol{Q}_e = \boldsymbol{Q}$.

Step 1. Calculate the partial solution $\boldsymbol{N}_e$ considering only equality constraints from Equation (13).

Step 2. Let the number of negative contact forces in the solution $\boldsymbol{N}_e$ be d_n. Case $d_n > 0$ go to *Step 3.* Otherwise, this is the optimal solution. Calculate joint forces by Equation (18). Finish.

$$\boldsymbol{\tau}_e = \boldsymbol{H}_q + \boldsymbol{J}^T \boldsymbol{N}_e \tag{18}$$

Step 3. Update $d = d + d_n$. Case $d \leq$ (free variables − balance equations) go to *Step 4*. Otherwise the problem can not be solved. Finish.

Step 4. Set the desired contact force at the contact points where resulted in negative forces to zero and include in the equality constraint $\boldsymbol{P}_d\boldsymbol{N} = \boldsymbol{Q}_d$. Return to *Step 1*.

Although this algorithm is suited for real time applications, it does not search for all the combination of possible solutions. For this reason it might finish in *Step 3.* even a possible solution exists. However, for normal steering control, passing-over pipes and ditches, and attitude control of KR-II, a possible solution was always found after a limited number of iterations. An example will be later described in Section 5.

4. KR-II's Attitude Control

4.1. KR-II's variables

KR-II's motion freedoms can be grouped as: z-axes linear displacements $\boldsymbol{z} = [z_1 \quad z_2 \quad \cdots \quad z_6]^T \in \boldsymbol{R}^6$; θ-axes angular displacements $\boldsymbol{\theta} = [\theta_0 \quad \theta_1 \quad \cdots \quad \theta_6]^T \in \boldsymbol{R}^7$; wheel's angular displacements $\boldsymbol{s} = [s_0 \quad s_1 \quad \cdots \quad s_6]^T \in \boldsymbol{R}^7$; body's coordinate position $\boldsymbol{c}_0 = [x_0 \quad y_0 \quad z_0]^T$ and attitude $\boldsymbol{\phi} = [\phi_X \quad \phi_Y \quad \phi_Z]^T$ relative to the inertial coordinate. This accounts for 26 degrees of freedom. KR-II's inertial parameters are listed in **Table 1**. Note that the extra loads were accounted in the body's front part (FP).

In this work, balance and motion equations given by Equations (7)(8) were derived by Newton-Euler method, but other efficient virtual power methods [7] can also be used.

4.2. Simplifications

4.2.1. *Wheel modeling*

The wheel will be simplified to a simple model:

1. It is a thin circular plate with constant radius.
2. It contacts a horizontal plane even when moving on slopes.

However, the horizontal plane is set independently for each wheel so that this simplification is effective for motion over uneven terrains. Nonetheless, for stair climbing and step overcoming motions, a better contact point estimation algorithm is under investigation.

Table 1: KR-II's inertial parameters.

Seg	Part	mass [kg]	Inertia[kg m^2]			mass center [mm]		
			I_x	I_y	I_z	p_x	p_y	$-p_z$
0	FP	5.0	0.04	0.04	0.01	120	0	300
	SP	28.0	0.24	0.24	0.07	0	0	570
	RP	10.8	0.40	0.30	0.08	-100	0	270
	Wh	3.6	0.12	0.06	0.12	0	0	778
1	FP	35.4	1.27	1.27	0.42	64	9	273
2	FP	41.7	1.73	1.71	0.45	54	17	227
3	FP	32.1	1.27	1.28	0.35	70	0	278
4	FP	45.6	1.64	1.71	0.45	46	17	229
5	FP	31.6	1.11	1.13	0.35	70	0	291
6	FP	40.2	1.60	1.60	0.46	56	0	241
1∼5	RP	9.5	0.24	0.19	0.05	-230	0	170
6	RP	4.2	0.11	0.09	0.02	-225	0	186
	IP	4.5	0.04	0.01	0.03	218	0	150
1∼6	SP	7.2	0.03	0.04	0.03	0	80	744
	Wh	3.6	0.12	0.06	0.12	0	240	778

(Parts abbreviations)
FP: front part
RP: rear part
IP: intermediate plate
SP: steering plate
Wh: wheel part

(Extra internal loads [kg])
Seg1: extra servo-amp (5.8)
Seg2: on-board computer (12.1)
Seg3: attitude sensor (2.5)
Seg4: battery-pack (16.0)
Seg5: DC-DC converter (2.0)
Seg6: AC-DC converter (10.6)

4.2.2. *Other simplifications*

1. **External contact forces:** the wheel's lateral and longitudinal forces are small because optimal trajectory are planned by the steering control [1] and also abrupt acceleration and deceleration are avoided. Moreover, moments between the tire and the ground are also negligible. For these reasons, the tire normal force F_{zi} can be considered the only external force acting on the system. Hence the external contact force vector is given by

$$\boldsymbol{N} = [F_{z0} \quad F_{z1} \quad \cdots \quad F_{z6}]^T \in \boldsymbol{R}^7 \qquad (19)$$

2. **Joint forces:** z-axes and θ-axes motions can be independently planned because KR's z-axes orientations are controlled to be always vertical. In fact, θ-axes are position controlled and their desired angular displacements are planned by the steering control [1]. On the other hand, although s-axes motion can be used for the attitude control, it would involve undesirable acceleration and deceleration in the system. For these reasons, z-axes forces will be set as the variables to be optimized.

$$\boldsymbol{\tau} = [f_{z0} \quad f_{z1} \quad \cdots \quad f_{z6}]^T \in \boldsymbol{R}^7 \qquad (20)$$

Note that f_{z0} was included just for avoiding singularity in the calculation, but always result in $f_{z0} = 0$.

3. **Balance equations:** from the above considerations, force balance in the z direction and moment balance around x and y direction are enough to model our system. Hence, the dimension of the balance Equation $\boldsymbol{P}\,\boldsymbol{N} = \boldsymbol{Q}$ becomes $\boldsymbol{Q} \in \boldsymbol{R}^3$ and $\boldsymbol{P} \in \boldsymbol{R}^{3\times 7}$.

4. **Generalized accelerations:** only a part of the 26 degrees of freedom of KR-II, $\boldsymbol{q}_s = [\,\boldsymbol{z}^T \quad \boldsymbol{\theta}^T \quad \phi_X \quad \phi_Y\,]^T$ and its time derivative $\dot{\boldsymbol{q}}_s = [\,\dot{\boldsymbol{z}}^T \quad \dot{\boldsymbol{\theta}}^T \quad \dot{\phi}_X \quad \dot{\phi}_Y\,]^T$ is used in the calculation. The acceleration variables are further simplified to

$$\ddot{\boldsymbol{q}}_a = [\,\ddot{x}_0 \quad \ddot{y}_0 \quad \ddot{z}_0 \quad \ddot{\phi}_X \quad \ddot{\phi}_Y\,]^T \tag{21}$$

and used as $\ddot{\boldsymbol{q}} \equiv \ddot{\boldsymbol{q}}_a$.

5. **Other parameters:** other dimensions are as follows: $\boldsymbol{H} \in \boldsymbol{R}^{7\times 5}$; $\boldsymbol{C} \in \boldsymbol{R}^7$; $\boldsymbol{G}_g \in \boldsymbol{R}^7$; $\boldsymbol{J} \in \boldsymbol{R}^{7\times 7}$; $\boldsymbol{P}_d \in \boldsymbol{R}^{d\times 7}$; $\boldsymbol{Q}_d \in \boldsymbol{R}^d$.

4.3. Attitude feedback law

The formulation described so far, solves for joint forces which balance the system in a given desired posture. This is fundamentally an inverse dynamics problem. A feedback control law shown below is added into Equation (21)

$$\ddot{\phi}_X = \ddot{\phi}_{X_d} + K_{P_X}(\phi_{X_d} - \phi_{X_m}) - K_{D_X}\dot{\phi}_{X_m} \tag{22}$$
$$\ddot{\phi}_Y = \ddot{\phi}_{Y_d} + K_{P_Y}(\phi_{Y_d} - \phi_{Y_m}) - K_{D_Y}\dot{\phi}_{Y_m} \tag{23}$$

where K_P, K_D are proportional and derivative gain and the indexes d, m stands for desired and measured values. This control law is equivalent to the (*Computed Torque Method*)[20] so that the closed-loop system stability can be analyzed in the same way.

5. Computer Simulation and Experimental Results

Computer simulation and experiment using the real robot KR-II, were evaluated for an "obstacle passing over (without touching them)" where a box shape obstacle with width 300mm and height 150mm was considered. This motion was performed at a constant forward velocity of 100mm/s. The vertical motion of each segment is shown in **Fig.5**(a). Note that the calculated displacement includes a 10mm displacement for safety, resulting in a 160mm total vertical displacement.

5.1. Continuity of calculated forces

Discontinuities in the calculated forces occurs when topological changes are caused by lifting-up or touching-down of the wheels. In this paper these discontinuities are avoided by introducing desired contact forces using the equality constraints $\boldsymbol{P}_d\boldsymbol{N} = \boldsymbol{Q}_d$ in *Step 0*. The desired forces when lifting-up is given as

$$F_{d_n} = F_{Up_n}\frac{(50 - Z_n)}{50} \tag{24}$$

and when touching-down the ground is given as

$$F_{d_n} = F_{Down_n}\frac{(50 - Z_n)}{50} \tag{25}$$

F_{Up_n} is the optimal force calculated just before the wheel lift-up, F_{Down_n} is the optimal force calculated considering that the wheel has completely touch-down the ground, Z_n is the segment vertical diplacement as shown in **Fig.5**(a). These equations are applied only in the interval $Z_n = 0 \sim 50$mm. The constant 50 was derived considering KR-II's spring suspension stroke. For vertical displacements above 50, the desired contact force is set to zero. The simulation results shown in **Fig.5**(b)-(c) demonstrate the validity of the proposed method.

5.2. Experimental results

The experiment was held applying the feedforward command shown in **Fig.5**(c) and feedback command given by Equations (22) and (23). The feedback gains were $K_{P_X} = 65$, $K_{D_X} = 18$, $K_{P_Y} = 95$, $K_{D_Y} = 16$ and all the computation were performed in real-time with a sampling-time of 20ms using a 486DX2-50MHz CPU based PC. The experiment overview is shown in **Fig.6**.

Fig.7(a) shows the performance of attitude control. Large attitude changes occur at times when more than one segment is lifted-up at the same time, but the overall performance is acceptable for finishing the passing-over motion. The sum of squares of z-axes joint forces measured during the experiment is shown in **Fig.7**(b), which has the same tendency as the simulation result in **Fig.5**(d).

6. Summary and Conclusions

An attitude control scheme based in optimal force distribution using quadratic programming, which minimize joint energy consumption was derived in this paper. Similarities with force distribution for multifingered hands, multiple coordinated manipulators and

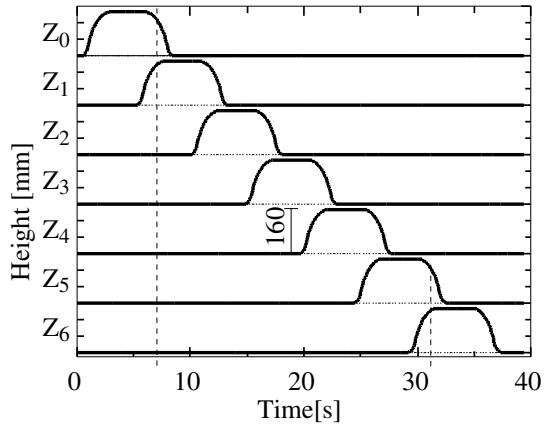

(a) Wheels vertical displacements

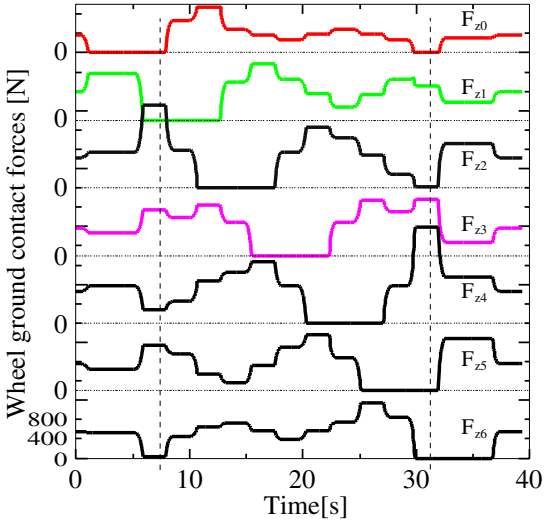

(b) Wheel-ground contact forces

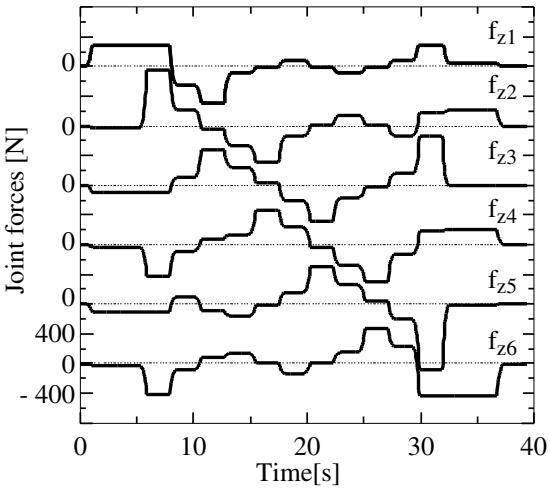

(c) z-axes joint forces

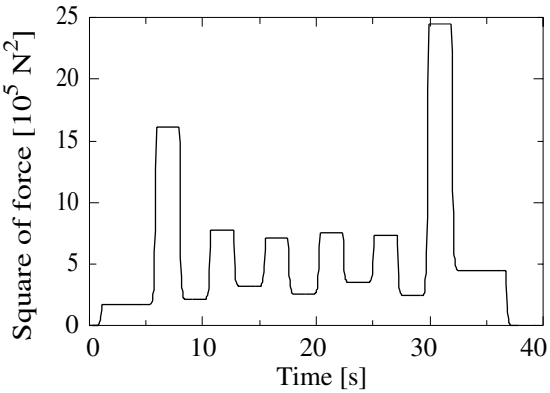

(d) Sum of squares of z-axes joint forces

Figure 5: Obstacle passing over simulation.

legged walking robots were demonstrated. The attitude control scheme was introduced inside this force distribution problem, and successfully implemented for control of the articulated body mobile robot KR-II. Validity and effectiveness of proposed methods were verified by computer simulation and also experimentally using the actual mechanical model KR-II.

References

[1] E. F. Fukushima, S. Hirose, "Efficient Steering Control Formulation for The Articulated Body Mobile Robot "KR-II"," *Autonomous Robots*, Vol. 3, No. 1, pp. 7-18, 1996.

[2] E. F. Fukushima, S. Hirose, and T. Hayashi, "Basic Manipulation Considerations For The Articulated Body Mobile Robot," *Proc. of the 1998 IEEE/RSJ Int. Conf. on Intelligent Robotics and Systems*, pp. 386-393, 1998.

[3] K. J. Waldron, V. Kumar and A. Burkat: "An actively coordinated mobility system for a planetary rover," *Proc. 1987 ICAR*, pp.77-86, 1987.

[4] Commissariat A I'Energie Atomique: "Rapport d'activite 1987," *Unité de Génie Robotique Avancé*, France, 1987.

[5] J. W. Burdick, J. Radford and G. S. Chirikjian: "Hyper-redundant robots: kinematics and experiments," *International Symposium on Robotics Research*, pp.1-16, 1993.

[6] D. Tilbury, O. J. Sordalen and L. Bushnell: "A Multisteering Trailer System: Conversion

Figure 6: Experiment overview.

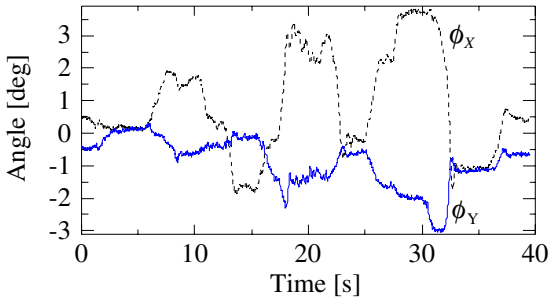

(a) Attitude displacements

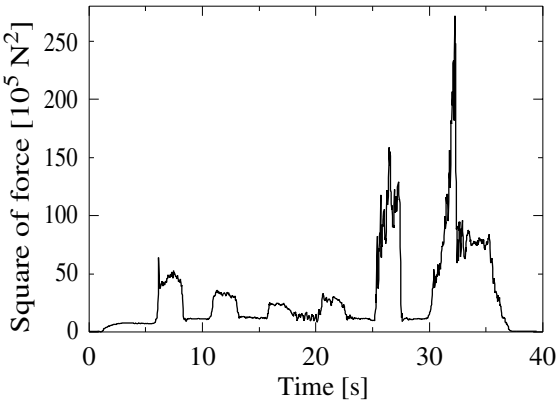

(b) Sum of squares of z-axes joint forces

Figure 7: Obstacle passing over experiment results.

into Chained Form Using Dynamic Feedback," *IEEE Transactions on Robotics and Automation*, Vol.11, No.6, pp.807-818, 1995.

[7] K. Thanjavur and R. Rajagopalan: "Ease of Dynamic Modelling of Wheeled Mobile Robots (WMRS) using Kane's Approach," *Proc. of IEEE Intl. Conference on Robotics and Automation*, pp.2926-2931, 1997.

[8] Y. Shan and Y. Koren: "Design and Motion Planning of a Mechanical Snake," *IEEE Transactions on System, Man and Cybernetics*, Vol.23, No.4, pp.1091-1100, 1993.

[9] Martin Nilsson, "Snake Robot Free Climbing," *Proc. IEEE Intl. Conference on Robotics and Automation*, pp.3415-3420, 1997.

[10] G. Migads and J. Kyriakopoulos, "Design and Forward Kinematic Analysis of a Robotic Snake," *Proc. IEEE Intl. Conference on Robotics and Automation*, pp.3493-3497, 1997.

[11] Jeffrey Kerr and Bernard Roth, "Analysis of Multifingered Hands," *The Intl. Journal of Robotics Research*, Vol.4, No.4, pp.3-17, 1986.

[12] Ian D. Walker, Robert A. Freeman and Steven I. Marcus: "Dynamic Task Distribution for Multiple Cooperating Robot Manipulators," *Proc. IEEE Intl. Conf. on Robotics and Automation*, pp.1288-1290, 1988.

[13] Y. Nakamura, K. Nagai, T. Yoshikawa: "Dynamics and Stability in Coordination of Multiple Robotic Mechanisms," *The Intl. Journal of Robotics Research*, Vol.8, No.2, pp.44-61, 1989.

[14] F. T. Cheng and D. E. Orin, "Optimal Force Distribution in Multiple-Chain Robotic Systems," *IEEE Transactions on Systems, Man, and Cybernetics*, Vol. 21, No.1, pp. 13-24, 1991.

[15] Meyer A. Nahon and Jorge Angeles, "Real-Time Force Optimization in Parallel Kinematic Chains under Inequality Constraints," *IEEE Trans. on Robotics and Automation*, Vol.8, No.4, pp.439-450, Aug. 1992.

[16] M. Buss, H. Hashimoto and J. Moore, "Dextrous Hand Grasping Force Distribution," *IEEE Transactions on Robotics and Automation*, Vol.12, No.3, pp.406-418, 1996.

[17] Jeng-Shi Chen, Fan-Tien Cheng, Kai-Tarng Yang, Fan-Chu Kung and York-Yin Sun, "Solving the Optimal Force Distribution Problem in Multilegged Vehicles," *Proc. of the 1998 IEEE Intl. Conf. on Robotics and Automation*, pp.471-476, Belgium, May 1998.

[18] Duane W. Markefka and David E. Orin, "Quadratic Optimization of Force Distribution in Walking Machines," *Proc. of the 1998 IEEE Intl. Conf. on Robotics and Automation*, pp.477-483, Belgium, May 1998.

[19] D. Goldfarb, A. Idnami, "A numerically stable dual method for solving strictly convex quadratic programs", *Math. Programming*, Vol. 27, pp.1-33, 1983.

[20] B. R. Markiewics, "Analysis of the Computer Torque Drive Method and Comparison with Conventional Position Servo for a Computer-Controlled Manipulator," *Jet Propulsion Laboratory, California Institute of Technology*, TM 33-601, March 1973.

Session

Behavior and Motion of Humans & Humanoids

Proceedings of the International Symposium on
Adaptive Motion of Animals and Machines,
Montreal, Aug.8-12, 2000

Analysis of Hemiparetic Gait by Using Mechanical Models

Ch. Lutzenberger[1], **F. Pfeiffer**[1]

[1]Lehrstuhl B für Mechanik, Technische Universität München, D-85747 Garching
cl@lbm.mw.tu-muenchen.de, pfeiffer@lbm.mw.tu-muenchen.de

Abstract

Clinical gait analysis is applied to analyse the disturbed gait pattern of a patient and to define a suitable therapy. Up to now, mostly measured kinematic gait parameters are considered. The usefulness of kinetic quantities has been recognised, but only scarcely applied. This paper presents a method, derived from robotics, to calculate kinetic quantities of human gait without using expensive force platforms. Kinetic quantities help to better analyse the disturbed gait pattern, to refine diagnosis and assess outcome of therapy. The application of this method in a neurological clinic for analysis of hemiparetic gait is shown.

1. Introduction

Hemiparesis with violent impairment of motricity of one side of the body occurs after stroke or skull-brain trauma. At the beginning and during rehabilitation hemiparetic patients undergo analysis of their gait. In clinical gait analysis the pathological state of the disturbed gait pattern is evaluated first qualitatively and quantitatively, in order to obtain a diagnosis and to determine a suitable therapy. Up to now mostly temporal variables such as stride length, gait speed, walking symmetry [1], kinematic quantities such as joint angles [2] and electromyograms [3] were considered. Despite a large amount of studies, the analysis of kinetic quantities like joint torques, power, work and ground reaction forces was considered only in few studies [4]. The reason therefore resides in the great effort to determine kinetic quantities, because they cannot be directly measured but have to be calculated by inverse models using expensive force platforms. Kinetic quantities, however, enable a further refinement of diagnosis and a better understanding of pathological gait. [5] point out, that kinetic quantities significantly help to separate primary abnormalities (caused by the neurological deficit) from secondary abnormalities (adaptations to circumvent the primary). [6] emphasises, that a multifactorial gait analysis, where kinematic, kinetic and myographic quantities are analysed should be aspired. Furthermore investigations about progression of rehabilitation and specific therapies are missing [4], [7]. [8] describes a method in robotics, which calculates and optimises kinetic quantities when the trajectory of the robot is given.

2. Mechanical Model

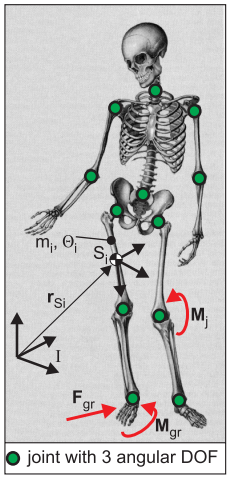

Figure 1: Mechanical model

The human locomotor apparatus is modelled as a three-dimensional system of multiple rigid bodies, connected by ideal ball-and-socket links. Segmentation of the human body respects the anatomy of the locomotor apparatus and the characteristics of human walking. Figure 1 shows the mechanical model, consisting of 13 segments and 12 links, each with 3 degrees of freedom (DOF). With 6 DOF for the trunk, defining its position and orientation in space, the model comprises 42 DOF. The joints are assumed frictionless. A coordinate frame is assigned to each segment, the x axis pointing in the anatomical (upright standing) position forward, the y axis upward and the z axis laterally. In the anatomical position, the coordinate axes of the segments are parallel. The sequence of rotation of each joint is internal/external rotation - adduction/abduction - flexion/extension [9]. The origin of the coordinate system lies in the center of mass of each segment.

The segments are described by their mass, moment of inertia with respect to the body fixed coordinate axes, the vector to the center of gravity and the vector to the distal link. Muscles are not taken into consideration, therefore the mechanical model of the human locomotor apparatus is just a skeletal one.

Several external forces and torques act on the human body when walking, see figure 1. Ground reaction forces $\boldsymbol{F}_{gr}$ and torques $\boldsymbol{M}_{gr}$, which result from the interaction of the foot with the floor, act on the foot in contact. Joint torques $\boldsymbol{M}_j$ summarise all the torques which are generated by the joint spanning muscles.

The mass and inertia properties of the legs and arms are calculated by approximating their shapes with geometric bodies and using average body densities, as described by [10]. By this means, the thigh, shank, upper and underarm are approximated by frustums with circular sections. For the trunk, pelvis, feet and head the regression equations of [11] and [12] are used. By this means the general model of the locomotor apparatus is adapted to each patient. The use of this technique is obligatory because parameters of subjects vary within a wide range, e.g. hemiplegics after stroke who suffer from heavy reductions of the muscle mass in contrast to healthy well-trained persons.

3. Mathematical Formulation

The dynamics of the locomotor apparatus is described in configuration space by the equations of motion. The Newton-Euler method, see [13], with the reference points in the centers of gravity of the segments yields

$$\begin{aligned} \boldsymbol{M}(\boldsymbol{q},t)\,\ddot{\boldsymbol{q}}(t) \quad - \quad \boldsymbol{h}(\boldsymbol{q},\dot{\boldsymbol{q}},t) = \sum_{i=1}^{2} \Big(\boldsymbol{J}_{T,i}^{T}\,\boldsymbol{F}_{gr,i} + \\ + \quad \boldsymbol{J}_{R,i}^{T}\,\boldsymbol{M}_{gr,i} \Big) + \sum_{k=1}^{12} \boldsymbol{J}_{R,k}^{T}\,\boldsymbol{M}_{j,k} \end{aligned} \tag{1}$$

The vectors $\boldsymbol{q}, \dot{\boldsymbol{q}}, \ddot{\boldsymbol{q}} \in \mathbb{R}^{42}$ denote the generalized coordinates, velocities and accelerations, $\boldsymbol{M} \in \mathbb{R}^{42\times 42}$ is the mass matrix and accounts for the inertial properties of the system, $\boldsymbol{h} \in \mathbb{R}^{42}$ contains all gravitational and gyroscopic forces and torques. As above mentioned, muscle properties are not taken into consideration. Consequently the external forces acting on the multibody system, see figure 1, are the ground reaction forces $\boldsymbol{F}_{gr,i} \in \mathbb{R}^3$ and torques $\boldsymbol{M}_{gr,i} \in \mathbb{R}^3$ and the 12 joint torques $\boldsymbol{M}_{j,k} \in \mathbb{R}^3$, which are multiplied with the corresponding Jacobian matrices of translation $\boldsymbol{J}_T \in \mathbb{R}^{3\times 42}$ and rotation $\boldsymbol{J}_R \in \mathbb{R}^{3\times 42}$.

The equations of motion (eq. (1)) can be solved in two different ways. First, assuming given forces and torques, the movement of the body is computed using numerical integration (direct dynamics). Unfortunately, control laws to compute forces and torques of normal and impaired human walking are unknown. Therefore only the second method, called inverse dynamics, can be used. Inverse dynamics method supposes given movement and yields forces and torques.

In single support phase, when only one foot is on the ground, we deal with one ground reaction force and one ground reaction moment. Assuming given generalized coordinates and their derivatives, eq. (1) yields 42 known quantities on the left side. 3 components of $\boldsymbol{F}_{gr}$, 3 of $\boldsymbol{M}_{gr}$ and 3 of the 12 joint torques lead to 42 unknowns on the right side. We calculate the unknown quantities by matrix inversions and multiplications.

In double support phase, when both feet are on the ground, we deal with 2 unknown ground reaction forces and torques and 36 unknown joint torques, so that the number of unknowns (48) exceeds the number of available equations. Additional equations are delivered using optimization techniques, when we require that some objective functions has to be minimized. Since human walking is an optimized movement, not only the equations of motion have to be fulfilled, but also biological principles have to be taken into account. This method has already been applied to the walking cycle of a grasshopper by [14]. We assume the optimization criterion C linear in the squares of the unknown forces and torques:

$$\begin{aligned} C \quad = \quad & f\left(\boldsymbol{F}_{gr}^{2}, \boldsymbol{M}_{gr}^{2}, \boldsymbol{M}_{j}^{2}\right) = \frac{1}{2}\boldsymbol{F}_{gr}^{T}\boldsymbol{C}_1\boldsymbol{F}_{gr} + \\ + \quad & \frac{1}{2}\boldsymbol{M}_{gr}^{T}\boldsymbol{C}_2\boldsymbol{M}_{gr} + \frac{1}{2}\boldsymbol{M}_{j}^{T}\boldsymbol{C}_3\boldsymbol{M}_{j} \end{aligned} \tag{2}$$

with the matrices $\boldsymbol{C}_i$ which weight the forces and torques.

The Lagrange multiplicators $\boldsymbol{\lambda}$ combine the criterion eq. (2) with the equations of motion in eq. (1) and lead to the Lagrangian function L

$$\begin{aligned} L = C \quad + \quad & \boldsymbol{\lambda}^{T}\left\{ \left[\boldsymbol{J}_{T,gr}^{T} \mid \boldsymbol{J}_{R,gr}^{T}\right] \begin{pmatrix} \boldsymbol{f}_{gr} \\ \boldsymbol{t}_{gr} \end{pmatrix} + \boldsymbol{J}_{R,j}^{T}\boldsymbol{t}_j \right. \\ - \quad & \left. \boldsymbol{M}\,\ddot{\boldsymbol{q}} + \boldsymbol{h} \right\}. \end{aligned} \tag{3}$$

According to Lagrange theory, a necessary condition for the minimisation of the criterion is that all partial derivatives of L with respect to the unknowns $\boldsymbol{f}_{gr}$, $\boldsymbol{t}_{gr}$, $\boldsymbol{t}_j$ and $\boldsymbol{\lambda}$ have to be zero, see [15]. This leads to the following system of linear equations

$$\begin{aligned} & \boldsymbol{J}\,\boldsymbol{f} = \boldsymbol{m} \\ & \boldsymbol{f} = \left(\boldsymbol{f}_{gr}^{T}, \boldsymbol{t}_{gr}^{T}, \boldsymbol{t}_{j}^{T}\right)^{T} \end{aligned} \tag{4}$$

which can easily be solved for the unknown ground reaction forces $\boldsymbol{f}_{gr}$, torques $\boldsymbol{t}_{gr}$ and joint torques $\boldsymbol{t}_j$ by inverting $\boldsymbol{J}$.

4. Measurements

In the “Neurologische Klinik Bad Aibling”, Germany, the disturbed gait patterns of hemiparetic patients are measured using the Optotrak System. This movement analysis system, depicted in figure 2, uses 58 active markers, which are applied on the skin of the patient. Two cameras measure the cartesian coordinates of the markers and a PC calculates relative angles between joints, using geometric relations. Joint velocities and accelerations are computed by differentiating twice joint angles and filtering with a 4th order Butterworth filter. The heel and toe markers are employed to determine stance and swing phase of the legs and thus single and double support phase.

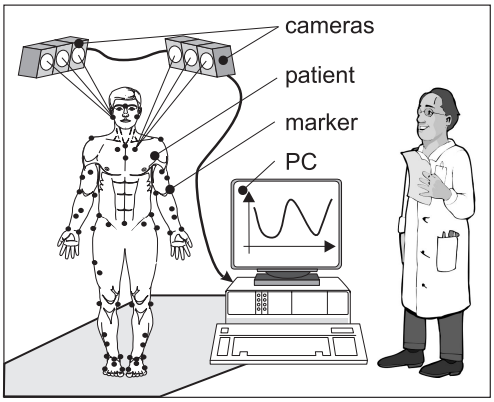

Figure 2: Measurement of human gait by a 3D movement analysis system

5. Verification

Calculated ground reaction forces and joint torques show good agreement with measurements and calculations from literature. As an example, figure 3 shows the calculated ground reaction force of a healthy subject during the single and double support phase of the right leg in comparison to data from other authors. The abscissa is time, normalized with the duration of the gait cycle and expressed in percent. A gait cycle starts with right heel contact (0%), the double stance phases are between 0% and 10% and between 50% and 60%. From 10% to 50% only the right foot and from 60% to 100% only the left foot is on the ground. The ordinate in figure 3 is the ground reaction force normalized with body weight. The calculated ground reaction force in vertical direction (bold solid line in figure 3) shows good agreement with measured data by [16] (dotted line) and calculations done by [17] (solid line).

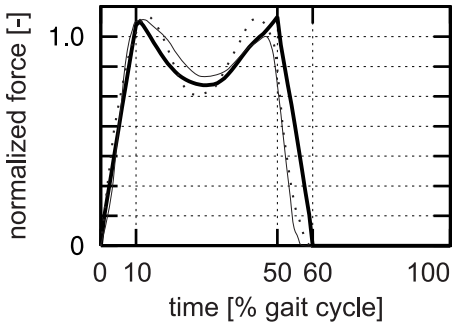

Figure 3: Vertical ground reaction forces by [16] (dotted line) and [17] (solid line) in comparison with simulation results (bold solid line)

6. Results and Conclusions

The following sections show how the method of inverse dynamics is used in the above-mentioned neurological clinic for analysis of hemiparetic gait.

6.1. Animation

Movement of the patient is automatically animated with “XAnimate” [18]. The animation offers many advantages over common recording techniques like video tapes. The doctor or physical therapist can easily, quickly and at each time view the disturbed gait pattern under different angles and zoom on single segments. Furthermore the disturbed and a normal gait pattern can be opposed on the same screen and thus differences are quickly recognised. Animation of the body’s center of mass reveals excessive lateral movements of the patient. Two sample pictures of the animation of a healthy subject and a patient with severe left-sided hemiparesis are depicted in figure 4.

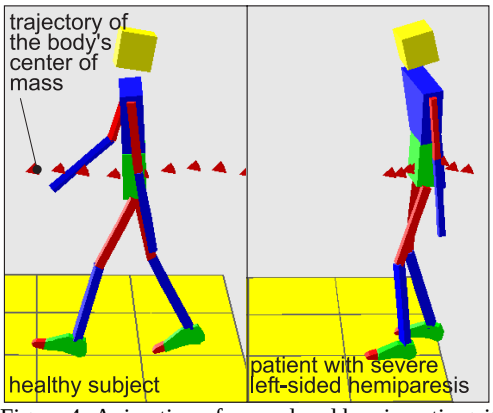

Figure 4: Animation of normal and hemiparetic gait

6.2. Evaluation of Degree of Hemiparesis and Outcome of Therapy

Calculated kinetic quantities are used to quantify the degree of hemiparesis of the patients and to control outcome of therapy.

Figure 5 shows for example peek ankle plantar flexion torque for a healthy subject A, patients with moderate (B) and severe (C and D) hemiparesis. One realises a close correlation between the degree of hemiparesis and this kinetic quantity. The more normal the gait pattern is, the higher and the more equal torques on the right and left side are.

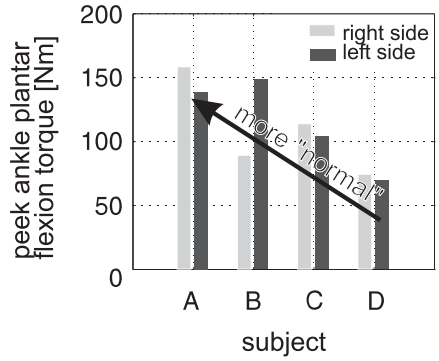

Figure 5: peak ankle plantar flexion torque for 4 subjects

Figure 6 depicts the calculated mechanical work in ankle for two steps for a hemiparetic patient at the beginning (D1), after 3 weeks (D2) and 7 weeks (D3) of physiotherapy in comparison to a healthy subject (A). One states an evident evolution of very low values of flexion work at the beginning to more normal values in course of rehabilitation. Here the outcome of therapy is evaluated by the method of inverse dynamics.

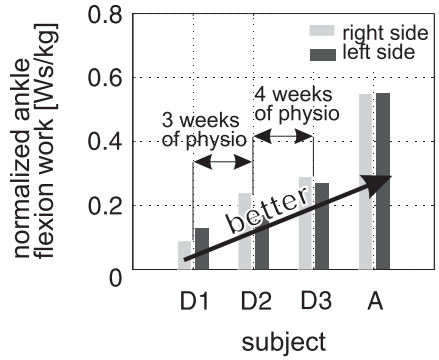

Figure 6: Normalized ankle flexion work in course of rehabilitation (physio=physiotherapy)

6.3. Detailed Analysis of One Patient's Gait Pattern

Inverse dynamics method yields time course of all kinetic quantities for one gait cycle. These data are the base for a detailed analysis of the impaired gait. Time course of left knee flexion/extension torque for a healthy subject (solid line in figure 7) and a patient with severe left-sided hemiparesis (dotted line in figure 7) are for example studied. The patient exhibits in single support phase of the left leg (between 60 and 100 % in gait cycle) a high and constant knee extension torque, whereas for the healthy subject the torque decreases very quickly to low values. Figure 8 shows the healthy subject and hemiparetic patient at 80 % in gait cycle. In single support phase the left knee of the healthy subject is completely extended.

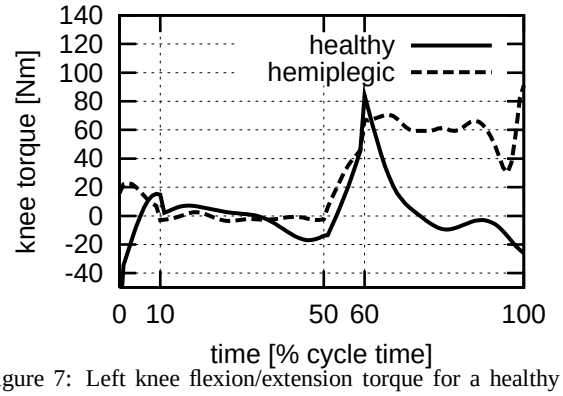

Figure 7: Left knee flexion/extension torque for a healthy subject (solid line) and a hemiplegic patient (dotted line)

Due to the intact neural control of walking, the body is well controlled falling forward in order to reduce knee torques. In contrast to this perfect neural control of movement, the hip and knee of the patient, see figure 8, are flexed, neural control of movement is impaired and the patient has to generate a very high extension torque at the knee to maintain body upright and to progress. Here kinetic quantities give insight into impaired neural control of movement.

6.4. Kinematic Characteristics of Hemiparetic Gait

Furthermore it was found that hemiparetic gait is characterised by excessive lateral movement of body's centre of mass, high lateral ground reaction forces on affected side, low peak torques in all joints of the lower extremity in comparison to healthy subjects, lower peak torques on the affected than on the unaffected side and that energy for propulsion of the body results mainly from the unaffected side.

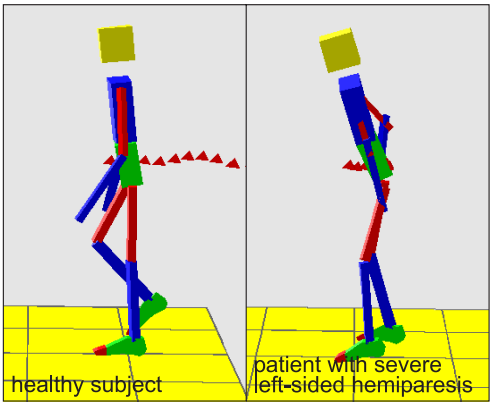

Figure 8: Animation of the two subjects of figure 7

7. Future research work

Future research work is directed towards therapy of hemiparetic patients by model-based functional electrical stimulation (FES), see figure 9.

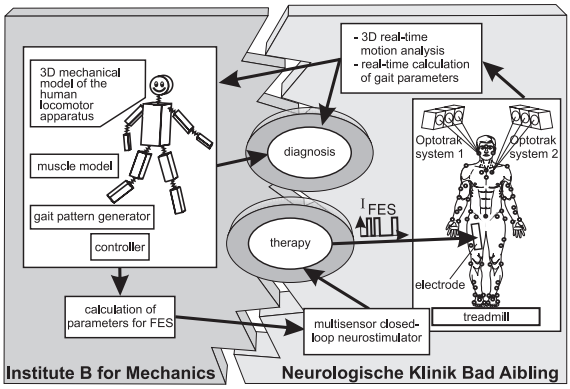

Figure 9: Diagnosis and therapy of hemiparesis: project overview

8. Summary and Conclusions

The goal of clinical gait analysis is to analyse the impaired gait pattern of the patient and to define a suitable therapy. In common gait analysis, only the kinematic data of the gait pattern are analysed, although kinetic quantities enable a further refinement of diagnosis and a better understanding of pathological gait. This paper presents a general method, derived from robotics, to calculate non-measurable kinetic quantities of human gait. In contrast to methods described in literature, expensive force platforms are superfluous. The calculation of kinetic quantities is based on a mechanical model of the human locomotor apparatus. The Newton-Euler method yields the equations of motion. Using inverse dynamics and optimisation, ground reaction forces and joint torques are computed. Movement as input into the inverse mechanical model is measured with a contactless movement analysis system. Calculated kinetic quantities show good agreement with data from literature. The method is applied in the "Neurologische Klinik Bad Aibling", Germany for analysis of hemiparetic gait. Animation of the impaired gait pattern yields a better visualisation than video recordings. The degree of hemiparesis and outcome of therapy is evaluated and patient's gait is detailed analysed by kinetic quantities. More generally, a characterisation of hemiparetic gait by kinetic quantities was found. Future research work deals with therapy of hemiparesis by functional electrical stimulation.

Acknowledgements

The research work presented in this paper is supported by a contract with the DFG (Deutsche Forschungsgemeinschaft, SFB 462 "Sensomotorik").

References

[1] E. J. Roth, C. Merbitz, K. Mroczek, S. A. Dugan, W. W. Suh, "Hemiplegic Gait - Relationships Between Walking Speed and Other Temporal Parameters", *Am J Phys Med Rehabil*, Vol. 6, pp. 128-133, 1997.

[2] D. Wulf, E. Hartmann, S. Heller, G. Hoch, E. Koenig, "3D-Analyse des hemiparetischen Gangbilds mit OPTOTRAK am Beispiel einer Verlaufsdokumentation", *Aktuelle Neurologie*, Vol. 25, p. 197, 1998.

[3] R. Shiavi, H. J. Bugle, T. Limbird, "Electromyographic gait assessment, part 2: Preliminary assessment of hemiparetic synergy patterns", *J Rehabil Res*, Vol. 24, pp. 24-30, 1987.

[4] S. J. Olney, C. L. Richards, "Hemiparetic gait following stroke. Part I: Characteristics", *Gait and Posture*, Vol. 4, pp. 136-148, 1996.

[5] J. R. Gage, S. E. Koop, "Clinical Gait Analysis: Application to Management of Cerebral Palsy", In: P. Allard, I. A. F. Stokes, J-P. Blanchi, *Three Dimensional Analysis of Human Movement*, pp. 349-362, Human Kinetics Publishers, 1994.

[6] A. Pedotti, "Future Perspectives in Europe for Quantitative Analysis of Movement", in: U. Boenick, M. Näder, *Gait Analysis - State of the Art of Measuring Systems and Their Importance*

for Prosthetic and Orthotic Technology, pp. 322-332, Mecke Druck und Verlag, 1990.

[7] S. J. Olney, C. L. Richards, “Hemiparetic gait following stroke. Part II: Recovery and Physical Therapy”, *Gait and Posture*, Vol. 4, pp. 149-162, 1996.

[8] F. Pfeiffer, *Roboterdynamik*, B. G. Teubner, Stuttgart, 1987.

[9] C. Lutzenberger, F. Pfeiffer, “A Three-dimensional Model of the Human Locomotor Apparatus for Analysis of Hemiplegic Gait”, Proceedings of International Conference of the IEEE Engineering in Medicine and Biology Society (EMBS ’98), Hongkong, pp. 2407-2410, 1998.

[10] J. Apkarian, S. Naumann, B. Cairns, “A Three-Dimensional Kinematic and Dynamic Model of the Lower Limb”, *J Biomech*, Vol. 22, pp. 143-155, 1989.

[11] D. J. Pearsall, J. G. Reid, R. Ross, “Inertial Properties of the Human Trunk of Males Determined from Magnetic Resonance Imaging”, *Ann Biomed Eng*, Vol. 22, pp. 692-706, 1994.

[12] V. Zatsiorsky, V. Seluyanov, “The Mass and Inertia Characteristics of the Main Segments of the Human Body.” *Biomechanics VIII-B*, University Park Press, pp. 1152-1159, 1983.

[13] F. Pfeiffer, *Einführung in die Dynamik,* B. G. Teubner, Stuttgart, 1992.

[14] J. Eltze, *Biologisch orientierte Entwicklung einer sechsbeinigen Laufmaschine*, VDI Fortschrittberichte, Reihe 17, Nr. 110, Düsseldorf, 1994.

[15] H. Bremer, *Dynamik und Regelung mechanischer Systeme*, B. G. Teubner, Stuttgart, 1988.

[16] D. A. Winter, *The Biomechanics and Motor Control and Human Gait*, University of Waterloo Press, Waterloo, 1987.

[17] B. Koopman, H. J. Grootetnboer, H. J., H. J. de Jongh, “An Inverse Dynamics Model for the Analysis, Reconstruction and Prediction of Bipedal Walking”, J Biomech, Vol. 28, pp. 1369-1376, 1995.

[18] D. W. Marhefka, D. E. Orin, “XAnimate”, program and documentation under http://eewww.eng.ohio-state.edu/∼orin/XAnimate/XAnimate.html.

Proceedings of the International Symposium on
Adaptive Motion of Animals and Machines,
Montreal, Aug.8-12, 2000

Dynamics and Control of a Simulated 3-D Humanoid Biped

Kemal Sari, Gabriel M. Nelson, and Roger D. Quinn

Case Western Reserve University, Department of Mechanical and Aerospace Engineering,
Cleveland, USA, kxs13@po.cwru.edu

Abstract

In this paper, we present an algorithm for controlling the walking of a humanoid biped. The algorithm is hierarchical with local Joint Space Control (JSC) and global Virtual Model Control (VMC). VMC plays an important role in the stance phase of the legs and provides postural stability during locomotion. JSC is used at all times, but is essential during the swing phase and for placement of the foot to obtain or change the speed of the robot. A simulation of walking of a three dimensional humanoid biped is achieved through the superposition of these two control schemes.

1. Introduction

Humanoid locomotion is one of the most complex problems to achieve by robots due to mechanical complexity and instabilities. However, solving this problem has many benefits. Humans can locomote over complex terrain that current commercial vehicles can not navigate. A humanoid biped with this locomotion capability could maneuver itself into position to conduct tasks too dangerous for humans. For this purpose, it would be beneficial to have a robot to perform those tasks.

Honda developed a humanoid robot that can walk on a planned path autonomously and perform simple tasks via wireless teleoperation [1]. The pre-defined joint angles of the desired walking pattern are used as reference points for local control of the Honda robot. The desired joint angles are defined via motion studies of human walking. This method is time consuming and not robust. For general locomotion, we can not consider the desired joints angles for JSC to be pre-defined.

In this paper, superposition of Joint Space Control (JSC) and Virtual Model Control (VMC) is used to drive the locomotion of a three dimensional humanoid biped in simulation. For the single support case, the VMC uses an inverted pendulum model. For the double support case this model is modified to generate forces which maintain the center of pressure inside the foot region because of the importance of stability. JSC is implemented using PD Control on desired joint angles obtained from the integration of Cartesian velocities. JSC is used during both stance and swing phases of the legs. Limited walking of the biped is realized by this control model.

To control lateral stability in the frontal plane, J.E. Pratt, and G.A. Pratt [2] use a simple pendulum model for determining the foot placement. Foot placement becomes a function of the velocity in their approach, but velocity control is not seen explicitly. JSC resembles this. On the other hand, JSC has an explicit velocity control component.

2. The Model and Dynamics

Our simulation models the trunk and legs of a human subject and has 18 degrees of freedom. It has two limbs, each with 3 segments, connected to the trunk for a total of 7 segments. The trunk (base body) is defined as a general 6 Degree of Freedom (DOF) body in space. Each limb has a three DOF hip, a one DOF knee, and a 2 DOF ankle.

As shown in Figure 1, each body has a reference frame with its origin located at the proximal joint center. The trunk's reference frame is located at its Center of Mass (COM).

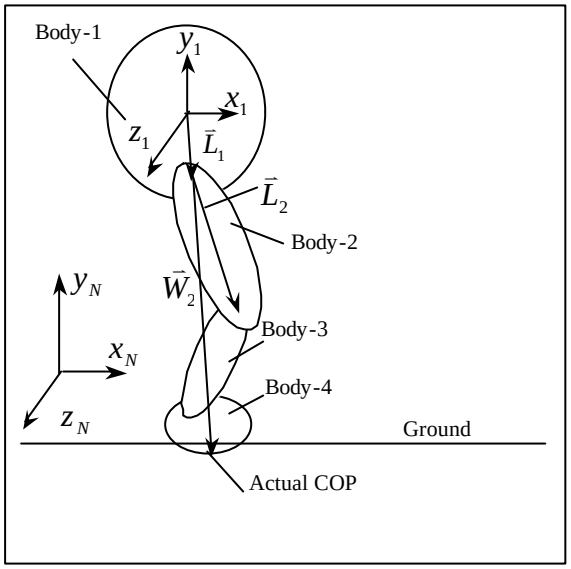

Figure 1: Notation of a Single Leg.

The authors developed a dynamic formulation for a three-dimensional humanoid biped based upon Lagrange's Equations in terms of quasicoordinates [3]. The ground is modeled using stiffness, damping and Coulomb friction. The foot is modeled with many points that can contact the ground. Using these points, the actual center of pressure (COP) can be calculated.

3. Virtual Model Control for the Biped

The posture controller is a global controller based upon VMC and it maintains body stability in all regimes of locomotion, including standing, walking, and running. VMC is presented by Pratt et al. [4]. Contributing research fields are also described well by Pratt [5]. Nelson and Quinn [7] have applied this approach to a cockroach-like hexapod robot. In this paper VMC is applied to control the posture of a three dimensional biped.

3.1. Single limb stance

In the single limb support phase of walking, one leg contacts the ground and provides the force to control the body's motion. The force on the body is produced by pushing on the ground. The limb consists of four links starting from body(1) to foot(4) with body fixed reference frames (1-frame to 4-frame).

The forces at the points on the foot that contact the ground can be resolved into the COP of the foot. The foot can be considered to have a point contact with the ground at the COP and the "unactuated ankle" constraint may be used [7]. Note that the COP is equivalent to the Zero Moment Point (ZMP). This constraint generates a required relationship between the forces and moments applied by the leg, *l*, on the body 1,

$$\vec{M}_l = \tilde{\vec{W}}_{1l} C_{1N} \vec{F}_l = \bar{J}_l \vec{F}_l, \qquad l = L, R \quad (1)$$

where $\vec{F}_l$ and $\vec{M}_l$ are these force and moment vectors, respectively. The force vector is expressed with respect to an inertial reference frame (N-frame) while the moment vector is expressed with respect to the body reference frame (1-frame). $\vec{W}_{1l}$ is a position vector of the foot in the body's reference frame, and $\tilde{\vec{W}}_{1l}$ represents a cross product which is equivalent to a skew operation on this vector:

$$\tilde{\vec{W}} = \begin{bmatrix} 0 & -W_Z & W_Y \\ W_Z & 0 & -W_X \\ -W_Y & W_X & 0 \end{bmatrix} \quad (2)$$

C_{1N} is a coordinate rotation matrix from the N-frame to the 1-frame. A recursive relationship of $\vec{W}$ can be expressed as follows:

$$\begin{aligned} \vec{W}_1 &= \vec{L}_1 + C_{12}\vec{W}_2 \\ \vec{W}_2 &= \vec{L}_2 + C_{23}\vec{W}_3 \\ \vec{W}_3 &= \vec{L}_3 + C_{34}\vec{W}_4 \\ \vec{W}_4 &= \vec{L}_4 \end{aligned} \quad (3)$$

where $\vec{L}_i$ represents the position vector from the origin of the i-frame to the origin of the (i+1)-frame measured in the i-frame. Thus the

transpose of the translational Jacobian for limb 1 with 4 links is expressed as

$$J^T = D^T \begin{bmatrix} \tilde{W}_2^T C_{2N} \\ \tilde{W}_3^T C_{3N} \\ \tilde{W}_4^T C_{4N} \end{bmatrix} \quad (4)$$

where D is a nonlinear function of joint angles.

3.2. Double limb stance

When the right and left legs are both in stance, the relationship between the forces and moments can be expressed as

$$\begin{bmatrix} F \\ M' \end{bmatrix} = \begin{bmatrix} I & I \\ \tilde{W}_1^R C_{1N} & \tilde{W}_1^L C_{1N} \end{bmatrix} \begin{bmatrix} F_R \\ F_L \end{bmatrix}$$

or

$$\begin{bmatrix} F \\ M \end{bmatrix} = \begin{bmatrix} I & I \\ \tilde{p}_f^R & \tilde{p}_f^L \end{bmatrix} \begin{bmatrix} F_R \\ F_L \end{bmatrix} = A \begin{bmatrix} F_R \\ F_L \end{bmatrix} \quad (5a,b)$$

where

$$\tilde{p}_f = C_{N1} \tilde{W}_1 C_{1N} = Skew\left[C_{N1} \vec{W}_1\right]$$

Where F and M are vectors representing the total forces and moments on the body from the stance legs. While M' is represented in the body frame and M is represented in the inertial reference frame, they represent the same vector. $\tilde{p}_f$ is the skew symmetric matrix of the position vector of the foot's contact point with respect to the body in the inertial reference frame. The subscripts R and L represent the right and left feet and I is a 3x3 identity matrix. The matrix A is defined by Eq. (5b).

3.2.1. Solving for the Force Distribution

Given F and M from the VMC, the forces on the right and left legs, F_R and F_L, need to be resolved to distribute the load between the legs. Attempted inversion of the matrix A in Eq. (5b) yields a singularity, because the third and sixth rows of the matrix A are linearly dependent. To solve this under constrained problem we use an optimization. To simplify the problem, we introduce dimensionless parameters that represent the lateral forces and the vertical force as follows:

$$c_{xl} = \frac{F_{xl}}{F_{yl}}, \quad d_{zl} = \frac{F_{zl}}{F_{yl}} \quad (6)$$

$$n_l = \frac{F_{yl}}{F_y}, \quad \sum n_l = 1, \quad l = R, L \quad (7a,b)$$

Introducing Eqs. (6) and (7a) into the six scalar equations represented by Eq. (5b), we have 5 equations, two of them being linearly dependent, and Eq. (7b). When the COP is expressed as

$$\begin{bmatrix} x_{cp} \\ z_{cp} \end{bmatrix} = \begin{bmatrix} p_{xR} & p_{xL} \\ p_{zR} & p_{zL} \end{bmatrix} \begin{bmatrix} n_R \\ n_L \end{bmatrix} \quad (8)$$

then, those linearly dependent equations yield [7]

$$x_{cp} = \frac{M_z}{F_y} + y\frac{F_x}{F_y}, \quad z_{cp} = -\frac{M_x}{F_y} + y\frac{F_z}{F_y} \quad (9a,b)$$

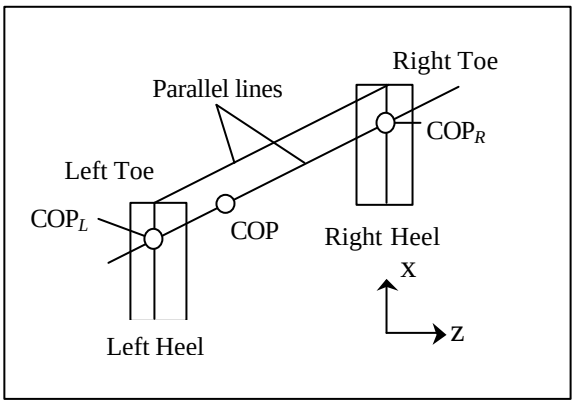

Figure 2: The COP Distribution for the Double Stance

Figure 2 represents the double stance case showing the common COP and distribution of the COP to the right and left legs, COP_L and COP_R. The total biped COP location corresponds to a single leg model of the biped on a flat surface. Note that y is the average of P_L and P_R. For the given F and M, x_{cp} and z_{cp} can be solved from Eq. (9a,b). The COP for double stance is projected to the right and left feet by drawing a line parallel to the line of the right and left toes from the COP as shown in Figure 2. This determines COP_L and COP_R. Now, we can solve Eq. (8) for the vertical weight distribution. This solution has a singularity when the COP's of the individual feet are symmetric about the origin of the trunk-frame. This is avoided by simply enforcing the sum of the vertical force coefficients to be equal to one when this singularity occurs. Now, we are left with three equations and four unknowns to complete the solution of the force distribution problem. We could add an additional constraint [4] or use an optimization [7]. We use optimization to solve the problem with the following cost function

$$E = \frac{1}{2}[(c_{xR} - \bar{c}_{xR})^2 + (c_{xL} - \bar{c}_{xL})^2 + (d_{xR} - \bar{d}_{xR})^2 + (d_{xL} - \bar{d}_{xL})^2] \quad (10)$$

where symbols with the over score represent the desired dimensionless force directions. Minimizing E, using the above three linearly independent equations from Eq. (5b) as constraints, solves the force distribution problem completely and encourages each leg to push in a preferred direction.

3.3. Virtual Forces and Moments

An inverted pendulum model is used to find the desired virtual forces and moments that produce a stable posture. In this model a spring and damper in parallel are connected to the origin of the trunk from the COP with length L. The desired virtual force in the direction of L can be computed as

$$F = K_p(L_d - L) + K_v(\dot{L}_d - \dot{L}) \quad (11)$$

where L_d is the desired length of one limb and K_p , and K_v are the proportional and derivative gains. For the single stance phase, L_d is defined as the height of origin of the trunk when the robot is standing up straight. For the double support phase L_d is calculated from a desired moving point that satisfies the initial condition of the inverted pendulum mode for the next single stance leg. F can be projected into the x, y and z directions to obtain the force components.

The desired torques acting on the main body can also be expressed as

$$t_{ti} = K_{pi}(a_{di} - a_i) + K_{vi}(\dot{a}_{di} - \dot{a}_i), \quad i = 1,2,3 \quad (12)$$

where K_p, and K_v are the proportional and derivative gains. $\boldsymbol{a}$, and $\boldsymbol{a}_d$ are the trunk's actual and desired orientations. The $\vec{M} = C_{N1}D_1^{-T}\vec{t}_t$ relation is used to transform $\boldsymbol{t}_{ti}$ to $\vec{M}$.

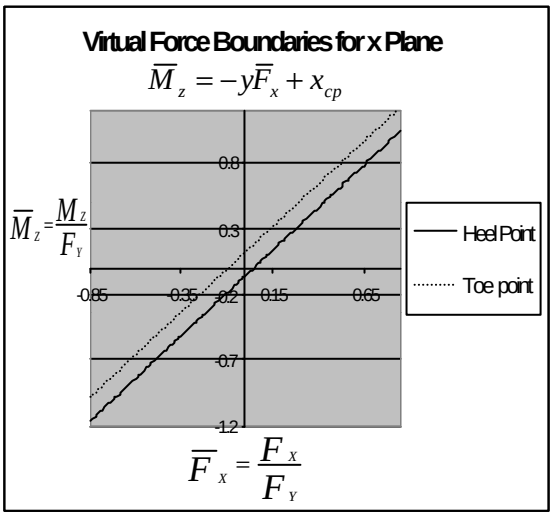

Figure 3: Virtual Force Boundaries for the xz Plane, vertical axis in meters, and horizontal axis in dimensionless units.

Using these sets of forces and moments, the desired COP can be calculated from Eq. (9a,b). The result may be outside of the foot region and therefore impossible to realize.

This led us to develop a scheme that changes the sets of desired virtual forces to realizable sets of forces and moments. In Figure 3, Eq. (9a) is transformed into a plot of virtual force boundaries for the xz plane. The region between the two lines represents the realizable sets of virtual force F_x and moment M_z. When the desired virtual force and moment fall outside of this region, they are modified to be brought into the boundaries at the closest point. The modified force and moment are the input force and moment for the VMC. Similarly, Eq. (9b) is evaluated in order to get a realizable set of F_z and M_z. The above applies to both single stance and double stance in a similar manner.

4. Joint Space Control

JSC is responsible for the swing phase and for placement of the foot at the end of the swing phase. In order to implement JSC using proportional control, we need to obtain some desired joint angles. In this respect, we will introduce a Jacobian that maps the foot cartesian velocity with respect to the trunk to the joint speeds. Let us express the angular velocity of the ground as follows:

$$\vec{w}_g = C_{N1}D_1\dot{\vec{a}}_1 + C_{N2}D_2\dot{\vec{a}}_2 + C_{N3}D_3\dot{\vec{a}}_3 + C_{N4}D_4\dot{\vec{a}}_4 + \vec{\Omega}_g = 0 \quad (13)$$

which is zero because the ground is fixed. $\vec{\Omega}_g$ is the angular velocity of the ground with respect to the foot. D_i is a nonlinear function of the i^{th} joint angles $\boldsymbol{a}_i$ Solving for the trunk angular speeds yields

$$D_1\dot{\vec{a}}_1 + \vec{\Omega}_g = \begin{bmatrix} -C_{12}D_2 & -C_{13}D_3 & -C_{14}D_4 \end{bmatrix} \begin{bmatrix} \dot{\vec{a}}_2 \\ \dot{\vec{a}}_3 \\ \dot{\vec{a}}_4 \end{bmatrix}$$

or (14a,b)

$$D_1\dot{\vec{a}}_1 + \vec{\Omega}_g = J_{fa} \begin{bmatrix} \dot{\vec{a}}_2 \\ \dot{\vec{a}}_3 \\ \dot{\vec{a}}_4 \end{bmatrix}$$

where J_{fa} is a rotational Jacobian (3x6) matrix.

Furthermore, the foot velocity with respect to the trunk can be expressed as

$$\dot{\vec{p}}_f = \begin{bmatrix} \tilde{L}_1^T & C_{12}\tilde{L}_2^T & C_{13}\tilde{L}_3^T & C_{14}\tilde{L}_4^T \end{bmatrix} \begin{bmatrix} I & 0 & 0 & 0 \\ C_{21} & I & 0 & 0 \\ C_{31} & C_{32} & I & 0 \\ C_{41} & C_{42} & C_{43} & I \end{bmatrix} \begin{bmatrix} D_1 & 0 & 0 & 0 \\ 0 & D_2 & 0 & 0 \\ 0 & 0 & D_3 & 0 \\ 0 & 0 & 0 & D_4 \end{bmatrix} \begin{bmatrix} \dot{\vec{a}}_1 \\ \dot{\vec{a}}_2 \\ \dot{\vec{a}}_3 \\ \dot{\vec{a}}_4 \end{bmatrix}$$

or

$$\dot{\vec{p}}_f - \tilde{W}_1^T D_1\dot{\vec{a}}_1 = \begin{bmatrix} C_{12}\tilde{W}_2^T D_2 & C_{13}\tilde{W}_3^T D_3 & C_{14}\tilde{W}_4^T D_4 \end{bmatrix} \begin{bmatrix} \dot{\vec{a}}_2 \\ \dot{\vec{a}}_3 \\ \dot{\vec{a}}_4 \end{bmatrix}$$

or (15a,b,c)

$$\dot{\vec{p}}_f - \tilde{W}_1^T D_1\dot{\vec{a}}_1 = J_{ft} \begin{bmatrix} \dot{\vec{a}}_2 \\ \dot{\vec{a}}_3 \\ \dot{\vec{a}}_4 \end{bmatrix}$$

where J_{ft} is 3x6 Jacobian matrix. Combining Eq. (14b) and (15c), yields

$$\begin{bmatrix} D_1\dot{\vec{a}}_1 + \vec{\Omega}_g \\ \dot{\vec{p}}_f - \tilde{W}_1^T D_1\dot{\vec{a}}_1 \end{bmatrix} = \begin{bmatrix} J_{fa} \\ J_{ft} \end{bmatrix} \begin{bmatrix} \dot{\vec{a}}_2 \\ \dot{\vec{a}}_3 \\ \dot{\vec{a}}_4 \end{bmatrix}$$

or (16a,b)

$$b = J_f\dot{\vec{a}}_c$$

where J_f is a 6x6 Jacobian matrix. By inverting J_f, we can obtain the joint angular velocities as functions of b, then we can integrate to find joint angles. When we prescribe b, a desired set of joint angles and velocities can be determined. These are equilibrium points for PD control. The following choices for the b vector are used in our controller:

$$b_{st} = \begin{bmatrix} 0 \\ 0 \\ 0 \\ -v_x \\ -v_y \\ -v_z \end{bmatrix}, \quad b_{sw} = \begin{bmatrix} 0 \\ 0 \\ 0 \\ v_x + K_{\dot{x}}(v_{xbsw} - v_{xd})/T \\ BCos(\pi t/T) \\ v_z + K_{\dot{z}}(v_{zbsw} - v_{zd})/T \end{bmatrix} \tag{17}$$

where $v_x, v_y, and\ v_z$ are the instantaneous velocities of the trunk in the x, y, and z directions. Also, T is the desired period of the swing phase, *B* is a constant for the swing leg's vertical travel, t is time, and *st* and *sw* represent the stance and swing legs, respectively. The additional terms $K_{\dot{x}}(v_{xbsw} - v_{xd})$, and $K_{\dot{z}}(v_{zbsw} - v_{zd})$ for the velocity control in the fourth and sixth rows of b_{sw} need to be explained in more detail. These terms are used by Raibert [8] as velocity control components for hopping robots. $K_{\dot{x}}, and\ K_{\dot{z}}$ are feedback gains. $v_{xd}, and\ v_{zd}$ are desired trunk velocities in the x and z directions. $v_{xbsw}, and\ v_{zbsw}$ are the trunk velocities at the beginning of the swing phase, however, previous average velocities can also be used. From simulation results, it was found that this solution produces a bended knee configuration at the end of the swing phase. In order to straighten the knee joint for transition to stance, we forced the knee to open during the swing phase. $\vec{\Omega}_g$ and $\dot{\alpha}_1$ are set to zero.

5. Simulation

A simulation of standing, and some trunk motion was performed using the posture controller based on VMC. The results are stable. A walking simulation of the biped robot was also conducted by combining VMC and JSC. In the forward (x) direction, a stable walking was observed. However, in the side-to-side (z) direction an instability occurs after several steps. We believe that the system can be made to be stable through the right choice of the *b* vector component in the lateral direction. In Figs. 4, and 5, measured COP, and desired COP

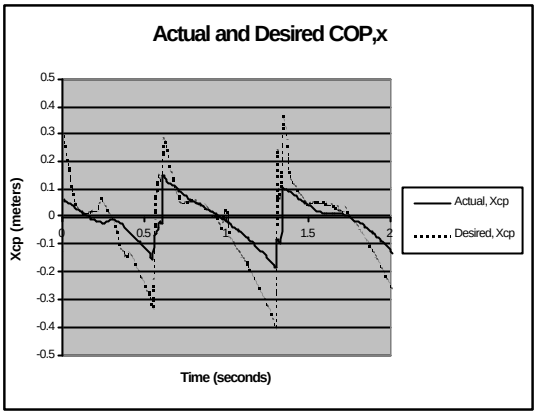

Figure 4: Actual and Desired COP of the Biped in the x direction.

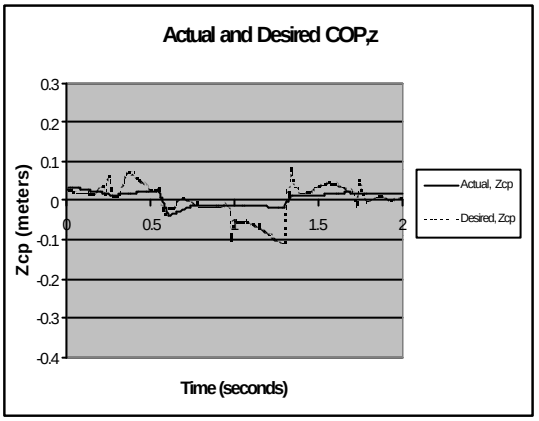

Figure 5: Actual and Desired COP of the Biped in the z direction.

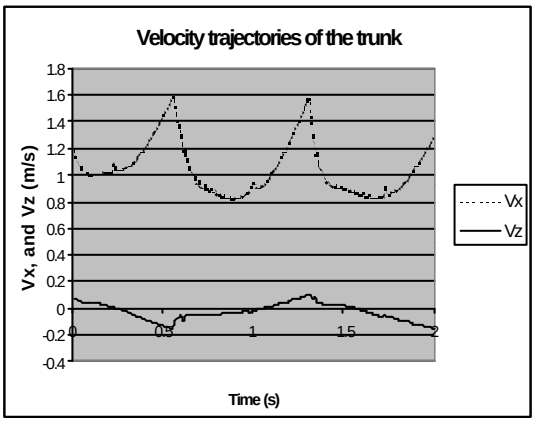

Figure 6: Velocity Trajectories of the Trunk.

with respect to the trunk are plotted versus time. Velocity trajectories in the x and z directions are shown in Fig. 6.

6. Conclusions

In legged locomotion, posture control plays a central role for stability. This is particularly important for a humanoid biped which is statically unstable. When its stability is disturbed, such as by a push, the robot may need to take a step to prevent it from falling. Therefore, foot placement by a swing leg on the ground must be chosen properly. These concepts can be realized by implementing VMC and JSC schemes.

References

[1] K.Hirai, M. Hirose, Y. Haikawa, and T. Takenaka, "The Development of Honda Humanoid Robot," *Proc. 1998 IEEE Int. Conf. Robot. Automat.*, Leuven, Belgium, May 1998.

[2] J.E. Pratt, and G.A. Pratt, "Exploiting Natural Dynamics in the Control of a 3D Bipedal Walking Simulation," *CLAWAR99*, Potsmouth, UK, September 1999.

[3] G.M. Nelson, and R.D. Quinn, "A Quasicoordinate Formulation for Dynamic Simulations of Complex Multibody Systems With Constraints," Dynamics and Control of Structures in Space III, C.L. Kirk and D.J. Inman, (ed) pp. 523-538, Computational Mechanics Publications, Southampton, UK, 1996.

[4] J. Pratt, P. Dilworth, and G. Pratt, "Virtual Model Control of a Bipedal Walking Robot," *Proc. 1997 IEEE Int. Conf. Robot. Automat.*, Albuquerque, New Mexico, 1997.

[5] J. Pratt, "Virtual Model Control of a Biped Walking Robot," Master's Thesis, Massachusetts Institute of Technology, Aug., 1995.

[6] G.M. Nelson, and R.D. Quinn, "Posture Control of a Cockroach-Like Robot," *IEEE Control Systems*, Vol. 19, No. 2, pp. 9-14, April 1999.

[7] M.H. Raibert, *Legged Robots That Balance*. MIT Press, Cambridge, MA, 1986.

[8] J.K. Hodgings, "Biped Gait Transitions," *Proc. 1991 IEEE Int. Conf. Robot. Automat.*, Sacramento, California, April 1991.

[9] S. Kajita, and K. Tani, "Study of Dynamic Biped Locomotion on Rugged Terrain," *Proc. 1991 IEEE Int. Conf. Robot. Automat.*, Sacramento, California, April 1991.

[10] S. Kajita, and K. Tani, "Expermental Study of Biped Dynamic Walking in the Linear Inverted Pendulum Mode," *Proc. 1995 IEEE Int. Conf. Robot. Automat.*, 1995.

[11] O. Bruneau, F.B. Ouezdou, and P.B. Wieber, "Dynamic Transition Simulation of a Walking Anthropomorhic Robot," *Proc. 1998 IEEE Int. Conf. Robot. Automat.*, Leuven, Belgium, May 1998.

[12] J.H. Park, and K.D. Kim, "Biped Robot Walking Using Gravity-Compensated Inverted Pendulum Mode and Computed Torque Control," *Proc. 1998 IEEE Int. Conf. Robot. Automat.*, Leuven, Belgium, May 1998.

[13] Y. Fujimoto, and A. Kawamura, "Three Dimensional Digital Simulation and Autonomous Walking Control for Eight-Axis Biped Robot," *Proc. 1995 IEEE Int. Conf. Robot. Automat.*, 1995.

[14] Y. Fujimoto, S. Obata, and A. Kawamura, "Robust Biped Walking with Active Interaction Control between Foot and Ground," *Proc. 1998 IEEE Int. Conf. Robot. Automat.*, Leuven, Belgium, May 1998.

[15] G.M. Nelson "Modeling and Simulation of an Insect Like Hexapod," Master's Thesis, Case Western Reserve University, Aug., 1995.

Proceedings of the International Symposium on
Adaptive Motion of Animals and Machines,
Montreal, Aug.8-12, 2000

Real-Time Interactive Motion Generator of Human Figures

Yoshihiko NAKAMURA[*1*2] and Katsu YAMANE[*1]
(E-mail: [nakamura, katz]@ynl.t.u-tokyo.ac.jp)

[*1] Department of Mechano-Informatics, University of Tokyo
7-3-1 Hongo Bunkyo-ku Tokyo, 113-8656 JAPAN

[*2] CREST, Japan Science and Technology Corporation

Abstract

This paper summarizes our research related to motions of human figures. Our final goal is to develop a motion generating system that creates realistic motions of human figures interacting with the user in real time, based on computational methods for the dynamics and kinematics of kinematic chains. Toward this goal, we propose the concept of dynamics filter which generates physically natural motions from any reference motion allowing interactive inputs by the user. Dynamics filter has a potential ability to generate virtually infinite variety of motions from a relatively small motion database or even motions captured from a human in real time. We have also developed a prototype of the real-time dynamics filter, which makes use of our efficient computing methods for the dynamics of human figures.

1. Introduction

Human figures are defined as kinematic models of the human body with links connected by mechanical joints (Figure 1). Motion generation of human figures is of great interest in robotics as well as in computer graphics. Humanoid robots are expected to work in place of human in various fields such as welfare, plant maintenance, entertainment, and so on. In computer graphics, the demand for high quality content with human characters is growing stronger along with the development and spread of multimedia technologies. The common keyword connecting these two issues is the motion of human figures. Motions of humanoid robots are neither simple nor predefined as in conventional industrial robots — we have to control the unstable body of robots to create almost infinite variation of motions. This situation is quite similar to human characters in computer animations, where we have to make various motions according to their role in virtual environments.

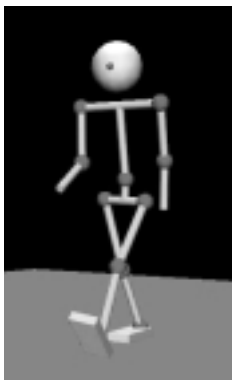

Figure 1: A human figure

To achieve this goal, we propose the concept of a dynamics filter, a real-time and interactive motion generator for human figures. The basic function of the filter is to convert a physically inconsistent motion into a consistent one, to which the following features are added:

1. Take human motions, either captured or drawn, as reference instead of created from scratch, in order to generate expressive human-like motions that convey emotion.

2. Execute the computation in real time in order to allow interactive inputs or adapt to dynamically changing environments

In this paper, we propose the concept of dynamics filter and introduce our first implementation based on our previous research on dynamics of structure-varying kinematic chains [1]. Before describing the implementation of a dynamics filter in detail, we first provide a summary of the methods for computing the dynamics of human figures, followed by the details on our dynamics filter. We also provide some examples of applying the dynamics filter to various motions. In the last section, we introduce our ongoing projects along with the conclusions of this paper.

2. The Concept of Dynamics Filter

Many methods have been proposed for generating motions for humanoid robots [2, 3, 4] and animations [5, 6, 7]. However, most of them have problems from the standpoint of interactivity:

1. Poor flexibility — Each method is only applicable to limited motions, walking in most cases, which means that we need to prepare many motion generators corresponding to different motions.
2. Off-line computation — The whole sequence of motion is required before generating motion. This would be a fatal disadvantage in interactive motion generation because we cannot modify the reference motion once the computation starts.
3. Long computation time — Another problem is that they require much computation to generate a single sequence of motion.

A dynamics filter is expected to provide a solution for these problems. The procedure for generating motion by dynamics filter is illustrated in Figure 2. First, several properties, such as the motion (walk / run / sit, ...), the model (mass / link length, ...), character (male / female, adult / child, ...) and emotion (happy / angry / sad, ...) are selected and combined kinematically. Next, the combined reference motion is input to the dynamics filter, which outputs a physically consistent motion close to the reference. Users may take some trial-and-error experiments with the dynamics filter to meet their taste. In interactive systems, the reference motion may change during the computation according to user inputs.

This approach is reasonable from the viewpoint of learning process of human. We first imitate just the kinematics of a motion watching the others — then adapt the motion to the dynamics of our own body and the environment.

Implementation of the filter may be off-line or on-line. An off-line filter, making use of the whole sequence of the input motion prior to the filtering, will generate motions of high quality and stability. This type of dynamics filter would be good for creating artistic films in computer graphics, or a motion library for humanoid robots. Previous research has already realized this type of dynamics filter [4, 5, 6, 7].

An on-line version of a dynamics filter is more difficult because only limited informations are provided to the filter, but interesting from the viewpoint of interactive motion generation. This feature is essential for humanoid robots moving in dynamically changing environments and human characters in some applications such as games.

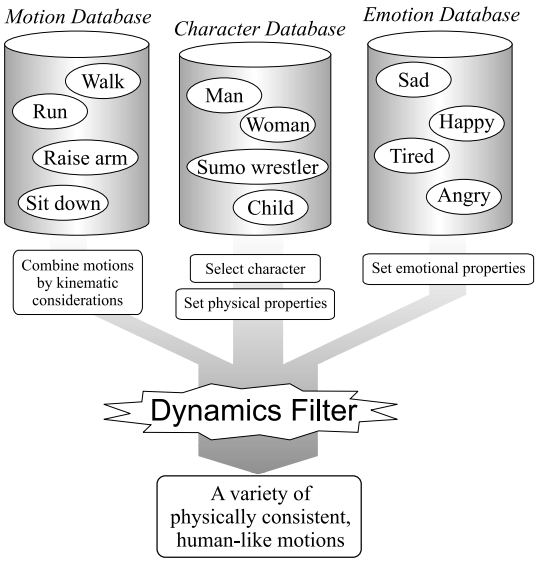

Figure 2: Motion generation via dynamics filter

We provide an on-line implementation of a dynamics filter in this paper. This is difficult and constitutes a contribution because others only have built off-line filters. The filter is based on the equation of motion of closed and structure-varying kinematic chains developed for dynamics simulation of human figures [1].

3. Dynamics Computation of Human Figures

3.1. Previous Work and Requirements

Since the human figure can be modeled in terms of kinematic chains, we can apply algorithms developed in multibody dynamics and robotics [8, 9, 10, 11] to human figures [12, 13, 14]. However, human figures have quite different properties compared to conventional robot manipulators from the point of view of dynamics computation as listed below:

1. Many degrees of freedom (DOF) — Human figures usally contain many DOF's, even the simplest model has more than 20 DOF.

2. Complicated closed kinematic chains — Human figures often form complicated closed kinematic chains by holding links in the environment, their own body, or other figures, for which most dynamics algorithms require a large computational load.

3. Structural changes — On catch or release of links by hands, human figures change their link structure dynamically during the motion.

4. Collisions and contacts — A human figure frequently collides with the environments, other human figures, or even itself during motion.

5. Under actuation — Since human figures have no fixed link, they are always under actuated, that is, the DOF of motion is larger than the number of actuators. Therefore, we need to consider the physical consistency of motion in generating motions for human figures.

6. Requirement for interactivity — Interactivity is likely to be the most important feature of future applications of human figures. Human figures move in dynamically changing environment interacting with humans, in contrast to conventional manipulators.

Considering these points, we decided to take a new approach toward the dynamics computation of human figures. Our objectives are:

1. To compute the dynamics of complicated kinematic chains efficiently, in real time

2. To handle open and closed kinematic chains seamlessly to enable on-line computation of structure-varying kinematic chains

3. To compute the dynamics of collisions and contacts efficiently

3.2. Closed Kinematic Chains

Dynamics of closed kinematic chains requires consideration of reaction forces in closed loops. Lagrange multipliers are often applied to compute the reaction force [8, 9]. However, the computational cost of Lagrange multipliers is too large to be applied to real-time or interactive simulation.

An alternative approach is to apply the principle of virtual work [15, 16], which is a mostly used to control robots with closed kinematic chains such as a planar five-bar linkage or parallel mechanisms [17]. This method has the advantage of high computational efficiency which enables real-time control of manipulators. Until recently no general algorithm was known for computing the Jacobian matrix essential for applying the principle of virtual work. We have found a solution for this problem [18] and extended this approach to general closed kinematic chains.

The basic equation of motion of human figures is described as:

$$\begin{pmatrix} \boldsymbol{A} & -\boldsymbol{H}_C^T & -\boldsymbol{H}_J^T \\ \boldsymbol{H}_C & \boldsymbol{O} & \boldsymbol{O} \end{pmatrix} \begin{pmatrix} \ddot{\boldsymbol{\theta}}_G \\ \boldsymbol{\tau}_C \\ \boldsymbol{\tau}_J \end{pmatrix} = \begin{pmatrix} -\boldsymbol{b} \\ -\dot{\boldsymbol{H}}_C \dot{\boldsymbol{\theta}}_G \end{pmatrix} \tag{1}$$

which can be summarized as:

$$\boldsymbol{W}\boldsymbol{x} = \boldsymbol{u} \tag{2}$$

where

$\boldsymbol{A}$	:	inertial tensor
$\boldsymbol{b}$	:	centrifugal, Coriollis and gravitational forces
$\boldsymbol{\theta}_G$	:	the generalized coordinates
$\boldsymbol{\tau}_C$	:	constraint forces at connected joints
$\boldsymbol{\tau}_J$	:	joint torques
$\boldsymbol{H}_C$	=	$\partial\boldsymbol{\theta}_C/\partial\boldsymbol{\theta}_G$
$\boldsymbol{H}_J$	=	$\partial\boldsymbol{\theta}_J/\partial\boldsymbol{\theta}_G$
$\boldsymbol{\theta}_J$	:	joint angles

and $\boldsymbol{\theta}_C$ is the variable that represents the constraint condition by $\ddot{\boldsymbol{\theta}}_C = \boldsymbol{O}$. If the joint torques $\boldsymbol{\tau}_J$ are known, we can compute the generalized acceleration $\ddot{\boldsymbol{\theta}}_G$ and constraint forces $\boldsymbol{\tau}_C$ by equation (1).

Figure 3 shows an example of a dynamics simulation of a closed kinematic chain, where a human figure is trying to raise its body with its arms. The human figure has 28 DOF, and each rope consists of spherical and rotational joints. The figure holds the ends of ropes by spherical joints, forming a closed kinematic chain. Forward dynamics computation for this 48 DOF system, including the 6 DOF of the base body, takes approximately 32 ms on DEC Alpha 21264 500 MHz processor.

3.3. Structure-Varying Kinematic Chains

Most conventional methods for dynamics computation of kinematic chains assume that the link connectivity of the system does not change during the simulation. However, this is obviously not the

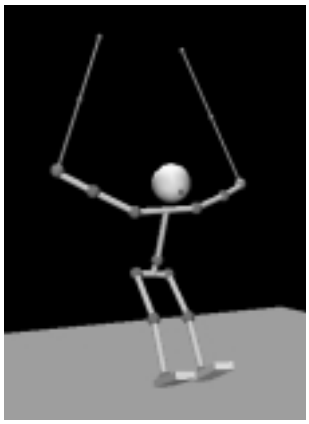

Figure 3: Simulation of a closed kinematic chain

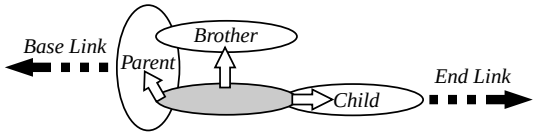

Figure 4: Three pointers to describe link connectivity

case in human motions. In fact, walking, the most common motion of human, can be said to have three different kinematic chains. We call such systems structure-varying kinematic chains and regard this as one of the key issues in the dynamics of human figures. To handle such situations by conventional methods, we would need to prepare all the possible structures in advance and switch among them during the simulation.

To solve this problem, we developed two techniques regarding the description of link connectivity [1]. The first is the method of description itself, where we use three pointers ("parent," "child," and "brother") per link to indicate its neighboring links as illustrated in Figure 4. However, these pointers are not capable of describing closed kinematic chains because the parent-child relationship makes an infinite loop. To describe closed kinematic chains, we virtually cut a joint in a loop and introduce an additional link called virtual link to describe the connection at the virtually cut joint. Another pointer, real, is added to the three pointers, to hold the relationship of real and virtual links. The concept is illustrated in Figure 5.

The second technique is the maintenance of pointers, that is, how to update the connectivity data in response to structural changes. Thanks to

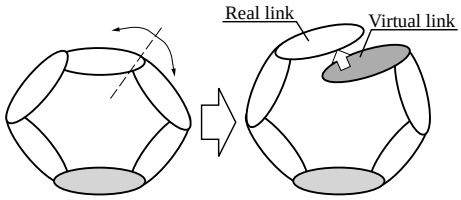

Figure 5: Virtual link to describe closed kinematic chains

the introduction of virtual links, the procedure is quite simple:

1. Link connection — If two links are connected by a new joint, create a new virtual link whose parent is one of the connected links, and set its real pointer to the other.

2. Joint cut — If a joint is cut, delete the virtual link associated with the cut joint.

By these simple procedures, link connectivity data is automatically updated according to the change in the kinematic chain.

The dynamics computation part is programmed to generate the equation of motion automatically based on the link connectivity. Thus, arbitrary structural changes are allowed and simulated without any manual tasks by the user. For the dynamics filter also, this description enables the filter to use the same strategy throughout the motion without concern for the change of structure.

Figure 6 is an example of an interactive application that makes use of these techniques. When the user clicks the mouse button, the monkey releases his hands one by one and finally falls down.

3.4. Collisions and Contacts

Contacts may be viewed as a structural change, because additional constraints appear at the contact point. They differ from joint connection in two points: transition of constraint and unilateral conditions. Therefore, modeling of collisions and contacts is still an open research issue in multibody dynamics area[19].

Collision and contact models are categorized into two types. The visco-elastic body model, or penalty model, places a virtual spring and damper at the point at which contact forces are exerted[20, 21]. The rigid body model, on the other hand, finds the contact force that satisfies

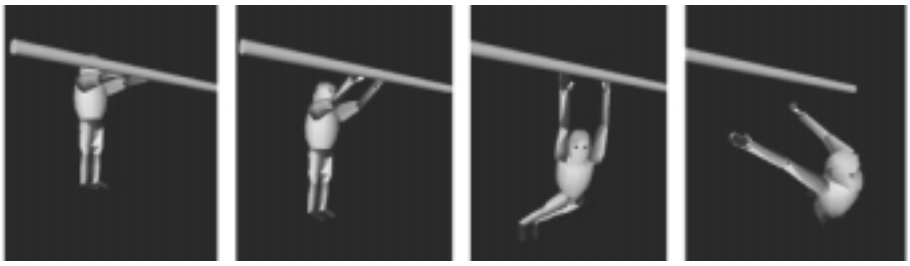

Figure 6: Dynamics simulation of structure-varying kinematic chain

the unilateral conditions through some optimization processes [19].

Our method is based on a rigid body model in the sense that we do not consider the deformation of links. However, to reduce the compuational load, we take the advantage of the fact that the precision of the contact model is not very important in human figures and apply a simplified computation with an iterative procedure:

1. Compute the discontinuous change of joint velocities using conservation of linear and angular momentum and Newton's impact law[19]. This approach has the advantage of numerical stability because large impact forces are not handled.
2. Set full constraint at each contact point.
3. Compute the constraint force to maintain the constraint condition $\ddot{\boldsymbol{\theta}}_C = \boldsymbol{O}$ by equation (1).
4. Check the feasibility of the constraint force.
5. If infeasible constraint forces were found, modify the constraint and return to 3, otherwise accept the constraint.

This method is more efficient than usual rigid body methods for two reasons: (1) it does not exceed four iterations, and (2) the computation for each iteration is very small.

4. Dynamics Filter Implementation

4.1. Basic Equations

The developed filter consists of two parts — feedback control and optimization based on equation (1). The control part computes the desired joint accelerations considering the reference motion, current state, and stability. Then the optimization part computes the optimal solution of equation (1) to generate the joint accelerations close to those computed in the control part.

First, initial desired acceleration of generalized coordinates $\ddot{\boldsymbol{\theta}}_G^{d0}$ is computed by simple joint angle and velocity feedback:

$$\ddot{\boldsymbol{\theta}}_G^{d0} = \ddot{\boldsymbol{\theta}}_G^{ref} + \boldsymbol{K}_D(\dot{\boldsymbol{\theta}}_G^{ref} - \dot{\boldsymbol{\theta}}_G) + \boldsymbol{K}_P(\boldsymbol{\theta}_G^{ref} - \boldsymbol{\theta}_G) \quad (3)$$

where $\boldsymbol{\theta}_G^{ref}$ is the generalized coordinates in reference motion, and $\boldsymbol{K}_D$ and $\boldsymbol{K}_P$ are constant gain matrices.

Then, in order to consider the global stability, the feedback of position and orientation of a specified point $\boldsymbol{P}$ in the upper body are included as follows. The desired acceleration of $\boldsymbol{P}$, $\ddot{\boldsymbol{\theta}}_P^d$, is computed by a similar feedback law as:

$$\ddot{\boldsymbol{r}}_P^d = \ddot{\boldsymbol{r}}_P^{ref} + \boldsymbol{K}_{DP}(\dot{\boldsymbol{r}}_P^{ref} - \dot{\boldsymbol{r}}_P) + \boldsymbol{K}_{PP}(\boldsymbol{r}_P^{ref} - \boldsymbol{r}_P) \quad (4)$$

where $\boldsymbol{r}_P^{ref}$ is the position and orientation of $\boldsymbol{P}$ in the reference motion, which can be obtained by forward kinematics computation, $\boldsymbol{K}_{DP}$ and $\boldsymbol{K}_{PP}$ are constant gain matrices, and $\boldsymbol{r}_P$ is the current position and orientation of $\boldsymbol{P}$. The initial desired acceleration of the generalized coordinates $\ddot{\boldsymbol{\theta}}_G^{d0}$ is modified into $\ddot{\boldsymbol{\theta}}_G^d$, so that the desired acceleration of $\boldsymbol{P}$, $\ddot{\boldsymbol{r}}_P^d$, is realized :

$$\ddot{\boldsymbol{\theta}}_G^d = \ddot{\boldsymbol{\theta}}_G^{d0} + \Delta\ddot{\boldsymbol{\theta}}_G^d \quad (5)$$

$$\Delta\ddot{\boldsymbol{\theta}}_G^d = \boldsymbol{J}_P^\sharp(\ddot{\boldsymbol{r}}_P^d - \ddot{\boldsymbol{r}}_P^{d0}) \quad (6)$$

where $\ddot{\boldsymbol{r}}_P^{d0} \triangleq \boldsymbol{J}_P\ddot{\boldsymbol{\theta}}_G^{d0} + \dot{\boldsymbol{J}}_P\dot{\boldsymbol{\theta}}_G$, $\boldsymbol{J}_P \triangleq \partial\boldsymbol{J}_P/\partial\boldsymbol{\theta}_G$, and $\boldsymbol{J}_P^\sharp$ is the weighted pseudo-inverse of $\boldsymbol{J}_P$.

Now we proceed to the optimization part. Solutions of equation (1) represents all the feasible combination of $\ddot{\boldsymbol{\theta}}_G, \boldsymbol{\tau}_C$ and $\boldsymbol{\tau}_J$. The task of the optimization part is to find the optimal solution of equation (1) to realize the desired acceleration. The optimized accelerations are integrated to derive the joint angle data.

First, in preparation for the optimization, we derive the weighted least-square solution of equation (2) and the null space of $\boldsymbol{W}$ regardless of the desired acceleration:

$$\boldsymbol{x} = \boldsymbol{W}^{\sharp}\boldsymbol{u} + (\boldsymbol{E} - \boldsymbol{W}^{\sharp}\boldsymbol{W})\boldsymbol{y} \tag{7}$$

where $\boldsymbol{W}^{\sharp}$ is the pseudo inverse of $\boldsymbol{W}$, $\boldsymbol{y}$ an arbitrary vector, and $\boldsymbol{E}$ the identity matrix of the appropriate size. Picking up the upper rows of equation (7) corresponding to the generalized accelerations, we get:

$$\ddot{\boldsymbol{\theta}}_G = \ddot{\boldsymbol{\theta}}_G^0 + \boldsymbol{V}_G\boldsymbol{y} \tag{8}$$

where $\ddot{\boldsymbol{\theta}}_G^0$ is the generalized acceleration in the least-square solution.

Next, we determine the arbitrary vector $\boldsymbol{y}$ to minimize the acceleration error by

$$\boldsymbol{y} = \boldsymbol{V}_G^*(\ddot{\boldsymbol{\theta}}_G^d - \ddot{\boldsymbol{\theta}}_G) \tag{9}$$

where $\boldsymbol{V}_G^*$ is the singularity-robust inverse[22] of $\boldsymbol{V}_G$.

Finally, substituting $\boldsymbol{y}$ into equation (7), we get the optimized solution of $\boldsymbol{x}$. Since $\boldsymbol{x}$ includes the generalized acceleration, joint torques and constraint forces all in one, the optimization part plays three roles at the same time: (1) computation of optimized motion, (2) computation of joint torques to realize the computed acceleration, and (3) dynamics simulation of the result.

4.2. Applications

In the following examples, the additional control point $\boldsymbol{P}$ was taken at the neck and its position and orientation were computed off-line, although it is easy to compute them on-line.

4.2.1. Filtering Raw Motion Capture Data

Figure 7 compares the captured (above) and filtered (below) walking motions. Although small latency is observed in the filtered motion, the result is satisfactory. This method is applicable to any motion as shown in Figure 8, which means that we do not need to prepare different filters for different motions.

4.2.2. Filtering Kinematically Synthesized Motion

The dynamics filter accepts not only raw captured data but also kinematic combinations of captured motions. The human figure in Figure 9 makes a turn of 30 degrees, by simply giving motion obtained by smoothly connecting two walking motions heading different directions as reference, considering no dynamic effects such as centrifugal force. This result shows that we can make a human figure walk along any path by indicating the direction using some input device.

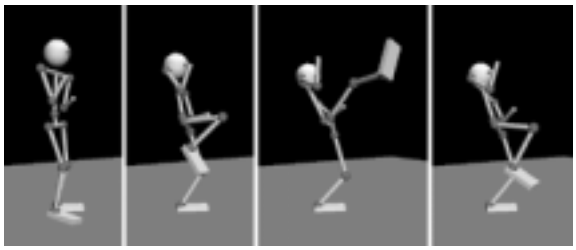

Figure 8: Karate kick generated by the dynamics filter

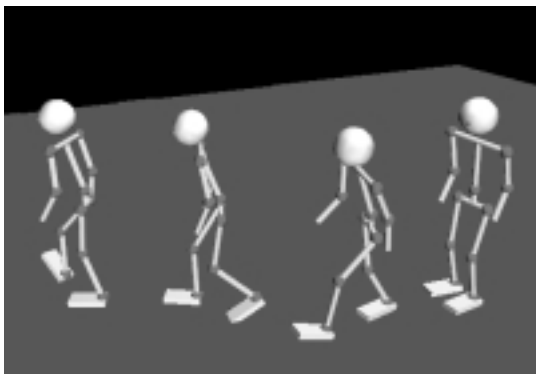

Figure 9: Motion generated from kinematically combined motion

4.2.3. Interactive Motion Generation

Note that the optimization applied here is strictly local to each frame, which means that this filter has the ability to realize a real-time and interactive motion generator. Although we cannot call it a "real-time dynamics filter" because the computation takes 70 to 80 ms per frame with an Alpha 21264 500MHz processor, we tried to interact with the figure filter as in Figure 10, where the figure is controlled to keep standing by the dynamics filter, and pushed in various directions by the user.

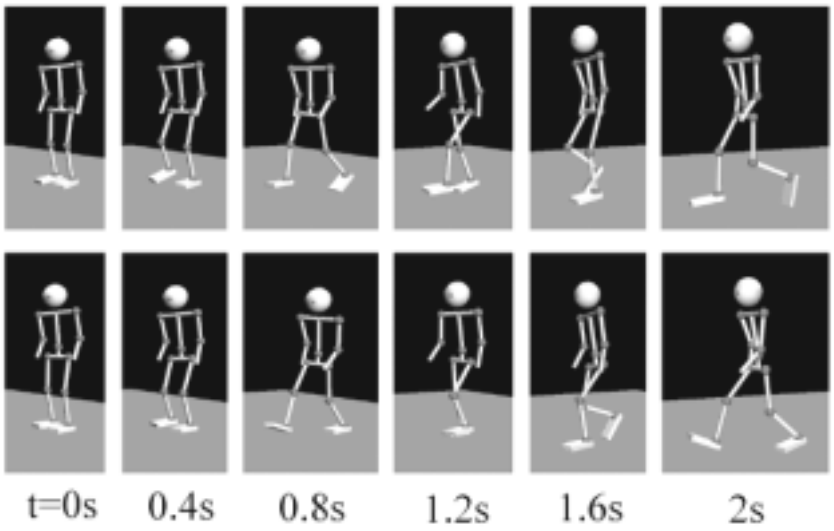

Figure 7: Captured (above) and filtered (below) walking motions

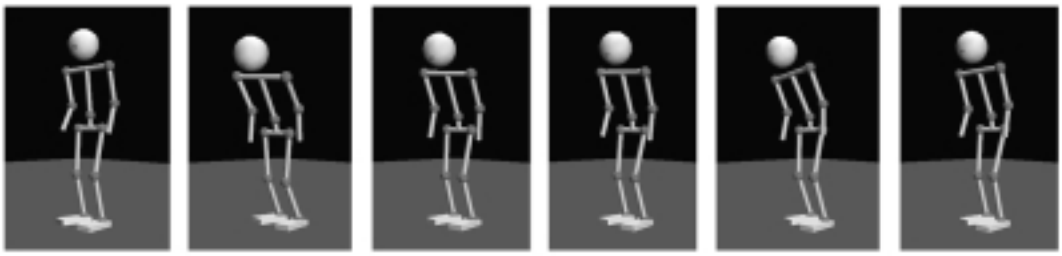

Figure 10: Example of interactive motion generation: push a standing figure

5. Conclusion

This paper presents our research issues toward a motion generator for human figures. The conclusions of this paper are summarized as follows:

1. The concept of a dynamics filter is proposed. A dynamics filter is a motion generator that creates a physically consistent motion from any reference motion, allowing interactive inputs from the user.

2. Basic dynamics computation methods used in the implementation of dynamics filter were presented. The methods can handle various phenomena observed in the motions of human figures, such as:

   (a) general closed kinematic chains;

   (b) structure-varying kinematic chains; and

   (c) collisions and contacts.

3. An implementation of an on-line dynamics filter was also introduced and proved the potential ability of the dynamics filter by examples of motions generated from motion capture data.

Currently we have several projects related to this issue:

1. Improvement of dynamics filter in its ability and computation time toward a real-time interactive system

2. Development of a behavior capture system, which not only captures the motion of humans but also their 3D shape, interaction with the environments, and mental state via various sensors

3. Controlling a real humanoid robot using the behavior capture system as an input device to make the robot imitate the motion of humans

Acknowledgements

This research was supported by the Humanoid Robotics Project, NEDO, Japan, and the CREST Program of the Japan Science and Technology Corporation.

References

[1] K. Yamane and Y. Nakamura: "Dynamics Computation of Structure-Varying Kinematic Chains for Motion Synthesis of Humanoid," Proceedings of IEEE International Conference on Robotics and Automation, pp.714–721, 1999.

[2] J.H. Park and Y.K. Rhee: "ZMP Trajectory Generation for Reduced Trunk Motions of Biped Robots," Proceedings of the 1998 IEEE/RSJ International Conference on Intelligent Robots and Systems, vol.1, pp.90–95, 1998.

[3] Q. Huang and S. Kajita et al.: "A High Stability, Smooth Walking Pattern for a Biped Robot," Proceedings of International Conference on Robotics and Automation, pp.65–71, 1999.

[4] A. DasGupta and Y. Nakamura: "Making Feasible Walking Motion of Humanoid Robots from Human Motion Captured Data," Proceedings of International Conference on Robotics and Automation, pp.1044–1049, 1999.

[5] Z. Popovic and A. Witkin: "Physically Based Motion Transformation," Proceedings of SIGGRAPH'99, pp.11–20, 1999.

[6] H. Ko and N.I. Badler: "Animating Human Locomotion with Inverse Dynamics," IEEE Transactions on Computer Graphics, vol.16, no.2, pp.50–59, 1996.

[7] Michiel van de Panne: "From Footprints to Animation," Computer Graphics Forum, vol.16, no.4, pp.211–223, 1997.

[8] E.J. Haug: Computer Aided Kinematics and Dynamics of Mechanical Systems, Allyn and Bacon Series in Engineering, 1989.

[9] J. G. de Jalon and E. Bayo: Kinematic and Dynamic Simulation of Multibody Systems – the Real-Time Challenge, Springer – Verlag, 1993.

[10] R. Featherstone: Robot Dynamics Algorithm, Kluwer, 1987.

[11] K.S. Chang and O. Khatib: "Efficient Algorithm for Extended Operational Space Inertia Matrix," Proceedings of IEEE International Conference on Robotics and Automation, pp.350–355, 1999.

[12] S. McMillan and D.E. Orin: "Forward Dynamics of Multilegged Vehicles Using the Composite Rigid Body Method," Proceedings of IEEE International Conference on Robotics and Automation, pp.464–470, 1998.

[13] O. Bruneau and F.B. Ouezdou: "Dynamic Walk Simulation of Various Bipeds via Ankle Trajectory," Proceedings of the 1998 IEEE/RSJ International Conference on Intelligent Robots and Systems, vol.1, pp.58–63, 1998.

[14] B. Perrin, C. Chevallereau, and C. Verdier: "Calculation of the Direct Dynamics Model of Walking Robots: Comparison Between Two Methods," Proceedings of IEEE International Conference on Robotics and Automation, vol.2, pp.1088–1093, 1997.

[15] Y. Nakamura and M. Ghodoussi: "Dynamics Computation of Closed-Link Robot Mechanisms with Nonredundant and Redundant Actuators," IEEE Transactions on Robotics and Automation, vol.5, no.3, pp.294–302, 1989.

[16] A. Codourey and E. Burdet: "A Body-Oriented Method for Finding a Linear Form of the Dynamic Equation of Fully Parallel Robots," Proceedings of IEEE International Conference on Robotics and Automation, pp.1612–1618, 1997.

[17] K. Yamane, M. Okada, N. Komine, and Y. Nakamura: "Parallel Dynamics Computation and H_∞ Acceleration Control of Parallel Manipulators for Acceleration Display," Proceedings of 1998 IEEE International Conference on Robotics and Automation, pp.2301–2308, 1998.

[18] K. Yamane and Y. Nakamura: "Dynamics Computation of Closed Kinematic Chains for Motion Synthesis of Human Figures," Proceedings of IEEE/RSJ International Conference on Intelligent Robots and Systems, pp.1108–1114, 1999.

[19] F. Pfeiffer and C. Glocker: Multibody Dynamics with Unilateral Contacts, Wiley Series in Nonlinear Science, 1996.

[20] D.W. Marhefka and D.E. Orin: "Simulation of Contact Using a Nonlinear Damping Model," Proceedings of the 1996 IEEE International Conference on Robotics and Automation, pp.1662–1668, 1996.

[21] P.R. Kraus, V. Kunmar, and P. Dupont: "Analysis of Frictional Contact Models for Dynamic Simulation," Proceedings of the 1998 IEEE International Conference on Robotics and Automation, pp.976–981, 1998.

[22] Y. Nakamura and H. Hanafusa: "Inverse Kinematics Solutions with Singularity Robustness for Robot Manipulator Control," Journal of Dynamic Systems, Measurement, and Control, vol.108, pp.163–171, 1986.

Proceedings of the International Symposium on
Adaptive Motion of Animals and Machines,
Montreal, Aug.8-12, 2000

Adaptive Motions by the Endocrine System Model in An Autonomous Robot

Tetsuya OGATA* *and* Shigeki SUGANO**
Department of Mechanical Engineering, Waseda University
3-4-1, Okubo, Shinjuku-ku, Tokyo 169-8555, Japan
Phone: +81-3-5286-3264, Fax: +81-3-5272-0948
E-mail: {ogata*, sugano**} @paradise.mech.waseda.ac.jp

ABSTRACT*: This paper describes an application of the model of human's endocrine system in a real robot hardware. The robot has four kinds of hormone parameters to adjust to various internal conditions such as motor output, cooling fan output and sensor gain etc. As the result of the experiments, the hormone parameters enabled the robot to adjust its conditions (homeostasis) and generate primitive adaptive motions.*

1. INTRODUCTION

To date, various “emotion models” have been proposed in fields of the human interface (HI) in order to realize human friendliness of machines etc. [1] In these studies, some explicit emotional states are implemented to the emotion models by designer a priori, such as “anger,” “pleasure” and “sadness” etc. The research theme of these studies is to determine the methodology to categorize emotion, the methodology to express each emotion, the methodology to change the emotional state in the model, and the methodology to improve the recognition rate for human to observe the emotion model etc.

Recently, much attention is paid to the application of the emotional mechanism into autonomous robots [2-4] in some fields represented by the “New AI.” These studies do not treat the emotional states categorized explicitly, but the intelligent behaviors which are similar to “emotional behaviors” of living creatures. The motivation for these studies is to construct the machine intelligence rather than the human interface. Therefore, the research theme for these studies is to propose the architecture of a variety of emerging behavior.

The behavior variety of living creatures (human) are assumed to emerge from biological changes in the body, for example, respiratory rhythm, muscle tension, pupils diameter, and skin temperature, etc. These biological changes do not depend on the reflection system such as the spinal cord and the brainstem but the autonomic nervous system and the endocrine system.

The objective of this study is to realize an emotion model without the need of defining the classified emotional states, but introducing a model based on the endocrine system. To date, we have developed an autonomous mobile robot named WAMOEBA-1R (Waseda Amoeba, Waseda Artificial Mind On Emotion BAse), and implemented the software of the endocrine system using fuzzy set theory, and some effects of the system were confirmed based mainly on the obstacle avoidance simulation experiments. [5, 10] Through the experiments, it was clarified the importance of the consideration of the robot hardware architecture such as the internal sensors and the internal adjusters which are the components of “the endocrine system” in order to realize the environment adaptability of the robot.

Based on above consideration, this paper discuss the robot hardware architecture which refers to human biological system. WAMOEBA-2R developed in this study obtained two possible functions by introducing the engineering model of the endocrine system. One is the adjustment function of the internal condition, and the other is the emotional expression function.

2. MORPHOLOGY OF THE ENDOCRINE SYSTEM IN ROBOTS

In this chapter the outline of the autonomic nervous system and the endocrine system is described. [6] The human nervous system is categorized into two nerve systems. One is the ‘motor system’ which has been conventionally implemented into robots as the joint servo control, and second is the autonomic nerve system and the endocrine system for the adjustment of the body.

These systems do not belong to a reflection system but a limbic system such as the amygdala and the hypothalamus in human brain where all sensing information are integrated. These parts of the brain are comparatively old;

they appeared after the reflection systems such as the brainstem and the vertebras. The endocrine system posses hormones to adjust various internal organs.

The autonomic nervous system and the endocrine system has two principle functions. One function is called 'homeostasis,' which maintains the internal condition of the living organisms. The other function is adjustment of body states in order to drive primitive emotions such as "anger" and "fear," so the being will survive in its environment. [7]

It is thought that the criteria of this adjustment would be the most primitive instinct of creatures; "self-preservation." [8] For example, when the conditions of the environment and/or the body change rapidly, the hormones, such as the noradrenaline and the dopamine etc. are secreted and the sympathetic nervous system is driven. Then, the muscles are tense, the pupils shrink and the activity of the internal organs are suppressed. As the result of these effects, the states of the body are prepared for the "fighting or flighting" behavior. [9]

If such endocrine systems are introduced into a robot, it is expected for the robot to adapt the environmental changes by the adjustments of the motor outputs, the viewing angles of the cameras, and the circuit temperatures, etc. As a result of these effects, the robot is expected to generate more flexible behaviors than the simple reflection systems that behavior based robots [10] generate in future. Furthermore, the behavior morphology of the robot has the possibility to become extremely similar to emotional expressions of human. For example, even the changes of the motor outputs are expected to cause psychological impressions to the observer in a sense of "excitement" or "quietness," for example.

3. THE MODEL OF THE ENDOCRINE SYSTEM

3.1 HARDWARE OF WAMOEBA-2R

In this chapter, an autonomous mobile robot developed in this study: WAMOEBA-2R shown in Fig. 1, 2 is described. WAMOEBA-2R is an independent robot into which the batteries and the control systems are built. The dimensions are 990 (L) x 770 (W) x 1390 (H) [mm], and the weight is approximately 130 [kg]. Since a motor powered wheel chair is adopted to the mobile vehicle of WAMOEBA-2R, the activity area is wide and not limited to the indoors. Moreover, using the battery equipped in the motor powered wheel chair, the total system of WAMOEBA-2R can be driven for about half an hour.

To detect the external information, the head is equipped with four ultrasonic range sensors, two color CCD cameras, two microphones, and the vehicle is equipped with eight touch sensors.

The breast portion of WAMOEBA-2R's body has two arms which has four D. O. F. (degree of freedom) with gripper which has one D. O. F. Total reach of this arm is 450 [mm] , the weight is 3.8 [kg], and the electric consumption is 50.5 [W]. Each arm can hold an object with a maximum weights of 2 [kg], and make emotional expressions by making gestures. A strain gage is installed directly on each joint axis to detect the torque of each joint.

Further, the head and breast are each equipped with the LCD for the expression of emotional information, monitoring of technical parameters and command inputs, etc.

However, the characteristic unique to WAMOEBA-2R are not the sensors or D.O.F. but the internal mechanisms for modeling the human's endocrine system. The endocrine system, control the entire state of the living organism. It is thought that, in the case of robot hardware,

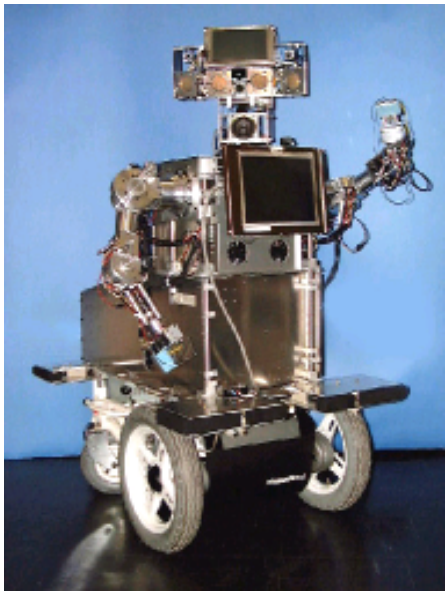

Fig. 1 WAMOEBA-2R (Photgraph)

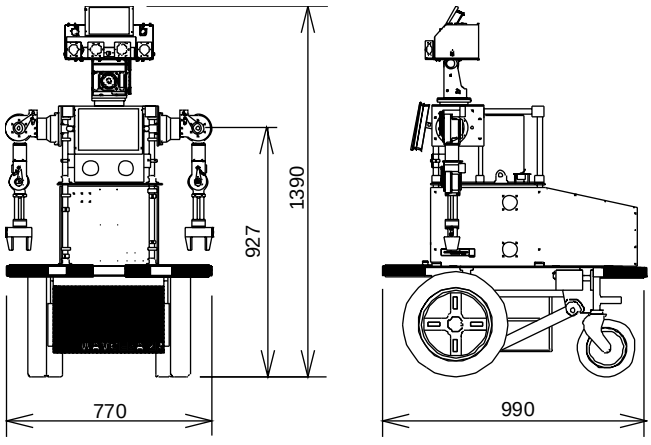

Fig. 2 Assembly Drawing of WAMOEBA-2R

Table 1 The correlation between the autonomic nervous system and Robot hardware mechanisms

Influence of Autonomic Nervous System in Human	Mechanical System		
	Influenced Part	Input Information	Adjustor
Heart Beat Sugar Density in Blood	Actuator Battery	Torque Sensor Voltage, Current Sensor	Actuator Output
Gastrointestinal Activity	Battery	Battery Load (Fruid Level Sensor)	Charging Current
Sweat, Cowlick Musclar tiredness	CPU, Electiric Curcuit, Actuator	Temperature Sensor	Cooling Fan
Arousal	Program Cycle Speed	Data Processing Times	Occupaton Memory
Pupillary Light Reflex	Camera	Optical Sensor	Squeezing
Excretion	Structural Part Electric Curcuit	Rust and/or Dirt	-
Self-Restoration of Organization	Wiring	Test for continuity (Tester, Voltmetor)	-
	Structural member	Deformations (Strain Gage etc.)	-
	Sensors	Referrence to Input Information	-

Table 2 Specification of WAMOEBA-2R

Dimensions		1390(H) x 990(L) x 770(W) mm
Weight		Approx. 130 kg
Operating Time		Approx. 50 min
Max speed		3.5 km/h
Payload		2 kgf/hand
External DOF	Neck	2
	Vehicle	2
	Arm	4 x 2 = 8
	Hand	1 x 2 = 2
Internal DOF	Cooling Fan	10
	Power Switches	4
External Sensors	Image Input Audio Input Audio Output Distance Detection Joint Torque Grip Detection Object Detection	CCD Cameras x 2 Microphones x 2 Speaker Ultrasonic Sensors x 4 Torque Sensers x 6 Pressure Sensors x 2 Photoelectric Sensors x 2 Touch Sensors x 8
Internal Sensors	Temperature Battery Voltage Motor Current	Thermometric Sensors x 8 Voltage Sensor Current Sensor
Material		Duralumin, Aluminum
CPU		Pentium III (500MHz) x 2
OS		RT-Linux

these organisms correspond to the control mechanisms of electric power consumption and circuit temperature etc. Table 1 shows the results of the consideration of correspondences between human's autonomic nerve system and the hardware mechanisms. Based on this assumption, we constructed the original hardware architecture in WAMOEBA-2R.

WAMOEBA-2R acquires the voltage of the battery in the motor powered wheel chair directly through the A/D converter and the driving current through the current sensor. Also, using the temperature sensors IC, which are fixed to each body part with silicon, WAMOEBA-2R can measure temperature at eight positions including the motors (the head, the neck, the shoulder, the elbow, and the motor chair) and the electrical circuits (the image processing board and A/D boards etc.).

WAMOEBA-2R can cool these circuit boards by switching the number of driven cooling fans. Moreover, WAMOEBA-2R can control the ON/OFF power supply of the motor powered wheel chair, the neck motor and the arm motor, etc., by itself. WAMOEBA-2R can adjust the entire electric power consumption and the temperature of the motor and the circuit by these functions.

WAMOEBA-2R has two CPU boards which are connected via a LAN, and each CPU connects various I/O boards such as the image processing board and A/D board (ISA and PCI bus). Table 2 shows the hardware specification of WAMOEBA-2R.

3.2 ENDOCRINESYSTEMSOFTWARE

In earlier work [5, 11], the original evaluation method was presented; "evaluation function of self-preservation" using fuzzy set membership function to simulate the endocrine system in robots. In this chapter, the concrete methodology for applying the model to the robot hardware is described.

Each evaluation function converts the sensor input into the evaluation value of durability (breakdown rate) of the robot between 0-1. This function consists of two sigmoid functions with one minimum value which stands for the best state for self-preservation. When this value is close to zero, the state of self-preservation is good, and if this value gets close to one, the state is bad. WAMOEBA-2 has seven kinds of self-preservation evaluation functions which correspond to eleven internal and external sensors. The shape of these functions are decided depending on the basic hardware specs. For example, the evaluation function of the voltage of battery is shown in Fig. 3. In

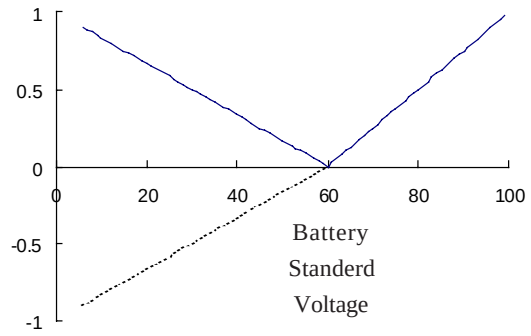

Fig.3 Evaluation Function of Voltage Battery

this case, the shape of the function is decided depending on the lowest voltage of the circuit drive, the standard voltage of the battery.

WAMOEBA-2R calculates the total value *P* of these evaluation functions and outputs four hormone parameters [*H*1 to *H*4] corresponding to four conditions, i.e. whether the evaluation value *P* is good or bad (mood), and whether the *P* changes dynamically or not (arousal), using the four sigmoid functions. These hormone parameters influence many hardware conditions and properties such as the sensor gains, the motor outputs, the temperatures of the circuits and the energy consumption etc. The influences of each hormone are decided by referring to the physiology [6] (Table 3).

The behaviors of WAMOEBA-2R are generated based on the original reflection mechanism called the "motor agent." [12] In the motor agent algorithm, each motor acquires all sensory information and other motor drive conditions through the network with in the robot hardware. Based on this information, each motor decides its own actions autonomously. Based on only the implicit expressions, the "motor agent," which is described as the weight of the network, WAMOEBA-2R can generate the behavior using the whole body, e.g. imitation of the movement area, the sound origin, and avoidance behavior, etc. Fig. 4 shows the structure of the hardware and software of WAMOEBA-2R.

Table 3 Influences of the Hormone Parameters

		H1	H2	H3	H4
Actuator Output		Up	Down	Down	Up
Cooling Fan Output		Down	Up	Up	Down
CCD Camera Viewing Angle		Decrease	Increase	Increase	Decrease
Ultrasonic Sensors Sensing Area		Narrow	Wide	Wide	Narrow
Sound	Volume	Up	Down	Down	Up
	Speed	Up	Down	Down	Up
	Loudness	Down	Down	Up	Up
LCD Color		Red	Blue	Yellow	

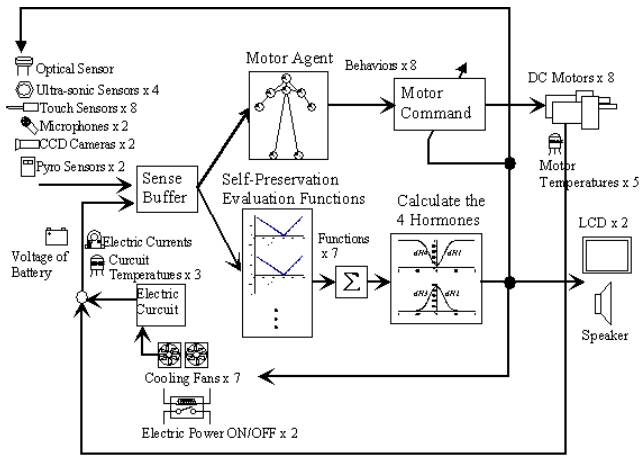

Fig. 4 System Structure of WAMOEBA-2R

4. AFFECTS OF ENDOCRINE SYSTEM

To verify the effects of the presented hardware and software architecture, we performed the experiments using WAMOEBA-2R. The experimental environment was set in an indoor room with a size of 6.0 (L) x 7.4 (W) [m]. There is an obstacle, of which the size is 1200 (L) x 20 (W) x 1080 (T) [mm]. WAMOEBA-2R performed simple collision avoidance behaviors by using the motor agent architecture.

We performed forty sets of experiments with WAMOEBA-2R, first with the presented model and then without the model. Each experiment takes approximately five minutes. In each of the experiments, thirteen kinds of data ,such as the temperature of the motors and the movement distance were sampled every two seconds.

4-1 ADJUSTMENT OF INTERNAL CONDITION

1) Stabilization of Electrical Current Consumption

Fig. 5 shows the history of the motor current value in WAMOEBA-2R in the collision avoidance behavior. When the hormone parameters were not used (No use), it is confirmed that the motor current value changes rapidly according to the mechanical behavior changes of WAMOEBA-2R. These could be regarded as the unstable states. On the other hand, when the parameters were used (Use) , the motor current was stabilized because the behavior changes smoothly by the effects of the hormone

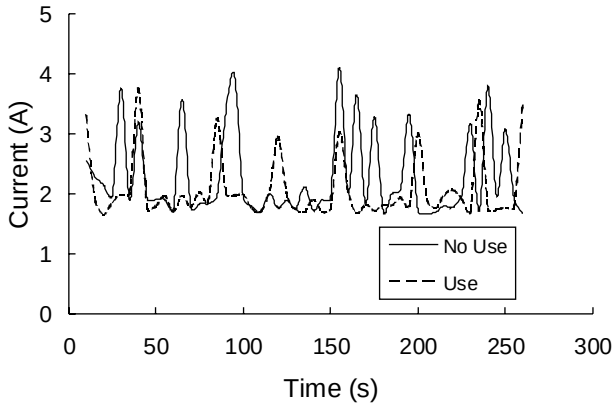

Fig. 5 The Comparison of the Motor Currents

parameters.

Referring to Table 3, if the motor output increases by the hormone parameters *H*1 and *H*4, then the cooling fan output decreases. On the other hand, if the motor output decreases by the hormone parameters *H*2 and *H*3, then the cooling fan output increases. WAMOEBA-2R achieves the stabilization of the current consumption of the entire system not by the suppression of the moving distance or the changing of the behavior form, but by the control adjustment between the motor and the cooling fan.

2) Stabilization of Temperature of Circuit

Based on the above relationship between the stabilization of the motor current and the cooling fan output, we investigated the influences of the temperature adjustment of the cooling fan on the electrical boards.

Fig. 6 shows the cooling fan output and the temperatures of each board. Though the alternation of the motor output influences each cooling fan's output, the H2 hormone parameter is an output due to rising temperature of each board and the output increases of the cooling fan. In this case the temperature of each board tends to converge around just under 26 [℃].

The following statements are the results of the experiments. When the temperatures of circuits are low, the hormone parameters increase the motor output and WAMOEBA-2R can move aggressively. On the contrary, when the temperatures of the electrical circuits are high, the hormone parameters suppress the motor output and increase the output of the cooling fan for the stabilization of the circuits.

From these experiments, it can be said that the proposed model of the endocrine system controls various conditions of WAMOEBA-2R simultaneously. These adjustments are decided not by the rules designed a priori, but by four hormone parameters which constitute the state of excitement or a state of calm for WAMOEBA-2R based on the evaluation value of self-preservation. These can be regarded as results of the realization of a part of the function "homeostasis," which stabilizes the entire system of the living organism.

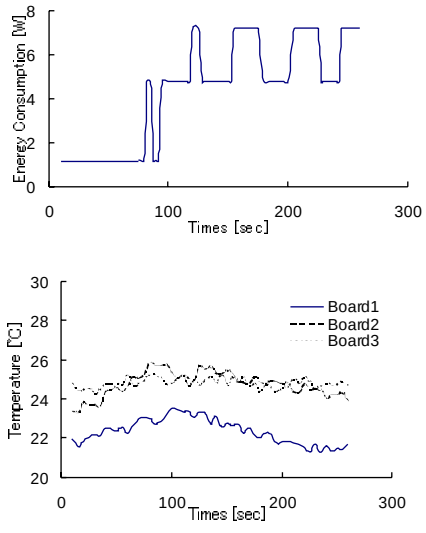

Fig. 6 The Cooling Fans Output and the Temperature of Curcuit Boards (System Used)

4.2 GENERATION OF ADAPTIVE MOTIONS

In this chapter, the adaptability of the arm motion is described. WAMOEBA-2R can detect the moving object by the cameras, and move the arm to the object by the motor agent architecture. Using this properties, we carried out some experiments to confirm the influence of the model of the endocrine system of WAMOEBA-2R. Concretely, we set the obstacle on the trajectory of the arm shown in Fig. 7, and observed the left arm motions according to the output of hormone parameters.

Fig 8 shows one of the results of the motions of WAMOEBA-2R arm without the effects of the endocrine system model. The data were sampled every one second for 485 [sec]. It is confirmed that the end of the arm made the collision with the obstacle, and the motion failed into the "dead lock" loop.

Fig. 9 shows one of the results of the motions of WAMOEBA-2R arm with the effects of the proposed model. It is confirmed that the arm could reach the moving object detected by the cameras. Though the data were sampled for 411 [sec], it took only 172 [sec] of the arm to reach the target. This motion was generated by the following process.

The condition of the hormone parameter was changed according to the output of the self-preservation evaluation function of the joint torques caused by the collisions between the end of the arm and the obstacle. Then WAMOEBA-2R became exciting condition and the mo-

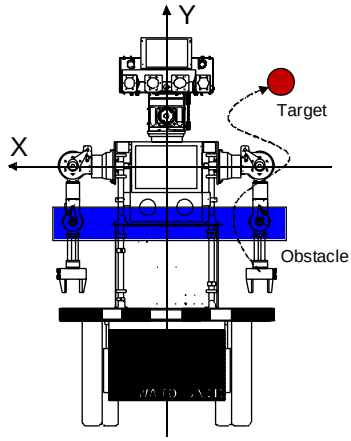

Fig. 7 The Experiment of the Arm Reaching

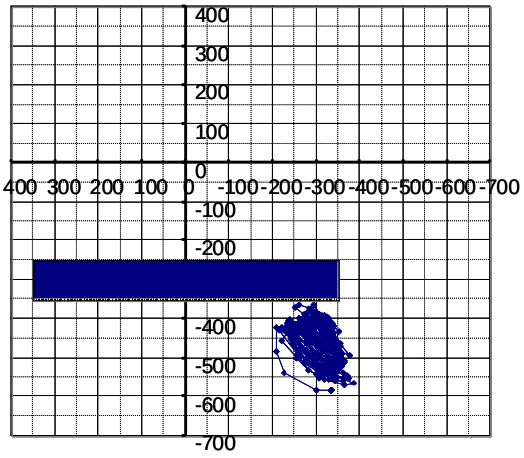

Fig. 8 The trajectory of the arm (without the proposed model)

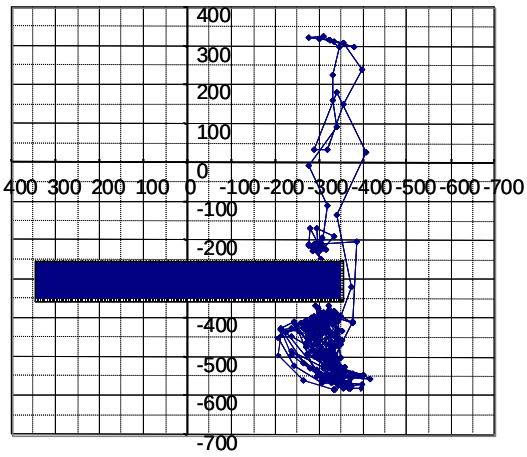

Fig. 9 The trajectory of the arm (with the proposed model)

tion speed and the trajectory of the arm were changed by the effects of the hormone parameters, and the diversity of the motion was generated.

It is thought that the results is one example of the adaptability of the endocrine system.

5. SUMMARY AND FURTHER WORK

In this study, the correlation between a human's endocrine system and the hardware mechanisms were described. Also, we showed the hardware mechanism for modeling the endocrine system in the independent autonomous mobile robot, WAMOEBA-2R developed in this research to realize the emotional communication between humans and robots. WAMOEBA-2R can acquire the internal information such as the voltage of the battery, the consumption current, and the circuit temperature etc. Moreover, WAMOEBA-2R is implemented four kinds of hormone parameters which control the internal conditions by using the cooling fans and electrical switches. These parameters are calculated from the original algorithm "the evaluation function for self-preservation." The parameters influence various parts, such as motor outputs and sensor gains due to the results of these functions. It is found that WAMOEBA-2R can adjust the internal conditions such as the motor current and the temperature of the circuit and produce adaptive behaviors accordingly.

In the future, it would be an interesting study to obtain evaluations concerning the psychological impressions which WAMOEBA-2R gives to humans.

REFERENCE

[1] F.Hara and H.Kobayashi: "Computer graphics for expressing robot- Artificial Emotions," in Proc. of IEEE Int. Workshop on Robot and Human Communication (ROMAN'92), pp.155-160, 1992.

[2] R.Pfeifer: "Emotions in Robot Design," in Proc. of IEEE International Workshop on Robot and Human Communication (ROMAN'93), pp.408-413, 1993.

[3] T.Gomi, and J.Ulvr: "Artificial Emotions as Emergent Phenomena," in Proc. of Robot and Human Communication (ROMAN'93), pp.420-425, 1993.

[4] T.Shibata, K.Inoue and R.Irie, "Emotional Robot for Intelligent system -Artificial Emotional Creature Project-," in Proc. of Robot and Human Communication (ROMAN96), pp.466-471, 1996.

[5] S.Sugano and T.Ogata: "Emergence of Mind in Robots for Human Interface -Research Methodology and Robot Model-," in Proc. of IEEE Int. Conf. of Robotics and Automation, pp.1191-1198, 1996.

[6] R.Nieuwenhuys, J.Voogd and Chr.Huijzen, ceremony he Human Central Nervous System-A Synopsis and Atlas, and Springer-Verlag, 1988 nine

[7] M.Toda: "Man, robot, and society," The Hague, Nijhoff, 1982.

[8] I.Kato: "Homini-Robotism," in Proc of Int. Conf. on Advanced Robotics (ICAR'91), pp.1-5, 1991.

[9] W. Cannon: "Bodily Changes in Pain," Hunger and Rage (2 nd ed), Appleton (New York), 1929.

[10] R. Brooks: "A robust layered control system for a mobile robot," in Proc. of IEEE Journal of Robotics and Automation, RA-2, April, and pp.14-23, 1986.

[11] T.Ogata and S.Sugano, "Emotional Behavior Adjustment System in Robots," in Proc. of IEEE International Workshop on Robot and Human Communication (ROMAN'97), pp.352-357, 1997.

[12] T. Ogata and S. Sugano, "Emotional Communication Between Humans and the Autonomous Robot which has the Emotion Model," in Proc. of IEEE Int. Conf. on Robotics and Automation (ICRA'99), pp.3177-3182, 1999.

Proceedings of the International Symposium on
Adaptive Motion of Animals and Machines,
Montreal, Aug.8-12, 2000

Self-Excited Walking of a Biped Mechanism

Kyosuke Ono[1], Ryutaro Takahashi[2], Toru Shimada[3] and Atsushi Imadu[4]

[1]Dept. of Mechanical Engineering and Science, Tokyo Institute of Technology
2-12-1 Ookayama, Meguro-ku, Tokyo, 152-8552, ono@mech.titech.ac.jp
[2]Dept. of Mechanical Engineering and Science, Tokyo Institute of Technology, ryutaro@stu.mech.titech.ac.jp

Abstract

This paper present a self-excited walking of a four-link biped mechanism which possesses an actuated hip joint and passive knee joints. First we manifested that this self-excitation control enables 3-DOF planar biped model to walk on a level ground, by numerical simulation. Next we showed experimental study of a manufactured planar biped walking robot. We demonstrated that stable walking can be realized on a slightly inclined plane by the self-excitation control.

1. Introduction

Biped locomotion is regarded as a combined motion of an inverted pendulum and a 2-DOF pendulum. Here the inverted pendulum represents motion of a support leg and body, while the 2-DOF pendulum represents motion of swing leg. Only when those movements are synchronized, biped locomotion can be stabilized.

Over the past few decades, a large number of studies have been made on bipedal walking. Among many researchers, McGeer [1] [2] studied passive dynamic walking mechanisms on a downhill slope without actuating and controlling. In connection with his research, a close study on stability and complexity of simple walking model was done by Garcia [3]. Goswami [4] [5] investigated the passive gait of a compass-like biped robot especially about symmetry and chaos. Spong [6] [7] studied on the switching control applied to passive gait. One of the purpose of their researches is to enlarge the basin of the limit cycles. The remarkable feature of these passive gait is its anthropomorphic motion and energy efficiency because those passive mechanisms utilize its inherent natural motion.

Based on the similar idea of utilizing natural mode, one of the authors has already proposed self-excitation control [8] which can efficiently and robustly drive natural mode of the mechanical system. Ono and Okada [9] [10] applied the Van der Pole type self-excitation to drive an insect wing model and the asymmetric stiffness-matrix type to drive a rolling biped mechanism. Further, Ono and Imadu [11] showed a possibility that a human like planar 3-DOF biped mechanism can be driven by the latter method. In this paper, we show this self-excitation control strategy enables 3-DOF planar biped mechanism to walk. Then we verify the numerical simulation experimentally by using a manufactured biped robot.

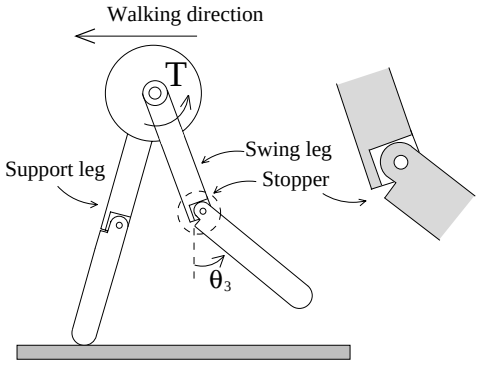

Figure 1: 3-DOF walking mechanism

2. Control Method of Biped Walking

2.1. Conditions for stable walking

Figure 1 shows a planar biped walking mechanism which has no ankle and trunk. This mechanism consists of two legs which are connected in series at hip joint by an actuator. Each leg consists of a thigh and a shank connected at a passive knee joint which has a rotary damper and a knee stopper. By this knee stopper, an angle of knee rotation is restricted like a human knee so that it cannot rotate forward. Five conditions are required to realize a stable biped walking on a sagittal plane

by this simple mechanism.

1. The period of the mechanism as a inverted pendulum should synchronize with half period of swing leg as a 2-DOF pendulum.

2. Kinematic energy loss which is consumed during swing leg's foot collision and each knee stopper collision should be actively supplied by the actuator.

3. Synchronized motion of inverted pendulum and 2-DOF swing leg pendulum, and energy supply and consumption have a stable characteristics against deviations from the synchronized motion.

4. At the support leg's knee joint, knee stopper have to be locked (support leg condition).

5. The swing leg should bend to keep the clearance (swing leg condition).

In this study, we show that these requirements can be satisfied by self-excitation control. By the linearized theory and simulation of nonlinear system, we already confirmed that 2-DOF swing link system is efficiently self-excited by asymmetric stiffness-matrix-type self-excitation control. Based on the previous study, we defined feedback torque at the hip joint as such,

$$T = -k\theta_3 \tag{1}$$

where k is a feedback gain and θ_3 is absolute angle of the swing leg shank. Because it is difficult to analytically show that this control method can generate a walking motion which satisfies the above mentioned requirements, we show this self-excitation control can fulfill the required conditions and make the mechanism walk stably on level plane by numerical simulation.

2.2. Algorithm of self-excitation control

In order to derive basic equation of motion to simulate the walking gait of the 4-link biped mechanism, we divide one step walking motion into three phases from view point of difference of freedom and governing equation. Figure 2 shows three different phases of one step walking.

1. From start of swinging leg to collision of knee stopper (First phase).

2. From collision of knee stopper to touchdown of swing leg (Second phase).

3. Double support phase and exchange between support leg and swing leg (Third phase).

In the following analysis, we assumed that during the first and second phases, the knee stopper

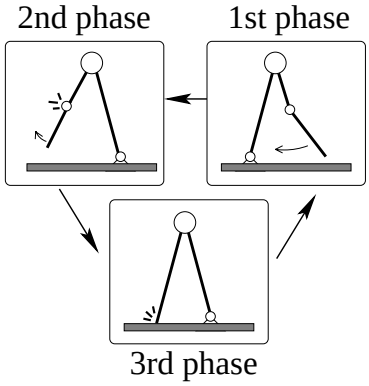

Figure 2: Different phases of biped walking

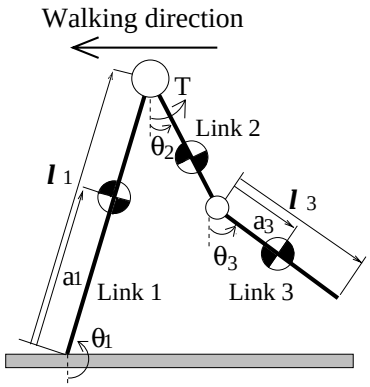

Figure 3: Analytical model of 3-DOF walking mechanism

of support leg can be locked by negative internal force. The validity of this assumption is discussed in the next chapter. From this assumption we can regard the biped mechanism as 3-DOF which consists of 1-DOF support leg and 2-DOF swing leg.

In the first phase, the feedback torque $T = -k\theta_3$ is applied at hip joint. By this feedback torque, swing leg is naturally bent at knee joint. Then it can swing forward without hitting the ground.

In the second phase, the feedback torque is not supplied ($T = 0$). Therefore it moves freely until it collides with a ground. We considered these foot collision and knee stopper collision as perfect inelastic one. Hence we calculate angular velocity of each links just after the collisions by the law of conservation of angular momentum.

2.3. Analysis of the model

First Phase: Figure 3 shows the analytical model of the biped mechanism. Equation of motion of

Table 1: Link parameter values

m_1	$[kg]$	4.0	$m_{2,3}$	2.0	2.0
l_1	$[m]$	0.8	$l_{2,3}$	0.4	0.4
I_1	$[kgm^2]$	0.21	$I_{2,3}$	0.027	0.027
a_1	$[m]$	0.2	$a_{2.3}$	0.2	0.2

this system is written as follows:

$$[M]\begin{pmatrix}\ddot{\theta}_1\\ \ddot{\theta}_2\\ \ddot{\theta}_3\end{pmatrix}+[C]\begin{pmatrix}\dot{\theta}_1^2\\ \dot{\theta}_2^2\\ \dot{\theta}_3^2\end{pmatrix}+\begin{pmatrix}K_1\\ K_2\\ K_3\end{pmatrix}=\begin{pmatrix}k\theta_3\\ -k\theta_3\\ 0\end{pmatrix} \quad (2)$$

Second Phase: During the second phase there is no feedback torque, and the swing leg can be considered as 1-DOF because the knee stopper is naturally locked by walking motion.

Third Phase: We assumed this phase takes place instantaneously. From the law of conservation of momentum and angular momentum, we derive the angular velocity just after the foot collision.

3. Results of Numerical Simulation

3.1. Nature of self-excited walking

Based on the analysis described above, we performed numerical simulations. In this self-excitation control strategy, the variable parameter is only feedback gain k. Therefore we examined the effect of feedback gain on characteristics of biped walking motion.

Figure 4 shows a typical result of numerical simulation of stable walking motion by using link parameter values shown in Table 1. Those parameter values are obtained under the assumption that the linear density of the robot's link is 5 [kg/m] and the length of leg l_1 is 0.8 [m]. Figure 5 shows phase plane of the shank during one cycle of the gait. From $t = T_0$ to $t = T_2^-$, the shank is support leg phase, from $t = T_2^+$ to $t = T_4^+$ the shank is swing leg phase. T_1^-, T_3^- and T_1^+, T_3^+ indicate before and after the knee stopper collision, respectively. T_2^-, T_4^- and T_2^+, T_4^+ show before and after the foot collision with the ground, respectively.

If the feedback gain and initial conditions are adequate, the gait of biped mechanism converges to the stable limit cycle. By inverse dynamics of

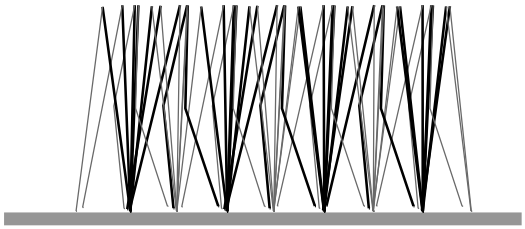

Figure 4: Stick figure of stable walking (k=6.3 [Nm/rad], $r = 0.0$ [m], Period=1.18 [s])

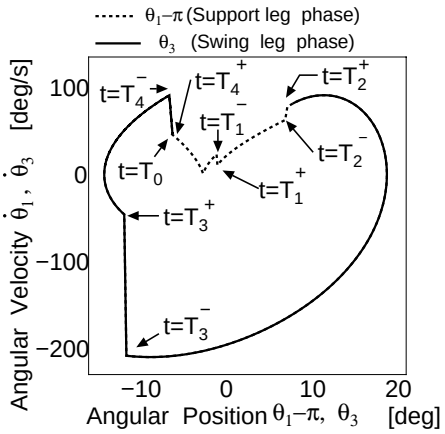

Figure 5: Phase plane of the shank

the simulation result, we confirmed that the knee stopper of the support leg is naturally locked by walking motion if there is $1 \sim 2[deg]$ offset at the knee joint. Therefore the knee joint of the experimental robot does not need a locking mechanism.

3.2. Effect of feedback gain

In this section, we explain the effect of feedback gain on biped walking motion. As the result of numerical simulation, we found that stable walking is possible over the wide range of feedback gain value, from $k = 4.8$ to $k = 7.2[Nm/rad]$. Figure 6 shows the effect of feedback torque on walking velocity, input energy and periods. We defined the input energy P such that

$$P = \frac{1}{t_{end}}\int_0^{t_{end}} |\dot{\theta}_2 k\theta_3| dt \quad (3)$$

where t_{end} is simulation term. As seen in this figure, even if feedback gain k increases, the walking periods change little, velocity increases slightly, but input energy increases proportional to the k.

The walking motion of the biped mechanism with high feedback gain become soldier-march-like

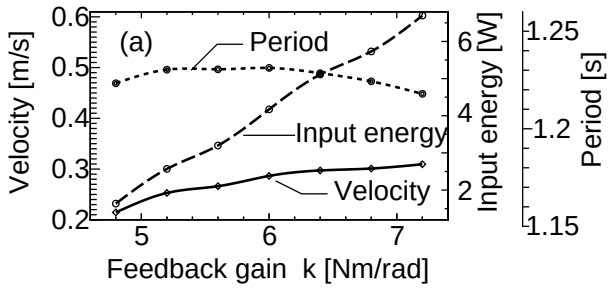

Figure 6: Feedback gain effect on velocity, input energy and period

gait, swinging up the swing leg high. This is the reason why energy consumption increases proportionally to the feedback gain. Therefore it can be said that walking period and velocity are not affected so much by feedback gain, but in terms of energy consumption, a smaller feedback gain walking is better. However the feedback gain should also be determined from the robustness of walking motions against the irregularity of the ground.

4. Experiment

4.1. Manufactured biped walking mechanism

The manufactured biped walking robot is shown in Figs.7 and 8. The Biped Walking Robot (BWR) has a couple of outer leg and single inner leg. These legs are connected in series by AC servo motor. Each leg consists of thigh and shank connected at knee joint which has optical encoder, rotary damper and knee stopper.

We carefully designed and adjusted the robot so as to meet the requirement of "dynamically equivalent to the analytical model". Therefore both the outer leg thighs are connected by the hip joint shaft. The shanks are also connected by the light weight frame which does not interfere the motion of inner leg. By means of the connected outer leg, the rolling motion of the robot was perfectly constrained so that the robot could behave as a biped mechanism on a sagittal plane.

4.2. Experimental results

In experiment the most difficult problem is to learn how we lead the initial state of BWR into a basin where BWR's walking motion converges to a limit cycle. Another problem is to reduce disturbances from ground, cable and irregularity of the mechanism. Optimization and symmetry of mechanical parameters are also important. As the results of trial learning of the initial condition and modification of the system, we have finally succeeded in realizing biped walking on a slightly inclined plane of about 0.8[*deg*]. Video of the self-excited biped walking will be shown in the presentation. Figure 9 shows experimental data and simulation data of relative angle α between support leg and swing leg. This experimental result approximately agreed with simulated one. Although it is not clear why the robot cannot walk on a complete level plane, main reason seems to be that the energy consumption at collision is much larger than the simulation results.

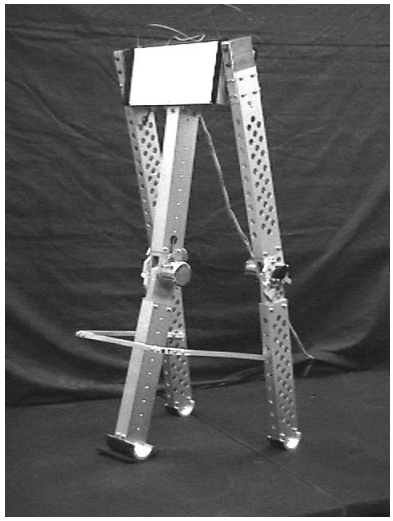

Figure 7: Picture of biped walking robot (BWR)

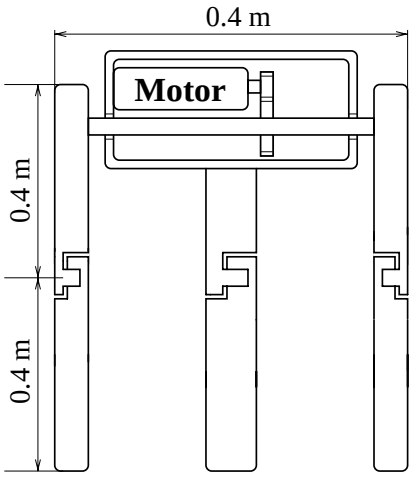

Figure 8: Outline of biped walking robot (BWR)

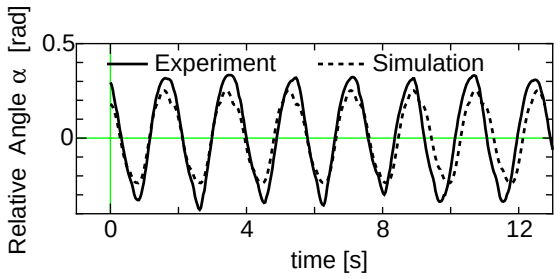

Figure 9: Experimental and simulation data of robot's walking

5. Conclusion

We proposed a self-excited biped walking mechanism which can generate its natural walking motion on a level ground. The control strategy is based on the asymmetric stiffness-matrix-type self-excitation.

Using simple analytical model and basic equation in each phase, we numerically showed self-excited biped walking. As a result, it was found that stable walking motion is possible over the wide range of feedback gain. The walking velocity and period were not so affected by feedback gain because this control strategy utilize the natural motion of the biped mechanism.

To verify the simulation results, we manufactured planar biped robot which has a couple of outer leg, inner leg and one actuator between them. After adjusting the mechanical parameters, we succeeded in making BWR walk on a plane with $0.8[deg]$ inclination. Our future goals are realization of biped walking on complete level plane and improvement of robustness against disturbances.

Acknowledgments

This research is supported by COE / SMS (Center of Excellence / Super Mechano-Systems Research Project) Grant of Aid Japanese Ministry of Education, Science, Culture and Sports.

References

[1] Tad McGeer, "Passive Dynamic Walking", The International Journal of Robotics Research, Vol.9, No.2, April 1990.

[2] Tad McGeer, "Passive Walking with Knees", Proc. 1990 IEEE Robotics and Automation Conference, May 1990. Cincinnati.

[3] Mariano Garcia et al, "The Simplest Walking Model: Stability, Complexity, and Scaling",ASME J. of Biomechanical Engineering, Vol.120, No.2, April 1998. pp.281∼288.

[4] Ambarish Goswami, Benoit Thuilot and Bernard Espiau, "A Study of the Passive Gait of a Compass-Like Biped Robot: Symmetry and Chaos", Int. J. of Robotics Research Vol.17, No.12, December 1998, pp.1282∼1301.

[5] Ambarish Goswami, Bernard Espiau and Ahmed Keramane, "Limit Cycles in a Passive Compass Gait Biped and Passivity-Mimicking Control Laws", Autonomous Robots 4, 273-286 (1997).

[6] Mark W. Spong, "Passivity Based Control of the Compass Gait Robot", IFAC World Congress, Beijing, China.

[7] Mark W. Spong, "Applications of Switching Control in Robot Locomotion", IFAC World Congress, Beijing, China.

[8] K.Ono, T.Okada, "Self-Excited Vibratory Actuator (1st Report, Analysis of Two-Degree-of- Freedom Self-Excited Systems)", Trans. JSME(C), 60-577, pp.92-99, (1994).

[9] K.Ono and T.Okada, "Self-Excited Vibratory Actuator (2nd Report, Self-Excitation of Insect Wing Model)", Trans. JSME(C), 60-579, pp.117-124, (1994), International journal of JSME.

[10] K.Ono and T.Okada, "Self-Excited Vibratory Actuator (3rd Report, Biped Walking Mechanism by Self-Excitation)", Trans. JSME(C), 60-579, pp.125-132, (1994), Proceeding of 4th Movic.

[11] K.Ono and A.Imadu, "Self-Organization of Biped Walking by Self-Exciting Feedback", Proceedings of the 75th JSME Spring Annul Meeting, No.98-1(1),pp.129-130, (1998).

Keynote Speech VIII

Proceedings of the International Symposium on
Adaptive Motion of Animals and Machines,
Montreal, Aug.8-12, 2000

Dynamic locomotion with four and six-legged robots[1]

M. Buehler[1], U. Saranli[2], D. Papadopoulos[1] and D. Koditschek[2]

[1] Centre for Intelligent Machines, Ambulatory Robotics Laboratory, McGill University
[2]Department of Electrical Engineering and Computer Science, University of Michigan
http://www.cim.mcgill.ca/~arlweb http://www.eecs.umich.edu/~ulucs/rhex/

Abstract

Stable and robust autonomous dynamic locomotion is demonstrated experimentally in a four and a six-legged robot. The Scout II quadruped runs on flat ground in a bounding gait, and was motivated by an effort to understand the minimal mechanical design and control complexity for dynamically stable locomotion. The RHex 0 hexapod runs dynamically in a tripod gait over flat and badly broken terrain. Its design and control was motivated by a collaboration of roboticists, biologists, and mathematicians, in an attempt to capture specific biomechanical locomotion principles. Both robots share some basic features: Compliant legs, each with only one actuated degree of freedom, and reliance on (task space) open loop controllers.

1. Introduction

Designers of statically stable autonomous legged robots in the past have paid careful attention to minimize negative work by minimizing vertical body movements during locomotion. This required complex leg designs with at least three degrees of freedom per leg, more if an ankle/foot combination is required. The resulting cost, mechanical complexity, and low reliability make it difficult for these robots to be profitably deployed in real world tasks.

In contrast, dynamic locomotion with compliant legs permits not only higher speeds and the potential for drastically improved mobility compared to statically stable machines, but at the same time permits these improvements with greatly simplified leg mechanics. With compliant legs, instantaneously controlled body motion can no longer be achieved, and energy efficient locomotion must utilize intermittent storage and release of energy in the passive leg compliances. It is remarkable that despite their mechanical simplicity, outstanding dynamic mobility is obtained in both machines described in this paper, based on very simple (task space) open loop controllers.

In the Scout II quadruped we have attempted to demonstrate the limits of mechanical simplicity, while still obtaining a range of useful dynamic mobility. Even with only one actuator per leg, we obtained full mobility in the plane on flat ground, and running speeds of up to 1.2 m/s with a bounding gait [7]. These preliminary results and ongoing research suggest that further speed and mobility improvements, including compliant walking, leaping, and rough terrain handling are within reach.

The extension of the basic engineering design principles of Scout II to the fundamentally different hexapedal running of RHex 0 is based on insights from biomechanics, whose careful consideration exceeds the scope of this paper. In a paper documenting the performance of cockroach locomotion in a setting similar to our recreation in Figure 11, R. J. Full et al., state “Simple feedforward motor output may be effective in negotiation of rough terrain when used in concert with a mechanical system that stabilizes passively. Dynamic stability and a conservative motor program may allow many-legged, sprawled posture animals to miss-step and collide with obstacles, but suffer little loss in performance. Rapid disturbance rejection may be an emergent property of the mechanical system." In particular, Full's video of a Blaberus cockroach racing seemingly effortlessly over a rough surface, shown at an interdisciplinary meeting [6] motivated and initiated the development of RHex.

Though morphologically quite distinct from its biological counterparts, RHex emulates the basic principles of insect locomotion as articulated by Full. The robot’s sprawled posture with properly designed compliant legs affords strong passive stability properties, even on badly broken terrain. These stability properties, combined with a rugged mechanical design forgiving to obstacle collisions permits controllers based on open loop (“clocked”) leg trajectories to negotiate a large variety of terrains.

[1] The Scout project was supported by IRIS (A Federal Network of Centers of Excellence of Canada) and NSERC (The National Science and Engineering Research Council of Canada). The RHex project was supported by DARPA (The U.S. Defense Advanced Research Projects Agency) under grant number DARPA/ONR N00014-98-1-0747.
Portions of this paper have appeared in the Proc. of the International Conference on Robotics and Automation, 2000 [7,9].

2. Scout II Quadruped

Figure 1: Scout II.

Scout II, shown in Fig. 1, has a main body and four compliant legs. The body contains all elements for autonomous operation, including computing, I/O, sensing, actuation, and batteries. Each leg is a passive prismatic joint with compliance and rotates in the sagittal plane, actuated at the hip by one motor. Without leg articulation, toe clearance during the swing phase can be achieved with any running gait that includes a flight phase, for example, pronking, trotting and bounding. We have chosen the bounding gait (Fig. 2) since it permits a smooth transition from a bounding walking gait, the subject of current research.

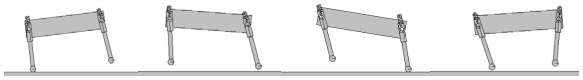

Figure 1: Illustration of a bounding gait.

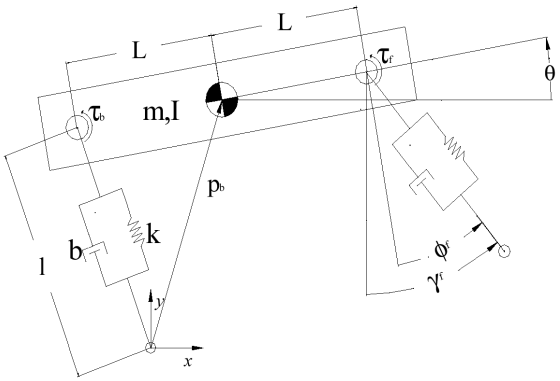

Figure 2: Scout II model

The sagittal plane model, shown in Fig. 3, is a four degree-of-freedom system in each single stance phase, and a five degree-of-freedom system during flight, with only two hip torque control inputs.

Control

The bounding controller accomplishes running at a desired forward speed, $\dot{x}_d$, by placing each leg at the desired angle, ϕ_d,

$$\begin{cases} XCG_d = \dot{x} T_S / 2 + k_{\dot{x}} (\dot{x} - \dot{x}_d) + a \\ \gamma_d = \arctan\left(\dfrac{XCG_d}{\sqrt{l^2 - XCG_d^2}} \right) \\ \phi_d = \gamma_d - \theta \end{cases}, \qquad (1)$$

and applying a leg torque $\tau = k_v (\dot{x} - \dot{x}_d)$ during stance. This controller is motivated by the foot placement algorithm in Raibert's three-part controller [8]. The key differences in our controller are necessitated by the absence of a linear leg thrusting actuator, and thus the lack of a direct means to add energy to the vertical (body pitching) dynamics. First, the offset term, *a*, in (1), diverts some forward energy to the vertical dynamics in each step. This reduced forward energy (the robot slows down) is then compensated during stance phase via the explicit velocity control.

There is no explicit control of the body pitch oscillation - front and back leg controllers are independent. They only rely on the individual leg states, and make no use of an overall body state. Computer simulations show that this controller, despite its simplicity, succeeds not only in stable velocity control, but also in tracking rapid set point changes in forward velocity, as shown in Fig. 4.

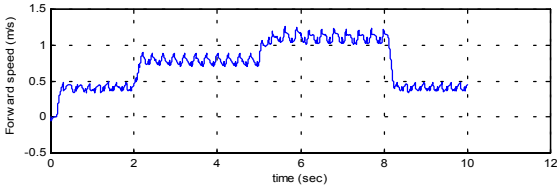

Figure 3: Step changes in forward velocities controlled by the hip actuator torque.

An open loop version of this controller is an attempt to demonstrate the simplest form of compliant quadruped running control without any explicit feedback control of body oscillation and forward speed. It simply commands a constant desired hip torque, τ_d, during stance and a constant desired leg angle, ϕ_d, controlled during flight via a set point PD algorithm. With two values for front and back legs, this controller is determined by only four parameters.

Fig. 5 shows a Working Model 2D® [4] simulation of the open loop controller, with fixed values of touchdown leg angles (18° for the back legs and 22° for the front legs) and stance torques (40 Nm for the back legs and 10 Nm for the front legs). The result is steady running with 1.2 m/s forward speed with body oscillation with an amplitude of 6.5° and a period of 0.29 s.

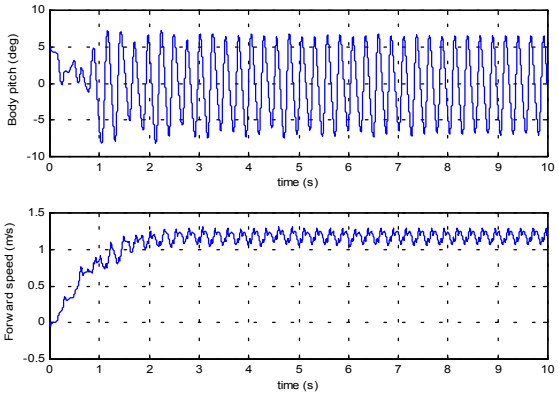

Figure 4: Body pitch and forward velocity during running with the open loop controller.

Thus, surprisingly, compliant quadruped running is possible without explicit feedback control of forward speed or stance time. The disadvantage of this controller is that each particular speed requires the selection of the appropriate touchdown leg angles and stance torques. However, this could be implemented in a straightforward fashion as a lookup table, and could serve as a potentially robot-saving backup controller in case of sensor failure.

Experiments

As suggested by the simulations, it is possible to achieve a steady bounding gait by choosing a suitable set of constant motor torques during stance and leg touchdown angles during flight. Even though there is no active control of the body roll dynamics in the experimental four-legged robot, the damping in the leg springs was sufficient for passive roll stability.

We have implemented the open loop controller on Scout II. A back torque of 35 Nm per leg and a front torque of 10 Nm per leg was used. A touchdown angle of 22° with respect to the vertical for the front legs and 18° for the back legs was commanded for the flight phases.

A slip prevention torque limit (described in [7] and omitted here for brevity) was implemented in simulation and experiments. The only difference in the experimental slip prevention function is that it dealt with each of the two front and back legs independently.

Both simulation and experimental runs started at zero speed and accelerated until steady state speeds were achieved. While the first two to three seconds transition phase is different in simulation and experiment, the remaining operating time is comparable. Both speeds reach a steady value of about 1.2 m/s. The large experimental speed fluctuations in Fig. 6 are primarily an artifact of our speed calculation, based on the hip angular velocities, which suffers due to the combined backlash of the gear and the belt transmission of several degrees.

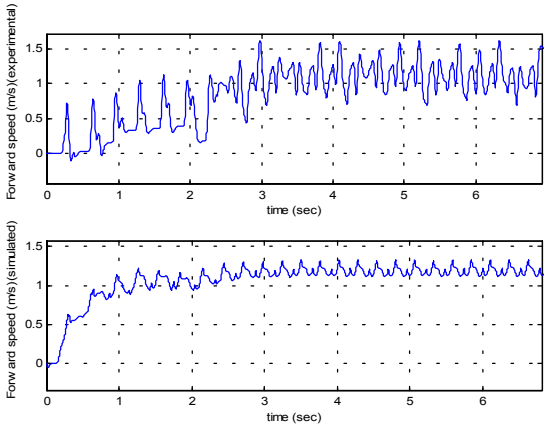

Figure 5: Forward velocity. Top: Experiment. Bottom: Simulation.

Turning while running is accomplished via a simple modification to the open loop bounding controller. The idea is to apply differential torques to the left and right sides of the legs during the stance phases. Implementation of the turning algorithm resulted in rapid turns as illustrated in Fig. 7.

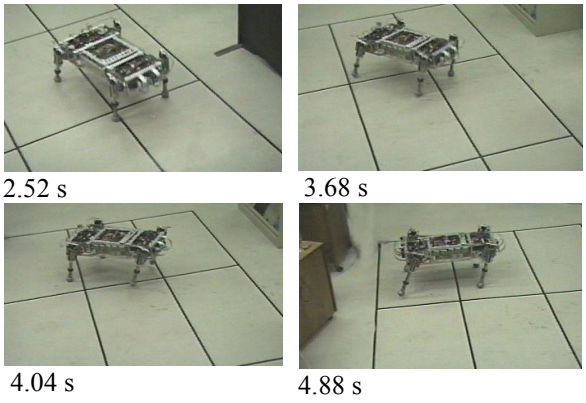

Figure 6: Turning experiment.

3. RHex 0 Hexapod

Figure 7: RHex 0.

RHex 0, shown in Fig. 8, has a main body and six compliant legs. As in Scout II, the body contains all elements for autonomous operation, including computing, I/O, sensing, actuation, and batteries. Unlike most hexapodal robots built to date, RHex 0 has compliant legs, and was built to be a runner. Each leg rotates in the sagittal plane, actuated at the hip by one motor. Since a bounding type walking gait is not feasible with six legs, RHex walks with a compliant tripod gait, and eliminates any toe clearance problems by rotating the legs in a full circle.

Control

Since the present prototype robot has no external sensors by which its body coordinates may be estimated, we have used joint space closed loop ("proprioceptive") but task space open loop control strategies. These are tailored to demonstrate the intrinsic stability properties of the compliant hexapod morphology and emphasize its ability to operate without a sensor-rich environment. Specifically, we present a four-parameter family of controllers that yields stable running and turning of the hexapod on flat terrain, without explicit enforcement of quasi-static stability. All controllers generate periodic desired trajectories for each hip joint, which are then enforced by six local PD controllers, one for each hip actuator. As such, they represent examples near one extreme of possible control strategies, which range from purely open-loop controllers to control laws that are solely functions of the leg and rigid body state. It is evident that neither one of these extremes is the best approach and a combination of these should be adopted. An alternating tripod pattern governs both the running and turning controllers, where the legs forming the left and right tripods are synchronized with each other and are 180° out of phase with the opposite tripod, as shown in Fig. 9.

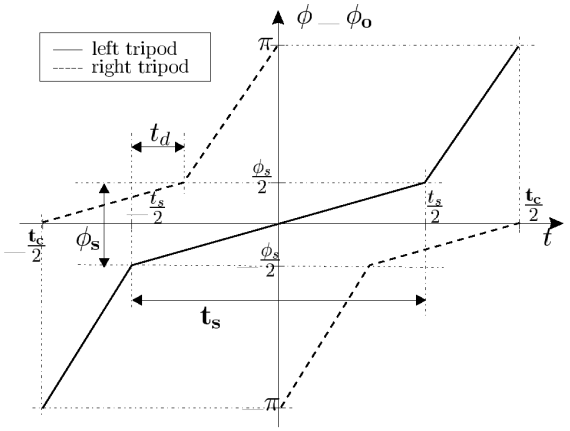

Figure 9: Motion profiles for left and right tripods.

The running controller's target trajectories for each tripod are periodic functions of time, parametrized by four variables: t_c, t_s, ϕ_s and ϕ_o. The period of both profiles is t_c. In conjunction with t_s, it determines the duty factor of each tripod. In a single cycle, both tripods go through their slow and fast phases, covering ϕ_s and 2π - ϕ_s of the complete rotation, respectively. The duration of double support t_d, when all six legs are in contact with the ground, is determined by the duty factors of both tripods. Finally, the ϕ_o parameter offsets the motion profile with respect to the vertical. Note that both profiles are monotonically increasing in time; but they can be negated to obtain backward running. Simulations (Fig. 10) demonstrate that control of average forward running velocity is possible with these controller outputs.

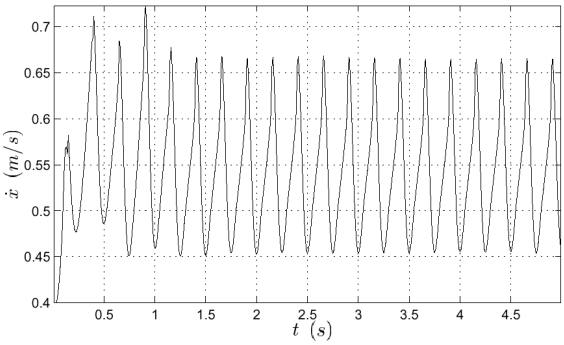

Figure 10: Simulation of forward body velocity.

We have developed two different controllers for two qualitatively different turning modes: turning in place

and turning during running. The controller for turning in place employs the same leg profiles as for running except that contralateral sets of legs rotate in opposite directions. This results in the hexapod turning in place. Note that the tripods are still synchronized internally, maintaining three supporting legs on the ground. Similar to the control of forward speed, the rate of turning depends on the choice of the particular motion parameters, mainly t_c and ϕ_s. In contrast, we achieve turning during forward locomotion by introducing differential perturbations to the forward running controller parameters for contralateral legs. In this scheme, t_c is still constrained to be identical for all legs, which admits differentials in the remaining profile parameters, ϕ_o and t_s, while ϕ_s remains unchanged. Two new gain parameters, Δt_s and $\Delta\phi_o$ are introduced. Consequently, turning in +x (right) direction is achieved by using $u_l = [t_c;\ t_s+\Delta t_s;\ \phi_s;\ \phi_o+\Delta\phi_o]$ and $u_r = [t_c;\ t_s-\Delta t_s;\ \phi_s;\ \phi_o-\Delta\phi_o]$ for the legs on the left and right sides, respectively.

Experiments

We have implemented the open loop controller on the RHex prototype. Extensive testing demonstrated that RHex was able to negotiate a variety of challenging obstacle courses, with obstacles well exceeding the robot's ground clearance, all with fixed (unchanged) open loop control trajectories, and with only minor velocity variations between 0.45 m/s and 0.55 m/s. Detailed statistical performance documentation over all the terrains will be the subject of a forthcoming publication. On flat ground (carpet), the forward speed (averaged over ten runs) is, as predicted by the simulation, slightly above 0.5 m/s, or about one body length/s. On this surface, the average total electrical power consumption is 80 W.

As simulation study had predicted as well, steering is possible, even though the leg actuation is limited to motion in the sagittal plane only, via differential motion between left and right legs. We selected control parameters that resulted in turns in place and robot speeds up to about 0.4 m/s. The maximum forward velocity is reduced during turning, because the differential leg motion precipitates the onset of the speed limiting vertical body oscillations. The maximum yaw angular velocities increase almost linearly with forward velocity up to 0.19 rad/s at 0.39 m/s. Interestingly, the resulting turn radius is almost constant with approximately 2 m. Turning in place provides the highest yaw angular velocity of 0.7 rad/s.

One particular rough terrain experiment was an attempt to evaluate RHex's performance in a similar environment to that negotiated by a Blaberus cockroach in [2]. Our efforts at re-creating such a surface at RHex's scale are shown in Figure 11. To our surprise, RHex was able to traverse this surface with random height variations of up to 20.32 cm (116% leg length) with relative ease at an average velocity of 0.42 m/s (averaged over ten successful runs).

Figure 11: Locomotion on rough terrain.

Accumulating evidence in the biomechanics literature suggests that agile locomotion is organized in nature by recourse to a controlled bouncing gait wherein the "payload", the mass center, behaves mechanically as though it were riding on a pogo stick [1]. While Raibert's running machines were literally embodied pogo sticks, more utilitarian robotic devices such as RHex must actively anchor such templates within their alien morphology if the animals' capabilities are ever to be successfully engineered [3]. A previous publication showed how to anchor a pogo stick template in the more related morphology of a four degree of freedom monopod [10]. The extension of this technique to the far more distant hexapod morphology surely begins with the adoption of an alternating tripod gait, but its exact details remain an open question, and the minimalist RHex design (only six actuators for a six degree of freedom payload!) will likely entail additional compromises in its implementation. Moreover, the only well understood pogo stick is the Spring Loaded Inverted Pendulum [12], a two-degree of freedom sagittal plane template that ignores body attitude and all lateral degrees of freedom. Recent evidence of a horizontal pogo stick in sprawled posture animal running [5] and subsequent analysis of a proposed lateral leg spring template to represent it [11] advance the prospects for developing a spatial pogo stick template in the near future. Much more effort remains before a functionally biomimetic six degree of freedom "payload" controller is available, but we believe that

the present understanding of the sagittal plane can already be used to significantly increase RHex's running speed, and, as well, to endow our present prototype with an aerial phase.

Acknowledgments

The Scout project was supported by IRIS (A Federal Network of Centers of Excellence of Canada) and NSERC (The National Science and Engineering Research Council of Canada). The RHex project was supported by DARPA (The U.S. Defense Advanced Research Projects Agency) under grant number DARPA/ONR N00014-98-1-0747. We also acknowledge the generous and talented help of L. Mitrea, G. Hawker, D. McMordie, and S. Obaid. Close collaboration with R. J. Full of UCB has provided many of the biomechanical insights which motivated the design and control of RHex 0.

Bibliography

1. R. Blickhan and R. J. Full, “Similarity in multilegged locomotion: bouncing like a monopode,” J. Comparative Physiology, vol. A. 173, pp. 509-517, 1993.
2. R. J. Full, K. Autumn, J. I. Chung, and A. Ahn, “Rapid negotiation of rough terrain by the death-head cockroach,” American Zoologist, vol. 38, pp. 81A, 1998.
3. R. J. Full and D. E. Koditschek, ”Templates and Anchors: Neuromechanical Hypotheses of Legged Locomotion on Land,” Journal of Experimental Biology, vol. 202, pp. 3325-3332, 1999.
4. Knowledge Revolution. *Working Model 2D User’s Guide*. San Mateo, CA, 1996.
5. T. M. Kubow and R. J. Full, “The role of the mechanical system in control: A hypothesis of self-stabilization in hexapedal runners,” Phil. Trans. R. Soc. Lond., vol. B. 354, pp. 849-862, 1999.
6. NSF Institute for Mathematics and Its Applications Spring 1998 Workshop on Animal Locomotion and Robotics. June 1-5 1998, www.ima.umn.edu/dynsys/spring/dynsys10.html.
7. D. Papadopoulos and M. Buehler, "Stable Running in a Quadruped Robot with Compliant Legs," IEEE Int. Conf. Robotics and Automation, April 2000.
8. M. H. Raibert. *Legged Robots That Balance*. MIT Press, Cambridge, MA, 1986.
9. U. Saranli, M. Buehler, and D. E. Koditschek, “Design, Modeling and Preliminary Control of a Compliant Hexapod Robot,” IEEE Int. Conf. Robotics and Automation, April 2000.
10. U. Saranli, W. J. Schwind, and D. E. Koditschek, “Toward the Control of a Multi-Jointed, Monoped Runner,” IEEE Int. Conf. Robotics and Automation, Leuven, Belgium, May 1998.
11. J. Schmitt and P. Holmes, “Mechanical models for insect locomotion I: Dynamics and stability in the horizontal plane,” Biol. Cybernetics, submitted, 1999.
12. W. J. Schwind and D. E. Koditschek, “Approximating the Stance Map of a 2 DOF Monoped Runner,” J. Nonlinear Science, to appear.

Session

Technical Development of Mechanism and Control

Proceedings of the International Symposium on
Adaptive Motion of Animals and Machines,
Montreal, Aug.8-12, 2000

Partial Leg Exchange and Active CG Control of Twin-Frame Walking Machine

Kan YONEDA, Yusuke OTA, Fumitoshi ITO and Shigeo HIROSE

Tokyo Institute of Technology, Department of Mechano-Aerospace Engineering,
2-12-1 O-okayama Meguro-ku, Tokyo 152-8552, JAPAN
{yoneda, ohta, fito, hirose}@hikari.mes.titech.ac.jp

Abstract

In this paper, partial leg exchange gait for twin-frame walking robot is proposed. This twin-frame walking robot doesn't have the degrees of freedom (DOF) for moving the center of gravity (CG). Thus, it is impossible to increase the stability margin actively. But using this proposal method, CG can move in the leg exchange phase and obtain enough stability margins. Proposal gait motion is verified through experiments using mechanical model ParaWalker-II.

1. Introduction

It is desired to be developed the practical robots which have both high terrain adaptability and high manipulability for moving on uneven terrain and performing various tasks. We have been developing twin-frame mobile robot named "ParaWalker-II" as with these abilities [1]. And until now, it is confirmed its practical use through the experiment of walking on uneven terrain [1], force control [2] and stair climbing [3].

In this paper, we propose the partial leg exchange motion, which is the method for obtaining high mobility with keeping high stability. Using this method, the position of CG can be moved during the leg exchange motion. Therefore the wider strides and more mobility can be obtained.

2. Twin-Frame Walking Robot "ParaWalker-II"

The indispensable abilities for practical moving and task performing robot are 1) mobility. 2) ability for performing tasks. and 3) ability for assisting for performing other tasks. As such a robot we proposed the twin-frame mobile robots [4].

Twin-frame mobile robots consist of two frames and 6-DOF mechanism connecting each frames. **Figure 1** shows twin-frame walking robot, which is walking type robot in the category of twin-frame mobile robot, named "ParaWalker-II." ParaWalker-II consists of two frames (leg-bases) with three legs. Each leg-base is connected by 6-DOF mechanism named "S/P Hybrid Platform." Therefore the swing leg-base can be move with 6-DOF motion against the supporting leg-base, that is against the ground. So using this DOF motion, ParaWalker-II has enough task performing abilities shown in **Fig. 1** as a 6-DOF manipulator.

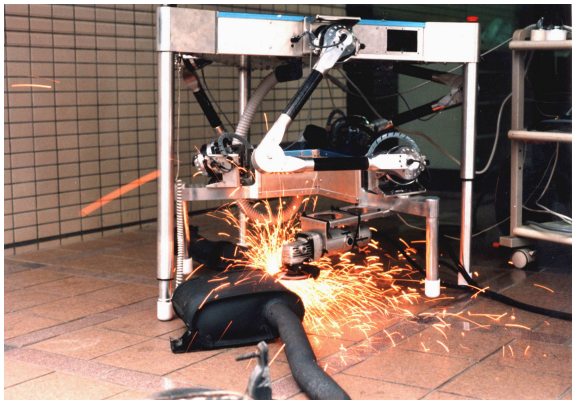

Figure 1: Twin-frame walking robot "ParaWalker-II", which can perform various tasks (performing the grinding task)

And using this DOF motion, ParaWalker-II can produce the walking motion. ParaWalker-II can walk with keeping its stability because each leg-base touch the ground with 3 points (legs) and the CG always stay inside the supporting area that is made by grounded points.

Twin-Frame mobile robot performs both tasking and moving using the same mechanism. So the necessary DOF, that is the actuators, for tasking and moving can be minimized. As a result of this, total weight can be reduced. Furthermore, reduction of DOF, actuators, makes control of the robot easy because amount of necessary calculation for the robots becomes small.

And the ParaWalker-II equips only one extendable leg [3] because of achieving higher terrain adaptability. But this is no relation between this paper. We don't explain and handle in this paper.

3. Partial Leg Exchange Motion

The gait motion for ParaWalker-II is produced by alternate motion. Each leg-base becomes swing/support leg-base alternatively. So this gait motion is equivalent to the biped with wide sole.

In bipedal walking motion like human beings, the position of the CG makes smooth transitions. That is because the smooth CG motion is produced by the motion of the upper part of the body. But the CG motion of twin-frame walking robot ParaWalker-II is intermittent motion. And ParaWalker-II doesn't have extra DOF for moving only CG actively because ParaWalker-II is constructed with minimized DOF. This makes some disadvantages. First, the position of CG is determined by relative position of each leg-bases explicitly. And second, the stability margin, that is almost equivalent to the mobility, is determined by robot's structure. For example in ParaWalker-II, the maximum stride (horizontal distance between each frames) is determined the 400 [mm] by its structural geometry. And if leg exchange motion is carried out at near this stride length the stability margin becomes very small and leg exchange motion is performed unstable. Therefore securing stability margin, one step is limited about 200 [mm] in the case of normal walking motion. Thus, the problem how to obtain high stability in leg exchange phase should be resolved for obtaining higher mobility.

So we proposed partial leg exchange motion. As using this method, the leg exchange motion is performed with high stability margin and robots realize wider strides. Furthermore, this method has the possibility that the robot is also able to move with smooth CG transition that is similar to the movement of the animals. Process of the partial leg exchange motion is explained next.

3.1 Process of the partial leg exchange motion

Motion difference between proposal partial leg exchange motion and previous motion is shown in **Fig. 2**. The process of proposal partial leg exchange motion is:

1: Lift up the frame and go forward
2: Rotate frame centered by frame's CG
3: Down the frame (two legs are touched down)
4: Rotate frame and all legs are touched down

At the process 2, CG doesn't move because center of the rotation is match with the center of frame, that is CG of each frame. At the process 3, grounded point of the leg goes forward with inclination of the frame.

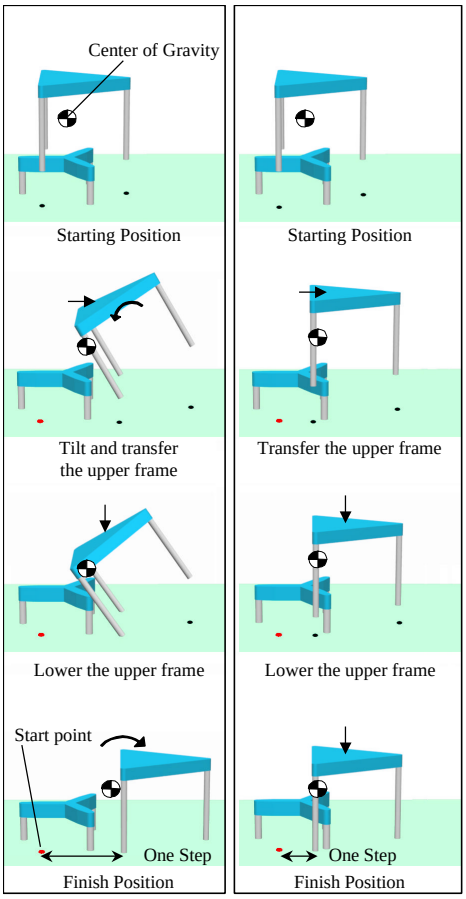

Figure 2: Comparison between (**a**)**:** proposal partial leg exchange motion and (**b**)**:** previous normal gait motion

So stride length can be changed by the inclination angle of the frame with the same stability margin. Therefore, it is possible to take a wide stride walk with enough stability margins.

This motion is resemble to animals' walking motion. Animals make their CG move smoothly in walking motion using these sequences, at first touch their heel to the ground, then whole sole and finally only tow. As taking this proposal walking motion the twin-frame walking robot ParaWalker-II can produce the smooth CG transition that was moved alternatively taking the previous walking motion.

4. Walking Experiment

Figure 4 shows the walking experiment using partial leg exchange motion by the ParaWalker-II. This confirms the realization of stable static walk with about 500 [mm] step using partial leg exchange motion.

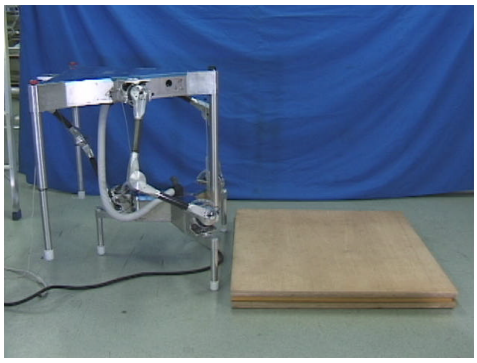

Step1: Lift the upper-leg-base

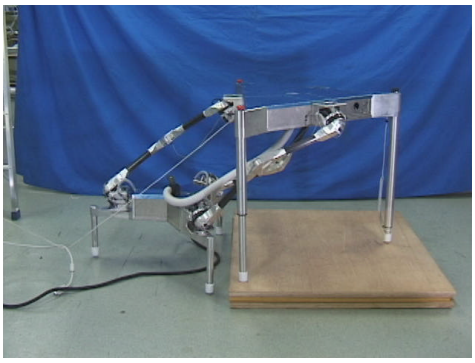

Step4: Rotate the upper-leg-base (all legs are touched down)

Step2: Forward the upper-leg-base and rotate

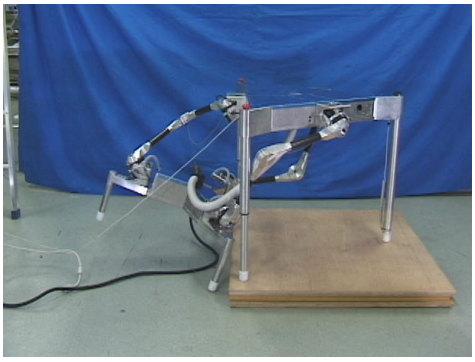

Step5: Rotate the lower-leg-base (1 leg left the ground)

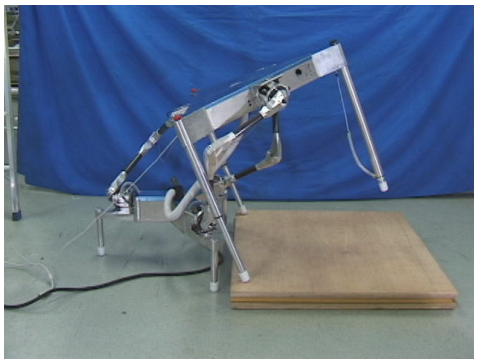

Step3: Down the upper-leg-base (2 legs are touched down)

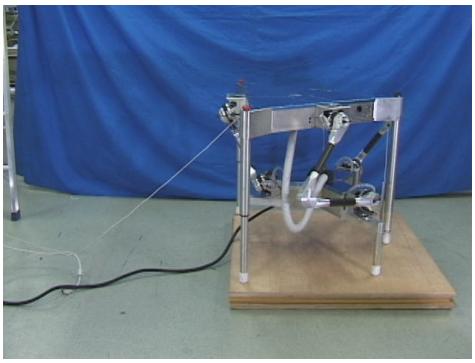

Step6: Lift. rotate, forward and grounded the lower-leg-base

Figure 3: Partial leg exchange walking experiment

5. Applications

5.1 For various walking gait motions

Partial leg exchange motion produces the CG actuation that seems impossible at the leg exchange phase. Therefore, using this motion makes some variations of pattern for walking gait motion.

5.1.1 3-6-3 gait motion (previous normal gait pattern)

This is previous gait motion. This gait sequence is shown in **Fig. 2** (**b**). So the number of the grounded legs changes from 3 to 6 and 3. From the problem of CG position that doesn't go out the supporting area, the state like **Fig.3 step4** cannot be taken. Therefore the maximum stride in this walking motion is limited by about 200 [mm].

5.1.2 3-5-6-5-3 gait motion

This is the partial leg exchange motion shown in **Fig. 3**. The number of grounded point is transfer from 3 to 5, 6, 5, and 3.

5.1.3 3-5-4-5-3 gait motion

This walking motion is shown in **Fig.4**. In this motion, grounded points change from 3 to 5, 4, 5 and 3 without all legs are grounded. As there is no state in all legs are in contact, the CG motion may become smooth and walking velocity could be faster than 3-5-6-5-3 gait motion that is before proposed.

5.1.4 2-4-2 gait motion (dynamic walk)

Furthermore, it is considered that a twin-frame walking robot can make a dynamic walk using an active CG control with 2,4,2 points contact sequence. In this gait, only two contact points of each frame are used, and the gait motion is like a pace or bound gait of quadruped.

5.2 For constructing biped

Since using the partial leg exchange motion, the supporting area is not overlapped. Therefore, supporting area can be taken some distance and produced separately each other. This state is equal to bipedal walking style. The walking motion shown in **Fig. 4** is obviously one type of bipedal walking motion with static balance. This means that the biped that is a twin-frame type structure can be constructed with only 6-DOF taking the strategy as a partial leg exchange motion. This result suggests that the biped, that seems to be necessary of 12 DOF for walking any direction, can be constructed by only 6-DOF.

Therefore, this proposal moving method is efficient as a constructing technique for walking robot with reduced degrees of freedom.

6. Conclusions

In this paper, the partial leg exchange motion which produces the CG actuation in leg exchange phase is proposed. As using this proposal method ParaWalker-II, that is the twin-frame walking robot that frames are connected by 6-DOF mechanism, is achieved CG transition in leg exchange phase that seems to be difficult, maximum strides with keeping stability and smooth CG motion. And this proposal method is verified through the walking experiment.

As a future work the dynamic walk in our proposal partial leg exchange motions will be applied to the ParaWalker-II.

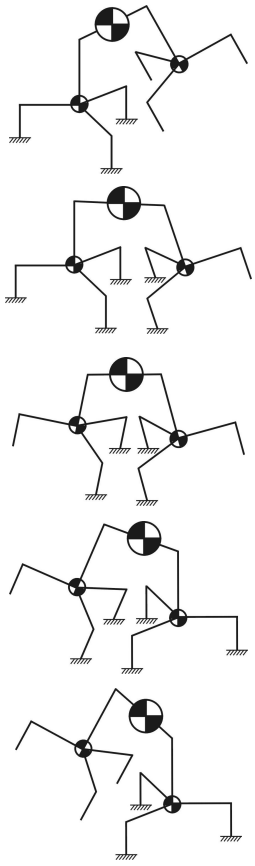

Figure 4: Process of 3-5-4-5-3 gait motion

Acknowledgement

This research is supported by The Grant-in Aid for COE Research Project of Super Mechano-Systems by The Ministry of Education, Science, Sport and Culture.

References

[1] Yusuke OTA, Yoshihiko INAGAKI, Kan YONEDA *and* Shigeo HIROSE; “Research on a Six-Legged Walking Robot with Parallel Mechanism”, Proc. of the IROS 98, pp.241-248 (1998)

[2] Yusuke OTA, Kan YONEDA, Shigeo HIROSE *and* Fumitoshi ITO; “Six-Axis Force Control for Walking Robot with Serial/Parallel Hybrid Mechanism”, Proc. of IEEE Int.Conf. on Robotics and Automation, pp.1469-1474 (1999)

[3] Kan YONEDA, Fumitoshi ITO, Yusuke OTA *and* Shigeo HIROSE; “Steep Slope Locomotion and Manipulation Mechanism with Minimum Degrees of Freedom”, Proc. of the IROS 99, pp.1896-1901 (1999)

[4] Yusuke OTA, Kan YONEDA, Fumitoshi ITO *and* Shigeo HIROSE; “Design Concept for a Walking Machine with Reduced Degree of Freedom”, Proc. of 2nd International Workshop and Conference on Climbing and Walking Robots, pp.485-496 (1999)

Proceedings of the International Symposium on
Adaptive Motion of Animals and Machines,
Montreal, Aug.8-12, 2000

3D Posture Control by Using the Cat-turn Motion

Akira MIYAJIMA, Kazuo YAMAFUJI and Takayuki TANAKA

Department of Mechanical Engineering and Intelligent Systems,
University of Electro-Communications
1-5-1 Chofugaoka, Chofu, Tokyo, 182-8585 JAPAN Tel/Fax:+81-424-43-5430
E-mail : akira@yama.mce.uec.ac.jp, yamafuji@mce.uec.ac.jp, tanaka@mce.uec.ac.jp

Abstract

In our previous paper, we made clear the principle of the cat-turning motion and realized the cat-turning by a robot. The robot can control three dimensional (3D) posture using cat-turning motion. It utilizes double cat-turning motion in order to conduct 3D posture change. This paper describes the principle of 3D posture control using double cat-turning motion and simulation result.

1. Introduction

Recently, many researches and developments of the space structure have been carrying out. Especially, its posture control is regarded as one of most important topics. However, in order to control the posture of space structure in the space, most of them need a lot of energy, such as the solid fuel, the nuclear fuel, the solar sell and so on. We consider that an innovative posture control with little energy will be required to create a new space generation in 21st century.
In this study, we conduct the development of a 3 dimensional (3D) cat-turning robot, which can control its posture by using its own internal power. When a cat falls upside down in the air, it turns its own body and makes a perfect landing. We apply such a cat-turning motion to the posture control of space structure without a lot of energy.
Firstly, we propose the 3D posture conversion method using the cat-turn motion in this paper. Secondly, the mechanism of the developed 3D cat-turning robot and the methodology of its posture control are described. Finally, by simulation and experimental results, it is shown that the proposed posture control method is very useful.

2. The Cat-Turn Motion

We made clear the principle of cat-turn motion. When a cat falls upside down in the air, as shown in Fig 1. When a cat starts to fall, its initial angular momentum is zero. (2) A cat bends over, (3) and twists both

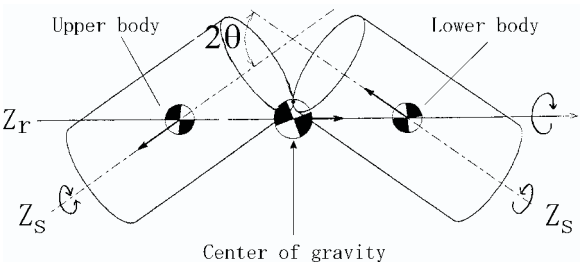

Fig. 1 Concept of a image of cat-turning motion

of upper and lower bodies around each central pivot. (4) It revolves on an axis, which links two centers of gravity of the upper and lower bodies. (5) Then, it makes a perfect landing from its paws.
This motion is explained by the following equation based on the law of conservation of angular momentum.

$$_r \cdot \ _r + \ _s \cdot \ _s \cdot \sin \ = 0 \qquad (1)$$

$_r$, $_r$: Internal moment and angular verocity around the $_r$ axis.
$_s$, $_s$: Internal moment and angular verocity around the $_s$ axis.
: The angle across the upper and lower body.

Where, the first term in the left side is an angler momentum around the $_r$ axis, and the second term is one around the $_s$ axis generated by twisting upper and lower bodies. The right side is constantly zero. This equation shows that the body rotates around the $_r$ axis, because removing angler momentum around the $_s$ axis generates an angler momentum around the $_r$ axis.

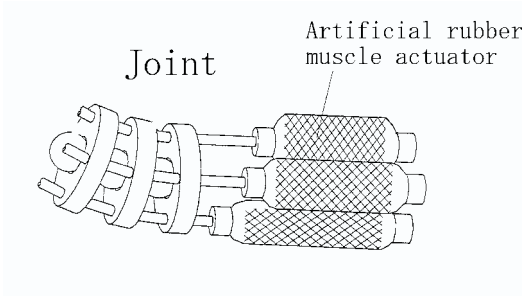

ig e 2 ec anism o t e at ning o ot

3. Development of Cat-Turning Robot

e s o a at r obot

In 1991, we conducted the development of a 2 dimensional (2D) cat-turning robot based on cat-turning motion, which was the fastest development in the world.[1][2] This robot has two links, which emulate upper and lower body of a cat. A link consists of four pneumatic actuators, as artificial rubber muscles, which emulate two pairs of antagonist muscles as shown in Fig.2. And a backbone type joint connect two links.
We succeeded to control 2D posture of the developed robot without a lot of energy, based on the principle of cat-turning motion as shown in Eq.(1).

e e o e t at r obot

In order to realize 3D posture control of the robot, we develop a 3D cat-turning robot as shown in Fig.(3). This robot is achieved by four links, which are basically equipped every 90 degrees on a joint base in the identical 2D plane. Three gyro sensors mounted on a joint base detect three eulerian angles of each links to recognize 3D posture of the robot.
Each of links, which has same mechanism of a link of 2D cat-turning robot, can rotate around a joint base. Then the robot can take two patterns of 2D cat-turning robot as shown in Fig.(4). Therefore, it can revolve around two axes, which lay at right angle each other, and realize 3D rotation in the air. Moreover, the robot needs little energy by using this 3D posture control based on cat-turning motion, because of the law of conservation of angular momentum.

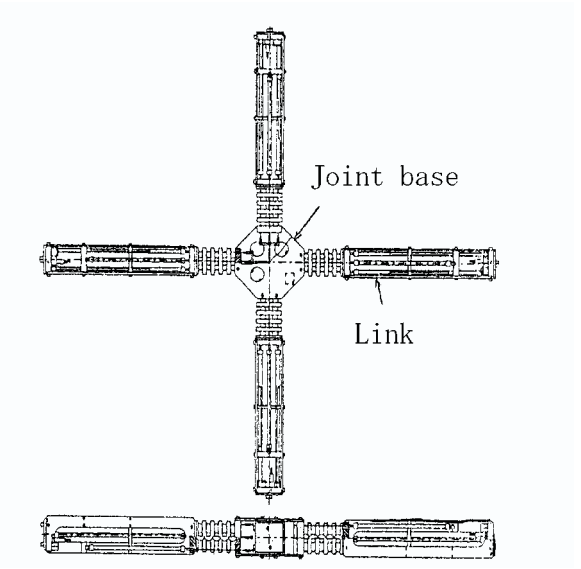

ig e 3 e de e o ment 3 at ning o ot

4. Methodology of 3D Posture Control

To control the posture, we have to control the link's angle and the base's three eulerian angles. There are three gyro sensors in one leg, the total sum are twelve in this robot. So we can detect the link's angles in the air, and calculate the base's eulerian angles by measurement of gyro sensors. The joint between base and link, there are four wires connecting the artificial rubber muscle actuators. So the link's angle ($_r$) is controlled by the wire's length (Δ), as shown in Eq.(2).

$$\Delta = 2 \quad _r \tag{2}$$

Δ : Variation of wire length
: Wire length between bottom and center of wire
$_r$: Reference angle

And the Δ is controlled by the difference of respective internal pressure of artificial rubber muscle actuators (Δ), there is the linear relation as shown in Eq.(3).

$$\Delta = 2 \quad \Delta \quad : \quad n \quad n \tag{3}$$

The Δ is detected by strain type pressure sensors at every sampling time. Therefore, we can control the $_r$ by controlling the Δ as shown in Eq.(4).

$$_r = \quad \Delta \tag{4}$$

And we use the 16 bit PC for the controller, and control program is written by C language.

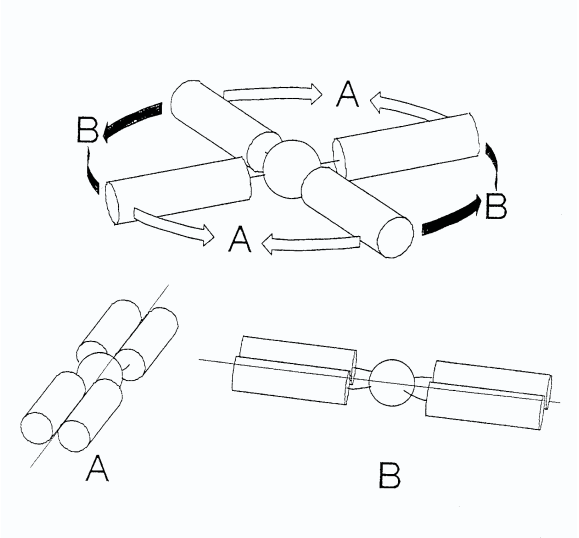

ig e 4 once t a image o 3 at ning o ot

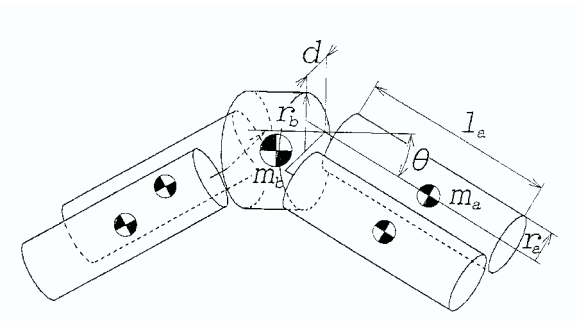

ig e 5 3 at t ning mode

5. Computer Simulation

To evaluate the characteristic motion, we make the simulation for that robot model, as shown in Fig.(5).

We enable to check the cat-turning motion and evaluate the effect of the system parameter for the simulation. To assess the cat-turning motion, we define the rate TR (Turning Rate) for the cat-turning motion shown in Eq.(5).

$$= 1 - \frac{2\ _{ax} \quad + \ _{bx} + 4 \quad _a{}^2}{4\ _{ax} \quad ^2 + 4 \quad _{ay} \quad n^2 \quad + \quad _{bx} + \frac{m_a m_b}{m_a \quad m_b} \quad ^2 + 4 \quad _a{}^2}$$

$$= \ _a(1 - \quad) + \frac{a}{2} \quad n \qquad (5)$$

$_{ax}$: Internal moment around the center of link.
$_{ay}$: Internal moment around the axis vertical of the center of link.
$_{bx}$: Internal moment around the center of joint.
$_a$: mass of a link. $_b$: mass of a joint bace.
: radius of joint bace.
$_a$: radius of link. $_a$: length of link.

For this simulation, we check the cat-turning motion. Fig.(6) is 3D stereo-pair of the motion. And we confirm the effect of parameters, TR is gradually much big in those conditions,

- Less small the radius of body $_b$ (shown in Fig.(5)).
- Less short between the gravitational point of body and the central pivot of the leg .
- Much long the length of leg $_a$.
- Much big the angle across the body and leg .

And the TR is about 0.23 in our developed robot.

6. Experimental Results

The experiment by a robot requires recreation of zero gravity condition in the robot. To substitute that condition, we need to provide the holonomic constrains force, which magnitude is equal but direction is opposite to the gravitation. Given that constrains force, the robot needs to fall down or be push up by the air. But for that experiment needs very big devices, and it is very difficult to gain the reproducibility. So we didn't experiment in that condition.
In our experiment, we hang up the robot by wire at the gravity center of body. Because we can check controllability of the motion in this position. In this experiment, we confirm that developed robot is enables to moving the legs along a two axes. Performing final time is about one second. In Fig.(7),(8), are body's eulerian angles measured by gyro sensors. Because of the constraints from the wire, it cannot change the body posture perfectly to cat-turning motion, we confirm to realize its motion.

7. Conclusion

We reach these conclusions for this report.

- The cat-turning motion is very effective to control the posture by using only internal power, in not only 2-dimensions but also 3-dimensions.
- It is possible in 3-dimensions to exchange one mechanism and axis using cat-turning motion, and it is very effective because the mechanism is much simple than having two axes.
- The joint modeled vertebrate's backbone is very effective by cat-turning motion. And it enables to exchange the axis for same mechanism, it is much simple than having two axes.

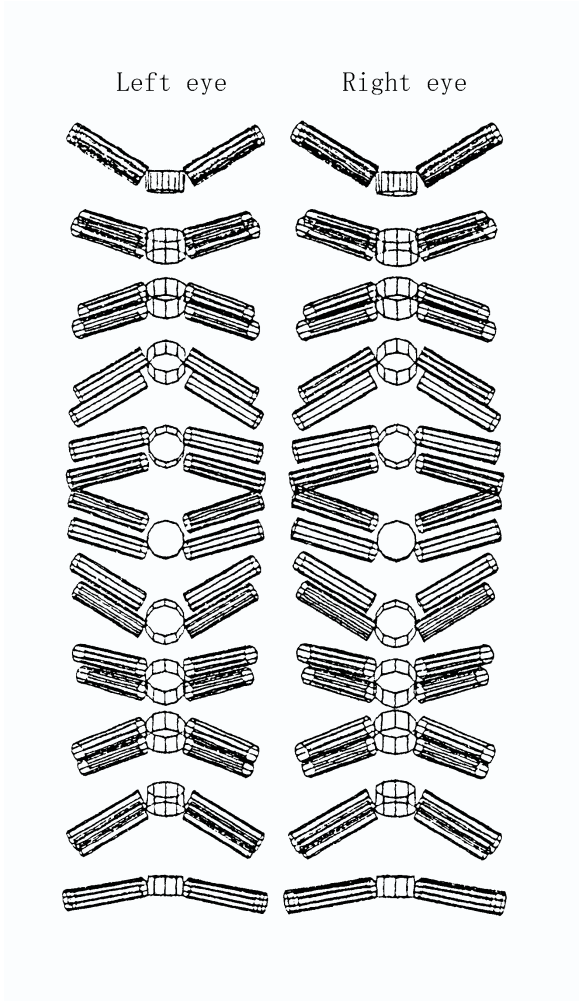

ig e 6 e es ts o sim ation (3 ste eo ai)

- Using three gyro censers, easily we can detect the 3-dimension posture.

This study, we develop the 3 dimensional cat-turning robot which can control its posture by using its own internal power in the zero gravity. Next study, we evolve this motion, and interlace other motion and mechanism. And we hope to develop much effective mechanism which can control its posture in the any 3 dimensional situations.

References

[1] T.Kawamura, K.Yamafuji and T.Kobayashi, Physical Explication and Realization of the Turning Motion of a Cat by Analysis and Experiment Using a Robot Cat, Journal of Robotics and Mechatronics, Vol.3, No.5, 437-442 (1991) .

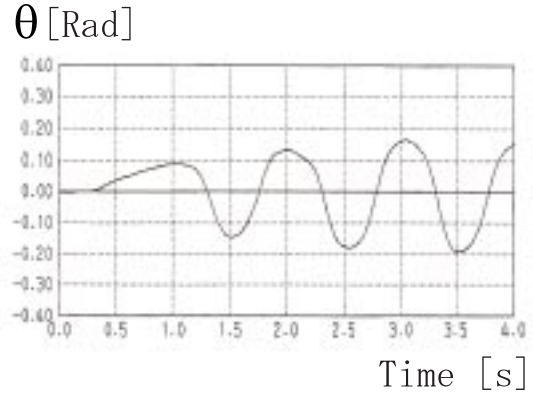

ig e x e imenta es ts o cat t ning mo tion θ

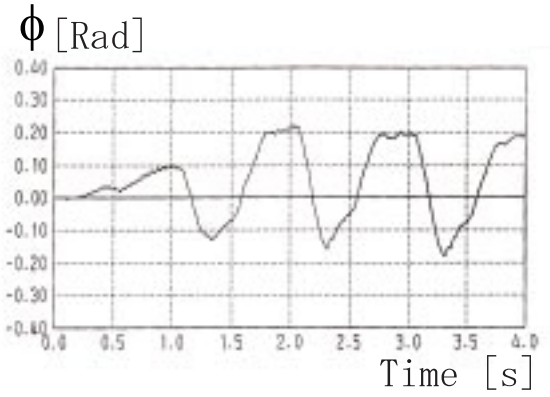

ig e 8 x e imenta es ts o cat t ning mo tion ϕ

[2] T.Kawamura, K.Yamafuji and T.Kobayashi, A Study on the Posture Control and Soft Landing of a Free Falling Robot (3rd Report, Fall Experiment with Cat-Turn Motion)(in Japanese),Trans. of JSME (Series C), Vol.58, No.52, 2495-2500 (1992)

[3] T.Kawamura, K.Yamafuji and N.Murayama, A Study on the Posture Control and Soft Landing of a Free Falling Robot (2nd Report, Posture Control and Soft Landing by Gas Jet)(in Japanese),ibid., Vol.58, No.545, 151-155 (1992)

[4] K.Yamafuji, T.Kawamura, T.Tanaka and M.Feng, Elcucidation of Twisiting Motion of a Falling Cat and its Realization by a Robot, Proc. of 30th Intern. Symposium on Robotics, Tokyo, 527-533 (1999).

Proceedings of the International Symposium on
Adaptive Motion of Animals and Machines,
Montreal, Aug.8-12, 2000

Development of MEL HORSE

Hiroki TAKEUCHI

Ministry of International Trade and Industry
Agency of Industrial Science and Technology
Mechanical Engineering Laboratory Robotics Department, NAMIKI 1-2, 305-8564 Japan
m4890@mel.go.jp

Abstract

Development of Quadruped Robot which has a high mobility performance provides a significant challenge to the robotics engineer. MEL HORSE II is aimed to be such an experimental robot consisting a mechanism for high mobility.

Using the front part of MEL HORSE II, a biped robot could be also developed; it is named MEL Deinonychus II. The characteristic of this robot is that it is equipped with oblong fuselage like as cursorial dinosaurs. In this paper, RHC (Receding Horizon Control) is applied into biped ZMP (Zero Moment Point) control.

1. Introduction

In the case of quadruped robot, Fig.1 shows reptile type and mammal type. Many studies about quadruped robots had been done. Both types have their own advantages. It is depend on the purposed application. If the robot is designed for a construction robot which works on rough terrain, the quadruped reptile type is more advantageous than mammal type. It has the static stability at holding a posture. Reptile type has the advantage in use to move heavy weight at low speed and low consumption. It is like as truck in automobile field.

However, mammal type has the other advantage. It is the fast mobility with long stride and high frequency at any cost. It is like as sports car in automobile field. Studies of this type is few, the study of MEL HORSE is aimed to this type. In this paper, LFD idea, V/H ratio as its measurement of this idea, simulations, high mobility gait are mentioned.

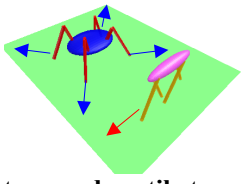

Fig.1 mammal type and reptile type in quadruped

On the other hand, many studies about humanoid (biped) robot are focused recently. One of the problems about these robots is how to control it and how to generate reference leg trajectory. These problems baffle almost designer of legged robots. In this paper, RHC (Receding Horizon Control) is applied onto control biped robot MEL Deinonychus II.

2. MEL HORSE II

2.1 MEL HORSE II

A legged machine named “MEL HORSE” had been developed. MEL HORSE is a quadruped machine and has distinct leg-function between forefeet and hind-feet. The forefeet have the gravity support function and the hind-feet have the generating forward force function. Such distinction of the functions is made by simple counter balance mechanism. Using counter balance, the center of gravity is assigned around front part of the body. Simply it makes the distinct distribution of the leg functions.

Each aluminum pipe frame supports the structure. Aluminum-Duralumin material is adopted at many parts for lightweight. Front part 8.4kg, rear part 6.0kg,fuserage 2.8kg, these are achieved to be lighter weight than MEL HORSE I. Body size 800 * 600 * 250mm. LFD (Leg Functions Distribution) makes main idea of MEL HORSE II mechanism. Linear mechanism using ball screw actuates each rotational joint. Power of the each servomotor is 190W.

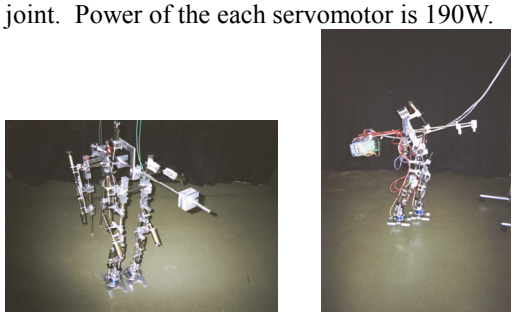

Fig.2.1 MEL HORSE II and MEL Deinonychus II

RT-Linux is adopted for real-time OS. This PC UNIX machine includes interface board “RIF-01”. Encoders at each joint of MEL HORSE II output (2000 pls/r) into up/down counter in RIF-01.

2.2 LFD

The functions required for a leg are discerned gravitational support function and generating forward

force function. Previous legged robot has leg combined with these 2 functions, particularly biped robot.

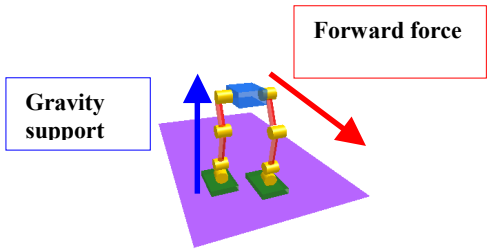

Fig.2.2.1 Leg functions

Quadruped robot has redundancy in number of legs, could be there advanced use of legs for these functions? LFD (Leg Functions Distribution) idea solute this problem. . This idea is simply realized by counter balance mechanism. Fig.2.2.2 shows this idea. The C.G. (centre of gravity) is assigned at front part of the body, and forefeet mainly cover gravitational support function, hind-feet mainly covers generating forward force function.

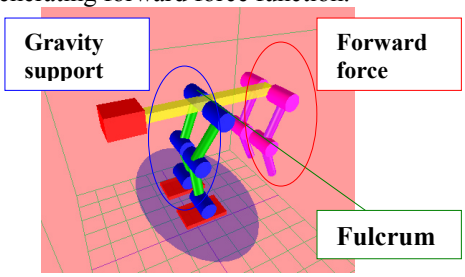

Fig.2.2.2 LFD2.3 Leg posture using DME

In this chapter, numerical analysis using DME (Dynamic Manipulability Ellipsoid) is described. In an analysis of manipulator DME is popular and useful tool, and it is also useful to evaluate LFD. DME is more effective than ME (Manipulability Ellipsoid) because that ME does not include model dynamics. DME is more effective for fast, frequent motion like as leg motion. State space equation of motion is described as;

$$\tau = M(\Theta)\ddot{\Theta} + V(\Theta,\dot{\Theta}) + G(\Theta) \quad (1)$$

$$\Theta = \begin{bmatrix} \theta_1(t) \\ \vdots \\ \theta_n(t) \end{bmatrix}, \boldsymbol{\tau} = \begin{bmatrix} \tau_1(t) \\ \vdots \\ \tau_n(t) \end{bmatrix}$$

Θ :Joint vecor, τ :joint torque vector, M:Inertial matrix, V:centrifugal force, coriolis force term, G:gravity term

Velocity at the tip of the leg v and joint angle velocity $\dot{\Theta}$ are related as;

$$v = J(\Theta)\dot{\Theta} \quad (2)$$

J is jacobian matrix. Derivate both side,

$$\dot{v} = J(\Theta)\ddot{\Theta} + \dot{J}(\Theta)\dot{\Theta} \quad (3)$$

From equation (1) and (3),

$$\dot{v} - (I - J^{+}J)\dot{J}\dot{\Theta} = JM(\Theta)^{-1}[\tau - V(\Theta,\dot{\Theta}) - G(\Theta) + MJ^{+}\dot{J}\dot{\Theta}] \quad (4)$$

J^{+} is pseudo inverse of J. Here,

$$\tilde{\tau} = \tau - V(\Theta,\dot{\Theta}) - G(\Theta) + M(\Theta)J^{+}\dot{J}\dot{\Theta} \quad (5)$$

$$\dot{\tilde{v}} = \dot{v} - (I - J^{+}J)\dot{J}\dot{\Theta} \quad (6)$$

And equation (4) is;

$$\dot{\tilde{v}} = JM(\Theta)^{-1}\tilde{\tau} \quad (7)$$

DME describes the maximum joint torques $\tau_{i\max}$ as the maximum acceleration $\dot{\tilde{v}}_{j\max}$ at the tip of the leg. $\tilde{\tau},\dot{\tilde{v}}$ are normalized by $\tilde{\tau}_{i\max},\dot{\tilde{v}}_{j\max}$.

$$\hat{\tau} = \left[\frac{\tilde{\tau}_1}{\tilde{\tau}_{1\max}},\cdots,\frac{\tilde{\tau}_n}{\tilde{\tau}_{n\max}}\right]^T \quad (8)$$

$$\dot{\hat{v}} = \left[\frac{\dot{\tilde{v}}_1}{\dot{\tilde{v}}_{1\max}},\cdots,\frac{\dot{\tilde{v}}_m}{\dot{\tilde{v}}_{m\max}}\right]^T \quad (9)$$

and then,

$$\dot{\hat{v}} = \hat{J}\hat{M}(\Theta)^{-1}\hat{\tau} \quad (10)$$

Here,

$$\hat{J} = T_a J \quad (11)$$

$$\hat{M}(\Theta) = T_\tau M(\Theta) \quad (12)$$

$$T_a = diag[\frac{1}{\dot{\tilde{v}}_{1\max}},\frac{1}{\dot{\tilde{v}}_{2\max}},\ldots\ldots,\frac{1}{\dot{\tilde{v}}_{m\max}}] \quad (13)$$

$$T_\tau = diag[\frac{1}{\tilde{\tau}_{1\max}},\frac{1}{\tilde{\tau}_{2\max}},\ldots\ldots,\frac{1}{\tilde{\tau}_{m\max}}] \quad (14)$$

$$\tilde{\tau}_{i\max} = \tau_{i\max} - |v(\Theta,\dot{\Theta})| - |G(\Theta)| \quad (15)$$

Inertial matrix used in simulation is;

$$M(\Theta) = \begin{bmatrix} l_{1c}^2 m_1 + l_1^2 m_2 + l_{2c}^2 m_2 + 2l_1 l_{2c} m_2 \mathrm{Cos}(\theta_2) & l_{2c}^2 m_2 + l_1 l_{2c} m_2 \mathrm{Cos}(\theta_2) \\ l_{2c}^2 m_2 + l_1 l_{2c} m_2 \mathrm{Cos}(\theta_2) & l_{2c} m_2 \end{bmatrix} \quad (16)$$

Centrifugal force and Coriolis force term is;

$$V(\Theta,\dot{\Theta}) = \begin{bmatrix} -2l_1 l_{2c} m_2 \dot{\theta}_1 \dot{\theta}_2 \mathrm{Sin}(\theta_2) - l_1 l_{2c} m_2 \dot{\theta}_2^2 \mathrm{Sin}(\theta_2) \\ l_1 l_{2c} m_2 \dot{\theta}_1 \mathrm{Sin}(\theta_2) \end{bmatrix} \quad (17)$$

Gravitational term is;

$$G(\Theta) = \begin{bmatrix} gl_{1c} m_1 \mathrm{Cos}(\theta_1) + gl_{2c} m_2 \mathrm{Cos}(\theta_1)\mathrm{Cos}(\theta_2) + \\ gl_1 m_2 \mathrm{Cos}(\theta_1)\mathrm{Cos}(\theta_2)^2 - 2l_1 l_{2c} m_2 \dot{\theta}_1 \dot{\theta}_2 \mathrm{Sin}(\theta_2) - \\ l_1 l_{2c} m_2 \dot{\theta}_2^2 \mathrm{Sin}(\theta_2) - gl_{2c} m_2 \mathrm{Sin}(\theta_1)\mathrm{Sin}(\theta_2) + \\ gl_1 m_2 \mathrm{Cos}(\theta_1)\mathrm{Sin}(\theta_2)^2 \\ \\ l_{2c} m_2 (g\mathrm{Cos}(\theta_1)\mathrm{Cos}(\theta_2) - g\mathrm{Sin}(\theta_1)\mathrm{Sin}(\theta_2)) \end{bmatrix} \quad (18)$$

2.4 V/H ratio

In this chapter, V/H ratio (Vertical/Horizontal Ratio) is proposed as index of LFD. From LFD idea, vertical force is maximized in gravitational support

function and horizontal force is maximized in generating forward force function as possible. V/H ratio measures this fact. V/H ratio describes what the part of the major axis of the ellipsoid could contribute into vertical direction or horizontal direction.

V/Hx ratio is the proportion between the length of the major axis and the length projected from the length of the ellipsoid along X axis onto the major axis (Fig.2.4.1).

V/Hz ratio is the proportion between the length of the major axis and the length projected from the length of the ellipsoid along Z axis onto the major axis (Fig.2.4.1).

$$V/H_x = X\cos\alpha \quad (19)$$

$$V/H_z = Z\sin\alpha \quad (20)$$

For example, V/H ratio does not indicate good value at Fig.3.3.

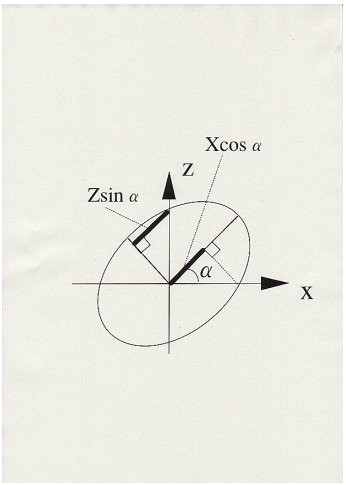

Fig2.4.1 V/H ratio

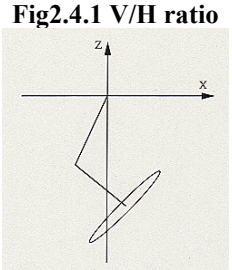

Fig.2.4.2 Negative example

2.5 Numerical Simulation

From Fig2.5.2.1 to Fig2.5.5.2 shows numerical simulation results. Parameters are shown in table2.1. Case1 is $l_1 < l_2$,Case2 is $l_1 > l_2$,Case3 is $l_1 = l_2$.

To define maximum moving velocity, fluid number is adopted. A virtual leg is assumed for whole the robot. The height of C.G. is defined as r;

$$\frac{mv^2}{mgr} \quad (21)$$

luid number is proportion between gravity acceleration and centrifugal force at its speed. The maximum moving velocity is assigned at fluid number = 1. In the case of $r = 0.5(m)$, vmax=2.23(m/s), if the robot accelerate than this speed, then the body is posed.

Case(1) : Fig2.5.2.1,Fig2.5.2.2 shows the ellipsoids. V means horizontal moving velocity. In this case, v= 2(m/s). Fig2.5.2.2 shows the case that τ_{max} =10(Nm). The direction of the major axis is not uniformed.

Case(2): Fig2.5.3.1,Fig2.5.3.2shows ellipsoids. In the case that the second link is shorter than first link, particularly Fig2.5.3.2, the ellipsoid is slender, and it is no use for both leg functions.

Case(3): Fig2.5.4.1,Fig2.5.4.2,Fig2.5.4.3,Fig2.5.4.4 shows ellipsoids. In the case that τ_{max} =10(Nm), the direction of the major axis is relatively uniformed. Altogether, in the area which x < 0 and z < 0, the ellipsoids are adapted for generate vertical acceleration. In the area which x > 0 and z < 0, the ellipsoids are adapted for generate horizontal acceleration.

When value of τ_{max} is large value, the ellipsoid is slender, then the direction of the ellipsoid is important factor. This means that LFD is important for a robot equipped with large torque actuators.

Fig. 2.5.5.1,Fig. 2.5.5.2 shows V/H ratio about case (3). The postures adapted for vertical acceleration and horizontal acceleration are distinctive. In Fig2.5.5.1, the posture adapted for V/Hx ratio aims generating forward force function. In Fig2.5.5.2, the posture adapted for V/Hz ratio aims gravitational support function.

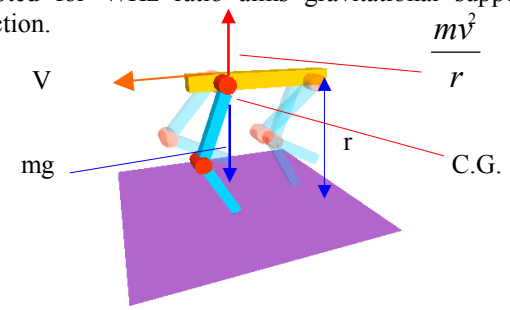

Fig.2.5.1 Definition of Fluid Number

Table 2.1 parameters of 2 link

case1	case2	case3
m_1=1.0 kg	m_1=1.0 kg	m_1=1.0 kg
m_2=1.0 kg	m_2=1.0 kg	m_2=1.0 kg
l_1=0.125 m	l_1=0.375m	l_1=0.25 m
l_{1c}=0.0625 m	l_{1c}=0.1875m	l_{1c}=0.125 m
l_2=0.375 m	l_2=0.125 m	l_2=0.25 m
l_{2c}=0.1875 m	l_{2c}=0.0625m	l_{2c}=0.125m

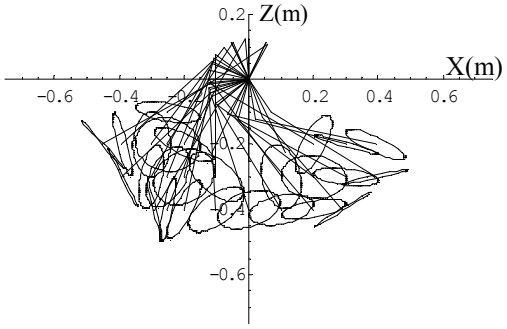

Fig2.5.2.1 Case1 V=2(m/s), τ_{max} =1(Nm)

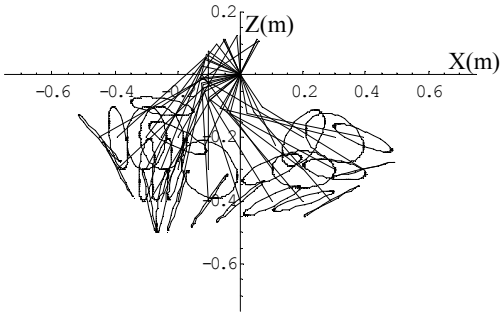

Fig2.5.2.2 Case1 V=2(m/s), τ_{max} =10(Nm)

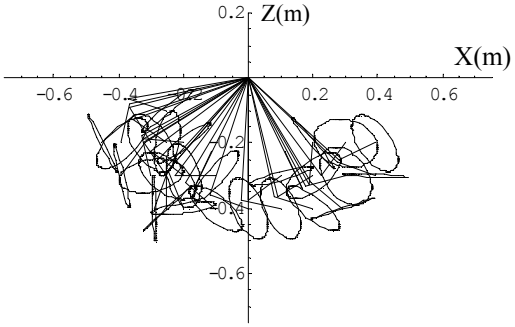

Fig2.5.3.1 Case2,V=2(m/s), τ_{max} =1(Nm)

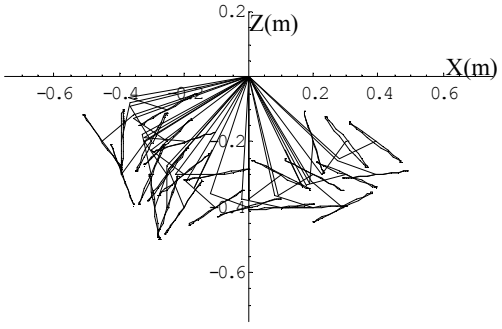

Fig2.5.3.2 Case2 ,V=2(m/s), τ_{max} =10(Nm)

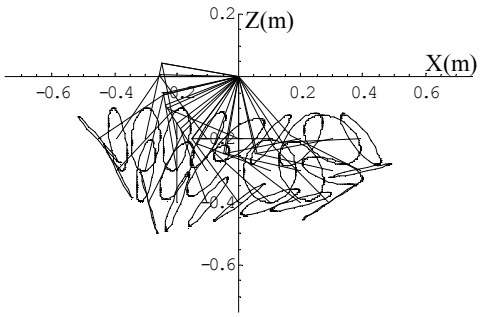

Fig2.5.4.1 Case3,V=2(m/s), τ_{max} =1(Nm)

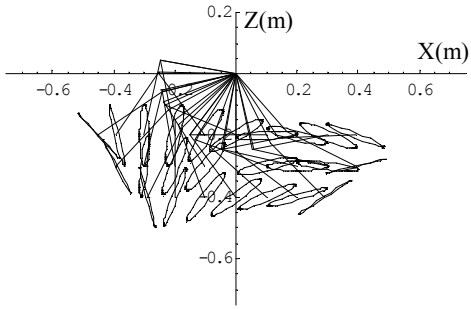

Fig2.5.4.2 Case3,V=2(m/s), τ_{max} =10(Nm)

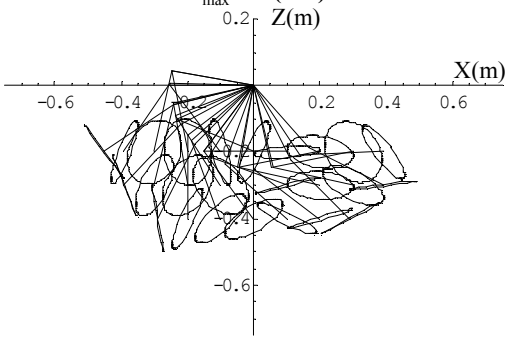

Fig.2.5.4.3 Case3,V=0.5(m/s), τ_{max} =10(Nm)

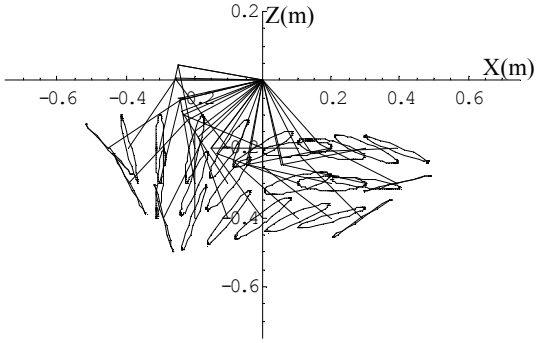

Fig2.5.4.4 Case3 ,V=0.5(m/s), τ_{max} =10(Nm)

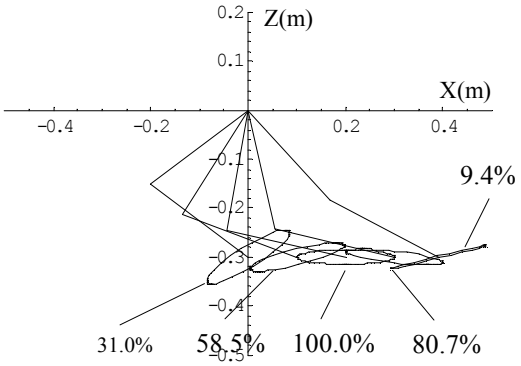

Fig.2.5.5.1 V/Hx Ratio Case3, V=2(m/s), τ_{max}=10(Nm)

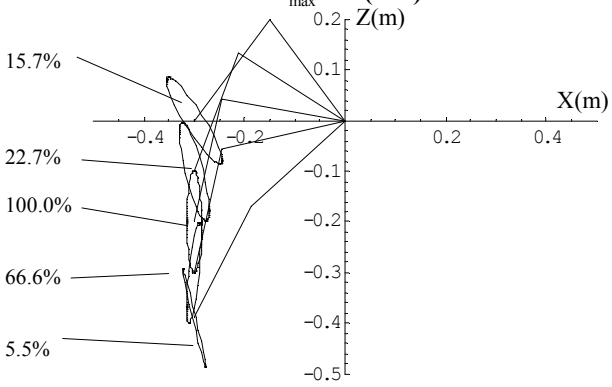

Fig.2.5.5.2 V/Hz Ratio Case3, V=2(m/s), τ_{max}=10(Nm)

3. High Mobility Gait

The gait of quadruped animal change along moving velocity. In this chapter, bound gait which is in high mobility area is considered. In bound gait, it is not effective that the legs merely act the robot upward like as hopping robot. It means that the robot waste the energy for it. In hopping robot, using spring mechanism can avoid this fact.

In this paper, it is proposed to use turnover moment for getting the robot upward in bound gait. Fig3.1 which a horse over a hurdle is helpful to understand this idea.

(Phase I) In Fig.3.2, inertial force $-m\ddot{x}$ rises when hind-feet accelerate the body forward. At this time,

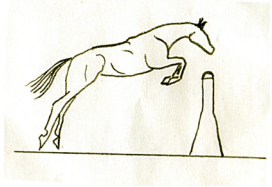

Fig.3.1 Horse jump over a hurdle

the moment around the tip of hind-feet is described as;

$$I\ddot{\theta} = -m\ddot{x}z + mgx \qquad (22)$$

If the first term > the second term, the body starts to overturn backward, take off, and the C.G. moves forward.

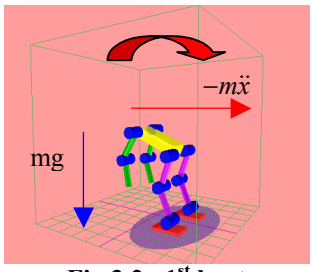

Fig.3.2 1st beat

(Phase II) At the moment of touch down like as Fig.3.3, the overturn moment forward rise because of decelerate force. At this time, if the tip of hind-feet return to front part of the body, then frequent legs motion is available. Ideally, the momentum between these 2 phases is conserved, it is supposed that this motion can be executed without spring mechanism. Off course, the performance of the motion upgrades.

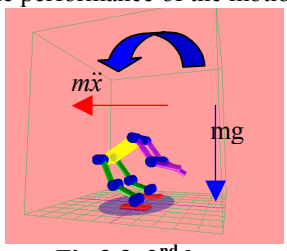

Fig.3.3 2nd beat

4.Receding Horizon Control for Biped

4.1 Receding Horizon Control

In this chapter, let consider how to control ZMP for the biped robot MEL Deinonychus II. The walking sequence is divided into dual support phase and single support phase. At the single support phase in sagittal plane, the robot model behaves like as Fig.4.1. This figure implies TPBVP(Two Point Baundary Value Problem) between initial attitude and final attitude in the single support phase. However, these problem was only available in off-line computing, because gradient method (SCGRA or MQA algorithm) was necessary for solving, then it waste huge calculating time. This is patient of real time control, and fore-running studies divert into a method explicated in the chapter4.2.

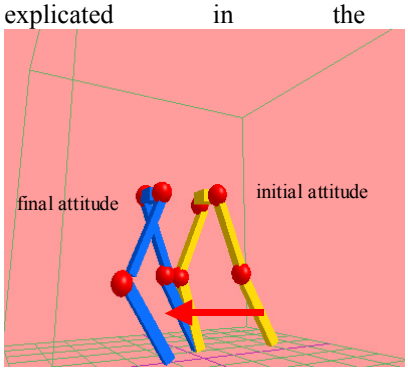

Fig.4.1 TPBVP in single support phase

4.2 Precedent technique of ZMP Control

Generally, the definition of ZMP is described as,

$$x_{zmp} = \frac{\sum_{i=0}^{n} m_i(g+\ddot{z}_i)x - \sum_{i=0}^{n} m_i \ddot{x}_i z_i}{\sum_{i=0}^{n} m_i(g+\ddot{z}_i)x} \quad (23)$$

For brief, these are represented as,

$$x_{zmp} = \frac{(g+\ddot{z})x - z\ddot{x}}{g+\ddot{z}} \quad (24)$$

If z is constant value and $\ddot{z} = 0$,then,

$$x_{zmp} = \frac{gx - h_{ref}\ddot{x}}{g} \quad (25)$$

In the most ordinarily used ZMP control, the height is not able to solve for x axis and z axis simultaneously. It is not able to solve by one on one, then the height of "z" is assumed as a constant. If the reference of ZMP value is larger than real ZMP value, then $\ddot{x}$ is accelerated into forward. If the reference of ZMP value is smaller than real ZMP value, then $\ddot{x}$ is decelerated. Thus it is available to control ZMP by most recently used method. However, this control is not innate, it is dependence of solution on extemporaneous technique.

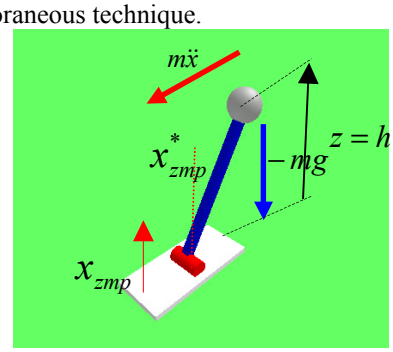

Fig.4.2 Accelerate

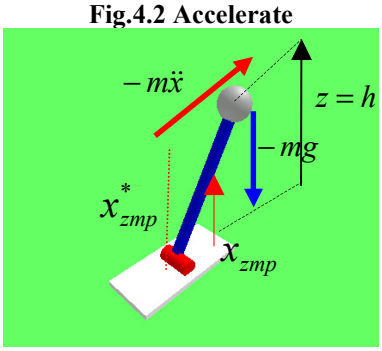

Fig.4.3 Decelerate

In this paper , solution using RHC with equal constraint is proposed, this is essentially solving technique and has real-time performance.

4.3 RHC with equal-constraint

The state equation of the model is described as;

$$\dot{x}^*_\tau(\tau,t) = f_1[x^*(\tau,t), u^*(\tau,t)] \quad (26)$$

The system has to followed the equal constraint,

$$(-g+\ddot{z})x_{zmpref} - (-g+\ddot{z})x + z\ddot{x} = \mathrm{O} -> f_2[x(t),u(t)] = \mathrm{O} \quad (27)$$

In this equation, the second and 3rd term are described as ZMP * $(-g+\ddot{z})$ state. And we have the Hamiltonian,

$$H = L + \lambda^* f_1[x^*(t),u^*(t)] + \rho^* f_2[x^*(t),u^*(t)] \quad (28)$$

Where, we have to consider the performance index moving on τ time axis. "*" means that it is on the τ time axis[12].

$$J = \varphi[x^*(t+T)] + \int_t^{t+T} L d\tau \quad (29)$$

The solution is derived from TPBVP(Two Point Boundary Value Problem) bellow,

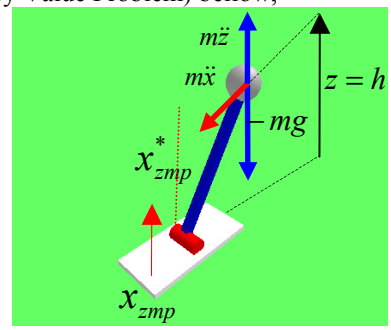

Fig.4.4 ZMP control by RHC

$$\begin{aligned} \dot{x}^*(\tau,t) &= H^T_\lambda ; x^*(0,t) = x(t) \\ \dot{\lambda}^*(\tau,t) &= -H^T_x ; \lambda^*(T,t) = \varphi^T_x[x^*(T,t)] \\ H_u &= 0 \end{aligned} \quad (30)$$

4.4 Index function for numerical solutions

The model for numerical solutions is defined as ,

$$\frac{d}{dt}\begin{bmatrix} \dot{\theta}_1(t) \\ \dot{\theta}_2(t) \\ \theta_1(t) \\ \theta_2(t) \end{bmatrix} = \begin{bmatrix} M^{-1}(\Theta)\left(\begin{bmatrix} u_1(t) \\ u_2(t) \end{bmatrix} - V(\Theta,\dot{\Theta}) - G(\Theta)\right) \\ \dot{\theta}_1(t) \\ \dot{\theta}_2(t) \end{bmatrix} \quad (31)$$

This is 2link model in sagittal plane. The performance index of this numerical solution is for the norm of each joint torque.

$$J = \varphi[x^*(t+T)] + \int_t^{t+T} u^*(t)^T u^*(t) d\tau \quad (32)$$

4.5 Enhanced ZMP for slope terrain

On step or slope, un-even terrain , it is not possible to use ZMP , because ZMP is defined around an ankle on horizontal terrain. At this point , ZMP should be enhanced for un-even terrain. It is assumed an un-even terrain in Fig.4.5. A virtual plane is set like from one foot to the other as the figure. This is same technique of HONDA humanoid robot. If the virtual plane is assigned, it can be to set the origin of the axis on the virtual plane, then ZMP is available to move on the plane to other foot.

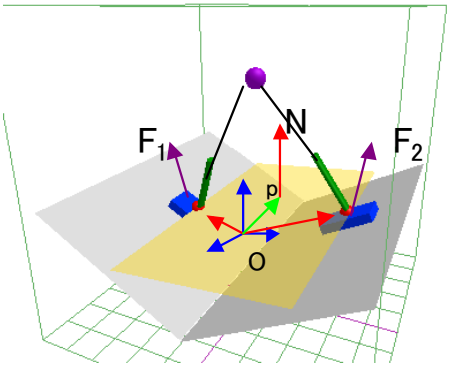

Fig.4.5 virtual plane for enhanced ZMP

References

[1]T.Yoshikawa : Dynamic Manipulability of Robotic Mechanisms, J.Robotic Systems, 2, 1, p.p.113-124, 1985

[2]A.E.Bryson Jr,Y.C.Ho: Applied Optimal Control, Hemisphere,1975

[3]R.M.Murray,Z.Li,S.S.Sastry: A Mathematical Introduction ROBOT to IC MANIPULATION, CRC Press,1994

[4]M.H.Raibert:"Legged Robot that balance", MIT Press, 1986

[5]P.M.Galton: The Posture of hadrosaurian dinosaurs, J. of Paleontology 44,p.p.464-473

[6]M.Alexander:Dynamics of Dinosaurs & other extinct giants, Colombia University Press, 1989

[7]D.J.Todd: Walking Machines-An Introduction , Kogan Page Ltd,1985

[8]M.Alexander: Exploring Biomechanics -Animals in Motion- , W.H.Freeman and Company, 1992

[9]H.TAKEUCHI : Development of Leg-Functions Coordinated Robot “MEL HORSE”,European Center Peace and Development Conference on Advanced Robotics,p.p.288-294,1996

[10]M.Buehler,A.CoCosco, K.Yamazaki, R.Battagria : Stable Open Loop Walking in Quadruped Robot with Stick Legs, International Conference on Robotics and Automation `99 Proceedings, p.p. 2348-2354,1999

[11]H.TAKEUCHI : Development of MEL HORSE, IEEE International Conference on Robotics and Automation `99 Proceedings, p.p. 1057-1062,1999

[12]H.TAKEUCHI, T.OHTSUKA : Optimization applied into Mechanical Link system using Receding Horizon Control -Consideration for solutions using Continuation Method-, RSJ journal, vol.17,No.3,1999, (Japanese language)

[13]M.Vukobratovic, et al : "Biped Locomotion", Springer Verlag, 1990

Session

Super Mechano-Systems

Proceedings of the International Symposium on
Adaptive Motion of Animals and Machines,
Montreal, Aug.8-12, 2000

Unit Design of Hyper-redundant Snake Robots Based on a Kinematic Model

Fumitoshi Matsuno and Kazutaka Mogi

Department of Computational Intelligence and Systems Science,
Interdisciplinary Graduate School of Science and Engineering,Tokyo Institute of Technology,
Nagatsuta, Midori, Yokohama 226-8502, Japan, {matsuno,mogi}@cs.dis.titech.ac.jp

Abstract

We define the redundancy controllable system of hyper-redundant mechanical systems. We derive the condition that the hyper-redundant snake robots become redundancy controllable, and the control law with considering the redundancy. We also propose a concept of a unit and the system design strategy of the snake robots. Simulation results are shown.

1. Introduction

Unique and interesting gait of the snakes makes them able to crawl, climb a hill, climb a tree by winding and move on very slippery floor [1]. It is useful to consider and understand the mechanism of the gait of the snakes for mechanical design and control law of snake robots.

Hirose has long investigated snake robots and produced several snake robots, and he models the snake by a wheeled link mechanism with no side slip [2]. Some other snake-like mechanisms are developed in [3] and [4]. Burdick and Chirikijian discuss the sidewinding locomotion of the snake robots based on the kinematic model [5]. Ostrowski and Burdick analyze the controllability of a class of nonholonomic systems that the snake robots are included on the basis of the gemotric approach [6]. The feedback control law for the snake head's position using Lyapunov method has been developed by Prautesch et al. on the basis of the wheeled link model [7]. They point out the controller can stabilize the head position of the snake robot to its desired value, but the configuration of it converges to a singular configuration. From the model we find that the snake robot does not have the redundant degrees of freedom, and this leads to the difficulty in the control objective of the singular configuration avoidance.

In this paper we define the redundancy controllable system and propose control law and structure design methodology of redundant snake robots based on the wheeled link model. We find that introduction of links without wheels and shape controllable points in the snake robot's body makes the system redundancy controllable. In this case the head's velocity of the snake robot does not determine all joint velocities of the robot uniquely. We introduce the cost function related to the measure for the singularity and the manipulability of the system, and construct a controller with considering the redundancy. Using redundancy, it becomes possible to accomplish both the main objective of controlling the position and the posture of the snake robot head and the shape of the snake robot, and the sub-objective of the singular configuration avoidance and the obstacle avoidance.

We introduce an unit which is fundamental element of the snake robots. We assume that the serial connection of uniform units constructs a snake robot. We discuss the condition of the unit that the connected system becomes redundancy controllable. We propose the unit design and the connection law for constructing the snake robot.

From simulation results we find that the crawling motion of the snake robot is natural.

2. Redundancy Controllable System

Let $\boldsymbol{q} \in R^{\bar{n}}$ be generalized coordinates, $\boldsymbol{u} \in R^{\bar{p}}$ be the input vector, $\boldsymbol{w} \equiv S\boldsymbol{q} \in R^{\bar{q}}$ be the state vector to be controlled, S be a selection matrix, whose row vectors are independent unit vectors, related to generalized coordinates. We define that the system

$$A(\boldsymbol{q})\dot{\boldsymbol{w}} = B(\boldsymbol{q})\boldsymbol{u} \tag{1}$$

is redundancy controllable if the number of inputs $\bar{p}$ is greater than that of the state vector to be controlled $\bar{q}$ ($\bar{p} > \bar{q}$), the matrix A is full column rank, B is full row rank, and there exists an input $\boldsymbol{u}$ which accomplishes both the main objective of the convergence of the vector $\boldsymbol{w}$ to the desired state $\boldsymbol{w}_d$ ($\boldsymbol{w} \to \boldsymbol{w}_d, \dot{\boldsymbol{w}} \to \dot{\boldsymbol{w}}_d$) and the sub-objective of increase (or decrease) of a cost function $V(\boldsymbol{q})$.

For a snake robot based on the wheeled link model we discuss a condition that the system is redundancy controllable.

3. Kinematic Model of Hyper-redundant Snake Robots

We consider a redundant n-link snake robot. Let n be the number of links, m be the number of wheeled links, $[\,x_h \quad y_h \quad \theta_h\,]^T$ be the vector of the position and the posture of the snake head, $[\,\phi_1 \quad \cdots \quad \phi_{n-1}\,]^T$ be the vector of relative joint angles and $\boldsymbol{q} = [\,x_h \quad y_h \quad \theta_h \quad \phi_1 \quad \cdots \quad \phi_{n-1}\,]^T \in R^{n+2}$ be the generalized coordinates.

The length of each link is $2l$. The wheels are located on the middle point of the wheeled link. Let $[\,x_i \quad y_i\,]^T$ be the position vector of the middle point of the link i as shown in Fig. 1. As the wheel does not slip to the side direction, the velocity constraint condition should be satisfied. If the i-th link is wheeled, the constraint can be written as

$$\dot{x}_i \sin(\theta_h + \sum_{k=1}^{i-1} \phi_k) - \dot{y}_i \cos(\theta_h + \sum_{k=1}^{i-1} \phi_k) = 0. \quad (2)$$

From the geometric relation the position vector is expressed as

$$\begin{aligned} x_i &= x_h + 2l\cos\theta_h + 2l\sum_{k=1}^{i-2}\cos(\theta_h + \sum_{j=1}^{k}\phi_j) \\ &\quad + l\cos(\theta_h + \sum_{k=1}^{i-1}\phi_k) \quad (3) \\ y_i &= y_h + 2l\sin\theta_h + 2l\sum_{k=1}^{i-2}\sin(\theta_h + \sum_{j=1}^{k}\phi_j) \\ &\quad + l\sin(\theta_h + \sum_{k=1}^{i-1}\phi_k). \quad (4) \end{aligned}$$

Substituting (3), (4) into (2), gives the velocity constraint equation

$$A(\boldsymbol{q})\dot{\boldsymbol{w}} = B(\boldsymbol{q})\boldsymbol{u}, \quad \boldsymbol{u} = \dot{\boldsymbol{\theta}} \quad (5)$$

where $\boldsymbol{w}$ is the state vector to be controlled, $\boldsymbol{\theta}$ is the vector of the active joint angles, $A \in R^{m\times q}$, $B \in R^{m\times p}$, and the angular velocity of the active joint is regarded as the input of the system.

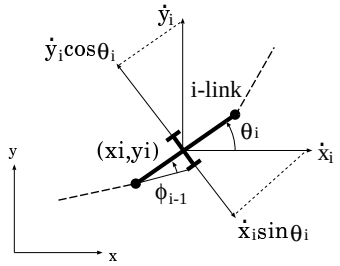

Fig. 1 Velocity constraint of the i-th wheeled link

As one wheeled link has one velocity constraint, the number m of the wheeled links is equal to the number of equations. We assume that at least the snake head's position and posture are controlled.

4. Condition for Redundancy Controllable System

We consider an n-link snake robot whose all links are wheeled as shown in Fig. 2. Let $\bar{\boldsymbol{w}} = [\,x_h \quad y_h \quad \theta_h\,]^T$ be the position and posture of the snake head, $\bar{\boldsymbol{\theta}} = [\,\phi_1 \quad \cdots \quad \phi_{n-1}\,]^T$ be relative angles of each link, $\boldsymbol{q} = \left[\,\bar{\boldsymbol{w}}^T \quad \bar{\boldsymbol{\theta}}^T\,\right]^T$ be generalized coordinates. We assume the angular velocity of an active joint is regarded as an input of the system

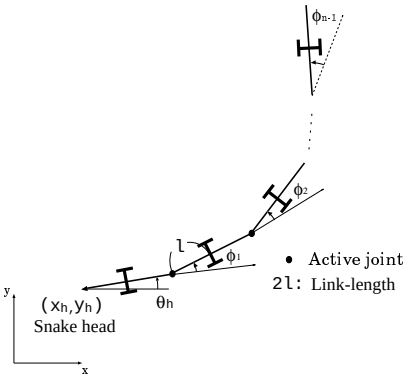

Fig. 2 An n-link snake robot

As in this case all links are wheeled link, the system can be written as

$$\bar{A}(\boldsymbol{q})\dot{\bar{\boldsymbol{w}}} = \bar{B}(\bar{\boldsymbol{\theta}})\bar{\boldsymbol{u}}, \quad \bar{\boldsymbol{u}} = \dot{\bar{\boldsymbol{\theta}}} \quad (6)$$

where $\bar{A} \in R^{n\times 3}, \bar{B} \in R^{n\times(n-1)}$. In the system (6), as the velocity constraint of the passive wheel of the head-link is expressed as $\dot{x}_h \sin\theta_h -$

$\dot{y}_h \cos\theta_h - l\dot{\theta}_h = 0$, we find that the matrix $\bar{B}$ is not full row rank. It is necessary that the first link is wheel free.

Next, we consider the system that only the head-link is wheel free. This system can be written as

$$\bar{A}'(\boldsymbol{q})\dot{\tilde{\boldsymbol{w}}} = \bar{B}'(\bar{\boldsymbol{\theta}})\bar{\boldsymbol{u}} \tag{7}$$

where $\bar{A}' \in R^{(n-1)\times 3}, \bar{B}' \in R^{(n-1)\times(n-1)}$ and

$$\bar{B}' = \begin{bmatrix} l & & & & \\ b_{21} & l & & O & \\ \vdots & & \ddots & & \\ \vdots & & & l & \\ b_{(n-1)1} & \cdots & \cdots & b_{(n-1)(n-2)} & l \end{bmatrix}.$$

We find that the matrix $\bar{B}'$ is invertible. As the velocity of the snake head $\dot{\tilde{\boldsymbol{w}}}$ determines the input $\bar{\boldsymbol{u}}$ uniquely, the system (7) is not redundant.

In this paper, as we control the shape of the snake robot body in addition to the position and posture of the snake head, some relative angles are included in the state vector to be controlled. We call the joint angle the shape controllable point and the number of the shape controllable points the shape controllability index. Let s be the shape controllability index.

Next, we consider that ϕ_i is introduced as the controlled state. Then the system can be written as

$$\hat{A}(\boldsymbol{q})\dot{\hat{\boldsymbol{w}}} = \hat{B}(\bar{\boldsymbol{\theta}})\hat{\boldsymbol{u}} \tag{8}$$

where $\hat{\boldsymbol{w}} = [\bar{\boldsymbol{w}}^T \quad \phi_i]^T$, $\hat{\boldsymbol{u}} = [\dot{\phi}_1 \cdots \dot{\phi}_{i-1} \; \dot{\phi}_{i+1} \cdots \dot{\phi}_{n-1}]$, $\hat{A} \in R^{(n-1)\times 4}, \hat{B} \in R^{(n-1)\times(n-2)}$ and

$$\hat{B} = \begin{bmatrix} l & & & & & \\ b_{21} & \ddots & & & O & \\ \vdots & & & & & \\ b_{(i-1)1} & \cdots & l & & & \\ b_{i1} & \cdots & b_{i(i-1)} & & & \\ b_{(i+1)1} & \cdots & b_{(i+1)(i-1)} & l & & \\ \vdots & & & & \ddots & \\ b_{(n-1)1} & \cdots & b_{(n-1)(i-1)} & b_{(n-1)(i+1)} & \cdots & l \end{bmatrix}.$$

We find possibility that the matrix $\hat{B}$ is not full row rank. For necessity of the full row rankness of the B matrix, the link which is introduced the shape controllable point should be wheel free.

Next, we consider the system which the $i+1$ $,\cdots,$ the n-th links are wheel free. This system can be written as

$$\tilde{A}(\tilde{\boldsymbol{q}})\dot{\tilde{\boldsymbol{w}}} = \tilde{B}(\bar{\boldsymbol{\theta}})\bar{\boldsymbol{u}} \tag{9}$$

where $\tilde{A} \in R^{(i-1)\times 3}, \tilde{B} \in R^{(i-1)\times(n-1)}$,

$$\tilde{B} = \left[\begin{array}{cccc|c} l & & & & \\ b_{21} & l & & O & \\ \vdots & & \ddots & & \\ \vdots & & & l & \\ b_{(i-1)1} & \cdots & \cdots & b_{(i-1)(i-2)} \quad l & \end{array}\right| O \Bigg].$$

As the column vectors after the $(i+1)$-th column of the matrix $\tilde{B}$ are zero, we find that the movement of links behind the last wheeled link does not contribute to the movement of the snake robot head. To satisfy the condition (B is full row rank) so that the system is redundancy controllable, we should introduce the assumptions.

[assumption 1] : The head link is wheel free.

[assumption 2] : The tail link is the wheeled link.

[assumption 3] : The link which is introduced the shape controllable point is wheel free.

[assumption 4] : The passive joint angle is equivalent to the state variable to be controlled as the shape controllable point.

We remark that the joints of the wheeled links are passive/active joints and that the link which has the passive joint is wheel free. If the assumptions 1-4 are satisfied, the matrix B is full row rank. The assumptions 1-4 are the sufficient condition for the full row rankness of the matrix B.

We consider a redundant n-link snake robot as shown in Fig. 3 with m wheeled links which satisfies the assumptions 1-4. In this case the system can be written as

$$A(\boldsymbol{q})\dot{\boldsymbol{w}} = B(\boldsymbol{q})\boldsymbol{u} \tag{10}$$

where $A \in R^{m\times(3+s)}, B \in R^{m\times(n-1-s)}$, $\boldsymbol{w} = S\boldsymbol{q} \in R^{(3+s)}, \boldsymbol{\theta} = \bar{S}\boldsymbol{q} \in R^{(n-1-s)}$ and $\boldsymbol{u} = \dot{\boldsymbol{\theta}}$. We find that exclusion of $\boldsymbol{w}$ from $\boldsymbol{q}$ gives $\boldsymbol{\theta}$. $\{\boldsymbol{w}\} \cup \{\boldsymbol{\theta}\} = \{\boldsymbol{q}\}, \{\boldsymbol{w}\} \cap \{\boldsymbol{\theta}\} = \boldsymbol{\phi}$.

The necessary and sufficiant condition for the existance of the solution of the system (10) is

$$rank[A, B\boldsymbol{u}] = rankA. \tag{11}$$

In the case of $m < dim(\boldsymbol{w}) = q$ for the system (10), if an input $\boldsymbol{u}$ is given, then the solution $\dot{\boldsymbol{w}}$ does not determine uniquely. From the necessity of the uniqueness of the solution of the system (10), we introduce the condition $m \geq q = 3 + s$. We set $m < p$ so as to satisfy the condition that the velocity vector $\dot{\boldsymbol{w}}$ does not determine the control input $\boldsymbol{u}$ uniquely. This condition means the redundancy of the input.

From two conditions $m \geq q$ and $m < p$ we find that the condition $p > q$ is satisfied. The condition that the system (10) is redundancy controllable can be written as

$$\begin{cases} m & \geq & 3+s \\ m & < & (n-1)-s \end{cases}. \tag{12}$$

Combining them gives

$$3+s \;\leq\; m \;<\; (n-1)-s. \tag{13}$$

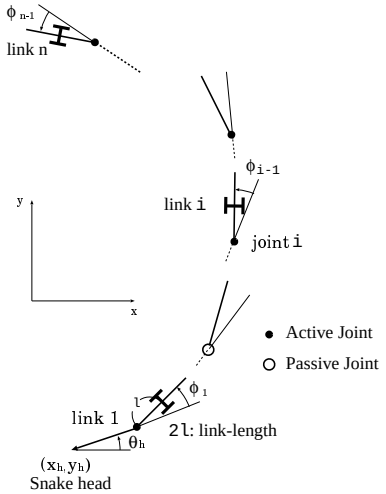

Fig. 3 A redundant n-link snake robot

5. Controller Design

Let us define the control input as follows:

$$\boldsymbol{u} = B^* A\{\dot{\boldsymbol{w}}_d - K(\boldsymbol{w} - \boldsymbol{w}_d)\} + (I_k - B^* B)\alpha\boldsymbol{\eta} \tag{14}$$

where B^* is a pseudo-inverse matrix of B, $\boldsymbol{\eta} = \nabla_{\boldsymbol{\theta}} V(\boldsymbol{q}) = [\partial V/\partial\theta_1 \cdots \partial V/\partial\theta_{n-1-s}]$ is the gradient of the cost function $V(\boldsymbol{q})$ with respect to the vector $\boldsymbol{\theta}$ related to the input vector $\boldsymbol{u}$, and $\alpha \geq 0$, $K > 0$. The first term of the right side of (14) is the control input term to accomplish the main objective of the convergence of the state vector $\boldsymbol{w}$ to the desired value $\boldsymbol{w}_d$. As the second term $(I - B^* B)\alpha\boldsymbol{\eta}$ belongs to the null space of the matrix B, we obtain

$$B\boldsymbol{u} = A\{\dot{\boldsymbol{w}}_d - K(\boldsymbol{w} - \boldsymbol{w}_d)\}. \tag{15}$$

As the vector $B\boldsymbol{u}$ can be expressed as a linear combination of column vectors of the matrix A, the condition of the existance of the solution (10) is satisfied. The second term in (14) does not disturb the dynamics of the controlled vector $\boldsymbol{w}$. As there is no interaction between $\boldsymbol{w}$ and $\boldsymbol{\theta}$, we find that the control law (14) accomplishes the sub-objective. Actually we can derive

$$\begin{aligned} \dot{V}(\boldsymbol{q}) &= (\partial V/\partial \boldsymbol{w})\dot{\boldsymbol{w}} + (\partial V/\partial\boldsymbol{\theta})\dot{\boldsymbol{\theta}} \\ &= (\partial V/\partial \boldsymbol{w})\dot{\boldsymbol{w}} + \boldsymbol{\eta}^T B^* A\{\dot{\boldsymbol{w}}_d - K(\boldsymbol{w} - \boldsymbol{w}_d)\} \\ &\quad + \boldsymbol{\eta}^T (I - B^* B)\alpha\boldsymbol{\eta}. \end{aligned} \tag{16}$$

As $(I - B^* B) \geq 0$ [8], we find that the third term of the input (14) accomplishes the increase of the cost function V.

The closed-loop system is expressed as

$$A\{(\dot{\boldsymbol{w}} - \dot{\boldsymbol{w}}_d) + K(\boldsymbol{w} - \boldsymbol{w}_d)\} = 0. \tag{17}$$

If the matrix A is full column rank, the uniqueness of the solution is guaranteed. The solution of (17) is given as

$$\dot{\boldsymbol{w}} - \dot{\boldsymbol{w}}_d + K(\boldsymbol{w} - \boldsymbol{w}_d) = 0$$

and we find that the controller ensures the convergence of the controlled state vector to the desired value ($\boldsymbol{w} \longrightarrow \boldsymbol{w}_d$). A set of joint angles which satisfies $rank A < q$ (A is not full column rank) means the singular configuration, for example a straight line ($\phi_i = 0, i = 1, \cdots, n-1$).

6. System Design based on Units

Let us introduce the concept of units. We define that a unit is a fundamental element for constructing the redundant snake robot. The serial connection of uniform units constructs a snake robot as shown in Fig. 4.

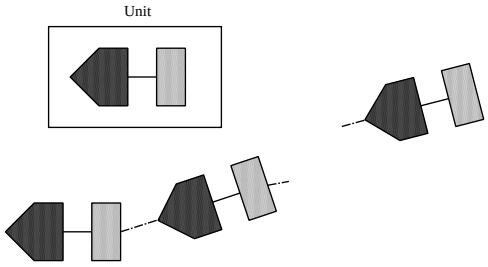

Fig. 4 Concept of unit and total system

6.1. Condition of unit

Let us introduce following [assumption U1] - [assumption U5].

[assumption U1] : A connected joint of two units is passive.

[assumption U2] : The head link of a unit is wheel free.

[assumption U3] : The tail link of a unit is the wheeled link.

[assumption U4] : The link which is introduced the shape controllable point in an unit is wheel free.

[assumption U5] : The passive joint is equivalent to the shape controllable point.

The assumption U1 means that a connection point of units is a free joint. The assumption is acceptable because the actuator can not be mounted on a connected point of units. The assumptions U2-U5 for the unit are related to the assumptions 1-4 for the total system, respectively.

Let n_u be the number of links, m_u be the number of wheeled links, s_u be the shape controllability index of one unit. We assume that same k units are connected serially. Fig. 5 shows an example of the connection of the units. From (12) the condition for the redundancy controllability of the total system of the connected k units can be expressed as

$$\begin{cases} km_u & \geq & 3 + (k-1) + ks_u \\ km_u & < & k(n_u - 1) - ks_u \end{cases}. \tag{18}$$

The condition for the unit so that the total system becomes redundancy controllable is given as follows

$$\frac{k+2}{k} + s_u \leq m_u < (n_u - 1) - s_u. \tag{19}$$

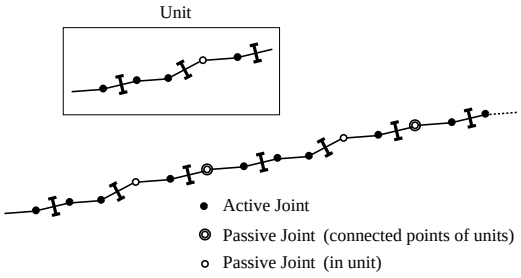

Fig. 5 An example of the connection of the units

We classify the units based on the number of the links n_u and the number of the wheeled links m_u and define $Type(n_u, m_u)$ as the type of units. From the assumptions U2 and U3 we find that the $Type(n_u, m_u)$ unit has ${}_{n_u-2}C_{m_u-1}$ different formations.

Next we discuss the minimum units. Setting $k = 1$ in (19) gives

$$3 + s_u \leq m_u < (n_u - 1) - s_u \tag{20}$$

If we set $s_u = 0$ and 1, from (20) the minimum number m_u, n_u are given as

$$\begin{cases} s_u = 0 : & n_u = 5, m_u = 3 \\ s_u = 1 : & n_u = 7, m_u = 4 \end{cases}.$$

For $k = 2$ the condition (13) is rewritten as

$$2 + s_u \leq m_u < (n_u - 1) - s_u. \tag{21}$$

If we set $s_u = 0$ and 1, from (21) the minimum number m_u, n_u are given as

$$\begin{cases} s_u = 0 : & n_u = 4, m_u = 2 \\ s_u = 1 : & n_u = 6, m_u = 3 \end{cases}.$$

We can derive the minimum units as follows:

1. The $Type(4,2)$ is the minimum unit which can construct the redundancy controllable system by connection.
2. The $Type(6,3)$ is the minimum unit which can construct the redundancy controllable system by connection and has a shape controllable point in the unit itself.
3. The $Type(5,3)$ is the minimum unit that the unit itself is the redundancy controllable.
4. The $Type(7,4)$ is the minimum unit that the unit itself is the redundancy controllable and has a shape controllable point in the unit itself.

From the second inequality of the condition (18) we obtain

$$s_u < n_u - m_u - 1$$

and we find the maximum number of the shape controllable points which can be indroduced in one unit is $n_u - m_u - 2$. If we set $s_u = n_u - m_u - 2 \geq 0$, the first inequality of the condition (18) is rewritten as

$$2m_u + 1 \geq n_u + \frac{2}{k}. \tag{22}$$

Combining $s_u \geq 0$ and (22) yields

$$m_u + 2 \leq n_u < 2m_u + 1. \tag{23}$$

Next we discuss the characteristic of the system which is constructed by connecting the $Type(n_u, m_u)$ units under the assumption that we introduce the maximum number of the shape controllable points in one unit. Let U be the total number of units, p be the total number of the inputs, $q = 3 + s$ be the total number of the states to be controlled, $r = p - q$ be the number of the redundancy, and s_c be the total number of the shape controllability index related to the connected joints of units. As the exclusion of the set of the shape controllable points in an unit means the set of active joints, we find that $p = k\{n_u - 1 - (n_u - m_u - 2)\} = k(m_u + 1)$. We obtain Table 1.

Table 1 Characteristic of the system which is constructed by the $Type(n_u, m_u)$ units

U	n	m	p	q
1	n_u	m_u	m_u+1	$(n_u-m_u-1)+2$
2	$2n_u$	$2m_u$	$2(m_u+1)$	$2(n_u-m_u-1)+2$
3	$3n_u$	$3m_u$	$3(m_u+1)$	$3(n_u-m_u-1)+2$
$\vdots$	$\vdots$	$\vdots$	$\vdots$	$\vdots$
k	kn_u	km_u	$k(m_u+1)$	$k(n_u-m_u-1)+2$

U	r	s_c	s_u
1	$2m_u-n_u$	0	n_u-m_u-2
2	$2(2m_u-n_u)+2$	1	$2(n_u-m_u-2)$
3	$3(2m_u-n_u)+4$	2	$3(n_u-m_u-2)$
$\vdots$	$\vdots$	$\vdots$	$\vdots$
k	$k(2m_u-n_u)+2(k-1)$	$k-1$	$k(n_u-m_u-2)$

U	s
1	n_u-m_u-2
2	$2(n_u-m_u-2)+1$
3	$3(n_u-m_u-2)+2$
$\vdots$	$\vdots$
k	$k(n_u-m_u-2)+k-1$

From Table 1 we obtain

$$\begin{cases} p = k(m_u+1) \\ r = k(-n_u+2m_u+2)-2 \\ s = k(n_u-m_u-1)-1 \end{cases}. \tag{24}$$

Eliminating k in (24) gives

$$r = (2-\frac{n_u}{m_u+1})p-2, \tag{25}$$

$$s = (\frac{n_u}{m_u+1}-1)p-1. \tag{26}$$

From (25) and (26) we obtain the relation

$$r+s+3=p \tag{27}$$

and we find the trade-off of p, r and s.

6.2. System design

We propose the system design strategy of the snake robot based on the units. The design problem is formulated as following.

[**Problem**] : Let n_u, m_u, k, p, r, s be natural numbers.

Given : p *and* r(*or* s)

Find : s(*or* r), n_u, m_u, k *which satisfy* (24)

The design procedure is as follows :

[**P1**] To give the number p_0 of the input.

[**P2**] To determine the number r_0 of the redundancy and the shape controllability index s_0 under the constraint (27).

[**P3**] To determine the type $Type(n_{u0}, m_{u0})$ and the number k_0 of units.

By using (24) we obtain

$$\frac{n_u}{m_u+1} = \frac{p_0+s_0+1}{p_0} = \frac{2p_0-r_0-2}{p_0} \tag{28}$$

In [P3], we should consider two cases.

(1) p_0+s_0+1 and p_0 are relatively prime

Let us define

$$\begin{aligned} n_{u0} &= p_0+s_0+1 = 2p_0-r_0-2 \\ m_{u0} &= p_0-1. \end{aligned} \tag{29}$$

If n_{u_0} and m_{u_0} satisfy the inequality (23), then the unit is defined as $Type(n_{u_0}, m_{u_0})$ and the number of the units as $k_0 = 1$. If not, go to [P2].

(2) p_0+s_0+1 and p_0 are not relatively prime

Let a be a common divisor of p_0+s_0+1 and p_0. From the condition $p_0+s_0+1 = an_{u_0}$, $p_0 = a(m_{u_0}+1)$ we obtain

$$\frac{p_0+s_0+1}{p_0} = \frac{an_{u_0}}{a(m_{u_0}+1)}$$

and

$$n_{u_0} = \frac{p_0+s_0+1}{a}, \quad m_{u_0} = \frac{p_0}{a}-1.$$

If n_{u_0} and m_{u_0} satisfy the inequality (23), then the unit is defined as $Type(n_{u_0}, m_{u_0})$ and the number of the units k_0 as

$$k_0 = \frac{p_0}{m_{u_0}+1} = \frac{p_0}{\frac{p_0}{a}} = a.$$

If not, choose another common divisor and take the same procedure (2). If the types for all common divisors do not satisfy the condition, go to [P2].

7. Simulation

To demonstrate the validity of the proposed control law simulations have been carried out. In this simulation we set $B^* = B^T(BB^T)^{-1}$ and

$$V = a'(det(A^TA)) + b'(det(BB^T)) \tag{30}$$

where $a', b' > 0$. The first term of the right side of (30) implies the measure of the singular configuration. The second term of the right side of (30) is related to the manipulability of the system.

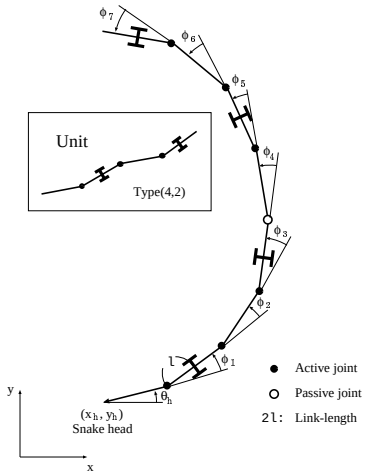

Fig. 6 A 8-link snake robot that is constructed by connecteing two $Type(4,2)$ units

We consider a 8-link snake robot that is constructed by connecteing two $Type(4,2)$ units as shown in Fig. 6. The $Type(4,2)$ unit has four links, two wheeled links and no shape controllable points The connected point is the shape controllable point. In this case $\boldsymbol{w} = [\, x_h \quad y_h \quad \theta_h \quad \phi_4 \,]^T$ and the matrix A is square.

We set the initial condition $\boldsymbol{w}(0), \boldsymbol{\theta}(0)$ and the desired condition $\boldsymbol{w}_d(t)$ as $\boldsymbol{w}(0) = [\, 0 \;\; 0 \;\; \frac{3\pi}{4} \;\; \frac{\pi}{90} \,]^T$, $\boldsymbol{\theta}(0) = [\, \frac{\pi}{120} \;\; \frac{\pi}{110} \;\; \frac{\pi}{100} \;\; \frac{\pi}{80} \;\; \frac{\pi}{70} \;\; \frac{\pi}{60} \,]^T$, $w_d = [\, t \;\; 0 \;\; \pi \;\; \phi_{4_d} \,]^T$, $\dot{w}_d = [\, 1 \;\; 0 \;\; 0 \;\; \dot{\phi}_{4_d} \,]^T$, and $l = 0.05[m]$, $K = diag(3,3,3,3)$. We set cofficients of the cost function V as $a' = a/l^4, b' = b/l^8$ in order to normalize with respect to the link length l. Figs.7-9 show the transient responses. The left column in each figure shows transient responses for $x_h - x_{h_d}[m], y_h - y_{h_d}[m], \theta_h - \theta_{h_d}[m], \phi_4[rad]$, $detA/l^2, \sqrt{det(BB^TT)}/l^4$ and the right column shows transient responses for $u_1, \cdots, u_6$. Fig. 10 shows the movement of the snake robot.

Fig. 7 shows the responses for $\alpha = 0, \phi_{4_d} = 0$ $(case\ 1)$. In this case the controller does not use the redundancy and the desired value for the shape controllable point is zero. From the figure we find that the snake head tracks the desired trajectory, but $detA$ converges to zero. In this case we find that the snake robot converges to a singular configuration of a straight line [9].

Fig. 8 shows the responses for $\alpha = 0, \phi_{4_d} = \frac{\pi}{10}\cos(9t)$ $(case\ 2)$. In this case the controller does not use the redundancy but the desired value of the shape controllable point is not zero. From the figure we find that the snake head tracks the desired trajectory without converging to the singular configuration and the movement of the snake robot is like *the side winding motion* [1] of snakes (Fig. 10).

Fig. 9 shows the responses for $\alpha = 1, a = 1, b = 0.85, \phi_{4_d} = 0$ $(case\ 3)$. In this case the controller uses the redundancy but the desired value of the shape controllable point is zero. From the figure we find that the snake head tracks the desired trajectory and the snake robot crawls without converging to the singular configuration (Fig. 10).

From simulation results we find that the second term of the control law (14) can ensure the singularity avoidance and the vibratory motion of the shape controllable point can avoid convergence of the singular configuration.

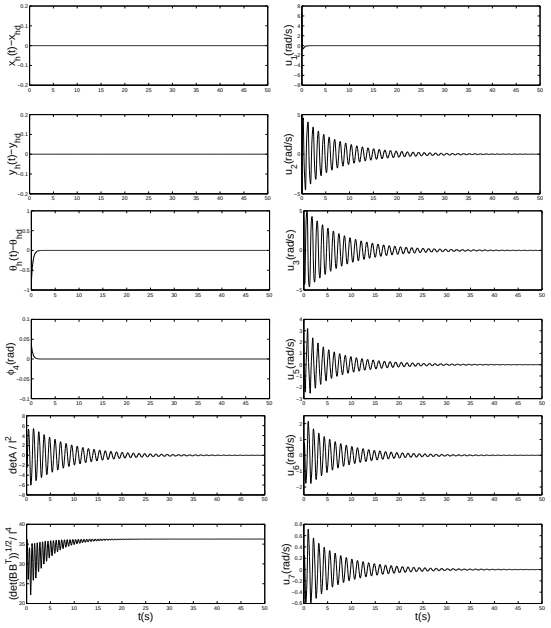

Fig. 7 Transient responses for the controller without considering redundancy $(\alpha = 0,\ \phi_{4_d} = 0)(case\ 1)$

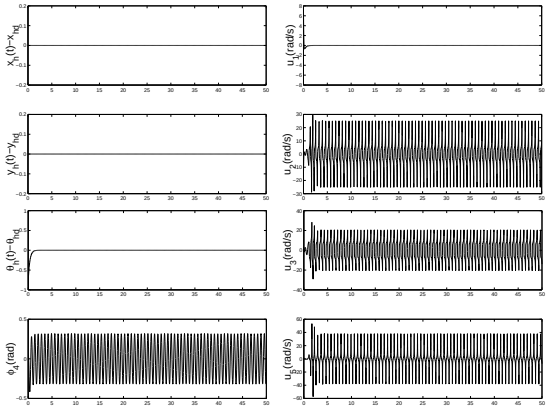

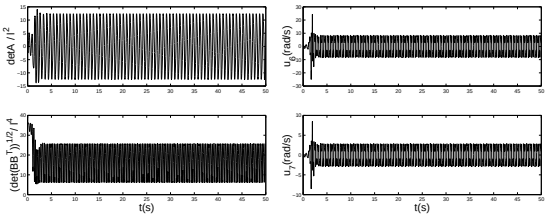

Fig. 8 Transient responses for the controller without considering redundancy ($\alpha = 0$, $\phi_{4_d} = \frac{\pi}{10}\cos(9t)$)($case$ 2)

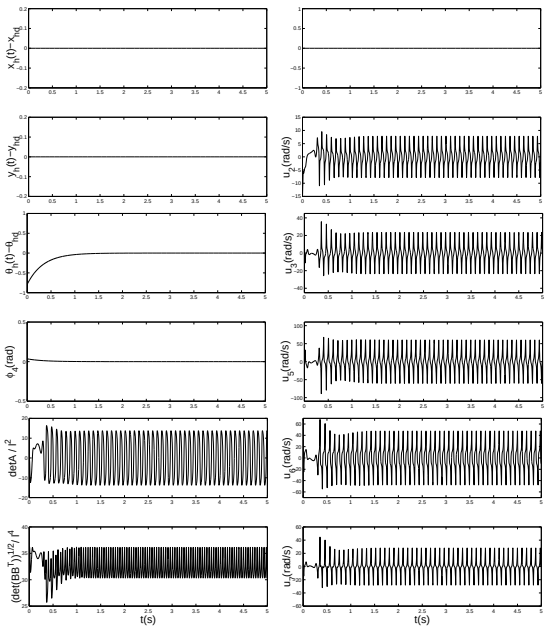

Fig. 9 Transient responses for the controller with considering redundancy ($\alpha = 1, a = 1, b = 0.85, \phi_{4_d} = 0$)($case$ 3)

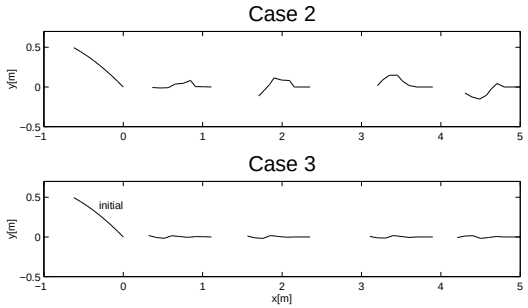

Fig. 10 Movement of the snake robot

8. Conclusion

We derive the condition that the snake robot system becomes redundancy controllable, and introduce the wheel free links in the snake robot body so as to satisfy the condition.

We introduce the concept of the unit and derive the minimum units for several categories. We also propose the system design strategy of the snake robots based on the units.

From simulation results we find that it is possible to accomplish the singular configuration avoidance by giving the appropriate desired value to the shape controllable point or using the redundancy.

As the future works, we should expand the obtained results to the dynamic model.

This research is supported by The Grant-in Aid for COE Research Project of Super Mechano-Systems by The Ministry of Education, Science, Sport and Culture, Japan.

References

[1] J. Gray, *Animal Locomotion*, pp. 166-193, Norton, 1968

[2] S. Hirose, *Biologically Inspired Robots (Snake-like Locomotor and Manipulator)*, Oxford University Press, 1993

[3] S. Shiotani, S. Hamada, T. Oomichi, Y. Ozawa and S. Tsuzuki, Development of Hyper-Degree of Freedom Control Method for Holonic Mechanism, *Proc. COE Super Mechano-Systems Workshop'99*, pp. 89-92, 1999

[4] N. Takanashi, S. Yashima, K. Aoki, T. Nishizawa, Complete Modular Links for Hyper Redundant Robots, *Proc. COE Super Mechano-Systems Workshop'99*, pp. 93-98, 1999

[5] G. S. Chirikijian and J. W. Burdick, The Kinematics of Hyper-Redundant Robotic Locomotion, *IEEE Trans. on Robotics and Automation*, Vol. 11, No. 6, pp. 781-793, 1995

[6] J. Ostrowski and J. Burdick, The Geometric Mechanics of Undulatory Robotic Locomotion, *Int. J. of Robotics Research*, Vol. 17, No. 6, pp. 683-701, 1998

[7] P. Prautesch, T. Mita, H. Yamauchi, T. Iwasaki and G. Nishida, Control and Analysis of the Gait of Snake Robots, *Proc. COE Super Mechano-Systems Workshop'99*, pp. 257-265, 1999

[8] Y. Nakamura, H. Hanafusa and T. Yoshikawa, Task-Priority Based Redundancy Control of Robot Manipulators, *Int. J. of Robotics Research* , Vol. 6, No. 2, pp. 3-15, 1987

[9] K. Mogi and F. Matsuno, Control of a Snake Robot with Redundancy Based on Kinematic Model, *Proc. 5th. Int. Symposiume of Artificial Life and Robotics*, pp. 507-510, 2000

[10] F. Matsuno and K. Mogi Design and Control of Snake Robots with Redundancy Based on Kinematic Model, *Proc. COE Super Mechano-Systems Workshop 2000*, pp. 249-258

Proceedings of the International Symposium on
Adaptive Motion of Animals and Machines,
Montreal, Aug.8-12, 2000

Dynamic Manipulability of a Snake-Like Robot with Consideration of Side Force and its Application to Locomotion Control

H. Date[1], Y. Hoshi[2] and M. Sampei[3]

[1,2,3]Tokyo Institute of Technology, Oh-Okayama 2-12-1, Meguro-ku, Tokyo 152-8552, sampei@mei.titech.ac.jp

Abstract

This paper discusses an autonomous locomotion control of a snake-like robot which consists of multiple links with passive wheels and active joints. Such a robot has quite different mechanism in locomotion from that of other locomotion systems. Since the robot has no driving wheel, the locomotability depends on its posture. Thus we utilize a notion of dynamic manipulability to evaluate the locomotability with consideration of the side force wheels. We also propose control method of locomotion control based on this manipulability. Simulation results show a certain periodic winding motion is automatically generated.

1. Introduction

This paper discusses an autonomous locomotion control of a snake-like articulated robot. Such a robot has been attracted attention of many researchers for capability of multiple functions such as grasping and locomotion by varying its shape. Particularly, the mechanism of locomotion is quite different from that of other mobile robots, that is to say, the robot has no driving wheel. There have been proposed several kinds of snake-like robots [3, 4, 5, 7, 9], and this research deals with one of them, an articulated robot with an actuator in each joint and a passive wheel in the middle of each link[7]. It is assumed that the wheels does not sideslip. In some appropriate postures, the robot can locomote using the constraining force of wheels against sideslip arising from actuating the joints. On the contrary, there exists singular postures in which the robot cannot move in some direction. Straight shape or single arc shape is known to be singular postures. Hence the locomotability of the robot largely depends on its posture and it is important to keep some suitable posture to control the locomotion.

Hirose suggested that actuating the joints with sinusoidal inputs generates typical winding motion of natural snakes [3]. A trace of such winding motion is called a serpenoid curve. He developed multi-link robots and applied some control based on the serpenoid curve. In this method, though singular postures can always be avoided, the gait of the robot is fixed beforehand and exact control of the position is difficult. On the contrary, Mita et al. proposed an autonomous locomotion control of the head's position based on Lyapnov function method [7]. In this method, winding motion is generated autonomously in real time and exact position control can be achieved. However, when the number of links is large, amplitude of winding motion tends to decrease, namely, tends to have a singular posture. Hence it is difficult to design a controller satisfying keeping good posture and tracking to a desired trajectory.

Our control objective in this paper is to achieve tracking to a desired trajectory avoiding singular postures without giving any gait beforehand. Since the robot has no driving wheel, locomotability is largely depends on the posture. Thus we utilize a notion of manipulability to evaluate the locomotability. Manipulability is used for a manipulator to evaluate the movability of the end effector [10]. Generally, manipulability is yielded from the relation between the joint torques and the acceleration of the end effector. However, in the case of snake-like robot, such manipulability is not always associated with actual locomotability. When the number of links is large, zigzag winding shape is associated with high manipulability, whereas the actual locomotability is not so good because large amplitude of constraining forces on the wheels are required for locomotion. Then we consider another manipulability for snake-like robot taking the side force on the wheels into consideration. We propose a simple controller capable of trajectory tracking and avoiding singular posture using this manipulability. Simulation results show that the robot spontaneously generates a suitable gait avoiding singular posture.

2. Model of a Snake-Like Robot

In this research, we use an n-link model as a model of snake-like robot [7] (Fig. 1). Each link has a passive wheel which does not sideslip at the middle. Mass, length, moment of inertia of each link are m, l, and J, respectively, and the center of gravity is placed at the

middle of the link; (x_F, y_F) and (x_i, y_i) denote position of the head and position of the i-th link respectively; θ_i is orientation of the i-th link and ϕ_i is relative angle of the $i-1$-th joint; D_{xy} and D_θ are coefficients of the friction of the translational and rotational motion, respectively, of the bottom of each wheel; D_ϕ is the coefficient of the friction in each joint.

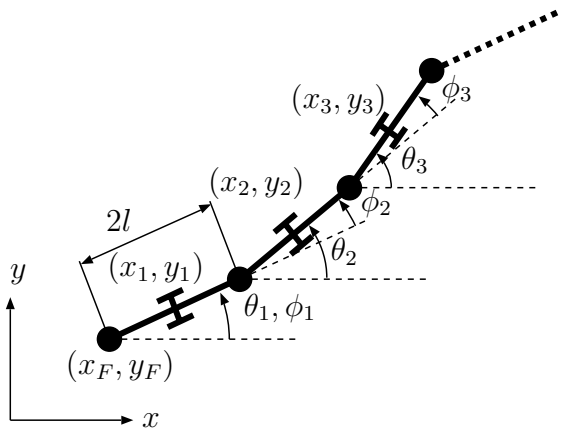

Figure 1: n-link model

2.1. Equation of Motion

Since derivation of equation of motion has previously been shown in the reference [7] in detail, only essential equations are shown. We first ignore the constraint of wheels. Then the equation of motion is similar to that of an n-link manipulator with the exception that no joint nor link is fixed on a base as

$$M(\boldsymbol{\theta})\ddot{\boldsymbol{q}} + C(\dot{\boldsymbol{\theta}}, \boldsymbol{\theta})\dot{\boldsymbol{\theta}} + D(\boldsymbol{\theta})\dot{\boldsymbol{q}} = \begin{bmatrix} E\boldsymbol{\tau} \\ 0 \end{bmatrix}, \qquad (1)$$

where $\boldsymbol{\theta} = [\theta_1, \cdots, \theta_n]^T \in R^n$, $\boldsymbol{\tau} \in R^{n-1}$ are joint torques, $\boldsymbol{q} = [\theta_1, \cdots, \theta_n, x_F, y_F]^T \in R^{n+2}$ are generalized coordinates, $M \in R^{n+2\times n+2}$ is an inertia matrix, $C \in R^{n+2\times n}$ is a centrifugal coefficient matrix, and $D \in R^{n+2\times n+2}$ is a frictional coefficient matrix. $E \in R^{n\times n-1}$ satisfies $\boldsymbol{\theta} = E\boldsymbol{\phi}$. Constraint of wheels is expressed as

$$A_\theta \dot{\boldsymbol{\theta}} = B_\theta \dot{\boldsymbol{r}} \qquad (2)$$

$$A_\theta = \begin{bmatrix} -l & 0 & \cdots & 0 \\ -2l\cos(\theta_2 - \theta_1) & -l & \cdots & 0 \\ \vdots & & \ddots & \vdots \\ -2l\cos(\theta_n - \theta_1) & \cdots & \cdots & -l \end{bmatrix} \in R^{n\times n}$$

$$B_\theta = \begin{bmatrix} -\sin\theta_1 & \cos\theta_1 \\ \vdots & \vdots \\ -\sin\theta_n & \cos\theta_n \end{bmatrix} \in R^{n\times 2},$$

and this equation yields Pfaffian non-holonomic constraint as

$$\begin{bmatrix} I_n & -F(\boldsymbol{\theta}) \end{bmatrix} \begin{bmatrix} \dot{\boldsymbol{\theta}} \\ \dot{\boldsymbol{r}} \end{bmatrix} = A(\boldsymbol{q})\dot{\boldsymbol{q}} = 0 \qquad (3)$$

where $\boldsymbol{r} = [x_F, y_F]^T$ is the position of the head and $F = -A_\theta B_\theta$ is a function of $\boldsymbol{\theta}$. The equation of motion under such constraint[6] can be described by adding a term of constraining force $A(\boldsymbol{q})^T\boldsymbol{\lambda}$ to (1) as

$$M\ddot{\boldsymbol{q}} + C\dot{\boldsymbol{\theta}} + D\dot{\boldsymbol{q}} + \begin{bmatrix} I_n \\ -F^T \end{bmatrix}\boldsymbol{\lambda} = \begin{bmatrix} E\boldsymbol{\tau} \\ 0 \end{bmatrix}, \qquad (4)$$

where $\boldsymbol{\lambda} \in R^n$ is the Lagrange's multiplier. By multiplying $\begin{bmatrix} F^T & I_n \end{bmatrix}$ from the left side of (4), we obtain the equation of the head's motion $\boldsymbol{r} = [x_F, y_F]^T$,

$$\tilde{M}\ddot{\boldsymbol{r}} + (\tilde{C} + \tilde{D})\dot{\boldsymbol{r}} = F^T E\boldsymbol{\tau} \qquad (5)$$

$$\begin{aligned} \tilde{M} &= [F^T\ I_2]M \begin{bmatrix} F \\ I_2 \end{bmatrix} \in R^{2\times 2} \\ \tilde{C} &= [F^T\ I_2]M \begin{bmatrix} F \\ 0 \end{bmatrix} + [F^T\ I_2]CF \in R^{2\times 2} \\ \tilde{D} &= [F^T\ I_2]D \begin{bmatrix} F \\ I_2 \end{bmatrix}. \end{aligned}$$

The whole motion of the robot is represented in this equation. (5) is a basic equation to discuss manipulability of the snake-like robot.

3. Dynamic Manipulability

In this section, we first show a brief summary of dynamic manipulability used for a manipulator, and then apply it to the snake-like robot. Motion of n-d.o.f manipulator, generally, is given by

$$M(\boldsymbol{\psi})\ddot{\boldsymbol{\psi}} + h(\dot{\boldsymbol{\psi}}, \boldsymbol{\psi}) + g(\boldsymbol{\psi}) = \boldsymbol{\tau}, \qquad (6)$$

where $\boldsymbol{\psi} \in R^n$ and $\boldsymbol{\tau} \in R^n$ denote joint angles, joint torques as control inputs, respectively. $M \in R^{n\times n}$ is the moment of inertia which is always nonsingular,

$h \in R^n$ and $g \in R^n$ is inertial force and gravity, respectively. Kinematic constraint due to the joints is expressed as

$$\dot{\boldsymbol{r}} = J(\boldsymbol{\psi})\dot{\boldsymbol{\psi}} \quad (7)$$

$$\ddot{\boldsymbol{r}} = J\ddot{\boldsymbol{\psi}} + \dot{J}\dot{\boldsymbol{\psi}}. \quad (8)$$

Elimination of $\ddot{\boldsymbol{\psi}}$ from (6) and (8), we have

$$\ddot{\boldsymbol{r}} = JM^{-1}[\boldsymbol{\tau} - h - g] + \dot{J}\dot{\boldsymbol{\psi}}. \quad (9)$$

Normalizing the input by

$$\boldsymbol{\tau} = N\boldsymbol{v} \quad (|v_i| \leq 1) \quad (10)$$

$$N = \mathrm{diag}(\tau_{i\max} - |h_i - g_i|), \quad (11)$$

we obtain

$$\ddot{\boldsymbol{r}} = JM^{-1}N\boldsymbol{v} + \dot{J}\dot{\boldsymbol{\theta}} \quad (12)$$

as a relation of normalized input $\boldsymbol{v}$ and the acceleration of the end effector $\ddot{\boldsymbol{r}}$. This implies that the maximum acceleration is characterized by an ellipsoid $JM^{-1}N\boldsymbol{v}$ ($\|\boldsymbol{v}\| \leq 1$) as long as $\dot{J}\dot{\boldsymbol{\psi}}$ is relatively small. This ellipsoid is called dynamic manipulability ellipsoid [10]. The larger and the more similar to a sphere the dynamic ellipsoid is, the higher the manipulability is. There have been proposed several measures of manipulability based on this dynamic manipulability ellipsoid as follows:

- the ratio of the length of the ellipsoid's minor axis to that of the major [2]
- the volume of the ellipsoid [10]
- the length of the ellipsoid's minor axis [1]

The choice of these measures varies according to what information of the dynamic ellipsoid is required.

Next, we will apply the notion of manipulability to the snake-like robot. The acceleration of the head caused by the input torques $\boldsymbol{\tau}$ is yielded from (5) as

$$\ddot{\boldsymbol{r}} = \tilde{M}F^T E\boldsymbol{\tau}. \quad (13)$$

The manipulability ellipsoid is characterized by singular values σ_1 and σ_2 of the matrix $\tilde{M}F^T E \in R^{2\times n-1}$. When the robot has a such shape that the acceleration of head is large with small input torques, the manipulability becomes high. However, zigzag winding shape is associated with high manipulability with this definition of manipulability. With large number of links, shape of high manipulability tends to be straight, namely, the singular posture. Under such posture, the side constraining force on each wheel against sideslip, which is necessary for locomotion, is required to be very large and non-slip assumption may be violated. Therefore, we consider another definition of manipulability taking the side constraining force into consideration.

3.1. Side Constraining Force on Wheels

The constraining force can be calculated from the Lagrange's multiplier $\boldsymbol{\lambda}$ in (4). First we consider coordinates u_i in direction perpendicular to i-th link. Virtual displacement of each link without constraint of wheels is expressed by

$$\delta\boldsymbol{u} = A_\theta\delta\boldsymbol{\theta} + B_\theta\delta\boldsymbol{r} \quad (14)$$

where $\delta\boldsymbol{u} = [\delta u_1, \cdots, \delta u_n]^T$, $\delta\boldsymbol{\theta}$, and $\delta\boldsymbol{r}$ are infinitesimal displacements along each u_i, θ_i, and $\boldsymbol{r}$, respectively. Let $\boldsymbol{f} = [f_1, \cdots, f_n]^T$ be the constraining forces along u_i axes respectively. Using principle of virtual work, we have

$$\boldsymbol{f} = (A_\theta^T)^{-1}\boldsymbol{\lambda}. \quad (15)$$

The Lagrange's multiplier $\boldsymbol{\lambda}$ can be calculated from (4) and (5). Thus we finally obtain

$$\boldsymbol{f} = Y(\boldsymbol{\theta}, \dot{\boldsymbol{r}}) + X(\boldsymbol{\theta})\boldsymbol{\tau}, \quad (16)$$

where

$$\begin{aligned} Y &= (A_\theta^T)^{-1}\left\{(M_{11}F + M_{12})\tilde{M}^{-1}[\tilde{C} + \tilde{D}]\right\} \\ &\quad -M_{11}\dot{F} - (C_1 + D_{11}F - D_{12})\dot{\boldsymbol{r}} \in R^n \\ X &= (A_\theta^T)^{-1}\left\{I_n - (M_{11}F + M_{12})\tilde{M}^{-1}F^T\right\}E \\ &\quad \in R^{n\times n-1}. \end{aligned}$$

This can be interpreted that $X\boldsymbol{\tau}$ is the side constraining forces cased by input torques $\boldsymbol{\tau}$ and Y is that cased by centrifugal force or frictional force.

3.2. Manipulability of a Snake-Like Robot

Ordinary dynamic manipulability becomes high when large acceleration of the head can be obtained with small input torques. On the contrary, in this paper, we consider another manipulability which becomes high when large acceleration of the head can be obtained with small side forces on wheels. From (16), side constraining force caused by input torques $\boldsymbol{\tau}$ is given by

$$X\boldsymbol{\tau} = \boldsymbol{f} - Y. \quad (17)$$

In order to limit the input torques lest each side force f_i exceeds the maximum $f_{i\max}$, we consider a normalized side force $\hat{\boldsymbol{f}}$ ($|\hat{f}_i| \leq 1$) and a matrix N such that

$$N = \mathrm{diag}[f_{i\max} - |Y_i|] \quad i = 1, \cdots, n \quad (18)$$

where Y_i is the i-th element of Y (Fig. 2). Notice that the dimension of the side force $\boldsymbol{f}$ is n whereas the

dimension of the input torques $\boldsymbol{\tau}$ is $n-1$, namely, the matrix X is not square. Hence limited input torque $\hat{\boldsymbol{\tau}}$ is expressed using X^+, pseudo inverse of X, as

$$\hat{\boldsymbol{\tau}} = X^+ N \hat{\boldsymbol{f}}. \tag{19}$$

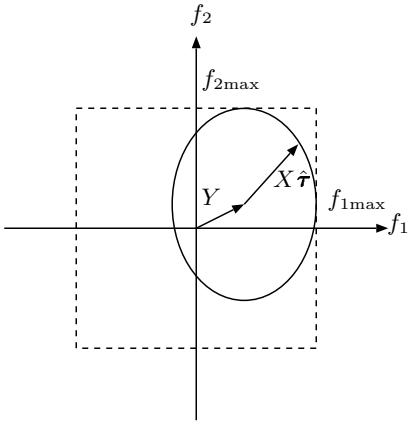

Figure 2: Normalization of side force

The acceleration of the head caused by $\hat{\boldsymbol{\tau}}$ is given by (13) as

$$\ddot{\boldsymbol{r}} = \tilde{M}^{-1} F^T E X^+ N \hat{\boldsymbol{f}}. \tag{20}$$

When the normalized side force $\hat{\boldsymbol{f}}$ is restricted in a unit sphere, the acceleration of the head $\ddot{\boldsymbol{r}}$ draws an ellipsoid $\tilde{M}^{-1} F^T E X^+ N \hat{\boldsymbol{f}}$ ($\|\hat{\boldsymbol{f}}\| \leq 1$). We regard this ellipsoid as the dynamic manipulability ellipsoid. The singular values σ_1 and σ_2 of the matrix $\tilde{M}^{-1} F^T E X^+ N$ characterize of the dynamic manipulability ellipsoid and smaller one σ_2 is taken as the measure of manipulability here.

Fig. 3-Fig. 6 show distributions of manipulability with sinusoidal oscillation of each joint angle ϕ_i as

$$\phi_i = a \sin\left(\omega t + \frac{2\pi T}{n}(i-1)\right) \tag{21}$$

where a, ω, and T is the amplitude of oscillation, the frequency, and period of undulation of the body shape. Such curve is known to be a serpenoid curve proposed by Hirose [3].

When the number of links is small, there are little differences between the ordinary manipulability and the proposed one (Fig. 3 and Fig. 4). In this case, both the manipulability becomes high around $T = 1$, where the body has winding shape of 1 period. On

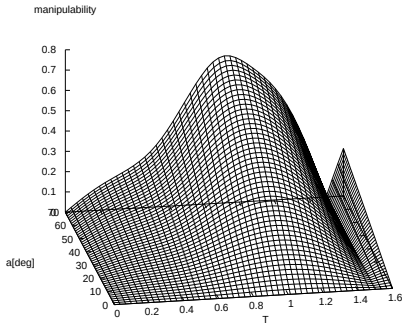

Figure 3: Distribution of ordinary manipulability (4-link)

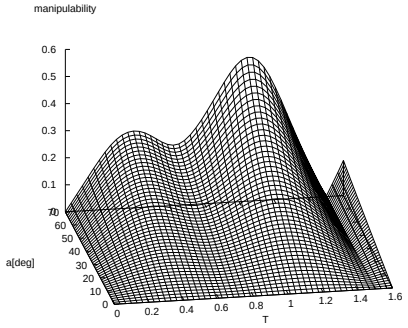

Figure 4: Distribution of proposed manipulability (4-link)

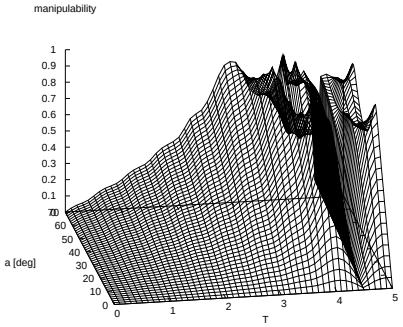

Figure 5: Distribution of ordinary manipulability (10-link)

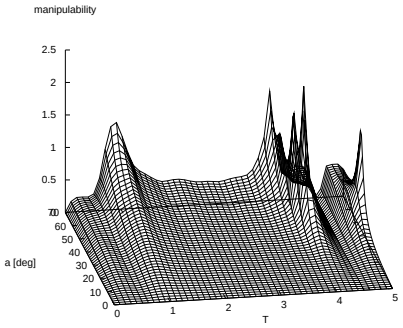

Figure 6: Distribution of ordinary manipulability (10-link)

the contrary, in the case of 10-link, i.e., larger number of links, the proposed manipulability becomes high around $T = 1$ while the ordinary manipulability is high with larger value T (Fig. 5 and Fig. 6). This implies that the proposed manipulability may have essential properties of winding motion of natural snakes.

4. Control of a Snake-Like Robot

The control objective is to achieve tracking to a line avoiding singular posture. Therefore, we propose a controller meeting the following demands.

1. The head of the robot follows a desired trajectory.
2. The posture of the robot should be kept with high manipulability.

Only the position of the head is controlled because the other dynamics is stable zero dynamics. Hence we set two acceleration vectors $\boldsymbol{\alpha}_t$ and $\boldsymbol{\alpha}_m$ of the head to satisfy the preceding requirements (Fig. 7). $\boldsymbol{\alpha}_t$ is an acceleration vector which make the current velocity of the head $\dot{\boldsymbol{r}}$ follow a desired trajectory as

$$\boldsymbol{\alpha}_t = k(\boldsymbol{v}_t - \dot{\boldsymbol{r}}) \tag{22}$$

where k is a constant and $\boldsymbol{v}_t$ ($\|\boldsymbol{v}_t\| = v$) is a desired velocity toward a desired trajectory. $\boldsymbol{\alpha}_m$ is an acceleration vector which improves the manipulability with constant norm. This vector is searched by a computing. Taking suitably weighed average of these two vectors, the desired acceleration of the head is determined as

$$\boldsymbol{\alpha}_{\rm next} = w_t\boldsymbol{\alpha}_t + w_m\boldsymbol{\alpha}_m \tag{23}$$

where w_t and w_m are design parameters.

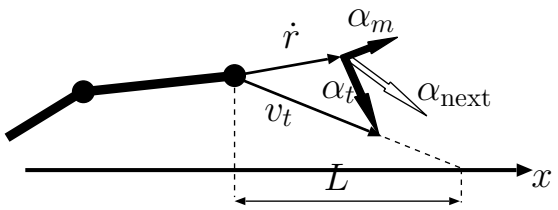

Figure 7: Two acceleration of the head

The input torques which realizes the desired acceleration can be computed from (5) as the inverse dynamics of the head motion as

$$\boldsymbol{\tau} = (F^T E)^+ \left[\tilde{M}\boldsymbol{\alpha}_{\rm next} + \tilde{C}\dot{\boldsymbol{r}} + \tilde{D}\dot{\boldsymbol{r}}\right] \tag{24}$$

where $(F^T E)^+$ is the pseudo inverse of $F^T E$.

Fig. 8-Fig. 10 show the simulation results of tracking control to a desired line, x-axis, toward the positive direction. The number of links is 10 and the desired trajectory is x axis. Parameters are given by

$$m = 0.68[\mathrm{kg}], l = 0.5[\mathrm{m}], J = 5.8 \times 10^{-3}[\mathrm{kgm}^2],$$
$$D_{xy} = 1.0 \times 10^{-3}[\mathrm{kg/s}], D_\phi = 0, v = 0.35[\mathrm{m/s}],$$
$$D_\theta = 8.4 \times 10^{-3}[\mathrm{kgm}^2/\mathrm{s}], f_{i\max} = 500[\mathrm{N}]$$

Design parameters are set as

$$k = 1,\ w_t = 1,\ w_m = 0.3\frac{\|\dot{\boldsymbol{r}}\|}{v}.$$

Fig. 8 and Fig. 9 show trace of the head and body shape at a certain moment. Fig. 8 is the result of tracking control based on the ordinary manipulability. Notice that The amplitude of winding motion is very small. (The vertical scale is magnified 5 times as large as the horizontal scale.) On the contrary, large winding motion can be observed in the results of the control based on the proposed manipulability (Fig. 9).

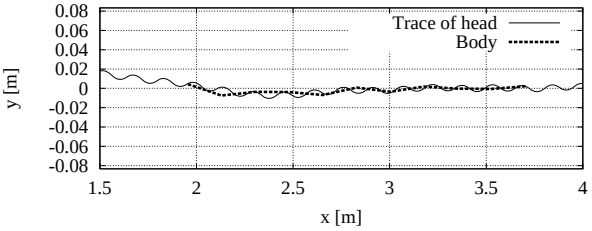

Figure 8: Trace of head; with ordinary manipulability

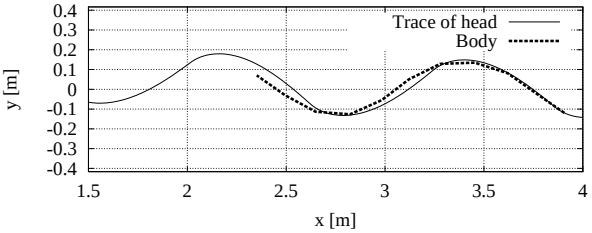

Figure 9: Trace of head; with proposed manipulability

Fig. 11 and Fig. 10 show time evolutions of Euclid norm of input torque $\|\boldsymbol{\tau}\|$ and that of side force $\|\boldsymbol{f}\|$. The norm of input torque is not so different between the ordinary manipulability and the proposed one (Fig. 10). However, the norm of side force in the case of the ordinary manipulability is much larger than that of the proposed manipulability (Fig. 11). From this, we can observe that large winding motion, which can be

seen in the locomotion of natural snakes, saves the side force of wheels.

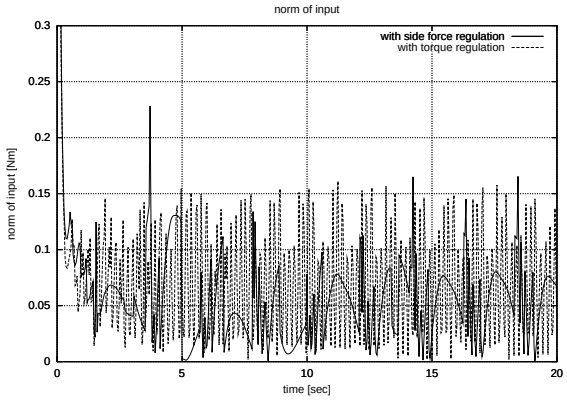

Figure 10: Norm of input

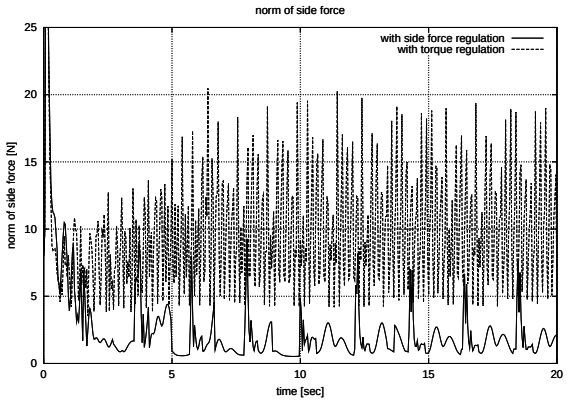

Figure 11: Norm of side force

5. Conclusion

In this paper, dynamic manipulability for a snake-like articulated robot was discussed. As a result, it turned out that such posture that saves the side constraining force on each wheel was associated with large winding shape independent of the number of links. We proposed a simple controller for an autonomous locomotion capable of tracking to a desired trajectory using the proposed manipulability.

Acknowledgement.

This work was supported in part by the Grant-in-Aid for COE Research No.09CE2004 of the Ministry of Education, Science, Sports and Culture, Japan.

References

[1] O. Khabit, 1985, “Dynamic optimazation in manipulator design: The operational space formulation,” presented at the ASME Winter Meeting.

[2] K. Kosuge and K. Furuta, 1985, “Kinematic and dynamic analysis of robot arm,” *Proc. IEEE Int. Conf. on Robotics and Automation*, pp. 1039–1044.

[3] S. Hirose, 1987, *Biomechanical Engineering*, Kougyou Tyousa Kai.

[4] S. Hirose and A. Morishima, 1990, “Design and Control of a Mobile Robot with an Articulated Body,” *The Int. Journal of Robotics Research*, Vol. 9, No. 2, pp. 99–114

[5] G. Migadis and J. Kyriakopoulos, 1997, “Design and forward kinematic analysis of a robotic snake,” *IEEE Int. Conf. on Robotics and Automation*, pp. 3493–3498.

[6] R.M. Murray, Z. Li, and S.S. Sastry, 1994, *A Mathematical Introduction to Robotic Manipulation*, CRC Press.

[7] P. Prautsch and T. Mita, 1999, “Control and Analysis of the Gait of Snake Robots,” *IEEE Int. Conf. on Conrol Applications*, pp.502–507.

[8] M. Sampei and K. Furuta, 1988, “Robot control in the neighborhood of singular points,” *IEEE Trans. on Robotics and Automation*, Vol. 4, No. 3, pp. 303–309.

[9] K. Sarrigeorgidis and K.J. Kyriakopoulos, 1998, “Stabilization and trajectory tracking of a robotic snake,” *IEEE Int. Conf. on Robotics and Automation*, pp. 2977–2981.

[10] T. Yoshikawa, 1983, “Analysis and control of manipulators with redundancy,” *Proceedings of the First Int. Symposium of Robotics Recearch*, pp. 735–747.

Proceedings of the International Symposium on
Adaptive Motion of Animals and Machines,
Montreal, Aug.8-12, 2000

Development and Running Control of a 3D Leg Robot

Takayuki IKEDA[1], Tetsuya TAMURA[1] and Tsutomu MITA[1]

[1]Department of Control and Systems Engineering
Tokyo Institute of Technology
2-12-1, Ohokayama, Meguro-ku, Tokyo 152-0033, Japan
ikeda@ctrl.titech.ac.jp

Abstract

In this research work, we will develop a 3D biped which simulates running motion of human. First, we will explain the mechanism of our 3D biped (Runbot 2). Next, we will show that the running motion pattern for the biped can be approximated by solutions of second or first order differential equations. Then we will derive a control strategy of the running biped which realizes these differential equations as motion pattern. Simulation results suggest that a biped having smooth running gait will be realized.

1. Introduction

In [1]-[3], we have developed three planar robots (Runbot-A, Runbot-B and Runbot-C) and succeeded to derive a control method such that they can run in the two dimensional space. In this paper, we will develop a control methodology of a biped which can run in the three-dimensional space by extending the mechanism and control of the previous results.

Static and dynamic walking have been realized using different and unique techniques by many researchers [4], [5], [6], [7], [8]. Several fundamental ideas toward realizing walking robots have been proposed in these research works. For example, the concept of ZMP and control technique based on the inverted pendulum were examined to obtain a control law which prevents turnover [4]. However, since the walking motion and running motion are really different from the viewpoint of speed and balancing, we think that a running motions are not obtained by direct applications of the results in these research works.

In particular, it is well known that Raibert and his group have created a running biped and quadruped using translated legs with spring action [9]. Although their results were very excellent, we think that it is not direct to switch the modes of the motions among walk, run and jump smoothly. To realize a walking robot moving supplely like living animals, we need to build running robots using articular joints. However, it is also difficult to extend and apply Raibert's results to running robots with articular joints since his result has been derived depending upon several ideal conditions of the mechanism, e.g, the leg motion does not affect the motion of the body.

The main reasons of the difficulties are considered to be the following: (1) The mechanism suitable for running has not been well investigated. This includes the actuation problem. (2) There is no effective control theory for the robot which can run. Raibert's results may restrict mechanisms as mentioned above.

In this paper, as a basic research work toward creating running biped composed of all articular joints, we will introduce our new running biped (Runbot 2) and propose a method which potentially control its running motion in 3D space. In order to simplify the control systems design, we assume that the three-dimensional movement of the biped can be decomposed into three motions in sagittal, lateral and horizontal planes. As the control strategy, the variable constraint control [1] is introduced. In this control, the motion patterns which the biped follows are described by differential equations. Several simulation results show that we can control Runbot 2.

2. Mechanism design and equation of motion

We will deal with a running biped depicted in Fig.1. Since direct analysis and design of the biped in 3D space is too complicated, we will introduce a coordination system shown in Fig.2 and assume that the running motion of the robot can be decomposed into three planar motions, i.e., motions in YOZ plane, XOZ plane and XOY plane which are known as the sagittal-plane, lateral-plane and horizontal-plane, respectively. In reality, each motion may interfere. In this research work, we will deal with such interference force as disturbances added to the control loops and we expect that they are controlled by our control strategy shown below.

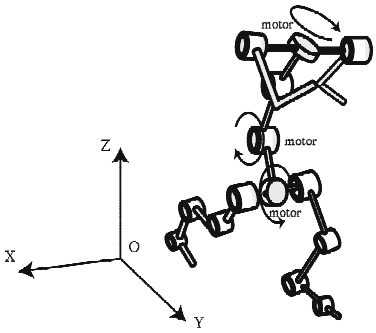

Figure 1: 3D biped robot

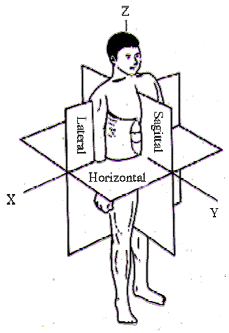

Figure 2: Axis and plains

2.1. Mechanism design of Runbot2

The three-dimensional biped Runbot2 (humanoid type) shown in Fig.1 was developed in our research lab this year. The configuration of the joints and actuators are shown in Fig.1. Fig. 3 shows the variables of the robot in the sagittal-plane; Fig. 4 and Fig.5 explain those in the lataral-plane and horizontal-plane, respectively. The overview of the designed Runbot2 is shown in Fig. 6.

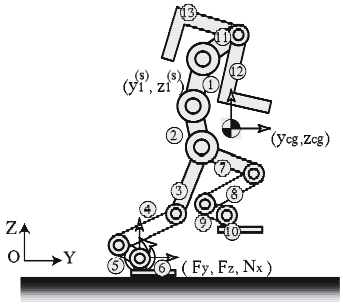

Figure 3: Sagital plane

The mechanism design has been done by taking the following assumptions and conditions into considerations.

[1] The motion in the sagittal-plane will be controlled by eight actuators of the both legs.

[2] The motion in the lateral-plane will be controlled by one waist actuator.

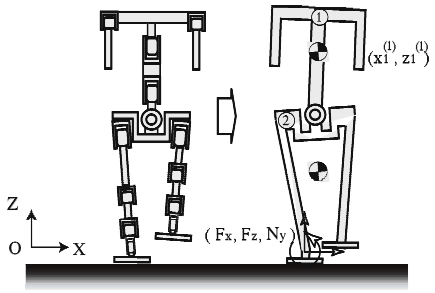

Figure 4: Lateral plane

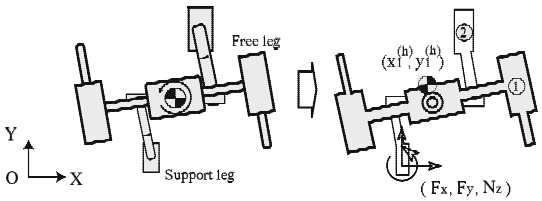

Figure 5: Horizontal plane

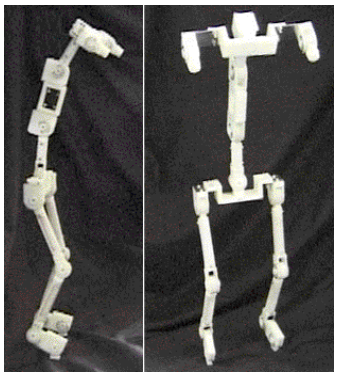

Figure 6: Runbot2 (humanoid type)

[3] The motion in the horizontal-plane will be controlled by one of the backbone actuator.

[4] The posture of the leg at the touchdown moment is selected to obtain the best manipulability.

[5] The foot toe will contact the surface.

[6] The shoulders are added as redundant DOF's.

The reason for the item [1] is that we will control the four fundamental characteristic variables shown below plus four joint angles of the swinging leg independently, just the same as the previous work [1]

Since we think that the motions in lateral and horizontal planes are not essential for the running, we have simply introduced the items [2] and [3].

In another previous work [3], we found that the concept of the manipulability of the leg posture at the touchdown moment is very important to reduce the magnitude of required force to keep running. This is the reason for the item [4]. Such a care is never taken for the mechanism introduced by Raibert.

The assumption in the item [5] makes the formulation of the motion and real control easier. Runbot2 has the force sensors at the foot toe to judge contact condition.

The shoulders in the item [6] are introduced for a future work. In the current research, the actuators of shoulders are not used.

2.2. The equation of motion of Runbot2

The motion in the saggital-plane will be described by 13 links and 12 joints as depicted in Fig. 3. The motion in the lateral-plane will be described by 2 link and 1 joint as depicted in Fig. 4. The motion in the horizontal-plane will be described by 2 link and 1 joint as depicted in Fig. 5.

Supposing that the robot does not jump long and its attitude can be recovered during the touchdown period, we only deal with the touchdown phase which starts from the landing of the toe and ends up with its lift-off. In this interval, the toe is assumed to be fixed, and the tip of foot and the absolute angle of the foot are kept zero. This leads to the following equation of motion [10], [11]:

$$M(q)\ddot{q} + h(q,\dot{q}) = \phi_q^T(q)\lambda + f_q^T(q)u \qquad (1)$$

$$\ddot{\phi}(q) + C\dot{\phi}(q) + K\phi(q) = 0 \qquad (2)$$

where $q(t) \in R^n$ is the generalized coordinates; $u(t) \in R^m$ is the control torques; $M(q)$ is inertia matrix; $h(q,\dot{q})$ is the gravity, centrifugal force and Coriolis force terms; $\phi(q) \in R^3$ is the position of the toe and the absolute angle of the foot; $\lambda(t) \in R^3$ is the force required to maintain the contact $\phi(q) = 0$ and is expressed in term of the Lagrange multiplier; $\phi_q = \frac{\partial \phi}{\partial q}$ gives the direction of the constraint force; $f_q = \frac{\partial f}{\partial q}$ is the Jacobian matrix which converts the direction of the input.

If we assume that $C > 0, K > 0$, $\phi(q_0) = 0$, $\dot{\phi}(q_0) = 0$, the constraint $\phi(q) = 0$ be expressed by (2).

The matrix and vector in the equation (1) and (2Åj are composed of the following matrix and vector, respectively.

$$q := \begin{bmatrix} u^{(s)} \\ q^{(\ell)} \\ q^{(h)} \end{bmatrix} \ , \ u := \begin{bmatrix} q^{(s)} \\ u^{(\ell)} \\ u^{(h)} \end{bmatrix} \ , \ ,\lambda := \begin{bmatrix} \lambda^{(s)} \\ \lambda^{(\ell)} \\ \lambda^{(h)} \end{bmatrix}$$

$$h := \begin{bmatrix} h^{(s)} \\ h^{(\ell)} \\ h^{(h)} \end{bmatrix} \ , \ f := \begin{bmatrix} f^{(s)} \\ f^{(\ell)} \\ f^{(h)} \end{bmatrix} \ , \ ,\phi := \begin{bmatrix} \phi^{(s)} \\ \phi^{(\ell)} \\ \phi^{(h)} \end{bmatrix}$$

$$M := diag([M^{(s)}, M^{(\ell)}, M^{(h)}]) \ ,$$
$$C := diag([C^{(s)}, C^{(\ell)}, C^{(h)}]) \ ,$$
$$K := diag([K^{(s)}, K^{(\ell)}, K^{(h)}])$$

where, index(s) and (ℓ), (h) mean the sagittal-plane, lateral-plane and horizontal-plane, respectively.

3. Control of the motion pattern via VCC

We will derive the control law which gives desired motion pattern to the motion of the biped described by (1) and (2). We assume that the required motion pattern of the robot is expressed by the following differential equation.

$$\ddot{\zeta}(t) = \eta(\zeta(t), \dot{\zeta}(t)) \qquad (3)$$

where $\zeta(t) \in R^k$ is called characteristic variables which express the motion of the robot. We will show the method to generate $\zeta(t)$ in the next section.

We can confirm that $\dot{\zeta}(t)$ is expressed by a function of the generalized velocity $\dot{q}$ as

$$\dot{\zeta} = g_q(q)\dot{q}, \qquad (4)$$

and (3) can also be written as

$$g_q(q)\ddot{q} + \dot{g}_q(q)\dot{q} + C\{\dot{\zeta}(t) - \dot{\bar{\zeta}}(t)\} + K\{\zeta(t) - \bar{\zeta}(t)\} = 0, \qquad (5)$$

if we want to derive the acceleration term $\ddot{q}$ explicitly.

Then arranging (1), (2) and (5) yield

$$\begin{bmatrix} M(q) & -\phi_q^T & -f_q \\ -\phi_q & 0 & 0 \\ -g_q & 0 & 0 \end{bmatrix} \begin{bmatrix} \ddot{q} \\ \lambda \\ u \end{bmatrix} = \begin{bmatrix} -h(q,\dot{q}) \\ \dot{\phi}_q\dot{q} + C\dot{\phi}(q) + K\phi(q) \\ \dot{g}_q(q)\dot{q} + \eta(\zeta,\dot{\zeta}) \end{bmatrix} \qquad (6)$$

Solving (6) leads to

$$\begin{bmatrix} \lambda \\ u \end{bmatrix} = \left\{ \begin{bmatrix} \phi_q \\ g_q \end{bmatrix} M^{-1} \begin{bmatrix} \phi_q^T & f_q^T \end{bmatrix} \right\}^{-1}$$
$$\left\{ \begin{bmatrix} \phi_q \\ g_q \end{bmatrix} M^{-1} h + \begin{bmatrix} -\dot{\phi}_q \dot{q} - C\phi_q \dot{q} - K\phi \\ -\dot{g}_q \dot{q} - \eta(\zeta, \dot{\zeta}) \end{bmatrix} \right\} \quad (7)$$

The existence condition of the control is that the matrix inside $\{\ \}^{-1}$ in (7) is of full row rank which can be satisfied in the present case since the mechanism is full actuated. As long as the constraint force λ can be supplied from the floor, the response of the closed loop system exactly simulates (3) since (7) is the decoupling control by regarding ζ as the output to follow. We call have called this control strategy as the *variable constraint control (VCC)* in [1].

3.1. Running motion pattern

In this section, we will derive three running motion patterns for the three planar motions.

3.2. Running motion pattern in the sagittal-plane

At the touchdown phase, we must control the kicking and balancing motions of the robot in the sagittal-plane. In this research work, we have paid attention to the following four fundamental *characteristic variables*;

[C1] y_{cg} [C2] z_{cg} [C3] L_{cg_x} [C4] L_{a_x}

where (y_{cg},z_{cg}) is the position of CG of the whole robot; L_{cg_x} is the total angular momentum with respect to CG of the total robot; L_{a_x} is the total angular momentum with respect to the toe.

In order to verify these arguments and derive the time response of C1∼C4, we have analyzed [1] the running motion of human using the sequence photographs [14] as shown in Fig. 7, Fig. 8 and Fig. 9.

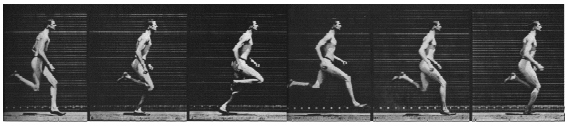

Figure 7: Consecutive photograph of human

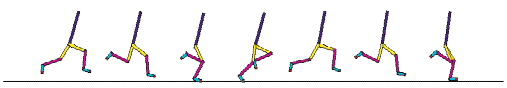

Figure 8: Motion of human

From this analysis, we have concluded that the motion of the CG of running human can be approximated

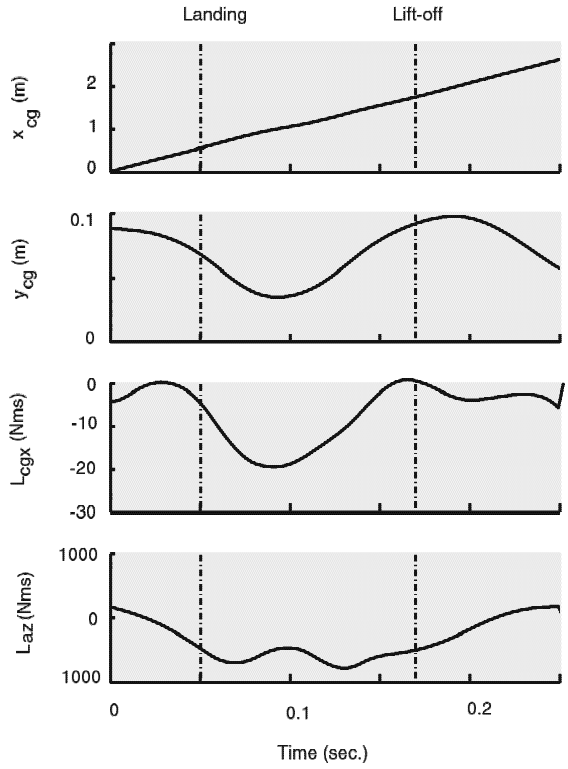

Figure 9: Center of gravity and Angular momentum

by a bouncing ball phenomenon. And the response of L_{cg_x} is described such that once becomes negative at the beginning of the touchdown and recovers to zero before the lift-off by regarding the first peak as an initial disturbance. The angular momentum L_{a_x} is just the same as L_{cg_x} except for the steady state. The steady state $\bar{L}_{a_x}$ of L_{a_x} is given by a nonzero value which means that the CG of the robot rotates after touchdown and the ZMP moves from the heel to the toe before the lift-off [1].

We modeled the motion pattern in the sagittal-plane as follows.

$$m\ddot{y}_{cg} + c_y\{\dot{y}_{cg} - \dot{\bar{y}}_{cg}\} + k_y\{y_{cg} - \bar{y}_{cg}\} = 0 \quad (8)$$
$$m\ddot{z}_{cg} + c_z\{\dot{z}_{cg} - \dot{\bar{z}}_{cg}\} + k_z\{z_{cg} - \bar{z}_{cg}\} = 0 \quad (9)$$
$$\dot{L}_{cg_x} + c_{cg_x} L_{cg_x} = 0 \quad (10)$$
$$\dot{L}_{a_x} + c_{a_x}\{L_{a_x} - \bar{L}_{a_x}\} = 0 \quad (11)$$

where $\bar{y}_{cg}(t) = \bar{v}t + y_{cg_-}$, $\bar{z}_{cg}(t) = z_{cg_-}$; (y_{cg_-}, z_{cg_-}) is the position of CG at the starting time t_- of the touchdown phase; $\bar{v}$ is the average speed of the velocity during the touchdown; k_y and k_z are spring coefficients; $c_{cg_x} > 0$ and $c_{a_x} > 0$ are damping coefficients.

We will control the posture of the swinging leg by regarding its four joint angles as additional characteristic variables of four dimensional, that is:

[C5-C8] $\hat{\theta} = [\theta_7, \theta_8, \theta_9, \theta_{10}]$

The posture is chosen to have the best manipulability in the next touchdown moment and is simply represented by

$$\bar{\theta} = [\bar{\theta}_7, \bar{\theta}_8, \bar{\theta}_9, \bar{\theta}_{10}] \quad (12)$$

Then, the motion pattern for the swinging leg is given by the following differential equation.

$$\ddot{\hat{\theta}} + C_{\hat{\theta}}\dot{\hat{\theta}} + K_{\hat{\theta}}\{\hat{\theta} - \bar{\theta}\} = 0 \ , \ C_{\hat{\theta}} > 0 \ , \ K_{\hat{\theta}} > 0 \quad (13)$$

We will control y_{cg}, z_{cg}, L_{cg_x}, L_{a_x} and $\theta_7 - \theta_{10}$ by eight actuators of both legs.

3.3. Running motion pattern in the lateral-plane

We will control the balance in the lateral-plane to keep the center of gravity to the toe center x_a. Then, the characteristic variable in the lateral-plane is defined as follows.

[C9] The center of gravity position x_{cg}

When we approximate the motion pattern of x_{cg} as that $x_{cg}(t) \to x_a$, it can be described as

$$\ddot{x}_{cg}(t) + c_x\dot{x}_{cg}(t) + k_x\{x_{cg}(t) - x_a\} = 0, \quad (14)$$

where $c_x > 0$ and $k_x > 0$.

3.4. Running motion pattern in the horizontal-plane

We think that the balance in the horizontal-plane is just like the above. In this case, the characteristic variable is chosen as

[C10] The horizontal angular momentum around the CG, L_{cg_z}

And the motion pattern is given by the differential equation

$$\ddot{L}_{cg_z}(t) + c_{cg_z}L_{cg_z}(t) = 0, \quad (15)$$

where $c_{cg_z} > 0$ is chosen to simulate the decay rate.

3.5. Total running motion pattern

Equation(8), (9), (10), (11), (13), (14) and (15) yield

$$\ddot{\zeta}(t) + \tilde{C}\{\dot{\zeta}(t) - \dot{\bar{\zeta}}(t)\} + \tilde{K}\{\zeta(t) - \bar{\zeta}(t)\} = 0, \quad (16)$$

when we define

$$\zeta(t) = [x_{cg}(t), y_{cg}(t), z_{cg}(t), \int_0^t L_{cg_x}(\tau)d\tau, \int_0^t L_{cg_z}(\tau)d\tau, \int_0^t L_{a_x}(\tau)d\tau, \hat{\theta}]^T. \quad (17)$$

Then substituting the derived ζ into (3) yields the variable constraint control for the running biped.

3.6. Simulation results

When an initial velocity is given to the robot, it can run several steps. The responses of the characteristic variables concerned with sagittal and lateral, horizontal plane are shown in 10, Fig. 11 and Fig. 12. These results show that a biped robot may be produced which has smooth running gaits. Stick diagram of the motion of the robot is shown in Fig. 13, Fig. 14 and Fig. 15.

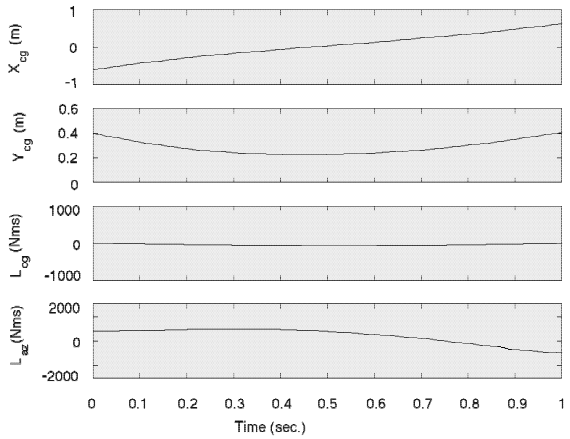

Figure 10: Simulation result (Sagittal Plane)

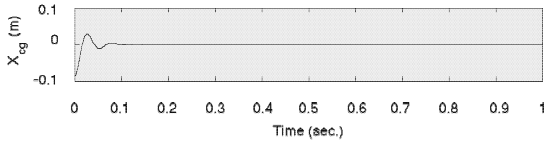

Figure 11: Simulation result (Lateral Plane)

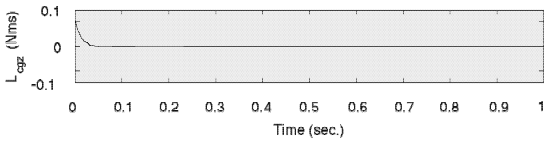

Figure 12: Simulation result (Horizontal Plane)

4. Conclusions

We have explained the mechanism of our 3D biped, Runbo2. We also have derived the running motion pattern for the biped and proposed a control strategy which can realize the running motion pattern. Simulation results suggest that a biped potentially can be produced which has smooth running gaits. We are now installing the experimental system and expect the positive results. Future research work includes realizing

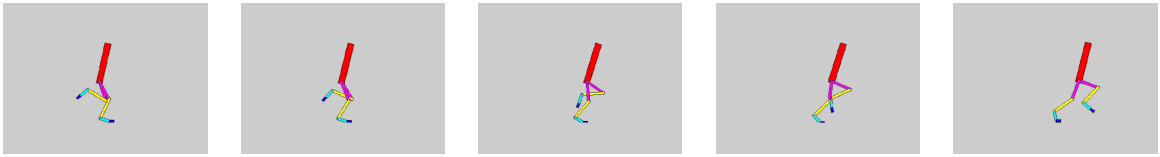

(a) t = 0.0 (sec.) (b) t = 0.2 (sec.) (c) t = 0.4 (sec.) (d) t = 0.6 (sec.) (e) t = 0.8 (sec.)

Figure 13: Stick diagram (Sagittal Plane)

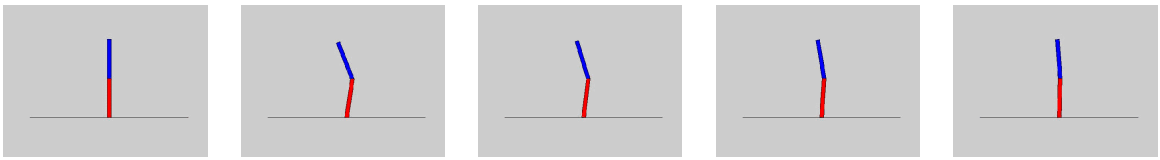

(a) t = 0.0 (sec.) (b) t = 0.2 (sec.) (c) t = 0.4 (sec.) (d) t = 0.6 (sec.) (e) t = 0.8 (sec.)

Figure 14: Stick diagram (Lateral Plane)

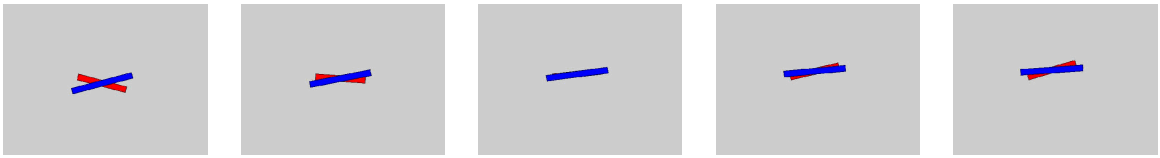

(a) t = 0.0 (sec.) (b) t = 0.2 (sec.) (c) t = 0.4 (sec.) (d) t = 0.6 (sec.) (e) t = 0.8 (sec.)

Figure 15: Stick diagram (Horizontal Plane)

quadruped robots in the three-dimensional space using the proposed control strategy.

5. Acknowledgement

This research work is carried out using the COE grant (COE: Super Mechano-Systems) supported by the Japanese Ministry of Education, Science, Culture and Sports.

References

[1] T. Ikeda, Y. Iwatani, K. Suse, T.Mita : Analysis and Design of Running Robots in Touchdown Phase, Proc. of CCA99, pp. 496-501 (1999)

[2] T. Mita, T. Ikeda, K. Suse, Y. Iwatani: Design of a quadruped robot which can run and jump –Basic analysis and control systems design–, IEEE Hong Kong Sympo. on Robotics and Control, July 2nd, pp. 393-398 1999.

[3] T. Ikeda, T. Mita: Posture Design of Running Robot based on Dynamic Manipulability, The 22th SICE Symposium on Dynamical System Theory (in Japanese), (1999)

[4] J. Yamaguchi, A. Takanishi, and I. Kato: ”Development of a Biped Walking Robot Compensating for Three-Axis Moment by trunk Motion,” Proceedings of the 1993 IEEE/RSJ Int. Conf. on Intelligent Robots and System pp. 561-566 (1993)

[5] Honda: http://www.honda.co.jp/english /technology/robot/index.html

[6] J. Furusho, M. Masubuchi : ”Control of a D ynamical Biped Locomotion System for Steady Walking,” Trans. ASME, J.of Dyn. Sys. Mes.and Control, vol. 108, no. 2, pp. 111-118 (1986)

[7] S. Kajita, K. Tani : ”Experimental Study of Bipe d Dynamics Walking,” IEEE Control Systems, vol. 16, no. 1, pp. 13-19 (1996)

[8] H. Kimura et al. ,Dynamic walking and running of the quadruped using neural oscillator, Proc. of IEEE &RSJ IROS98, pp.50-57, 1998.

[9] M. H. Raibert:” Legged Robots That Balance,” MIT Press, Cambridge, Massachusetts (1985)

[10] E. J. Haug: Computer-Aided Kinematics and Dynamics of Mechanical Systems. vol. 1, Basic Methods, Allyn and Bacon (1989)

[11] A. A. Shabana: Dynamics of Multibody Systems. Cambridge Univ. Pr. (1998)

[12] R. Margaria: Biomechanics and Energetics of Muscular Exercise. Oxford University Press (1976)

[13] M. Vukobratovic, B. Borovac, D. Surla, D. Stokic: Biped Locomotion - Dynamics, Stability, Control and Application - . Springer-Verlag (1990)

[14] E. Muybridge: Animals in motion. Dover (1957)

Proceedings of the International Symposium on
Adaptive Motion of Animals and Machines,
Montreal, Aug.8-12, 2000

Jumping Cat Robot with kicking a Wall

Masaki Yamakita[1] **Yasuhito Omagari** [1] **and Yasuaki Taniguchi**[1]

[1]Dept. of Control and Systems Engineering, Tokyo Institute of Technology
2-12-1 Oh-okayama Meguro-ku, Tokyo 152 Japan,
yamakita@ctrl.titech.ac.jp

Abstract

In this paper we study a robotic system moving in a vertical direction mimicking a cat's behavior as a cat kicks a wall to jump up to a roof, which may be an efficient mechanism for vertical movement and the robot system can be considered as one of the prototypes for Super Mechano Systems (SMS). Concept, modeling, controller design, simulation and experimental results are discussed.

1. Introduction

Cats sometimes jump toward a wall and kick it to get to a higher-place like a roof (Fig.1), and can move in a vertical direction as a result, and the motion seems to be very skillful and efficient. Considering the movement from a viewpoint of constraints, a robotic system, which realizes the motion to change its configuration according to the position (on the ground, kicking with one leg, in the air, etc), can be considered as one of the prototypes for Super-Mechano Systems.

Our purpose in this paper is to analyze and construct a control law for a real machine mimicking the cat's motion. In the considered robotic system, the robotic motion is assumed to be constrained in the sagittal plane to make the problem simple.

In section 2, the dynamic equation of the system is derived, and in the following section a control method will be discussed. In section 4, we will show some simulation results. Finally we will show some experimental results and future work will be discussed.

2. Modeling

2.1. System structure

Even though a real cat twists its body after jumping to get to a higher place(the roof), we restrict the jumping-motion in the sagittal plane in this paper so that we can analyze and consider fundamental control problems.

In order to realize the motions, jumping from the ground to a wall and from the wall to the roof, we consider a 7-link robot as in Fig.2 The feature of the system can be summarized as follows.
The robot has

- 6 rotational actuators at it's joints,
- when the toe makes contact with the floor or the wall, it is assumed that there is no slip between the toe and the contact point along the surfaces.

Figure 1: Motion of the jumping cat

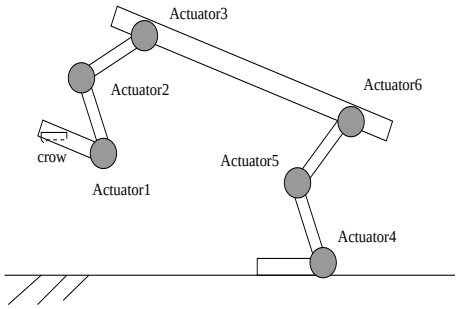

Figure 2: Robotic system

2.2. Modeling

The whole system is divided into two 4-link serial links at point X(Fig 3) virtually, and a holonomic body constraint $C_b(q) = 0$ to keep the body as one straight link is introduced.

As generalized coordinate systems, we use

$$q_F^T = [x_F, y_F, \theta_{F_1}, \theta_{F_2}, \theta_{F_3}, \theta_{F_4}], \quad (1)$$
$$q_R^T = [x_R, y_R, \theta_{R_1}, \theta_{R_2}, \theta_{R_3}, \theta_{R_4}], \quad (2)$$
$$q^T = [q_F^T, q_R^T]. \quad (3)$$

Though these coordinate systems are redundant and the system description becomes complex, the advantages are as follows:

- A 4-link dynamic equation is simpler than a 7-link one and we can use the same equation for each link,
- this coordinate system is very useful for judging the timing of switching the constraint on the toe, which will be mentioned later.

For the following discussion, Jacobian of the body constraint is defined as follows:

$$\frac{d}{dt}C_b(q) = J_b(q)\dot{q} = 0, \quad J_b(q) = \frac{\partial C_b(q)}{\partial q}. \quad (4)$$

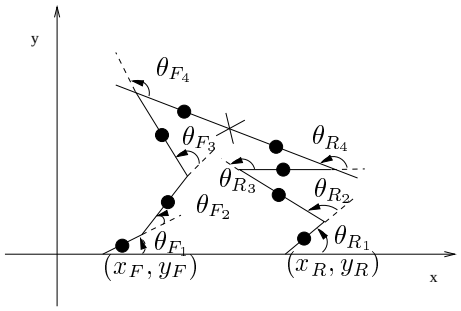

Figure 3: Robotic system and coordination

2.3. Variable constraints

We assume that enough constraint force is exerted when the toe makes contact with the ground or wall, and holonomic constraints $C_v(q, mode) = 0$ are introduced according to the state of the system, where mode is an index that indicates the state of the toe's contact.

For example, when only the hind toe is constrained to the floor or wall, $C_v(q, mode)$ becomes

$$C_v(q, mode) = \begin{bmatrix} x_R - X_R const \\ y_R - Y_R const \end{bmatrix}, \quad (5)$$

and we can calculate the Jacobian,as

$$\frac{d}{dt}C_v(q) = J_v(q)\dot{q} = 0, \quad J_v(q) = \frac{\partial C_v(q)}{\partial q}. \quad (6)$$

The problem here is how we can judge the mode. The answer lies in the understanding of the constraint force λ_v (Fig 4). In the case of toe being on the ground, λ_x is a horizontal constraint force and λ_y is vertical one, and if the λ_y is equal to zero and the acceleration upward is positive, the constraint should vanish($\lambda = 0$) and toe can move upward. When the toe is on the wall, switching timing depends on the λ_x vise versa.

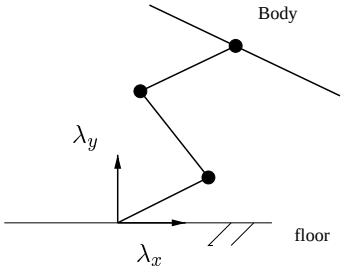

Figure 4: Constraint force

2.4. Dynamic equation

The dynamic equation for the system with the redundant coordinate systems is considered in this section. Ignoring the constraint, two 4-link manipulator's dynamic equations are described as

$$M(q)\ddot{q} + C(\dot{q}, q)\dot{q} + G(q) = \tau, \quad (7)$$

where

$$M = \begin{bmatrix} M_F & 0 \\ 0 & M_R \end{bmatrix}, \; C = \begin{bmatrix} C_F & 0 \\ 0 & C_R \end{bmatrix},$$
$$G = \begin{bmatrix} G_F \\ G_R \end{bmatrix}, \tau = \begin{bmatrix} \tau_F \\ \tau_R \end{bmatrix}.$$

In order to change position constraint to acceleration constraint, we differentiate (4) and (6), and in order to keep the constraint, constraint forces, $J_b^T\lambda_b$, and $J_v^T\lambda_v$ are introduced, and following simultaneous equations are used to express the system including all constraints:

$$M(q)\ddot{q} + C(\dot{q}, q)\dot{q} + G(q) = \tau - J_b^T\lambda_b - J_v^T\lambda_v, \quad (8)$$

$$J_b\ddot{q} = -\dot{J}_b\dot{q}, \quad (9)$$

$$J_v\ddot{q} = -\dot{J}_v\dot{q}. \quad (10)$$

From these equations, accelerating vector $\ddot{q}$, and constraint forces λ_b and λ_v can be calculated. Therefore, constraint force and acceleration can be used for judging the change of the mode.

Collision with the wall or other things is assumed to be perfectly inelastic, and the state will shift to that of the under constraint just after the collision which is modeled as effects of impulse forces.

3. Controller Design

Since the initial configuration is very important for the robot's jumping motion, it is determined by *stochastic dynamic manipulability measure*. For dynamic control of the robot's jump, we pay attention to the motion of the center of mass mainly, and the proposed method is derived as if the center of the gravity is moved by a spring connected to a virtual wall.

3.1. Stochastic dynamic manipulability measure

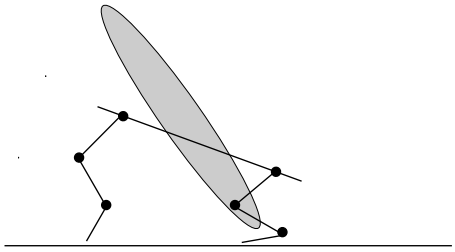

Figure 5: Realizable acceleration for the center of mass

There exists a lot of possible postures of the 7-link robot before the jump, and it is not easy to determine what kind of pose is suitable for the jump. Therefore, we use a measure to decide the position for jumping, i.e., *stochastic dynamic manipulability measure*, which evaluates an expected required torque to realize the desired acceleration.

Sub-optimal configuration for the jump from the ground and from the wall based on the stochastic dynamic manipulability measure can be determined by a numerical optimization.

In another words, at first we determine the pose which easily achieves the desired acceleration and angular acceleration, and the robot is set to the posture before the jump.

Let's assume that, (x_g, y_g) and θ_b indicate the coordinates of the center of mass, and angle of the body, respectively. By eliminating the constraint force λ from the system dynamics, we have

$$\tau_a = M_a\ddot{q} + C_a\dot{q} + G_a, \tag{11}$$

where

$$\dot{x_c} = J_q\dot{q}, \qquad x_c = \begin{bmatrix} x_g & y_g & \theta_b \end{bmatrix}^T, \tag{12}$$

and

$$\begin{aligned} M_a &\equiv M, \\ C_a &\equiv YC + J_r^T X^{-1}\dot{J}_r, \\ G_a &\equiv YG, \\ \tau_a &\equiv Y\tau, \\ X &\equiv J_r M^{-1} J_r^T, \\ Y &\equiv I - J_r^T M^{-1} J_r M^{-1}. \end{aligned}$$

For this description of the system, stochastic dynamic manipulability measure is defined as

$$w_{sd} = \begin{cases} \sqrt{\frac{tr[W^T W]}{tr[W^T\{(J_q M^{-1})(J_q M\ -1)\}^{-1} W]}} \\ \qquad\qquad (\det[J_q J_q^T] \neq 0) \\ 0 \\ \qquad\qquad (\det[J_q J_q^T] = 0), \end{cases} \tag{13}$$

where

w_{sd}: Stochastic dynamic manipulability measure

W: Weight matrix indicates the direction to accelerate

J_q: Jacobian matrix.

To determine the sub-optimal configuration with respect to the measure under the constraints, w_{sd} is updated by the following iteration:

$$w_{sd}(i+1) = w_{sd}(i) + \left(\frac{\partial w_{sd}(i)}{\partial q}\right)^T \Delta q, \tag{14}$$

$$\Delta q = Dq\epsilon, \tag{15}$$

$$\epsilon = \{(\frac{\partial w_{sd}(i)}{\partial q})^T Dq\}^T \cdot k, \tag{16}$$

where Dq is basis of $Ker(J_q)$. If we use the iteration and k is a semi-positive constant, W_{sd} is increased as

$$w_{sd}(i+1) = w_{sd}(i) + \|(\frac{\partial w_{sd}(i)}{\partial q})^T Dq\|^2 k \geq w_{sd}(i). \tag{17}$$

3.2. Jumping control

Only jumping with both legs or with only the hind leg is mentioned here. When the cat is in the air, we just adopt feedback control so that the posture of the legs converges to a desired one determined beforehand by the above method, which is ready for the next jump.

In order to derive a proposed control algorithm, we re-describe the system, and we pay attention to the center of mass and the body's angle. Using a coordinate change from q to $x_c = [x_g, y_g, \theta_b]$, the system can be expressed as

$$\ddot{x}_c = A(q,\dot{q})\tau + B(q,\dot{q}), \quad \tau = [\tau_F^T, \tau_R^T]^T, \tag{18}$$

where

$$A \equiv J_q M_a^{-1} Y,$$
$$B \equiv J_q M_a^{-1}(C_a + G_a) - \dot{J}_q \dot{q},$$
$$Y \equiv I - J_r^T M^{-1} J_r M^{-1},$$

and J_q is the tangential map of the coordinate transformation. For the system representation, $\ddot{x}_c$ is determined so that the motion of the mass center follows a simple mass-spring model.

3.2.1. *Jumping with both legs*

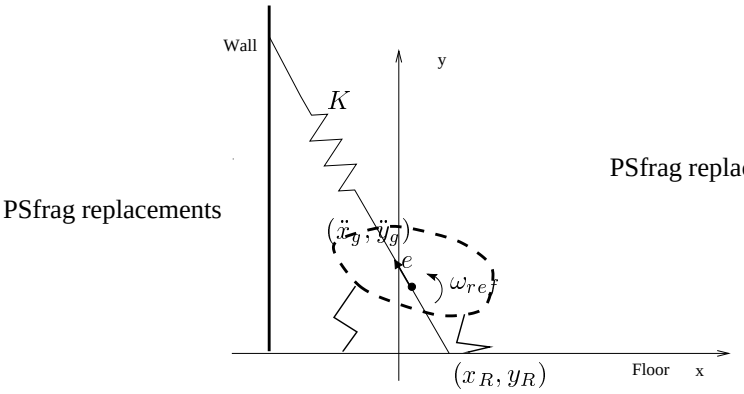

PSfrag replacements

PSfrag replacements

Figure 6: Model matching 1

ω_{ref}: Desired angular acceleration
θ_{ref}: Desired angle
e : Normal unit directional vector
K : Coefficient of the virtual spring
l : Length of the virtual spring
M : Mass of the virtual body

The desired acceleration of the body $\ddot{x}_{ref1} \in R^2$ is, as shown in Fig.6, determined so that the virtual mass concentrated to the mass center moves as if it is pulled by a strong spring stuck to the wall, and a desired angular acceleration of body $\ddot{x}_{ref2} \in R$ is designed to rotate in the desired direction as

$$\ddot{x}_{ref} = \begin{bmatrix} \ddot{x}_{ref1} \\ \ddot{x}_{ref2} \end{bmatrix} \quad (19)$$
$$= \begin{bmatrix} \frac{lK}{M} e \\ 0 \end{bmatrix} + \begin{bmatrix} \mathbf{0} \\ \dot{\omega}_{ref} - K_\theta(\dot{\theta}_b - \omega_{ref}) \end{bmatrix}, \quad (20)$$

where e is a unit vector toward the desired direction for jumping, and v is a vector from the center of mass to the wall along to the line from the toe to the center of mass, and $l =< e, v >$ indicates the spring's length. K_θ is an appropriate feedback gain.

Because of the redundant system, τ is selected to minimize the following criterion function as:

$$J_1 := \|W_c(A\tau - B - \ddot{x}_{ref})\|^2 + \frac{1}{2}\tau^T W_\tau \tau, \quad (21)$$

where

$$W_c = \begin{bmatrix} \alpha & 0 & 0 \\ 0 & \alpha & 0 \\ 0 & 0 & \beta \end{bmatrix}, \quad (22)$$

and α, β are positive constants, and W_τ is an appropriate positive weight matrix.

3.2.2. *Jumping only with the hind leg*

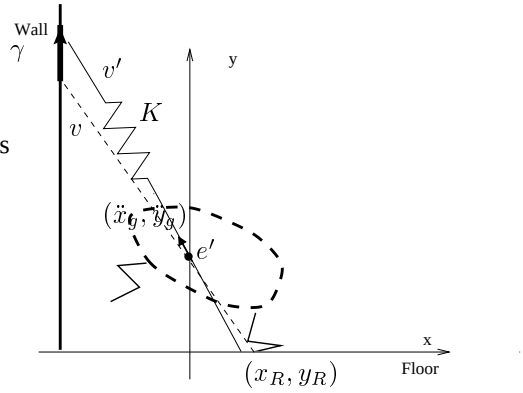

PSfrag replacements

Figure 7: Model matching 2

v : Normal directional vector of the spring
v' : Modified unit vector for desired direction
γ : Modifying ratio of the direction
e' : Normal unit directional vector
K : Coefficient of the virtual spring
l : Length of the virtual spring
M : Mass of the virtual body

After the motion with the two legs, the front leg will naturally lift. In order to control the center of mass, only the hind leg's actuators are mainly used, and as it is difficult to control all of the three degree of freedom,the spring-mass model is modified to control the body angle indirectly First, v is determined as a directional vector by connecting the toe and the center of mass, then, it is adjusted to a directional vector v' due to the sign of the error of the angular velocity by γ as follows:

$$v' = v - [0, \gamma sgn(\omega_{ref} - \dot{\theta}_b)]^T \quad (23)$$

and, desired acceleration x_{ref} is determined by

$$\ddot{x}_{ref1} = \begin{bmatrix} \frac{lK}{M} e' \\ 0 \end{bmatrix}, \quad (24)$$

$$l :=< v, e' >, \quad e' := v'/\|v'\|,$$

and the weight W_a is also changed to

$$W_a = \begin{bmatrix} \alpha & 0 & 0 \\ 0 & \alpha & 0 \\ 0 & 0 & 0 \end{bmatrix}. \tag{25}$$

As in the previous method, τ_R is determined to minimize the following criterion function:

$$J_2 := \|W_a(A\tau - B - \ddot{x}_{ref})\|^2 + \frac{1}{2}\tau^T W_\tau \tau, \tag{26}$$

where τ_L is determined locally.

4. Simulation

In order to examine the validity of the proposed method, we conducted numerical simulations of the jump for a model of an experimental system. In the optimization and the simulations,it is assumed that the fore leg and hind sub-systems have the same parameters.

4.1. Pose optimization

We obtained a sub-optimal posture, using the stochastic dynamic manipulability measure from some of the initial poses by a gradient search. One of the results is shown in Fig.8 and Fig.9. By the procedure, the manipulability measure increased by about 20%, from $s_{sd} = 37.6$ to $s_{sd} = 43.5$.

4.2. Cat jumping with kicking a wall

In the simulation, we assumed that a wall is located at $x = -0.4$[m], and the roof at $y = 0.5$[m].

For the values of control parameters, we used $K = 700$[N/m], $\omega = -40[rad/s]$, and when the cat jumps from the floor to the wall, we set $\omega = -800[rad/s]$, from the wall to the roof. Since there is no systematic rule to determine the value of parameters, they are determined by trial and error.

As shown in Fig.10 the sequence of the jumping motion is shown. It is shown that the robotic cat jumped up to a roof at y=0.5[m] after kicking the wall with a rotation.

5. Experimental Results

In order to check the validity of the proposed method, we constructed an experimental system.

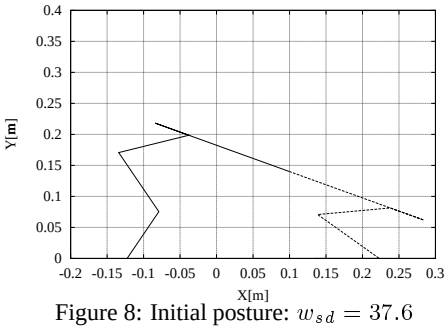

Figure 8: Initial posture: $w_{sd} = 37.6$

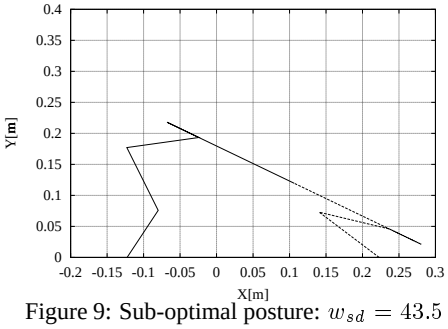

Figure 9: Sub-optimal posture: $w_{sd} = 43.5$

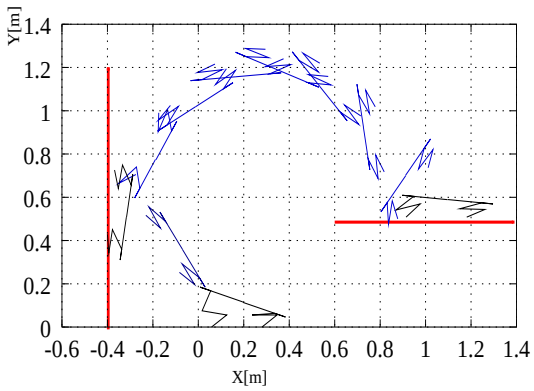

Figure 10: Simulation result: Jump kicking the wall

5.1. System configuration

We designed a 7-link robotic cat shown in Fig.11. The system configuration of the whole system is given in Fig.12. The following describes the details of the robotic system.

Since motors are too heavy to be installed in the robot, power of the actuators is supplied from outside by wires (Fig.13), and the weight of the wires is compensated for by a counter weight.

The position and the angle of the toe is measured by the CCD camera. In order to measure the angles of the joints, potentiometers are used since encoders of the motor are useless due to the extension of the

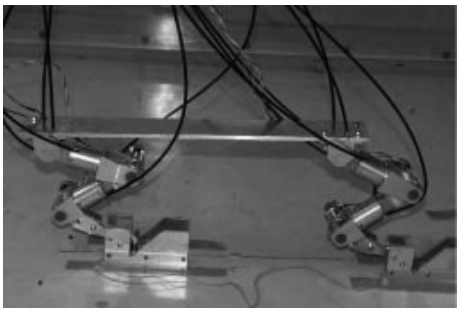

Figure 11: Cat robot

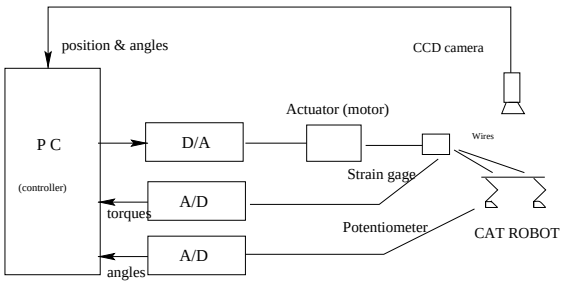

Figure 12: System configuration

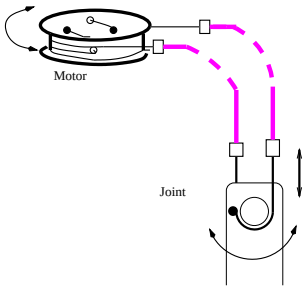

Figure 13: Motor and wire system

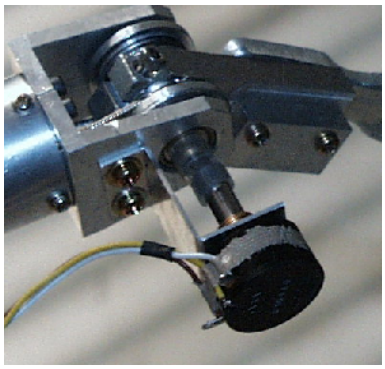

Figure 14: Potentiometer

wire. Because of the wires extension, there are a lot of time delays in the wire system. In order to control the angle in such a bad condition, sliding mode control are introduced as,

$$\tau_d = -K_{\text{outer}} sgn(S_1), \quad (27)$$

$$S_1 = \dot{e}_q + \lambda_{\text{outer}} e_q, \quad (28)$$

where $e_q = q - q_d$ and λ is a positive constant.

Furthermore, we introduced strain-gages in the wire system between motors and the body of the cat to measure the equivalent torques exerted to the joints(Fig.15), since the power applied by the motors is lost due to friction in the wire system. Tension of the wire is measured using the bending deformation of a plate stretched from both sides(Fig.16).

Using the information from the strain gage, a minor loop compensation is constructed as,

$$\tau = \tau_d - K_{minor} sgn(S_2), \quad (29)$$

$$S_2 = \int_0^t e_\tau dt, \quad (30)$$

where, $e_\tau = \tilde{\tau} - \tau_d$, $\tilde{\tau}$ is the measured torque.

5.2. Learning control

The problem due to the time loss and disturbance of the wire system is too serious, it was difficult to apply the proposed method directly, therefore the learning control [6] is applied as follows.

In the i-th trial, the sliding surface is modified as

$$S_1(t) = \dot{e}_q(t) + \lambda e_q(t) + u_i(t), \quad (31)$$

where u_i indicates the learning term which is updated by the following algorithm.

$$u_{i+1} = u_i - \gamma_i L(q_d - q_i), \quad (32)$$

where, L is a learning filter, q_i is the experimental data of the ith trial, and γ_i is positive coefficient. The desired angle q_d is determined based on the simulation data. (See the details in [6].)

One of the results is shown in the Fig.17. It is observed that the output of the latter trial is obviously improved.

6. Conclusion and Future Work

We proposed a jumping method of a robotic cat using spring-mass model matching, and we conformed the

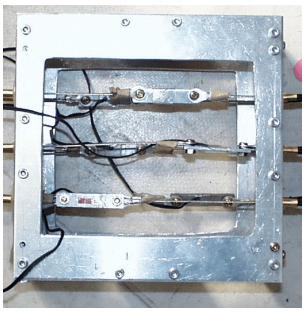

Figure 15: Strain gage system

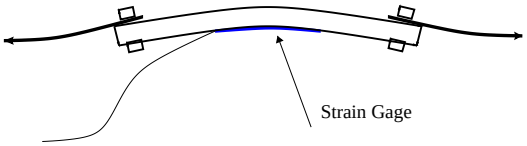

Figure 16: Principal of measuring torque

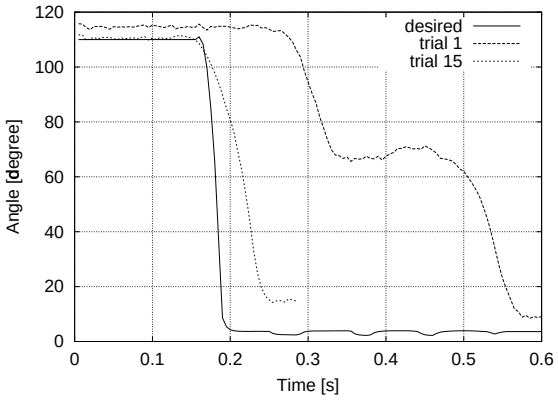

Figure 17: Learning result: Angle of the rear toe

effectiveness of the control law by simulation, in which the robotic cat could jump towards the wall and land on the wall. For it's initial posture evaluation, we used *stochastic dynamic manipulability measure*.

In order to realize the real robot, VSS control and learning control were applied and much progress are conformed. But the jumping has not completed yet, and future work should include:

- completion of the jumping with the real robot,
- learning control in the task space,
- realization of a 3D cat robot, and development of the control into the three-dimensional system.

Acknowledgment
This research was partially supported by the Scientific and Research Foundation of the Ministry of Education under Grant COE #09CE2004

References

[1] D.T.Greenwood, 1977, *Classical dynamics*, Prentice Hall.

[2] S.Tadokoro and T.Takamori, 1993, "On Dynamic Evaluation of Dexterity of Robot Manipulators Considering Deviation of Acceleration," Trans. of SICE, Vol.29, No.4, pp.419-428

[3] S.Tadokoro and T.Takamori, 1993, "An Evalutiong Method for Dexterity of Robot Manipulators Considering Deviation of Direction of Motions," Trans. of SICE, Vol.29, No.6, pp.668-676

[4] Xiaoping Yun and Nilanjan Sarkar, 1998, "Unified Formulation of Robotic Systems with Holonomic and Nonholonomic Constraints," Vol. 14, No.4, pp.640-450

[5] N.Ueno, 1999, "A Study on efficient vertical movement of Robotic Systems In spired by Cat's Jumping," Bachelor thesis, Dept. of Control and Systems Eng. Tokyo Inst. of Tech.

[6] M.Yamakita and K.Furuta, 1992, "A Design of Learning Control System for Multivariable Systems" Asia-Pacific Engineering Journal(Part A), Vol.2, No.1, pp.97-118

See you again!

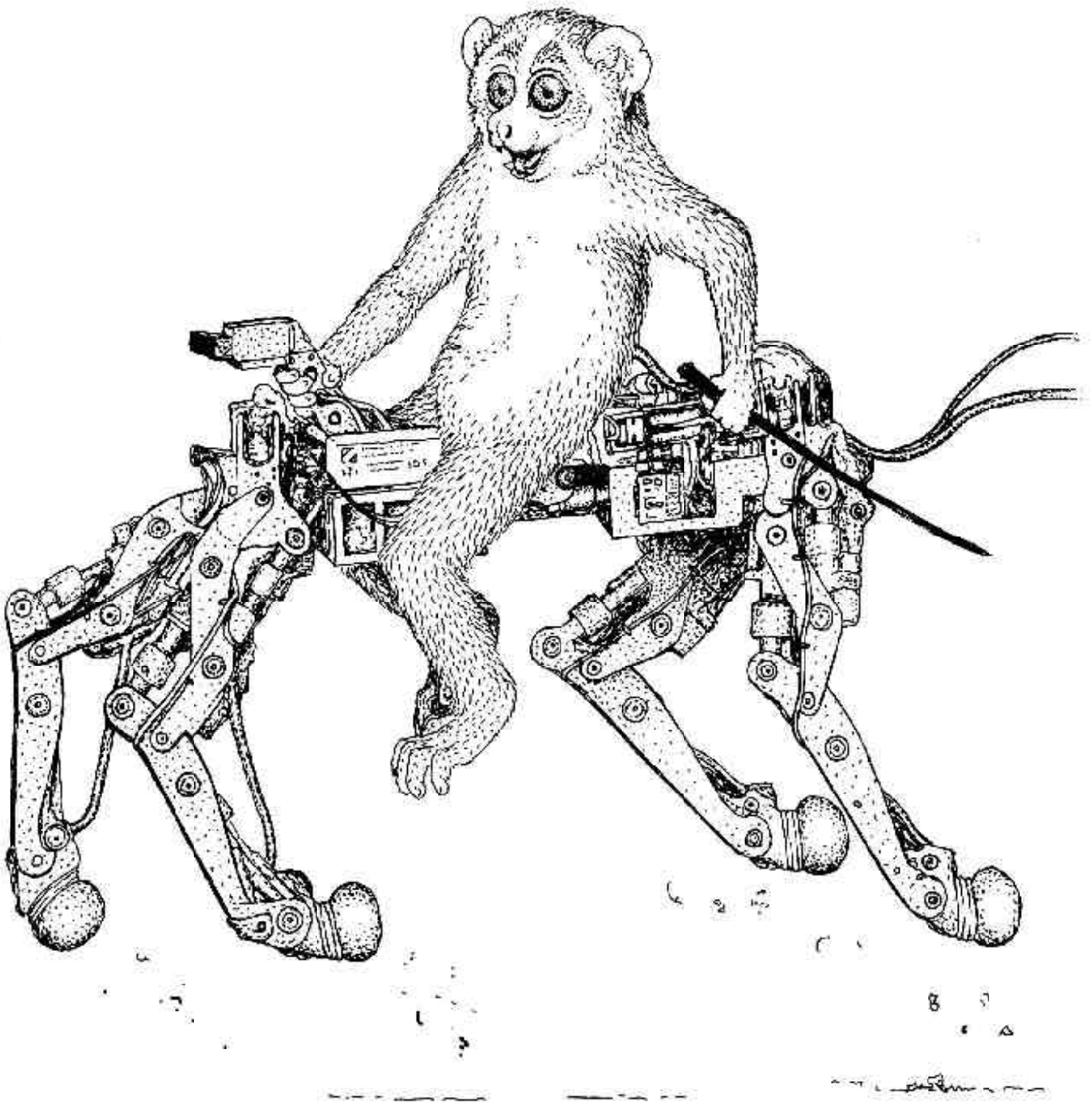

IPC:

H.Kimura (University of Electro-Communications)
H.Witte (Friedrich-Schiller-Universitat Jena)
G.Taga (University of Tokyo)